

bradscholars

Mechanistic approaches towards understanding particle formation in biopharmaceutical formations.

The role of surfactant type and level on protein conformational stability, as assessed by calorimetry, and on protein size stability as assessed by dynamic light scattering, micro flow imaging and HIAC

Item Type	Thesis
Authors	Vaidilaite-Pretorius, Agita
Rights	
The University of Bradford theses are licenced under a Creative Commons Licence.
Download date	2026-04-20 02:49:23
Link to Item	http://hdl.handle.net/10454/13482



University of Bradford eThesis

This thesis is hosted in [Bradford Scholars](#) – The University of Bradford Open Access repository. Visit the repository for full metadata or to contact the repository team



© University of Bradford. This work is licenced for reuse under a [Creative Commons Licence](#).

Mechanistic Approaches towards Understanding Particle Formation in
Biopharmaceutical Formulations

The role of surfactant type and level on protein conformational stability, as
assessed by calorimetry, and on protein size stability as assessed by dynamic light
scattering, micro flow imaging and HIAC

Agita VAIDILAITE-PRETORIUS

Submitted for the Degree
of Doctor of Philosophy

Faculty of Life Sciences
Department of Pharmacy and Pharmaceutical Innovation

University of Bradford

2013

Abstract

Agita Vaidilaite-Pretorius

Mechanistic Approaches towards Understanding Particle Formation in Biopharmaceutical Formulations

The role of surfactant type and level on protein conformational stability, as assessed by calorimetry, and on protein size stability as assessed by dynamic light scattering, micro flow imaging and HIAC

Keywords: Surfactant, High Sensitivity Differential Scanning Calorimetry (HSDSC), Liquid Particle Counter (HIAC), Micro-flow Imaging (MFI), Aggregation, Protein stabilization, Sub-visible particles, Antibody IgG2, Bovine serum albumin (BSA), Size distribution.

Control and analysis of protein aggregation is an increasing challenge to biopharmaceutical research and development. Therefore it is important to understand the interactions, causes and analysis of particles in order to control protein aggregation to enable successful biopharmaceutical formulations.

This work investigates the role of different non-ionic surfactants on protein conformational stability, as assessed by HSDSC, and on protein size stability as assessed by Dynamic Light Scattering (DLS), HIAC and MFI. BSA and IgG2 were used as model proteins. Thermal unfolding experiments indicated a very weak surfactant-immunoglobulin IgG2 interaction, compared to much stronger interactions for the BSA surfactant systems.

The DLS results showed that BSA and IgG2 with different surfactants and concentration produced different levels of particle size growth. The heat treatment and aging of samples in the presence of Tween 20, Tween 80, Brij 35 and Pluronic F-68 surfactants led to an increase in the populations of larger particles for BSA samples, whereas IgG2 systems did not notably aggregate under storage conditions

MFI was shown to be more sensitive than HIAC technique for measuring sub-visible particles in protein surfactant systems. Heat treatment and

storage stress showed a significant effect on BSA and IgG2 protein sub-visible particle size stability.

This work has demonstrated that both proteins with different Tween 20, Tween 80, Brij 35 and Pluronic F-68 concentrations, have different level of conformational and size stability. Also aging samples and heating stress bears the potential to generate particles, but this depends on surfactant type. Poor predictive correlations between the analytical methods were determined.

Acknowledgements

Firstly I would like to thank my Academic Supervisors Prof. Rob T. Forbes and Dr. Wendy L. Hulse for their support throughout the project and guidance through all the stages of this process. They have provided an accessible source for help when I required it and therefore made this project far easier to complete than it would have been otherwise.

I would like to thank MedImmune UK Ltd who provided financial support for this work. Many thanks are going to Shahid Uddin and his formulation group at Medimmune UK Ltd for their excellent technical assistance, support on many of the instruments used in this work and the opportunity to spend time at the company. Special thanks for the MedImmune formulation group research scientists Jamie Biddlecombe, Sarah Grasso and Smita Kumar for their assistance and training with the Dynamic Light Scattering, High Sensitivity Differential Scanning Calorimetry, Light Obscuration and Micro-flow imaging instruments.

Special thanks also go to my husband Mike, my mum, my dad and to my brother for their continual support over the last four years without which none of this would have been possible.

Table of Contents

Abstract.....	i
Acknowledgements.....	iii
Table of Contents.....	iv
List of Figures	viii
List of Tables.....	xxv
List of symbols and abbreviations.....	xxvii
Chapter 1 Introduction	1
1.1 General Introduction	2
1.2 Mechanisms of aggregation and particle formation.....	2
1.3 Conformational stability: Thermal unfolding	5
1.4 Analytical technique for characterising protein conformational stability – HSDSC	7
1.5 Analytical techniques to characterise aggregates and particulates.....	7
1.5.1 Laser Diffraction Technology	9
1.5.2 Analytical Ultracentrifugation (AUC).....	10
1.5.3 Field Flow Fractionation (FFF).....	12
1.5.4 Multiangle Light Scattering (MALS).....	13
1.5.5 Size Exclusion Chromatography (SEC)	13
1.5.6 Dynamic Light Scattering (DLS).....	15
1.5.7 Light Obscuration and Microscopic Particle Count.....	16
1.5.7.1 Light Obscuration (HIAC).....	17
1.5.7.2 Micro-flow imaging (MFI).....	18
1.5.7.3 Flow particle image analysis (FPIA).....	20
1.5.8 Visual Inspection.....	21
1.5.9 Raman Spectroscopy.....	22
1.6 Gaps in the control and analysis of particles.....	23
1.7 Protein formulation. Use of surfactants	29
1.7.1 Structure and behaviour of surfactants	30
1.7.2 Micellization. Critical Micelle Concentration (CMC).....	31
1.8 Choice of materials	33
1.8.1 Phosphate buffered saline	33
1.8.2 Bovine Serum Albumin.....	34

1.8.3	Antibody IgG2	34
1.8.4	Nonionic surfactants: Tween 20, Tween 80, Brij 35 and Pluronic F-68.....	36
1.9	Aims and objectives	39
1.10	Structure of thesis	40
	Chapter 2 Materials and Methods.....	42
2.1	Materials	43
2.1.1	Sources of materials	43
2.1.2	Material processing.....	44
2.1.2.1	Preparation of Bovine Serum Albumin (10 mg/ml) solution.....	44
2.1.2.2	Preparation of antibody IgG2 (10 mg/ml) solution.....	44
2.1.2.3	Preparation of BSA (10 mg/ml) and IgG2 (10 mg/ml) with non ionic Tween 20, Tween 80, Brij 35 and Pluronic F-68 surfactants solutions.....	44
2.1.2.4	Preparation of PBS buffer with Tween 20, Tween 80, Brij 35 and Pluronic F-68 solutions	45
2.2	Methods	45
2.2.1	Heat treatment stress method.....	45
2.2.2	Stability study.....	46
2.2.3	High Sensitivity Differential Scanning Calorimetry (HSDSC)	46
2.2.4	Dynamic Light Scattering (DLS).....	49
2.2.5	Light Obscuration (HIAC).....	51
2.2.6	Micro-flow Imaging (MFI)	52
2.2.7	Statistical data analysis.....	53
	Chapter 3 Effect of surfactant and surfactant concentration on the thermal unfolding of BSA and Igg2 in solution	55
3.1	Introduction	56
3.2	Objective.....	57
3.3	Experimental.....	57
3.4	Results and Discussion.....	58
3.4.1	Thermal unfolding experiments of bovine serum albumin.....	58
3.4.2	Thermal unfolding experiments of monoclonal antibody IgG2	65
3.5	General Discussion.....	75

Chapter 4 Effect of different concentrations of Tween 20, Tween 80, Brij 35 and PLuronic F-68 surfactants on size stability by Dynamic Light Scattering	76
4.1 Introduction	77
4.2 Objective	78
4.3 Experimental	79
4.4 Results and Discussion.....	79
4.4.1 Particle size distribution measurements for freshly prepared BSA-surfactants systems	79
4.4.2 Particle size distribution measurements for heat stressed BSA-surfactants systems	92
4.4.3 Particle size distribution measurements for aged BSA-surfactant systems.....	104
4.4.4 Particle size distribution measurements for freshly prepared IgG2-surfactants systems	115
4.4.5 Particle size distribution measurements for heated IgG2-surfactant systems.....	125
4.4.6 Particle size distribution measurements for aged IgG2-surfactants .	135
4.5 General Discussion	144
Chapter 5 Light Obscuration (HIAC) and Micro-flow Imaging (MFI) applied for subvisible particulate analysis of BSA and Igg2 with Tween 20, Tween 80, Brij 35 and Pluronic F-68 surfactants at below, around and above CMC levels	146
5.1 Introduction	147
5.2 Objective	148
5.3 Experimental	148
5.3.1 Light obscuration (HIAC) measurements	148
5.3.2 Micro-Flow Imaging (MFI) measurements.....	149
5.4 Results and Discussion.....	149
5.4.1 Light Obscuration (HIAC) measurements	149
5.4.1.1 Light Obscuration measurements for fresh, heated and aged BSA surfactant free and BSA with Tween 20, Tween 80, Brij 35 and Pluronic F-68 surfactants at below, around and above CMC levels	149

5.4.1.2	Light Obscuration measurements for fresh, heated and aged IgG2 surfactant free and IgG2 with Tween 20, Tween 80, Brij 35 and Pluronic F-68 surfactants at below, around and above CMC levels	177
5.4.2	Micro-flow imaging (MFI) measurements	202
5.4.2.1	Micro-flow measurements for fresh, heated and aged BSA surfactant free and BSA with Tween 20, Tween 80, Brij 35 and Pluronic F-68 surfactants at below, around and above CMC levels	202
5.4.2.2	Micro-flow measurements for fresh, heated and aged IgG2 surfactant free and IgG2 with Tween 20, Tween 80, Brij 35 and Pluronic F-68 surfactants present at below, around and above their CMC levels	226
5.5	General discussion	249
	Chapter 6 General Discussion	251
	Chapter 7 General Conclusions and Recommendations for Future Research	294
7.1	General Conclusions.....	295
7.2	Recommendations for future research.....	305
	References.....	307
	Appendices	323

List of Figures

Figure 1.1.	Aggregates and Particles size range (Krishnan, 2009).....	3
Figure 1.2.	Proteins aggregation and particle formation through different mechanisms (Krishnan, 2009).....	5
Figure 1.3.	Analytical methods to characterize and quantify protein aggregates and particles. Shaded region – sub-visible particles (Jiang, 2009).....	8
Figure 1.4.	Schematic picture of a laser diffraction instrument (Beckman Coulter, 2008).....	9
Figure 1.5.	Illustration of SEC experiment (Analytical Ventura, 2013).....	14
Figure 1.6.	Reported hydrodynamic diameter (Malvern Instruments Ltd, 2011).....	15
Figure 1.7.	Diagram of Light Obscuration particle counter (Solids Wiki, 2013).....	18
Figure 1.8.	Micro-flow imaging instrument configuration (Sharma et al., 2010).....	19
Figure 1.9.	FPIA sample dispersion and image capture (Malvern Instruments Ltd, 2010).....	20
Figure 1.10.	Scheme of particle flow (Malvern Instruments Ltd, 2010).....	21
Figure 1.11.	Aggregation process. N – native protein state, I – intermediate protein state, U – unfolded protein state, N* - non-native protein state (Das et al., 2007).....	24
Figure 1.12.	Figure of a surfactant monomer (Garq, 2012).....	30
Figure 1.13.	Micellization (Rangel-Yaguil et al., 2005).....	32
Figure 1.14.	The self assembly mechanism of micelle formation with increasing concentration of surfactant (Behan, 1999).....	33
Figure 1.15.	Schematic drawing of IgG antibody (Mayer, 2009).....	35
Figure 1.16.	Chemical structure of polysorbates 20 and 80. w+x+y+z refers to the total number of oxyethylene subunits on each surfactant molecule and may not exceed 20 (Kerwin, 2008).....	37
Figure 1.17.	Brij 35 structure (Stavroudis, 2009).....	37

Figure 1.18.	Pluronic F-68 structure (Santander-Ortega et al., 2006).....	38
Figure 2.1.	Differential scanning calorimetric unit (Microcal system user manual).....	46
Figure 2.2.	Microcal VP – capillary DSC 96 well plate (Edge Biosystems Inc.).....	47
Figure 2.3.	Low volume quartz batch cuvette for size and molecular weight measurements for use with the Zetasizer Nano series (The Nanobiotechnology Centre, 2009).....	50
Figure 2.4.	Typical image frame (Brightwell Technologies Inc., 2006).....	53
Figure 3.1.	Thermal unfolding profile of BSA (10 mg/ml in PBS buffer). Black line represents normalised calorimetric data for the thermal denaturation of BSA. Red line represents the results of fitting experimental curves to a non-two-state model.....	59
Figure 3.2.	Unfolding temperatures (T_m) of BSA (10mg/ml) with different Tween 20, Tween 80, Brij 35 and Pluronic F-68 concentrations.....	61
Figure 3.3.	The effect of different concentrations of Tween 20, Tween 80, Brij 35 and Pluronic F-68 surfactants on BSA (10 mg/ml) unfolding temperature T_m ($^{\circ}\text{C}$) measured by HSDSC. Data is expressed as the mean \pm Std. Deviation. ** $P < 0.01$ - *** $P < 0.001$; significant decrease in BSA with surfactants unfolding temperature T_m compared with BSA (10 mg/ml) surfactant free solutions.....	63
Figure 3.4.	Effect of surfactant concentration relative to CMC on the T_m of BSA for Tween 20, Tween 80, Brij 35 and Pluronic F-68 surfactants. (1 – 10 times below CMC; 2 – around CMC; 3 – 10 times above CMC).....	64
Figure 3.5.	Thermal unfolding profile of IgG2 (10 mg/ml). Black line represents normalised calorimetric data for the thermal denaturation of IgG2 (10 mg/ml). Red lines represent the two peaks of fitting experimental curves to a non-two-state model.....	66

Figure 3.6.	Thermal unfolding temperatures (T_{m1} and T_{m2}) of IgG2 (10 mg/ml) with different Tween 20, Tween 80, Brij 35 and Pluronic F-68 concentrations.....	68
Figure 3.7.	The effect of different CMC levels of Tween 20, Tween 80, Brij 35 and Pluronic F-68 surfactants on IgG2 unfolding temperature T_{m1} ($^{\circ}$ C) measured by HSDSC. Data are expressed as the mean \pm Std. deviation. NS – no significant difference, * - $P<0.05$, ** - $P<0.01$, *** - $P<0.001$ significant decrease in unfolding temperature T_{m1} for IgG2 with surfactants compared with IgG2 surfactant free solution.....	69
Figure 3.8.	The effect of different CMC levels of Tween 20, Tween 80, Brij 35 and Pluronic F-68 surfactants on IgG2 unfolding temperature T_{m2} ($^{\circ}$ C) measured by HSDSC. Data are expressed as the mean \pm Std. deviation. NS – no significant difference, ** - $P<0.01$, *** - $P<0.001$ significant decrease in T_{m2} for IgG2 with surfactants compared with IgG2 surfactant free solution.....	71
Figure 3.9.	The effect of different surfactant concentration levels on T_{m1} . (1 – below CMC; 2 – around CMC; 3 – above CMC).....	72
Figure 3.10.	The effect of different CMC concentration levels on T_{m2} . (1 – below CMC; 2 – around CMC; 3 – above CMC).....	73
Figure 3.11.	Scatter plot of unfolding temperatures T_{m1} and T_{m2} measured by HSDSC for IgG2-surfactant systems.....	74
Figure 4.1.	Particle size distribution by intensity obtained for freshly prepared BSA (10 mg/ml). Average $n=3$	80
Figure 4.2.	Particle size distribution by intensity obtained for BSA (10 mg/ml) fresh samples with: (A) Tween 20 below CMC; (B) Tween 20 around CMC; (C) Tween 20 above CMC.....	81
Figure 4.3.	The surfactant can exist as different phases depending upon the concentration of the sample (Malvern Instruments Ltd., 2006).....	83
Figure 4.4.	Particle size distribution by intensity obtained for BSA (10 mg/ml) with: (A) Tween 80 below CMC; (B) Tween 80 around CMC; (C) Tween 80 above CMC.....	84

Figure 4.5.	Particle size distribution by intensity obtained for BSA (10 mg/ml) with: (A) Brij 35 below CMC; (B) Brij 35 around CMC; (C) Brij 35 above CMC.....	86
Figure 4.6.	Particle size distribution by intensity obtained for BSA (10 mg/ml) with: (A) Pluronic F-68 below CMC; (B) Pluronic F-68 around CMC; (C) Pluronic F-68 above CMC.....	88
Figure 4.7.	Particle size diameter (nm) of the peak with greatest intensity (Peak 1) for fresh BSA (10 mg/ml) with below, around and above CMC levels of Tween 20, Tween 80, Brij 35 and Pluronic F-68 surfactants.....	90
Figure 4.8.	A plot of the highest intensity peak diameter (nm) obtained at below (1), around (2) and above (3) CMC levels for Tween 20, Tween 80, Brij 35 and Pluronic F-68 surfactants.....	91
Figure 4.9.	Particle size distribution by intensity obtained for heated (66°C) BSA (10 mg/ml).....	93
Figure 4.10.	Particle size distribution by intensity obtained for heated samples for BSA (10 mg/ml) with: (A) Tween 20 below CMC; (B) Tween 20 around CMC; (C) Tween 20 above CMC.....	94
Figure 4.11.	Particle size distribution by intensity obtained for heated samples for BSA (10 mg/ml) with: (A) Tween 80 below CMC; (B) Tween 80 around CMC; (C) Tween 80 above CMC.....	96
Figure 4.12.	Particle size distribution by intensity obtained for heated samples (66°C) for BSA (10 mg/ml) with: (A) Brij 35 below CMC; (B) Brij 35 around CMC; (C) Brij 35 above CMC.....	98
Figure 4.13.	Particle size distribution by intensity obtained for heated (66°C) samples for BSA (10 mg/ml) with: (A) Pluronic F-68 below CMC; (B) Pluronic F-68 around CMC; (C) Pluronic F-68 above CMC.....	100
Figure 4.14.	Particle size diameter (nm) of the peak with greatest intensity (Peak 1) for heated BSA (10 mg/ml) with below, around and above CMC levels of Tween 20, Tween 80, Brij 35 and Pluronic F-68 surfactants.....	102

Figure 4.15. A plot of the highest intensity peak diameter (nm) obtained at below (1), around (2) and above (3) CMC levels for Tween 20, Tween 80, Brij 35 and Pluronic F-68 surfactants.....	103
Figure 4.16. Particle size distribution by intensity for aged BSA (10 mg/ml).....	104
Figure 4.17. Particle size distribution by intensity obtained for aged BSA (10 mg/ml) with: (A) Tween 20 below CMC; (B) Tween 20 around CMC; (C) Tween 20 above CMC.....	106
Figure 4.18. Particle size distribution by intensity obtained for aged BSA (10 mg/ml) with: (A) Tween 80 below CMC; (B) Tween 80 around CMC; (C) Tween 80 above CMC.....	108
Figure 4.19. Particle size distribution by intensity obtained for aged BSA (10 mg/ml) with: (A) Brij 35 below CMC; (B) Brij 35 around CMC; (C) Brij 35 above CMC.....	110
Figure 4.20. Particle size distribution by intensity obtained for aged BSA (10 mg/ml) with: (A) Pluronic F-68 below CMC; (B) Pluronic F-68 around CMC; (C) Pluronic F-68 above CMC.....	112
Figure 4.21. Particle size diameter (nm) of the peak with greatest intensity (Peak 1) for aged BSA (10 mg/ml) with below, around and above CMC levels of Tween 20, Tween 80, Brij 35 and Pluronic F-68 surfactants.....	114
Figure 4.22. A plot of the highest intensity peak diameter (nm) obtained at below (1), around (2) and above (3) CMC levels for Tween 20, Tween 80, Brij 35 and Pluronic F-68 surfactants.....	115
Figure 4.23. Particle size distribution by intensity obtained for freshly prepared IgG2 (10 mg/ml). Average n=3.....	116
Figure 4.24. Particle size distribution by intensity obtained for IgG2 (10 mg/ml) with: (A) Tween 20 below CMC; (B) Tween 20 around CMC; (C) Tween 20 above CMC.....	117
Figure 4.25. Particle size distribution by intensity obtained for IgG2 (10 mg/ml) with: (A) Tween 80 below CMC; (B) Tween 80 around CMC; (C) Tween 80 above CMC.....	118

Figure 4.26. Particle size distribution by intensity obtained for IgG2 (10 mg/ml) with: (A) Brij 35 below CMC; (B) Brij 35 around CMC; (C) Brij 35 above CMC.....	119
Figure 4.27. Particle size distribution by intensity obtained for IgG2 (10 mg/ml) with: (A) Pluronic F-68 below CMC; (B) Pluronic F-68 around CMC; (C) Pluronic F-68 above CMC.....	121
Figure 4.28. Particle size diameter (nm) of the peak with greatest intensity (Peak 1) for fresh IgG2 (10 mg/ml) with below, around and above CMC levels of Tween 20, Tween 80, Brij 35 and Pluronic F-68 surfactants.....	123
Figure 4.29. A plot of the highest intensity peak diameter (nm) obtained at below (1), around (2) and above (3) CMC levels for Tween 20, Tween 80, Brij 35 and Pluronic F-68 surfactants.....	124
Figure 4.30. Particle size distribution by intensity obtained for heated (60°C) IgG2 (10 mg/ml).....	125
Figure 4.31. Particle size distribution by intensity obtained for heated IgG2 (10 mg/ml) with: (A) Tween 20 below CMC; (B) Tween 20 around CMC; (C) Tween 20 above CMC.....	127
Figure 4.32. Particle size distribution by intensity obtained for heated IgG2 (10 mg/ml) with: (A) Tween 80 below CMC; (B) Tween 80 around CMC; (C) Tween 80 above CMC.....	129
Figure 4.33. Particle size distribution by intensity obtained for heated IgG2 (10 mg/ml) with: (A) Brij 35 below CMC; (B) Brij 35 around CMC; (C) Brij 35 above CMC.....	130
Figure 4.34. Particle size distribution by intensity obtained for heated IgG2 (10 mg/ml) with: (A) Pluronic F-68 below CMC; (B) Pluronic F-68 around CMC; (C) Pluronic F-68 above CMC.....	132
Figure 4.35. Particle size diameter (nm) of the peak with greatest intensity (Peak 1) for heated IgG2 (10 mg/ml) with below, around and above CMC levels of Tween 20, Tween 80, Brij 35 and Pluronic F-68 surfactants.....	134
Figure 4.36. A plot of the highest intensity peak diameter (nm) obtained at below (1), around (2) and above (3) CMC levels for heated	

	IgG2 with Tween 20, Tween 80, Brij 35 and Pluronic F-68 surfactants.....	135
Figure 4.37.	Particle size distribution by intensity obtained for aged samples for IgG2 (10 mg/ml).....	136
Figure 4.38.	Particle size distribution by intensity obtained for aged samples for IgG2 (10 mg/ml) with: (A) Tween 20 below CMC; (B) Tween 20 around CMC; (C) Tween 20 above CMC.....	137
Figure 4.39.	Particle size distribution by intensity obtained for aged samples for IgG2 (10 mg/ml) with: (A) Tween 80 below CMC; (B) Tween 80 around CMC; (C) Tween 80 above CMC.....	138
Figure 4.40.	Particle size distribution by intensity obtained for aged samples for IgG2 (10 mg/ml) with: (A) Brij 35 below CMC; (B) Brij 35 around CMC; (C) Brij 35 above CMC.....	139
Figure 4.41.	Particle size distribution by intensity obtained for aged samples for IgG2 (10 mg/ml) with: (A) Pluronic F-68 below CMC; (B) Pluronic F-68 around CMC; (C) Pluronic F-68 above CMC...	140
Figure 4.42.	Particle size diameter (nm) of the peak with greatest intensity (Peak 1) for aged IgG2 (10 mg/ml) with below, around and above CMC levels of Tween 20, Tween 80, Brij 35 and Pluronic F-68 surfactants.....	142
Figure 4.43.	A plot of the highest intensity peak diameter (nm) obtained at below (1), around (2) and above (3) CMC levels for aged Tween 20, Tween 80, Brij 35 and Pluronic F-68 surfactants.....	143
Figure 5.1.	Particle concentrations measured by HIAC for fresh, heated and aged BSA samples. Data are expressed as the mean \pm Std. Deviation. * P<0.05, ** P<0.01, *** P<0.001; significant difference in particles per ml compared with fresh BSA samples.....	150
Figure 5.2.	Particle concentrations in size ranges: (A) $\geq 2 \mu\text{m}$ and $\geq 5 \mu\text{m}$, (B) $\geq 10 \mu\text{m}$ and $\geq 25 \mu\text{m}$, (C) $\geq 50 \mu\text{m}$ and $\geq 100 \mu\text{m}$ per ml measured by HIAC for fresh BSA samples with Tween 20, Tween 80, Brij 35 and Pluronic F-68 surfactants at below,	

- around and above CMC levels. Data are expressed as the mean \pm Std. Deviation.....153
- Figure 5.3. Particle concentrations in size ranges: (A) $\geq 2 \mu\text{m}$ and $\geq 5 \mu\text{m}$, (B) $\geq 10 \mu\text{m}$ and $\geq 25 \mu\text{m}$, (C) $\geq 50 \mu\text{m}$ and $\geq 100 \mu\text{m}$ per ml measured by HIAC for heated BSA samples with Tween 20, Tween 80, Brij 35 and Pluronic F-68 surfactants at below, around and above CMC levels. Data are expressed as the mean \pm Std. Deviation.....155
- Figure 5.4. Particle concentrations in size ranges: (A) $\geq 2 \mu\text{m}$ and $\geq 5 \mu\text{m}$, (B) $\geq 10 \mu\text{m}$ and $\geq 25 \mu\text{m}$, (C) $\geq 50 \mu\text{m}$ and $\geq 100 \mu\text{m}$ per ml measured by HIAC for aged BSA samples with Tween 20, Tween 80, Brij 35 and Pluronic F-68 surfactants at below, around and above CMC levels. Data are expressed as the mean \pm Std. Deviation.....158
- Figure 5.5. Particle concentrations at size ranges of: (A) $\geq 2 \mu\text{m}$, (B) $\geq 5 \mu\text{m}$, (C) $\geq 10 \mu\text{m}$, (D) $\geq 25 \mu\text{m}$, (E) $\geq 50 \mu\text{m}$ and (F) $\geq 100 \mu\text{m}$ measured by HIAC for fresh, heated and aged BSA with Tween 20 at below, around and above its CMC. Data are expressed as the mean \pm Std. Deviation. * $P < 0.05$, ** $P < 0.01$, *** $P < 0.001$; significant difference in particles per ml compared with fresh BSA with Tween 20 samples.....162
- Figure 5.6. Particle concentrations at size ranges of: (A) $\geq 2 \mu\text{m}$, (B) $\geq 5 \mu\text{m}$, (C) $\geq 10 \mu\text{m}$, (D) $\geq 25 \mu\text{m}$, (E) $\geq 50 \mu\text{m}$ and (F) $\geq 100 \mu\text{m}$ measured by HIAC for fresh, heated and aged BSA with Tween 80 at below, around and above its CMC. Data are expressed as the mean \pm Std. Deviation. * $P < 0.05$, ** $P < 0.01$, *** $P < 0.001$; significant difference in particles per ml compared with fresh BSA with Tween 80 samples.....166
- Figure 5.7. Particle concentrations at size ranges of: (A) $\geq 2 \mu\text{m}$, (B) $\geq 5 \mu\text{m}$, (C) $\geq 10 \mu\text{m}$, (D) $\geq 25 \mu\text{m}$, (E) $\geq 50 \mu\text{m}$ and (F) $\geq 100 \mu\text{m}$ measured by HIAC for fresh, heated and aged BSA with Brij 35 at below, around and above its CMC. Data are expressed as the mean \pm Std. Deviation. * $P < 0.05$, ** $P < 0.01$, *** $P < 0.001$;

- significant difference in particles per ml compared with fresh BSA with Brij 35 samples.....171
- Figure 5.8. Particle concentrations at size ranges of: (A) $\geq 2 \mu\text{m}$, (B) $\geq 5 \mu\text{m}$, (C) $\geq 10 \mu\text{m}$, (D) $\geq 25 \mu\text{m}$, (E) $\geq 50 \mu\text{m}$ and (F) $\geq 100 \mu\text{m}$ measured by HIAC for fresh, heated and aged BSA with Pluronic F-68 present at below, around and above its CMC. Data are expressed as the mean \pm Std. Deviation. * $P < 0.05$, ** $P < 0.01$, *** $P < 0.001$; significant difference in particles per ml compared with fresh BSA with Pluronic F-68 samples.....175
- Figure 5.9. Particle concentrations measured by HIAC for fresh, heated and aged IgG2 samples. Data are expressed as the mean \pm Std. Deviation. * $P < 0.05$, ** $P < 0.01$, *** $P < 0.001$; significant difference in particles per ml compared with fresh IgG2 samples.....177
- Figure 5.10. Particle concentrations in size ranges: (A) $\geq 2 \mu\text{m}$ and $\geq 5 \mu\text{m}$, (B) $\geq 10 \mu\text{m}$ and $\geq 25 \mu\text{m}$, (C) $\geq 50 \mu\text{m}$ and $\geq 100 \mu\text{m}$ per ml measured by HIAC for fresh IgG2 samples with Tween 20, Tween 80, Brij 35 and Pluronic F-68 surfactants present at below, around and above their CMC levels. Data are expressed as the mean \pm Std. Deviation.....180
- Figure 5.11. Particle concentrations in size ranges: (A) $\geq 2 \mu\text{m}$ and $\geq 5 \mu\text{m}$, (B) $\geq 10 \mu\text{m}$ and $\geq 25 \mu\text{m}$, (C) $\geq 50 \mu\text{m}$ and $\geq 100 \mu\text{m}$ measured by HIAC for heated IgG2 samples with Tween 20, Tween 80, Brij 35 and Pluronic F-68 surfactants at below, around and above their CMC levels. Data are expressed as the mean \pm Std. Deviation.....182
- Figure 5.12. Particle concentrations in size ranges: (A) $\geq 2 \mu\text{m}$ and $\geq 5 \mu\text{m}$, (B) $\geq 10 \mu\text{m}$ and $\geq 25 \mu\text{m}$, (C) $\geq 50 \mu\text{m}$ and $\geq 100 \mu\text{m}$ per ml measured by HIAC for aged IgG2 samples with Tween 20, Tween 80, Brij 35 and Pluronic F-68 surfactants present at below, around and above their CMC. Data are expressed as the mean \pm Std. Deviation.....184
- Figure 5.13. Particle concentrations at size ranges of: (A) $\geq 2 \mu\text{m}$, (B) $\geq 5 \mu\text{m}$, (C) $\geq 10 \mu\text{m}$, (D) $\geq 25 \mu\text{m}$, (E) $\geq 50 \mu\text{m}$ measured by HIAC

for fresh, heated and aged IgG2 with Tween 20 below, around and above its CMC levels. Data are expressed as the mean \pm Std. Deviation. * P<0.05, ** P<0.01, *** P<0.001; significant difference in particles per ml compared with fresh IgG2 with Tween 20 samples.....188

Figure 5.14. Particle concentrations at size ranges of: (A) $\geq 2 \mu\text{m}$, (B) $\geq 5 \mu\text{m}$, (C) $\geq 10 \mu\text{m}$, (D) $\geq 25 \mu\text{m}$, (E) $\geq 50 \mu\text{m}$ measured by HIAC for fresh, heated and aged IgG2 with Tween 80 present below, around and above CMC. Data are expressed as the mean \pm Std. Deviation. * P<0.05, ** P<0.01, *** P<0.001; significant difference in particles per ml compared with fresh IgG2 with Tween 80 samples.....192

Figure 5.15. Particle concentrations at size ranges of: (A) $\geq 2 \mu\text{m}$, (B) $\geq 5 \mu\text{m}$, (C) $\geq 10 \mu\text{m}$, (D) $\geq 25 \mu\text{m}$, (E) $\geq 50 \mu\text{m}$ measured by HIAC for fresh, heated and aged IgG2 with added Brij 35 below, around and above its CMC level. Data are expressed as the mean \pm Std. Deviation. * P<0.05, ** P<0.01, *** P<0.001; significant difference in particles per ml compared with fresh IgG2 with Brij 35 samples.....196

Figure 5.16. Particle concentrations at size ranges of: (A) $\geq 2 \mu\text{m}$, (B) $\geq 5 \mu\text{m}$, (C) $\geq 10 \mu\text{m}$, (D) $\geq 25 \mu\text{m}$, (E) $\geq 50 \mu\text{m}$ measured by HIAC for fresh, heated and aged IgG2 samples with Pluronic F-68 added below, around and above CMC level. Data are expressed as the mean \pm Std. Deviation. * P<0.05, ** P<0.01, *** P<0.001; significant difference in particles per ml compared with fresh IgG2 with Pluronic F-68 samples.....200

Figure 5.17. Representative micro-flow imaging (MFI) example images for BSA (10 mg/ml) particles.....202

Figure 5.18. Particle concentrations measured by MFI for fresh, heated and aged BSA samples. Data are expressed as the mean \pm Std. Deviation. * P<0.05, ** P<0.01, *** P<0.001; significant difference in particles per ml compared with fresh BSA samples.....203

- Figure 5.19. Particle concentrations in size ranges: (A) $\geq 2 \mu\text{m}$ and $\geq 10 \mu\text{m}$, (B) $\geq 25 \mu\text{m}$, $\geq 50 \mu\text{m}$ and $\geq 100 \mu\text{m}$ per ml measured by MFI for fresh BSA samples with added Tween 20, Tween 80, Brij 35 and Pluronic F-68 surfactants at levels below, around and above their CMC. Data are expressed as the mean \pm Std. Deviation.....205
- Figure 5.20. Particle concentrations in size ranges: (A) $\geq 2 \mu\text{m}$ and $\geq 10 \mu\text{m}$, (B) $\geq 25 \mu\text{m}$, $\geq 50 \mu\text{m}$ and $\geq 100 \mu\text{m}$ per ml measured by MFI for heated BSA samples with added Tween 20, Tween 80, Brij 35 and Pluronic F-68 surfactants at below, around and above their CMC levels. Data are expressed as the mean \pm Std. Deviation.....207
- Figure 5.21. Particle concentration for size ranges: (A) $\geq 2 \mu\text{m}$ and $\geq 10 \mu\text{m}$, (B) $\geq 25 \mu\text{m}$, $\geq 50 \mu\text{m}$ and $\geq 100 \mu\text{m}$ measured by MFI for aged BSA samples with Tween 20, Tween 80, Brij 35 and Pluronic F-68 surfactants at below, around and above their CMC levels. Data are expressed as the mean \pm Std. Deviation.....209
- Figure 5.22. Particle concentrations at size ranges of: (A) $\geq 2 \mu\text{m}$, (B) $\geq 10 \mu\text{m}$, (C) $\geq 25 \mu\text{m}$, (D) $\geq 50 \mu\text{m}$ measured by MFI for fresh, heated and aged BSA with added Tween 20 below, around and above its CMC level. Data are expressed as the mean \pm Std. Deviation. * $P < 0.05$, ** $P < 0.01$, *** $P < 0.001$; significant difference in particles per ml compared with fresh BSA with Tween 20 samples.....212
- Figure 5.23. Particle concentrations at size ranges of: (A) $\geq 2 \mu\text{m}$, (B) $\geq 10 \mu\text{m}$, (C) $\geq 25 \mu\text{m}$, (D) $\geq 50 \mu\text{m}$ and (E) $\geq 100 \mu\text{m}$ measured by MFI for fresh, heated and aged BSA with added Tween 80 below, around and above its CMC level. Data are expressed as the mean \pm Std. Deviation. * $P < 0.05$, ** $P < 0.01$, *** $P < 0.001$; significant difference in particles per ml compared with fresh BSA with Tween 80 samples.....216
- Figure 5.24. Particle concentrations at size ranges of: (A) $\geq 2 \mu\text{m}$, (B) $\geq 10 \mu\text{m}$, (C) $\geq 25 \mu\text{m}$, (D) $\geq 50 \mu\text{m}$ and (E) $\geq 100 \mu\text{m}$ measured by MFI for fresh, heated and aged BSA with added Brij 35 at

below, around and above its CMC. Data are expressed as the mean \pm Std. Deviation. * $P < 0.05$, ** $P < 0.01$, *** $P < 0.001$; significant difference in particles per ml compared with fresh BSA with Brij 35 samples.....220

Figure 5.25. Particle concentrations at size ranges of: (A) $\geq 2 \mu\text{m}$, (B) $\geq 10 \mu\text{m}$, (C) $\geq 25 \mu\text{m}$, (D) $\geq 50 \mu\text{m}$ and (E) $\geq 100 \mu\text{m}$ measured by MFI for fresh, heated and aged BSA with added Pluronic F-68 at concentrations below, around and above its CMC. Data are expressed as the mean \pm Std. Deviation. * $P < 0.05$, ** $P < 0.01$, *** $P < 0.001$; significant difference in particles per ml compared with fresh BSA with Pluronic F-68 samples.....224

Figure 5.26. Particle concentrations measured by MFI for fresh, heated and aged IgG2 samples. Data are expressed as the mean \pm Std. Deviation. * $P < 0.05$, ** $P < 0.01$, *** $P < 0.001$; significant difference in particles per ml compared with fresh IgG2 samples.....226

Figure 5.27. Particle concentrations in size ranges of $\geq 2 \mu\text{m}$, $\geq 10 \mu\text{m}$ and $\geq 25 \mu\text{m}$ per ml measured by MFI for fresh IgG2 samples with added Tween 20, Tween 80, Brij 35 and Pluronic F-68 surfactants at below, around and above their CMC levels. Data are expressed as the mean \pm Std. Deviation.....228

Figure 5.28. Particle concentrations in size range: (A) $\geq 2 \mu\text{m}$ and $\geq 10 \mu\text{m}$; (B) $\geq 25 \mu\text{m}$, $\geq 50 \mu\text{m}$ and $\geq 100 \mu\text{m}$ per ml measured by MFI for heated IgG2 samples with Tween 20, Tween 80, Brij 35 and Pluronic F-68 surfactants at below, around and above their CMC levels. Data are expressed as the mean \pm Std. Deviation.....230

Figure 5.29. Particle concentrations in size range: (A) $\geq 2 \mu\text{m}$ and $\geq 10 \mu\text{m}$; (B) $\geq 25 \mu\text{m}$, $\geq 50 \mu\text{m}$ and $\geq 100 \mu\text{m}$ per ml measured by MFI for aged IgG2 samples with added Tween 20, Tween 80, Brij 35 and Pluronic F-68 surfactants at below, around and above their CMC. Data are expressed as the mean \pm Std. Deviation.....232

Figure 5.30. Particle concentrations at size ranges of: (A) $\geq 2 \mu\text{m}$, (B) $\geq 10 \mu\text{m}$, (C) $\geq 25 \mu\text{m}$, (D) $\geq 50 \mu\text{m}$ and (E) $\geq 100 \mu\text{m}$ measured by

	MFI for fresh, heated and aged IgG2 with Tween 20 at concentrations below, around and above CMC. Data are expressed as the mean \pm Std. Deviation. * P<0.05, ** P<0.01, *** P<0.001; significant difference in particles per ml compared with fresh IgG2 with Tween 20 samples.....	235
Figure 5.31.	Particle concentrations at size ranges of: (A) $\geq 2 \mu\text{m}$, (B) $\geq 10 \mu\text{m}$, (C) $\geq 25 \mu\text{m}$, (D) $\geq 50 \mu\text{m}$ and (E) $\geq 100 \mu\text{m}$ measured by MFI for fresh, heated and aged IgG2 with Tween 80 present below, around and above CMC. Data are expressed as the mean \pm Std. Deviation. * P<0.05, ** P<0.01, *** P<0.001; significant difference in particles per ml compared with fresh IgG2 with Tween 80 samples.....	239
Figure 5.32.	Particle concentrations at size ranges of: (A) $\geq 2 \mu\text{m}$, (B) $\geq 10 \mu\text{m}$, (C) $\geq 25 \mu\text{m}$, (D) $\geq 50 \mu\text{m}$ and (E) $\geq 100 \mu\text{m}$ measured by MFI for fresh, heated and aged IgG2 with Brij 35 below, around and above CMC levels. Data are expressed as the mean \pm Std. Deviation. * P<0.05, ** P<0.01, *** P<0.001; significant difference in particles per ml compared with fresh IgG2 with Brij 35 samples.....	243
Figure 5.33.	Particle concentrations at size ranges of: (A) $\geq 2 \mu\text{m}$, (B) $\geq 10 \mu\text{m}$, (C) $\geq 25 \mu\text{m}$, (D) $\geq 50 \mu\text{m}$ measured by MFI for fresh, heated and aged IgG2 with Pluronic F-68 below, around and above CMC levels. Data are expressed as the mean \pm Std. Deviation. * P<0.05, ** P<0.01, *** P<0.001; significant difference in particles per ml compared with fresh IgG2 with Pluronic F-68 samples.....	247
Figure 6.1.	Comparison of particle count per ml measured by HIAC and MFI methods for fresh BSA protein.....	260
Figure 6.2.	Comparison of particle count per ml measured by HIAC and MFI methods for fresh IgG2 protein.....	261
Figure 6.3.	Scatter plots of particle count per ml at $\geq 2 \mu\text{m}$, $\geq 10 \mu\text{m}$, $\geq 25 \mu\text{m}$ and $\geq 50 \mu\text{m}$ as measured by HIAC and MFI for fresh BSA – surfactant formulations.....	262

Figure 6.4.	Scatter plots of particle count per ml at $\geq 2 \mu\text{m}$, $\geq 10 \mu\text{m}$, $\geq 25 \mu\text{m}$ and $\geq 50 \mu\text{m}$ as measured by HIAC and MFI for heated BSA – surfactant formulations.....	263
Figure 6.5.	Scatter plots of particle count per ml at $\geq 2 \mu\text{m}$, $\geq 10 \mu\text{m}$, $\geq 25 \mu\text{m}$ and $\geq 50 \mu\text{m}$ measured by HIAC and MFI for aged BSA – surfactant formulations.....	264
Figure 6.6.	Scatter plots of particle count per ml at $\geq 2 \mu\text{m}$, $\geq 10 \mu\text{m}$, $\geq 25 \mu\text{m}$ and $\geq 50 \mu\text{m}$ as measured by HIAC and MFI for fresh IgG2 – surfactant formulations.....	265
Figure 6.7.	Scatter plots of particle count per ml at $\geq 2 \mu\text{m}$, $\geq 10 \mu\text{m}$, $\geq 25 \mu\text{m}$ and $\geq 50 \mu\text{m}$ as measured by HIAC and MFI for heated IgG2 – surfactant formulations.....	266
Figure 6.8.	Scatter plots of particle count per ml at $\geq 2 \mu\text{m}$, $\geq 10 \mu\text{m}$, $\geq 25 \mu\text{m}$ and $\geq 50 \mu\text{m}$ as measured by HIAC and MFI for aged IgG2 – surfactant formulations.....	267
Figure 6.9.	The Pearson Correlation Coefficient between HSDSC unfolding temperature T_m and main peak diameter (nm) measured by DLS for: (1) fresh, (2) heated and (3) aged BSA with Tween 20, Tween 80, Brij 35 and Pluronic F-68 surfactants.....	268
Figure 6.10.	The Pearson Correlation Coefficient between HSDSC unfolding temperature T_{m1} and main peak diameter (nm) measured by DLS for: (1) fresh, (2) heated and (3) aged IgG2 with Tween 20, Tween 80, Brij 35 and Pluronic F-68 surfactants.....	269
Figure 6.11.	The Pearson Correlation Coefficient between HSDSC unfolding temperature T_{m2} and main peak diameter (nm) measured by DLS for: (1) fresh, (2) heated and (3) aged IgG2 with Tween 20, Tween 80, Brij 35 and Pluronic F-68 surfactants.....	270
Figure 6.12.	The Pearson Correlation Coefficient measured between T_m (HSDSC) and particle count (HIAC) for fresh BSA with Tween 20, Tween 80, Brij 35 and Pluronic F-68 surfactants at (1) $\geq 2 \mu\text{m}$, (2) $\geq 5 \mu\text{m}$, (3) $\geq 10 \mu\text{m}$, (4) $\geq 25 \mu\text{m}$, (5) $\geq 50 \mu\text{m}$ and (6) $\geq 100 \mu\text{m}$ particle size ranges.....	272
Figure 6.13.	The Pearson Correlation Coefficient measured between T_m (HSDSC) and particle count (HIAC) for heated BSA with Tween	

	20, Tween 80, Brij 35 and Pluronic F-68 surfactants at (1) ≥ 2 μm , (2) ≥ 5 μm , (3) ≥ 10 μm , (4) ≥ 25 μm , (5) ≥ 50 μm and (6) ≥ 100 μm particle size ranges.....	273
Figure 6.14.	The Pearson Correlation Coefficient measured between T_m (HSDSC) and particle count (HIAC) for aged BSA with Tween 20, Tween 80, Brij 35 and Pluronic F-68 surfactants at (1) ≥ 2 μm , (2) ≥ 5 μm , (3) ≥ 10 μm , (4) ≥ 25 μm , (5) ≥ 50 μm and (6) ≥ 100 μm particle size ranges.....	274
Figure 6.15.	The Pearson Correlation Coefficient measured between T_{m1} (HSDSC) and particle count (HIAC) for fresh IgG2 with Tween 20, Tween 80, Brij 35 and Pluronic F-68 surfactants at (1) ≥ 2 μm , (2) ≥ 5 μm , (3) ≥ 10 μm , (4) ≥ 25 μm , (5) ≥ 50 μm and (6) ≥ 100 μm particle size ranges.....	275
Figure 6.16.	The Pearson Correlation Coefficient measured between T_{m2} (HSDSC) and particle count (HIAC) for fresh IgG2 with Tween 20, Tween 80, Brij 35 and Pluronic F-68 surfactants at (1) ≥ 2 μm , (2) ≥ 5 μm , (3) ≥ 10 μm , (4) ≥ 25 μm , (5) ≥ 50 μm and (6) ≥ 100 μm particle size ranges.....	276
Figure 6.17.	The Pearson Correlation Coefficient measured between T_{m1} (HSDSC) and particle count (HIAC) for heated IgG2 with Tween 20, Tween 80, Brij 35 and Pluronic F-68 surfactants at (1) ≥ 2 μm , (2) ≥ 5 μm , (3) ≥ 10 μm , (4) ≥ 25 μm , (5) ≥ 50 μm and (6) ≥ 100 μm particle size ranges.....	277
Figure 6.18.	The Pearson Correlation Coefficient measured between T_{m2} (HSDSC) and particle count (HIAC) for heated IgG2 with Tween 20, Tween 80, Brij 35 and Pluronic F-68 surfactants at (1) ≥ 2 μm , (2) ≥ 5 μm , (3) ≥ 10 μm , (4) ≥ 25 μm , (5) ≥ 50 μm and (6) ≥ 100 μm particle size ranges.....	278
Figure 6.19.	The Pearson Correlation Coefficient measured between T_{m1} (HSDSC) and particle count (HIAC) for aged IgG2 with Tween 20, Tween 80, Brij 35 and Pluronic F-68 surfactants at (1) ≥ 2 μm , (2) ≥ 5 μm , (3) ≥ 10 μm , (4) ≥ 25 μm , (5) ≥ 50 μm and (6) ≥ 100 μm particle size ranges.....	279

- Figure 6.20. The Pearson Correlation Coefficient measured between T_{m2} (HSDSC) and particle count (HIAC) for aged IgG2 with Tween 20, Tween 80, Brij 35 and Pluronic F-68 surfactants at (1) $\geq 2 \mu\text{m}$, (2) $\geq 5 \mu\text{m}$, (3) $\geq 10 \mu\text{m}$, (4) $\geq 25 \mu\text{m}$, (5) $\geq 50 \mu\text{m}$ and (6) $\geq 100 \mu\text{m}$ particle size ranges.....280
- Figure 6.21. The Pearson Correlation Coefficient measured between T_m (HSDSC) and particle count (MFI) at (1) $\geq 2 \mu\text{m}$, (2) $\geq 10 \mu\text{m}$, (3) $\geq 25 \mu\text{m}$, (4) $\geq 50 \mu\text{m}$ and (5) $\geq 100 \mu\text{m}$ particle size ranges for fresh BSA with Tween 20, Tween 80, Brij 35 and Pluronic F-68 surfactant.....281
- Figure 6.22. The Pearson Correlation Coefficient measured between T_m (HSDSC) and particle count (MFI) for heated BSA with Tween 20, Tween 80, Brij 35 and Pluronic F-68 surfactants at (1) $\geq 2 \mu\text{m}$, (2) $\geq 10 \mu\text{m}$, (3) $\geq 25 \mu\text{m}$, (4) $\geq 50 \mu\text{m}$ and (5) $\geq 100 \mu\text{m}$ particle size ranges.....282
- Figure 6.23. The Pearson Correlation Coefficient measured between T_m (HSDSC) and particle count (MFI) for aged BSA with Tween 20, Tween 80, Brij 35 and Pluronic F-68 surfactants at (1) $\geq 2 \mu\text{m}$, (2) $\geq 10 \mu\text{m}$, (3) $\geq 25 \mu\text{m}$, (4) $\geq 50 \mu\text{m}$ and (5) $\geq 100 \mu\text{m}$ particle size ranges.....283
- Figure 6.24. The Pearson Correlation Coefficient measured between T_{m1} (HSDSC) and particle count (MFI) for fresh IgG2 with Tween 20, Tween 80, Brij 35 and Pluronic F-68 surfactants at (1) $\geq 2 \mu\text{m}$, (2) $\geq 10 \mu\text{m}$, (3) $\geq 25 \mu\text{m}$, (4) $\geq 50 \mu\text{m}$ and (5) $\geq 100 \mu\text{m}$ particle size ranges.....284
- Figure 6.25. The Pearson Correlation Coefficient measured between T_{m2} (HSDSC) and particle count (MFI) for fresh IgG2 with Tween 20, Tween 80, Brij 35 and Pluronic F-68 surfactants at (1) $\geq 2 \mu\text{m}$, (2) $\geq 10 \mu\text{m}$, (3) $\geq 25 \mu\text{m}$, (4) $\geq 50 \mu\text{m}$ and (5) $\geq 100 \mu\text{m}$ particle size ranges.....285
- Figure 6.26. The Pearson Correlation Coefficient measured between T_{m1} (HSDSC) and particle count (MFI) for heated IgG2 with Tween 20, Tween 80, Brij 35 and Pluronic F-68 surfactants at (1) ≥ 2

	μm , (2) $\geq 10 \mu\text{m}$, (3) $\geq 25 \mu\text{m}$, (4) $\geq 50 \mu\text{m}$ and (5) $\geq 100 \mu\text{m}$ particle size ranges.....	286
Figure 6.27.	The Pearson Correlation Coefficient measured between T_{m2} (HSDSC) and particle count (MFI) for heated IgG2 with Tween 20, Tween 80, Brij 35 and Pluronic F-68 surfactants at (1) ≥ 2 μm , (2) $\geq 10 \mu\text{m}$, (3) $\geq 25 \mu\text{m}$, (4) $\geq 50 \mu\text{m}$ and (5) $\geq 100 \mu\text{m}$ particle size ranges.....	287
Figure 6.28.	The Pearson Correlation Coefficient measured between T_{m1} (HSDSC) and particle count (MFI) for aged IgG2 with Tween 20, Tween 80, Brij 35 and Pluronic F-68 surfactants at (1) ≥ 2 μm , (2) $\geq 10 \mu\text{m}$, (3) $\geq 25 \mu\text{m}$, (4) $\geq 50 \mu\text{m}$ and (5) $\geq 100 \mu\text{m}$ particle size ranges.....	288
Figure 6.29.	The Pearson Correlation Coefficient measured between T_{m2} (HSDSC) and particle count (MFI) for aged IgG2 with Tween 20, Tween 80, Brij 35 and Pluronic F-68 surfactants at (1) ≥ 2 μm , (2) $\geq 10 \mu\text{m}$, (3) $\geq 25 \mu\text{m}$, (4) $\geq 50 \mu\text{m}$ and (5) $\geq 100 \mu\text{m}$ particle size ranges.....	289
Figure 6.30.	Scatter plot for aged IgG2 samples between main peak diameter (nm) (DLS) and particle count per ml (HIAC) at $\geq 2 \mu\text{m}$ size range using Pearson correlation test.....	292
Figure 6.31.	Scatter plot for aged IgG2 samples between main peak diameter (nm) (DLS) and particle count per ml (MFI) at $\geq 2 \mu\text{m}$ size range using Pearson correlation test.....	292

List of Tables

Table 2.1.	Table showing all the materials used in this study and their respective sources.....	43
Table 2.2.	Tween 20, Tween 80, Brij 35 and Pluronic F-68 CMC concentrations.....	45
Table 2.3.	Microcal VP – capillary DSC plate lay-out.....	48
Table 2.4.	Low volume quartz cuvette (ZEN2112) description (The Nanobiotechnology Centre, 2009).....	50
Table 3.1.	Results of thermal unfolding profiles of BSA (10 mg/ml in PBS buffer) and BSA (10 mg/ml) with different Tween 20, Tween 80, Brij 35 and Pluronic F-68 concentrations.....	60
Table 3.2.	Results of thermal unfolding profiles of IgG2 (10 mg/ml) and IgG2 (10 mg/ml) with different Tween 20, Tween 80, Brij 35 and Pluronic F-68 concentrations.....	67
Table 4.1.	Particle size diameter (nm) of the peak with greatest intensity (Peak 1) for fresh BSA (10 mg/ml) with below, around and above CMC levels of Tween 20, Tween 80, Brij 35 and Pluronic F-68 surfactants.....	89
Table 4.2.	Particle size diameter (nm) of the peak with greatest intensity (Peak 1) for heated BSA (10 mg/ml) with below, around and above CMC levels of Tween 20, Tween 80, Brij 35 and Pluronic F-68 surfactants.....	101
Table 4.3.	Particle size diameter (nm) of the peak with greatest intensity (Peak 1) for aged BSA (10 mg/ml) with below, around and above CMC levels of Tween 20, Tween 80, Brij 35 and Pluronic F-68 surfactants.....	113
Table 4.4.	Particle size diameter (nm) of the peak with greatest intensity (Peak 1) for fresh IgG2 (10 mg/ml) with below, around and above CMC levels of Tween 20, Tween 80, Brij 35 and Pluronic F-68 surfactants.....	122
Table 4.5.	Particle size diameter (nm) of the peak with greatest intensity (Peak 1) for heated IgG2 (10 mg/ml) with below, around and	

	above CMC levels of Tween 20, Tween 80, Brij 35 and Pluronic F-68.....	133
Table 4.6.	Particle size diameter (nm) of the peak with greatest intensity (Peak 1) for aged IgG2 (10 mg/ml) with below, around and above CMC levels of Tween 20, Tween 80, Brij 35 and Pluronic F-68 surfactants.....	141
Table 6.1.	Hydrophilic-Lipophilic Balance values for Tween 20, Tween 80, Brij 35 and Pluronic F-68 surfactants (Anatrace, 2006; Griffin, 1954; Sigma Aldrich).....	258
Table 6.2.	Pearson Correlation Coefficient measured between main peak diameter (nm) (DLS) and particle count per ml (HIAC) for fresh, heated and aged BSA samples.....	290
Table 6.3.	Pearson Correlation Coefficient measured between main peak diameter (nm) (DLS) and particle count per ml (MFI) for fresh, heated and aged BSA samples.....	290
Table 6.4.	Pearson Correlation Coefficient measured between main peak diameter (nm) (DLS) and particle count per ml (HIAC) fresh, heated and aged IgG2 samples. (*) – Pearson Correlation is significant at 0.05 level (P<0.05).....	291
Table 6.5.	Pearson Correlation Coefficient measured between main peak diameter (nm) (DLS) and particle count per ml (MFI) for fresh, heated and aged IgG2 samples. (*) – Pearson Correlation is significant at 0.05 level (P<0.05).....	291

List of symbols and abbreviations

μl	microlitre
μm	micrometer
μW	microwatt
ANOVA	Analysis of Variance
AUC	Analytical Ultracentrifugation
BSA	Bovine Serum Albumin
CMC	Critical Micelle Concentration
DLS	Dynamic Light Scattering
FFF	Field Flow Fractionation
FPIA	Flow Particle Image Analysis
HIAC	Liquid particle counter
HLB	Hydrophilic-lipophilic balance
HSA	Human Serum Albumin
HSDSC	High sensitivity differential scanning calorimetry
IgG	Immunoglobulin
ISO	International Organization for Standardization
kDa	kiloDaltons
LD	Laser Diffraction technology
LO	Light Obscuration
MALS	Multiangle Light Scattering
MFI	Micro-flow imaging
nm	Nanometer
PBS	Phosphate Buffered Saline
rhGH	Recombinant human growth hormone
RPC	Reversed phase chromatography
rpm	Rotations per minute
SEC	Size Exclusion Chromatography
SPSS	Statistical Package for Social Sciences
T_m	Unfolding temperature (peak maxima)
VEGF	vascular endothelial growth factor

α

Alpha

β

Beta

Chapter 1
Introduction

1.1 General Introduction

Aggregation and particle formation have become the focus of increased attention for the biopharmaceutical industry recently due to increasing concerns about their impact on the safety and efficacy of biological products. The effect of surfactants on minimizing and preventing the formation of sub-visible and visible particles is not yet fully understood. This question is an open emphasis across the industry and academic organizations.

In the past two decades significant advances have been made in understanding the mechanism of many chemical degradation pathways of protein-based solutions. However to understand particle formation and prevention of particles forming still remains relatively poor. Protein aggregates and particulates form in a wide range of sizes from few nanometres to centimetre and shapes, which makes it extremely challenging to fully characterize particles in biopharmaceutical formulations.

1.2 Mechanisms of aggregation and particle formation

Proteins can form a large variety of aggregates starting from a dimer species to multimers. Dimers and other smaller size aggregates are soluble in nature and typically range in size from a few nanometres to tens of nanometres. Some of the multimers can grow large in size and may eventually appear as visible particles. Although all multimeric species including dimers are generally termed as aggregates, the phrase particles or particulates refers to the large size aggregates that are in the size range of tens of microns or

even larger species that are visibly detected. More broadly defined, particles refer to species encompassing both the visible and sub-visible size ranges.

Aggregates and particles cover a size range from few nanometers to hundreds of micrometers (Figure 1.1):

- Aggregates
10 nm – 0.1 μm (> dimers = oligomers, soluble)
- Particles
0.1 – 1 μm (sub-micron, often soluble aggregates)
10 – 150 μm (sub-visible, often soluble aggregates)
- Visible particles
125 μm (internal definition) to 1 mm (insoluble)

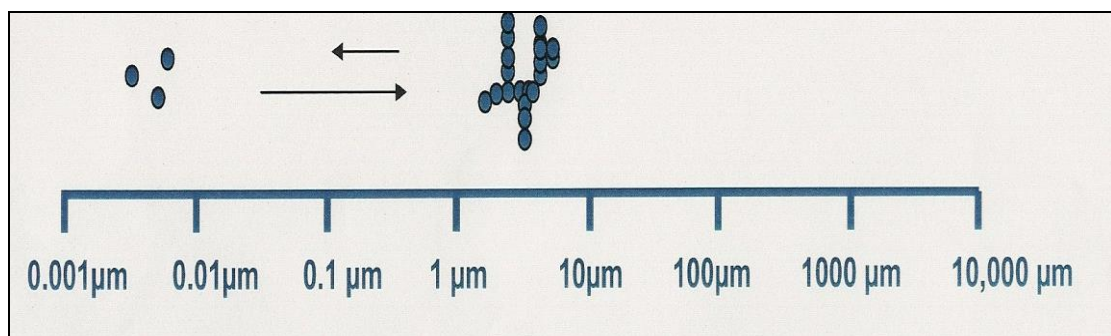


Figure 1.1. Aggregates and Particles size range (Krishnan, 2009).

Protein aggregates and particles can be induced by different mechanical stresses, therefore protein particles and aggregates have been classified based on different aspects. Cromwell et al. classified particles into 4 groups (Cromwell et al., 2006):

- Soluble/insoluble aggregates;
- Covalent/non-covalent aggregates;
- Reversible/irreversible aggregates;
- Native/denatured aggregates.

Soluble aggregates are usually described as discrete, not visible particles and may be easily removed by 0.22 μm pore size filters. Where insoluble aggregates are usually visible to unaided eye and can be removed by filtration.

Covalent aggregates can arise due to the chemical bond formation between 2 or more monomers (Cromwell et al., 2006). Most common mechanisms for covalent aggregation have been described as disulfide bond formation and oxidation of tyrosines (Andya et al., 2003; Shahrokh et al., 1994).

Reversible aggregates arise due to weak non covalent protein interactions. Cromwell et al. stated that reversibility can be indicative of the presence of equilibrium between the monomers and higher order forms and that this equilibrium can shift due to the change in solution conditions such as a decrease in protein concentration or pH change (Cromwell et al., 2006).

Protein denaturation is described as a change of protein shape which is caused by applying external stresses such as heat or acid.

Just as there are many types of interactions that can cause protein aggregation, particle formation can be induced by a variety of different conditions such as temperature, pH, protein concentration, ionic strength, mechanical stresses such as shaking, stirring, pumping, freezing and thawing and also formulation (Mahler et al., 2008).

Figure 1.2 shows that proteins can aggregate and form particles through different mechanisms.

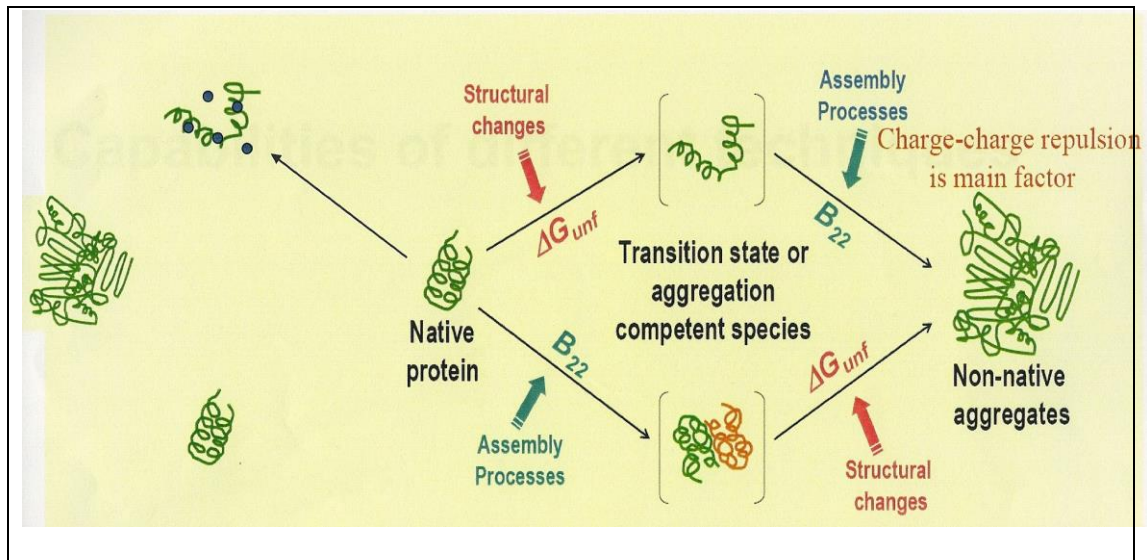


Figure 1.2. Proteins aggregation and particle formation through different mechanisms (Krishnan, 2009).

1.3 Conformational stability: Thermal unfolding

Thermal unfolding is often found to be a rate-limiting step for aggregation (Roberts et al., 2011). Most therapeutic proteins are prone to aggregation because of their partially or fully unfolded conformational states.

It has been previously reported (Flaugh et al., 2005 a, b; Feire et al., 1992), that proteins with multi domains have multi unfolding profiles which make it more difficult to investigate. Also it is more likely that just a small fraction of multi domain proteins can be aggregation prone. Therefore, it may be that increasing or decreasing in unfolding free energy may not have any effect on aggregate formation (Roberts et al., 2011).

Taking into account all the above issues, unfolding temperature T_m can still be predictive in protein aggregation. In this scenario, Roberts et al., (2011) described that “aggregation proceeds during thermal unfolding with the

aggregation prone monomer population”, which is “continuously being depleted as monomers convert to aggregates”.

However it is not known which unfolding transitions correspond to the region of aggregation prone protein and also which T_m values are potentially relevant for predicting protein aggregation. Scientists described few approaches to investigate the above. One of them is to consider that unfolding profiles are dependant on thermal scan rate and if aggregation will be forming during the unfolding then unfolding temperature T_m will shift to higher levels. However T_m values could also increase when the scan rate is too fast comparing to unfolding rates in the absence of aggregation (Roberts et al., 2011).

Another approach reported by Remmele et al. (1999) and Sahin et al. (2010) is to assess the reversibility and the extent of re-folding by reheating of the same sample. This approach is often used because the reversibility could inform if the unfolding endotherm is related to protein aggregation. This theory assures that T_m will not be indicative of relative aggregation due to other factors such as slow unfolding or sample misfolding without aggregation.

The alternative approach suggested by Sahin et al. (2010) and Btummitt et al. (2011) is to try to monitor aggregation for those samples, which have been thermally scanned to different temperatures and directly assign the unfolding transitions with the loss of monomer.

1.4 Analytical technique for characterising protein conformational stability – HSDSC

When proteins are being developed as therapeutics, it is important to evaluate protein conformational and long shelf-life stability. As mentioned before, there are many factors which could affect protein stability and reversibility and cause protein aggregation. Therefore it is very important to understand and investigate these effects in order to help developing new analytical methods to assist in protein and antibody formulation. High sensitivity differential scanning calorimetry (HSDSC) is a potential technique to do that.

HSDSC is commonly used method in assessing thermal and conformational stability in protein and antibody formulations. This analytical technique has an advantage not just by measuring the unfolding temperature and reversibility, but also it provides the unfolding profiles for multi domain proteins and antibodies, which have multi unfolding transitions.

1.5 Analytical techniques to characterise aggregates and particulates

There are a wide number of analytical methods available to characterize and quantify protein aggregates and particles (Figure 1.3). The methods include:

- Laser Diffraction Technology
- Analytical Ultracentrifugation (AUC)
- Field Flow Fractionation (FFF)
- Multiangle Light Scattering (MALS)

- Size Exclusion Chromatography (SEC)
- Dynamic Light Scattering (DLS)
- Light Obscuration
- Microscopy: Micro-flow imaging (MFI), Flow Particle Image Analysis (FPIA)
- Visual Inspection
- Raman Spectroscopy

In this review, an overview of some of the methods is presented.

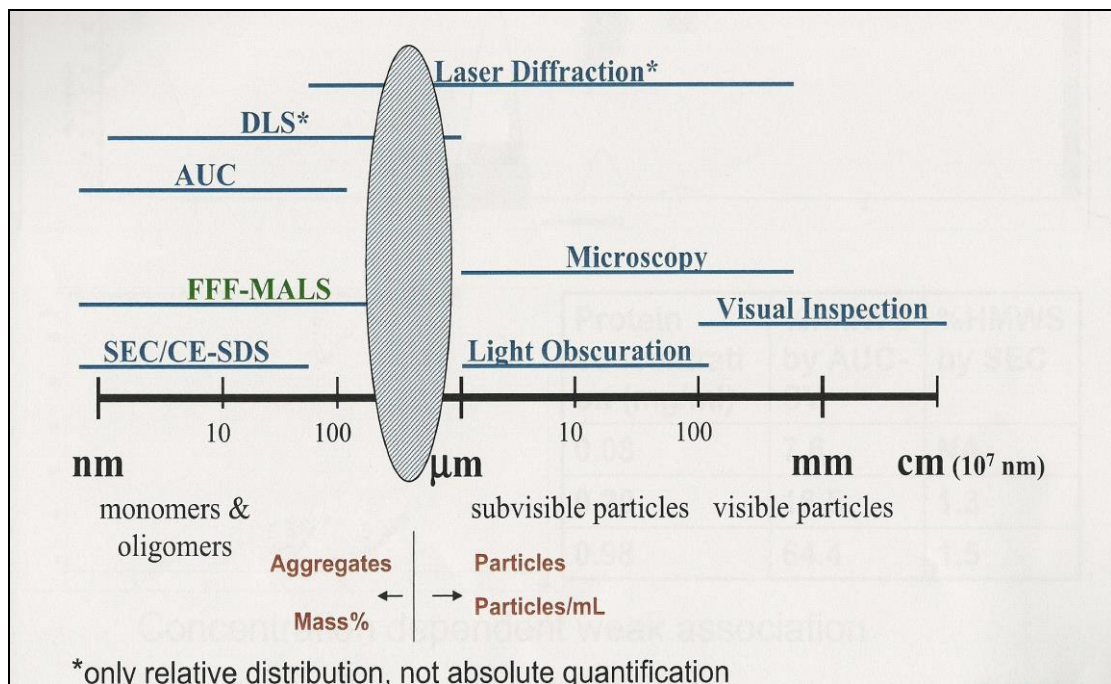


Figure 1.3. Analytical methods to characterize and quantify protein aggregates and particles. Shaded region – sub-visible particles (Jiang, 2009).

1.5.1 Laser Diffraction Technology

Laser Diffraction technology (LD) is an absolute technique, which doesn't need any calibration. This method is quick and easy to use, has a high reproducibility and covers a wide particle size range from few nanometres to millimetres. Virden describes this technique as a method which provides a result for the whole sample, rather than building up distributions from data for individual particles (Virden, 2010).

Figure 1.4 presents schematic structure of Laser Diffraction technology.

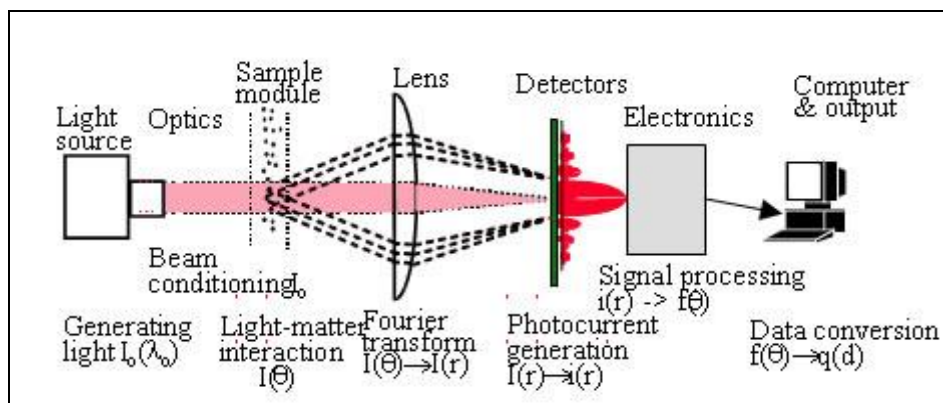


Figure 1.4. Schematic picture of a laser diffraction instrument (Beckman Coulter, 2008)

The LD instrument performing process starts when a light source generates monochromatic beam. Firstly, this beam goes through few optical components and gets conditioned. That creates an expanded and collimated beam which illuminates the particles. The particles scatter light over a range of different angles. Larger particles generate a high scattering intensity at

narrow angles and smaller particles generate lower intensity, but at wider angles to the incident beam (Virden, 2010).

These unique scattering patterns ($I(\theta)$) are Fourier transformed into a spatial intensity pattern ($I(r)$), which is detected by a photo detector array. Then data is processed and digitized creating an intensity flux pattern ($f(\theta)$), which is utilized and converted into a particle size distribution ($q(d)$) (Beckman Coulter, 2008).

There are two Laser Diffraction theories: Mie and Fraunhofer. Virden states that both models provide similar results for larger particles, but Mie method is more accurate for finer materials. Also inaccuracies arising from Fraunhofer model are unpredictable (Virden, 2010).

1.5.2 Analytical Ultracentrifugation (AUC)

Analytical Ultracentrifugation (AUC) is another technique widely used to study protein aggregation (Liu et al., 2006; Liu et al., 1999; Schuch, 2003; Berkowitz, 2006; Gabrielson et al., 2007; Mahler et al., 2008). AUC method measures the sedimentation rate, which provides information of molecular mass, the size and shape of molecules. Alliance Protein Laboratories scientists stated 8 points why AUC is a valuable method to use for (Alliance Protein Laboratories Inc, 2014):

- Verifying whether a sample is entirely homogeneous in mass and conformation;

- Detecting aggregates in protein samples and quantifying the amount of aggregate;
- Comparing the conformations for samples from different lots, manufacturing processes, or expression systems (comparability studies), or comparing different engineered variants of the sample protein/peptide;
- Establishing whether the native state of protein or peptide is a monomer, dimer, trimer, etc.;
- Determining the overall shape of non-glycosylated protein and peptide molecules in solution (are they approximately spherical or highly extended and rod-like);
- Measuring the distribution of sizes in samples which contain a very broad range of sizes;
- Detecting changes in protein conformation, for example partial unfolding or transitions to “molten globule” states;
- Studying the formation and stoichiometry of tight complexes between proteins.

The AUC method can be used for a wide range of pH, temperature and ionic strength conditions. There is very little or no sample preparation involved and technique can be used for a wide range of sample concentration up to 40 mg/ml (Mahler et al., 2009).

1.5.3 Field Flow Fractionation (FFF)

Field-flow fractionation (FFF) is a separation technique and is used to determine the size of particles. Fraunhofer et al, Reschiglian et al. and Giddings have described FFF as a technique which is able to separate particles in the range of small molecules measuring few nanometres to large particles measuring in micrometers (Fraunhofer et al., 2004; Reschiglian et al., 2005; Giddings, 1993).

FFF separates molecules depending on their molar mass and size by employing applied field force, which forces molecules to different velocity regions within a channel. The molecules separation process is initiated by injecting the sample into a carrier fluid within a thin channel and then the fluid is pumped through this channel and perpendicular to this parabolic flow an external generated field is applied (Mahler et al., 2008). Depending on the field applied FFF can be divided in few forms: flow FFF, Asymmetric Flow, Centrifugal, Sedimentation, Thermal, Electrical and Magnetic FFF.

When one of these fields is applied the sample components move towards accumulation wall where molecules closest to the wall are located in the slowest velocity of the flow and elute out slower compared to the molecules found in the fastest velocity region (Mahler et al., 2008).

1.5.4 Multiangle Light Scattering (MALS)

Multiangle light scattering (MALS) technique measures particles' average size and absolute molar mass (Mahler et al., 2008).

The MALS method has been extensively used by scientists to determine particles and aggregates molecular weight. This method detects laser scattered light at different angles. The technique doesn't require any calibration and the only parameters required to calculate absolute molecular weight are each elution fraction concentration and differential refractive index increment (Mahler et al., 2008).

1.5.5 Size Exclusion Chromatography (SEC)

Size-Exclusion Chromatography (SEC) is commonly used technique to detect and quantify protein aggregates. SEC separates particles depending on their hydrodynamic size, diffusion coefficient and surface properties.

Figure 1.5 illustrates SEC experimental process.

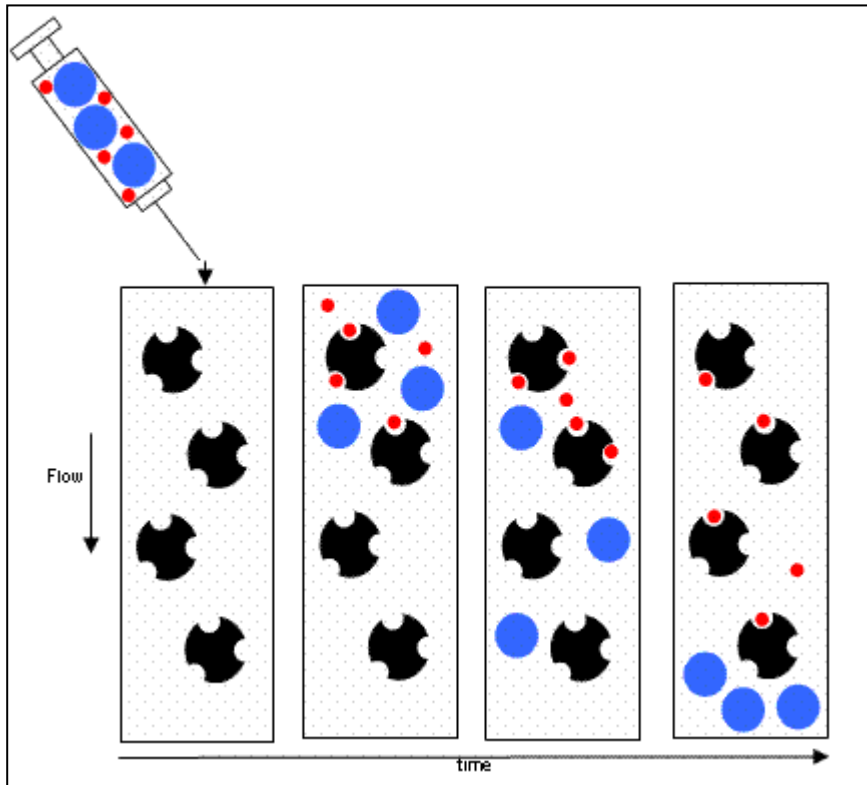


Figure 1.5. Illustration of SEC experiment (Analytical Ventura, 2013).

Figure 1.5 illustrates the principle by following a sample containing large (blue) and small (red) particles on injection into a size exclusion column, where stationary phase beads (black) were present. As the time passes, small (red) particles enter the pores on the stationary phase beads (black). However, the blue particles, because of their bigger size were not able to penetrate the pores of black beads, therefore they get excluded from the packing pore volume and get eluted (Barth, 2004).

There are various size exclusion columns available, depending on experimental needs, such as sample concentration, chemical and physical properties. The SEC technique, like some of the other particle counting techniques, should be used with light scattering methods as for example the previously mentioned MALS, and also combined with Light Obscuration or Dynamic Light Scattering techniques.

1.5.6 Dynamic Light Scattering (DLS)

Dynamic light scattering (DLS) is a well-established, commonly used technique to measure small molecules and particles from few nanometres size.

Arakawa et al. describes the DLS method as a technique which studies particle size distribution by intensity of light scattered from protein solution over time (Arakawa et al., 2007).

The principle of DLS Brownian motion is that larger particles move slower than smaller ones, therefore scattering fluctuations time scale gives particle size parameter – hydrodynamic diameter (Figure 1.6).

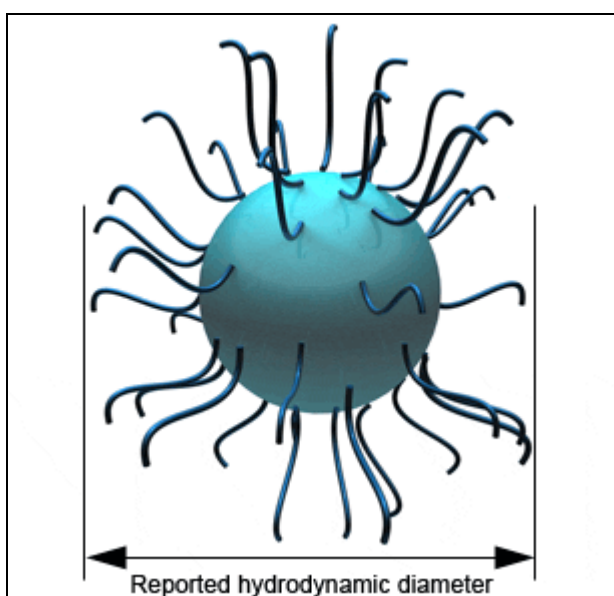


Figure 1.6. Reported hydrodynamic diameter (Malvern Instruments Ltd, 2011).

Hydrodynamic diameter is described as the radius of spherical particle, which has the same translational diffusion coefficient as protein molecule (particle) measured (Arakawa et al., 2007).

1.5.7 Light Obscuration and Microscopic Particle Count

There are two procedures to determine sub-visible particle contamination:

- Light Obscuration Particle Count;
- Microscopic Particle Count.

The Light Obscuration method is often used when only a sub-visible particle count is required. However it is usually necessary to additionally experiment with one of the Microscopic Count methods. Not all protein or antibody formulations can be examined for sub-visible particles by one of these methods, as an example due to sample high viscosity, Light Obscuration can not always be applied. Also if air or gas bubbles are present in the sample, Microscopic particle count testing is required.

Most analytical measurements for particle sizing use either a spherical approximation for shape or indirect methods and a mathematical algorithm to extract shape information. Microscopic methods, however, provide direct visualization of morphology in addition to size information. More recently, dynamic imaging capability is used by multiple manufacturers in sizing equipments for not only size and shape analysis but also for video imaging. The optical microscopes are generally limited to size particles of approximately 0.5 μm and higher (ISO, 2006). Dynamic imaging offers the benefits of measuring images in real time and under conditions when particles remain suspended - an advantage over static imaging. This may allow superior imaging of extremely irregular shaped particles, and monitoring the dynamic behaviour of particles if the size distribution is

changing over time. Such information is valuable during formulation development of biologics to characterize any particulates formed and to identify potential preventive measures. It should be noted, however, that it is inherently complex to determine a true size distribution from the dynamic/static imaging data, especially for biologic particles (for example, irregular shaped fibrils). It is not straightforward to directly compare size distribution (or counts) from dynamic imaging to that obtained from light obscuration or laser diffraction analyses (Das et al., 2007).

1.5.7.1 Light Obscuration (HIAC)

The light obscuration (LO) liquid particle counting system relies on light obscuration to detect and quantify the number of particles and their size range in a test sample. Introduced in 1969, the first and current instruments operate on the interaction of an intense collimated and focused beam of light with a particle suspended in a liquid medium (Barber, 2000). Particles are forced to pass through a narrow view volume between the light and photodiode detector (Figure 1.7). The presence of a particle is detected and measured by the variation in light intensity, which is then translated to a voltage signal.

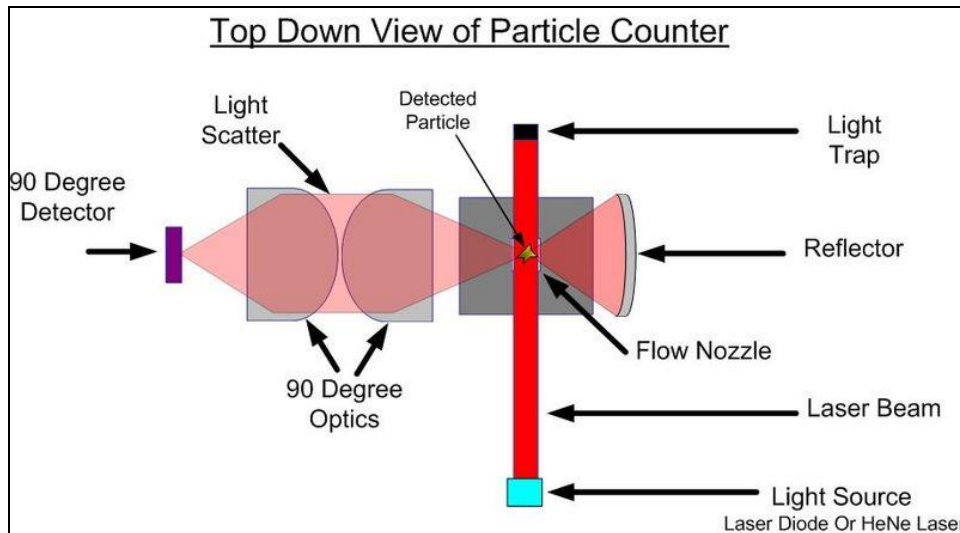


Figure 1.7. Diagram of Light Obscuration particle counter (Solids Wiki, 2013).

The principle of light obscuration is used to detect particles in the range of greater than 2 μm to up to 100 μm . The sensors are used to measure the size of the particles through their full dynamic range, resulting in unsurpassed resolution and count efficiency (Barber, 2000).

1.5.7.2 Micro-flow imaging (MFI)

Micro-flow imaging (MFI) is a flow microscopy technique, which captures bright field images in the frames while continuous sample stream passes through a flow cell (Sharma et al., 2010).

The instrument configuration is shown in Figure 1.8.

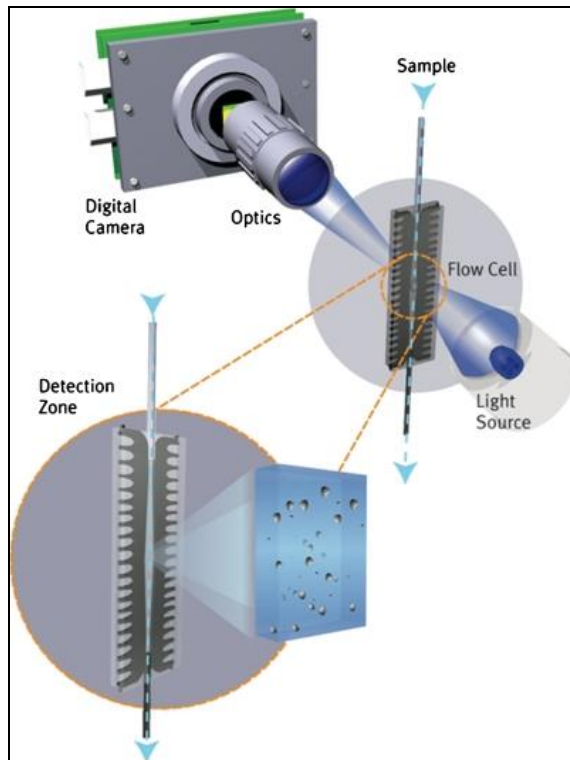


Figure 1.8. Micro-flow imaging instrument configuration (Sharma et al., 2010).

The MFI process starts when a sample is directly inverted from a pipette tip through the flow cell. Both, system magnification and flow-cell depth determine the accuracy of the concentration measurement. Concentration and parameter measurements are absolute but may be re-verified using particle standards. Usually sample volumes range from less than 0.25 mL to tens of millilitres. In the detection zone, immediate visual images of a particle population is provided.

The MFI system software is extracting particle images by using a sensitive threshold to identify and define each particle. All particle images are analysed straight away in real time. From the analysed images the MFI system provides particle count, size, concentration and shape information. Also this method is supported by image filtering to be able to selectively extract similar

particles from all the population, thus allowing the isolation and independent analysis of those sub-populations (Sharma et al., 2010).

In general, the MFI method has many advantages over indirect obscuration or scattering measurements. This method doesn't rely on a correlation between particle size and the scattered optical signal magnitude.

1.5.7.3 Flow particle image analysis (FPIA)

Flow particle image analysis (FPIA) method produces high resolution analysis of particle shape and size from 0.8 μm to 300 μm .

This technique requires minimal sample preparation and provides particle size and shape distributions in a short time.

Figure 1.9 illustrates the process of FPIA method.

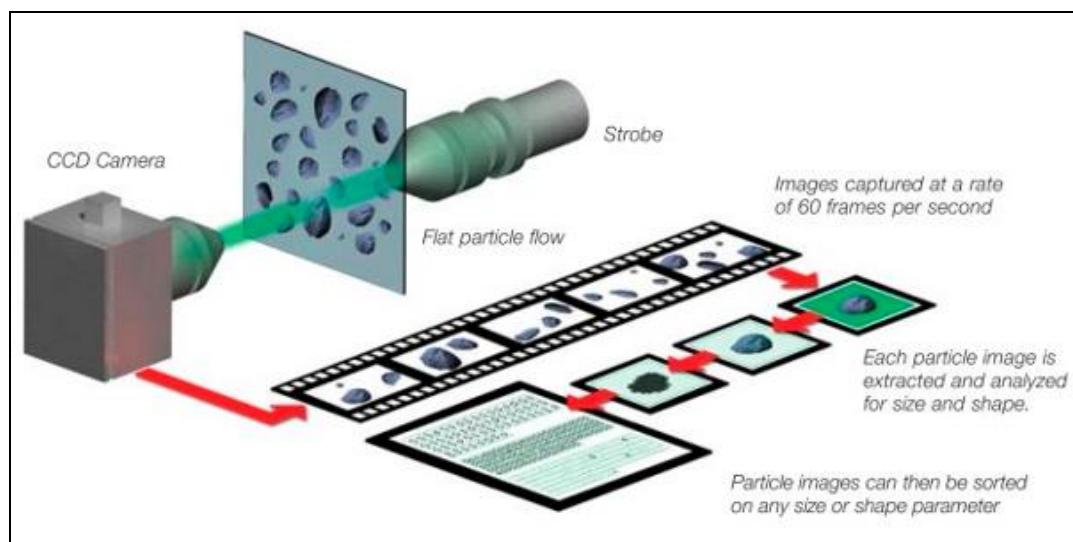


Figure 1.9. FPIA sample dispersion and image capture (Malvern Instruments Ltd, 2010).

After inverting the required sample through a jet nozzle, the sample goes through a sheath-flow cell, where a particle suspension is transformed into a flat flow. This ensures that particles present in a sample lie in the same line and are facing the CCD camera (Figures 1.9, 1.10).

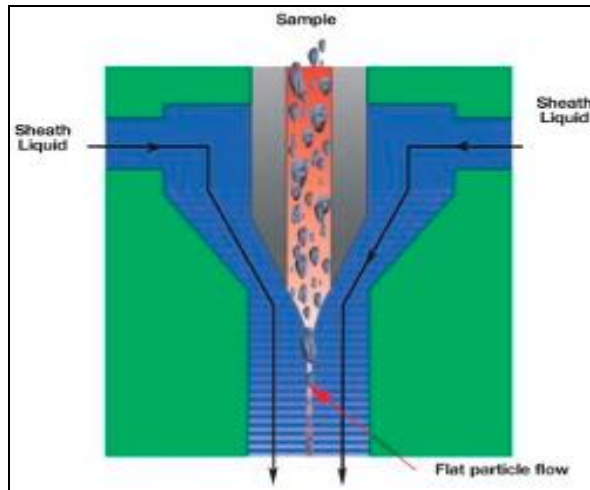


Figure 1.10. Scheme of particle flow (Malvern Instruments Ltd, 2010).

60 particle images per second are captured by FPIA and after removing the noise and the background correction, the number of morphological parameters are calculated: particle diameter, perimeter, length, width and distance.

FPIA software is able to analyse the data and to compare and identify multiple records (Malvern Instruments Ltd, 2010).

1.5.8 Visual Inspection

The visual inspection test is intended to provide a simple procedure for the visual inspection of larger aggregates.

The visual inspection apparatus consists of:

- a matt black panel;
- a non-glare white panel;
- an adjustable lamp holder (Mahler et al., 2008).

Visual inspection is often subjective and results are in high variability. Visualization of particles not only depends on an inspector's visual capability, but also on a size, number and type of particles, the light conditions, magnifying lenses used, observation time, distance from inspected samples, the background used.

Although no strict size limit can be assigned for when particles become visible to the human eye, it is generally recognized that particles of $> 100 \mu\text{m}$ size are detected with relatively high probability when appropriate testing conditions are employed (Das et al., 2007).

1.5.9 Raman Spectroscopy

The use of Raman spectroscopy has been a valuable approach to identify foreign particulates in parenteral dosage forms, especially in aqueous based systems due to non-interference of water in Raman measurements (unlike Infra-Red spectroscopy) (Warterwig et al., 2005). With recent advancements in this field, Raman spectrometers provide adequate sensitivity to collect good quality spectrum in a short period of time allowing better throughput in assays. One application of such a throughput method is the automated characterization of particulates (micron and larger size) by optical imaging and Raman identification. A parenteral formulation is filtered to collect the

foreign matter as well as intrinsic particulates, and Raman identification is conducted either for all or a statistically relevant number of particulates to understand the nature and distribution of particulates (Vankeirsblick et al., 2002). Most foreign particulates have unique Raman spectral fingerprint, and the protein particulates display backbone amide spectra characteristic of secondary structure. Fluorescence is often a problem (high background) with Raman measurements of biologics formulations, however, chemical identification of at least a part of the particulate populations can provide valuable clue to its source (Warterwig et al., 2005).

1.6 Gaps in the control and analysis of particles

Mechanisms of protein aggregation and its relevance to biopharmaceuticals has been reviewed and discussed by several researchers (Cromwell et al., 2006; Hermeling et al., 2004; Shire et al., 2004; Stefani et al., 2004; Wang et al., 2007 ; Chi et al., 2003). The biochemical events that are implicated to initiate aggregation include protein denaturation, misfolding, and partial unfolding. Quite often exposure of hydrophobic regions of proteins is believed to initiate aggregation. Additionally, the presence of trace quantity of non-native species may also provide nucleation; however, detection of such non-native species in native state (N) ensemble is very challenging by using classical analytical techniques. Figure 1.11 shows a simplified scheme depicting possible pathways of aggregation from non-native (N^*), intermediate (I), and unfolded (U) protein species. It should be noted that the aggregation process often follows more complicated pathways possibly

involving a wide variety of intermediates. Therefore figure 1.11 should be considered as a conceptual depiction of representative steps in the aggregation process. How small aggregates lead to formation of particulates is a debatable topic (Das et al., 2007).

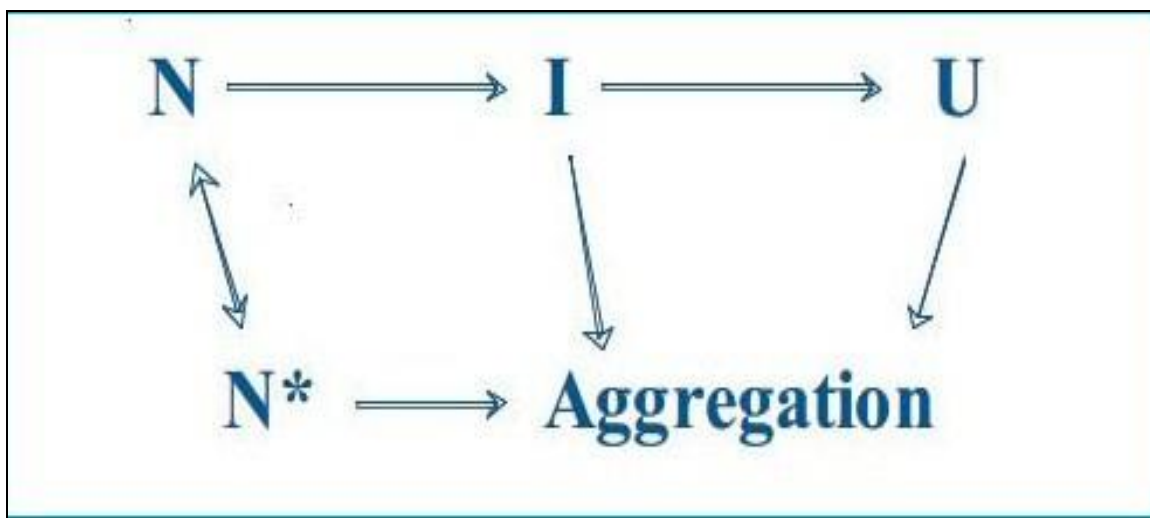


Figure 1.11. Aggregation process. N – native protein state, I – intermediate protein state, U – unfolded protein state, N* - non-native protein state (Das et al., 2007).

Researchers often use the nucleation concept in explaining particulate formation, although as discussed before in the General Introduction, the process of particulate formation via nucleation in biologic systems is poorly understood.

Usually the recommended tests by European Pharmacopoeia for particulate matter in parenteral solution (intravenous) are visual inspection, and sub-visible testing (light obscuration and light microscope). Light obscuration is the preferred method, and light microscopy is conducted when light obscuration test either fails or can not be applied.

Visual inspection is often subjective and results present a high variability of data. Visualization of particles not only depends on an inspector's visual acuity, but also on the nature of the particle (e.g. transparency) and test conditions used. Although no strict size limit can be assigned for when particles become visible to human eye, it is generally recognized that particles of $>100\ \mu\text{m}$ size are detected with relatively high probability when appropriate testing conditions (e.g. light intensity and background).

Small aggregates of proteins remain soluble in the formulation and are typically detectable by conventional separation techniques such as size-exclusion chromatography. For example, a monoclonal antibody (approximately 10 nm in size) and some of its aggregated species (say, dimer through tetramer) can be conveniently separated using standard size-exclusion columns. Between the sizes of a few tens of nanometres (small soluble) and 50-100 micron (visible) there exists a wide size range that is relatively more difficult to explore primarily because of a lack of robust techniques that can perform adequate detection and characterization for the whole size range. For example, when particulates appear in a biologics formulation it might be natural to consider involvement of higher order structures and sub-visible intermediates (although not always detectable) in a mechanistic approach. The event that occur in the sub-visible size range might hold important clues to decipher the origin of visible particulate formation. Although the sub-visible range traditionally refers to a size range of tens of microns, for the purpose of this review the entire size range of submicron to tens of microns is being referred to as the sub-visible gap. Dynamic Light Scattering (DLS) is a convenient method for measurement of

soluble or suspended particles in solution. It is a useful technique - in principle - to cover a wide size range (nanometres to few microns), however it provides only limited information due to:

- (a) poor size resolution;
- (b) artefacts from dust particles;
- (c) "masking" of intensity from smaller size particles in the presence of significant quantity of larger particles;
- (d) lack of shape information.

In order to mitigate the 'sub-visible gap' it is important to detect and characterize the particulates with wider coverage of size range, and to identify composition when possible.

Therefore, with light scattering methods it is often necessary to have some means of knowing that the signals really come from protein and not dust. For static scattering, that is usually accomplished by using the detector in flow mode, following separation by SEC or FFF (which presumably separates dust from the protein) (Arakawa et al., 2007).

Laser diffraction analysis uses the principle that when a laser beam is incident on particles of differing size, light is scattered and the direction and intensity of scattered light are related to particle size. The traditional laser light diffraction analyzers typically use an array of detectors to cover a size range of approximately 0.5 μm – 2000 μm . The detectors when placed at low angle, can size large particles with good accuracy; however, their performance is inadequate for smaller size particles.

When conducting measurement in any of the size ranges, if aggregates and particulates are dynamic in nature, special care should be taken to study the reversibility and transience of formation.

Most analytical measurements for particle sizing (small or large) use either spherical approximation for shape or indirect methods and mathematical algorithm to extract shape information. Microscopy methods, however, provide direct visualization of morphology in addition to size information. More recently, dynamic imaging capability is made available for not only size and shape analysis but also for video imaging. The optical microscopes are generally limited to size of approximately 0.5 μm and higher. Dynamic imaging offers the benefits of measuring images in real time and under conditions when particles remain suspended - an advantage over static imaging. This may allow superior imaging of extremely irregular shaped particles, and monitoring the dynamic behaviour of particles if the size distribution is changing over time. Such information is valuable during formulation development of biologics to characterize the particles produced and in finding potential preventive measures. It should be noted, however, that it is inherently complex to determine a true size distribution from the dynamic/static imaging data. It is not straightforward to directly compare size distribution (or counts) from dynamic imaging to that obtained from light obscuration or laser diffraction analyses (ISO, 2006).

The use of Raman spectroscopy has been a valuable approach to identify foreign particulates, especially in aqueous based systems due to non-interference of water in Raman measurements (unlike InfraRed spectroscopy). With recent advances in this field, Raman spectrometers

provide adequate sensitivity to collect good quality spectrum in a short period of time allowing better throughput in assays. One application of such throughput method is automated characterization of particulates (micron and larger size) by optical imaging and Raman identification. A parenteral formulation is filtered to collect the foreign matter as well as intrinsic particulates, and Raman identification is conducted either for all or a statistically relevant number of particulates to understand the nature and distribution of particulates. Most foreign particulates have unique Raman spectral fingerprint, and the protein particulates display backbone amide spectra characteristic of secondary structure. Fluorescence is often a problem (high background) with Raman measurements, however, chemical identification of at least a part of the particulate populations can provide valuable clue to its source (Warterwig et al., 2005; Vankeirsblick et al., 2002).

Regarding the analysis of particles and their formation it is desirable to conduct suitable stress tests and use appropriate detection and characterization techniques.

Aggregation continues to be one of the major concerns in development of biopharmaceuticals. However, understanding of aggregation pathways and inhibition of aggregation remain relatively poorly understood. Protein particulates form in a wide range of size and shape, and it is extremely challenging to comprehensively characterize the whole size range of particulates.

1.7 Protein formulation. Use of surfactants

The formulation of recombinant proteins and their long stability and reproducible activity is very important in biopharmaceuticals.

Kerwin states, that in order to maintain biological activity proteins need to be maintained in their multi dimensional conformation and that this conformation is only marginally stable and that any minor disruptions can cause loss of biological activity (Kerwin, 2007). Author's described disruptions are usually induced when producing proteins by filtering, freeze-thawing, lyophilisation, spray drying. Also storage and transportation can have a negative effect on proteins stability and can induce protein aggregation (Kerwin, 2007).

Therefore non-ionic surfactants are widely used in formulation of protein pharmaceuticals to prevent protein aggregation and minimize surface absorption of proteins during their development (Maggio, 2012).

It has been reported that by adding surfactants into protein formulations, the surfactant can act to unfold protein and together they can form a protein – surfactant complex (Narayanan, 1999; Valstar et al., 1999; Valstar et al., 2000; Sahu et al., 2005). Chodankar stated that surfactant molecules while interacting with the non polar amino acids are responsible for causing the protein to unfold (Chodankar, 2007).

This author sated three main models for protein – surfactant complexes:

- “Rod-like model” – it describes the complex as a rigid rod with the length proportional to the molecular weight of the protein;

- “Flexible helix model” – it describes the complex as a flexible cylindrical micelle formed by the micelle on the surface of which hydrophilic segments of the protein are bound;
- “Necklace model” – proposes that protein is unfolded with micelle-like clusters bounded to the polypeptide chain of the protein (Chodankar, 2007).

1.7.1 Structure and behaviour of surfactants

Surfactants are usually described as surface active molecules with polar and nonpolar domains that have aqueous solubility as aggregate and monomers. Surfactants are very useful in protein delivery. They have capability to reduce interfacial surface tension in formulations by adsorbing to interfaces (Rosen, 2004). That is related to surfactant structure: the polar hydrophilic part of the surfactant molecule – “hydrophilic head group” and nonpolar – “hydrophobic tail” (Figure 1.12).

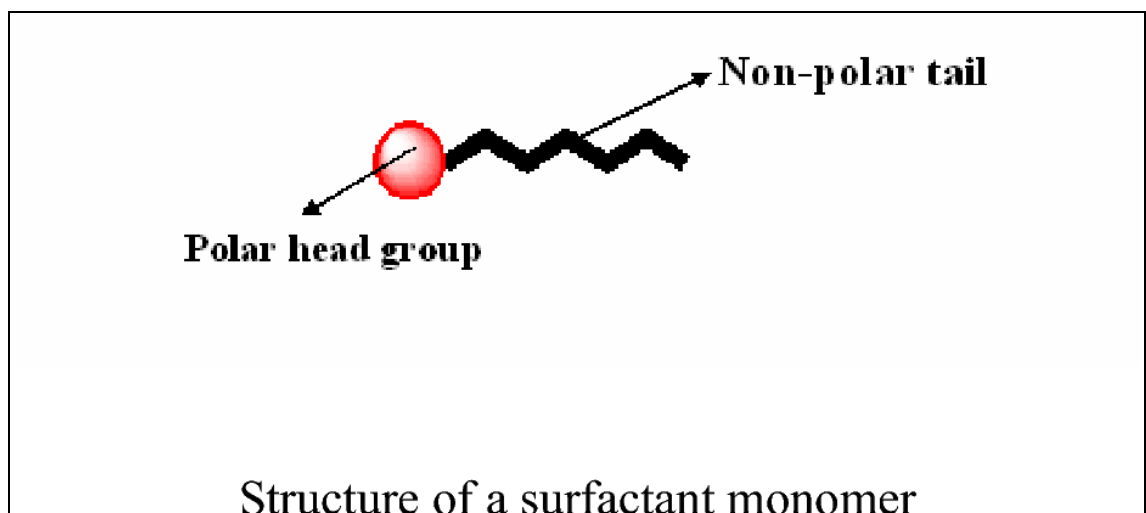


Figure 1.12. Figure of a surfactant monomer (Garq, 2012).

Depending on surfactant hydrophilic group surfactants can be divided into 3 groups:

- Ionic surfactants – denaturing surfactants. These type of surfactants disrupt molecular protein – protein interactions;
- Non ionic surfactants have uncharged hydrophilic head groups. They are non denaturing. These type surfactants disrupt protein-lipid and lipid-lipid interactions rather than protein-protein interactions.
- Zwitterionic surfactants contain both a positive and negative charge in their hydrophilic head group. These compounds are electrically neutral like the nonionic surfactants, but can often disrupt protein-protein interactions like the ionic surfactants (Malvern Instruments Ltd, 2006).

1.7.2 Micellization. Critical Micelle Concentration (CMC)

Surfactants interact with proteins as micelles. Micellization occurs when surfactant concentration is increased and molecules are forced to aggregate and form monolayers at interfaces and micelles (Figure 1.13).

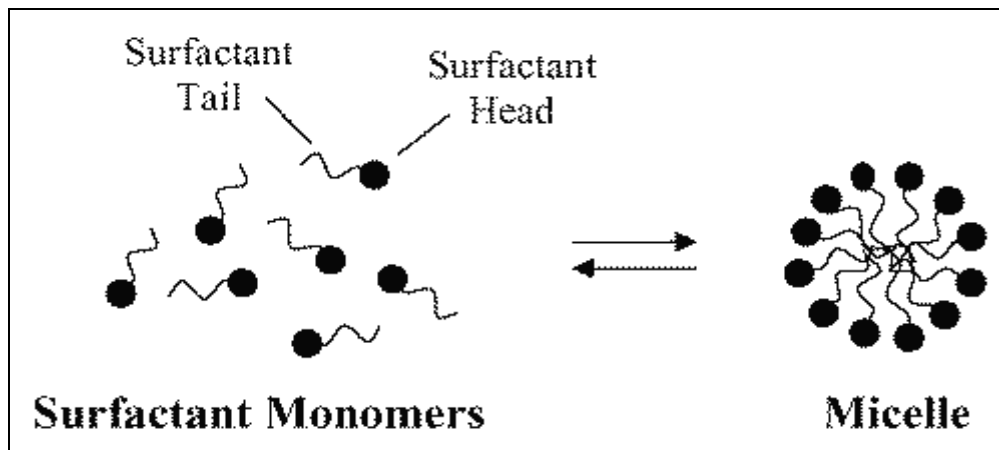


Figure 1.13. Micellization (Rangel-Yaguil et al., 2005).

This happens when a non polar group is inverted into the aqueous solution, the hydrogen bonding is disrupted and then water molecules put themselves around the non polar group to satisfy hydrogen bonds (Anatrace Inc, 2008).

Usually micelle diameter is just a few nanometres and micelles molecular weight is less than 100 kDa.

Each surfactant is characterised by its CMC, which is the surfactant concentration above which monomers self assemble and form non covalent aggregates as so called micelles.

When the total surfactant concentration is below CMC, monomers are free in bulk solution. However, as more surfactant is added above the CMC, all additional detergent monomers will go into micelles (Figure 1.14).

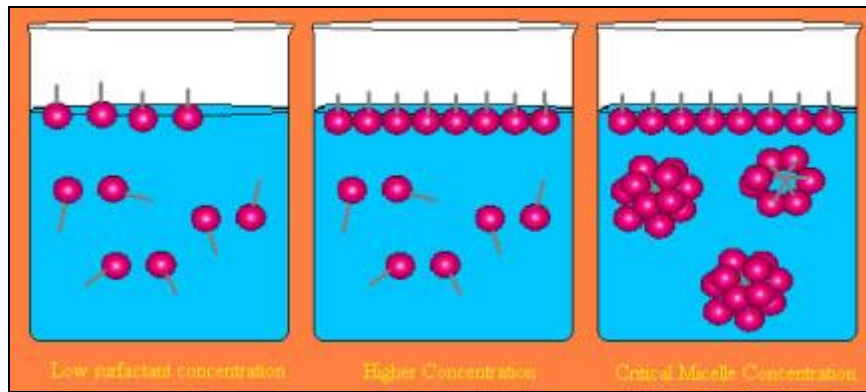


Figure 1.14. The self assembly mechanism of micelle formation with increasing concentration of surfactant (Behan, 1999).

There are several physical-chemical factors that can affect the CMC of surfactants. Generally, the CMC decreases as the hydrophobicity of the surfactant increases. Other properties that directly affect the CMC are the characteristics of the hydrophobic and hydrophilic groups and solution additives such as electrolytes (Malvern Instruments Ltd, 2006).

1.8 Choice of materials

1.8.1 Phosphate buffered saline

Phosphate buffered saline (PBS) is a buffer solution commonly used in pharmaceutical research. It is a water based salt solution containing sodium chloride, sodium phosphate, and in some formulations potassium chloride and potassium phosphate. The buffer helps to maintain a constant pH.

1.8.2 Bovine Serum Albumin

Bovine serum albumin (BSA) is one of the most widely used and studied single chain protein with a typical concentration of 5 g/100 ml (Das et al., 2004).

BSA is composed of 582 amino acids and has 3 homologous domains: I, II and III. All domains are connected through helical extensions creating the two longest helices in albumin. Also domains are divided into 9 loops by 17 disulfide bonds (Wei et al., 2006).

Much research has been conducted using BSA because of its stability and low cost. Also this protein is commonly used to determine the quantity and interactions with other proteins and in order to understand how BSA affects their functionality (Adel et al., 2007).

1.8.3 Antibody IgG2

The research and development of monoclonal antibodies is a rapidly progressing field. It has been reported that in the past years more than 30 immunoglobulins (IgGs) have been approved for use as biopharmaceuticals. Also many studies are looking at the different antibodies structure and interactions, investigating their stability and binding (Beck et al., 2008). However the avoidance of aggregation and particle formation in antibody formulations is a major issue that is a focus in drug development. IgG antibodies play a big role in mature immune response.

IgG antibodies are Y shaped molecules. Figure 1.15 illustrates the structure of IgG antibody.

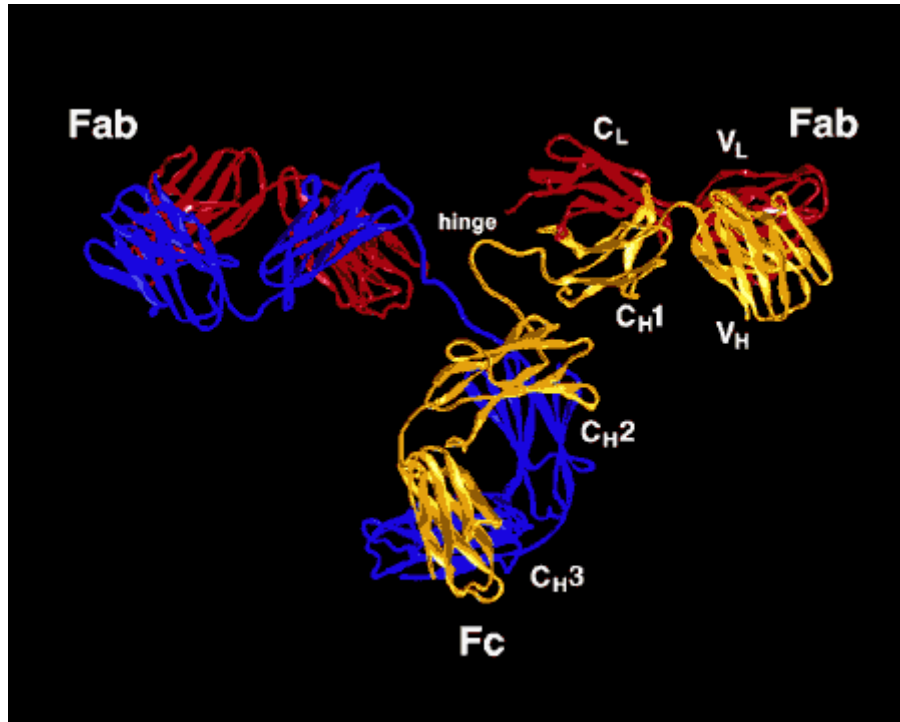


Figure 1.15. Schematic drawing of IgG antibody (Mayer, 2009).

IgG structure is divided into two heavy chains and two light chains, which are joined by disulfide linkages (Wang, 2006). The IgG molecule can be broken down into two regions, the Fc and Fab. The Fc region, so called because it is the fragment of the IgG molecule that most readily crystallizes, is involved in effecting the physiological roles the antibody must play. Two identical Fab fragment are present at the ends of the "Y" in every IgG structure. The Fab region is named as such because it is the IgG fragment that contains the antibody binding site. The Fab region contains a region of highly conserved amino acids as well as a region of highly variable amino acids (Fv). These variable sequences are confined to 6 protein loops (or complementarity

determining regions) that cluster together at the end of the Fab fragments to form a continuous hypervariable surface. It is this region that is responsible for the binding of foreign antigens (Wang, 2006).

1.8.4 Nonionic surfactants: Tween 20, Tween 80, Brij 35 and Pluronic F-68

Non-ionic surfactants are widely used in the formulation of protein pharmaceuticals to prevent aggregation and minimize surface adsorption of proteins, both during the manufacturing process and in the final product formulation (Maggio, 2012).

The most commonly used non-ionic surfactants in protein formulation are the polysorbates PS 20 and PS 80 also known as Tween 20 and Tween 80. It has been reported that more than 70 % of the marketed formulations of monoclonal antibody products contain one or both these two surfactants (Maggio, 2012). Tween 20 and Tween 80 are comprised of mixtures of structurally-related fatty acid esters of polyoxyethylene sorbitan and lauric acid or oleic acid. In the case of Tween 20, the monolaurate fraction comprises 40% to 60% of the alkyl chains, with alkyl groups of different chain length making up the remainder of the molecules. Tween 80 has approximately 60% of the alkyl chains which are derived from oleic acid with the remainder of the esters derived from other fatty acids. Tween 20 and Tween 80 structures are shown in Figure 1.16.

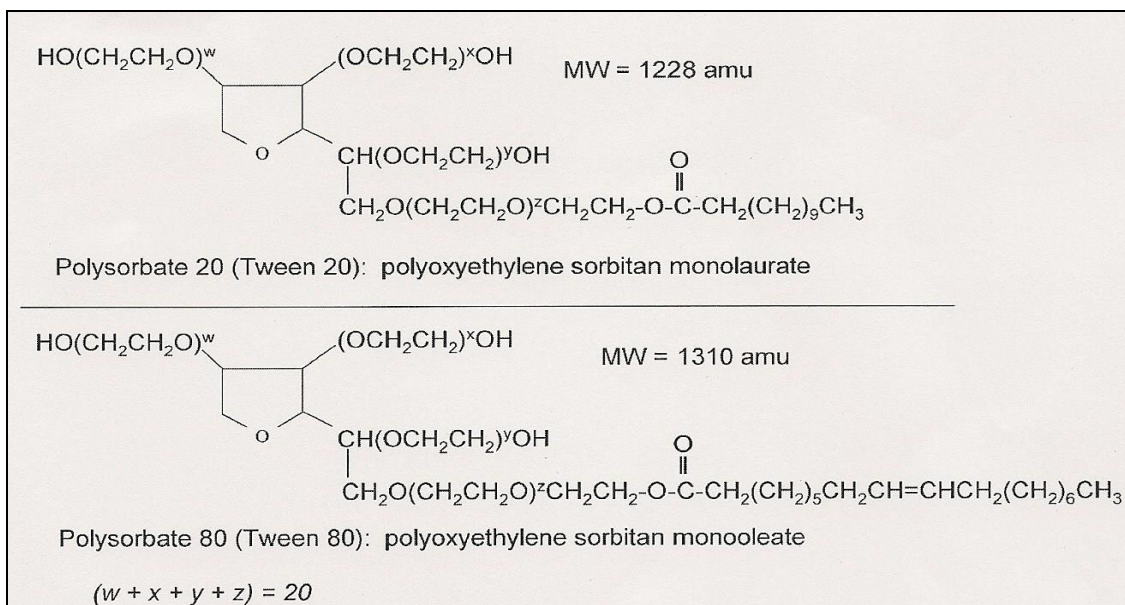


Figure 1.16. Chemical structure of polysorbates 20 and 80. $w+x+y+z$ refers to the total number of oxyethylene subunits on each surfactant molecule and may not exceed 20 (Kerwin, 2008).

Other non-ionic surfactants commonly used in pharmaceutical formulations include Brij 35 (polyoxy-ethylene alkyl ether) and Pluronic F-68.

Brij 35 is a polyethoxylated lauryl alcohol (yielding a lauryl ether). Lauryl is another name for a chain consisting of mostly a 12 carbons, straight chain, primary alcohol, dodecanol (Stavroudis, 2009). The ethoxylate chain averages 23 repeating units (Figure 1.17).

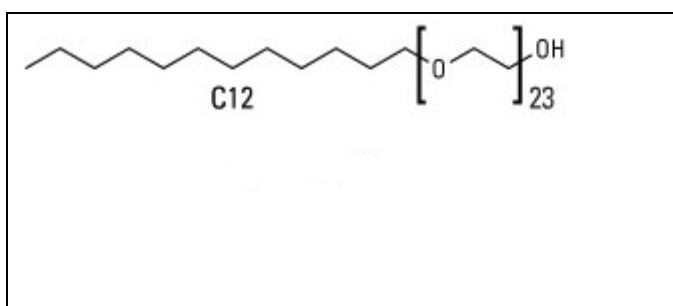


Figure 1.17. Brij 35 structure (Stavroudis, 2009).

Pluronic F-68 non-ionic surfactant has been used to stabilize recombinant human growth hormone (rhGH) against aggregation as injectable as well as

in the extended action formulation (Katakam et al., 1995; Wei et al., 2007). As a surfactant Pluronic F-68 has two hydrophilic poly (ethylene oxide) (PEO) chains and one hydrophobic poly (propylene oxide) (PPO) chain (Figure 1.18).

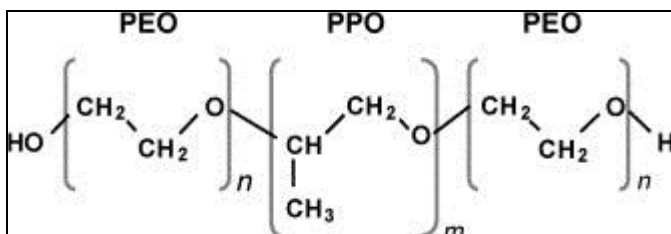


Figure 1.18. Pluronic F-68 structure (Santander-Ortega et al., 2006).

In general, the surfactants are very important and have a valuable role in pharmaceutical biotechnology. They are widely utilized in various drug dosage forms to stability and bioavailability. Also it is important to notice, that some surfactants are quite unstable from the thermodynamic point of view and frequently form large aggregates. Association colloids such as micelles, on the other hand, can form self-assembling systems, and are thermodynamically more stable towards both dissociation and aggregation (Rangel-Yagui et al., 2005). Therefore, the study of surfactants and their role in biopharmaceuticals is very important for protein aggregation. In this work we analyse the role of Tween 20, Tween 80, Brij 35 and Pluronic F-68 surfactants on proteins BSA and IgG2 conformational and size stabilities.

1.9 Aims and objectives

The overall aim of this project was to identify improved methods of particle characterisation and understanding of the mechanisms of their formation in protein formulations. The project scope would include evaluation of the effect of different surfactants on minimising and preventing the formation of sub visible particles. Moreover, characterising and understanding mechanisms of particle formation to improve drug development.

To achieve this, the effect of Tween 20, Tween 80, Brij 35 and Pluronic F-68 surfactants at below, around and above their CMC on bovine serum albumin (BSA) and immunoglobulin IgG2 conformational and particle size stability was studied.

Experiments were performed in order to achieve the following research questions:

- Do all four surfactants behave the same way regarding prevention/inhibition of particle formation;
- Is surfactant behaviour with regard to particulate formation protein specific;
- Is there a relationship between the structure of nonionic surfactants and particle formation;
- Is the concentration and CMC of the surfactants significant for the effect;
- Does T_m measured by HSDSC predict particle formation;
- Does level of small particle size measured by DLS predict levels of larger particles measured by HIAC and MFI;

- Which method is the most appropriate to examine biopharmaceutical particles.

1.10 Structure of thesis

The thesis is structured as follows:

- Chapter 2 gives details of all the materials used and methods employed during experimental work.
- Chapter 3 investigates the effect of Tween 20, Tween 80, Brij 35 and Pluronic F-68 surfactants and their below, around and above CMC levels on protein BSA and antibody IgG2 conformational stability employing HSDSC method in a series of unfolding experiments.
- Chapter 4 explores the sub-visible particle size range measured by Dynamic Light Scattering (DLS) method for BSA and IgG2. Investigating the effect of Tween 20, Tween 80, Brij 35 and Pluronic F-68 surfactants and their different CMC levels on particle size distributions. The effect of heat treatment and storage is also assessed.
- Chapter 5 investigates the effect of Tween 20, Tween 80, Brij 35 and Pluronic F-68 surfactants on BSA and IgG2 particle size per ml using Light Obscuration (HIAC) and Micro-Flow Imaging (MFI). The effect of heat treatment stress and storage on protein surfactant free and protein-surfactant systems is also investigated.
- Chapter 6 discusses general findings within the thesis.

- Chapter 7 presents general conclusions and gives suggestions of further work.

Chapter 2
Materials and Methods

2.1 Materials

2.1.1 Sources of materials

Table 2.1 shows all the materials used in the study and their suppliers.

All water used was double distilled and deionised.

Table 2.1. Table showing all the materials used in this study and their respective sources.

Material	Source	Batch/Lot number
Dulbecco's Phosphate Buffered Saline (PBS)	SIGMA Ltd, UK	RNBB6734
Bovine Serum Albumin (BSA)	Sigma Life Science, UK	029K1447
Antibody IgG2	MedImmune Ltd, Cambridge, UK	NUT-184
Polysorbate 20 (Tween 20)	Sigma-Aldrich Company Ltd, UK	STBB2028M9
Polysorbate 80 (Tween 80)	Sigma-Aldrich Company Ltd, UK	S398616419
Brij 35	Sigma-Aldrich Company Ltd, UK	BCBC6472
Pluronic F-68	Sigma-Aldrich Company Ltd, UK	020M0029

2.1.2 Material processing

2.1.2.1 Preparation of Bovine Serum Albumin (10 mg/ml) solution

The required amount of BSA was weighed and dissolved in PBS buffer. Samples were stored in the fridge.

2.1.2.2 Preparation of antibody IgG2 (10 mg/ml) solution

Antibody IgG2 was used as received from MedImmune Ltd (Cambridge) and was dissolved into filtered PBS buffer. Samples were stored in the fridge.

2.1.2.3 Preparation of BSA (10 mg/ml) and IgG2 (10 mg/ml) with non ionic Tween 20, Tween 80, Brij 35 and Pluronic F-68 surfactants solutions

Tween 20, Tween 80, Brij 35 and Pluronic F-68 surfactants at different concentrations (below, around and above CMC) were weighed by Mettler Toledo Micro Balance scale XP26 and were added separately to BSA (10 mg/ml) and IgG2 (10 mg/ml) solutions (Table 2.2). Samples were stored in the fridge.

CMC values for Tween 20, Tween 80, Brij 35 and Pluronic F-68 were taken from the literature (Malvern Instruments Ltd, 2006).

Table 2.2. Tween 20, Tween 80, Brij 35 and Pluronic F-68 CMC concentrations.

CMC levels	Tween 20	Tween 80	Brij 35	Pluronic F-68
10 times below CMC (mg/ml)	0.006	0.0015	0.009	0.004
Around CMC (mg/ml)	0.06	0.015	0.09	0.04
10 times above CMC (mg/ml)	0.6	0.15	0.9	0.4

2.1.2.4 Preparation of PBS buffer with Tween 20, Tween 80, Brij 35 and Pluronic F-68 solutions

Dulbecco's PBS was mixed separately with different Tween 20, Tween 80, Brij 35 and Pluronic F-68 concentrations (Table 2.2). Samples were stored in the fridge.

2.2 Methods

2.2.1 Heat treatment stress method

BSA (10 mg/ml) surfactant free and BSA (10 mg/ml) with Tween 20, Tween 80, Brij 35 and Pluronic F-68 surfactants were held at elevated 66°C temperature for 25 minutes using a Thermovac sample thermostat.

IgG2 (10 mg/ml) surfactant free and IgG2 (10 mg/ml) with all four surfactants were held at elevated 60°C temperature for 5 minutes.

2.2.2 Stability study

Freshly prepared BSA (10 mg/ml) and IgG2 (10 mg/ml) surfactant free and BSA and IgG2 with Tween 20, Tween 80, Brij 35 and Pluronic F-68 surfactants were stored in the fridge at +4°C temperature for 8 weeks.

2.2.3 High Sensitivity Differential Scanning Calorimetry (HSDSC)

HSDSC is a suitable method to follow the thermal denaturation of proteins and is more convenient than conventional assay methods (Izutsu et al., 1990). HSDSC is a very sensitive calorimetry technique that uses larger volume sample cells and slow heating rates which make it particularly suitable for the study of dilute solutions (Robson et al., 2000).

A schematic diagram of a calorimetric unit is shown in Figure 2.1.

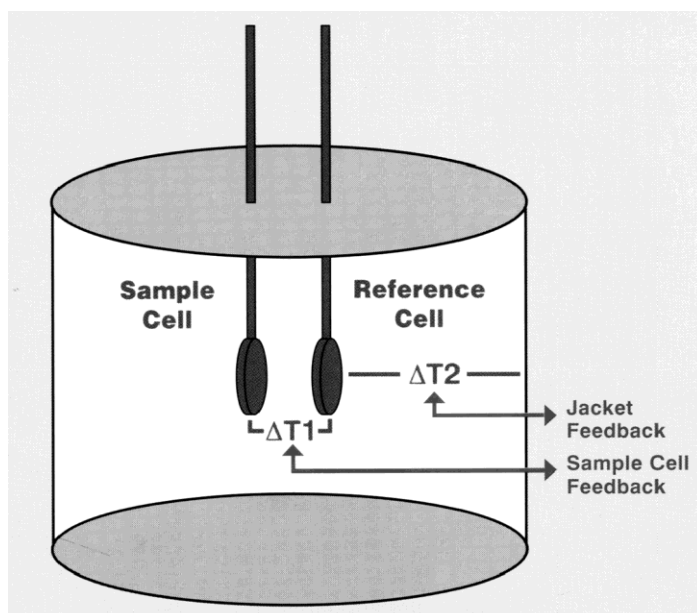


Figure 2.1. Differential scanning calorimetric unit (Microcal system user manual).

The samples and reference solutions were pipetted into one Microcal VP – capillary DSC 96 well plate (Figure 2.2).



Figure 2.2. Microcal VP – capillary DSC 96 well plate (Edge BioSystems Inc.).

At first water was placed in both sample and reference compartments (Table 2.3). HSDSC curve corresponding to water vs. lysozyme run was used as the instrumental calibration.

Table 2.3. Microcal VP – capillary DSC plate lay-out.

	1	2	3	4	5	6	7	8	9	10	11	12
A	Water	Water	Water	Water	Water	Lysozyme	PBS	PBS	PBS	PBS	PBS	Sample
B	PBS	PBS	PBS	Sample Tween 20 < CMC	PBS	PBS	PBS	Sample Tween 20 ~ CMC	PBS	PBS	PBS	Sample Tween 20 > CMC
C	PBS	PBS	PBS	Sample Tween 80 < CMC	PBS	PBS	PBS	Sample Tween 80 ~ CMC	PBS	PBS	PBS	Sample Tween 80 > CMC
D	PBS	PBS	PBS	Sample Brij 35 < CMC	PBS	PBS	PBS	Sample Brij 35 ~ CMC	PBS	PBS	PBS	Sample Brij 35 > CMC
E	PBS	PBS	PBS	Sample F-68 < CMC	PBS	PBS	PBS	Sample F-68 ~ CMC	PBS	PBS	PBS	Sample F-68 > CMC
F	Water	Water	Water	Lysozyme	Detergent	Detergent	Water	Water	Water	Water	Water	Water
G	Water	Water										
H												

During the scan the cells are heated with constant power and the difference in temperature between the cells is closely monitored. The difference in power that has to be supplied to the cells during scan is recorded as a function of time and is a measure of the difference between the heat capacity of the sample and the reference sample.

HSDSC analysis was performed using a Microcal VP-DSC.

The calorimetric data was analyzed by using the software Origin 5.0, MicroCal Inc.. The parameter obtained from this analysis was temperature at

which maximum heat exchange occurs (T_m). This was obtained by linear connection of the baseline, normalizing concentration and fitting a non-two-state model to the data after baseline correction.

2.2.4 Dynamic Light Scattering (DLS)

DLS measurements were performed using a Zetasizer nano-series (Malvern Instruments Ltd). The DLS instrument was left powered up for approximately 30 minutes before measurements were made. This was to prevent any thermal equilibration problems affecting the measurement results (The NanoBiotechnology Centre, 2009)

All experiments were performed at 173° scattering angle, which maximizes the detection of scattered light while maintaining signal quality. This provides exceptional sensitivity that is required for measuring the size of particles, such as surfactant micelles, at low concentration (Malvern Instruments Ltd, 2006). A monochromatic coherent He-Ne laser with a fixed wavelength of 633 nm was employed. The samples were measured un-filtered and un-diluted to ensure that the sample composition is maintained in its original state. Samples were directly poured into a low volume quartz cuvette ZEN2112 (Figure 2.3, Table 2.4) and placed inside a constant temperature holder. All measurements in this study were taken at a temperature of 25°C. Each sample was equilibrated for 10 minutes and had three measurements.



Figure 2.3. Low volume quartz batch cuvette for size and molecular weight measurements for use with the Zetasizer Nano series (The Nanobiotechnology Centre, 2009).

Table 2.4. Low volume quartz cuvette (ZEN2112) description (The Nanobiotechnology Centre, 2009).

LOW VOLUME QUARTZ CUVETTE ZEN2112	
Typical solvent	Water, most organic and inorganic solvents
Optical quality	Excellent
Minimum sample volume	12 μ l
Advantages	Highest optical quality Can use nearly any dispersant Low sample volume
Disadvantages	Requires cleaning after measurement Requires careful filling to avoid bubbles

The intensity size distributions were obtained from analysis of the correlations functions using the Multiple Narrow Modes algorithm in the instrument software.

2.2.5 Light Obscuration (HIAC)

Light obscuration analysis is based on the reduction of light intensity due to reflection, absorption and scattering, if a particle crosses an incident laser beam. As the decrease in light intensity is proportional to the size of particles, particle size distributions assuming spherical particles can be generated (Mahler et al., 2009).

All HIAC measurements were performed at Medimmune UK Cambridge Ltd formulation laboratory using the HIAC/ROYCO eight channel particle counter 8000A and liquid syringe sample 3000A instrument. It has been reported by Mahler et al. (2009) that the HIAC instrument contains a laser diode and a photodiode detector to determine the residual light intensity of laser beam, after particles have passed the sensor-zone (Mahler et al., 2009).

Between the measurements the HIAC instrument was cleaned and particle free fluid was flushed through the system to provide a clean baseline. The samples were gently inverted taking care not to introduce air bubbles. Six measurements were analyzed for each sample. The results from all measurements were reported as the number of particles per ml, and the average of the last three measurements was utilized for further evaluation. Appropriate negative controls were also measured to ascertain the effects of

sample handling. The instrument was set up to measure particles greater than or equal to 2, 5, 10, 25, 50 and 100 μm , as appropriate.

2.2.6 Micro-flow Imaging (MFI)

MFI is a flow microscopic technology which operates by capturing images of suspended particles in a flowing stream. Different magnification set-points are available to suit the desired particle size range and image quality (Brightwell Technologies Inc., 2006).

Micro-flow imaging (MFI) measurements were performed at Medimmune UK using the MFI DPA4200 series instrument. Samples and PBS buffer were allowed to stand for 10 minutes at atmospheric pressure and room temperature to assist in removing any air bubbles which may have been formed after sample preparation. Prior to each sample analysis, particle free fluid was flushed through the system to provide a clean baseline. Clean baselines were achieved by flushing for 2 minutes between sample runs. A typical image frame from a proteinaceous sample is shown in Figure 2.4. As described in the "Application of MFI to the Analysis of Particles in Parenteral Fluids", the sample volume in each frame is precisely defined by the flow cell geometry so the particle concentrations can be determined absolutely (Brightwell Technologies Inc., 2006).

No calibration is required and all critical system parameters are automatically pre-set to eliminate run-to run and user-dependent variations.

The system software proceeds measurement of area, equivalent circular diameter, perimeter, intensity, circularity and maximum Feret's diameter for each sample.



Figure 2.4. Typical image frame (Brightwell Technologies Inc., 2006).

Dulbecco's filtered PBS buffer was used to optimize the illumination. The samples were gently inverted taking care not to introduce air bubbles. For each sample two separate runs of 1 ml each were analysed and then averaged for further analysis. The MFI instrument measured particles greater than or equal to 2, 10, 25, 50 and 100 μm per ml.

2.2.7 Statistical data analysis

Collected data was analysed using SPSS (Statistical Package for the Social Sciences) software (Version 20.0).

Data normality was assessed.

Statistical tests were used:

- One-Way ANOVA, post-hoc Bonferroni test was applied for testing the significance of differences between different sample groups;

- Pearson Correlation test was used to measure the “degree of linearity” and relationship between pair of variables on a scale from -1.00 to +1.00;
- T-test – Student’s t-test was used to determine if two sets of data are significantly different from each other.

Chapter 3

Effect of surfactant and surfactant concentration on the thermal unfolding of BSA and Igg2 in solution

3.1 Introduction

One of the crucial problems of protein-based biopharmaceuticals is their long-term stability or so called shelf life. Comprehensive knowledge about prediction of protein stability can facilitate the development of optimal formulations (Ahrer et al., 2006). Protein stability is important for formulation development and also during the whole production process of the therapeutic protein to prevent process-induced aggregation. Aggregation is one of the major problems in pharmaceutical industry since proteins are relatively unstable in solution (Ahrer et al., 2006).

One of the common methods of protein solution stabilization is the addition of surfactants for their ability to prevent protein aggregation. Maximum protection occurs at concentrations close to the critical micelle concentration (CMC) independent of the initial protein concentration (Krielgaard et al., 2000).

High sensitivity differential scanning Calorimetry (HSDSC) is a powerful method, which can be used for optimising the stability of proteins in solution. It is therefore an essential tool in the development of pharmaceutical proteins (Remmele et al., 1998; Krielgaard et al., 2000; Vidanovic et al., 2003; Michnik 2003; Wissing et al., 2000). HSDSC operates on a similar principle to conventional DSC, but HSDSC is around 10 – 100-fold more sensitive and is able to detect baseline changes below 1 μ W (Wissing et al., 2000).

The T_m value measured by HSDSC is commonly used as a stability indicator for proteins (Cueto et al. 2003) and has been reported comprehensively in

the literature (Cueto et al., 2003; Branchu et al., 1999; Larsericsdotter et al., 2004; Michnik, 2003; Wissing et al., 2000; Ahrer et al., 2006; Garidel et al., 2009).

Given the sensitivity associated with HSDSC, it was accordingly decided to use HSDSC to investigate the effects that Tween 20, Tween 80, Brij 35 and Pluronic F-68 – (non-ionic surfactants) at different concentrations have on the thermal stability of bovine serum albumin and immunoglobulin IgG2.

3.2 Objective

The main objective of the HSDSC experiments was to investigate the effect of Tween 20, Tween 80, Brij 35 and Pluronic F-68 non-ionic surfactants and their different concentrations on the unfolding transition temperature of bovine serum albumin BSA and immunoglobulin IgG2.

3.3 Experimental

Thermal unfolding of proteins was monitored with a high sensitivity differential scanning calorimeter, model VP-DSC, from MicroCal Inc. Thermograms were obtained between 25 and 95°C, at a scan rate of 1°C/min. Both – bovine serum albumin and immunoglobulin IgG2 were analyzed at concentrations of 10 mg/ml.

Samples of BSA and IgG2 alone were scanned to produce a thermal profile along with protein samples containing surfactants at below, around and

above CMC levels to allow comparison of protein-surfactant free and protein-surfactant systems.

Thermal unfolding measurements were carried out as described in Chapter 2, Section 2.2.3.

The experiments were repeated two times to show reproducibility of the results.

The reversibility of the thermally induced transition was checked by reheating the sample solution in the calorimetric cell after cooling from the first run.

The calorimetric data was analyzed by using the software Origin 5.0, MicroCal Inc. as described in Chapter 2, Section 2.2.3.

3.4 Results and Discussion

3.4.1 Thermal unfolding experiments of bovine serum albumin

Figure 3.1 shows the HSDSC thermal unfolding profile of bovine serum albumin (10 mg/ml in PBS buffer). The T_m value for the protein was taken as the peak maxima.

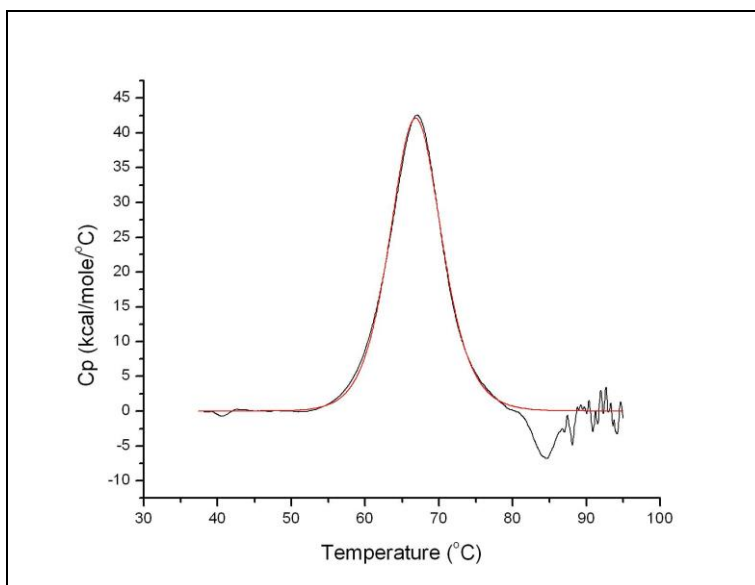


Figure 3.1. Thermal unfolding profile of BSA (10 mg/ml in PBS buffer). Black line represents normalised calorimetric data for the thermal denaturation of BSA. Red line represents the results of fitting experimental curves to a non-two-state model.

The average of the unfolding temperature T_m BSA was $66.91 \pm 0.085^\circ\text{C}$ this is similar to the published value of 67°C (Nishimura et al., 2001).

Thermal analysis of BSA (10mg/ml) alone and BSA (10mg/ml) with different added levels of Tween 20, Tween 80, Brij 35 and Pluronic F-68 surfactants showed that the denaturation process is irreversible, probably due to aggregation of unfolded protein molecules at high temperatures. This behaviour has been previously reported in the literature (Michnik, 2003, Pico, 1997, Giancola et al., 1997).

Table 3.1 shows the results obtained for the thermal unfolding profiles of BSA (10 mg/ml) and BSA (10 mg/ml) with different Tween 20, Tween 80, Brij 35 and Pluronic F-68 concentrations (See Appendix 1-12).

Table 3.1. Results of thermal unfolding profiles of BSA (10 mg/ml in PBS buffer) and BSA (10 mg/ml) with different Tween 20, Tween 80, Brij 35 and Pluronic F-68 concentrations.

SOLUTION	T_m (°C)	Standard deviation
BSA (10 mg/ml)	66.91	±0.085
BSA (10 mg/ml) with Tween 20 below CMC	61.79	±0.057
BSA (10 mg/ml) with Tween 20 around CMC	60.24	±0.255
BSA (10 mg/ml) with Tween 20 above CMC	60.68	±0.042
BSA (10mg/ml) with Tween 80 below CMC	61.09	±0.099
BSA (10 mg/ml) with Tween 80 around CMC	61.66	±0.184
BSA (10 mg/ml) with Tween 80 above CMC	64.70	±0.071
BSA (10 mg/ml) with Brij 35 below CMC	61.20	±0.042
BSA (10 mg/ml) with Brij 35 around CMC	65.54	±0.085
BSA (10 mg/ml) with Brij 35 above CMC	65.99	±0.028
BSA (10 mg/ml) with Pluronic F-68 below CMC	61.42	±0.042
BSA (10 mg/ml) with Pluronic F-68 around CMC	61.46	±0.042
BSA (10 mg/ml) with Pluronic F-68 above CMC	62.29	±0.071

Figure 3.2 represents the results from table 3.1 to identify if any trends are present.

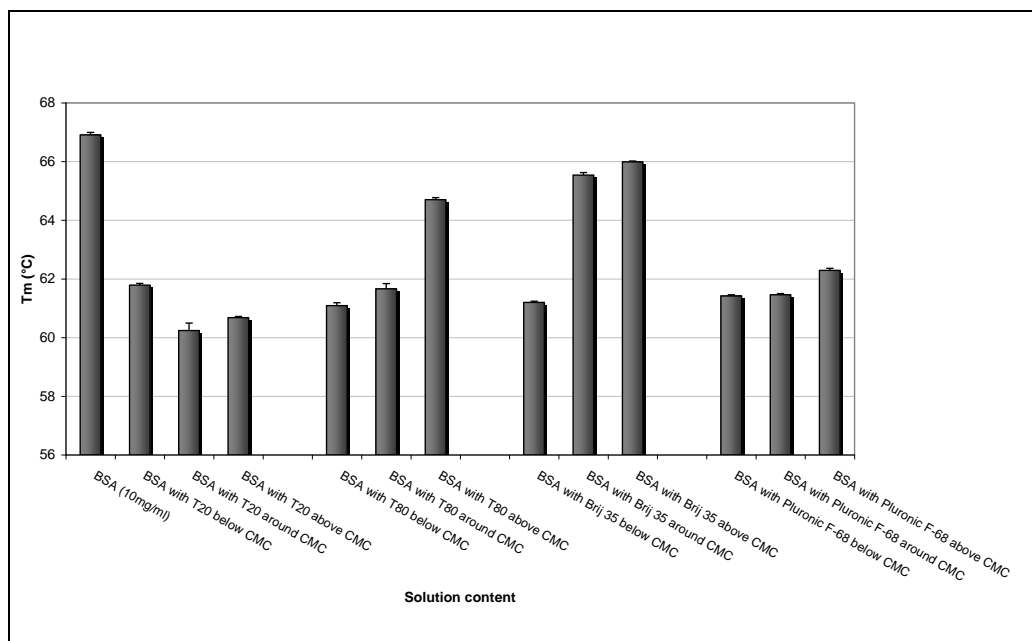


Figure 3.2. Unfolding temperatures (T_m) of BSA (10mg/ml) with different Tween 20, Tween 80, Brij 35 and Pluronic F-68 concentrations.

From the data shown in Table 3.1 and Figure 3.2 it can be clearly seen that the presence of all of the surfactants at any concentration lowers T_m and promotes the thermal unfolding of BSA. The average T_m of BSA with Tween 20 and Tween 80 surfactants are lower than that reported by Garidel et al. (Garidel et al., 2009). These discrepancies are due to the difference in used concentrations, which were higher. The other difference that may have contributed was the albumin sample. In the pre-cited study (Garidel et al., 2009) the sample was Human Serum Albumin (HSA).

At the concentrations employed, the average T_m of BSA (10 mg/ml) with Tween 20 and Pluronic F-68 was lower then that produced by Tween 80 and Brij 35. T_m was maximal for BSA in the presence of Tween 80 at a concentration above its CMC ($64.70 \pm 0.012^\circ\text{C}$) and similarly for Brij 35 at concentrations around ($65.54 \pm 0.019^\circ\text{C}$) and above its CMC ($65.99 \pm 0.015^\circ\text{C}$). This finding would indicate that Tween 80 and Brij 35 at

concentrations above their CMC had a weaker interaction with BSA than Tween 20 and Pluronic F-68 at higher concentrations relative to CMC, because they reduced T_m to the least extent compared to the surfactant-free BSA sample.

One-way ANOVA analysis showed a significant effect of all the surfactants at all concentrations on the unfolding temperature T_m of BSA (10 mg/ml) ($P < 0.01$). Post-hoc tests, using the Bonferroni correction, showed a significant reduction in the T_m ($^{\circ}\text{C}$) of BSA (10 mg/ml) with all four surfactants at the concentrations employed compared to BSA (10 mg/ml) surfactant free solution. The mean difference was significant at the 0.001 level ($P < 0.001$) for BSA with Tween 20, Tween 80, Pluronic F-68 surfactants at all CMC levels and Brij 35 at below and above CMC. Brij 35 around CMC the mean difference was significant at 0.01 ($P < 0.01$) level compared to BSA surfactant free solution. Figure 3.3 illustrates these findings.

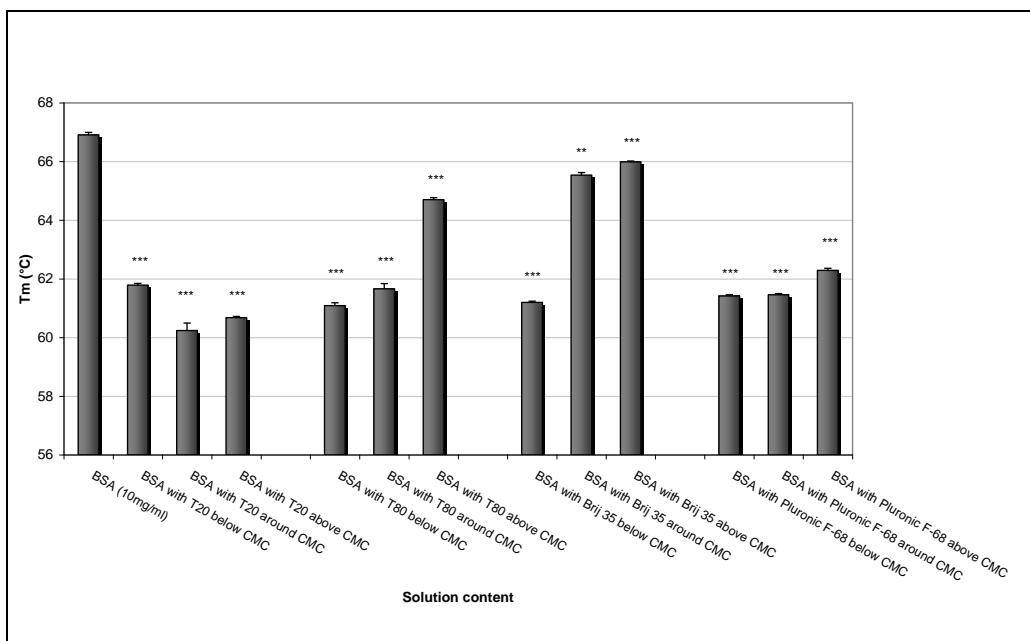


Figure 3.3. The effect of different concentrations of Tween 20, Tween 80, Brij 35 and Pluronic F-68 surfactants on BSA (10 mg/ml) unfolding temperature T_m (°C) measured by HSDSC. Data is expressed as the mean \pm Std. Deviation. ** $P < 0.01$ - * $P < 0.001$; significant decrease in BSA with surfactants unfolding temperature T_m compared with BSA (10 mg/ml) surfactant free solutions.**

In Figure 3.4 the effect on T_m of different surfactant concentration relative to CMC is shown.

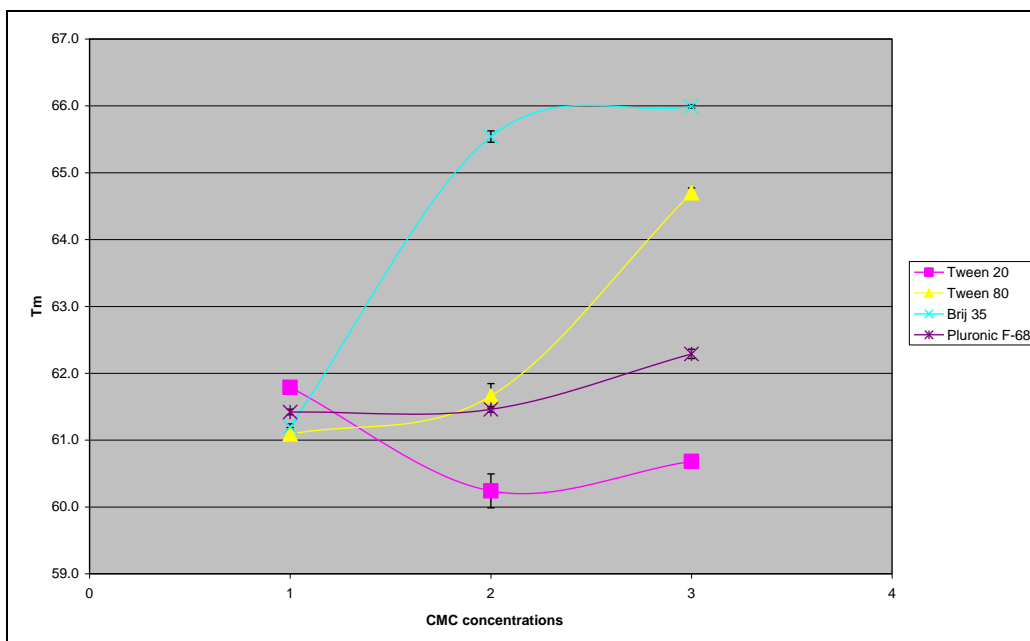


Figure 3.4 Effect of surfactant concentration relative to CMC on the T_m of BSA for Tween 20, Tween 80, Brij 35 and Pluronic F-68 surfactants. (1 – 10 times below CMC; 2 – around CMC; 3 – 10 times above CMC)

From Figure 3.4 BSA T_m values increased with increasing concentration for Tween 80, Brij 35 and Pluronic F-68 surfactants. Interestingly, for the Tween 20 system, T_m was maximal at its lowest concentration.

It is noticeable that when the concentration of surfactant in solution is below CMC there is a general decrease in T_m for Tween 80, Brij 35 and Pluronic F-68 surfactant systems.

One-way ANOVA analysis showed significant differences of T_m between the Tween 20, Tween 80, Brij 35 and Pluronic F-68 surfactant groups at concentrations below CMC, around CMC and above CMC levels. For all four surfactants at concentrations below their CMC, the T_m ($^{\circ}\text{C}$) difference was statistically significant at 0.01 level ($P < 0.01$). At around CMC and above CMC concentrations, the T_m difference between surfactants was statistically significant at 0.001 level ($P < 0.001$).

3.4.2 Thermal unfolding experiments of monoclonal antibody IgG2

The thermal unfolding of IgG2 (10 mg/ml), is notably different to that of bovine serum albumin (10 mg/ml), over the temperature range 30 – 95°C. It is characterised by two endothermic transitions (Figure 3.5), which is the result of the melting of two independent domains of the immunoglobulin (Ionescu et al., 2007). Typical applications concerning immunoglobulin are studies describing the complex unfolding of antibodies by the denaturation of two individual domains. The complexity of the unfolding is given by the structure of the IgG2 molecule, which consists of four polypeptide chains that are linked by disulphide bonds and grouped in two identical F_{ab} and one F_c fragment forming an Y-shaped conformation (Ahrer et al., 2006). These authors reported that immunoglobulin F_c fragments having different glycosylation pattern show differences in the thermodynamic properties (Ahrer et al., 2006).

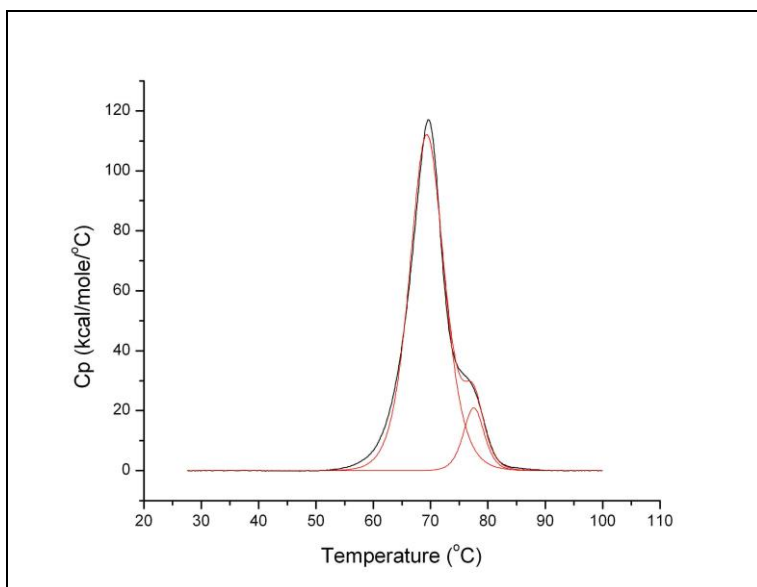


Figure 3.5. Thermal unfolding profile of IgG2 (10 mg/ml). Black line represents normalised calorimetric data for the thermal denaturation of IgG2 (10 mg/ml). Red lines represent the two peaks of fitting experimental curves to a non-two-state model.

Results of the thermal unfolding of IgG2 in absence and presence of different CMC levels of Tween 20, Tween 80, Brij 35 and Pluronic F-68 surfactants are shown in Appendixes 13-24 and are summarised in Table 3.2 and Figure 3.6.

The best fit parameters returned from the data fits are consistent with a transition at $69.38 \pm 0.057^{\circ}\text{C}$ (T_{m1}) and another at $77.53 \pm 0.113^{\circ}\text{C}$ (T_{m2}) (Table 3.2). Kravchuk et al., (1998) presented similar T_m unfolding peaks for IgG2.

Under these conditions, the transitions were irreversible and no thermal transitions were noted on subsequent scans of the same samples after cooling.

Table 3.2. Results of thermal unfolding profiles of IgG2 (10 mg/ml) and IgG2 (10 mg/ml) with different Tween 20, Tween 80, Brij 35 and Pluronic F-68 concentrations.

SOLUTION	T _{m1} (°C)	T _{m2} (°C)
	Mean ±STDEV	Mean ±STDEV
Igg2	69.38±0.057	77.53±0.113
Igg2 with Tween 20 below	69.61±0.042	77.50±0.141
Igg2 with Tween 20 around	69.22±0.311	77.60±0.042
Igg2 with Tween 20 above	69.13±0.042	77.63±0.071
Igg2 with Tween 80 below	69.31±0.057	76.70±0.156
Igg2 with Tween 80 around	69.61±0.169	77.65±0.071
Igg2 with Tween 80 above	69.60±0.057	77.63±0.028
Igg2 with Brij 35 below	68.60±0.042	76.49±0.099
Igg2 with Brij 35 around	69.11±0.028	76.78±0.042
Igg2 with Brij 35 above	68.88±0.014	76.68±0.057
Igg2 with F-68 below	68.82±0.042	76.93±0.071
Igg2 with F-68 around	68.12±0.042	76.12±0.028
Igg2 with F-68 above	68.75±0.071	77.02±0.028

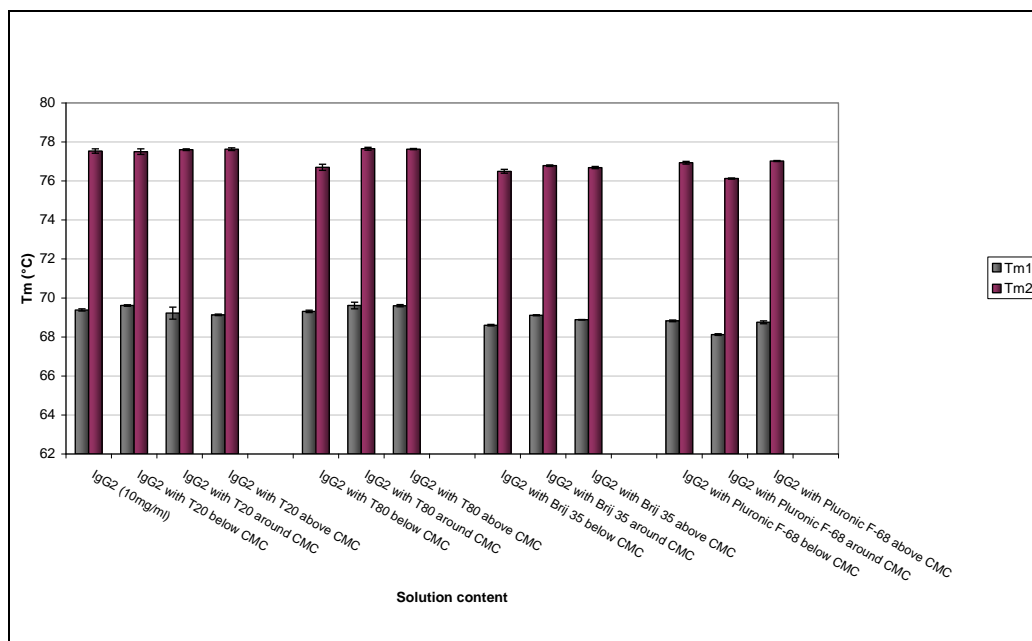


Figure 3.6. Thermal unfolding temperatures (T_{m1} and T_{m2}) of IgG2 (10 mg/ml) with different Tween 20, Tween 80, Brij 35 and Pluronic F-68 concentrations.

Data presented in Table 3.2 shows that the first thermal unfolding peak (T_{m1}) is shifted to lower temperatures, opposite to what is observed for the second peak (T_{m2}). In any case, the difference between T_{m1} and T_{m2} comprises around 9 degrees. This relates to thermal unfolding of two IgG2 individual domains (Tischenko et al., 1998, Tischenko et al., 2003).

In general, the different levels of Tween 20, Tween 80, Brij 35 and Pluronic F-68 surfactants lowered the T_m for IgG2. The analysis of the thermal unfolding curves shows that the presence of all surfactants at different concentrations is negligible (Figure 3.6).

One-way ANOVA analysis showed significant differences of T_{m1} between the IgG2 surfactant free and IgG2 with Tween 20, Tween 80, Brij 35 and Pluronic F-68 surfactants at different concentrations. However post-hoc comparison between individual groups corrected for repeated analysis using Bonferroni

test indicated no significant difference for Tween 20 and Tween 80 below, around and above CMC and Brij 35 around CMC surfactants comparing to IgG2 (10 mg/ml) surfactant free solution. Bonferroni test showed that the T_{m1} mean difference was significant: at the 0.001 level ($P < 0.001$) for Brij 35 below its CMC and Pluronic F-68 at around its CMC, at the 0.01 level ($P < 0.01$) for Pluronic F-68 above its CMC, at the 0.05 level ($P < 0.05$) for Brij 35 above and Pluronic F-68 below their CMC compared to the transition of IgG2 in surfactant free solution (Figure 3.7).

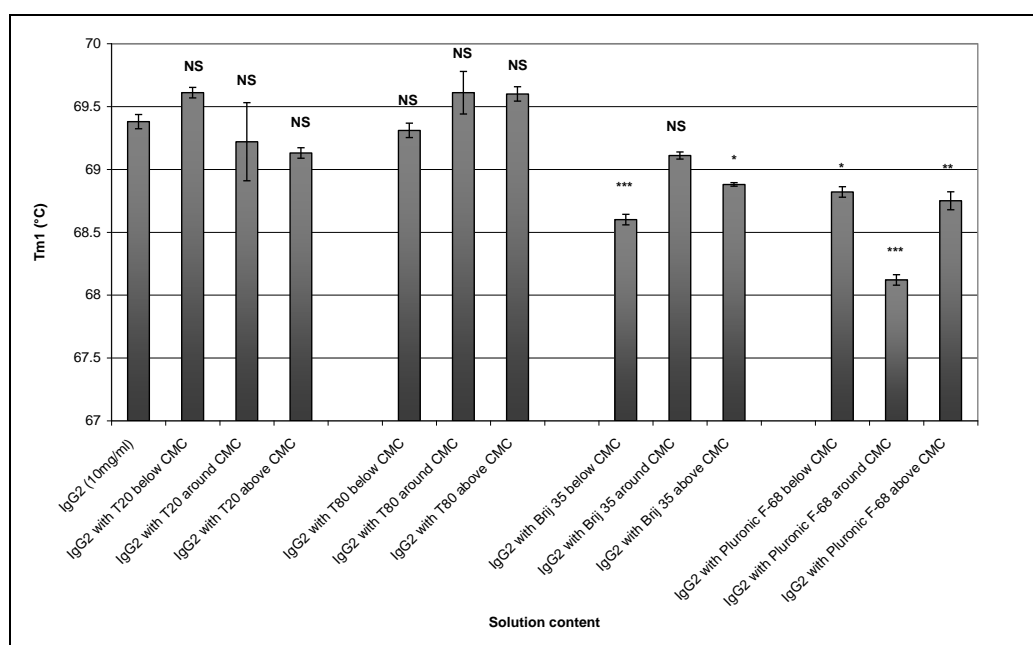


Figure 3.7. The effect of different CMC levels of Tween 20, Tween 80, Brij 35 and Pluronic F-68 surfactants on IgG2 unfolding temperature T_{m1} (°C) measured by HSDSC. Data are expressed as the mean \pm Std. deviation. NS – no significant difference, * - $P < 0.05$, ** - $P < 0.01$, * - $P < 0.001$ significant decrease in unfolding temperature T_{m1} for IgG2 with surfactants compared with IgG2 surfactant free solution.**

One-way ANOVA analysis showed a significant effect of all the surfactants at concentrations below, around and above their CMC levels on the IgG2 unfolding temperature T_m2 . However post-hoc, Bonferroni test showed that there is no significant difference in T_m2 between IgG2 surfactant free and IgG2 with Tween 20 below, around and above its CMC and Tween 80 at around and above its CMC solutions.

The unfolding temperature T_m2 difference was significant at the 0.001 ($P < 0.001$) level for Tween 80 below, Brij 35 below, around and above CMC and Pluronic F-68 around CMC levels compared to IgG2 surfactant free solution. The mean difference for Pluronic F-68 below and above concentrations was significantly different at 0.01 ($P < 0.01$) level compared to IgG2 (10 mg/ml) (Figure 3.8).

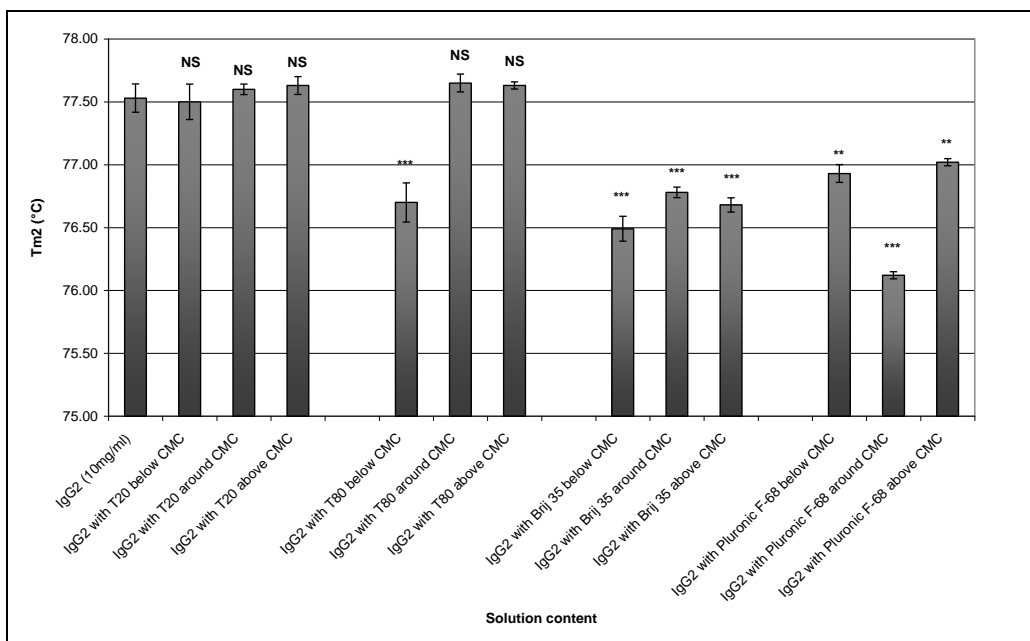


Figure 3.8. The effect of different CMC levels of Tween 20, Tween 80, Brij 35 and Pluronic F-68 surfactants on IgG2 unfolding temperature T_{m2} (°C) measured by HSDSC. Data are expressed as the mean \pm Std. deviation. NS – no significant difference, ** - $P < 0.01$, * - $P < 0.001$ significant decrease in T_{m2} for IgG2 with surfactants compared with IgG2 surfactant free solution.**

Figure 3.9 illustrates the effect on T_{m1} of different CMC levels of surfactants.

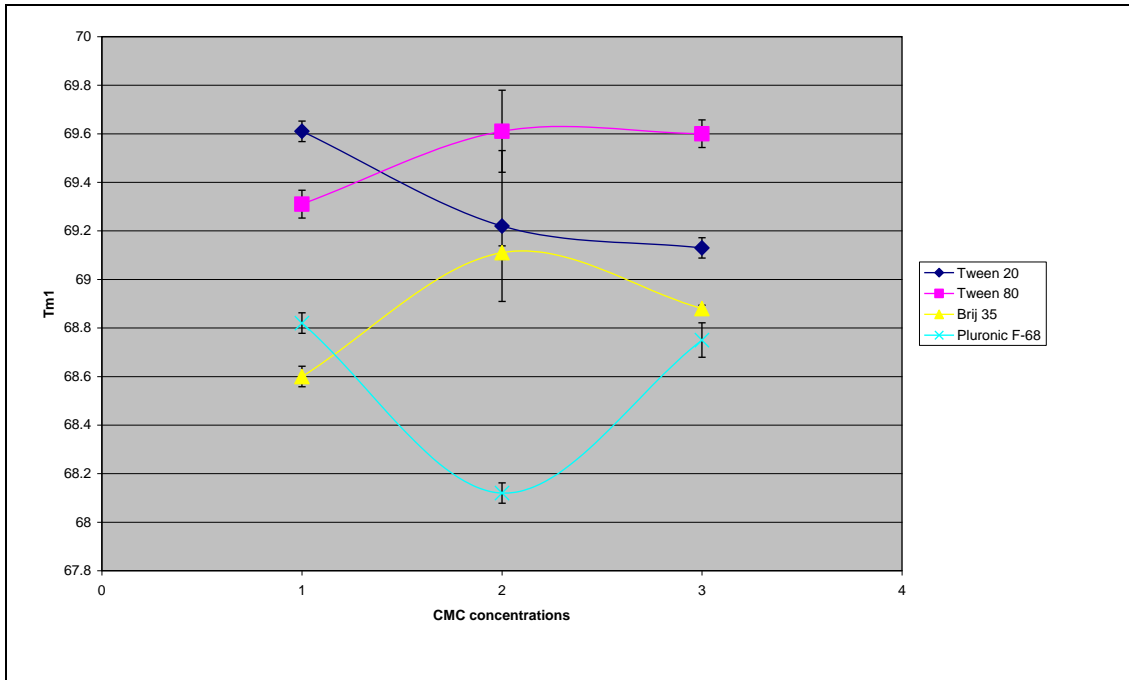


Figure 3.9. The effect of different surfactant concentration levels on T_{m1} . (1 – below CMC; 2 – around CMC; 3 – above CMC)

By introducing a trend line into the data it is possible to see that there are some differences between the behaviour of the surfactants over the range of concentrations. It is noticeable that at the lowest concentration level, Tween 20 and Tween 80 systems have the highest T_{m1} comparing with Brij 35 and Pluronic F-68 systems. However, with increase in surfactant concentration, T_{m1} values increased for Tween 80 systems, and decreased with Tween 20. For the Brij 35 system T_{m1} is maximal at around its CMC, whereas Pluronic F-68 has the lowest T_{m1} at around its CMC.

Similar results were obtained for T_{m2} with Brij 35 and Pluronic F-68 systems (Figure 3.10).

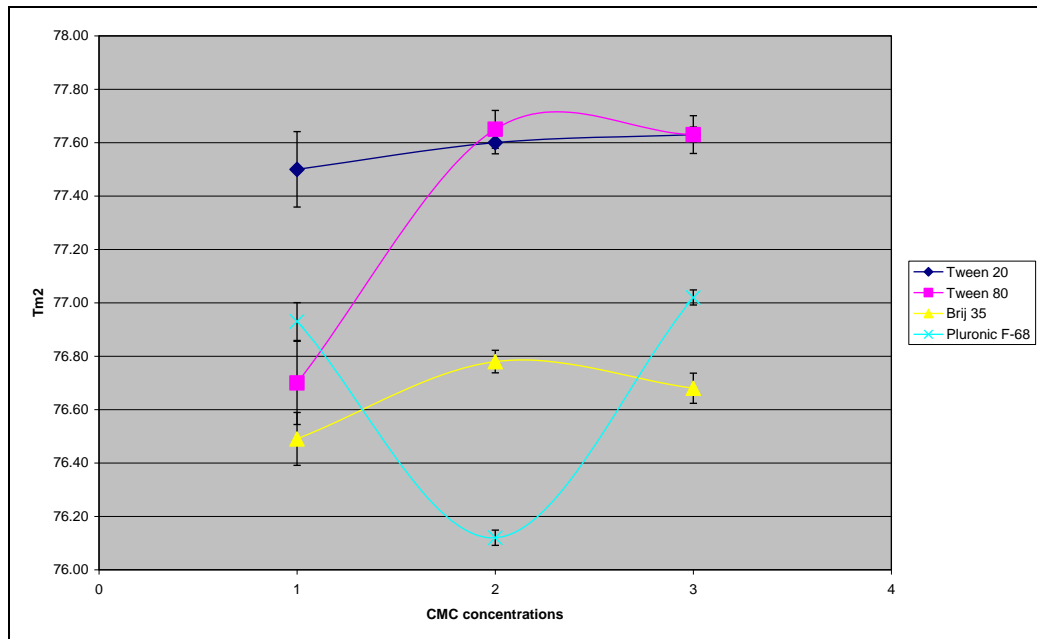


Figure 3.10. The effect of different CMC concentration levels on T_{m2} . (1 – below CMC; 2 – around CMC; 3 – above CMC)

T_{m2} values increase with increase in concentration of Tween 20 and Tween 80.

No notable changes of T_m are observed between different concentrations of surfactants. The present results indicate a very weak surfactant-immunoglobulin interaction, compared to the much stronger interactions described for bovine serum albumin-Tween 20, Tween 80, Brij 35 and Pluronic F-68 systems (Table 3.1, Figure 3.1).

One – way ANOVA analysis, post-hoc analysis showed significant differences for both T_{m1} and T_{m2} between BSA with Tween 20, Tween 80, Brij 35 and Pluronic F-68 surfactants groups at below, around and above CMC concentrations. The mean difference was significant at the 0.05 ($P < 0.05$) level.

A comparison of T_{m1} and T_{m2} measured by HSDSC for fresh IgG2 (10 mg/ml) with Tween 20, Tween 80, Brij 35 and Pluronic F-68 surfactants at below, around and above CMC levels are summarised in Figure 3.11.

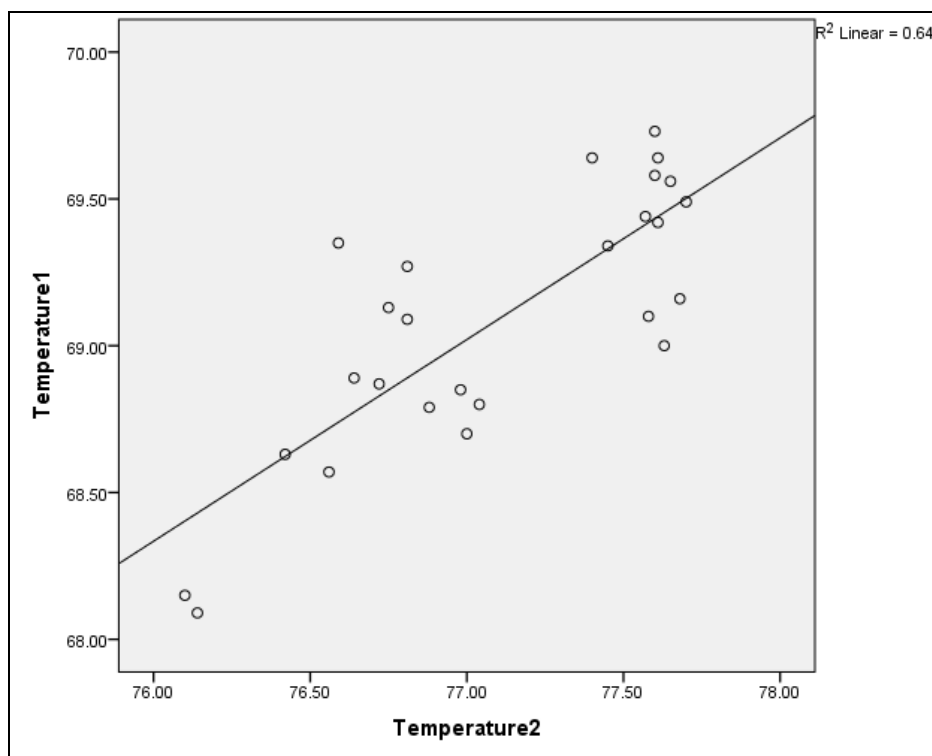


Figure 3.11. Scatter plot of unfolding temperatures T_{m1} and T_{m2} measured by HSDSC for IgG2-surfactant systems.

Statistical analysis, using Pearson correlation was used to describe the relationship between IgG2 unfolding temperatures T_{m1} and T_{m2} measured by HSDSC. The Pearson Correlation significance value was found to be 0.000, which means that correlation between variables is significant at 0.01 level ($P < 0.01$). The finding is indicative that for this protein both variables T_{m1} and T_{m2} rise and fall sympathetically and denotes a near-perfect linear relationship (Figure 3.11).

3.5 General Discussion

HSDSC thermal unfolding experiments showed that for BSA (10 mg/ml) in PBS a single unfolding peak is observed: $T_m=66.91 \pm 0.085^\circ\text{C}$. The presence of Tween 20, Tween 80, Brij 35 and Pluronic F-68 surfactants induced T_m -shifts to lower temperatures for bovine serum albumin. The interaction of Tween 80 at above its CMC and Brij 35 at around and above its CMC with BSA was less pronounced compared with other surfactants.

The thermal unfolding curve of the immunoglobulin IgG2 was represented by and best fitted by two overlapping endotherms: $T_{m1}=69.38 \pm 0.057^\circ\text{C}$ and $T_{m2}=77.53 \pm 0.113^\circ\text{C}$. The exact position of the unfolding temperatures is depending on the environmental conditions and immunoglobulin subtype (Weichel et al., 2008; Garidel et al., 2008).

The results showed that the presence of any surfactant at different concentrations with immunoglobulin IgG2 was negligible. No notable changes of the T_{m1} and T_{m2} were observed.

Thermal unfolding experiments indicated a very weak surfactant-immunoglobulin IgG2 interaction, compared to much stronger interactions for the bovine serum albumin-surfactant systems. These results are consistent with published results (Garidel et al., 2009), who found out that the binding of surfactants on IgG2 is negligible.

Chapter 4

Effect of different concentrations of Tween 20, Tween 80, Brij 35 and PLuronic F-68 surfactants on size stability by Dynamic Light Scattering

4.1 Introduction

In the biopharmaceutical industry, protein aggregation is encountered routinely during purification, refolding, sterilization, shipping, and storage processes because of the presence of chemical and physical stresses (Bermudez et al., 2004). The presence of aggregates in protein and antibody formulation influences a decrease in the efficiency of the drug and causes potential problems in its intravenous administration (Bermudez et al., 2004). Even if the protein preparation may be aggregate-free after a last polishing step has been completed, aggregates can form during storage (Bermudez et al., 2004).

Proteins are being utilized directly in the pharmaceutical industry as active agents in medicines. The size of the molecule and its association state can be used as a quality control measure. Also during the production of nanoparticles, the particle size can be used as a quality attribute in a quality control process (Kaszuba et al., 2007). It is obvious that if we want to provide accurate information on protein aggregation the use of light scattering technique is needed (Bermudez et al., 2004). In part, this is because there are only a few techniques available for the direct measurement of small molecules and particles in solution such as Analytical Ultracentrifugation (AUC), Field Flow Fractionation (FFF), Multiangle Light Scattering (MALS), Size Exclusion Chromatography (SEC) and Dynamic Light Scattering (DLS). Dynamic light scattering (DLS) is a technique for characterising the size of particles and particle size distribution, which utilizes the illumination of a

suspension of particles or molecules undergoing Brownian motion by a laser beam (Kaszuba, 2007).

DLS has been widely used to study various types of proteins (Mahler et al., 2005; Ye 2006; Demeule et al., 2007; Qian et al., 1997; Georgalis et al., 1993; Onuma et al., 2003; Onuma et al., 2005; Plakoutsi et al., 2005, Liu et al., 2009). DLS is mainly used to determine particle size by measuring the diffusion coefficient of the particles in a solution and then using the diffusion coefficient to determine the size. As DLS is used to determine particle size, it has become very useful to investigate protein aggregation (Bermudez et al., 2004). That is, in DLS we can achieve a mathematical separation of large from small components because they produce scattering fluctuations on different time scales. Also DLS is useful for comparing one formulation sample to another formulation approach (Arakawa et al., 2007).

The aim of this chapter is to explore that part of the sub-visible particle size range which is measurable by dynamic light scattering. The test systems used are bovine serum albumin (BSA) and immunoglobulin IgG2 treated with different levels of Tween 20, Tween 80, Brij 35, Pluronic F-68 surfactant systems under heat stress and storage conditions.

4.2 Objective

To study how particle size distribution measured by Dynamic light scattering is affected by the concentration of Tween 20, Tween 80, Brij 35 and Pluronic F-68 surfactants, and in relation to CMC.

To investigate how heat treatment stress affects the particle size distribution for different surfactants and at different concentration.

To investigate how particle size distribution changes under storage.

4.3 Experimental

Dynamic light scattering (DLS) measurements were performed at BSA and IgG2 concentrations of 10 mg/ml with below, around and above CMC levels of Tween 20, Tween 80, Brij 35 and Pluronic F-68 surfactants (See Table 2.2 Chapter 2 for details).

Measurements of all samples were made on a Malvern Zetasizer Nano series (Malvern Instruments Ltd., UK) as described in Section 2.2.4 Chapter 2.

4.4 Results and Discussion

4.4.1 Particle size distribution measurements for freshly prepared BSA-surfactants systems

DLS intensity particle size distribution histograms of freshly prepared samples of BSA (10 mg/ml) in the absence and presence of Tween 20, Tween 80, Brij 35 and Pluronic F-68 surfactants at different CMC levels are shown in figures 2 – 6. The plots have been configured using the software dialogue to display a size distribution by intensity histogram, with a

logarithmic x-axis and a linear y-axis. The x-axis is the absolute size of the scatter obtained by a multimodal fitting of the time correlation function. The y-axis is the intensity average of the scattered light. The distribution histograms show the percentage of the scattering intensity that arises from species at each size (d.nm).

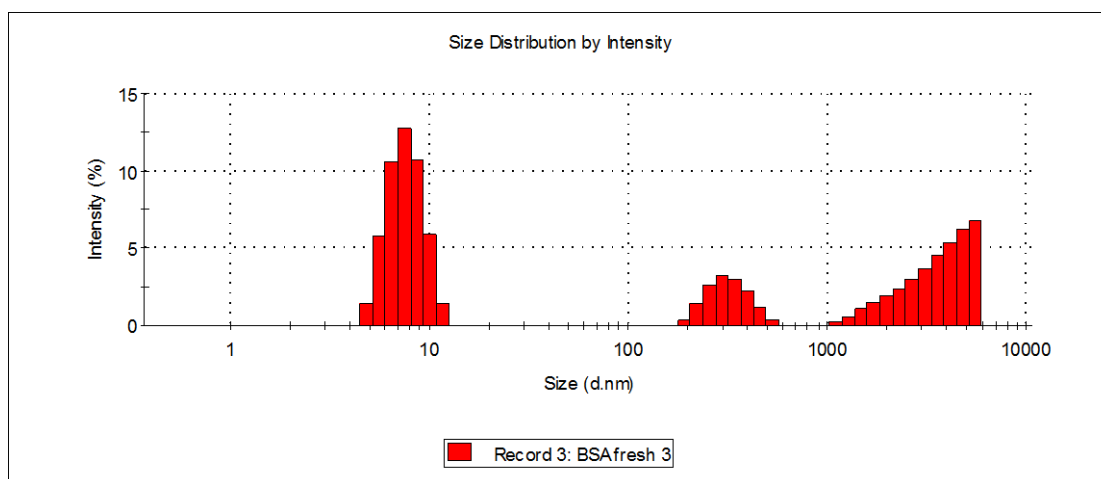
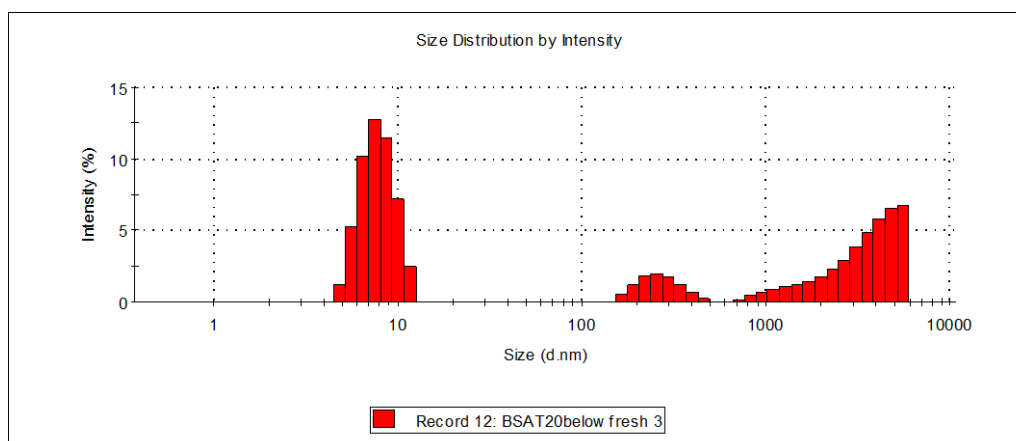


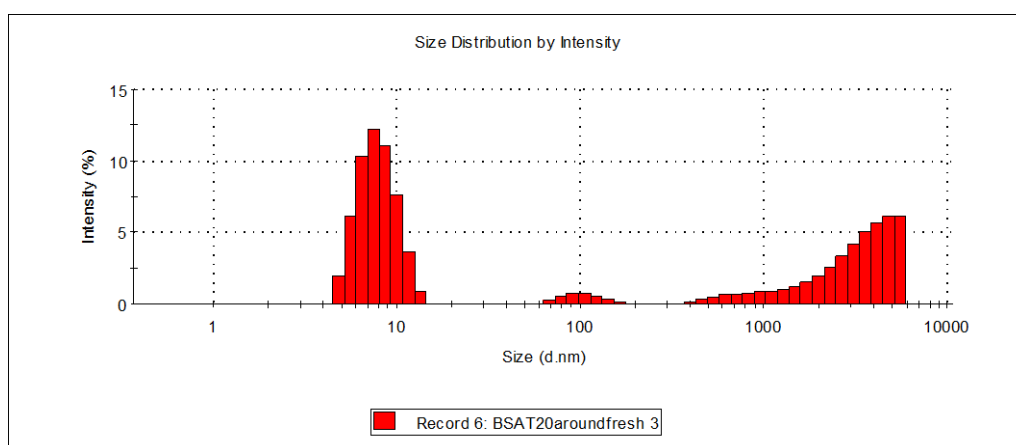
Figure 4.1. Particle size distribution by intensity obtained for freshly prepared BSA (10 mg/ml). Average n=3.

From figure 4.1 the particle size by intensity obtained for freshly prepared BSA (10 mg/ml) samples gave trimodal distribution with the main peak at 7.7 nm (48.5 % intensity), a second peak at 3755 nm (37.1 % intensity) and a third peak at 322.7 nm diameter (14.4 % intensity). Our findings are consistent with a main BSA protein peak of diameter at 7.8 nm as reported previously by Yu et al (2011).

(A)



(B)



(C)

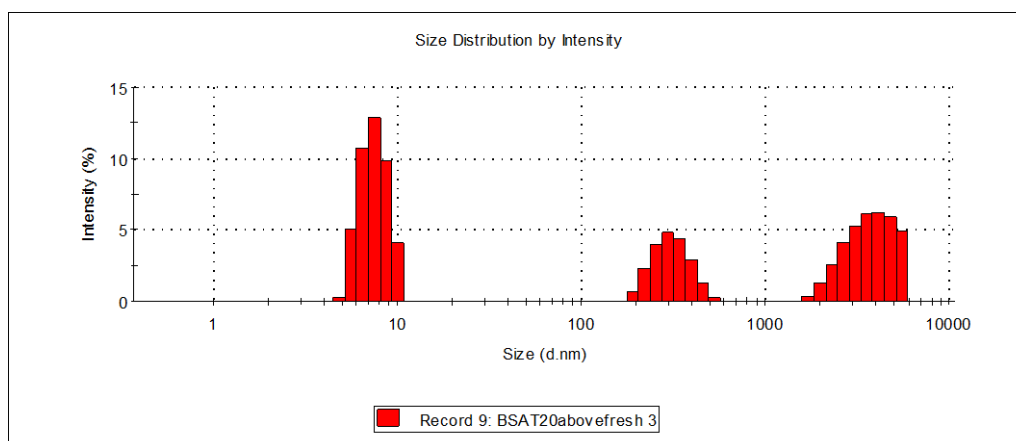


Figure 4.2. Particle size distribution by intensity obtained for BSA (10 mg/ml) fresh samples with: (A) Tween 20 below CMC; (B) Tween 20 around CMC; (C) Tween 20 above CMC.

From Figure 4.2 the particle size distributions for BSA (10 mg/ml) in the presence of Tween 20 surfactant at all CMC concentrations produced three peaks with the main peak mode consistently around 8 nm. When Tween 20 concentration was above CMC, a greater percentage of larger particles formed than Tween 20 below and around CMC and BSA alone (Figure 4.2 (C)).

Running DLS analysis on the Tween 20 surfactant alone in the presence of with PBS buffer, with no protein present, for Tween 20 below and around CMC levels no peak at around 10 nm was detected (See Appendix 25-27). At Tween 20 concentration around CMC, DLS results produced a 100 % intensity peak at an average of 499 nm diameter. The corresponding data for the Tween 20 concentration above CMC showed bimodal peaks with 59.5 % intensity peak at diameter of 7.0 nm, and 40.5 % intensity peak at 86.0 nm diameter. The control experiment suggests that some micellar interference at this concentration needs to be taken into account. Figure 4.3 schematically represents these findings that at low concentrations, surfactant molecules are unassociated monomers. As the concentration of surfactant is increased, the molecules cause self-aggregation to occur resulting in the formation of monolayers or micelles (Figure 4.3).

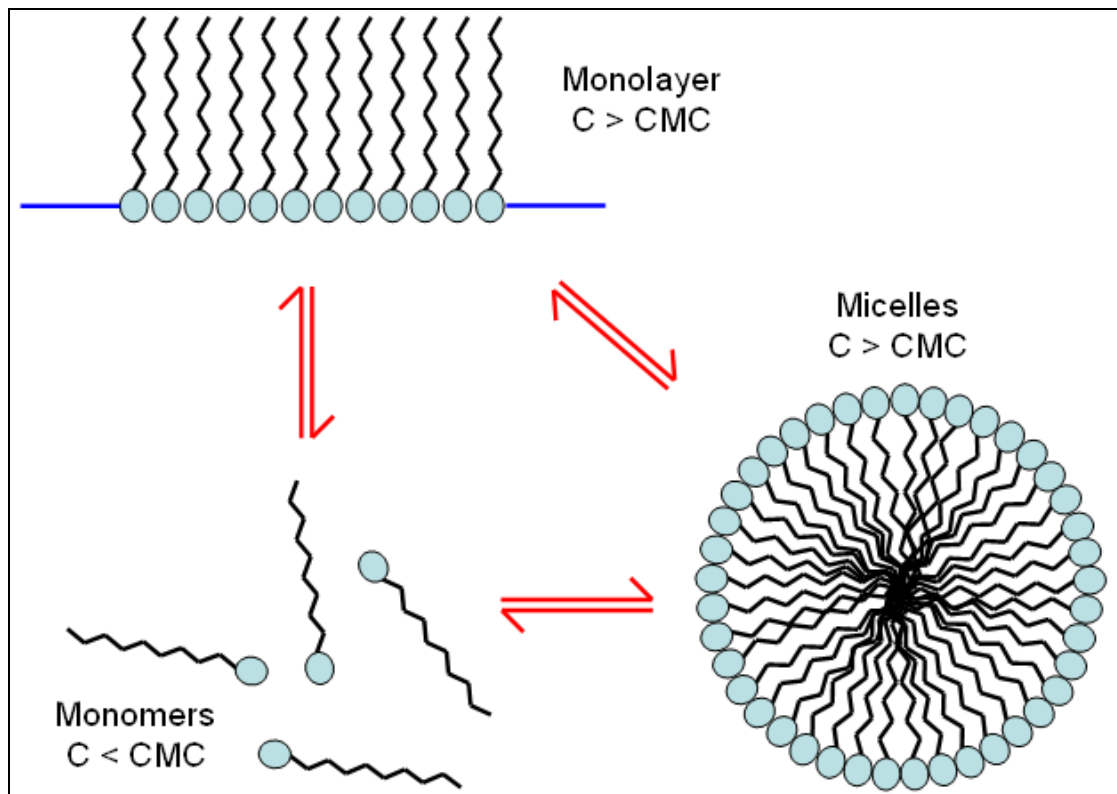
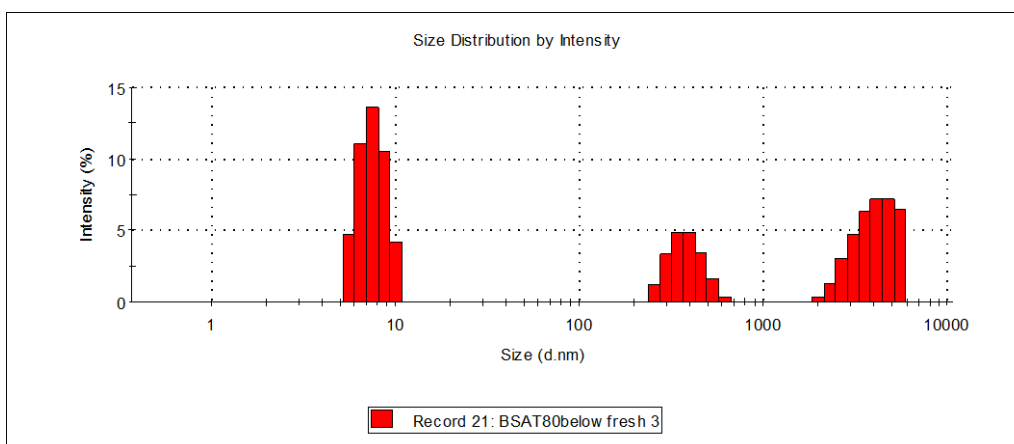


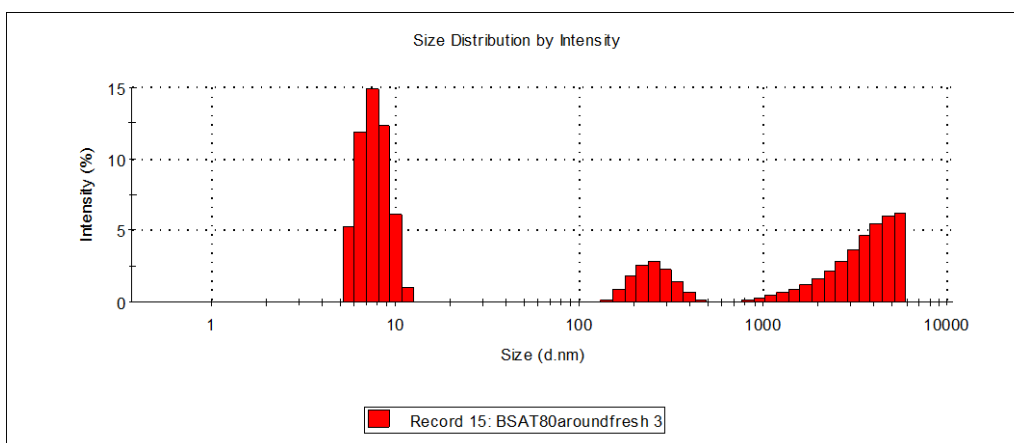
Figure 4.3. The surfactant can exist as different phases depending upon the concentration of the sample (Malvern Instruments Ltd., 2006).

BSA (10 mg/ml) with Tween 80 surfactant at below, around and above CMC, gave very similar trimodal distribution with the main peak consistently around 8 nm diameter (Figure 4.4).

(A)



(B)



(C)

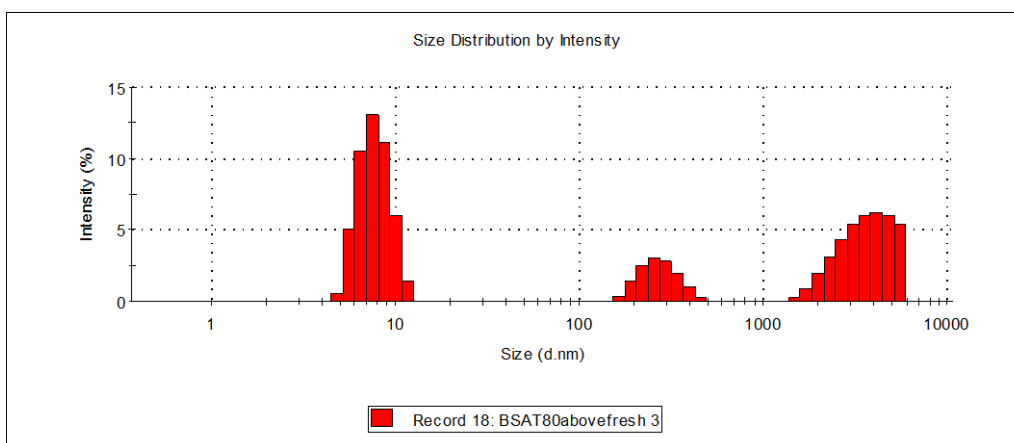
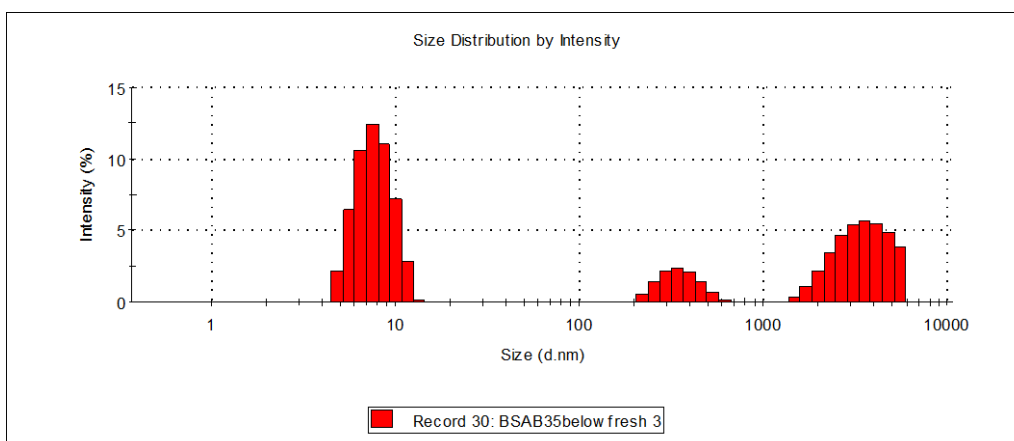


Figure 4.4. Particle size distribution by intensity obtained for BSA (10 mg/ml) with: (A) Tween 80 below CMC; (B) Tween 80 around CMC; (C) Tween 80 above CMC.

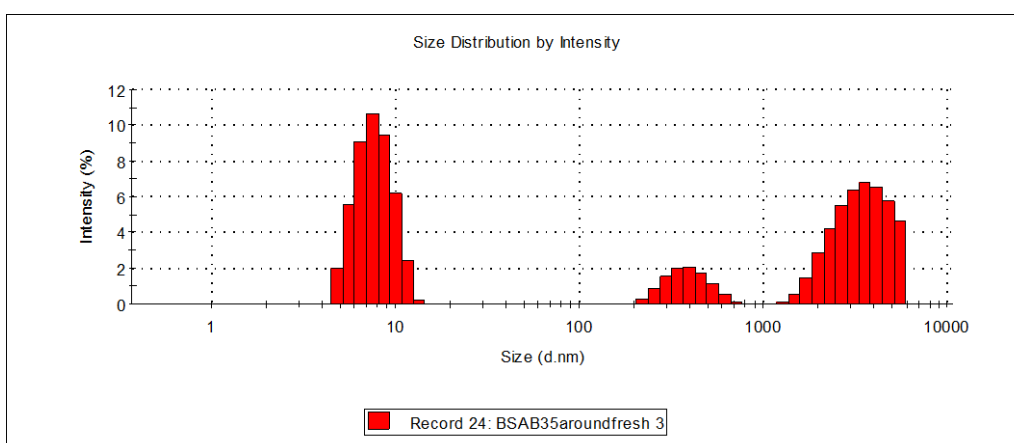
The second largest peak by intensity for BSA (10 mg/ml) with Tween 80 at all concentrations had a consistent diameter of around 4000 nm. BSA in the presence of Tween 80 above its CMC produced by DLS a main peak at 7.8 nm, the highest compared to BSA with added Tween 80 below its CMC (7.6 nm diameter) and BSA with Tween 80 at around its CMC (7.8 nm diameter). The finding may result from the contribution of surfactant micelles at the higher Tween 80 concentration, where the diameter of the Tween 80 micelle was determined to be 10.7 nm from control experiments (See Appendix 28-30) (Malvern Instruments Ltd., 2006).

Similar findings were obtained for BSA (10 mg/ml) with Brij 35 at different concentrations (Figure 4.5). The main DLS peak diameter for BSA obtained from surfactant concentrations below, around and above CMC was around 8 nm. Brij 35 above CMC had the highest diameter of 8.2 nm at the main peak intensity of 82 % comparing to below and around CMC concentrations. Once again surfactant micellar contribution at high Brij 35 levels may have contributed. Our evidence stems from that DLS analysis of Brij 35 above its CMC with PBS buffer and no protein produced a the main intensity peak at 8.8 nm diameter (88.9 % intensity), where Brij concentrations below and around its CMC did not produce any intensity peak around 10 nm diameter (See Appendix 31-33). The literature value for a Brij 35 micelle is 8 nm diameter (Malvern Instruments Ltd., 2006).

(A)



(B)



(C)

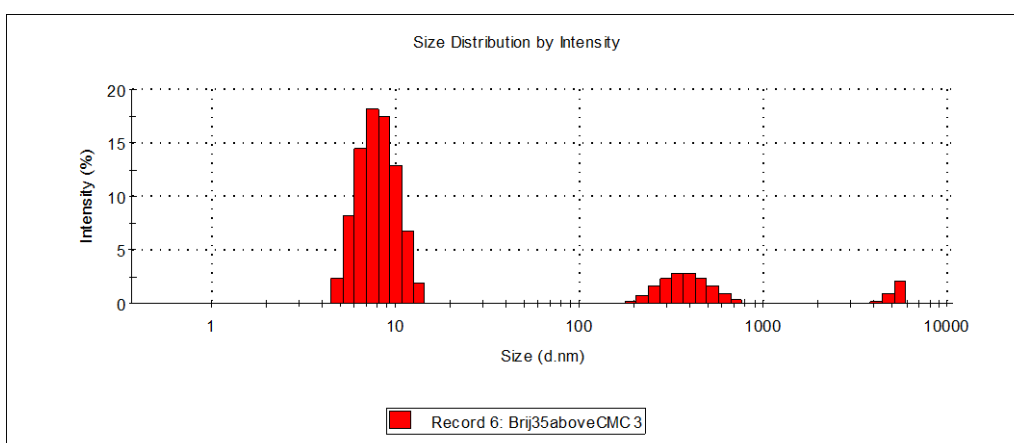
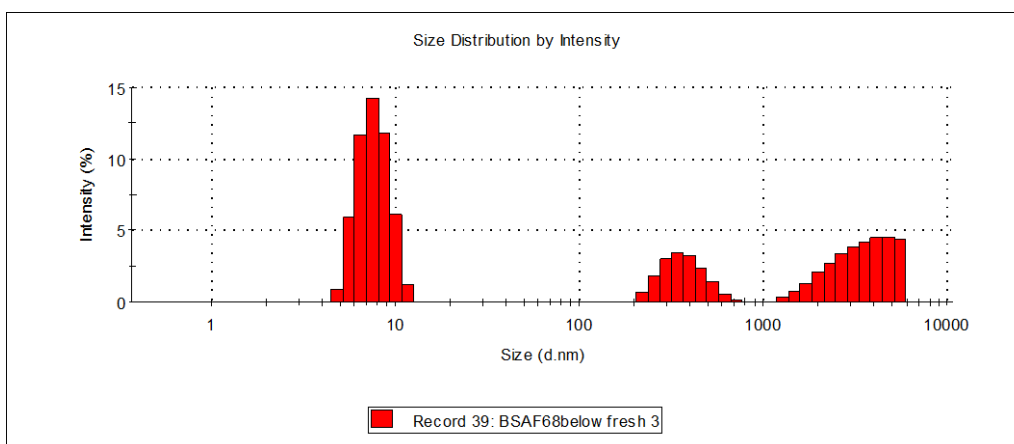


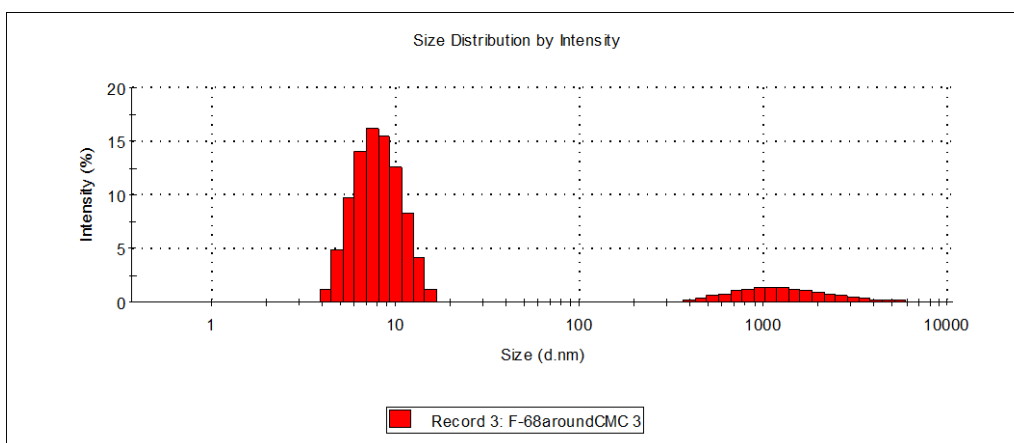
Figure 4.5. Particle size distribution by intensity obtained for BSA (10 mg/ml) with: (A) Brij 35 below CMC; (B) Brij 35 around CMC; (C) Brij 35 above CMC.

The DLS particle size distributions by intensity obtained for the analysis of BSA (10 mg/ml) in the presence of Pluronic F-68 are shown in Figure 4.6. Concentrations of Pluronic at below and above its CMC level produced a main peak at around 8 nm diameter. Pluronic F-68 at around and above CMC concentrations produced a main peak diameter and intensity that was higher than that obtained for Pluronic F-68 at below CMC levels (Figure 4.6).

(A)



(B)



(C)

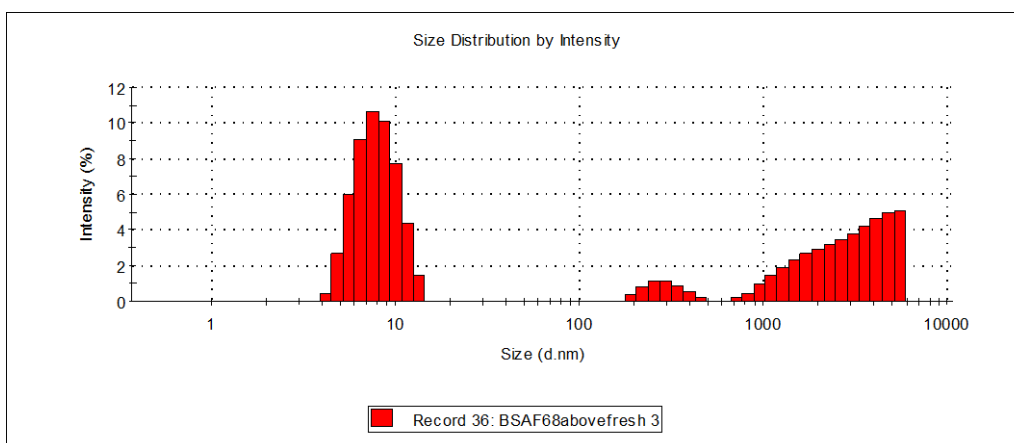


Figure 4.6. Particle size distribution by intensity obtained for BSA (10 mg/ml) with: (A) Pluronic F-68 below CMC; (B) Pluronic F-68 around CMC; (C) Pluronic F-68 above CMC.

Running F-68 at all concentrations just with PBS buffer no peak around 10 nm was detected (See Appendix 34-36). At below, around and above concentrations DLS results showed just one peak with 100 % intensity and 407.5 nm for below CMC, 286.8 nm for around CMC and 256.1 nm for above CMC concentrations. This finding is consistent with the increase in diameter of the second and third peaks shown in Figure 4.6.

The particle size diameter (nm) of the main peak with greatest intensity for fresh BSA (10 mg/ml) with below, around and above CMC levels of Tween 20, Tween 80, Brij 35 and Pluronic F-68 surfactants are summarised in Table 4.1 and Figure 4.7.

Table 4.1. Particle size diameter (nm) of the peak with greatest intensity (Peak 1) for fresh BSA (10 mg/ml) with below, around and above CMC levels of Tween 20, Tween 80, Brij 35 and Pluronic F-68 surfactants.

FRESH SAMPLES		PEAK POSITION WITH GREATEST INTENSITY DIAMETER (nm)
BSA (10mg/ml)		7.689
Tween 20	below CMC	7.895
	around CMC	8.004
	above CMC	7.549
Tween 80	below CMC	7.597
	around CMC	7.763
	above CMC	7.791
Brij 35	below CMC	7.823
	around CMC	7.811
	above CMC	8.224
Pluronic F-68	below CMC	7.700
	around CMC	8.322
	above CMC	8.089

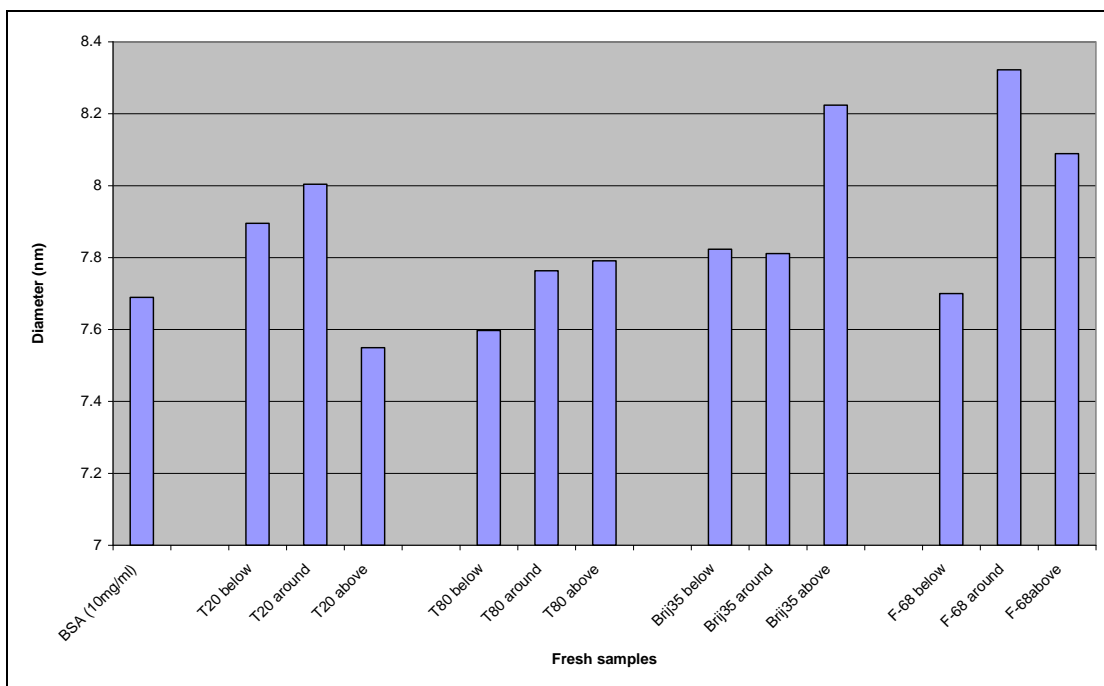


Figure 4.7. Particle size diameter (nm) of the peak with greatest intensity (Peak 1) for fresh BSA (10 mg/ml) with below, around and above CMC levels of Tween 20, Tween 80, Brij 35 and Pluronic F-68 surfactants.

Analysing particle size diameter of the main peak for fresh samples, it can be seen that the highest intensity peak diameter (nm) increased for concentration of Tween 20 below and around CMC and slightly decreased by 0.14 nm for Tween 20 above CMC compared to BSA alone (10 mg/ml). Tween 80 below CMC – main peak diameter was slightly smaller and Tween 80 around and above slightly bigger than that obtained for surfactant free BSA (10 mg/ml). The greatest increase in diameter (nm) was detected for samples with Brij 35 above its CMC and the sample containing Pluronic F-68 at around and above its CMC (Figure 4.7). It is likely that the high concentrations of Brij 35 and Pluronic F-68 surfactants produce larger micelle size of entities that contribute to this result.

Statistical analysis – t-test (See Chapter 2, Section 2.2.7) showed that the difference between fresh surfactant - free BSA (10 mg/ml) and Tween 20, Tween 80, Brij 35 and Pluronic F-68 surfactants at below, around and above CMC levels, was statistically significant at the 95 % level ($P < 0.05$).

Figure 4.8 illustrates the comparison of the diameter in nm of the main (highest intensity) peak at below, around and above CMC levels for Tween 20, Tween 80, Brij 35 and Pluronic F-68 surfactants.

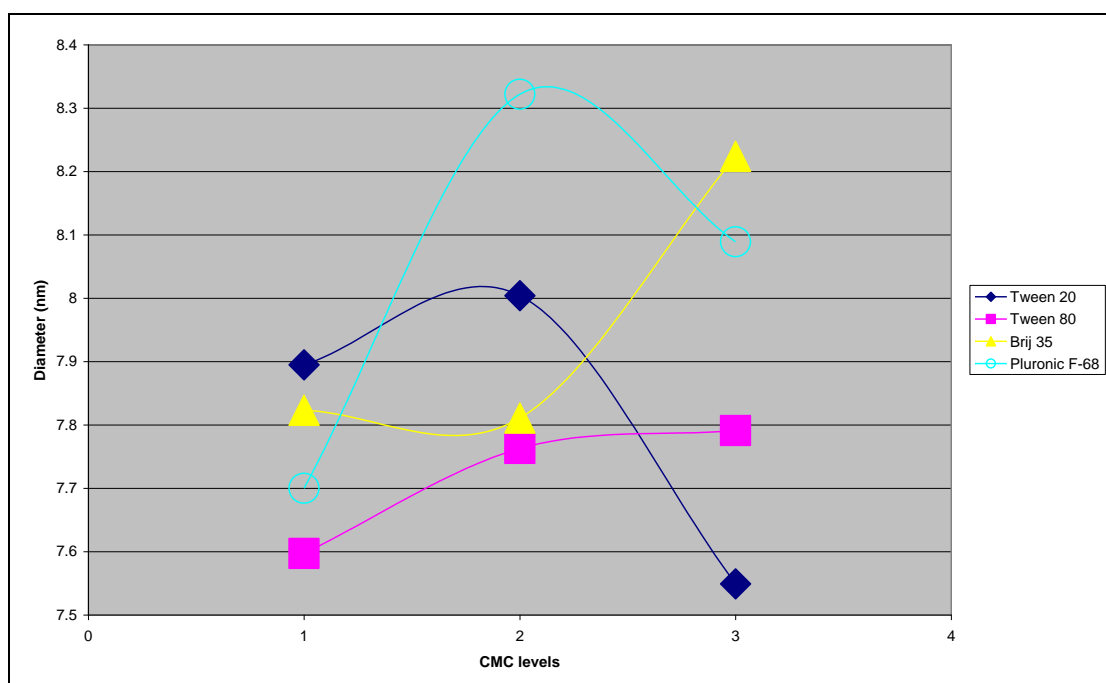


Figure 4.8. A plot of the highest intensity peak diameter (nm) obtained at below (1), around (2) and above (3) CMC levels for Tween 20, Tween 80, Brij 35 and Pluronic F-68 surfactants.

From Figure 4.8 it can be clearly seen that all four surfactants at below, around and above CMC levels differ in the particle size diameter (nm) for the highest intensity peak.

There is a decrease in the main peak measured size diameter as the Tween 20 surfactant concentration increases. Tween 80 shows gradual increase in

diameter (nm) with concentration. Similar results are observed for Brij 35 and Pluronic F-68. It can be seen the high concentration of Tween 20 produced the lowest main peak particle size diameter (nm) compared to other surfactants.

4.4.2 Particle size distribution measurements for heat stressed BSA-surfactants systems

Figure 4.9 shows data for BSA (10 mg/ml) after heat stress as described in Chapter 2 section 2.2.1. The scattering intensity for the main peak of the stressed BSA sample was almost double than that of the starting material. The main intensity peak reached 76.9 % intensity compared to fresh BSA main peak intensity at 48.5 % (Figure 4.1). As shown by the size distribution, the difference arises from an increase in scattering for main intensity peak. For this heat stressed BSA (10 mg/ml) sample the main peak was 26.9 nm diameter compared to a fresh BSA sample (10 mg/ml) of main peak diameter 7.7 nm. An increase in hydrodynamic size of heated BSA samples was previously reported by Kelly et al. (1993), Adel et al. (2008).

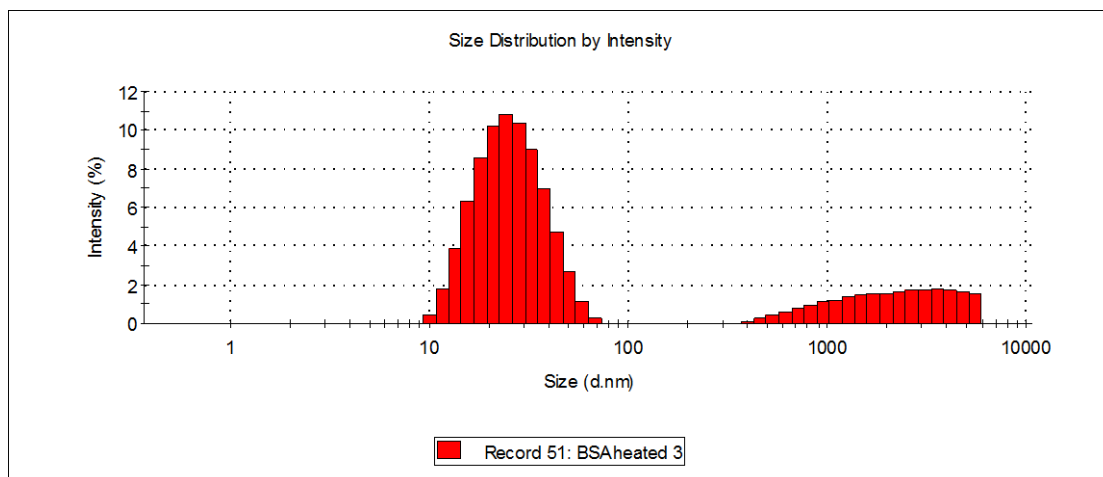
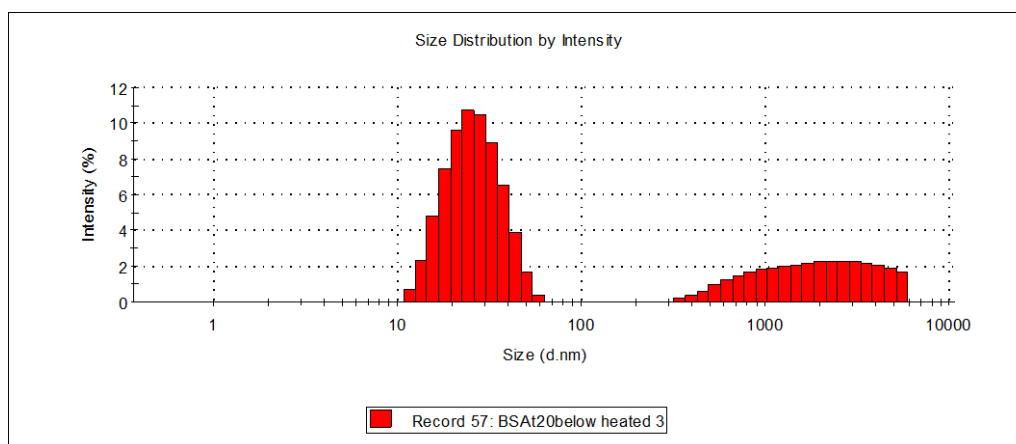


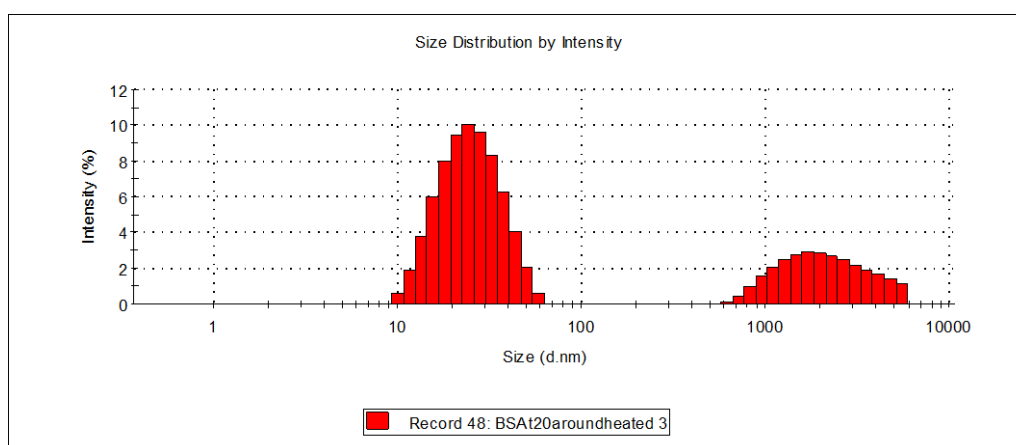
Figure 4.9. Particle size distribution by intensity obtained for heated (66°C) BSA (10 mg/ml).

Heat treatment of BSA (10 mg/ml) in the presence of Tween 20, Tween 80, Brij 35 and Pluronic F-68 surfactants led to an increase in the populations of larger particles compared to freshly prepared samples (Figures 4.10 – 4.13).

(A)



(B)



(C)

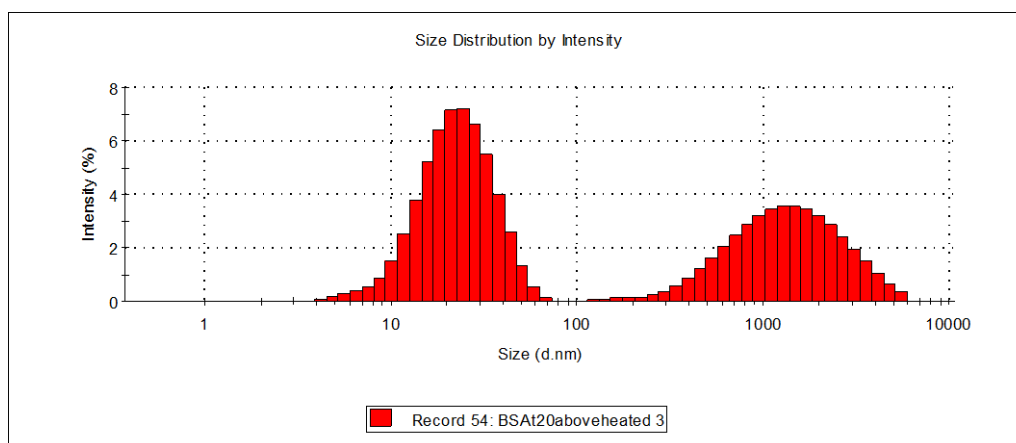
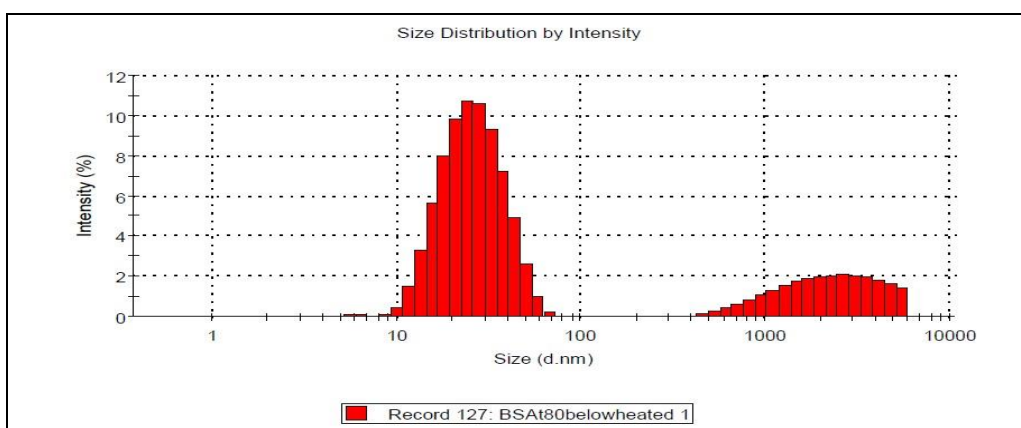


Figure 4.10. Particle size distribution by intensity obtained for heated samples for BSA (10 mg/ml) with: (A) Tween 20 below CMC; (B) Tween 20 around CMC; (C) Tween 20 above CMC.

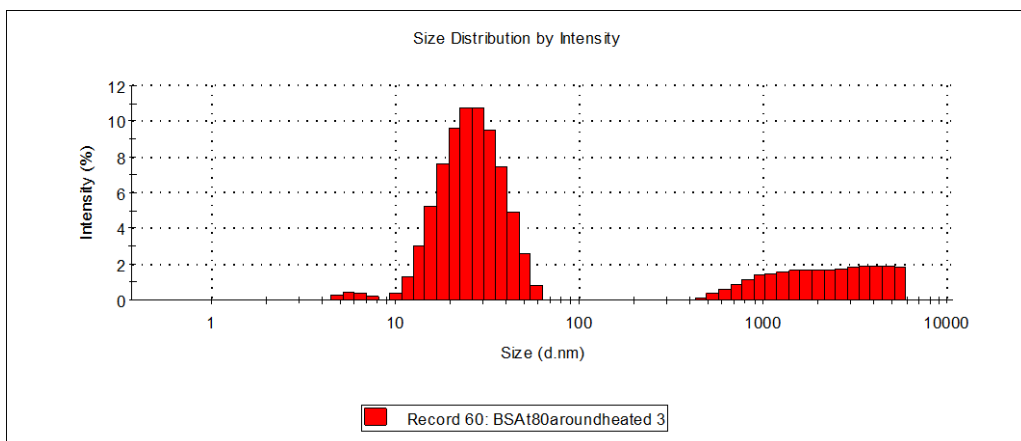
The main peak diameter increased to around 27 nm for heated BSA in the presence of Tween 20 at concentrations. Further, heated BSA with Tween 20 present showed bimodal size distributions, whereas unheated samples had produced a trimodal distribution (Figure 4.2). Moreover, there is a notable increase in intensity of the most intense peak (Figure 4.10), which has shifted to the right indicating an increase in particle size, probably due to aggregation of the heat stressed samples.

Similar results were observed for heated BSA with Tween 80 at concentrations below, around and above its CMC (Figure 4.11).

(A)



(B)



(C)

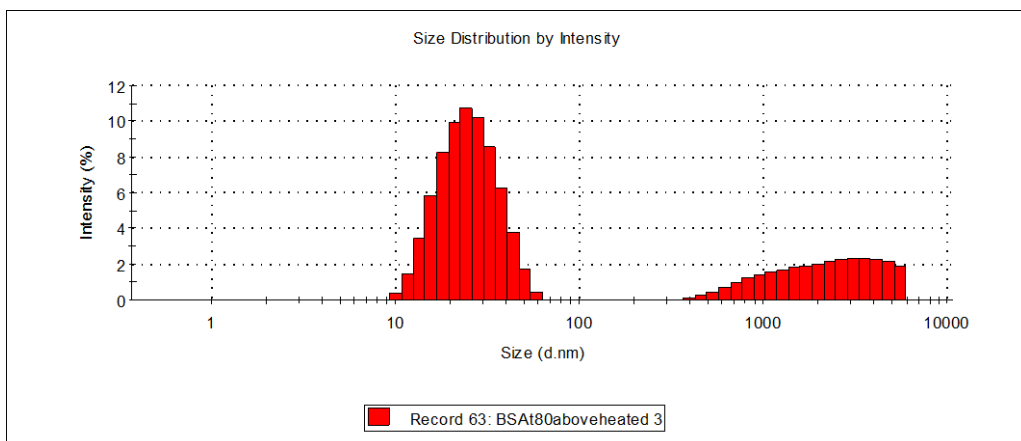
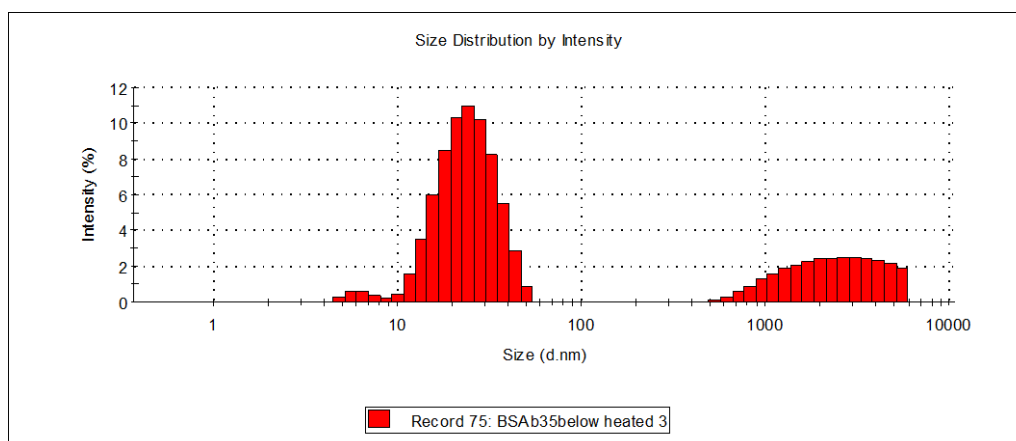


Figure 4.11. Particle size distribution by intensity obtained for heated samples for BSA (10 mg/ml) with: (A) Tween 80 below CMC; (B) Tween 80 around CMC; (C) Tween 80 above CMC.

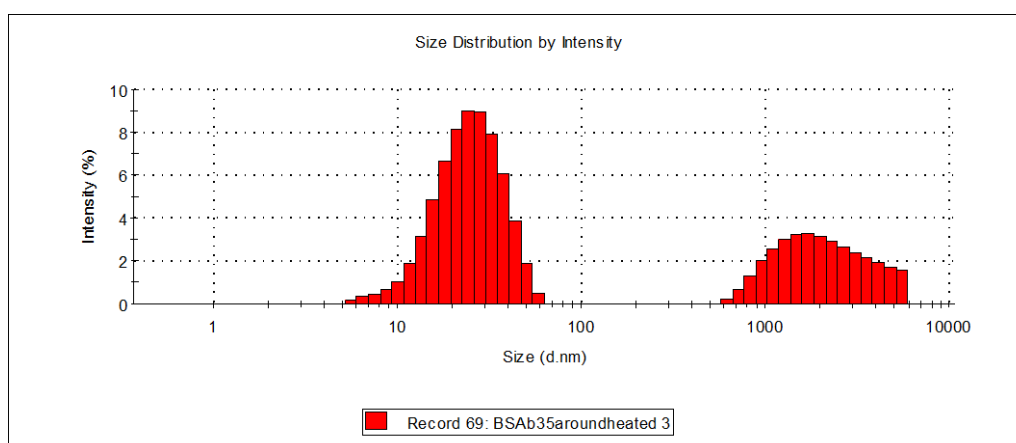
Again, the main peak diameter has increased to around 27 nm compared to unheated BSA with Tween 80 samples (Figure 4.11). Once again, a bimodal size distribution by intensity was detected by DLS.

Figure 4.12 shows particle size distribution by intensity for heated BSA (10 mg/ml) with Brij 35 present at concentrations below, around and above its CMC.

(A)



(B)



(C)

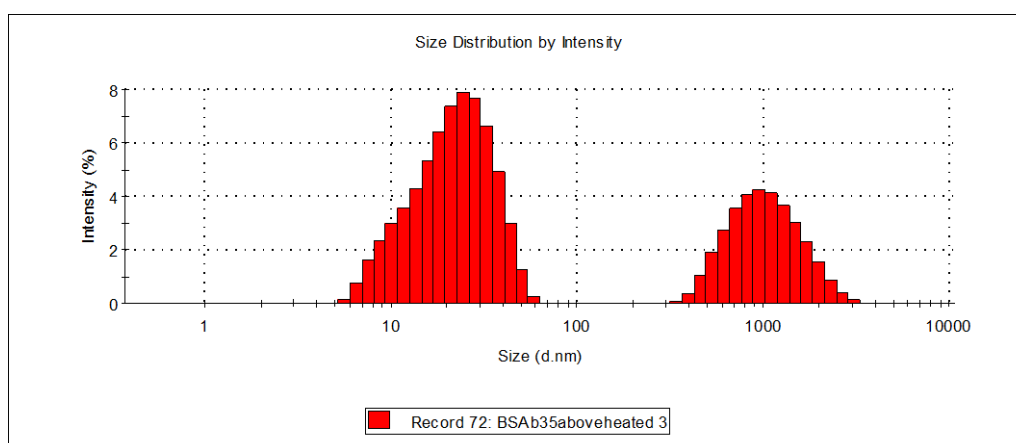
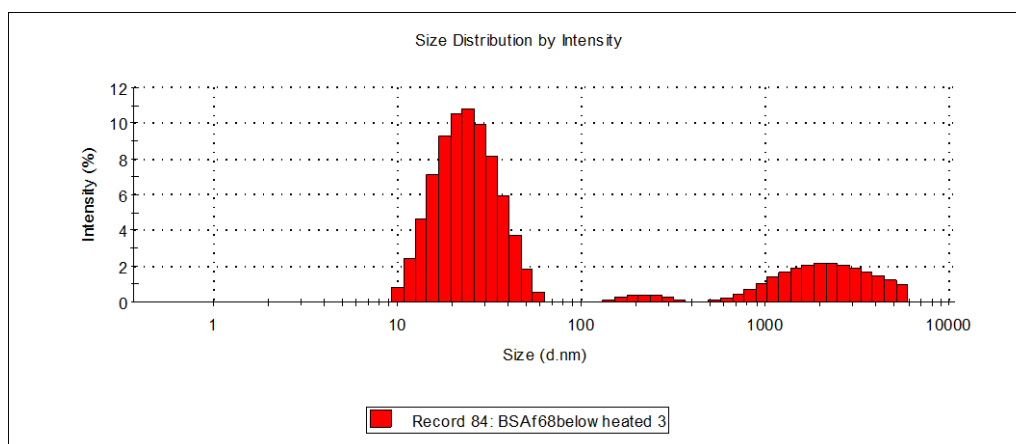


Figure 4.12. Particle size distribution by intensity obtained for heated samples (66°C) for BSA (10 mg/ml) with: (A) Brij 35 below CMC; (B) Brij 35 around CMC; (C) Brij 35 above CMC.

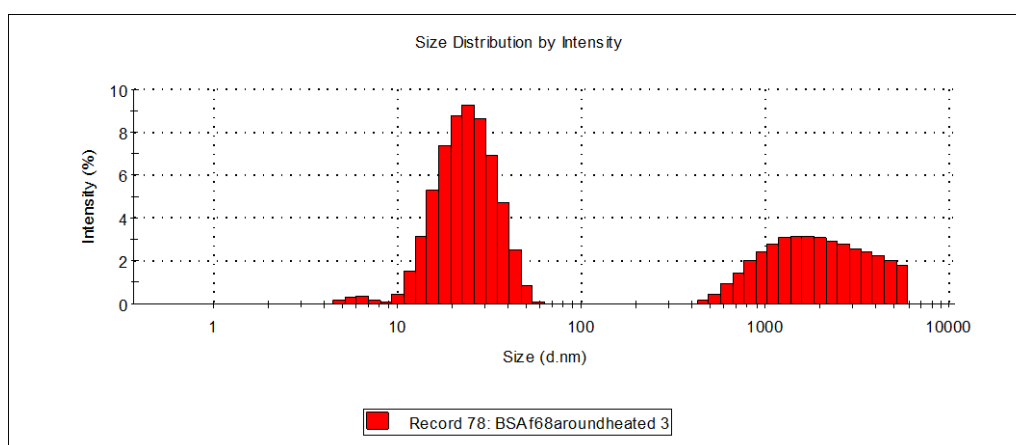
From Figure 4.12 there is a notable increase in the intensity of the most intense peak compared to unheated samples of BSA with Brij 35 present. Also the main peak has shifted to the right indicating an increase in particle size diameter to around 25 nm compared to around 8 nm diameter observed for unheated BSA with Brij 35 present (Figure 4.5).

In Figure 4.13 DLS measurements obtained for heated BSA (10 mg/ml) with Pluronic F-68 present at concentrations below, around and above its CMC are presented.

(A)



(B)



(C)

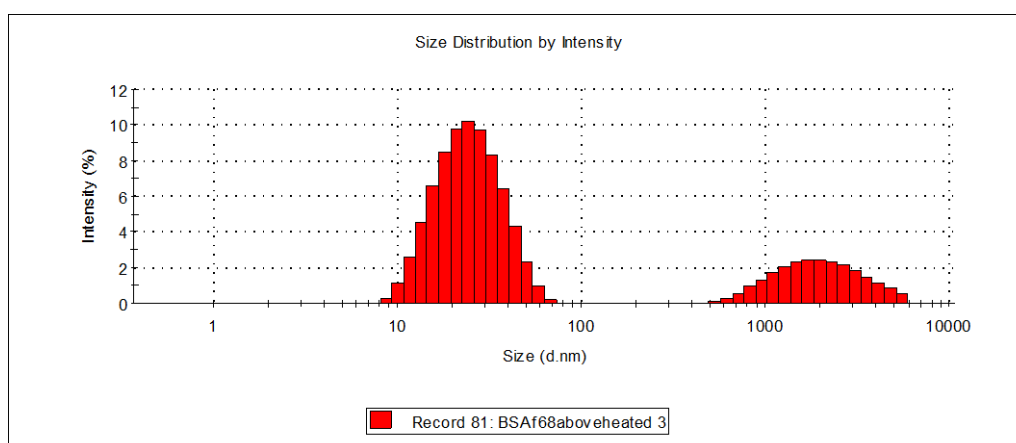


Figure 4.13. Particle size distribution by intensity obtained for heated (66°C) samples for BSA (10 mg/ml) with: (A) Pluronic F-68 below CMC; (B) Pluronic F-68 around CMC; (C) Pluronic F-68 above CMC.

Similar results showing an increase in main peak intensity and diameter (nm) were observed for heated BSA with Pluronic F-68 present compared to unheated samples (Figure 4.6). However heated BSA with Pluronic F-68 below CMC gave a trimodal distribution with a middle peak at 227.5 nm diameter and a very low intensity of 1.8 % (Figure 4.13).

The particle size diameter (nm) of the main peak with greatest intensity for heated BSA (10 mg/ml) with below, around and above CMC levels of Tween 20, Tween 80, Brij 35 and Pluronic F-68 surfactants are summarised in Table 4.2 and Figure 4.14.

Table 4.2. Particle size diameter (nm) of the peak with greatest intensity (Peak 1) for heated BSA (10 mg/ml) with below, around and above CMC levels of Tween 20, Tween 80, Brij 35 and Pluronic F-68 surfactants.

HEATED SAMPLES		PEAK POSITION WITH GREATEST INTENSITY DIAMETER (nm)
BSA (10mg/ml)		26.99
Tween 20	below CMC	26.99
	around CMC	26.33
	above CMC	24.22
Tween 80	below CMC	27.21
	around CMC	27.51
	above CMC	26.22
Brij 35	below CMC	25.12
	around CMC	26.08
	above CMC	23.28
Pluronic F-68	below CMC	25.41
	around CMC	25.17
	above CMC	26.10

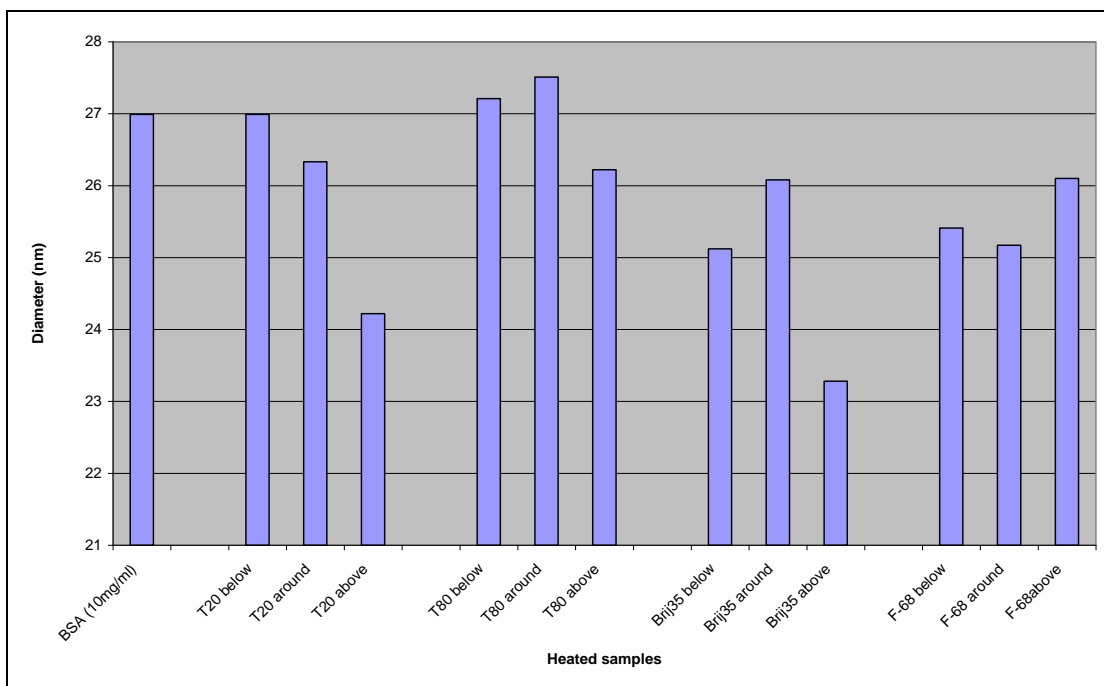


Figure 4.14. Particle size diameter (nm) of the peak with greatest intensity (Peak 1) for heated BSA (10 mg/ml) with below, around and above CMC levels of Tween 20, Tween 80, Brij 35 and Pluronic F-68 surfactants.

In the presence of Tween 20 below and around CMC the particle size for main intensity peak increased considerably compared to heated surfactant free BSA. This showed that BSA aggregates more strongly in the presence of Tween 20 below and around CMC concentrations. Analysing particle size diameter of the main peak for heated samples, it can be seen that the greatest increase in the size of the highest intensity peak diameter was found for the sample containing Tween 20 at above its CMC (24.2 nm) and for the sample containing Brij 35 at above its CMC (23.3 nm) when compared to the heated BSA surfactant free sample (Figure 4.14). It is likely that due to the heat treatment the protein unfolded leading to an increase in particle size comparing to fresh BSA samples.

Statistical analysis using the t-test showed that the difference between heated surfactant free BSA (10 mg/ml) and Tween 20 around and above CMC, Tween 80, Brij 35 and Pluronic F-68 at all concentrations, was statistically significant at the 95 % level ($P < 0.05$).

Figure 4.15 illustrates the comparison of the diameter (nm) of the main peak for heated BSA with Tween 20, Tween 80, Brij 35 and Pluronic F-68 surfactants present.

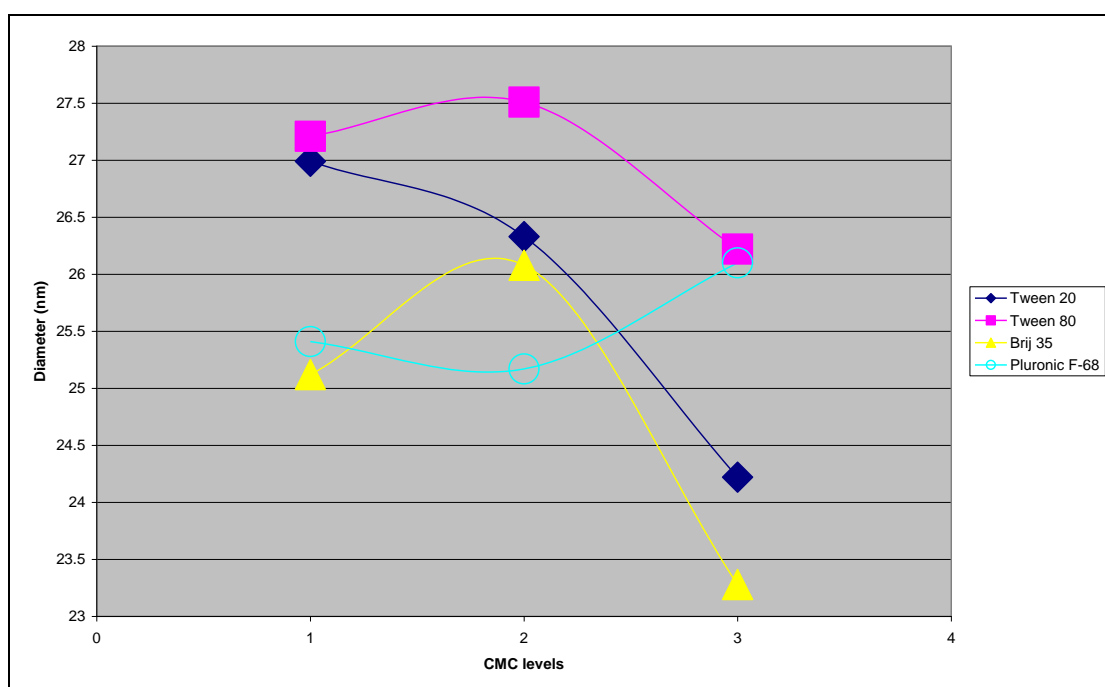


Figure 4.15. A plot of the highest intensity peak diameter (nm) obtained at below (1), around (2) and above (3) CMC levels for Tween 20, Tween 80, Brij 35 and Pluronic F-68 surfactants.

In general there is a decrease in the measured size diameter as the Tween 20 concentration increases. Both Tween 80 and Brij 35 had produced an increase in main peak diameter at around CMC and then a noticeable decrease in diameter (nm) at high CMC levels. The results show that Pluronic F-68 at around its CMC yielded particle diameters slightly decreased which then increased again at high concentration (Figure 4.15).

4.4.3 Particle size distribution measurements for aged BSA-surfactant systems

Figure 4.16 shows particle size distribution data by intensity for aged (See Chapter 2, Section 2.2.2) BSA (10 mg/ml).

As shown by the size distribution profiles, the main peak diminishes relative to the larger particle size populations. For example, a main peak at 1271 nm diameter is now observed on storage with a 68.2 % intensity suggesting that in aged BSA (10 mg/ml) many large particulates are present. There is a notable reduction in intensity of the most intense peak (compared to fresh BSA, Figure 4.1). There is an increase in peak width and intensity for the aged sample indicating that the BSA sample has physically changed.

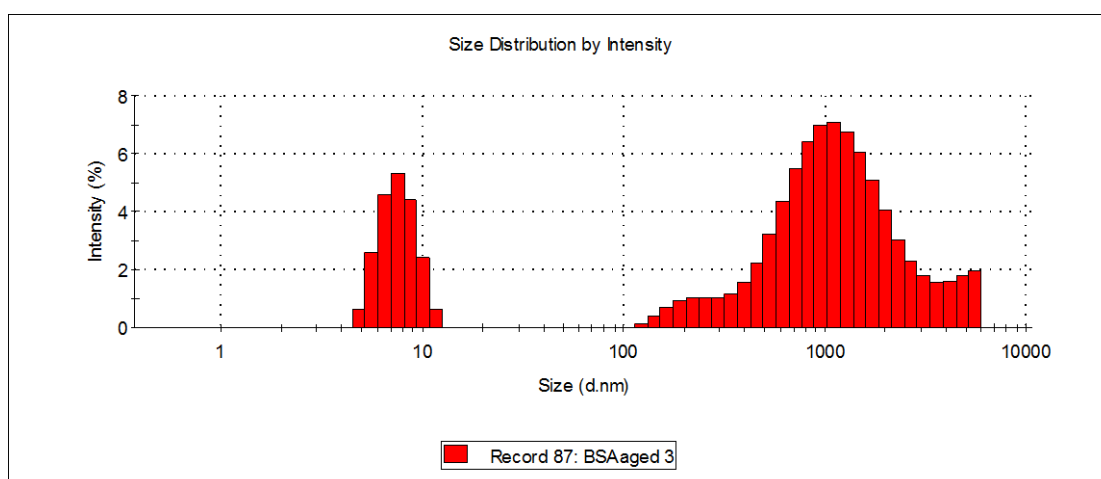


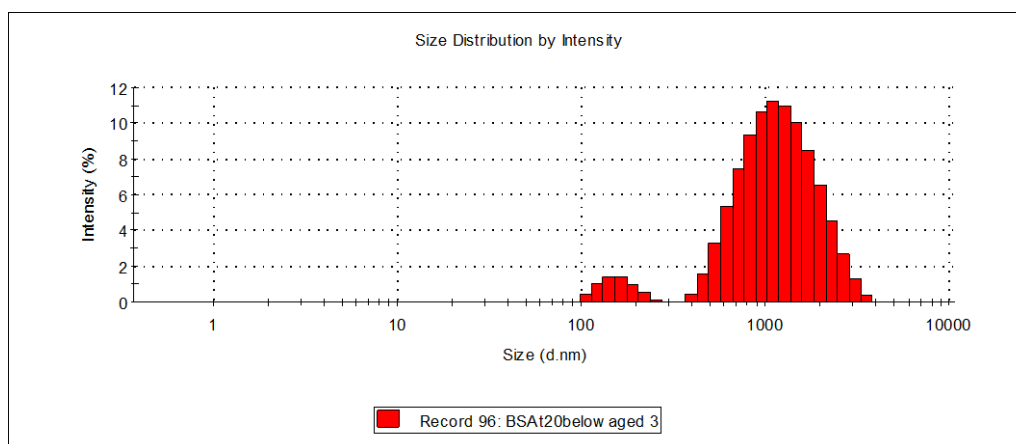
Figure 4.16. Particle size distribution by intensity for aged BSA (10 mg/ml).

Aged BSA samples in the presence of different concentrations of Tween 20 surfactant showed an increase in particle size (Figure 4.17). It is difficult to quantify, since precisely because the particles are so large, they scatter the

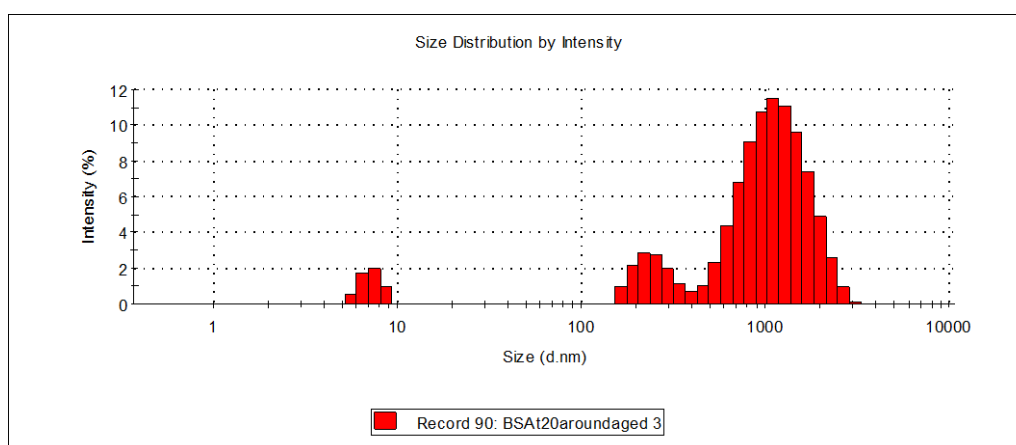
light very strongly and even though they represent two-thirds of the total protein scattering intensity, they in fact are present in very low amounts (Arakawa et al., 2007).

Only observed at Tween 20 concentrations around CMC (Figure 4.17 (B)) there is a small peak at around 7 nm with a low intensity of 5.2 %.

(A)



(B)



(C)

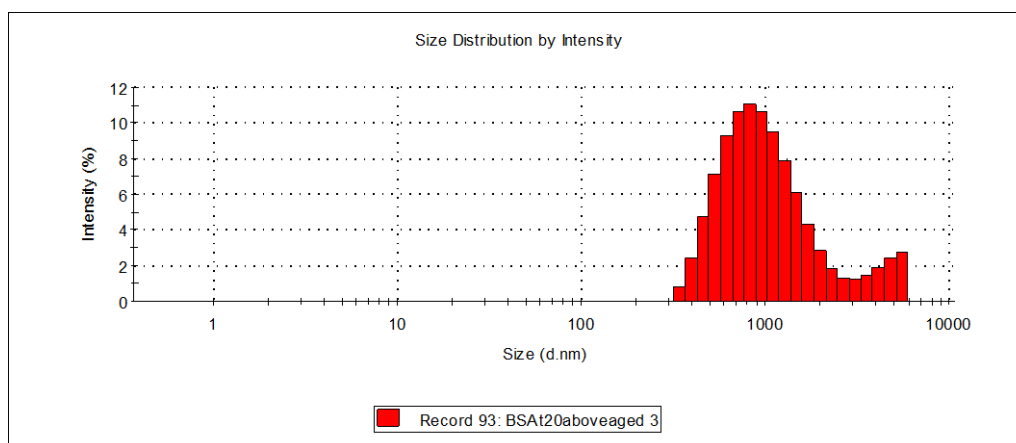
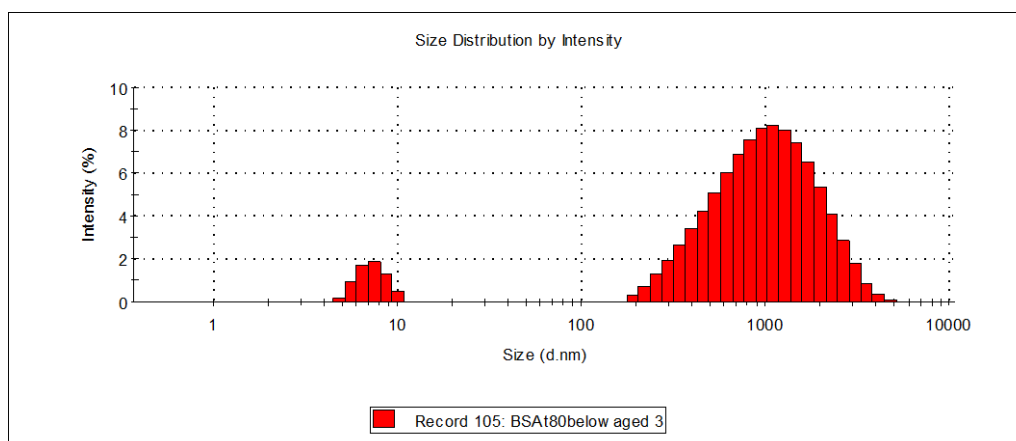


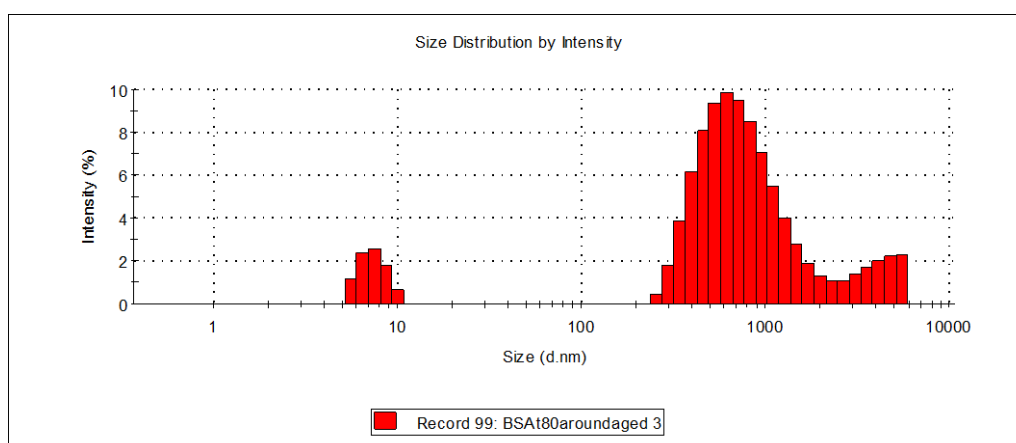
Figure 4.17. Particle size distribution by intensity obtained for aged BSA (10 mg/ml) with: (A) Tween 20 below CMC; (B) Tween 20 around CMC; (C) Tween 20 above CMC.

In the presence of Tween 80 above its CMC concentration just one peak at 100 % intensity with diameter at 1028 nm (Figure 4.18 (C)) was observed by DLS. Aged samples of BSA with Tween 80 below its CMC gave distributions showing bimodal peaks (Figure 4.18 (A)). Aged BSA with Tween 80 concentrations at around its CMC produced three peaks (Figure 4.18 (B)). Similarly, as observed for aged BSA with Tween 20 data presented in Figure 4.17, large particulates are present for BSA with Tween 80 concentrations below, around and above its CMC and that the most intense peak, comparing to fresh samples (Figures 4.2 and 4.3) has shifted to the right indicating an increase in particle size.

(A)



(B)



(C)

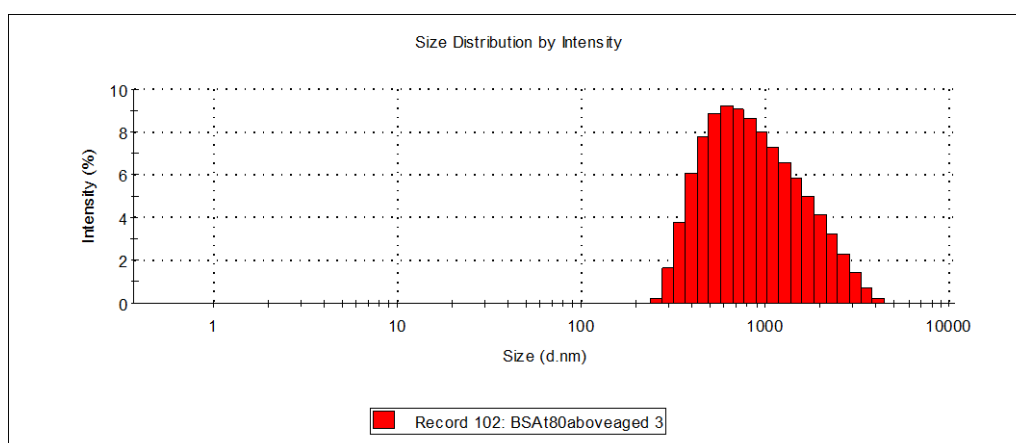
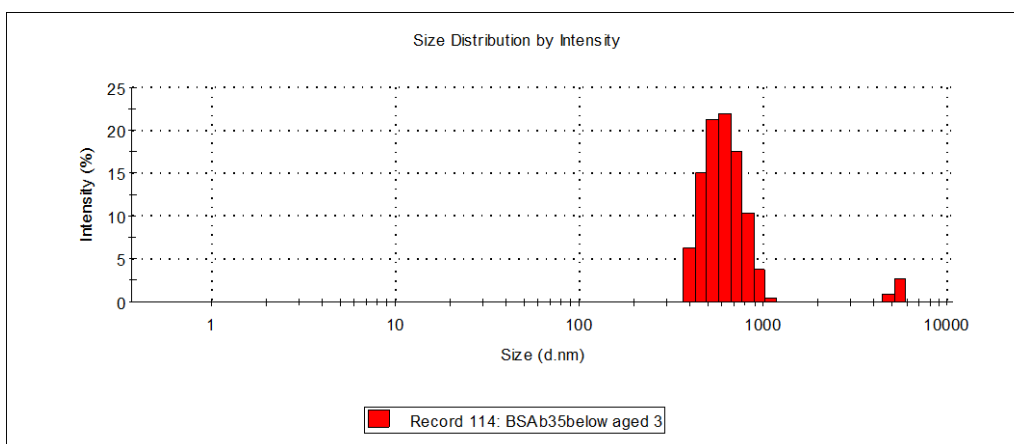


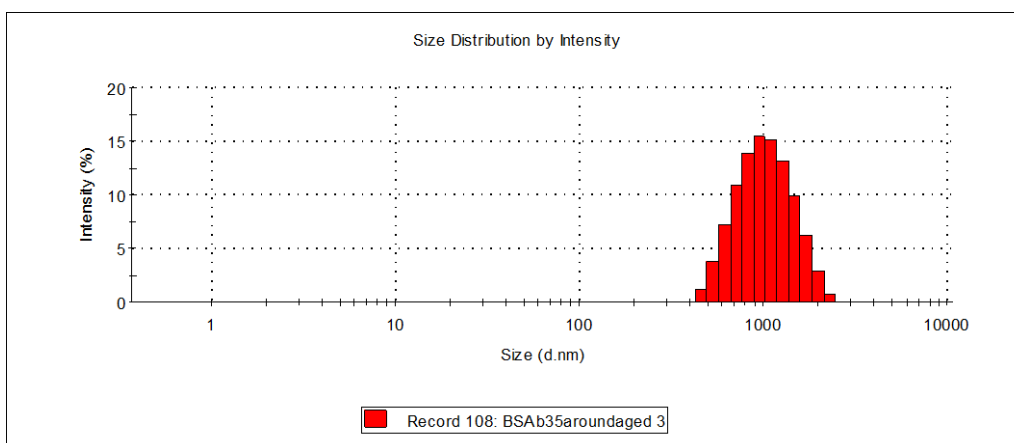
Figure 4.18. Particle size distribution by intensity obtained for aged BSA (10 mg/ml) with: (A) Tween 80 below CMC; (B) Tween 80 around CMC; (C) Tween 80 above CMC.

Figure 4.19 shows intensity particle size distribution data for aged BSA (10 mg/ml) with different Brij 35 concentration. As shown by the distribution profiles, the main peak with highest intensity is around 1000 nm diameter for the three concentrations employed.

(A)



(B)



(C)

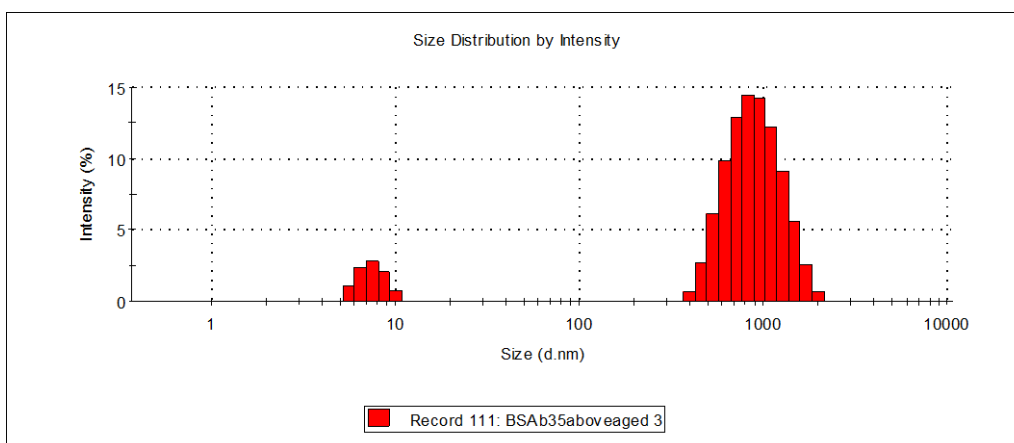
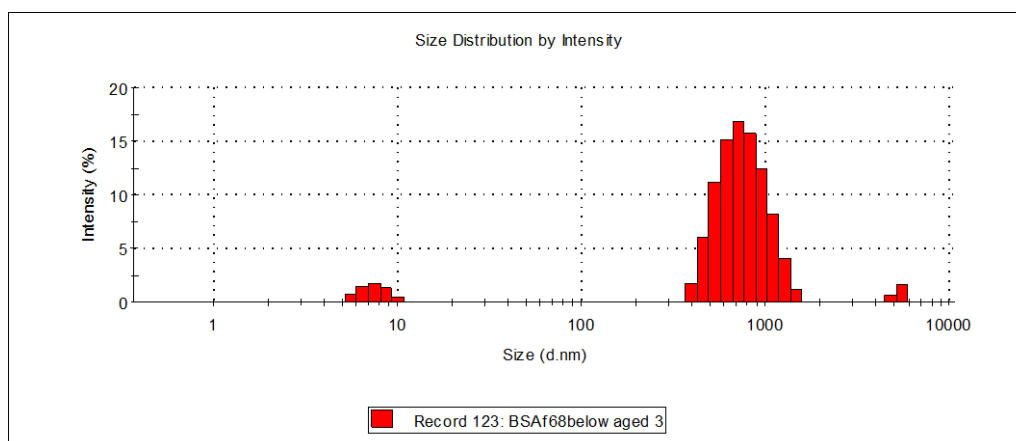


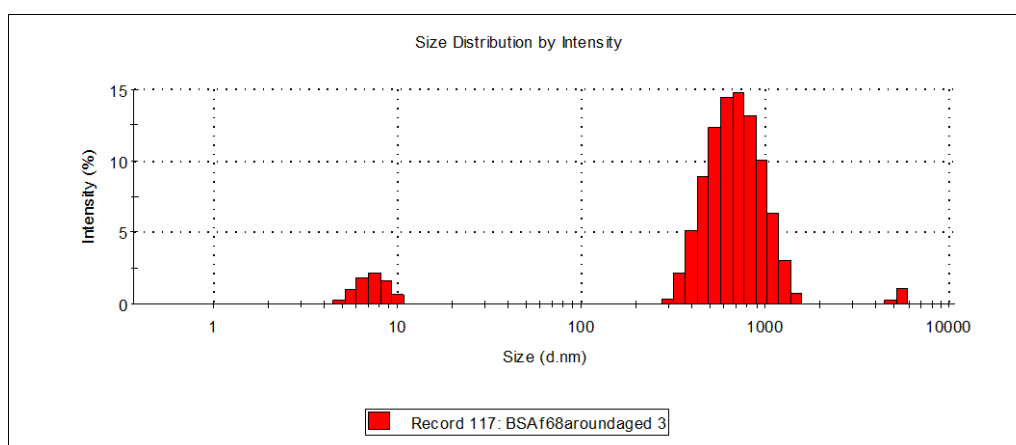
Figure 4.19. Particle size distribution by intensity obtained for aged BSA (10 mg/ml) with: (A) Brij 35 below CMC; (B) Brij 35 around CMC; (C) Brij 35 above CMC.

The DLS data returned peaks of the highest intensity for aged BSA with added Pluronic F-68 at around 700 nm diameter for concentrations below and around CMC (Figure 4.20 (A) and (B)) and 1219 nm for BSA with F-68 below CMC system.

(A)



(B)



(C)

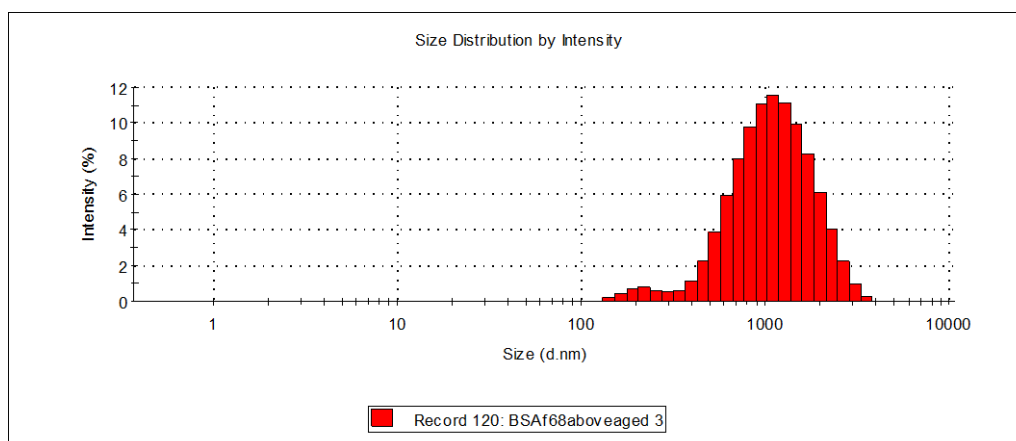


Figure 4.20. Particle size distribution by intensity obtained for aged BSA (10 mg/ml) with: (A) Pluronic F-68 below CMC; (B) Pluronic F-68 around CMC; (C) Pluronic F-68 above CMC.

Particle size diameter (nm) of the main peak with greatest intensity for aged BSA (10 mg/ml) with below, around and above CMC levels of Tween 20, Tween 80, Brij 35 and Pluronic F-68 surfactants are summarised in Table 4 and Figure 23.

Table 4.3. Particle size diameter (nm) of the peak with greatest intensity (Peak 1) for aged BSA (10 mg/ml) with below, around and above CMC levels of Tween 20, Tween 80, Brij 35 and Pluronic F-68 surfactants.

AGED SAMPLES		PEAK POSITION WITH GREATEST INTENSITY DIAMETER (nm)
BSA (10mg/ml)		1271
Tween 20	below CMC	1284
	around CMC	1200
	above CMC	1023
Tween 80	below CMC	1177
	around CMC	779
	above CMC	1028
Brij 35	below CMC	613
	around CMC	1067
	above CMC	931
Pluronic F-68	below CMC	773
	around CMC	714
	above CMC	1219

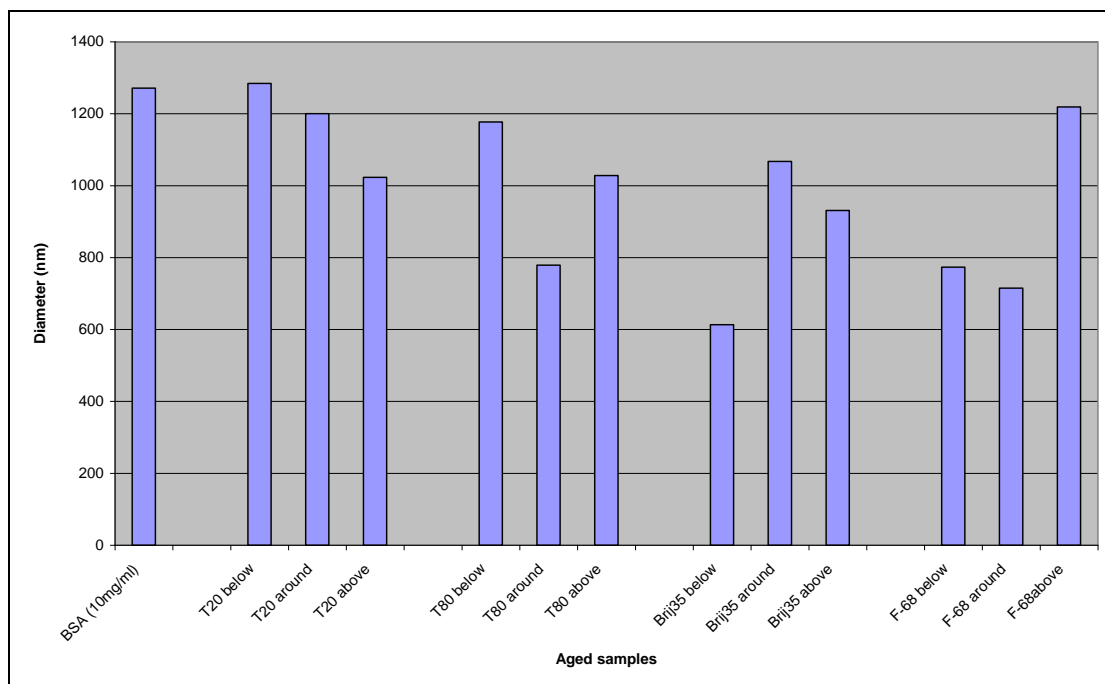


Figure 4.21. Particle size diameter (nm) of the peak with greatest intensity (Peak 1) for aged BSA (10 mg/ml) with below, around and above CMC levels of Tween 20, Tween 80, Brij 35 and Pluronic F-68 surfactants.

Comparing the particle size diameter of the main intensity peak for aged samples, it can be seen that highest intensity peak diameter in nm slightly increased for Tween 20 at concentrations below CMC compared to aged BSA alone (10 mg/ml) sample. All other surfactants lowered the particle diameter in nm with the greatest decrease seen for Brij 35 at a concentration below its CMC (613 nm diameter).

Statistical analysis using a t-test indicated that the difference between aged surfactant-free BSA (10 mg/ml) and Tween 20, Tween 80, Brij 35 and Pluronic F-68 surfactants at below, around and above CMC levels, was statistically significant at the 95 % level ($P < 0.05$).

Figure 4.22 illustrates the comparison of the diameter in nm of the main (highest intensity) peak at below, around and above CMC levels for Tween 20, Tween 80, Brij 35 and Pluronic F-68 surfactants.

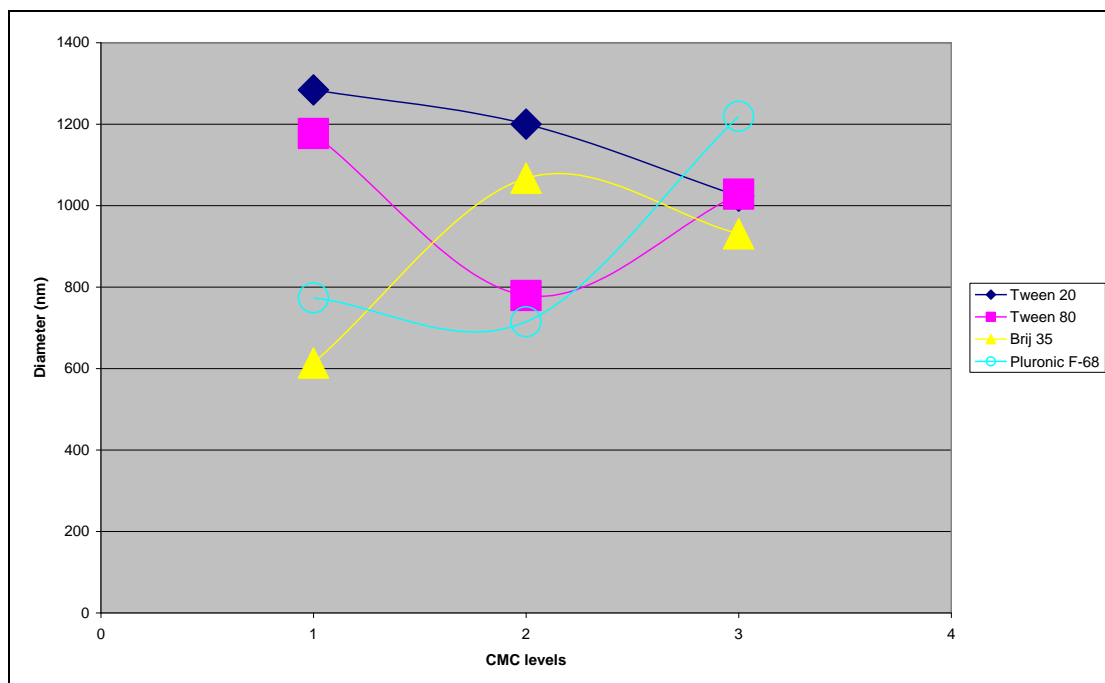


Figure 4.22. A plot of the highest intensity peak diameter (nm) obtained at below (1), around (2) and above (3) CMC levels for Tween 20, Tween 80, Brij 35 and Pluronic F-68 surfactants.

Data presented in Figure 4.22 shows that all aged four surfactants at below, around and above CMC failed to prevent increases in the levels of larger particles forming.

4.4.4 Particle size distribution measurements for freshly prepared IgG2-surfactants systems

Figure 4.23 illustrates size distribution histogram for fresh immunoglobulin IgG2 (10 mg/ml) sample. The reported size of native IgG is around 10 nm

(Song et al, 2001; Bermudez et al 2004), which is significantly lower compared to the 14.44 nm size of the variant obtained in this data for IgG2.

Figure 4.23 also indicates the presence of larger aggregates present in the IgG2 sample at 4532 nm diameter. However, the larger aggregates only represent a small fraction of the total number of molecules (~2 %). The presence of these large particles is common and has been previously reported (Bermudez et al., 2004).

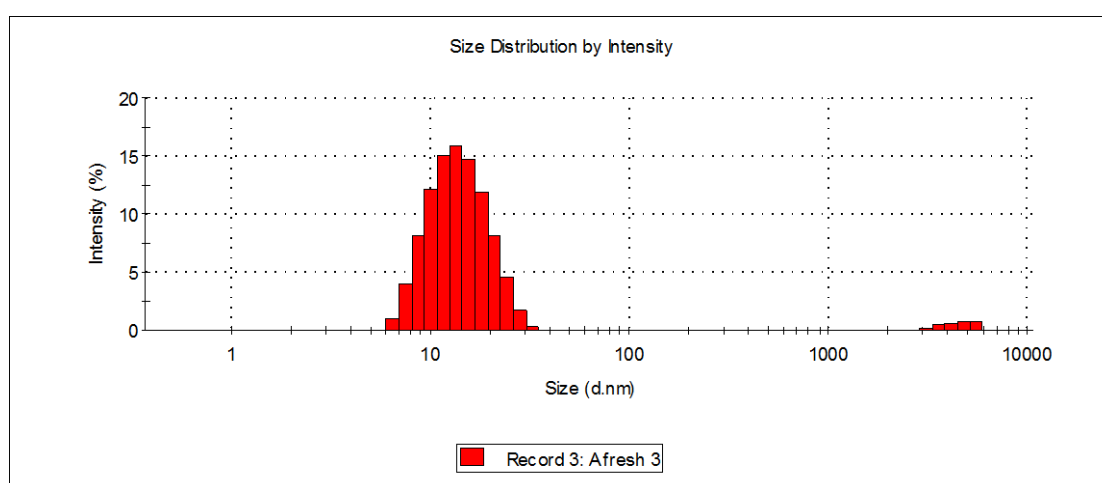
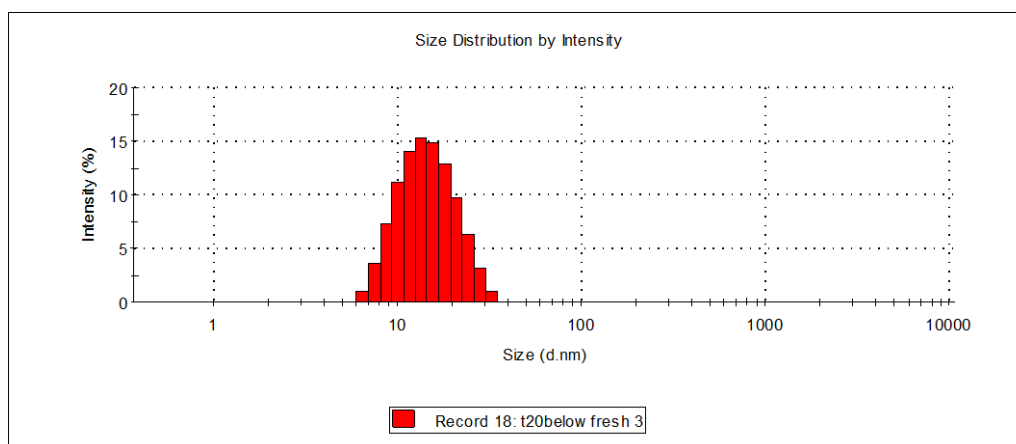


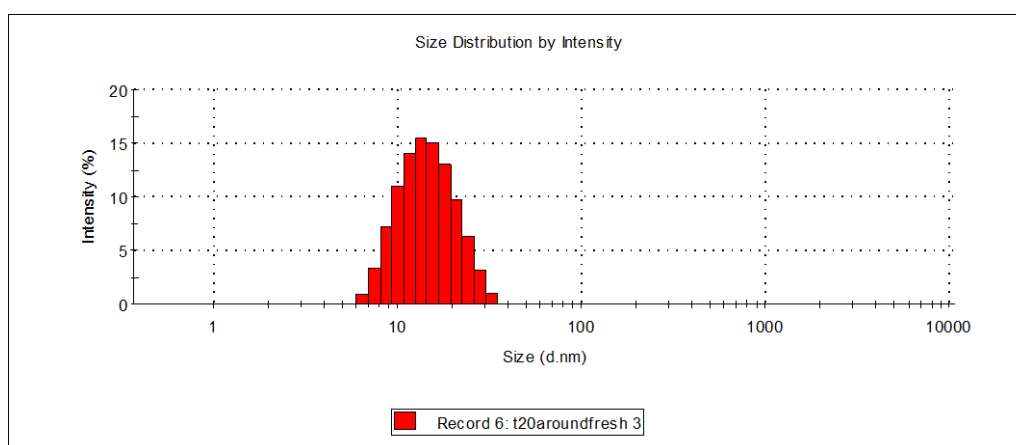
Figure 4.23. Particle size distribution by intensity obtained for freshly prepared IgG2 (10 mg/ml). Average n=3.

Comparison between Figure 4.23 and Figures 4.24 – 4.26 shows that IgG2 in the presence of different concentrations of Tween 20, Tween 80 and Brij 35 surfactants indicate a small increase in calculated particles size from 14.4 nm at its native state to the average of 15.2 nm diameter. It is also clear from Figures 4.24 – 4.26, that the presence of surfactant at any of the tested concentrations acts to remove the presence of the larger particles.

(A)



(B)



(C)

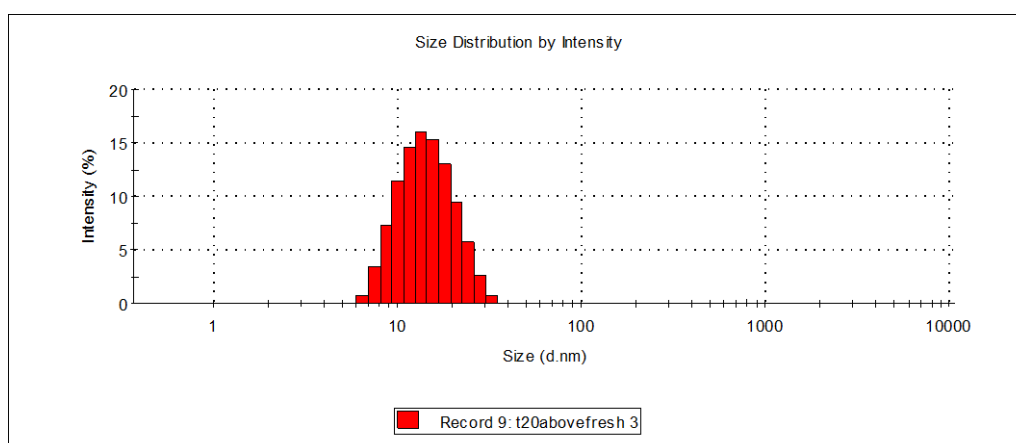
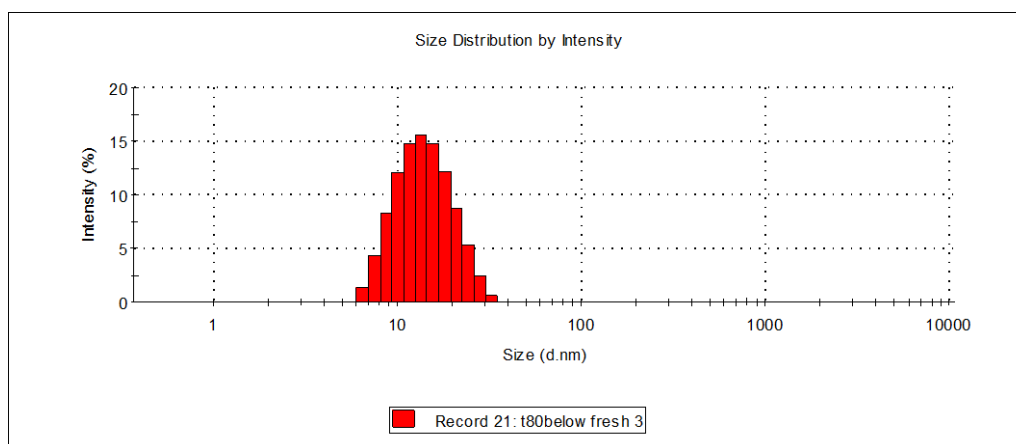
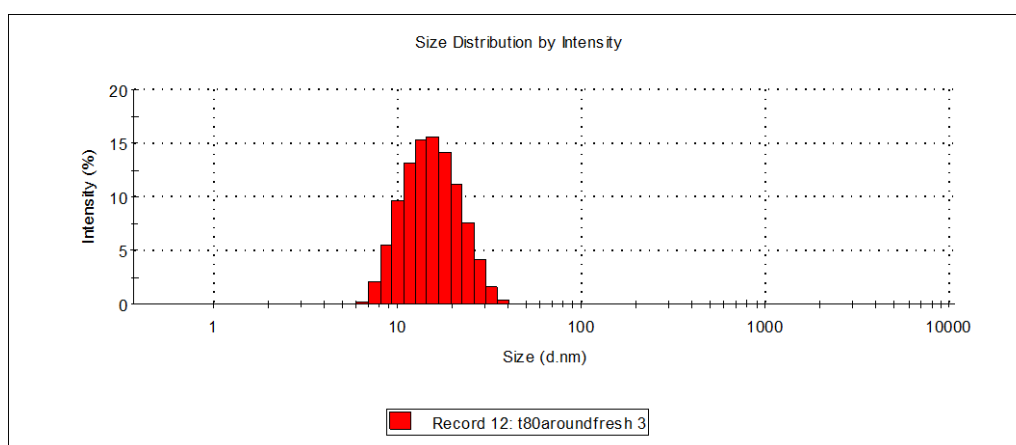


Figure 4.24. Particle size distribution by intensity obtained for IgG2 (10 mg/ml) with: (A) Tween 20 below CMC; (B) Tween 20 around CMC; (C) Tween 20 above CMC.

(A)



(B)



(C)

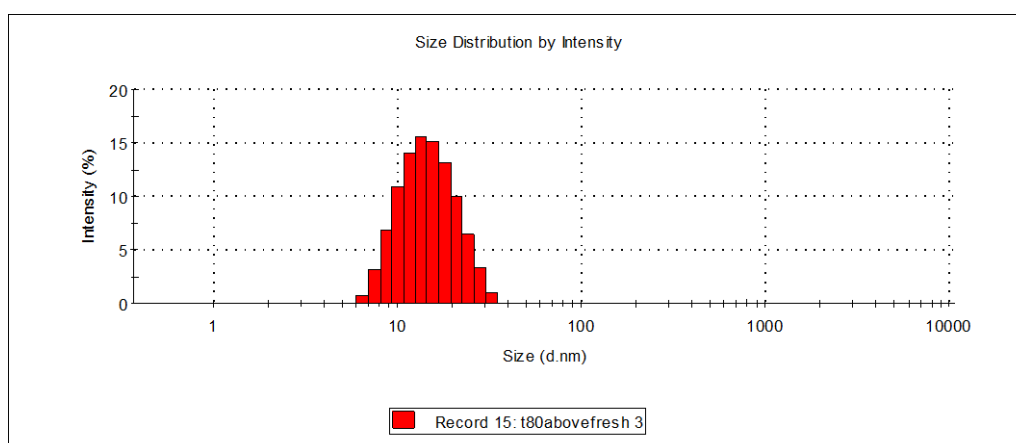
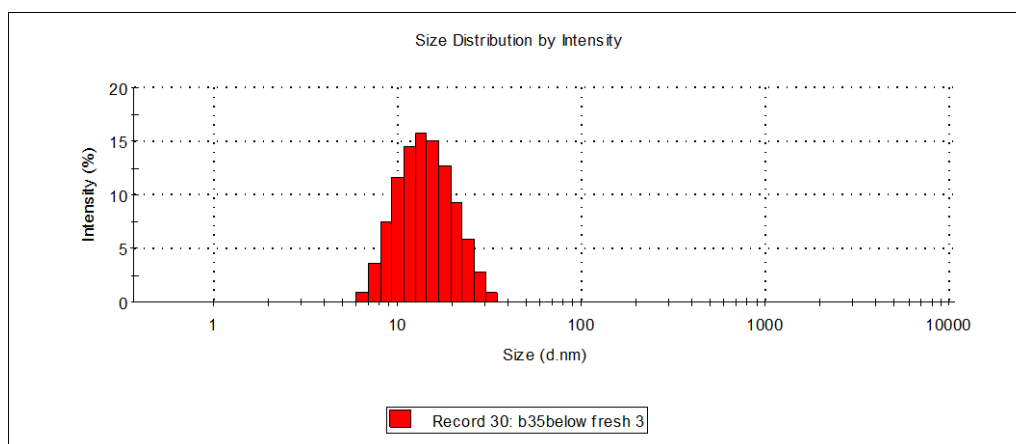
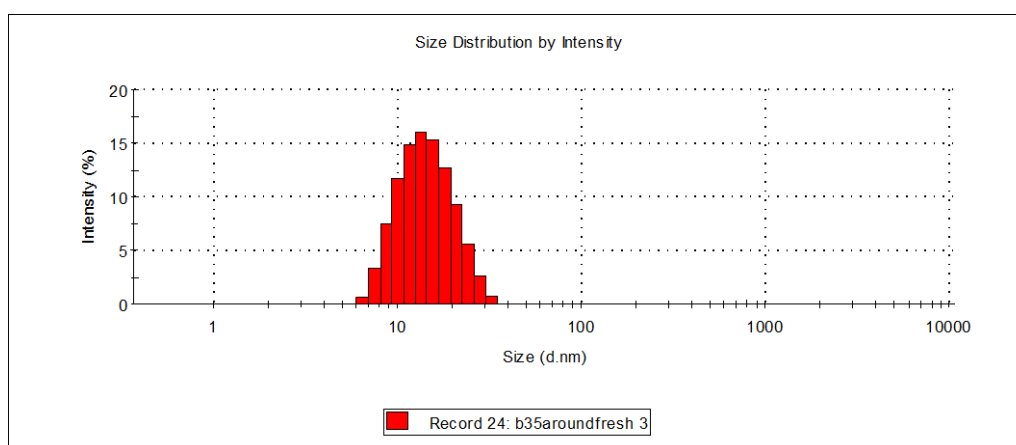


Figure 4.25. Particle size distribution by intensity obtained for IgG2 (10 mg/ml) with: (A) Tween 80 below CMC; (B) Tween 80 around CMC; (C) Tween 80 above CMC.

(A)



(B)



(C)

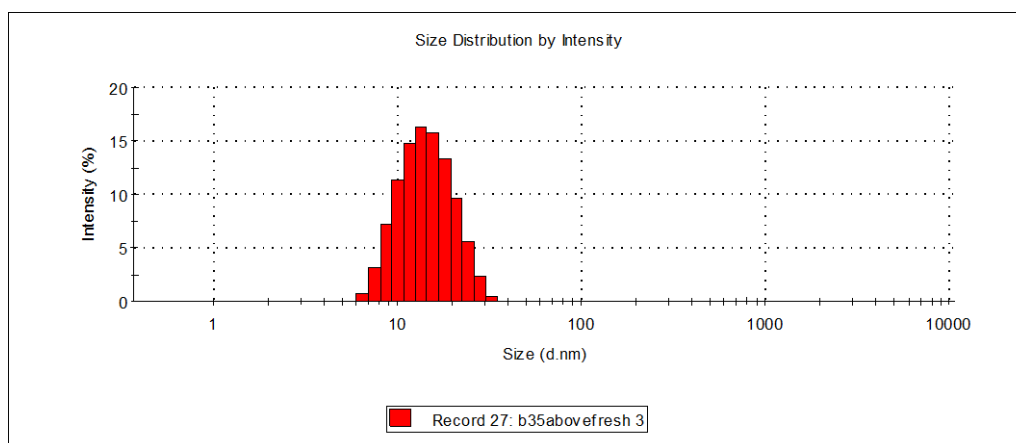


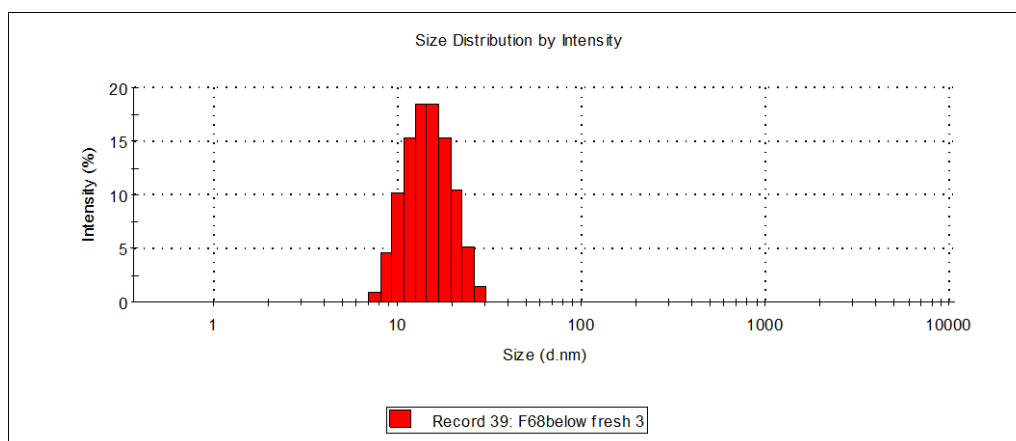
Figure 4.26. Particle size distribution by intensity obtained for IgG2 (10 mg/ml) with: (A) Brij 35 below CMC; (B) Brij 35 around CMC; (C) Brij 35 above CMC.

Similar results were observed for fresh IgG2 with Pluronic F-68 surfactant (Figure 4.27).

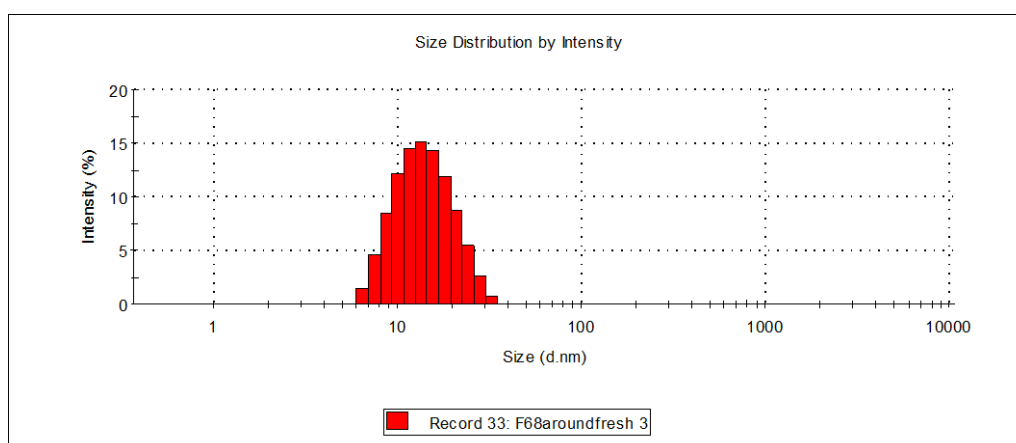
Fresh IgG2 with Pluronic F-68 at concentrations below CMC produced an increase in diameter at 15.3 nm, also F-68 at concentrations around CMC slightly increased diameter to 14.7 nm comparing to freshly prepared IgG2-surfactant free samples (Figure 4.23).

The high concentration of Pluronic F-68 produced an increase in size to 16.1 nm diameter. Data in Figure 4.27 (C) also indicates some larger aggregates are present with a diameter of 4569 nm and the peak intensity of 1.6% for this sample.

(A)



(B)



(C)

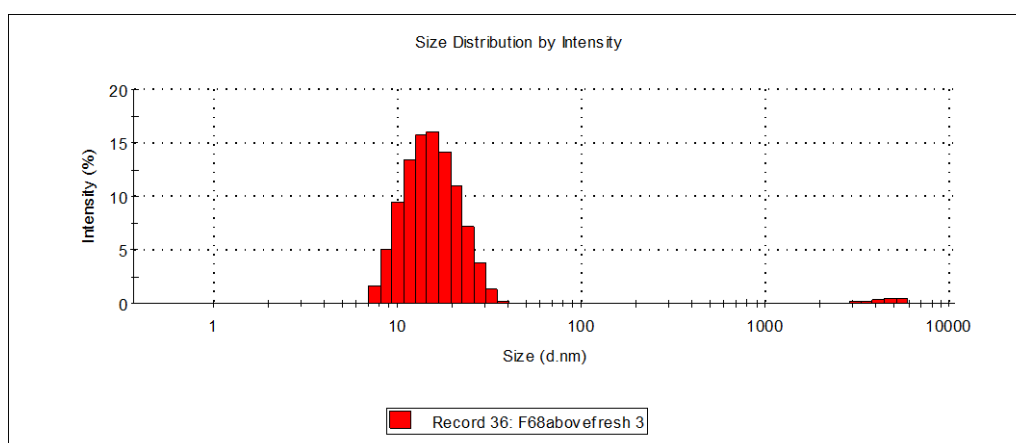


Figure 4.27. Particle size distribution by intensity obtained for IgG2 (10 mg/ml) with: (A) Pluronic F-68 below CMC; (B) Pluronic F-68 around CMC; (C) Pluronic F-68 above CMC.

Particle size diameter (nm) of the main peak with greatest intensity for fresh IgG2 (10 mg/ml) with below, around and above CMC levels of Tween 20, Tween 80, Brij 35 and Pluronic F-68 surfactants are summarised in Table 4.4 and Figure 4.28.

Table 4.4. Particle size diameter (nm) of the peak with greatest intensity (Peak 1) for fresh IgG2 (10 mg/ml) with below, around and above CMC levels of Tween 20, Tween 80, Brij 35 and Pluronic F-68 surfactants.

FRESH SAMPLES		PEAK POSITION WITH GREATEST INTENSITY DIAMETER (nm)
IgG2 (10 mg/ml)		14.44
Tween 20	below CMC	15.25
	around CMC	15.31
	above CMC	15.04
Tween 80	below CMC	14.69
	around CMC	16.20
	above CMC	15.40
Brij 35	below CMC	15.04
	around CMC	15.02
	above CMC	15.00
Pluronic F-68	below CMC	15.30
	around CMC	14.69
	above CMC	16.09

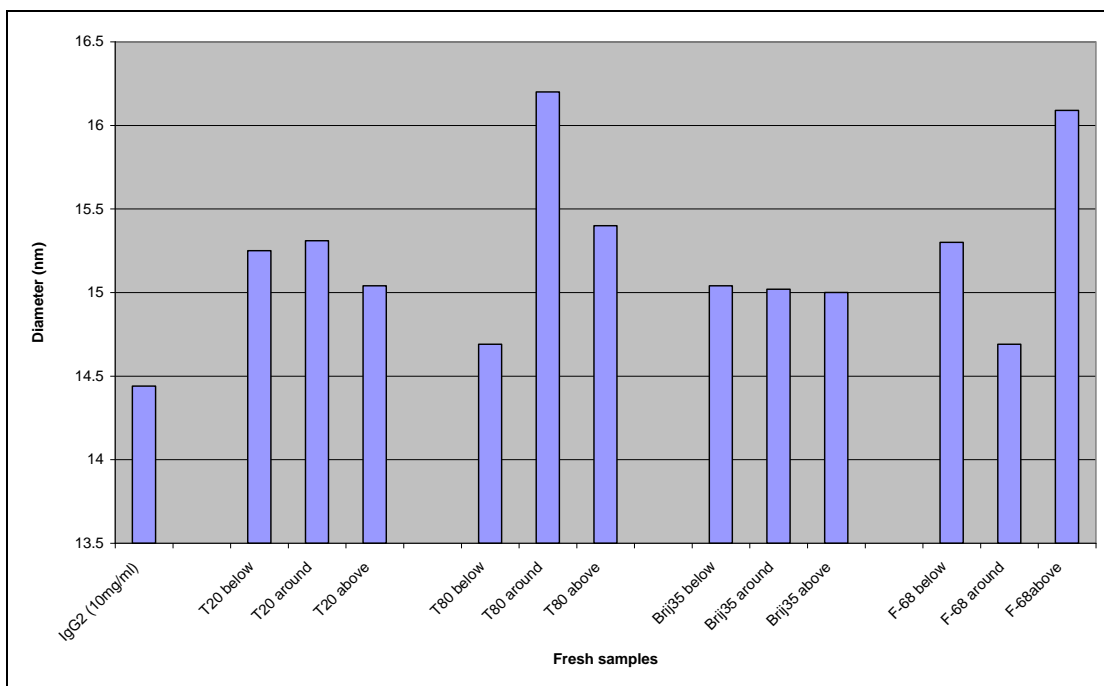


Figure 4.28. Particle size diameter (nm) of the peak with greatest intensity (Peak 1) for fresh IgG2 (10 mg/ml) with below, around and above CMC levels of Tween 20, Tween 80, Brij 35 and Pluronic F-68 surfactants.

On analysing the particle size diameter of the main intensity peak for fresh IgG2 – surfactant samples, it can be seen that highest intensity peak diameter is increased for all four surfactants at all concentration levels. The highest increase in diameter (nm) was detected for Tween 80 around CMC at 16.20 nm and Pluronic F-68 above CMC at 16.09 nm diameter (Table 4.4, Figure 4.28).

Statistical analysis using a t-test showed that the increase in diameter (nm) for all four surfactants at below, around and above CMC levels was statistically significant at the 95 % level ($P < 0.05$).

Figure 4.29 illustrates the comparison of the diameter in nm of the main (highest intensity) peak at below, around and above CMC levels for Tween 20, Tween 80, Brij 35 and Pluronic F-68 surfactants.

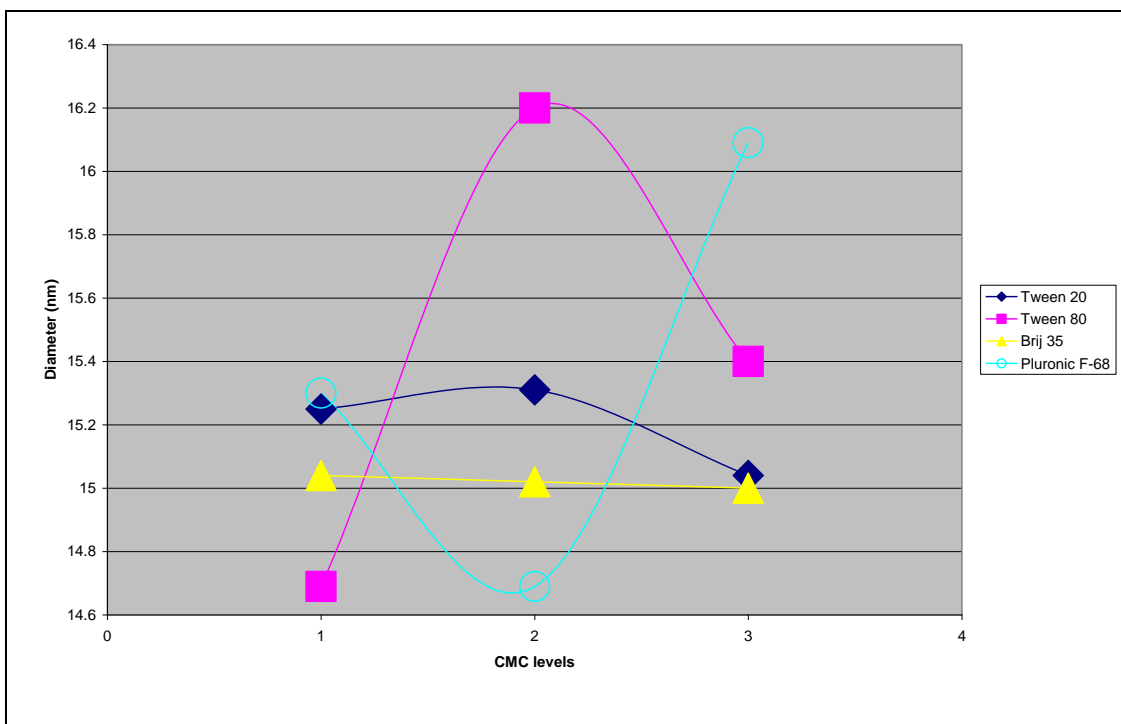


Figure 4.29. A plot of the highest intensity peak diameter (nm) obtained at below (1), around (2) and above (3) CMC levels for Tween 20, Tween 80, Brij 35 and Pluronic F-68 surfactants.

From Figure 4.29 it can be seen that all four surfactants at different concentrations in relation to their CMC produce different particle size diameters (nm) for the highest intensity peak. There is a gradual decrease in the measured particles size diameter (nm) as the Brij 35 surfactant concentration increases. Tween 20 and Tween 80 surfactants produced the highest diameter (nm) at around CMC, where Pluronic F-68 gave its lowest particle size diameter at around its CMC.

4.4.5 Particle size distribution measurements for heated IgG2-surfactant systems

Figure 4.30 illustrates particle size distribution by intensity for heated (see Chapter 2 Section 2.2.1) immunoglobulin IgG2 (10 mg/ml) samples. The particle size of heat stressed IgG2 sample increased by more than double that of the starting material (Figure 4.23). As shown by the size distribution histograms, the difference arises from an increase in the diameter from 14.4 nm for fresh IgG2 to 37.3 nm for heat stressed sample. Also it is noticeable that heat stressed IgG2 doesn't have larger aggregates present comparing to fresh sample.

It also has been previously reported that heat treatment of native IgG induces strong aggregation which results in precipitation of the protein (Vermeer et al., 2000).

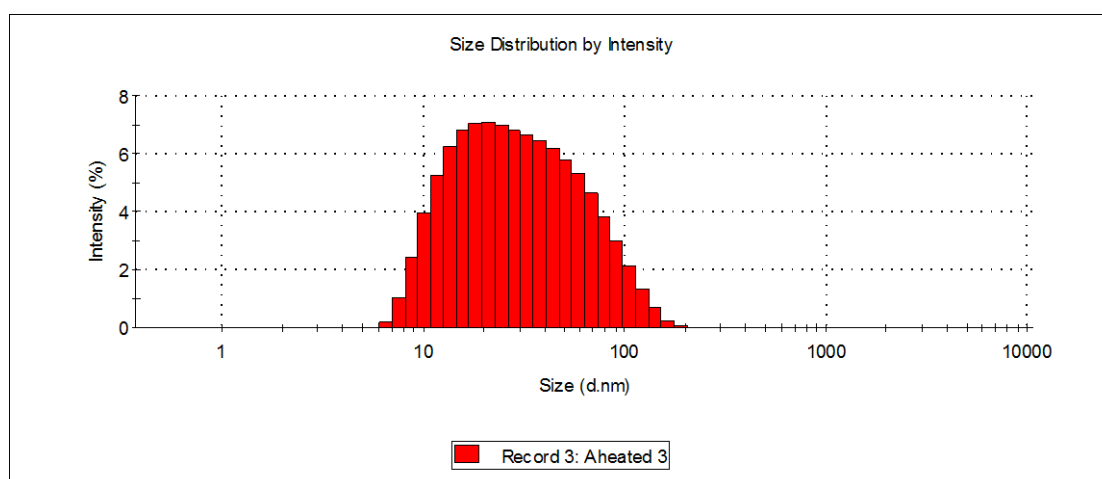
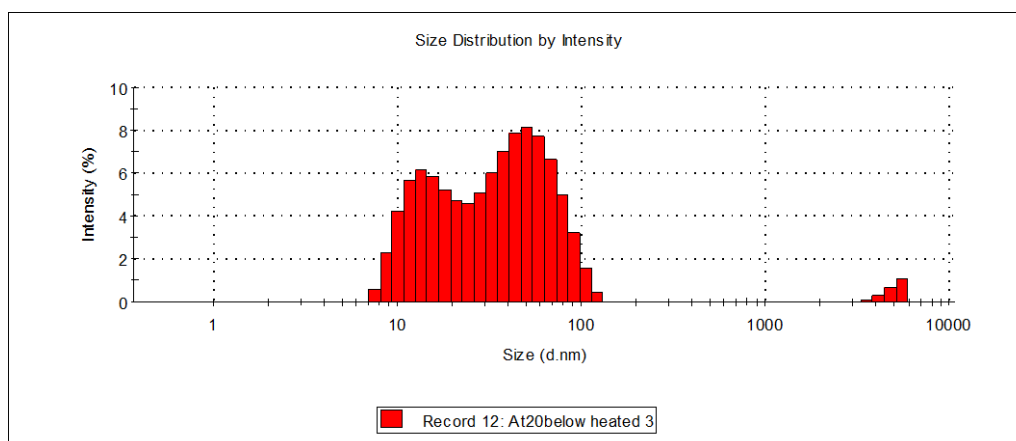


Figure 4.30. Particle size distribution by intensity obtained for heated (60°C) IgG2 (10 mg/ml).

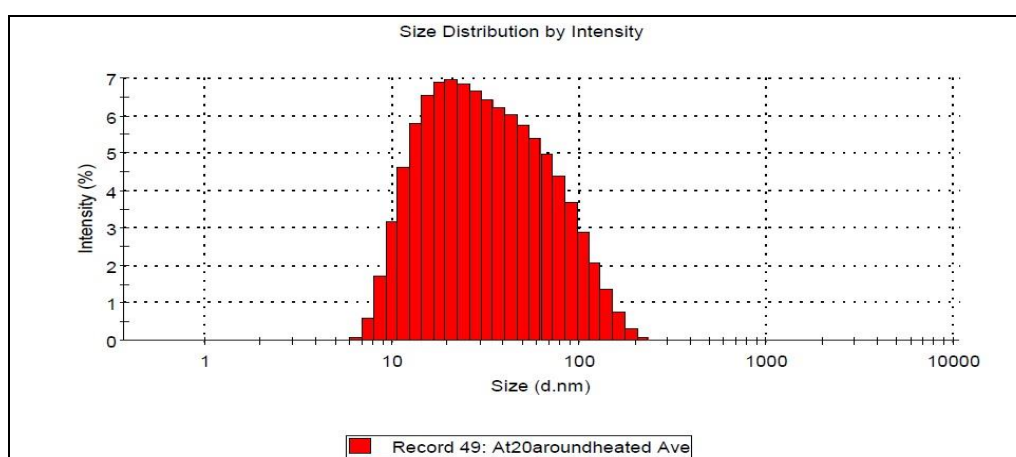
Figure 4.31 shows that heat treatment of IgG2 in the presence of different levels of Tween 20 led to an increase of the populations of larger particles comparing to freshly prepared samples.

The monoclonal sample containing Tween 20 at around its CMC showed a monomodal distribution with a peak diameter of 41.9 nm (Figure 4.31 (B)). At lower levels a trimodal distribution was obtained: Peak 1: 51.9 nm, Peak 2: 15.6 nm and Peak 3: 5036.0 nm. The monoclonal sample containing Tween 20 at above its CMC gave a DLS output which was bimodal with Peak 1 at 46.9 nm and Peak 2 at 13.1 nm.

(A)



(B)



(C)

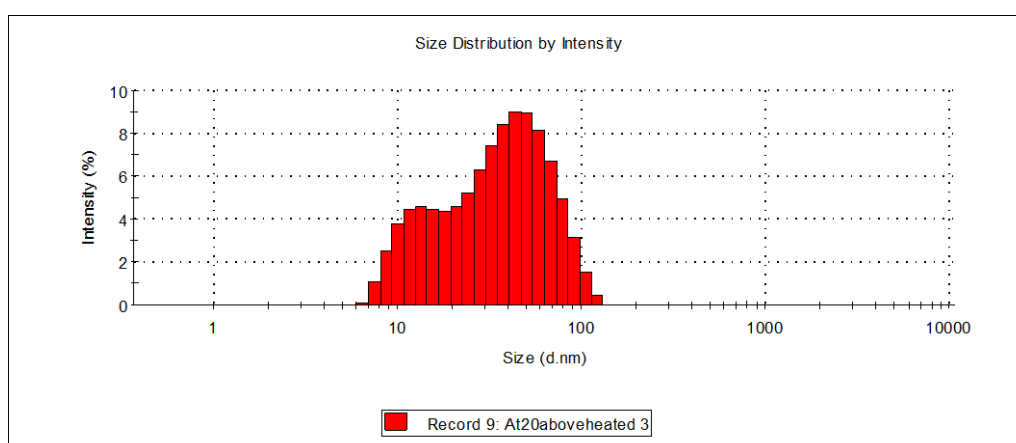
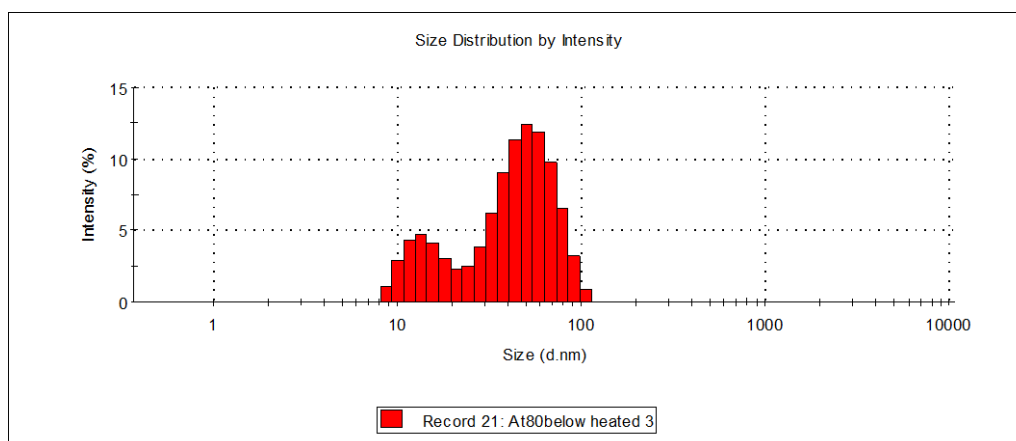


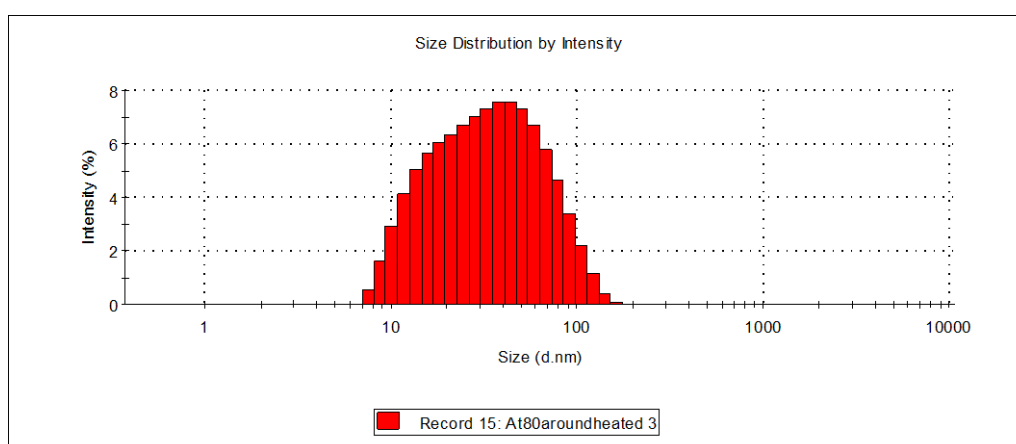
Figure 4.31. Particle size distribution by intensity obtained for heated IgG2 (10 mg/ml) with: (A) Tween 20 below CMC; (B) Tween 20 around CMC; (C) Tween 20 above CMC.

DLS histograms for heated samples containing the higher than CMC level of Tween 80 showed that greater numbers of larger particles were forming (Figure 4.32 (C)). Also samples at levels below and around CMC of Tween 80 produced an increase in particle size after heat stress (Figure 4.32 (A), (B)).

(A)



(B)



(C)

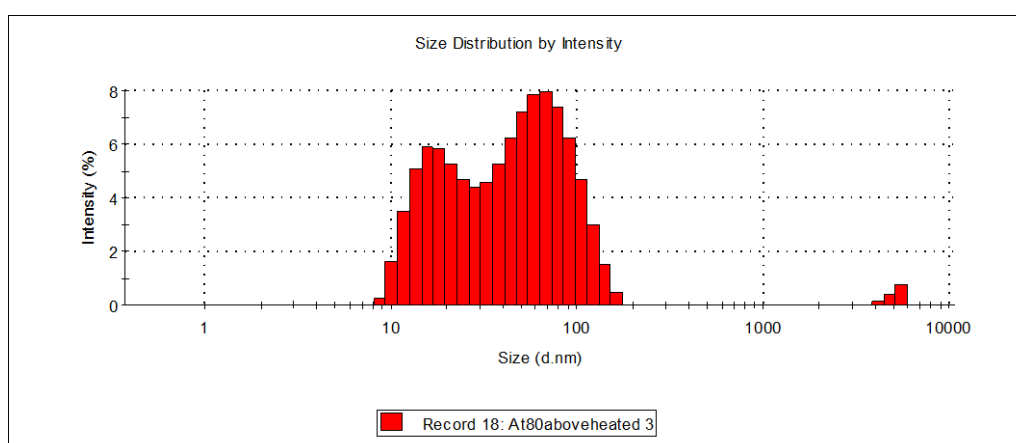
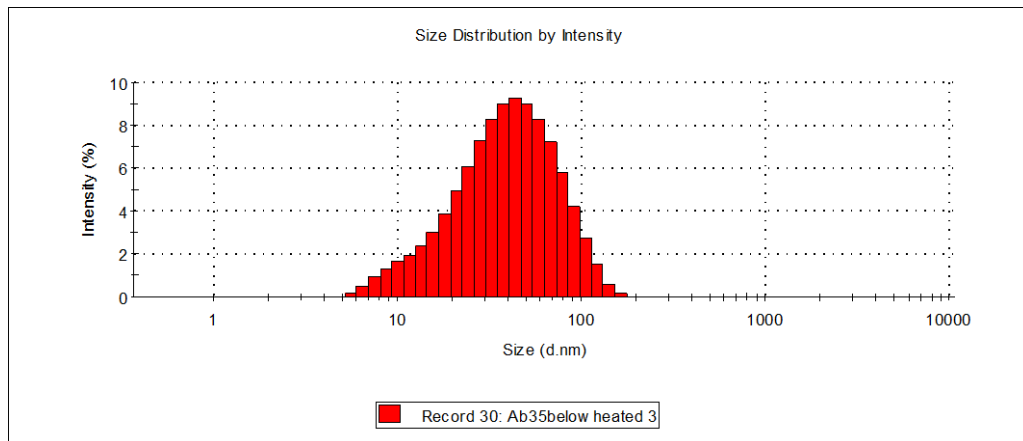
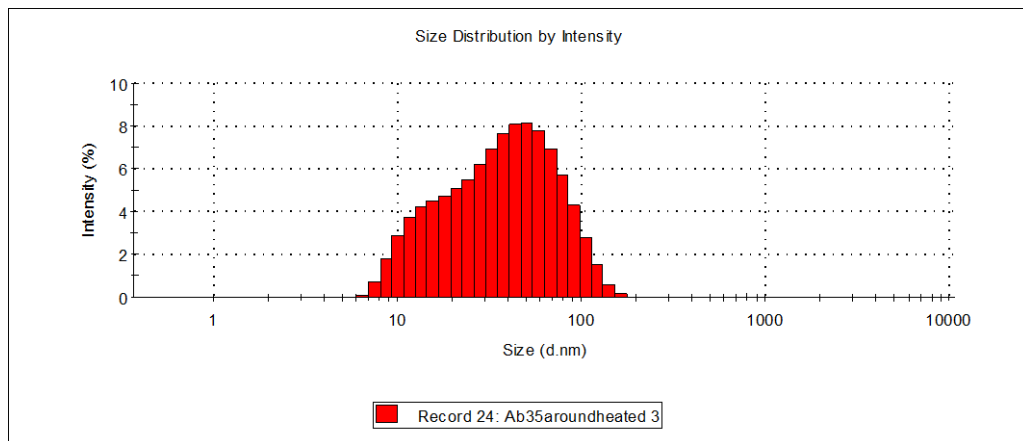


Figure 4.32. Particle size distribution by intensity obtained for heated IgG2 (10 mg/ml) with: (A) Tween 80 below CMC; (B) Tween 80 around CMC; (C) Tween 80 above CMC.

(A)



(B)



(C)

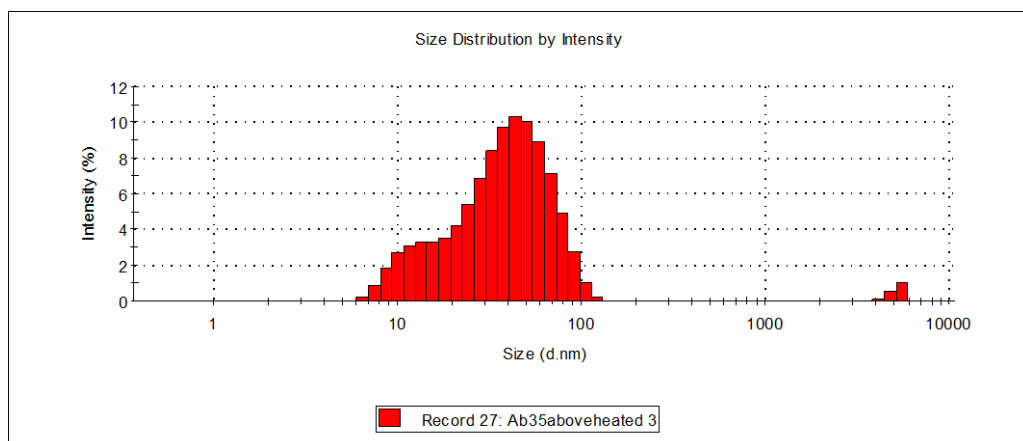
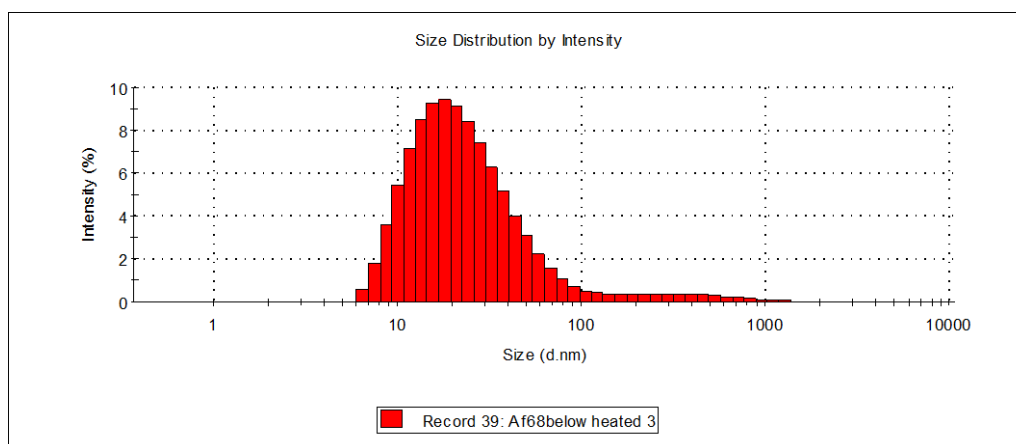


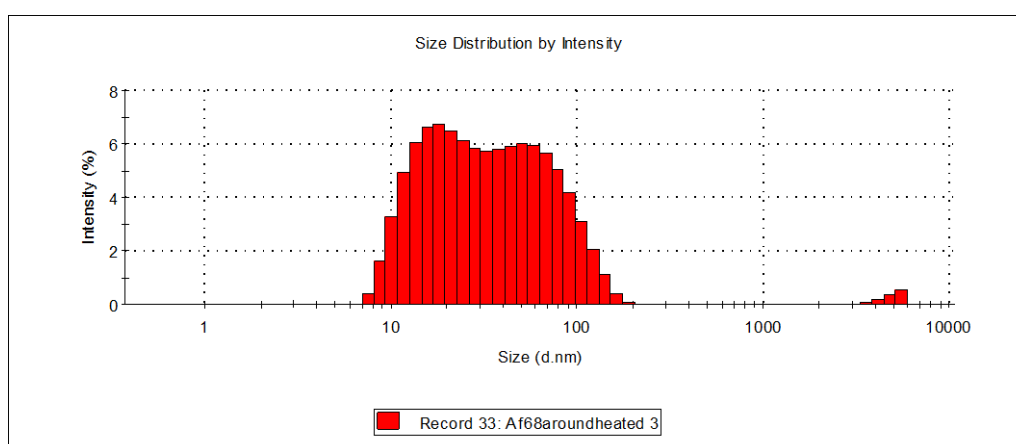
Figure 4.33. Particle size distribution by intensity obtained for heated IgG2 (10 mg/ml) with: (A) Brij 35 below CMC; (B) Brij 35 around CMC; (C) Brij 35 above CMC.

The Brij 35 surfactant produced similar results to Tween 80 (Figure 4.33 (C)). Heated IgG2 systems with Pluronic F-68 present gave an increase in particle size with all concentrations (Figure 4.34).

(A)



(B)



(C)

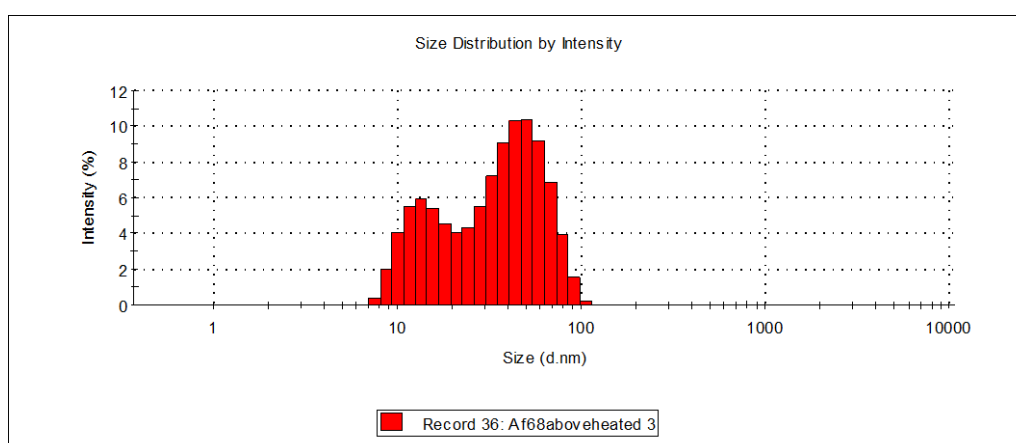


Figure 4.34. Particle size distribution by intensity obtained for heated IgG2 (10 mg/ml) with: (A) Pluronic F-68 below CMC; (B) Pluronic F-68 around CMC; (C) Pluronic F-68 above CMC.

The particle size diameter (nm) obtained using DLS of the peak with greatest intensity for heated IgG2 (10 mg/ml) with below, around and above CMC levels of Tween 20, Tween 80, Brij 35 and Pluronic F-68 surfactants are summarised in Table 4.5 and Figure 4.35.

Table 4.5. Particle size diameter (nm) of the peak with greatest intensity (Peak 1) for heated IgG2 (10 mg/ml) with below, around and above CMC levels of Tween 20, Tween 80, Brij 35 and Pluronic F-68.

HEATED SAMPLES		PEAK POSITION WITH GREATEST INTENSITY DIAMETER (nm)
IgG2 (10mg/ml)		37.25
Tween 20	below CMC	51.95
	around CMC	41.85
	above CMC	46.96
Tween 80	below CMC	51.98
	around CMC	39.78
	above CMC	66.13
Brij 35	below CMC	45.39
	around CMC	43.67
	above CMC	40.99
Pluronic F-68	below CMC	26.46
	around CMC	19.58
	above CMC	46.56

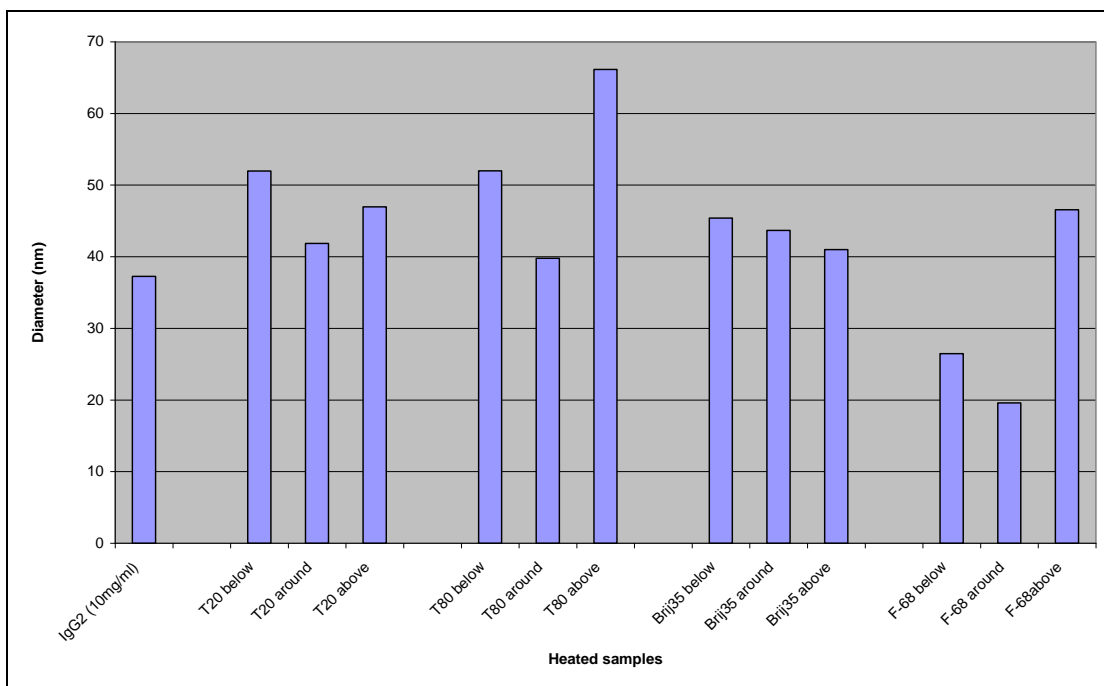


Figure 4.35. Particle size diameter (nm) of the peak with greatest intensity (Peak 1) for heated IgG2 (10 mg/ml) with below, around and above CMC levels of Tween 20, Tween 80, Brij 35 and Pluronic F-68 surfactants.

On analysing the particle size diameter of the main peak for heated samples, it can be seen that the highest intensity peak diameter increased for all Tween 20, Tween 80 and Brij 35 levels and for Pluronic F-68 at above its CMC comparing to heated IgG2-surfactant free sample. The highest increase in diameter (nm) was detected for Tween 80 above its CMC and the lowest for Pluronic F-68 around its CMC. Relative to data for all other samples, F-68 at the two lower concentrations, suggested a protective effect against heat stress.

Statistical analysis using a t-test showed that the difference between heated surfactant free IgG2 (10 mg/ml) and Tween 20, Tween 80, Brij 35 and Pluronic F-68 surfactants at all CMC levels, was statistically significant at the 95 % level ($P < 0.05$).

Figure 4.36 illustrates the comparison of the diameter in nm of the main peak at below, around and above CMC levels for Tween 20, Tween 80, Brij 35 and Pluronic F-68 surfactants.

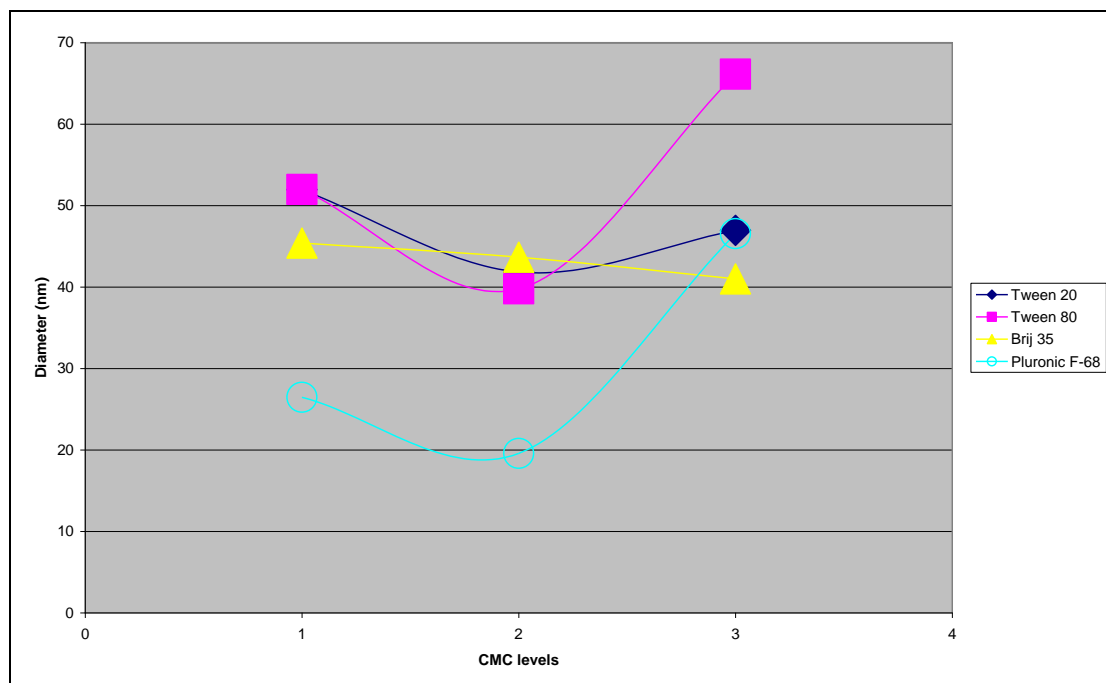


Figure 4.36. A plot of the highest intensity peak diameter (nm) obtained at below (1), around (2) and above (3) CMC levels for heated IgG2 with Tween 20, Tween 80, Brij 35 and Pluronic F-68 surfactants.

Figure 4.36 shows that all surfactants differ in particle size diameter for highest intensity peak. Brij 35 showed a gradual decrease in diameter (nm) with concentration. Surfactants Tween 80 and Pluronic F-68 showed increases in diameter at above CMC levels. Tween 20 produced its highest particle size diameter at below its CMC.

4.4.6 Particle size distribution measurements for aged IgG2-surfactants

Shown in Figure 4.37 is a size distribution histogram for aged (See Chapter 2, Section 2.2.2) IgG2 (10 mg/ml).

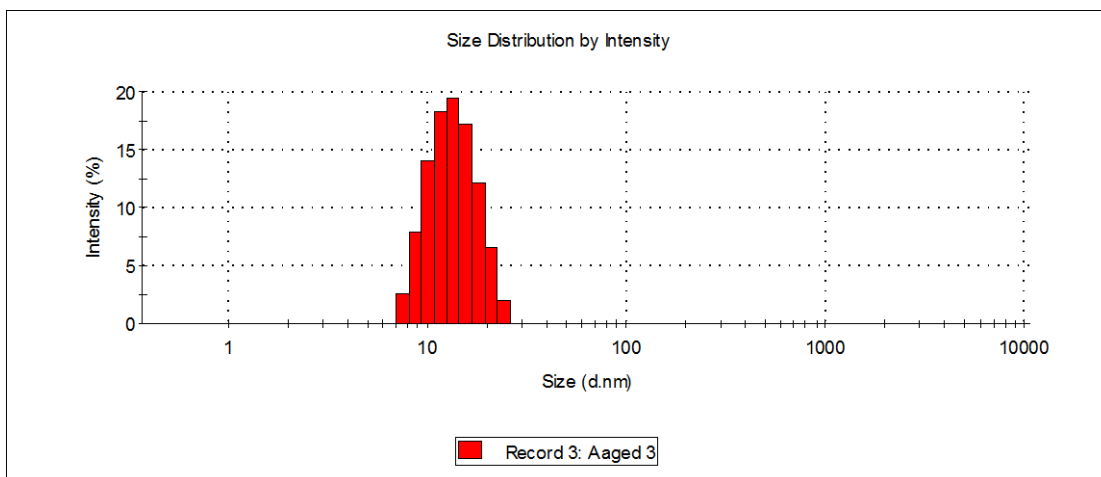
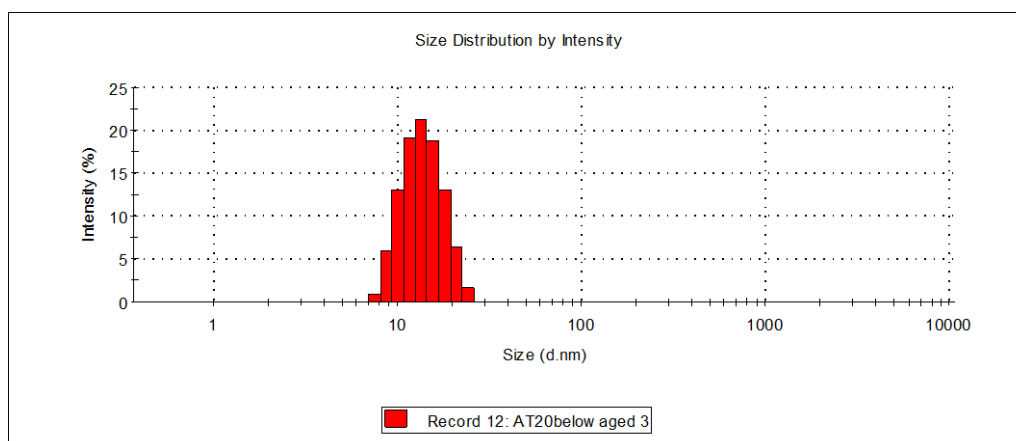


Figure 4.37. Particle size distribution by intensity obtained for aged samples for IgG2 (10 mg/ml).

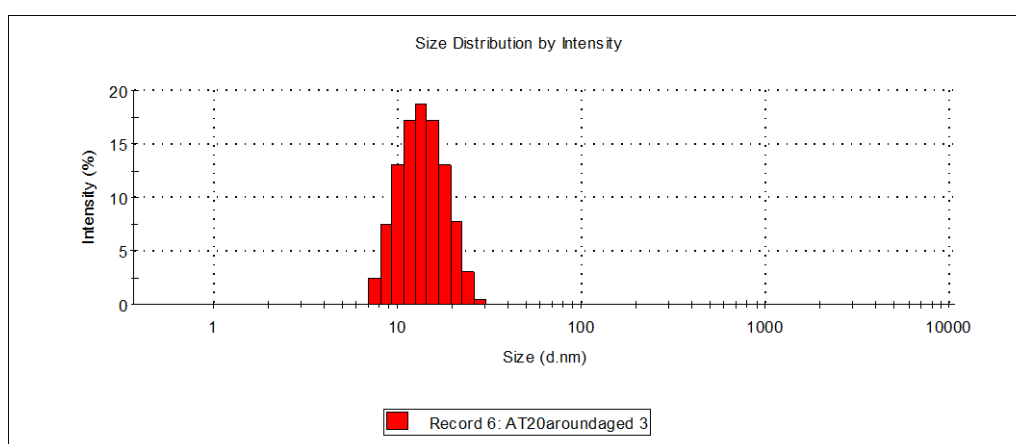
Data shows the monomodal peak 13.8 nm diameter, which is slightly lower to the one obtained for freshly prepared IgG2 samples (Figure 4.23).

In the presence of Tween 20 (Figure 4.38), Tween 80 (Figure 4.39), Brij 35 (Figure 4.40) and Pluronic F-68 (Figure 4.41) a size distribution of a monomodal peak at around 14-15 nm diameter was obtained.

(A)



(B)



(C)

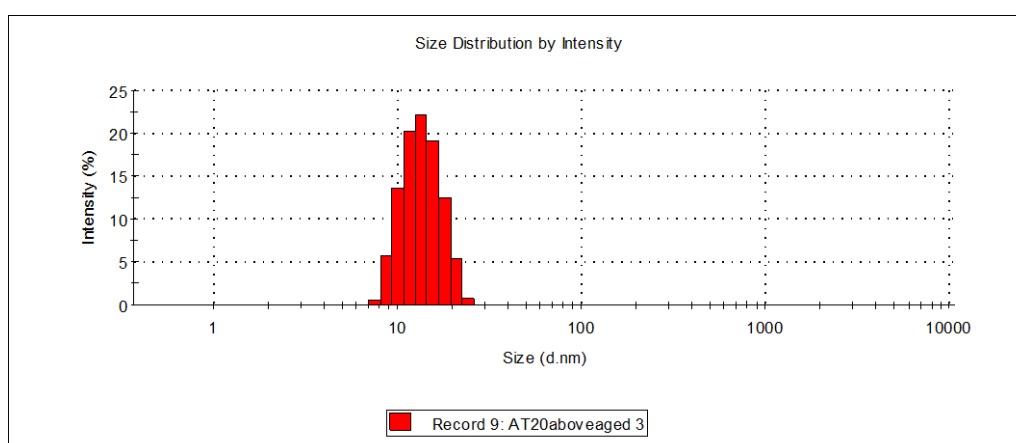
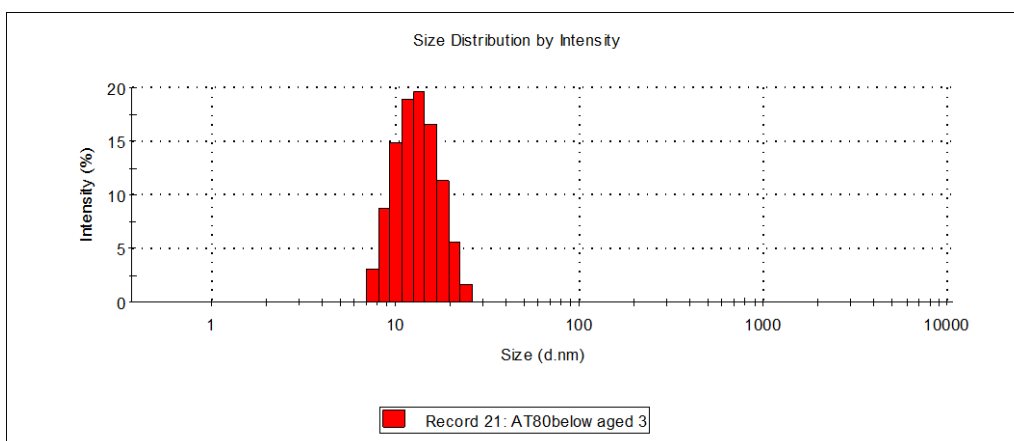
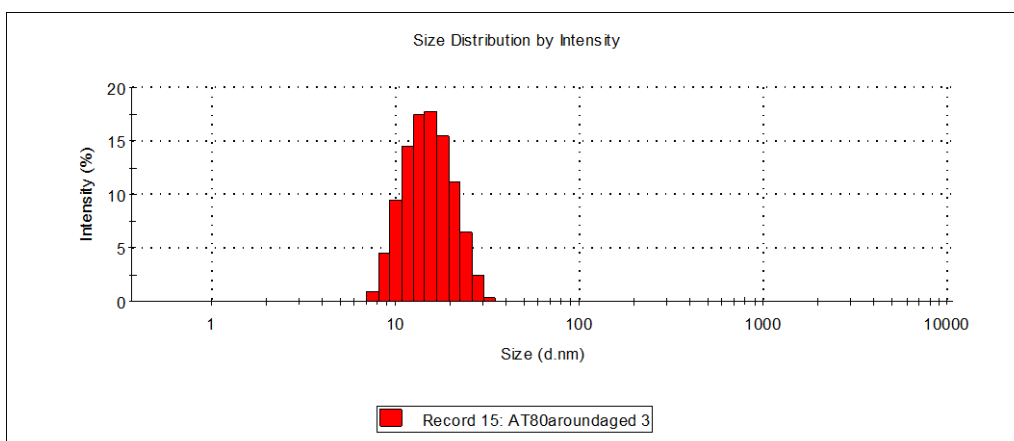


Figure 4.38. Particle size distribution by intensity obtained for aged samples for IgG2 (10 mg/ml) with: (A) Tween 20 below CMC; (B) Tween 20 around CMC; (C) Tween 20 above CMC.

(A)



(B)



(C)

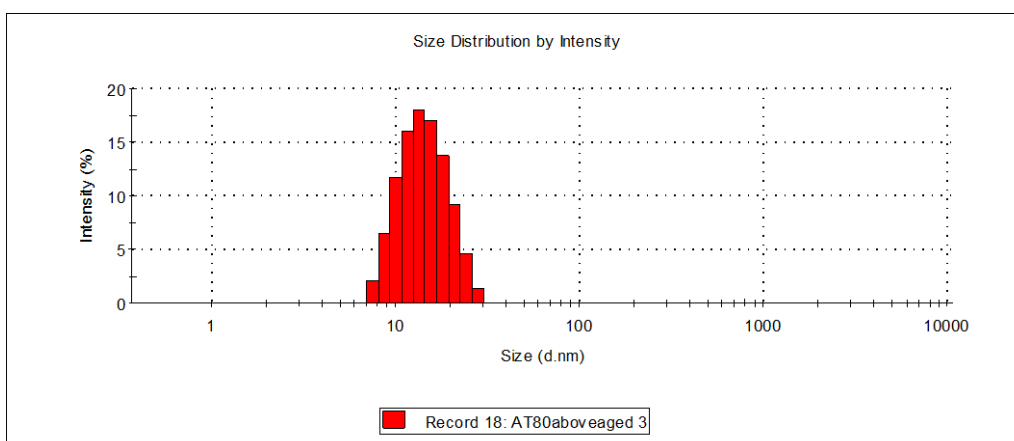
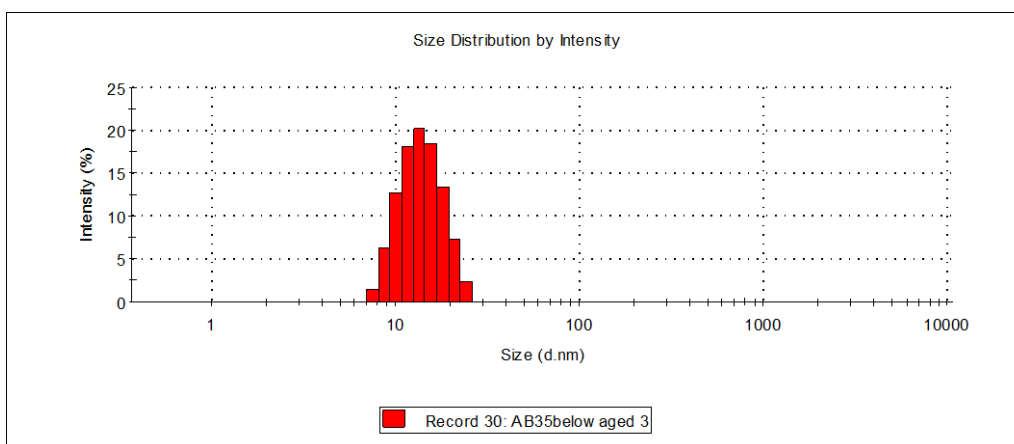
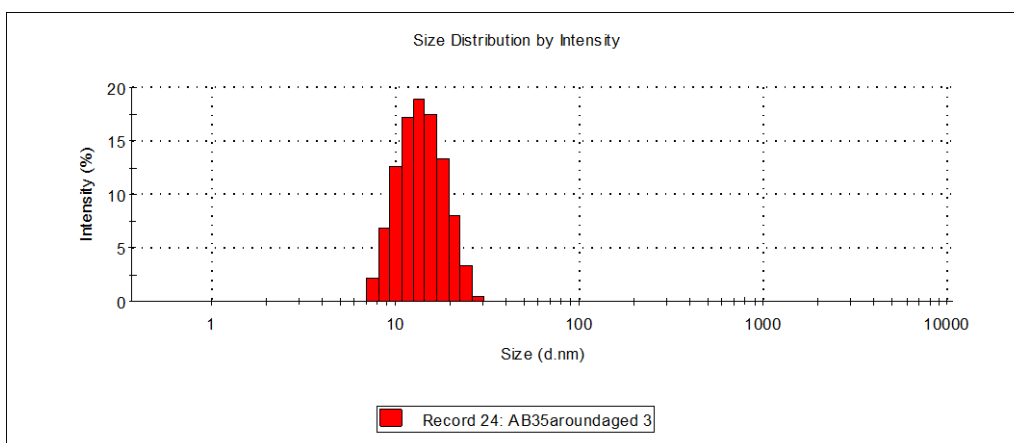


Figure 4.39. Particle size distribution by intensity obtained for aged samples for IgG2 (10 mg/ml) with: (A) Tween 80 below CMC; (B) Tween 80 around CMC; (C) Tween 80 above CMC.

(A)



(B)



(C)

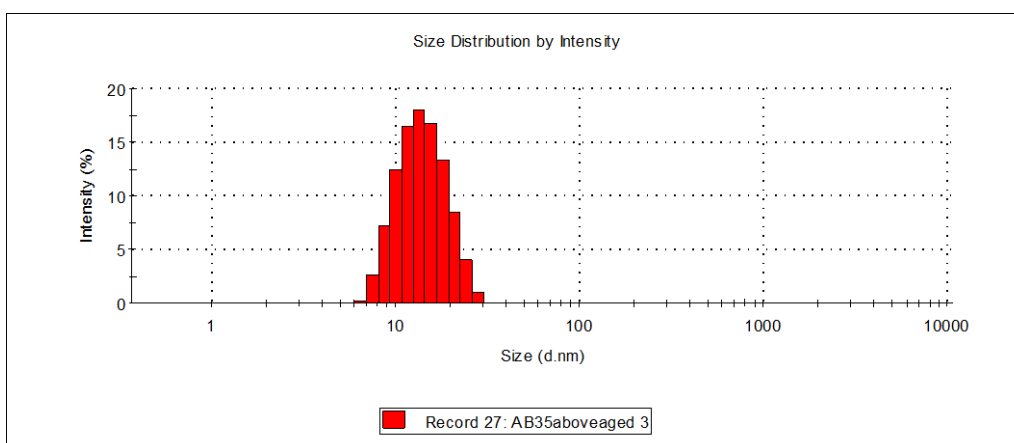
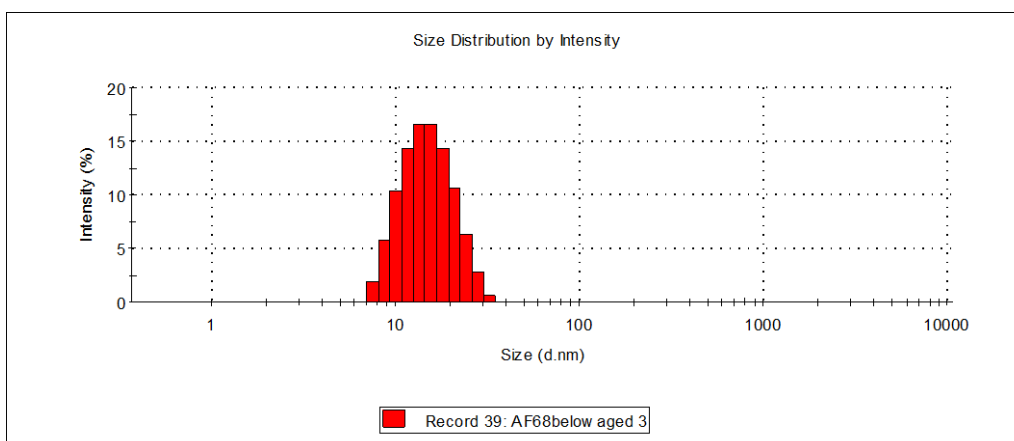
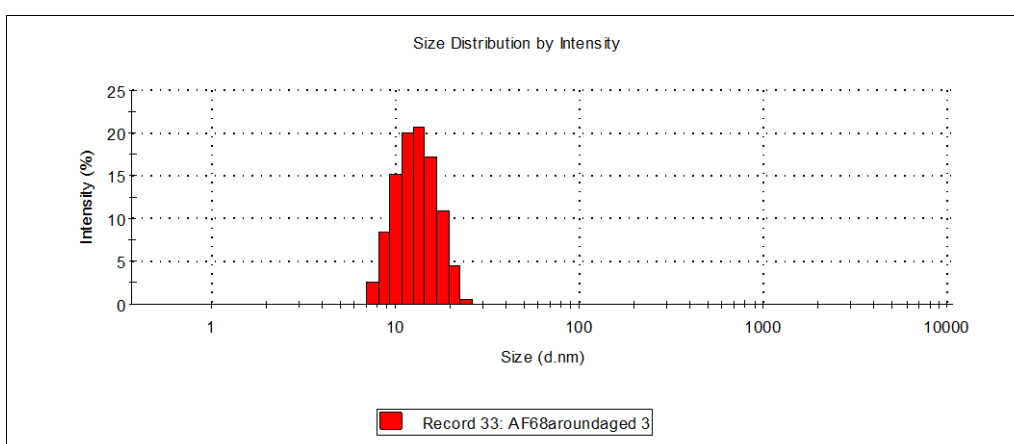


Figure 4.40. Particle size distribution by intensity obtained for aged samples for IgG2 (10 mg/ml) with: (A) Brij 35 below CMC; (B) Brij 35 around CMC; (C) Brij 35 above CMC.

(A)



(B)



(C)

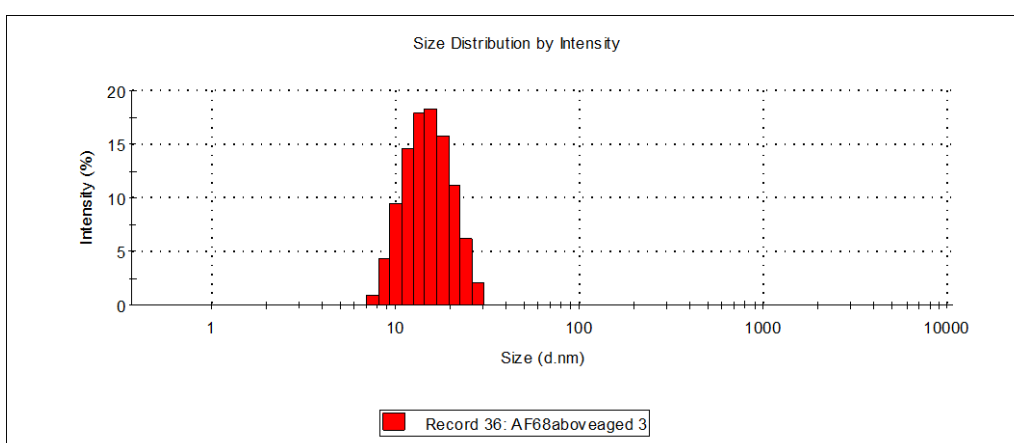


Figure 4.41. Particle size distribution by intensity obtained for aged samples for IgG2 (10 mg/ml) with: (A) Pluronic F-68 below CMC; (B) Pluronic F-68 around CMC; (C) Pluronic F-68 above CMC.

Particle size diameters (nm) of the main peak with greatest intensity for aged IgG2 (10 mg/ml) with below, around and above CMC levels of Tween 20, Tween 80, Brij 35 and Pluronic F-68 surfactants are summarised in Table 4.6 and Figure 4.42.

Table 4.6. Particle size diameter (nm) of the peak with greatest intensity (Peak 1) for aged IgG2 (10 mg/ml) with below, around and above CMC levels of Tween 20, Tween 80, Brij 35 and Pluronic F-68 surfactants.

AGED SAMPLES		PEAK POSITION WITH GREATEST INTENSITY DIAMETER (nm)
IgG2 (10mg/ml)		13.84
Tween 20	below CMC	14.06
	around CMC	14.20
	above CMC	13.86
Tween 80	below CMC	13.55
	around CMC	15.72
	above CMC	14.77
Brij 35	below CMC	14.21
	around CMC	14.33
	above CMC	14.48
Pluronic F-68	below CMC	15.52
	around CMC	13.38
	above CMC	15.60

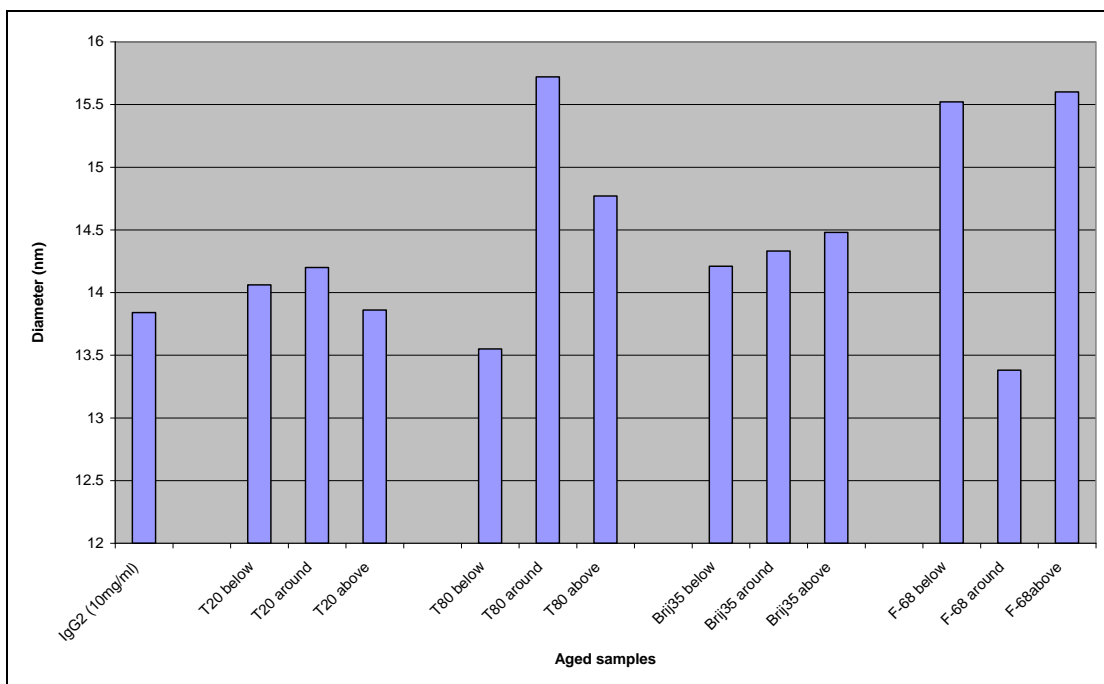


Figure 4.42. Particle size diameter (nm) of the peak with greatest intensity (Peak 1) for aged IgG2 (10 mg/ml) with below, around and above CMC levels of Tween 20, Tween 80, Brij 35 and Pluronic F-68 surfactants.

Analysing particle size diameter of the main peak for aged samples, it can be seen that highest intensity peak diameter in nm was obtained for Tween 80 around (15.72 nm) and Pluronic F-68 above (15.6 nm) comparing to aged IgG2 surfactant free sample. The highest decrease was obtained for Pluronic F-68 around concentrations.

Statistical analysis using a t-test showed that the difference between aged surfactant free IgG2 (10 mg/ml) and Tween 20 below and around CMC, Tween 80, Brij 35, Pluronic F-68 at all CMC levels, was statistically significant at the 95 % level ($P < 0.05$). Analysis between aged surfactant free IgG2 and Tween 20 above CMC showed no statistical significance.

Figure 4.43 illustrates the comparison of the diameter of the main highest intensity peak at below, around and above CMC levels for Tween 20, Tween 80, Brij 35 and Pluronic F-68 surfactants.

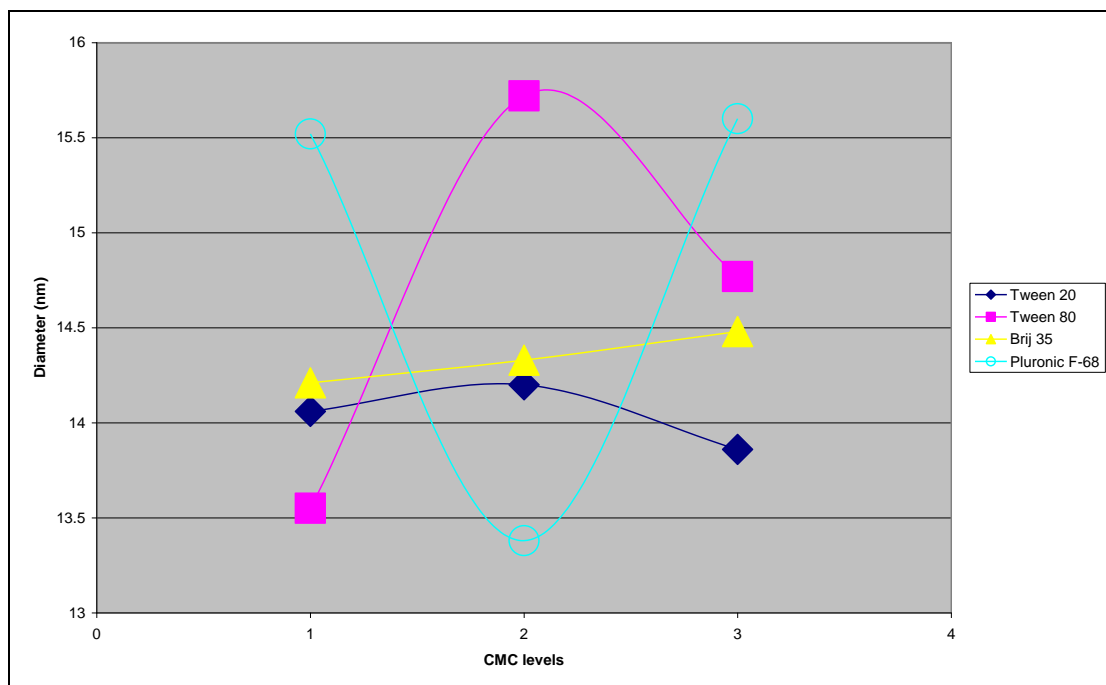


Figure 4.43. A plot of the highest intensity peak diameter (nm) obtained at below (1), around (2) and above (3) CMC levels for aged Tween 20, Tween 80, Brij 35 and Pluronic F-68 surfactants.

Figure 4.43 shows that DLS measured size of all aged surfactant systems at each concentration in relations to their CMC differs. There is a gradual increase in diameter when Brij 35 concentration increases. The presence of Tween 20 and Tween 80 surfactant produced their highest particle size when their concentration was around their CMC. At its highest concentration Pluronic F-68 produced its largest particle size for the aged samples.

4.5 General Discussion

Dynamic Light scattering measurements have been performed to study the effect of different CMC concentrations of Tween 20, Tween 80, Brij 35 and Pluronic F-68 surfactants on bovine serum albumin BSA and immunoglobulin IgG2 particle size.

The DLS results showed that BSA and IgG2 with different surfactants at below, around and above CMC concentrations produced different levels of particle size growth. The reported size of native BSA is 7.83 nm (Yu et al, 2011), which is similar to the 7.69 nm obtained for freshly prepared BSA for this study. BSA with added Tween 20, Tween 80 and Brij 35 surfactants at all concentrations and Pluronic F-68 at below and above its CMC, yielded trimodal distributions with the main peak consistently around 8 nm diameter.

DLS analysis of fresh samples of IgG2 surfactant free produced a bimodal distribution with a main peak at 14.44 nm diameter, which is significantly higher than the 10 nm reported for native IgG (Song et al., 2001, Bermudez et al., 2004). DLS results for the IgG2 in the presence of all four non-ionic surfactants produced a low increase in particle size.

Heat treatment of BSA and IgG2 surfactant free samples and in the presence of Tween 20, Tween 80, Brij 35 and Pluronic F-68 surfactants, led to an increase in the populations of larger particles compared to the freshly prepared samples. Under heat stress, main peak diameter (nm) dramatically increased. For BSA (10 mg/ml) samples it reached 27.2 nm with Tween 80 at concentrations of around CMC, where IgG2 (10 mg/ml) produced a maximum

diameter of 66.1 nm diameter in the presence of Tween 80 at a concentration above its CMC.

On storing BSA (10 mg/ml) and BSA-surfactant samples, the original main peak diminished and larger particles size populations formed compared to freshly prepared and heat stressed solutions. The increased levels of aggregates after storing BSA samples has been previously reported (Krishnan, 2009).

DLS data for aged IgG2-surfactant systems showed a monomodal peak at around 14 nm diameter and was relatively unchanged to that obtained for fresh IgG2 samples with all surfactants.

Compared to BSA, IgG2 did not aggregate under storage conditions. Obviously storing and heat stress bears the potential to generate aggregates and particles, but this depends on protein and surfactant type and concentration (Schmidt, 2009).

Chapter 5

Light Obscuration (HIAC) and Micro-flow Imaging (MFI) applied for subvisible particulate analysis of BSA and Igg2 with Tween 20, Tween 80, Brij 35 and Pluronic F-68 surfactants at below, around and above CMC levels

5.1 Introduction

Recent commentaries have stressed a need for characterizing sub-visible particle populations in protein drug formulations (Carpenter et al., 2008). Particles of primary concern are protein aggregates in the size range from approximately 0.1 μm to 50 μm . A complication in measuring protein particulates in many formulations is the simultaneous presence of other particle types such as silicone oil micro-droplets, air bubbles, and extrinsic contaminants. A measurement method which could isolate different particle sub-populations and allow an accurate characterization and quantification of sub-visible particles in protein formulation is highly desirable. These challenges led to an interest in Light obscuration (HIAC) and Micro-flow imaging (MFI) techniques.

Light obscuration (HIAC) and micro-flow imaging (MFI) are two commercially available particle-counting techniques able to characterize sub-visible particles in the range of 2 μm to 100 μm . Both methods have been recently reviewed (Narhi et al., 2009; Mahler et al, 2009) and used in work summarized in recent publications to study protein solutions (Kiese et al., 2010; Tyagi et al., 2009; Demeule et al, 2010; Sharma et al., 2010; Wuchner et al 2010). Micro-flow imaging has received a lot of attention for the characterization of protein formulations in the past few years (Sharma et al., 2010; Wuchner et al., 2010), while light obscuration analysis showed promising results for the quantification of sub-visible particles in carefully chosen conditions (Ives et al, 2007).

The use of Light obscuration and MFI for characterizing sub-visible particles in protein formulations has been applied to a variety of formulation and aggregate types which might be encountered in the development and manufacturing of bio-pharmaceuticals. Mechanistic approaches have been lacking.

5.2 Objective

The main objective is to characterize and quantify particles in BSA and IgG2 surfactant free solutions, and in BSA and IgG2 solutions with Tween 20, Tween 80, Brij 35 and Pluronic F-68 surfactants present at concentrations below, around and above their CMC levels, using light obscuration (HIAC) and micro-flow imaging (MFI) measurements.

5.3 Experimental

5.3.1 Light obscuration (HIAC) measurements

The concentration of BSA and IgG2 samples used in HIAC experiments was 5 mg/ml. All HIAC measurements were performed as described in Chapter 2, Section 2.2.5.

5.3.2 Micro-Flow Imaging (MFI) measurements

Micro-flow imaging (MFI) measurements were performed as described in Chapter 2, section 2.2.6. The concentration of BSA and IgG2 samples used in MFI experiments was 10 mg/ml.

5.4 Results and Discussion

5.4.1 Light Obscuration (HIAC) measurements

5.4.1.1 Light Obscuration measurements for fresh, heated and aged BSA surfactant free and BSA with Tween 20, Tween 80, Brij 35 and Pluronic F-68 surfactants at below, around and above CMC levels

Light obscuration (HIAC) analysis assesses the size of individual sub-visible particles and provides a particle size distribution.

Figure 5.1 illustrates particle concentration per ml measured for fresh, heated and aged BSA samples (See Chapter 2, Section 2.2 for preparation of samples).

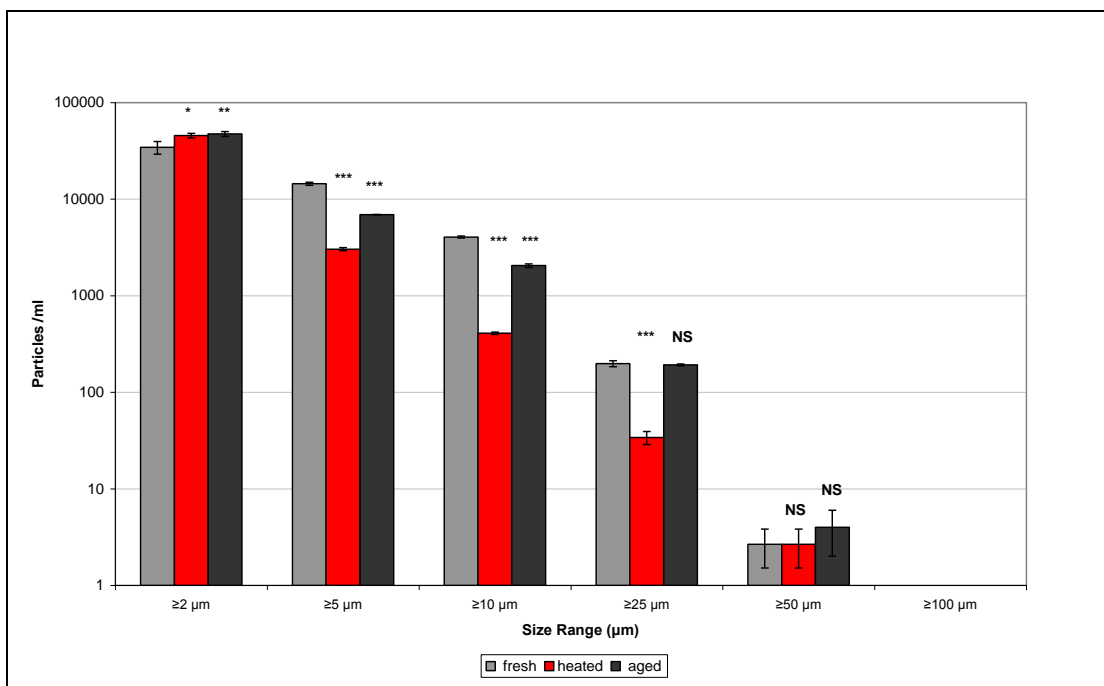


Figure 5.1. Particle concentrations measured by HIAC for fresh, heated and aged BSA samples. Data are expressed as the mean \pm Std. Deviation. * $P < 0.05$, ** $P < 0.01$, * $P < 0.001$; significant difference in particles per ml compared with fresh BSA samples.**

From Figure 5.1, HIAC analysis shows that heat stressed and aged BSA surfactant free formulations produced greater levels in terms of the amount of particles per ml greater than or equal to 2 μm compared to that determined for fresh BSA samples.

A slight increase in the number of particles $\geq 2 \mu\text{m}$ is detectable for heated BSA solutions, whereas, for size ranges $\geq 5 \mu\text{m}$, $\geq 10 \mu\text{m}$ and $\geq 25 \mu\text{m}$, heating did not induce an increase in the number of particles detected compared to fresh and aged BSA samples.

The total number of particles greater than or equal to 5 μm , 10 μm and 25 μm , respectively measured after storage (6913.3 ± 34.4 particles $\geq 5 \mu\text{m}$, 2050.7 ± 88.6 particles $\geq 10 \mu\text{m}$, 192.0 ± 4.0 particles $\geq 25 \mu\text{m}$ per ml) exceeds the number of particles of the same size determined after heat

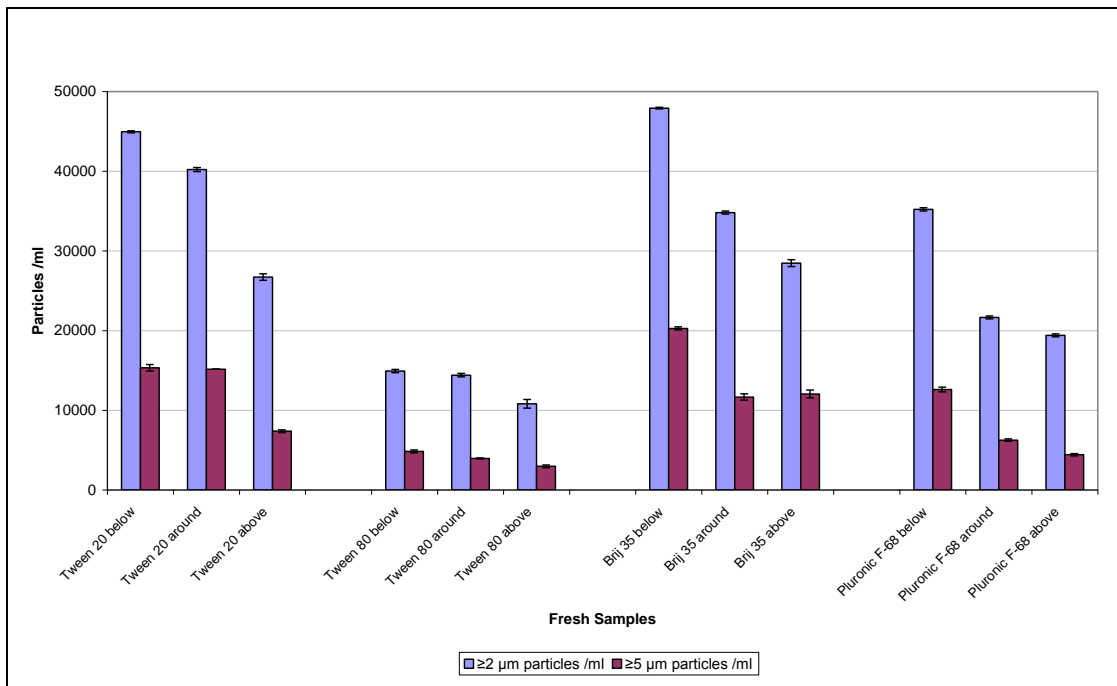
stress (3035.3 ± 114.3 particles $\geq 5 \mu\text{m}$, 408.0 ± 11.1 particles $\geq 10 \mu\text{m}$, 34.0 ± 5.3 particles $\geq 25 \mu\text{m}$ per ml).

One-way ANOVA analysis showed a significant effect of heat treatment and storage on the number of particles per ml at the size ranges of $\geq 2 \mu\text{m}$, $\geq 5 \mu\text{m}$, $\geq 10 \mu\text{m}$ and $\geq 25 \mu\text{m}$. Post-hoc tests, Bonferroni correction showed a significant increase in the number of particles per ml for the size range $\geq 2 \mu\text{m}$ at 0.05 level ($P < 0.05$) for heated samples and at 0.01 level ($P < 0.01$) for aged samples when compared to fresh BSA samples.

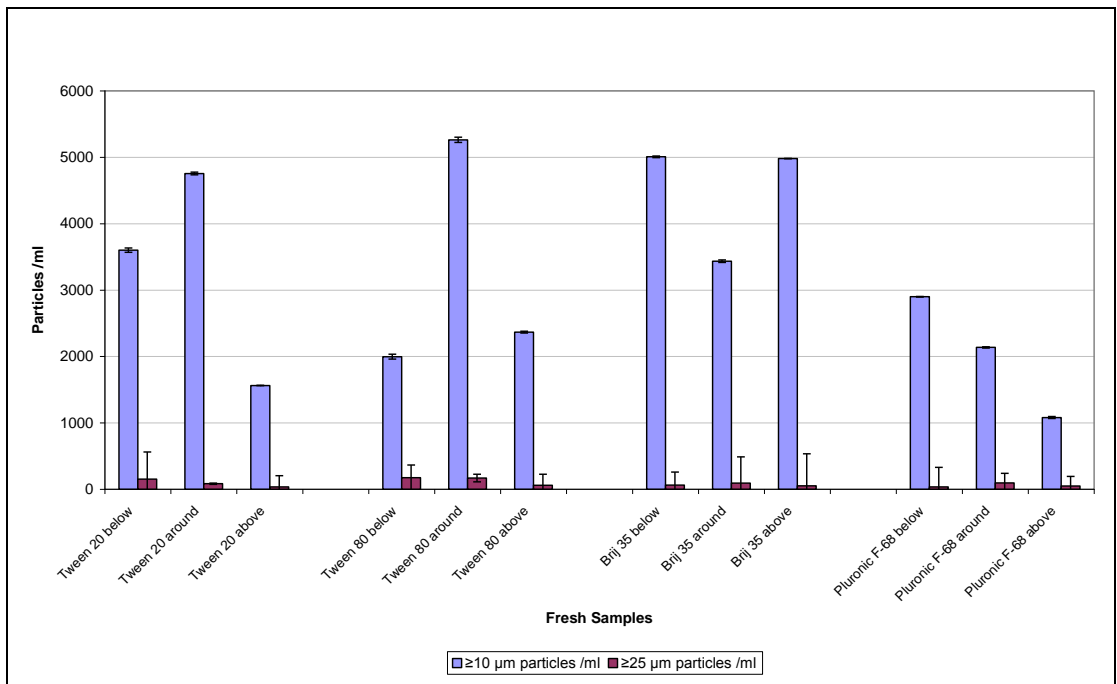
For the $\geq 5 \mu\text{m}$ and the $\geq 10 \mu\text{m}$ size range, Bonferroni statistical results showed that the mean decrease is significant at 0.001 level ($P < 0.001$) for both heated and aged BSA samples. At the size range $\geq 25 \mu\text{m}$ heated BSA samples showed a statistically significant decrease ($P < 0.001$), whereas aged BSA samples produced no statistically different particle numbers compared to fresh ones. Also at the size range $\geq 50 \mu\text{m}$ there was no significant difference in the number of particles per ml between samples (Figure 5.1).

Figure 5.2 shows number of particles in a size range of $\geq 2 \mu\text{m}$, $\geq 5 \mu\text{m}$, $\geq 10 \mu\text{m}$, $\geq 25 \mu\text{m}$, $\geq 50 \mu\text{m}$ and $\geq 100 \mu\text{m}$ per ml measured by Light Obscuration for fresh BSA with Tween 20, Tween 80, Brij 35 and Pluronic F-68 surfactants at below, around and above their CMC levels.

(A)



(B)



(C)

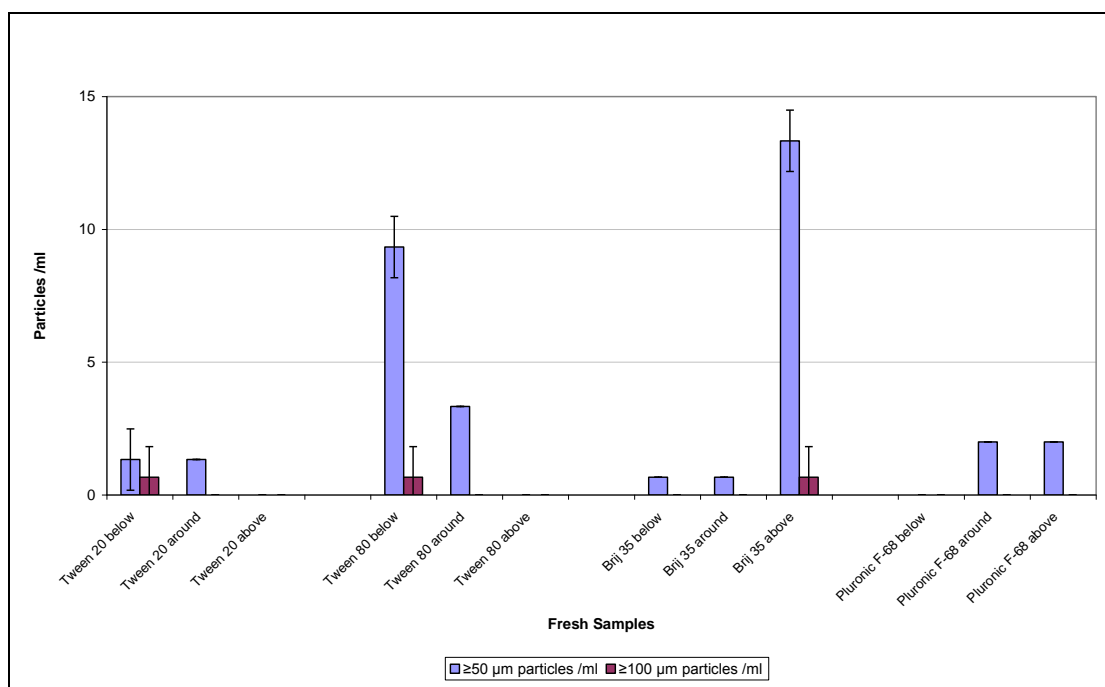


Figure 5.2. Particle concentrations in size ranges: (A) $\geq 2 \mu\text{m}$ and $\geq 5 \mu\text{m}$, (B) $\geq 10 \mu\text{m}$ and $\geq 25 \mu\text{m}$, (C) $\geq 50 \mu\text{m}$ and $\geq 100 \mu\text{m}$ per ml measured by HIAC for fresh BSA samples with Tween 20, Tween 80, Brij 35 and Pluronic F-68 surfactants at below, around and above CMC levels. Data are expressed as the mean \pm Std. Deviation.

In fresh formulations of BSA containing Tween 20 at concentrations below and around CMC, Brij 35 at below and around its CMC and Pluronic F-68 at below its CMC, an increase in the number of particles $\geq 2 \mu\text{m}$ is detectable. For samples containing Tween 20 above its CMC, for all Tween 80 levels, for Brij 35 above its CMC, and for Pluronic F-68 at around and above its CMC, the number of particles at this size range has decreased (Figure 5.2 A).

BSA formulations containing Tween 20 at below and around its CMC and formulations containing Brij 35 below its CMC showed an increase in the number of particles per ml greater than or equal to $10 \mu\text{m}$ (compared to fresh surfactant free BSA samples shown in Figure 5.1).

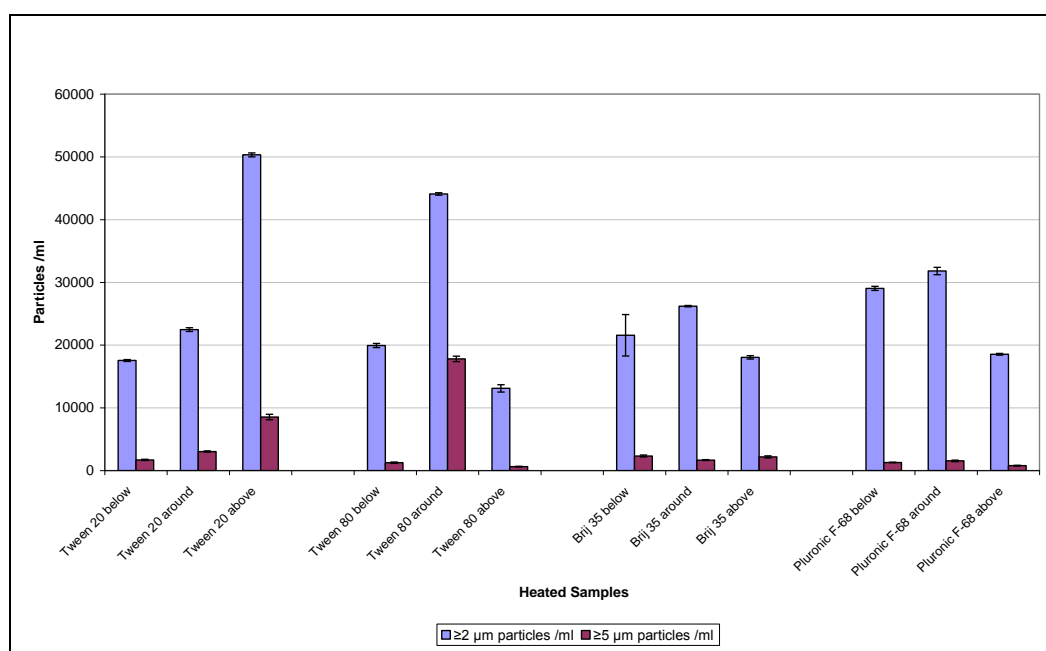
Formulations of BSA with Tween 20 and Tween 80 levels around their CMC and formulations of Brij 35 below its CMC, produced a slight increase in the number of particles $\geq 10 \mu\text{m}$ (Figure 5.2 A).

The number of particles per ml greater than or equal to $25 \mu\text{m}$, $50 \mu\text{m}$ and $100 \mu\text{m}$, in protein solutions of BSA with all four surfactants at below, around and above CMC levels has decreased by particle count compared to freshly prepared BSA surfactant free samples (Figure 5.2 B and C).

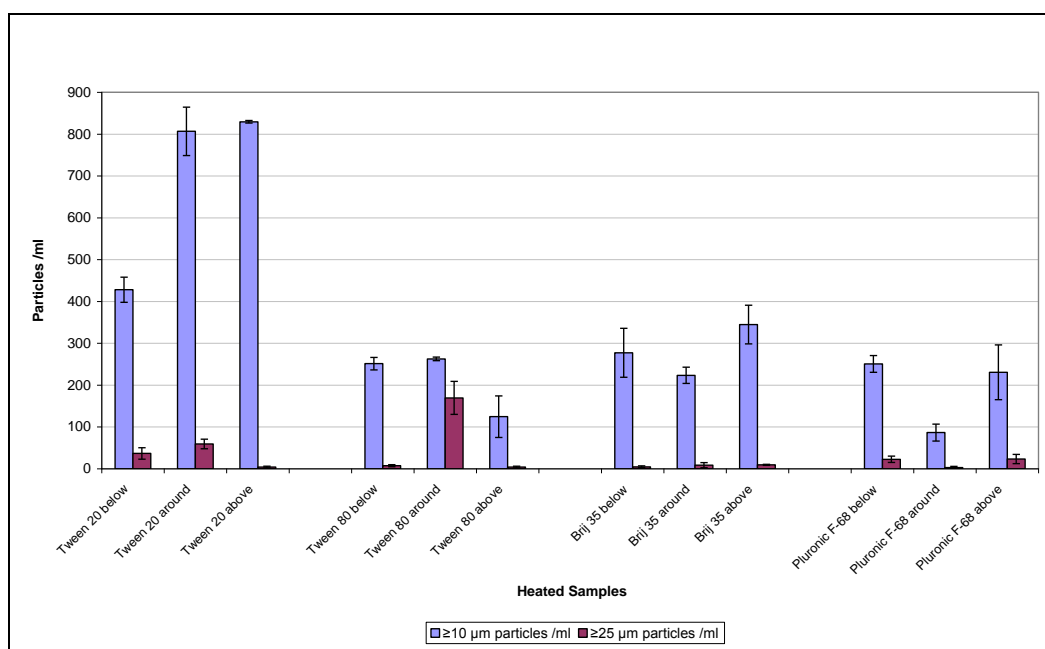
In general, freshly prepared BSA solutions with Tween 80 at all CMC levels contained significantly lower levels of particles than BSA solutions containing Tween 20, Brij 35 and Pluronic F-68 surfactants and surfactant free BSA samples (Figure 5.2).

Figure 5.3 shows particle count per ml measured for heated BSA with Tween 20, Tween 80, Brij 35 and Pluronic F-68 surfactants at below, around and above their CMC levels.

(A)



(B)



(C)

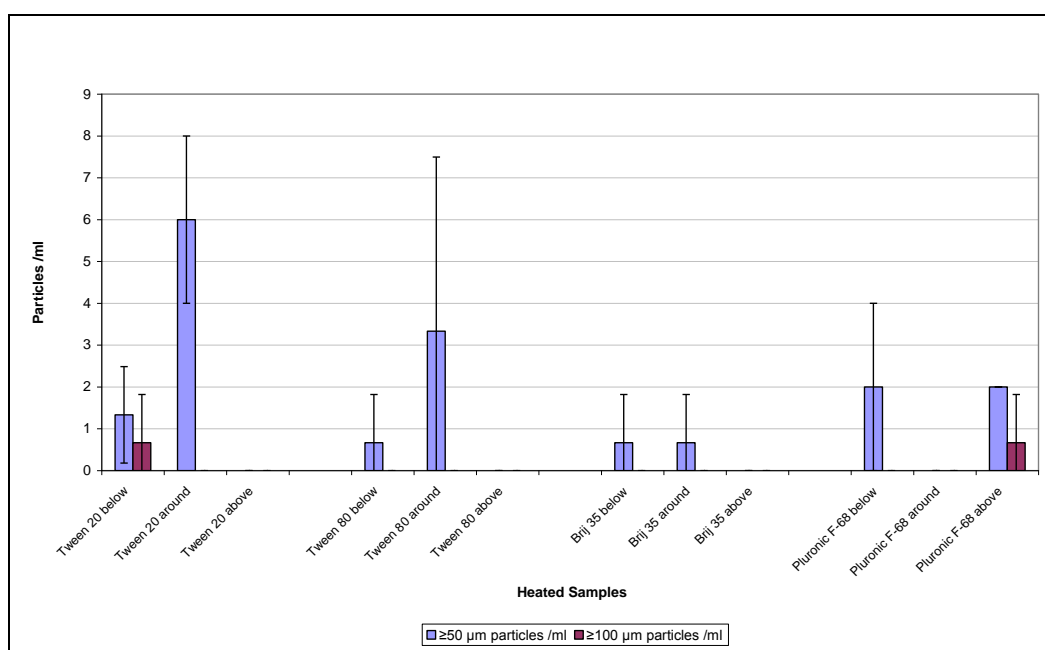


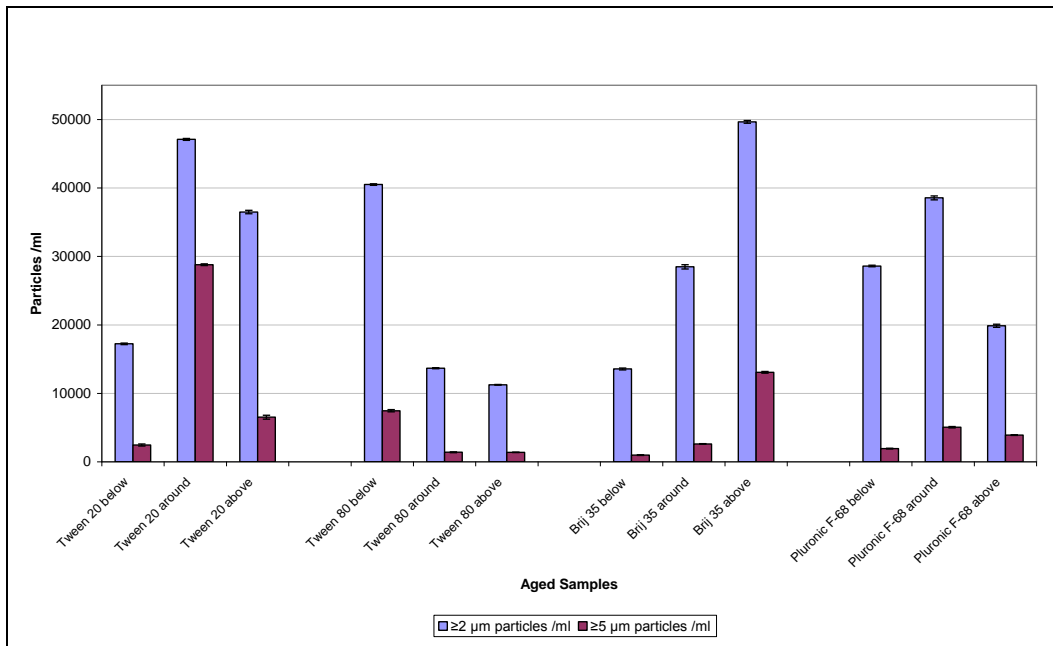
Figure 5.3. Particle concentrations in size ranges: (A) $\geq 2 \mu\text{m}$ and $\geq 5 \mu\text{m}$, (B) $\geq 10 \mu\text{m}$ and $\geq 25 \mu\text{m}$, (C) $\geq 50 \mu\text{m}$ and $\geq 100 \mu\text{m}$ per ml measured by HIAC for heated BSA samples with Tween 20, Tween 80, Brij 35 and Pluronic F-68 surfactants at below, around and above CMC levels. Data are expressed as the mean \pm Std. Deviation.

Heat stressed BSA formulations show an increase in the number of particles per ml greater than or equal to 2 μm with Tween 20 surfactant above CMC level. Also at the particle size range $\geq 5 \mu\text{m}$, samples of BSA with Tween 20 above and with Tween 80 around their CMC have increased particle counts compared to other surfactants and heat stressed surfactant free BSA (Figure 5.3 A; Figure 5.1).

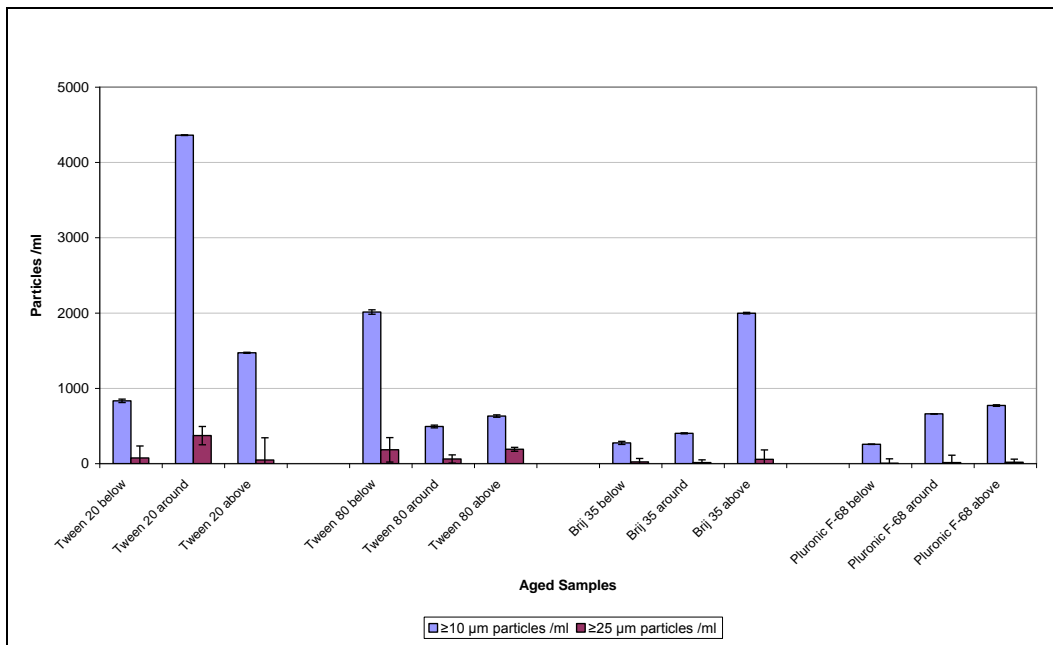
Heated BSA formulations with Tween 20 levels below, around and above its CMC show an increase in the number of particles greater than or equal to 10 μm compared to other surfactants.

At particle size $\geq 25 \mu\text{m}$, heated BSA with Tween 20 below (36.7 ± 13.6 particles) and around its CMC (59.3 ± 11.4 particles), and with Tween 80 around its CMC (169.3 ± 39.5 particles) produced the highest level of particles per ml (Figure 5.3 B). For particles $\geq 50 \mu\text{m}$ the formulation containing Tween 20 around (6.0 ± 2.0 particles) its CMC and for the sample with Tween 80 around its CMC (3.3 ± 4.2 particles) both produced an increase in particle count compared to the other surfactants and heated BSA surfactant free samples (Figure 5.3 C).

(A)



(B)



(C)

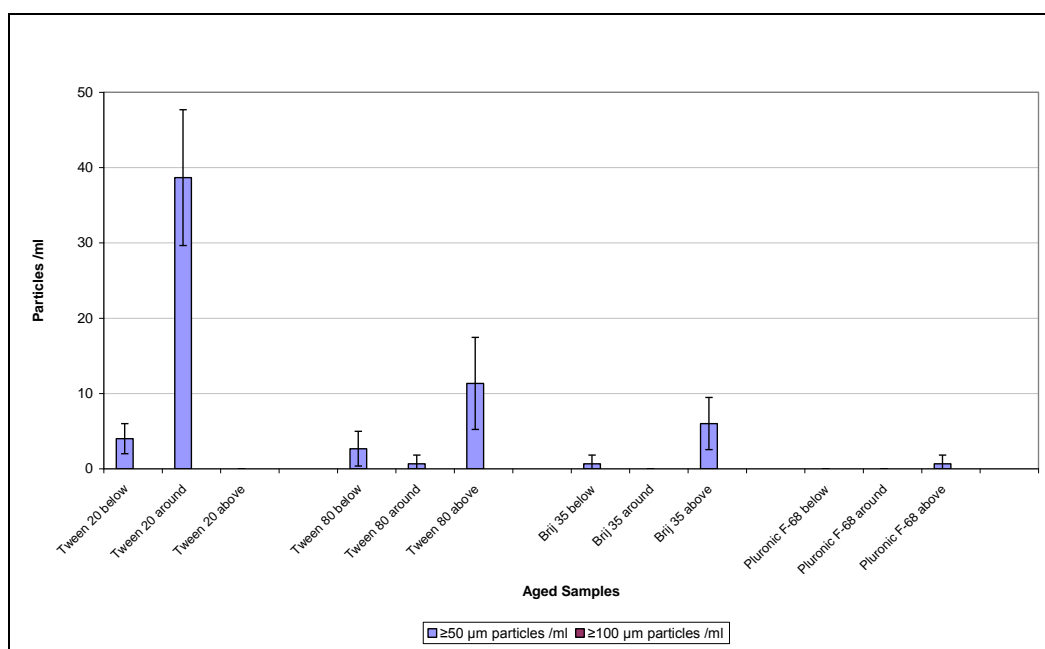


Figure 5.4. Particle concentrations in size ranges: (A) $\geq 2 \mu\text{m}$ and $\geq 5 \mu\text{m}$, (B) $\geq 10 \mu\text{m}$ and $\geq 25 \mu\text{m}$, (C) $\geq 50 \mu\text{m}$ and $\geq 100 \mu\text{m}$ per ml measured by HIAC for aged BSA samples with Tween 20, Tween 80, Brij 35 and Pluronic F-68 surfactants at below, around and above CMC levels. Data are expressed as the mean \pm Std. Deviation.

Figure 5.4 shows that in aged formulations of BSA containing all four surfactants at their different CMC levels, a decrease in the number of particles $\geq 2 \mu\text{m}$ was detected compared to aged surfactant-free BSA.

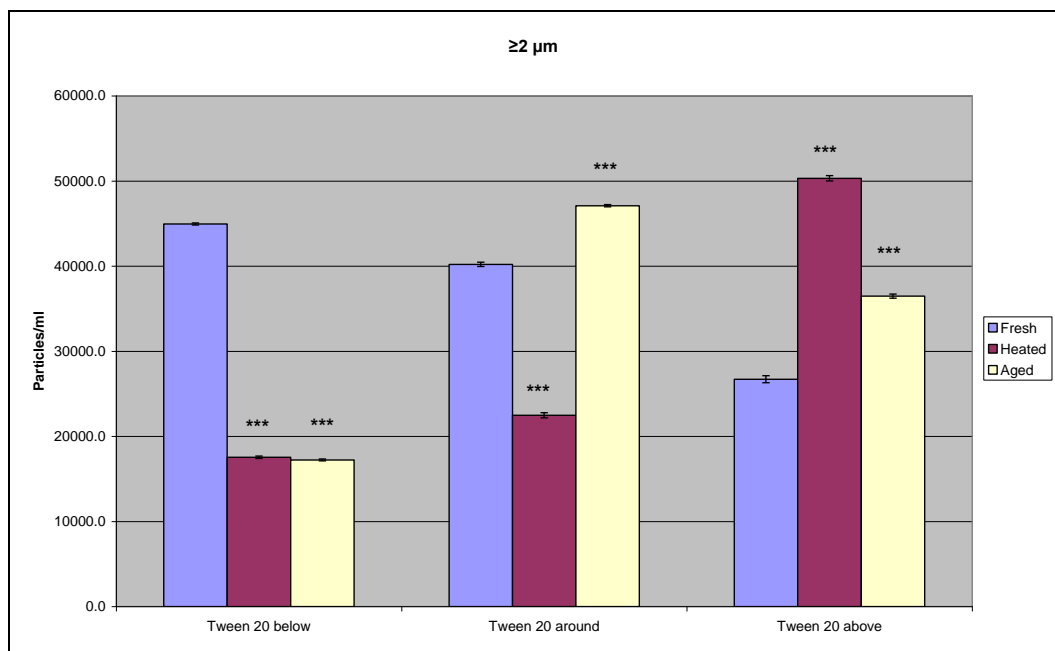
The number of particles $\geq 5 \mu\text{m}$ measured for aged BSA with Tween 20 around CMC, Tween 80 below CMC and Brij 35 above CMC has a noticeable increase (Figure 5.4 A). Considering particle counts for size ranges of $\geq 10 \mu\text{m}$ and $\geq 25 \mu\text{m}$, the aged formulation with Tween 20 at around its CMC has significantly a higher number of particles compared to the other surfactants and surfactant free aged BSA formulations (Figure 5.4 B).

Figure 5.4 (C) shows that particle count $\geq 50 \mu\text{m}$ for aged BSA with Tween 20 around its CMC and for Tween 80 above its CMC exceeded that of the aged surfactant free BSA solution shown in Figure 5.1.

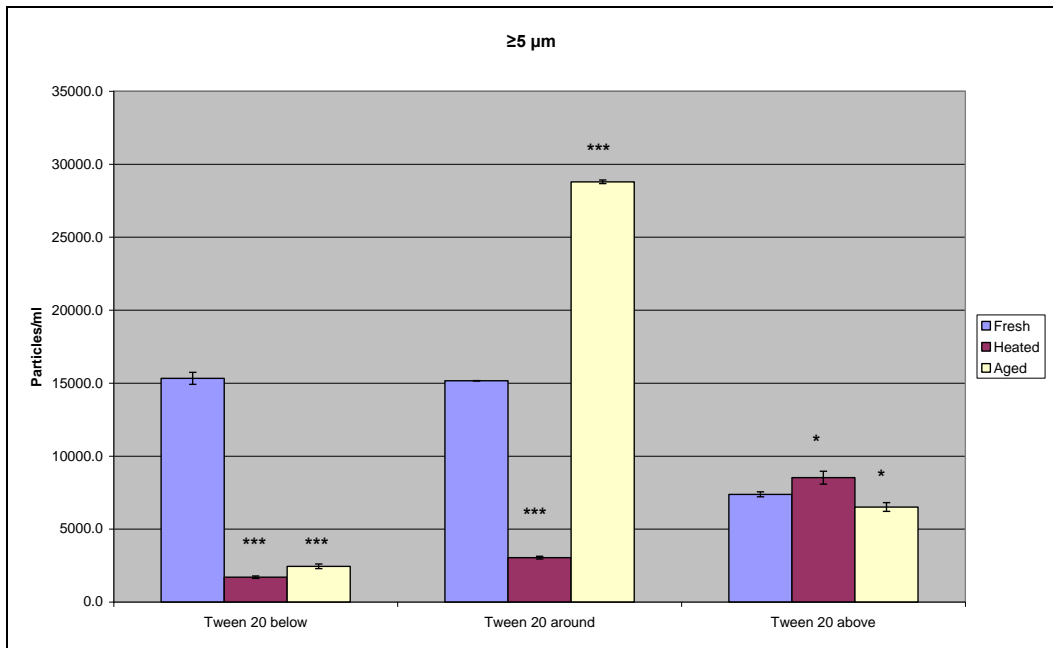
It can be clearly seen that particle levels vary for the fresh, heated and aged BSA samples and for the Tween 20, Tween 80, Brij 35 and Pluronic F-68 surfactant formulations (Figures 5.2 – 5.4).

Figures 5.5 to 5.8 illustrate how the particle counts per ml for the different size ranges of $\geq 2 \mu\text{m}$, $\geq 5 \mu\text{m}$, $\geq 10 \mu\text{m}$, $\geq 25 \mu\text{m}$, $\geq 50 \mu\text{m}$ and $\geq 100 \mu\text{m}$ change after heat stress and aging of BSA solutions with each surfactant.

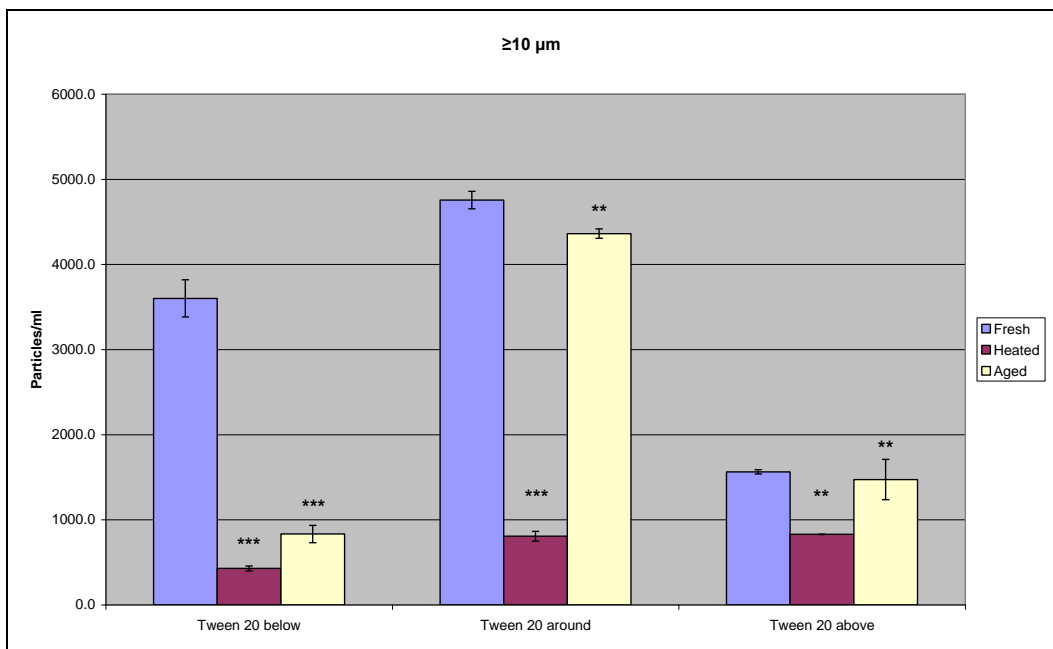
(A)



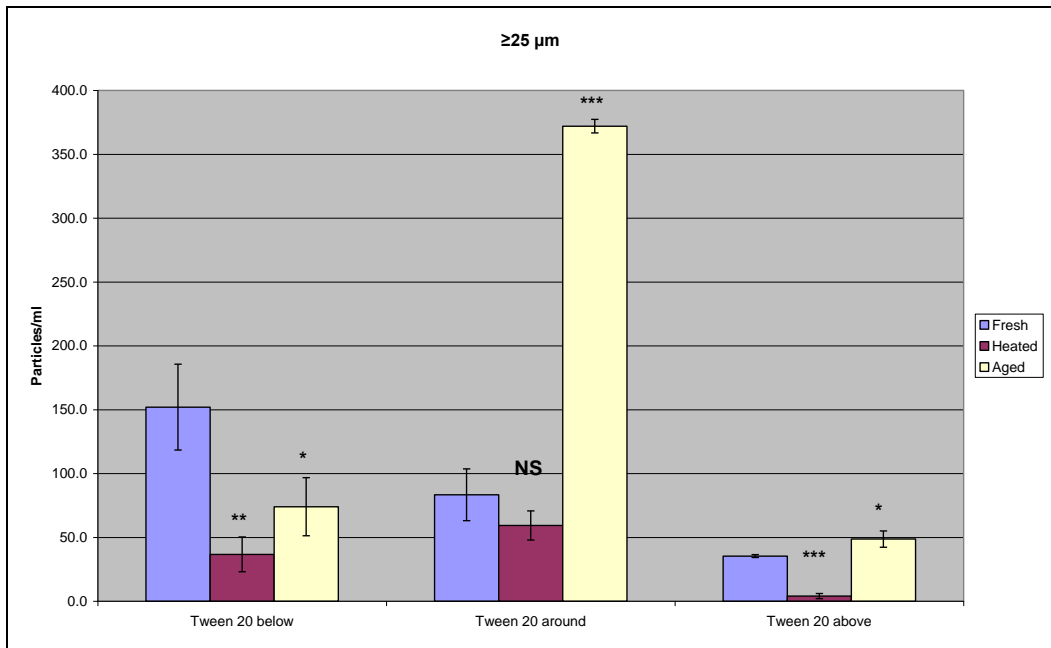
(B)



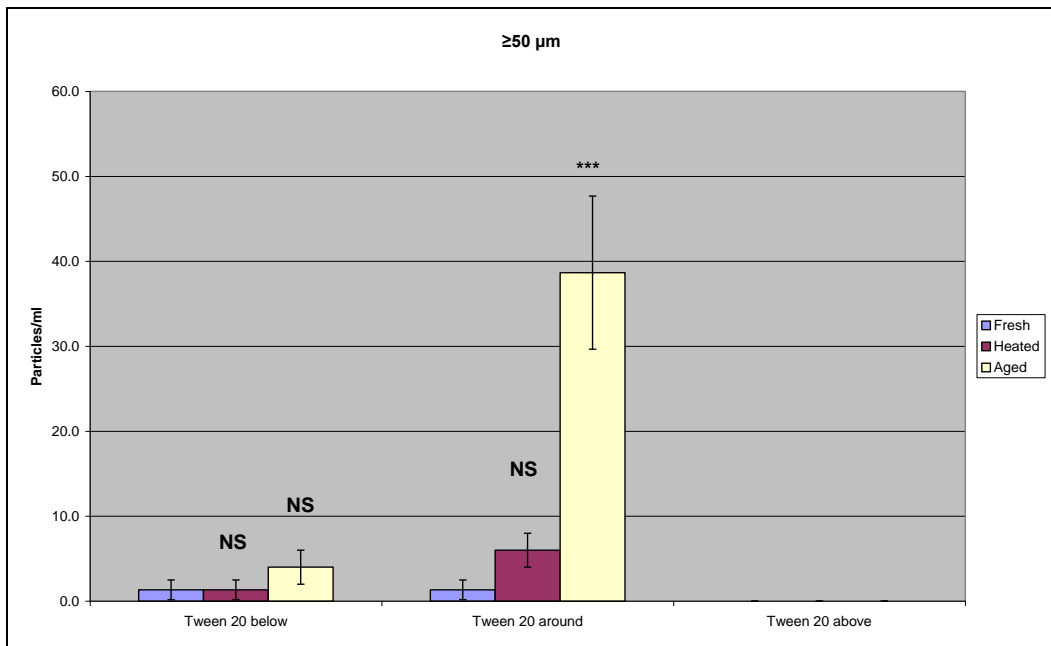
(C)



(D)



(E)



(F)

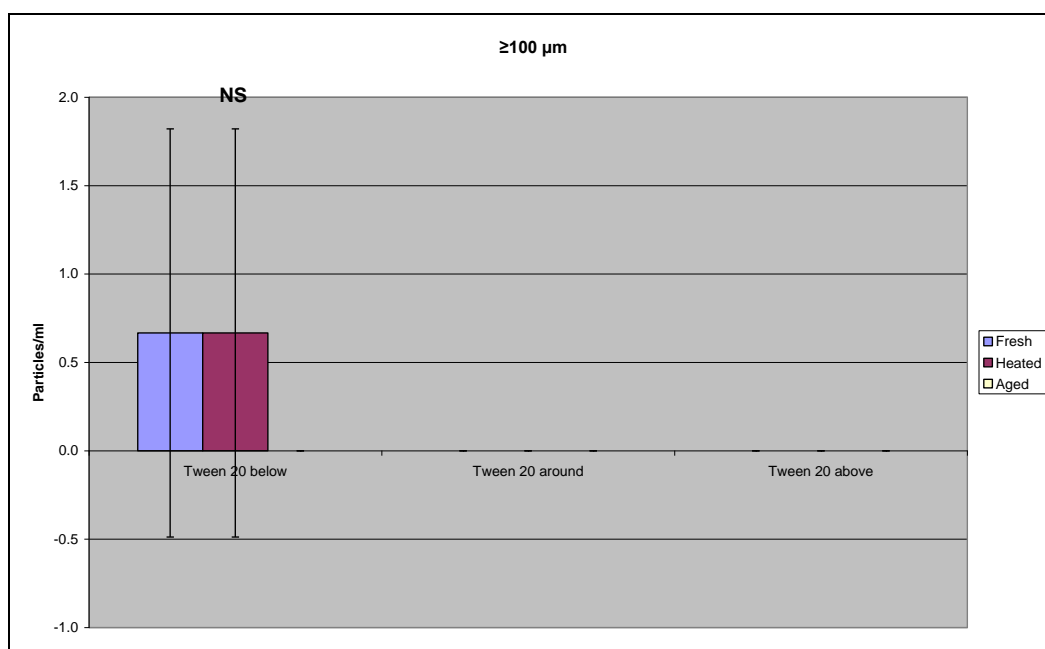


Figure 5.5. Particle concentrations at size ranges of: (A) $\geq 2 \mu\text{m}$, (B) $\geq 5 \mu\text{m}$, (C) $\geq 10 \mu\text{m}$, (D) $\geq 25 \mu\text{m}$, (E) $\geq 50 \mu\text{m}$ and (F) $\geq 100 \mu\text{m}$ measured by HIAC for fresh, heated and aged BSA with Tween 20 at below, around and above its CMC. Data are expressed as the mean \pm Std. Deviation. * $P < 0.05$, ** $P < 0.01$, * $P < 0.001$; significant difference in particles per ml compared with fresh BSA with Tween 20 samples.**

One-way ANOVA analysis, Bonferroni correction showed a significant effect of heat stress and aging samples for BSA with Tween 20 surfactant at below, around and above its CMC for particle counts $\geq 2 \mu\text{m}$. The mean difference is significant ($P < 0.001$) compared to the fresh samples (Figure 5.5 A).

Considering the particle count per ml of particles $\geq 5 \mu\text{m}$, statistical analysis showed that the difference is significant ($P < 0.001$) between fresh and heated, and between fresh and aged BSA with Tween 20 levels belows and around CMC. The mean difference is also significant ($P < 0.05$) for BSA with

Tween 20 concentrations above CMC. Figure 5.5 (B) illustrates these findings.

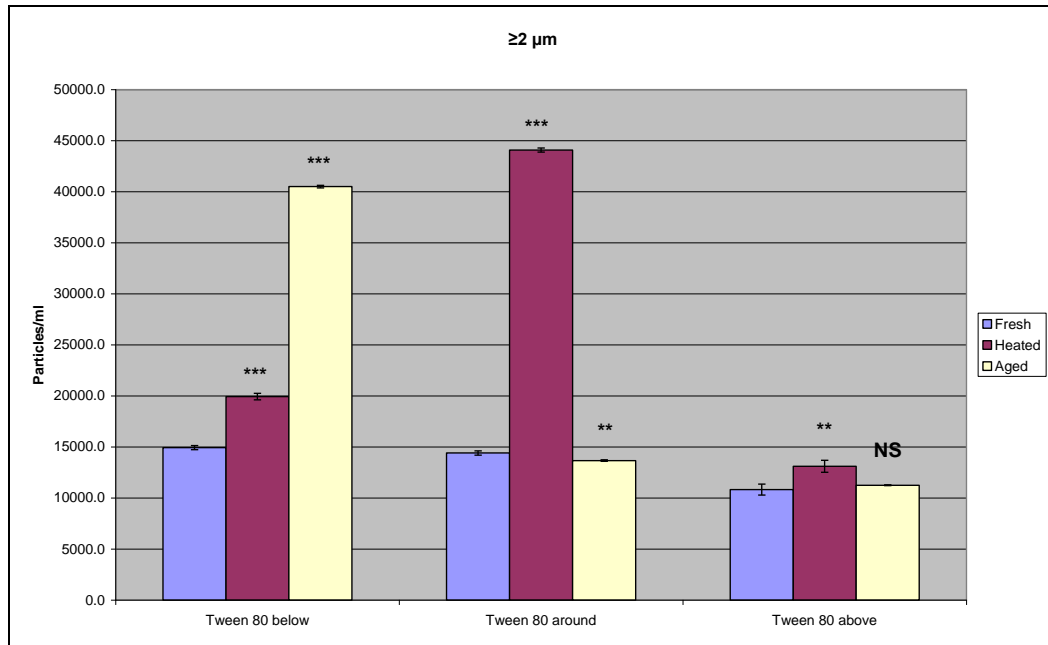
Similar statistical analysis was obtained for the particle counts per ml, sized at $\geq 10 \mu\text{m}$. The statistical difference between fresh and heat stressed, fresh and aged BSA with Tween 20 below its CMC was significant ($P < 0.001$). For the BSA sample with Tween 20 at around its CMC, a significant difference between fresh and heated samples was observed ($P < 0.001$) and also was observed between fresh and aged samples ($P < 0.01$). Higher CMC concentrations of Tween 20 with BSA showed statistical difference at 0.01 level ($P < 0.01$) between fresh and heated, fresh and aged samples (Figure 5.5 C).

For particle count data of size $\geq 25 \mu\text{m}$, the Bonferroni test showed that the difference in particle count is significant ($P < 0.01$) between fresh and heated BSA with Tween 20 below its CMC and also significant ($P < 0.05$) between fresh and aged BSA with Tween 20 below its CMC. No significant difference in particle count was detected between fresh and heated samples of BSA with Tween 20 around its CMC. The mean difference was significant at 0.05 level ($P < 0.05$) between fresh and aged samples of BSA with Tween 20 around its CMC. One-way ANOVA, Bonferroni test, showed statistical difference ($P < 0.001$) between fresh and heated samples particle count and between fresh and aged BSA ($P < 0.05$) particle count for the BSA sample containing Tween 20 above its CMC (Figure 5.5 D).

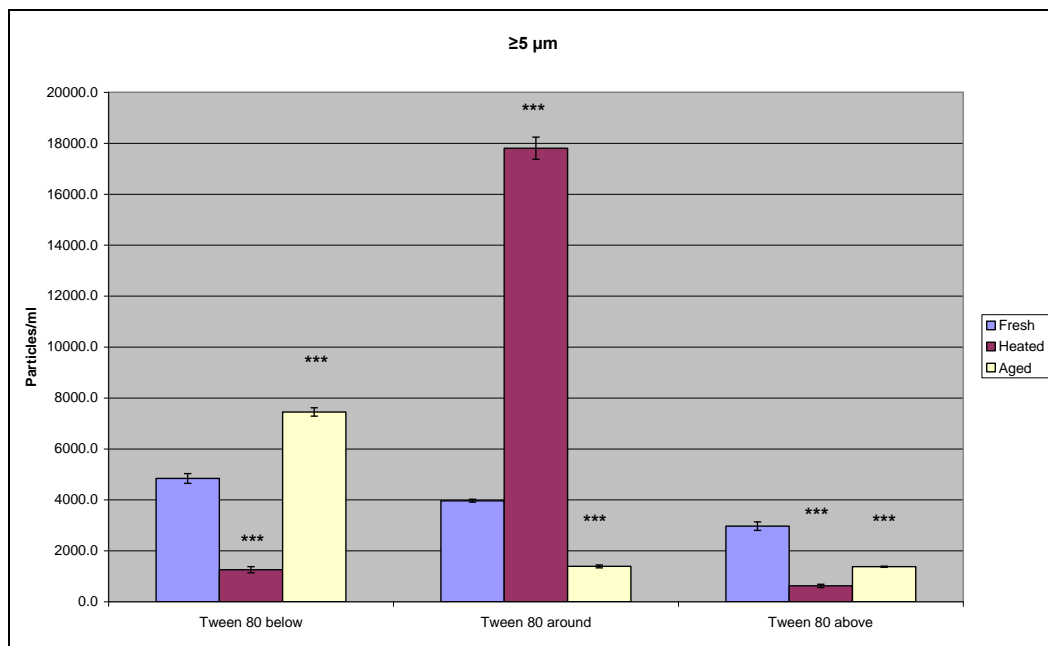
For particle sizes $\geq 50 \mu\text{m}$ and $\geq 100 \mu\text{m}$ no statistical difference in particle count was detected between fresh and heat stressed, and between fresh and aged BSA samples with Tween 20 present below its CMC. Post-hoc analysis

showed no statistical difference between fresh and heated BSA samples with Tween 20 at around its CMC ($P>0.05$) at these size ranges. Particle counts significantly different ($P<0.001$) were calculated between heated and aged BSA with Tween 20 around its CMC for particles $\geq 50 \mu\text{m}$ (Figure 5.5 F).

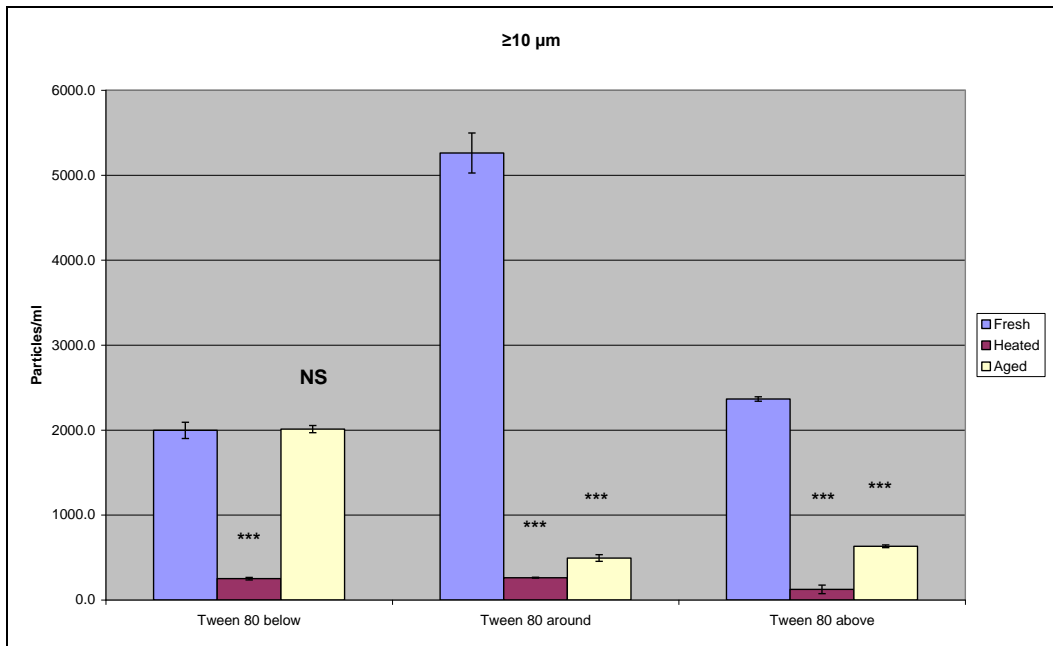
(A)



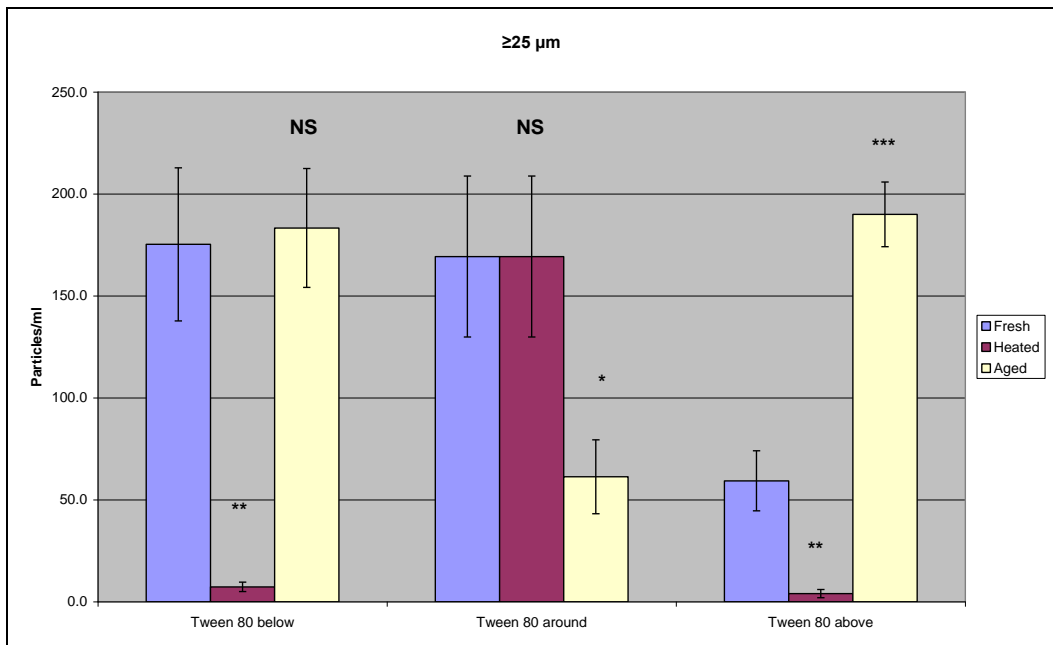
(B)



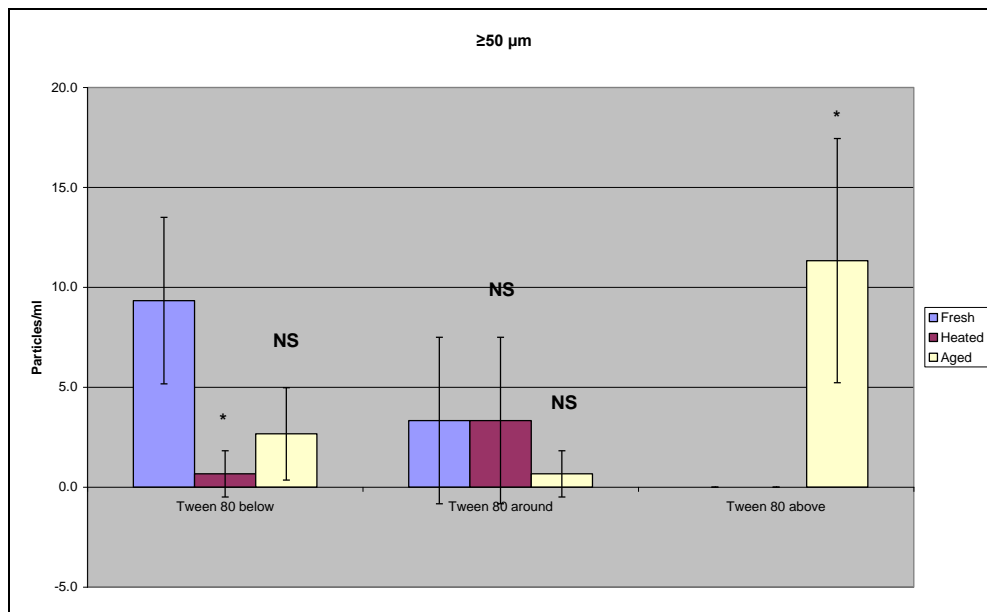
(C)



(D)



(E)



(F)

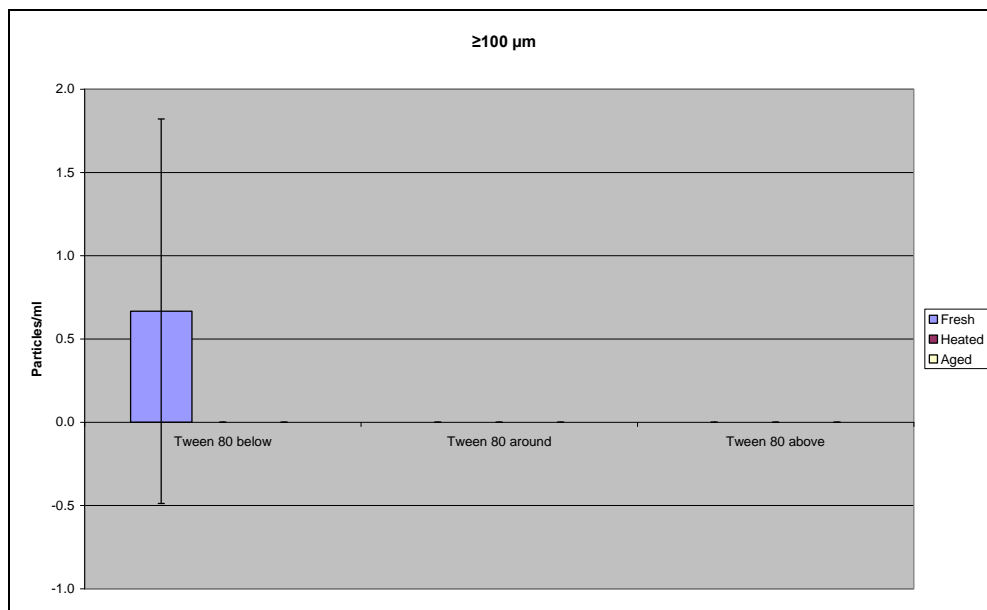


Figure 5.6. Particle concentrations at size ranges of: (A) $\geq 2 \mu\text{m}$, (B) $\geq 5 \mu\text{m}$, (C) $\geq 10 \mu\text{m}$, (D) $\geq 25 \mu\text{m}$, (E) $\geq 50 \mu\text{m}$ and (F) $\geq 100 \mu\text{m}$ measured by HIAC for fresh, heated and aged BSA with Tween 80 at below, around and above its CMC. Data are expressed as the mean \pm Std. Deviation. * $P < 0.05$, ** $P < 0.01$, *** $P < 0.001$; significant difference in particles per ml compared with fresh BSA with Tween 80 samples.

One-way ANOVA analysis, Bonferroni correction showed a significant effect of heat stress and aging samples of BSA with Tween 80 surfactant present at levels below and around its CMC on particle count of particles $\geq 2 \mu\text{m}$. The mean difference was significant ($P < 0.001$) between fresh and heated BSA with Tween 80 below and around its CMC. The difference was statistically significant ($P < 0.01$) for BSA with Tween 80 present at around its CMC between fresh and aged samples and for BSA with Tween 80 at above CMC between fresh and heat stressed samples. There was no statistical significance between fresh and aged samples of BSA with Tween 80 at high concentrations (Figure 5.6 A).

For particle count data of size $\geq 5 \mu\text{m}$, statistical analysis showed that the particle count difference is significant ($P < 0.001$) between fresh and heated, fresh and aged BSA with below, around and above CMC Tween 80 concentrations (Figure 5.6 B).

Similar statistical analysis was obtained for the particle size range of $\geq 10 \mu\text{m}$. The statistical difference between fresh and heat stressed, fresh and aged BSA with Tween 80 below, around and above CMC was significant ($P < 0.001$). However statistical analysis showed no significance between fresh and aged BSA with Tween 80 present below its CMC (Figure 5.6 C).

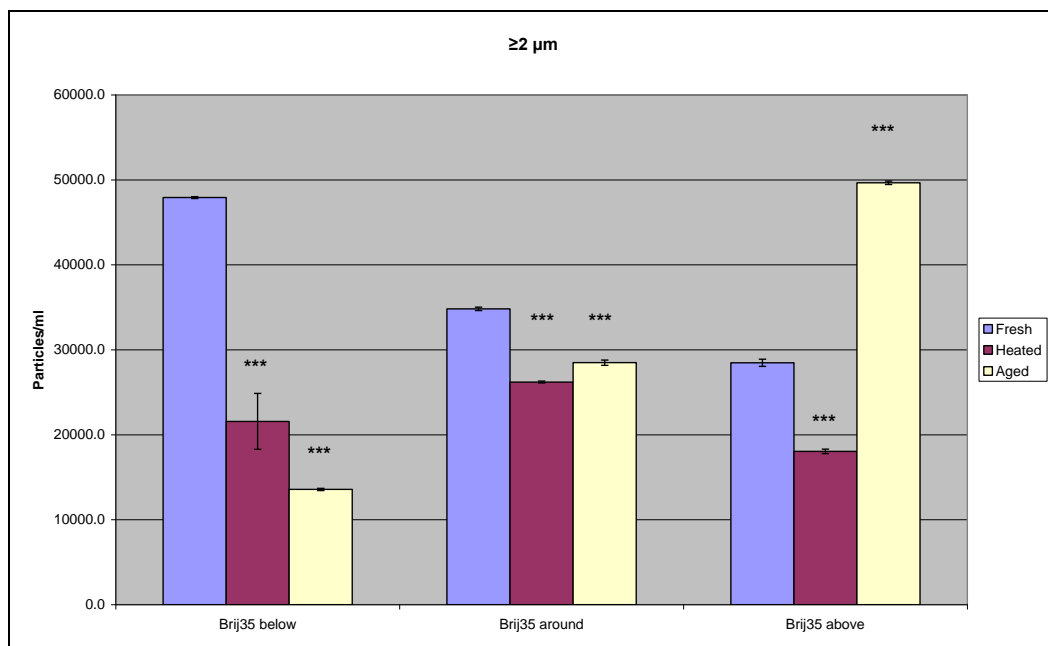
For particle count data of size ≥ 25 , Bonferroni test analysis showed that the count difference is significant ($P < 0.01$) between fresh and heated BSA with Tween 80 below and above CMC and the difference is statistically significant ($P < 0.001$) between fresh and aged BSA samples with Tween 80 above its CMC. The mean difference was significant ($P < 0.05$) between fresh and aged BSA samples with Tween 80 present at around CMC. No significant

difference was detected between fresh and heated samples of BSA with Tween 80 around CMC (Figure 5.6 D).

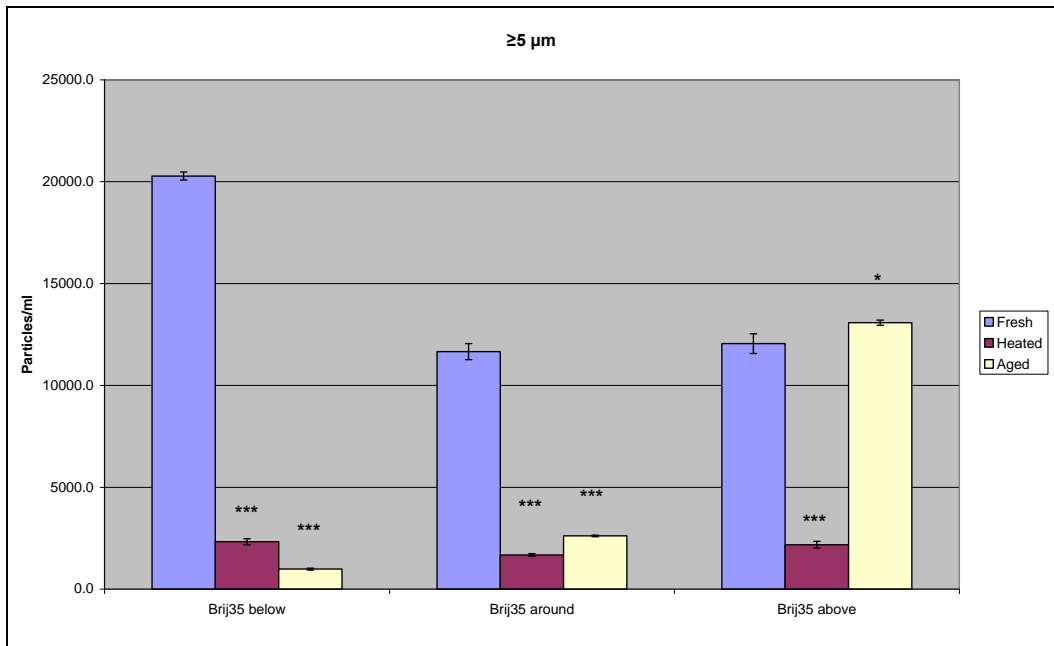
For particle count data of size $\geq 50 \mu\text{m}$ a statistical difference ($P < 0.05$) was detected between samples of fresh and heated BSA with Tween 80 below its CMC and between fresh and aged BSA samples with Tween 80 above its CMC (Figure 5.6 E).

For particle count data of size $\geq 100 \mu\text{m}$ no statistical difference was detected between fresh and heat stressed, fresh and aged BSA for samples containing Tween 80 at all concentrations employed (Figure 5.6 F).

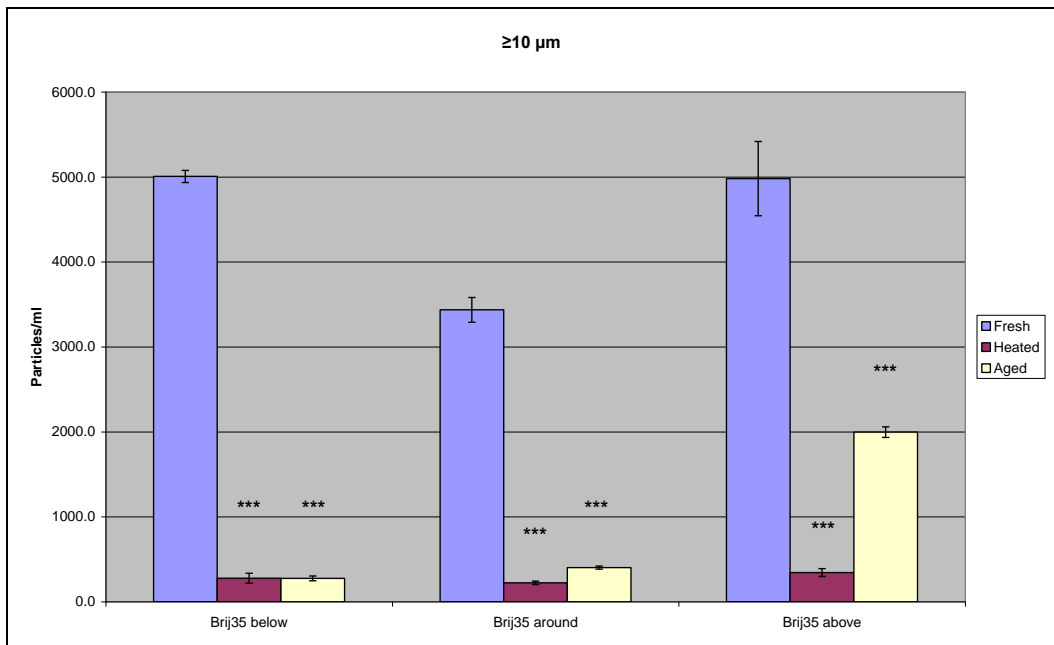
(A)



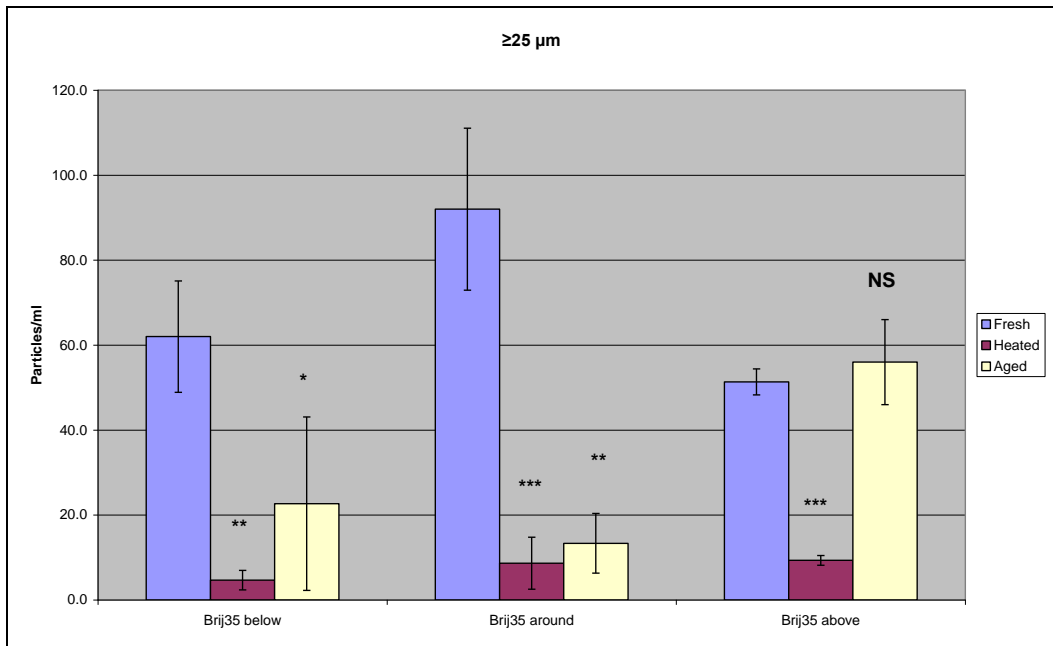
(B)



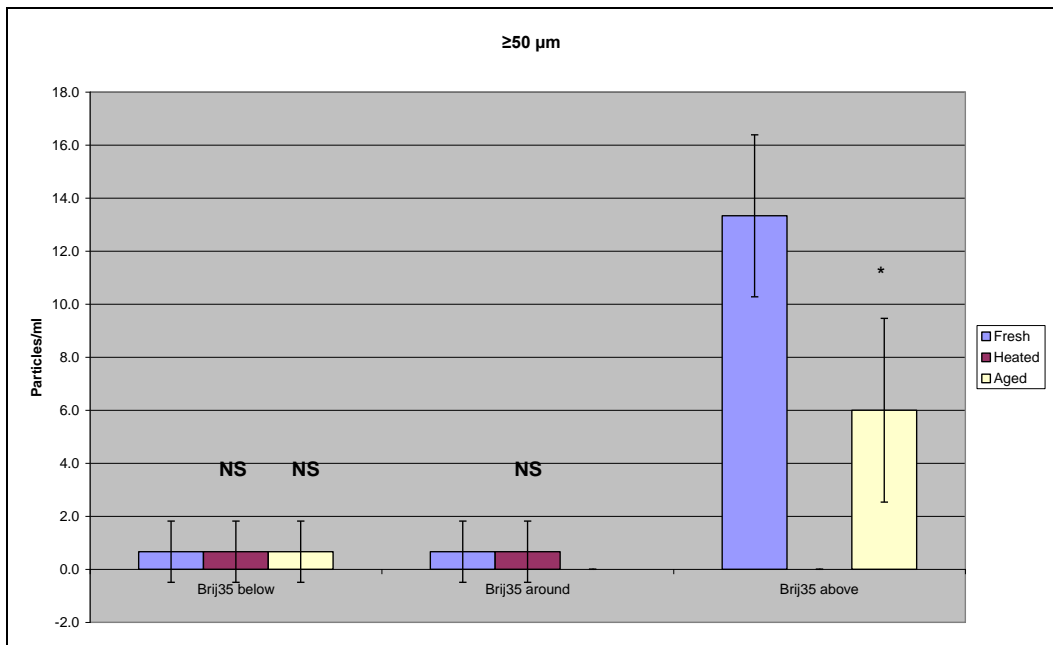
(C)



(D)



(E)



(F)

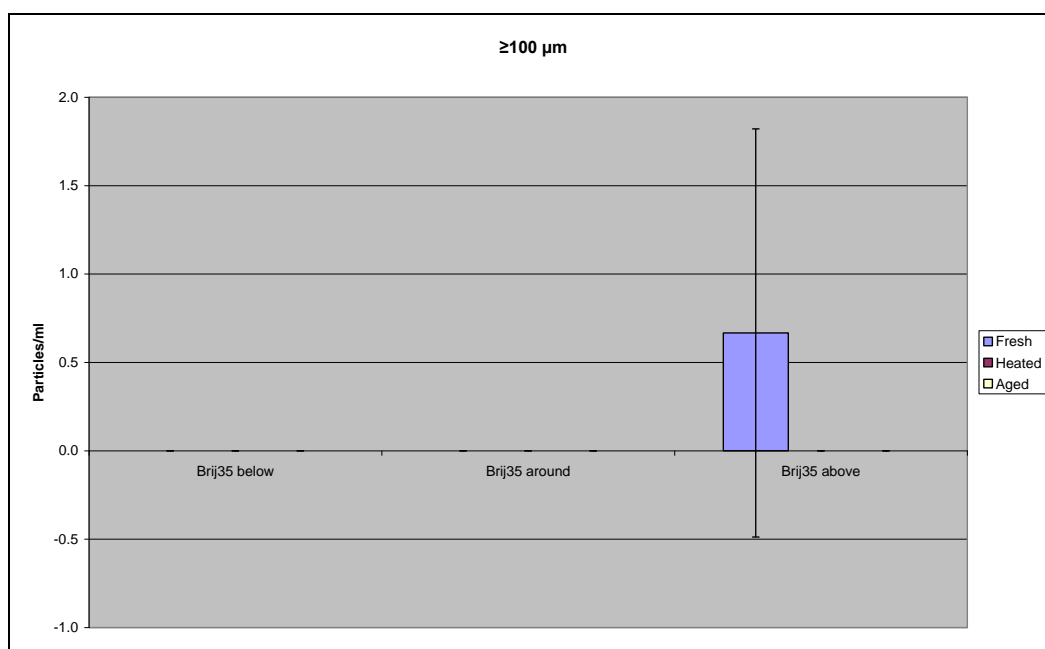


Figure 5.7. Particle concentrations at size ranges of: (A) $\geq 2 \mu\text{m}$, (B) $\geq 5 \mu\text{m}$, (C) $\geq 10 \mu\text{m}$, (D) $\geq 25 \mu\text{m}$, (E) $\geq 50 \mu\text{m}$ and (F) $\geq 100 \mu\text{m}$ measured by HIAC for fresh, heated and aged BSA with Brij 35 at below, around and above its CMC. Data are expressed as the mean \pm Std. Deviation. * $P < 0.05$, ** $P < 0.01$, * $P < 0.001$; significant difference in particles per ml compared with fresh BSA with Brij 35 samples.**

One-way ANOVA analysis, using the Bonferroni correction, showed a significant effect of heat stress and aging of BSA in the presence of Brij 35 surfactant at below, around and above its CMC on particle numbers $\geq 2 \mu\text{m}$. The mean difference is significant ($P < 0.001$) compared to fresh samples (Figure 5.7 A).

For particle count data of size $\geq 5 \mu\text{m}$, statistical analysis showed that the difference is significant ($P < 0.001$) between fresh and heated, and between fresh and aged BSA with Brij 35 present below and around its CMC, and also between fresh and heated BSA with Brij 35 present at a level above CMC.

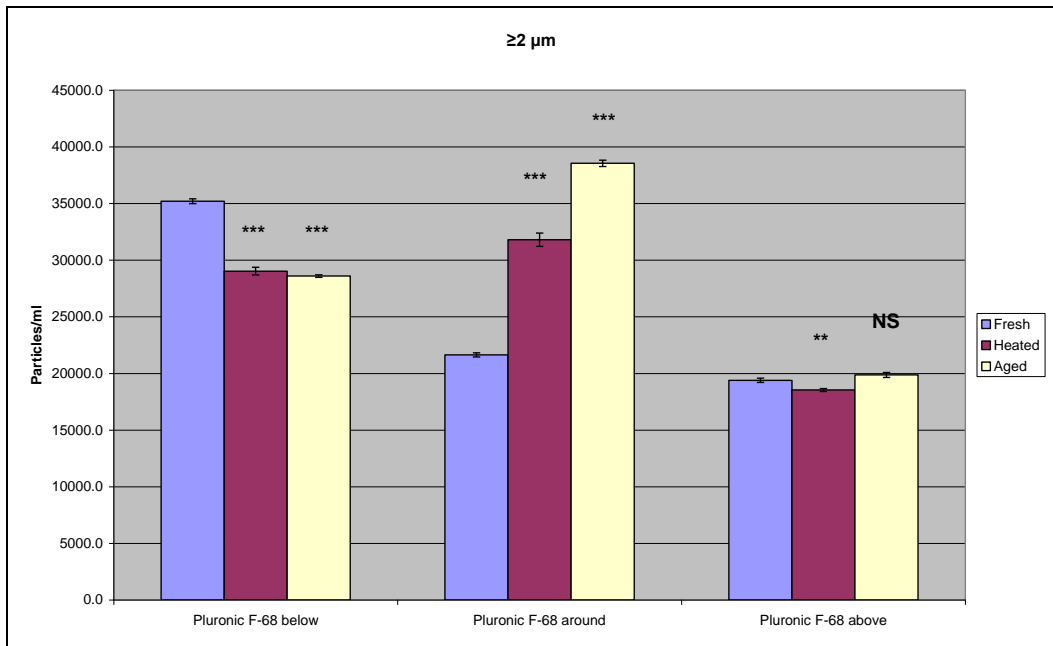
The mean difference between fresh and aged BSA with Brij 35 present above CMC is significant at 0.05 level ($P < 0.05$). Figure 5.7 (B) illustrates these findings.

For particle count data of size $\geq 10 \mu\text{m}$, the statistical difference between fresh and heat stressed, fresh and aged BSA with Brij 35 below, around and above its CMC was significant ($P < 0.001$) (Figure 5.7 C).

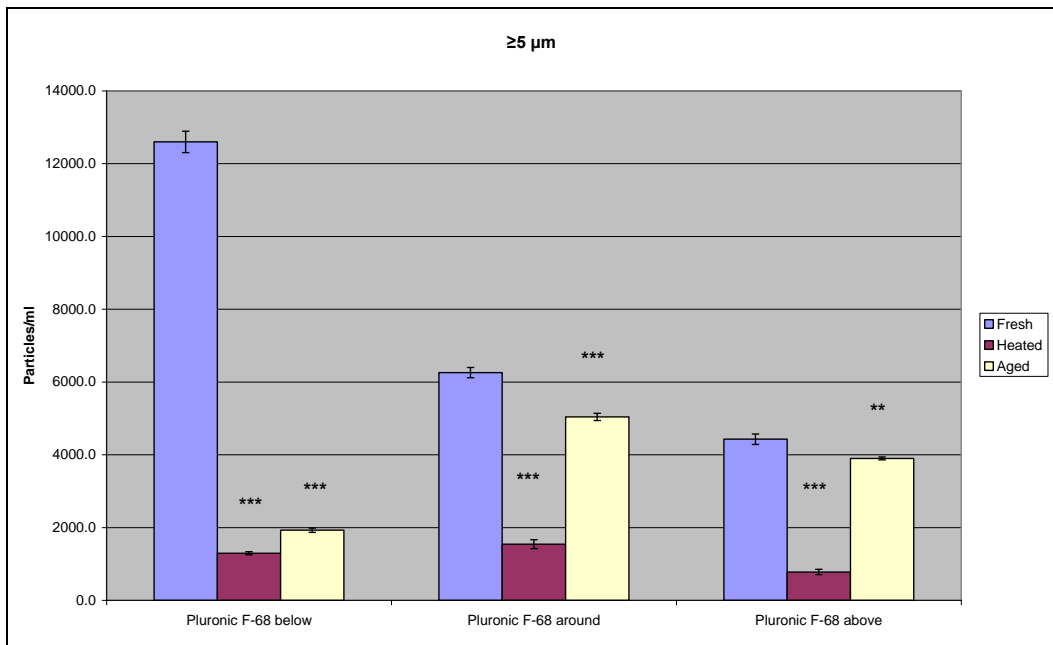
For particle count data of size $\geq 25 \mu\text{m}$, Bonferroni correction test showed that the difference is significant ($P < 0.001$) between fresh and heated BSA with Brij 35 present below its CMC ($P < 0.05$) and between fresh and heated BSA with Brij 35 present at around and above its CMC. No significant difference was detected between fresh and aged samples of BSA with Brij 35 present at above its CMC. The mean difference was significant ($P < 0.01$) between fresh and heated BSA samples with Brij 35 present below CMC and between fresh and aged BSA samples with Brij 35 present at around its CMC. One-way ANOVA, Bonferroni test analysis showed a statistical difference ($P < 0.05$) between fresh and aged BSA with Brij 35 used at below CMC (Figure 5.7 D).

For particle count data of size $\geq 50 \mu\text{m}$ no statistical difference was detected between fresh and heat stressed, and between fresh and aged BSA with Brij 35 below and around its CMC. Post-hoc analysis showed a significant difference level ($P < 0.05$) between fresh and aged BSA samples with Brij 35 present above CMC (Figure 5.7 E).

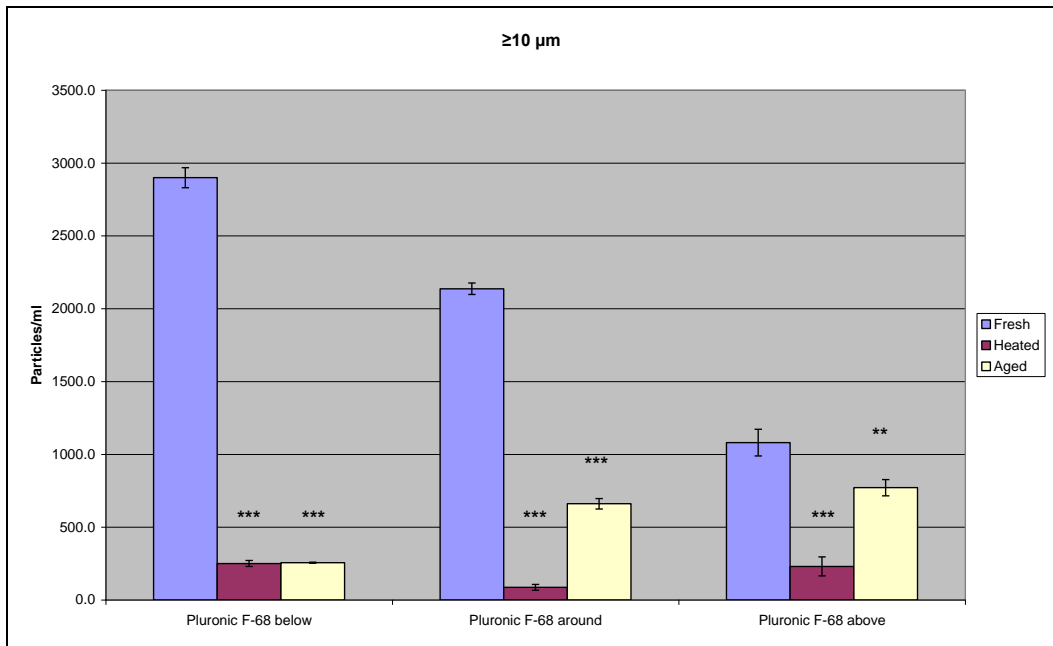
(A)



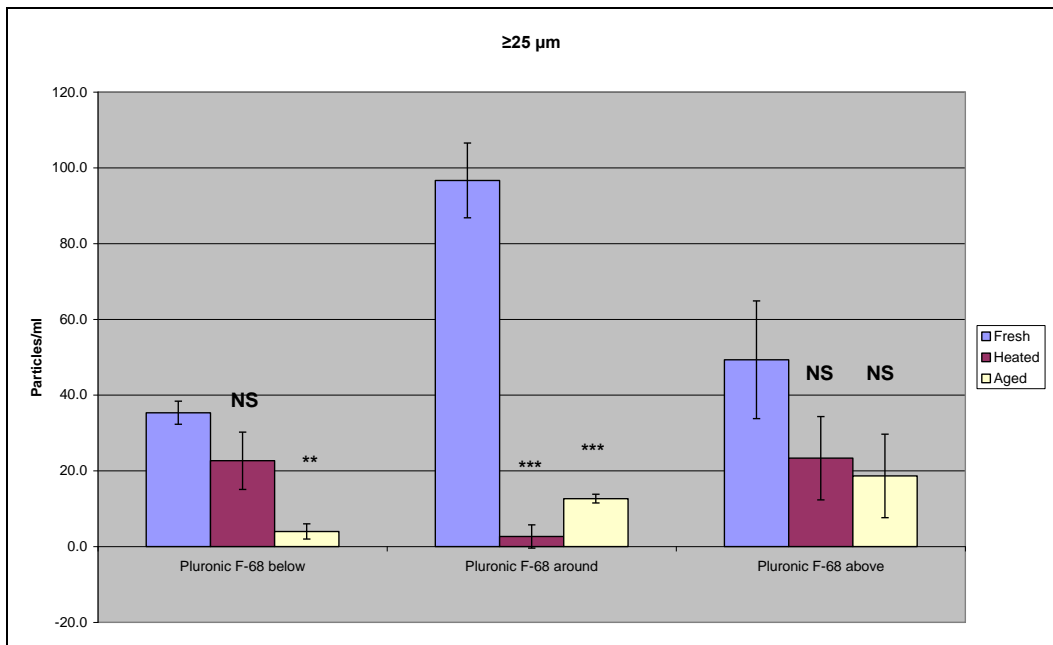
(B)



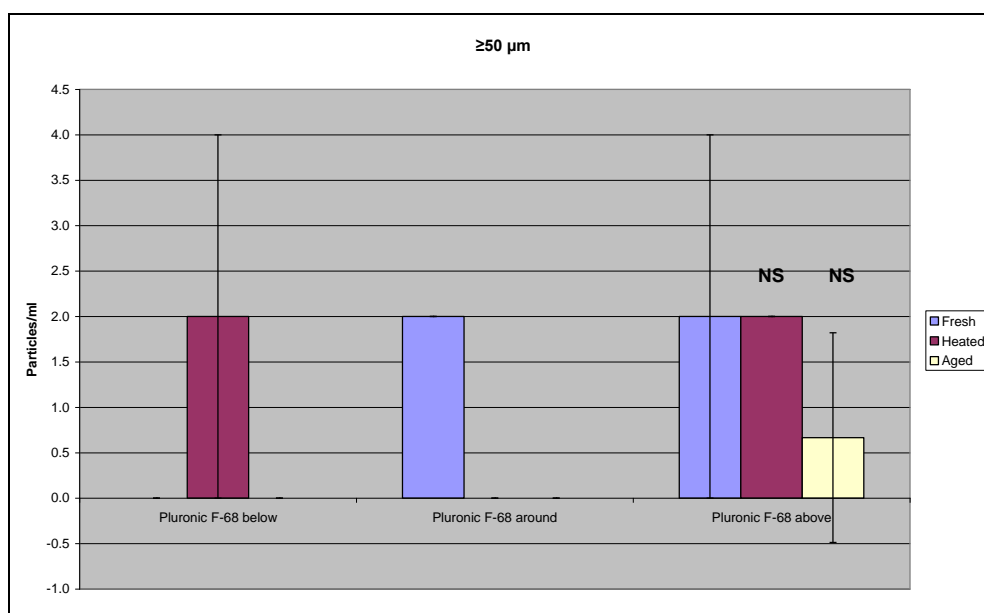
(C)



(D)



(E)



(F)

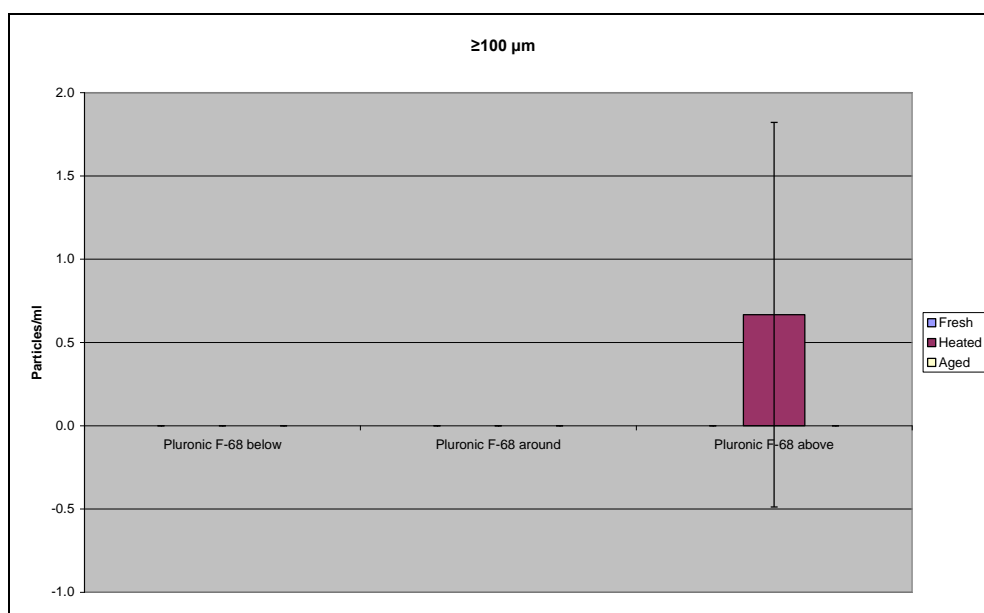


Figure 5.8. Particle concentrations at size ranges of: (A) $\geq 2 \mu\text{m}$, (B) $\geq 5 \mu\text{m}$, (C) $\geq 10 \mu\text{m}$, (D) $\geq 25 \mu\text{m}$, (E) $\geq 50 \mu\text{m}$ and (F) $\geq 100 \mu\text{m}$ measured by HIAC for fresh, heated and aged BSA with Pluronic F-68 present at below, around and above its CMC. Data are expressed as the mean \pm Std. Deviation. * $P < 0.05$, ** $P < 0.01$, * $P < 0.001$; significant difference in particles per ml compared with fresh BSA with Pluronic F-68 samples.**

One-way ANOVA analysis, Bonferroni correction, showed a significant effect of heat stress and aging samples for BSA with Pluronic F-68 surfactant present at below and around its CMC on particle count data for particles ≥ 2 μm particles. The mean difference is significant ($P < 0.001$) compared to fresh samples. For the same particle size data, the mean difference between fresh and heated BSA samples with Pluronic F-68 above its CMC is statistically significant ($P < 0.01$). There is no statistical difference ($P > 0.05$) between fresh and aged BSA samples with Pluronic F-68 above its CMC (Figure 5.8 A).

For particle count data of size ≥ 5 μm and ≥ 10 μm , statistical analysis showed that the difference is statistically significant ($P < 0.001$) between fresh and heated BSA with Pluronic F-68 present at all levels and between fresh and aged BSA samples with Pluronic F-68 present below and around CMC. The mean difference in particle data is significant ($P < 0.01$) between fresh and aged BSA samples with Pluronic F-68 employed above its CMC. Figure 5.8 (B and C) illustrates these findings.

For particle count data of size ≥ 25 μm , Bonferroni test analysis showed that the difference is statistically significant ($P < 0.001$) between fresh and heated, and between fresh and aged BSA samples with Pluronic F-68 present at around CMC and significantly different ($P < 0.01$) between fresh and aged BSA with Pluronic F-68 used below its CMC. No significant difference ($P > 0.05$) was detected between fresh and heated BSA samples with Pluronic F-68 used below its CMC and between fresh and heated, fresh and aged BSA with Pluronic F-68 present at above CMC levels. (Figure 5.8 D).

For particle count data of size $\geq 50 \mu\text{m}$, no statistical difference ($P>0.05$) was detected between fresh and heat stressed, and between fresh and aged BSA samples with Pluronic F-68 at above CMC (Figure 5.8 E).

5.4.1.2 Light Obscuration measurements for fresh, heated and aged IgG2 surfactant free and IgG2 with Tween 20, Tween 80, Brij 35 and Pluronic F-68 surfactants at below, around and above CMC levels

Figure 5.9 illustrates particle concentration per ml measured for fresh, heated and aged IgG2 surfactant free samples.

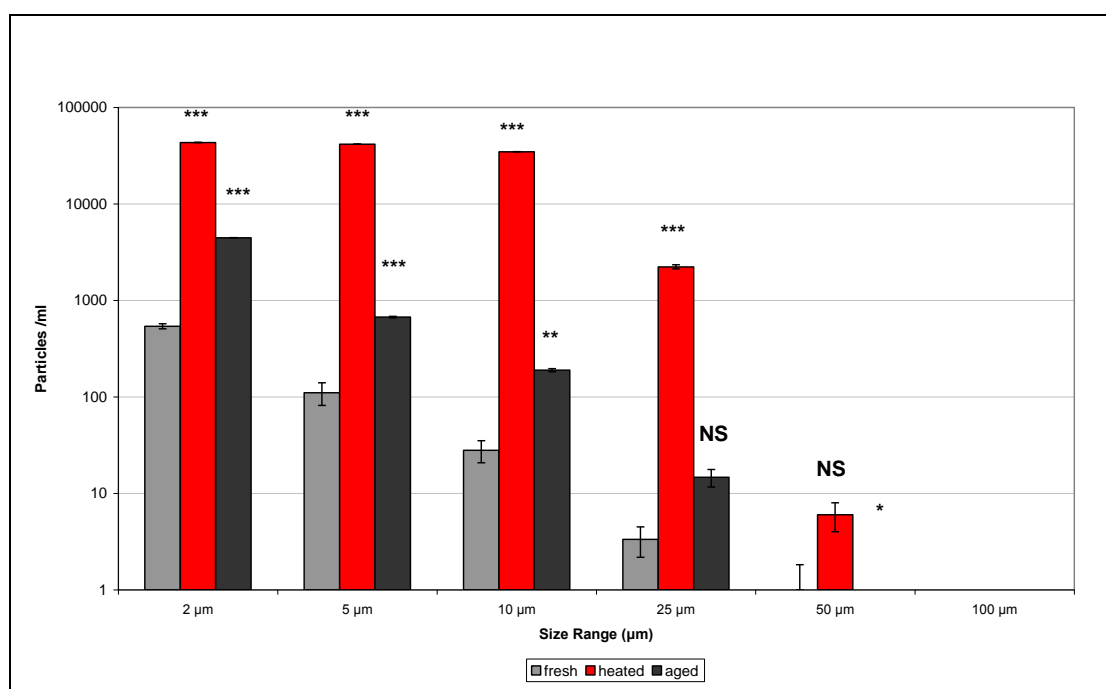


Figure 5.9. Particle concentrations measured by HIAC for fresh, heated and aged IgG2 samples. Data are expressed as the mean \pm Std. Deviation. * $P<0.05$, ** $P<0.01$, * $P<0.001$; significant difference in particles per ml compared with fresh IgG2 samples.**

Heated IgG2 formulations show an increase in the number of particles per ml at all particle size ranges compared to fresh and aged IgG2 samples (Figure 5.9).

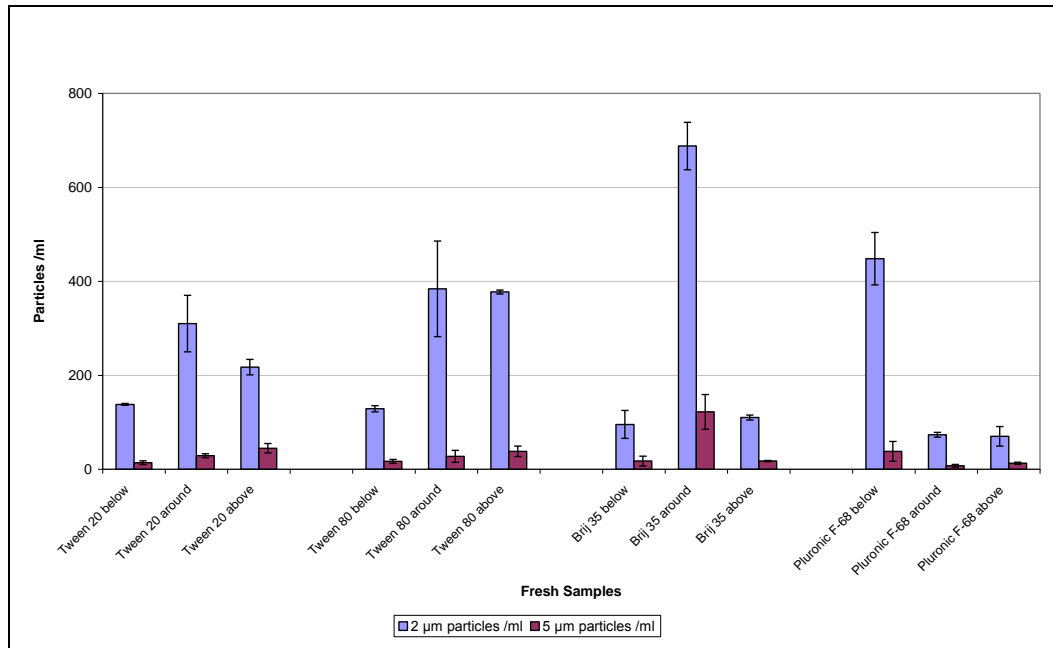
Both heated and aged samples caused the formation of immunoglobulin aggregation to a similar extent. The total number of particles greater or equal to 2 μm , 5 μm , 10 μm , 25 μm and 50 μm , respectively measured after heat stress (43334.0 ± 84.6 particles $\geq 2 \mu\text{m}$, $41570.0 \pm 44.5 \geq 5 \mu\text{m}$, $34748.0 \pm 61.0 \geq 10 \mu\text{m}$, $2227.3 \pm 111.3 \geq 25 \mu\text{m}$ and $6 \pm 2.0 \geq 50 \mu\text{m}$) and aged samples (4460.7 ± 21.4 particles $\geq 2 \mu\text{m}$, $670.7 \pm 13.3 \geq 5 \mu\text{m}$, $189.3 \pm 7 \geq 10 \mu\text{m}$, $14.7 \pm 3.1 \geq 25 \mu\text{m}$) exceeded the number of particles found for the same size range of freshly prepared samples.

One-way ANOVA analysis showed a significant effect of heat treatment and storage on particles count at the size ranges of $\geq 2 \mu\text{m}$, $\geq 5 \mu\text{m}$, $\geq 10 \mu\text{m}$. Post-hoc tests, Bonferroni correction analyses showed a significant increase in particle concentration at the size ranges $\geq 2 \mu\text{m}$ and $\geq 5 \mu\text{m}$ ($P < 0.001$) for heated and aged samples compared to fresh IgG2 samples.

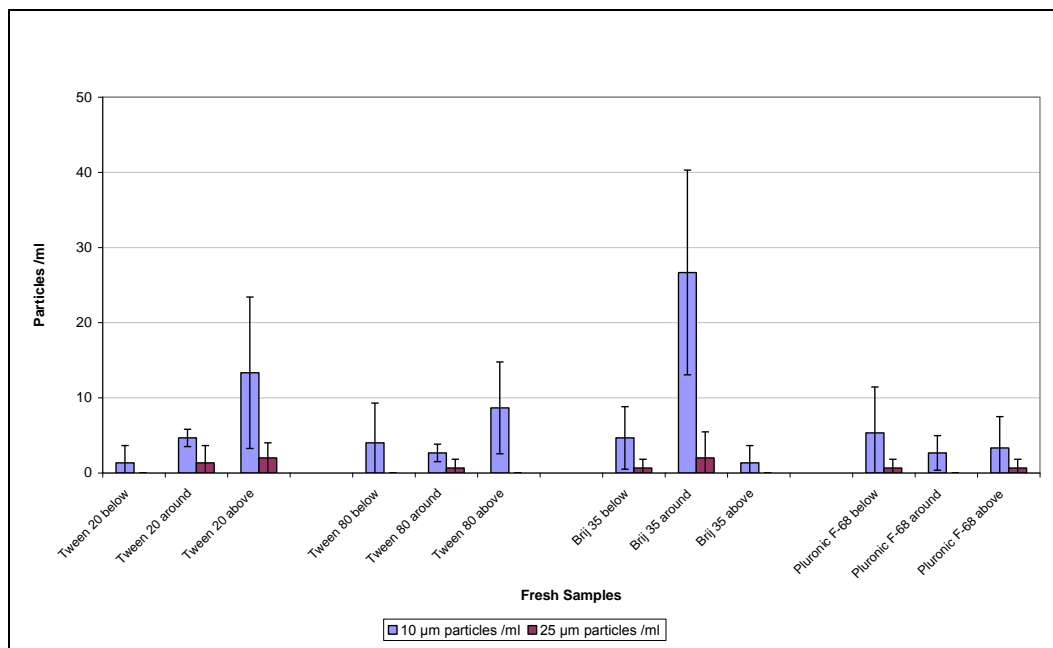
For particle count data of size $\geq 10 \mu\text{m}$, Bonferroni statistical results showed that the mean increase is significant ($P < 0.001$) for heated IgG2 samples and aged ($P < 0.01$) IgG2 samples. For particle count data of size $\geq 25 \mu\text{m}$, heated IgG2 samples showed a statistically significant increase ($P < 0.001$), whereas aged IgG2 samples showed no statistical difference ($P > 0.05$) compared to fresh samples. Moreover, for particle count data of size $\geq 50 \mu\text{m}$ there was no significant difference in particle count for heated samples, but there was a significant difference ($P < 0.05$) between fresh and aged IgG2 samples (Figure 5.9).

Figure 5.10 illustrates the quantity of particles in a size range of $\geq 2 \mu\text{m}$, $\geq 5 \mu\text{m}$, $\geq 10 \mu\text{m}$, $\geq 25 \mu\text{m}$ and $\geq 100 \mu\text{m}$ measured by Light Obscuration for fresh IgG2 with Tween 20, Tween 80, Brij 35 and Pluronic F-68 surfactants present .

(A)



(B)



(C)

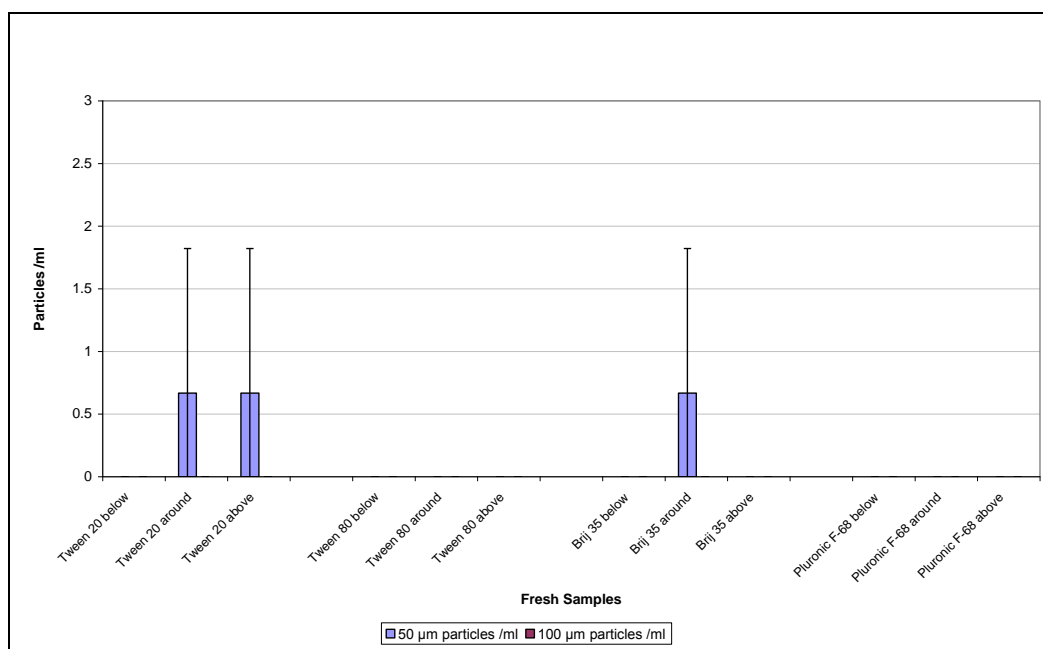
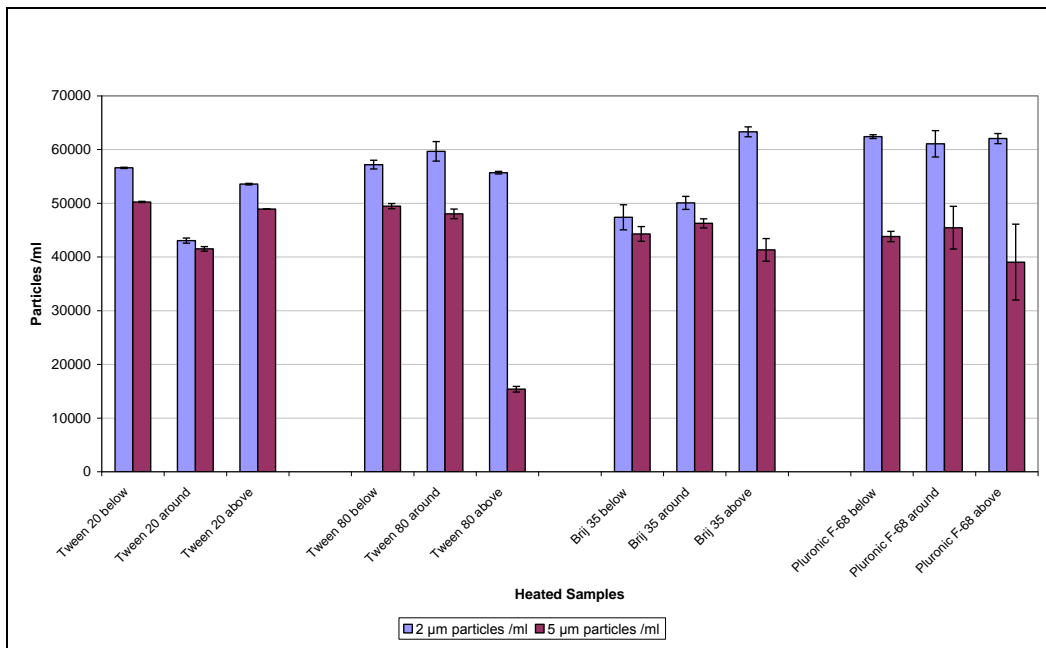


Figure 5.10. Particle concentrations in size ranges: (A) $\geq 2 \mu\text{m}$ and $\geq 5 \mu\text{m}$, (B) $\geq 10 \mu\text{m}$ and $\geq 25 \mu\text{m}$, (C) $\geq 50 \mu\text{m}$ and $\geq 100 \mu\text{m}$ per ml measured by HIAC for fresh IgG2 samples with Tween 20, Tween 80, Brij 35 and Pluronic F-68 surfactants present at below, around and above their CMC levels. Data are expressed as the mean \pm Std. Deviation.

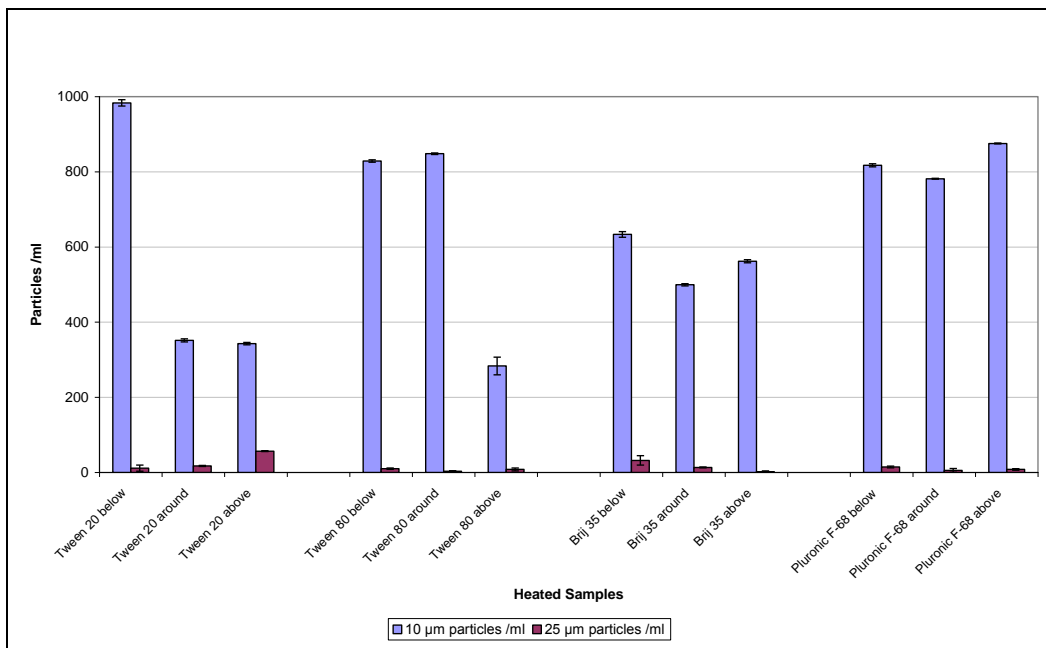
In formulations of fresh IgG2 containing Brij 35 around CMC, a slight increase in the number of particles $\geq 2 \mu\text{m}$ and $\geq 5 \mu\text{m}$ was detectable (6880.0 ± 50.5 particles $\geq 2 \mu\text{m}$ and 122.0 ± 37.0 particles $\geq 5 \mu\text{m}$ per ml), compared to fresh IgG2 surfactant free solutions (540.0 ± 33.0 particles $\geq 2 \mu\text{m}$ and 110.7 ± 29.1 particles $\geq 5 \mu\text{m}$ per ml).

Fresh IgG2 formulations with Tween 20, Tween 80 and Pluronic F-68 surfactants at all levels and for samples containing Brij 35 below and above CMC, showed lower particle counts at all particle size classifications (Figure 5.10).

(A)



(B)



(C)

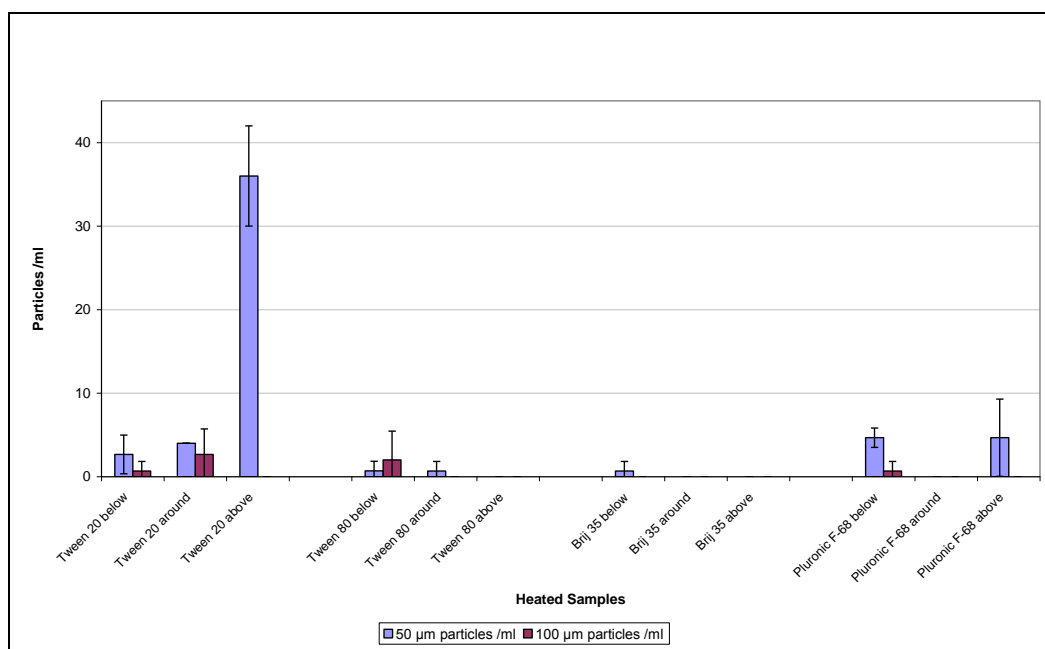


Figure 5.11. Particle concentrations in size ranges: (A) $\geq 2 \mu\text{m}$ and $\geq 5 \mu\text{m}$, (B) $\geq 10 \mu\text{m}$ and $\geq 25 \mu\text{m}$, (C) $\geq 50 \mu\text{m}$ and $\geq 100 \mu\text{m}$ measured by HIAC for heated IgG2 samples with Tween 20, Tween 80, Brij 35 and Pluronic F-68 surfactants at below, around and above their CMC levels. Data are expressed as the mean \pm Std. Deviation.

Heated IgG2 formulations containing Tween 20 at around its CMC revealed a slight decrease in the number of particles at $\geq 2 \mu\text{m}$ (43047.3 ± 485.5 particles) whereas IgG2 with Tween 20 present at below and above its CMC, and with Tween 80, Brij 35 and Pluronic F-68 present at below, around and above their respective CMC showed noticeable increases in particle numbers compared to heated immunoglobulin without any surfactant present (Figure 5.11 A).

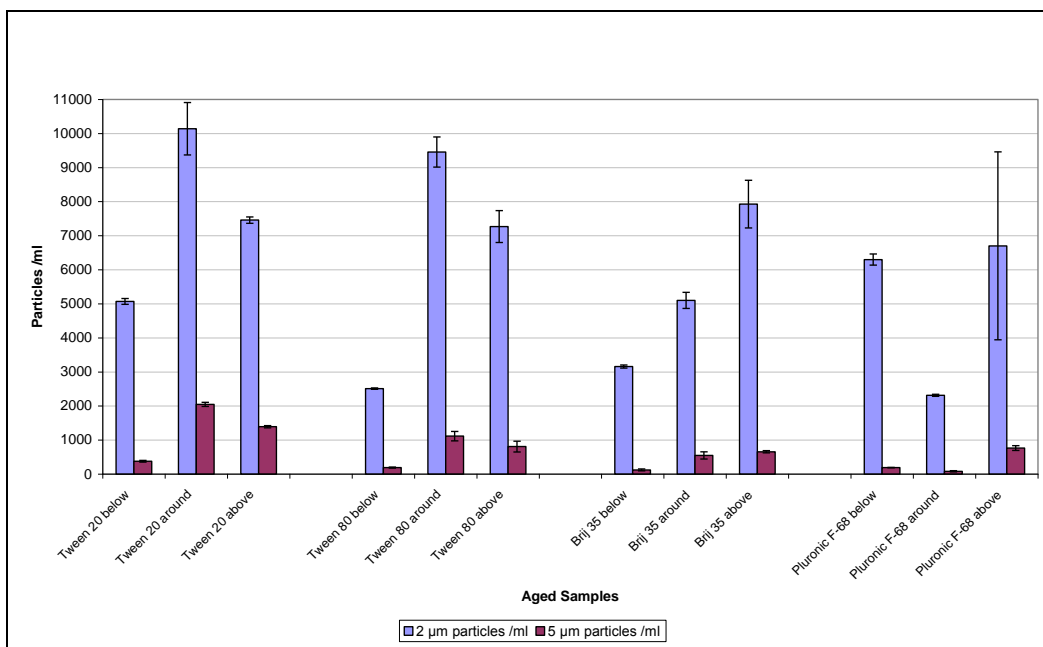
A similar effect was noted for the data of particles $\geq 5 \mu\text{m}$ where IgG2 with Tween 20 present at around, Tween 80 present at above, Brij 35 at above

and Pluronic F-68 present at above their CMC levels showed decreases in particle counts.

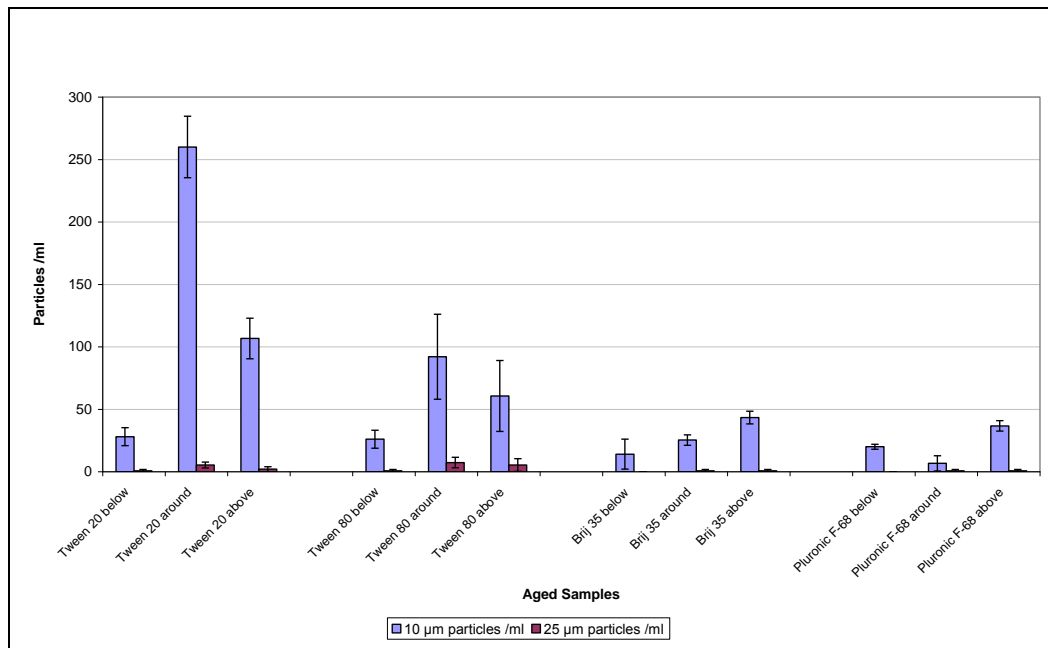
All four surfactants at below, around and above their CMC showed a decrease in particle count at $\geq 10 \mu\text{m}$, $\geq 25 \mu\text{m}$ and $\geq 50 \mu\text{m}$ particle size classes (Figure 5.11 B and C).

Figure 5.12 illustrates particle concentrations for aged IgG2 with Tween 20, Tween 80, Brij 35 and Pluronic F-68 surfactants.

(A)



(B)



(C)

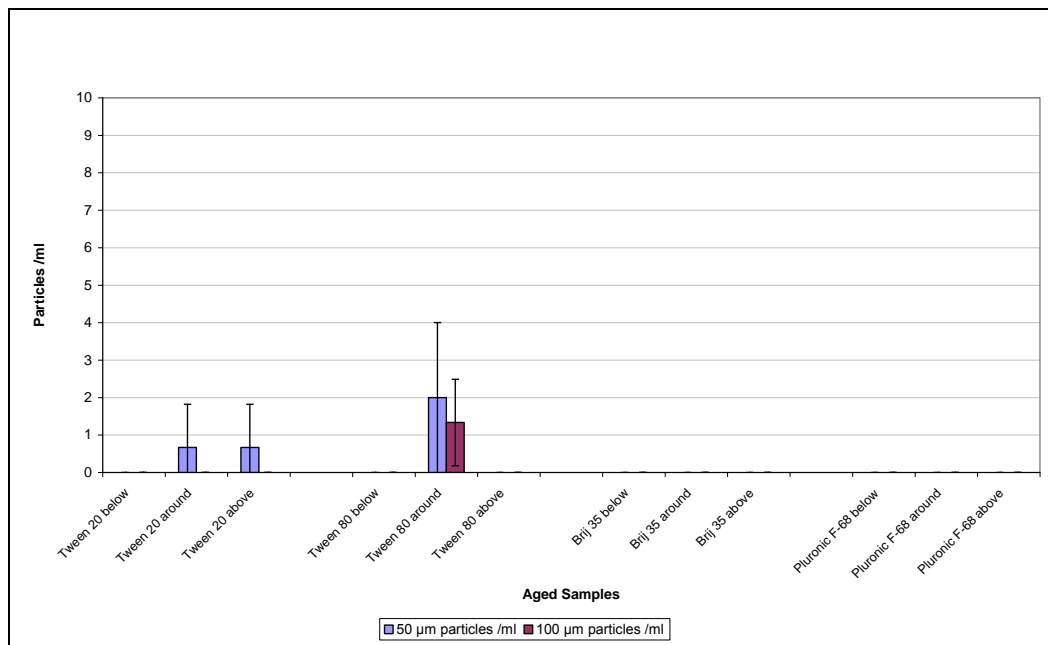


Figure 5.12. Particle concentrations in size ranges: (A) $\geq 2 \mu\text{m}$ and $\geq 5 \mu\text{m}$, (B) $\geq 10 \mu\text{m}$ and $\geq 25 \mu\text{m}$, (C) $\geq 50 \mu\text{m}$ and $\geq 100 \mu\text{m}$ per ml measured by HIAC for aged IgG2 samples with Tween 20, Tween 80, Brij 35 and Pluronic F-68 surfactants present at below, around and above their CMC. Data are expressed as the mean \pm Std. Deviation.

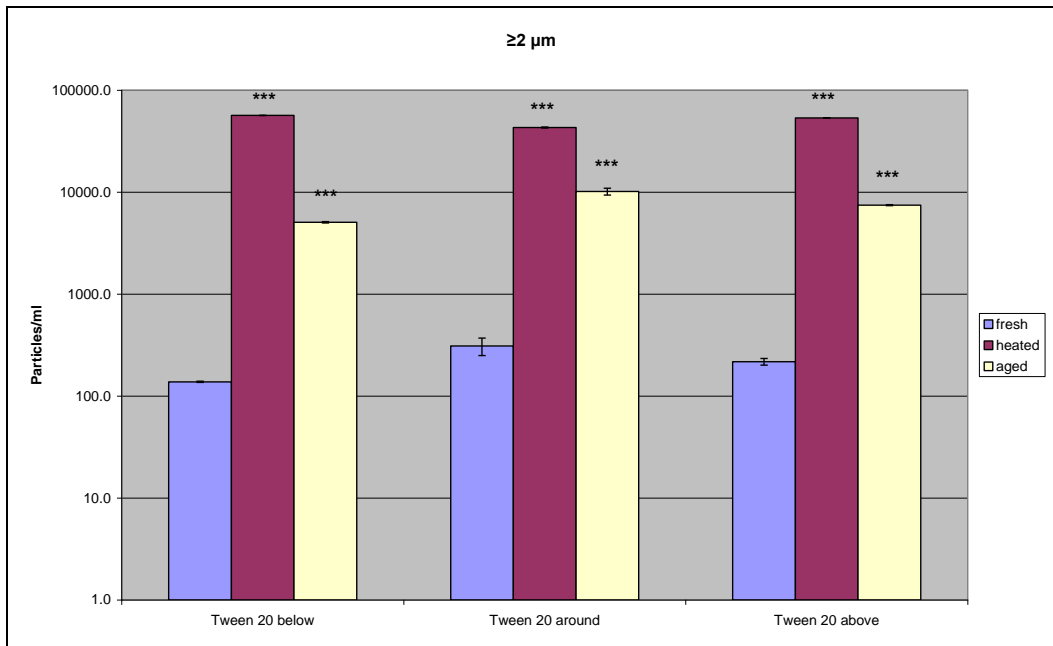
For aged IgG2 formulations containing Tween 80 below its CMC, Brij 35 below its CMC and Pluronic F-68 around its CMC, a decrease in the number of particles $\geq 2 \mu\text{m}$ was detected (Figure 5.12 A).

IgG2 formulations with Tween 20 around and above its CMC, Tween 80 around and above its CMC, and Pluronic F-68 above its CMC, an increase in the number of particles $\geq 5 \mu\text{m}$ was detected. Solutions with Tween 20 present below, Tween 80 present below, Brij 35 present below, around and above and Pluronic F-68 present below and around their respective CMC's did not induce formation of large aggregates.

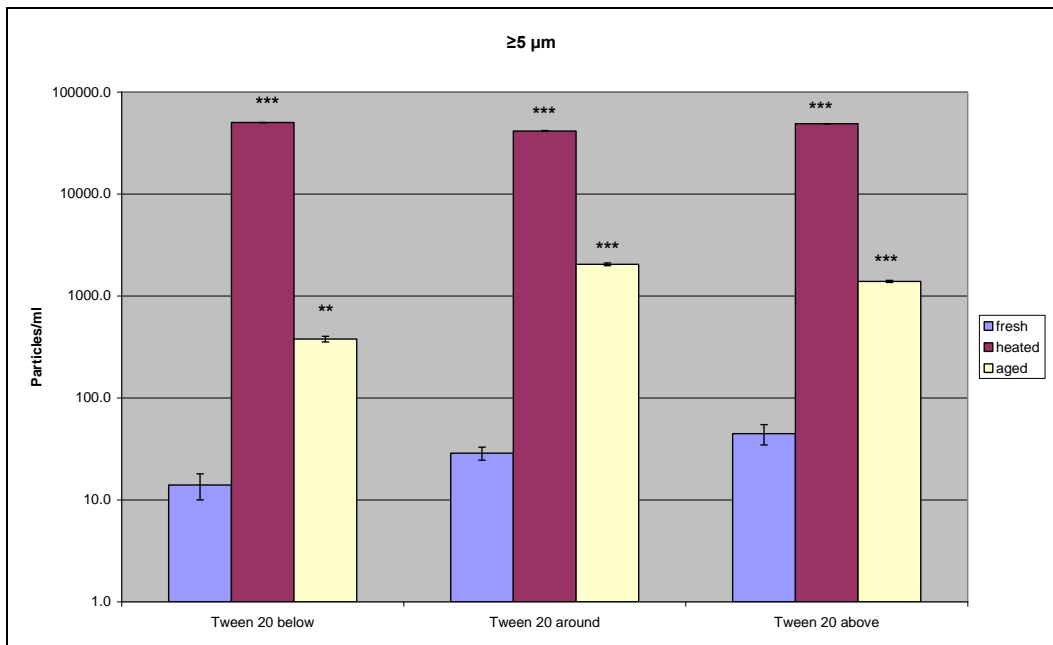
For particle count data of size $\geq 10 \mu\text{m}$ only Tween 20 at around CMC produced an increase in particle count. Particle count data for Tween 80, Brij 35 and Pluronic F-68 surfactants at particle size $\geq 10 \mu\text{m}$, and all surfactants at particle sizes $\geq 25 \mu\text{m}$ and $\geq 50 \mu\text{m}$ contained significantly fewer particles than aged surfactant free IgG2 samples (Figure 5.12 B and C).

Figures 5.13 to 5.16 illustrate how the particle counts with different size ranges of $\geq 2 \mu\text{m}$, $\geq 5 \mu\text{m}$, $\geq 10 \mu\text{m}$, $\geq 25 \mu\text{m}$, $\geq 50 \mu\text{m}$ and $\geq 100 \mu\text{m}$ change after heat stress and aging of IgG2 with each surfactant at below, around and above their respective CMC levels.

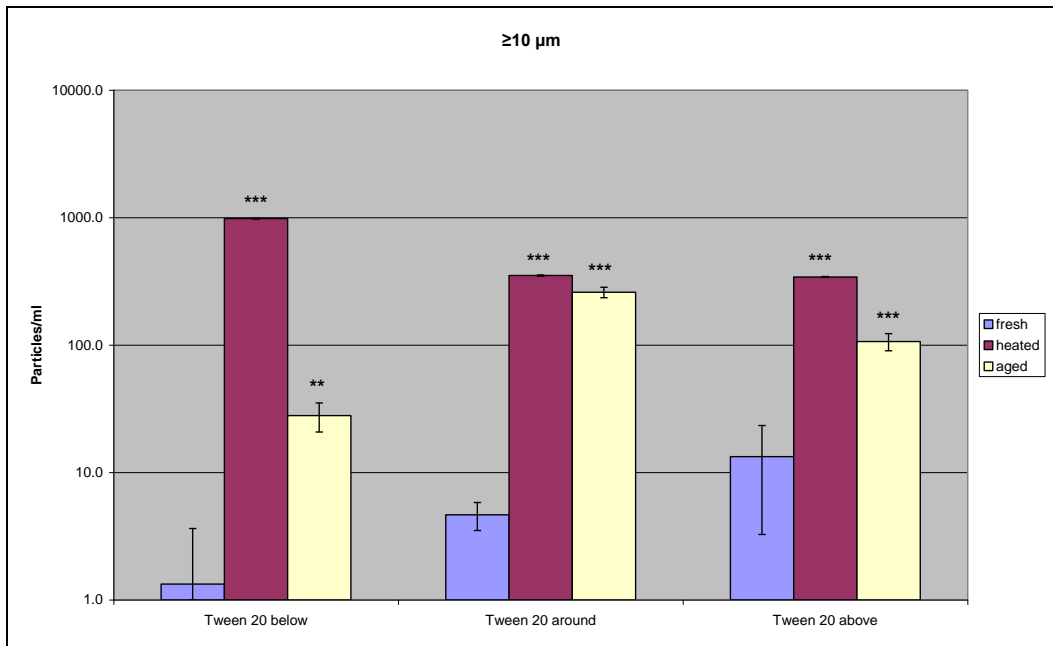
(A)



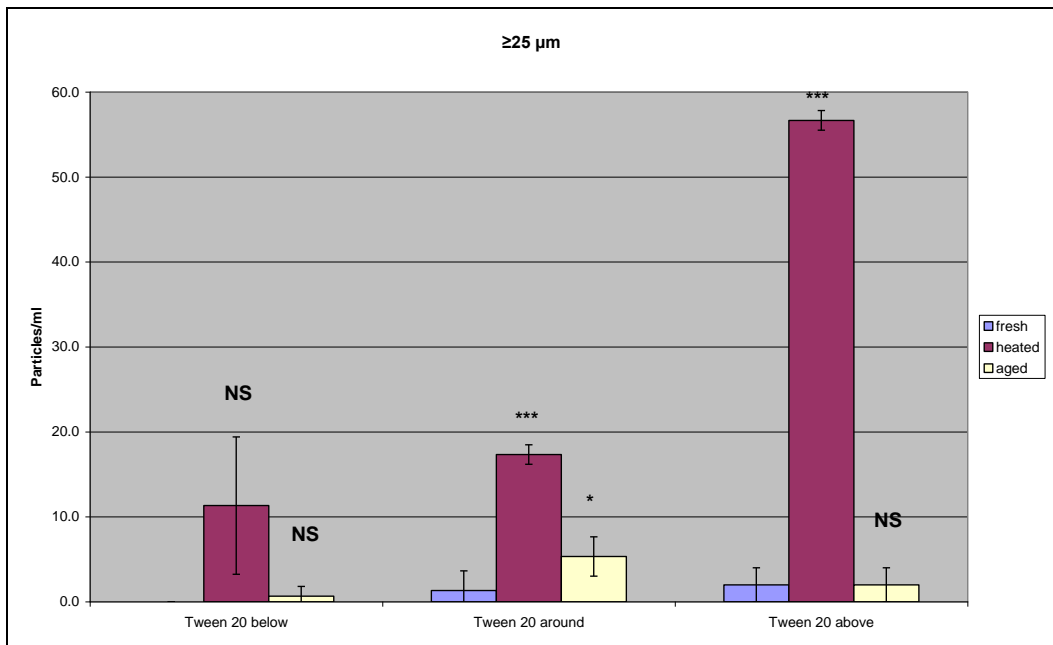
(B)



(C)



(D)



(E)

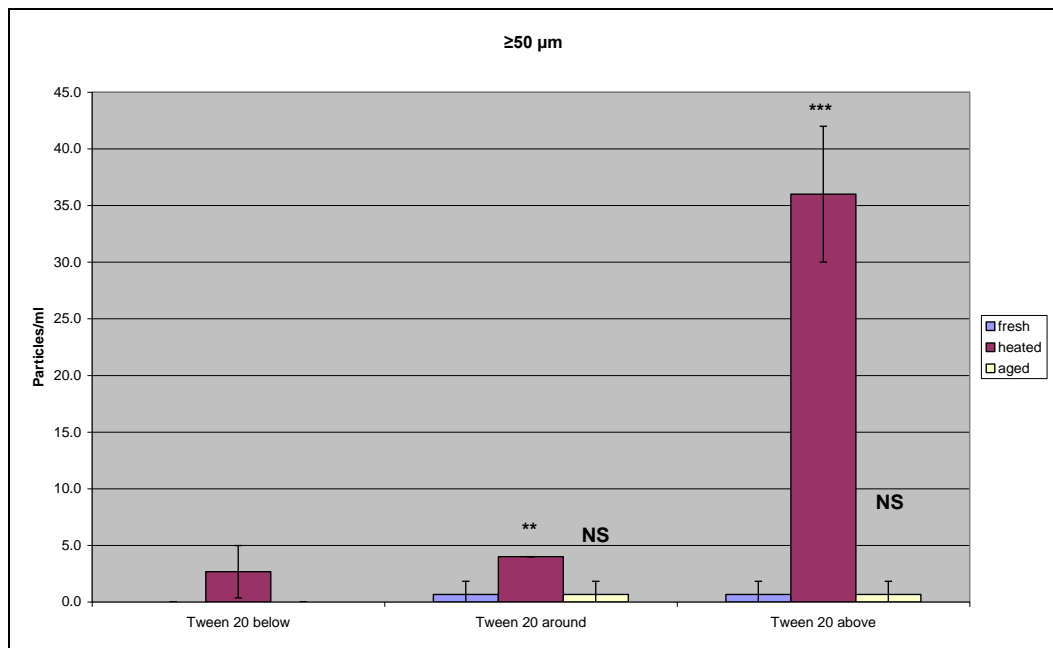


Figure 5.13. Particle concentrations at size ranges of: (A) $\geq 2 \mu\text{m}$, (B) $\geq 5 \mu\text{m}$, (C) $\geq 10 \mu\text{m}$, (D) $\geq 25 \mu\text{m}$, (E) $\geq 50 \mu\text{m}$ measured by HIAC for fresh, heated and aged IgG2 with Tween 20 below, around and above its CMC levels. Data are expressed as the mean \pm Std. Deviation. * $P<0.05$, ** $P<0.01$, * $P<0.001$; significant difference in particles per ml compared with fresh IgG2 with Tween 20 samples.**

One-way ANOVA analysis, post-hoc Bonferroni correction showed a significant effect of heat stress and aging on samples for IgG2 with Tween 20 surfactant at below, around and above its CMC for particle count data of size $\geq 2 \mu\text{m}$. The mean difference is significant ($P<0.001$) compared to fresh samples (Figure 5.13 A).

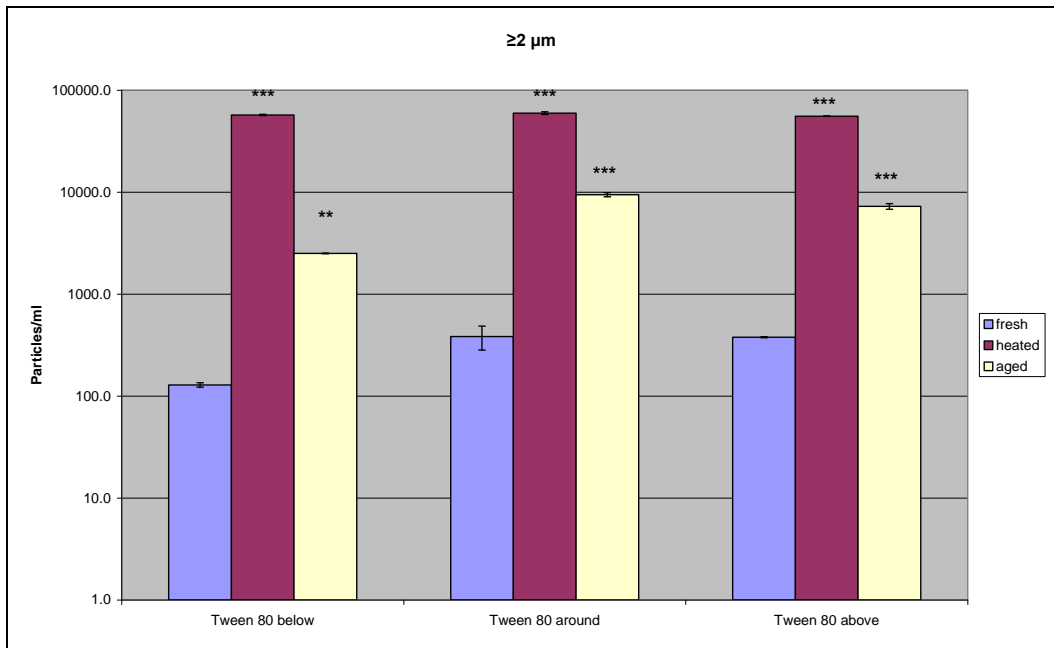
For particle count data of size $\geq 5 \mu\text{m}$ and $\geq 10 \mu\text{m}$, statistical analyses showed that the difference is significant ($P<0.001$) between fresh and heated, and between fresh and aged IgG2 with Tween 20 present at around and above CMC and also between fresh and heated IgG2 with Tween 20

present below CMC. The mean difference is significant ($P < 0.01$) between fresh and aged IgG2 with Tween 20 below CMC. Figure 5.13 (B) and (C) illustrates these findings.

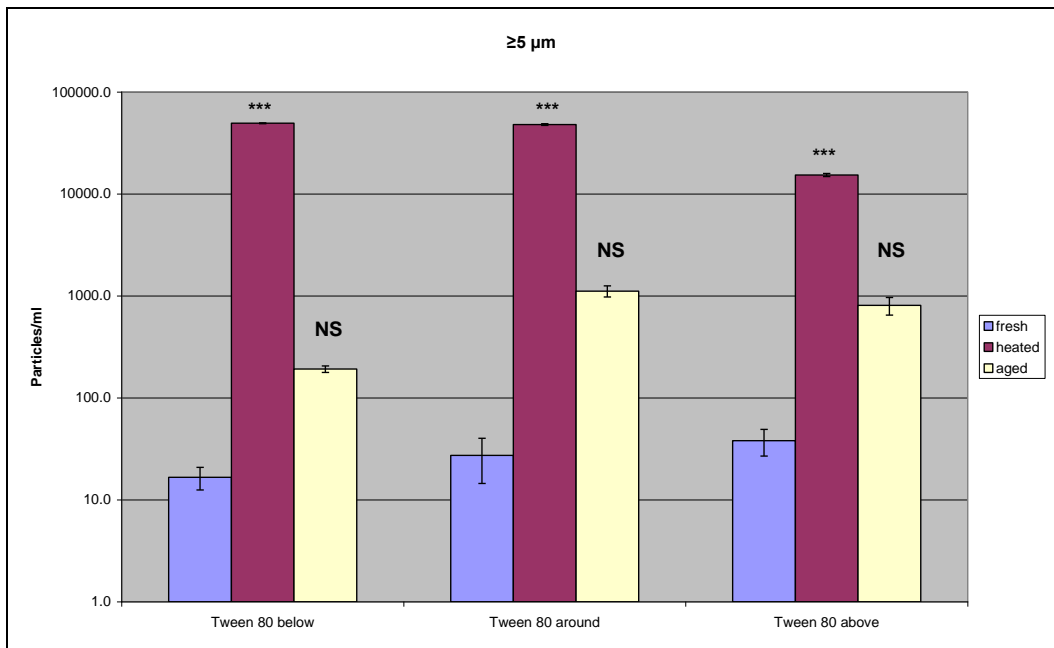
For particle count data of size ≥ 25 , Bonferroni test analysis showed that the difference is statistically significant ($P < 0.001$) between fresh and heated IgG2 samples with Tween 20 present at around and above CMC and between fresh and aged samples of IgG2 with Tween 20 present around CMC ($P < 0.05$). No significant difference was detected between fresh and heated, and between fresh and aged samples of IgG2 with Tween 20 below CMC and between fresh and aged Tween 20 above CMC (Figure 5.13 D).

For particle count data of size $\geq 50 \mu\text{m}$ no statistical difference ($P > 0.05$) was detected between fresh and aged IgG2 with Tween 20 around and above its CMC. Post-hoc analysis showed significant difference ($P < 0.001$) between fresh and heated IgG2 with Tween 20 added above CMC and was also significantly different between fresh and heated samples of IgG2 with Tween 20 present at around CMC ($P < 0.01$) (Figure 5.13 E).

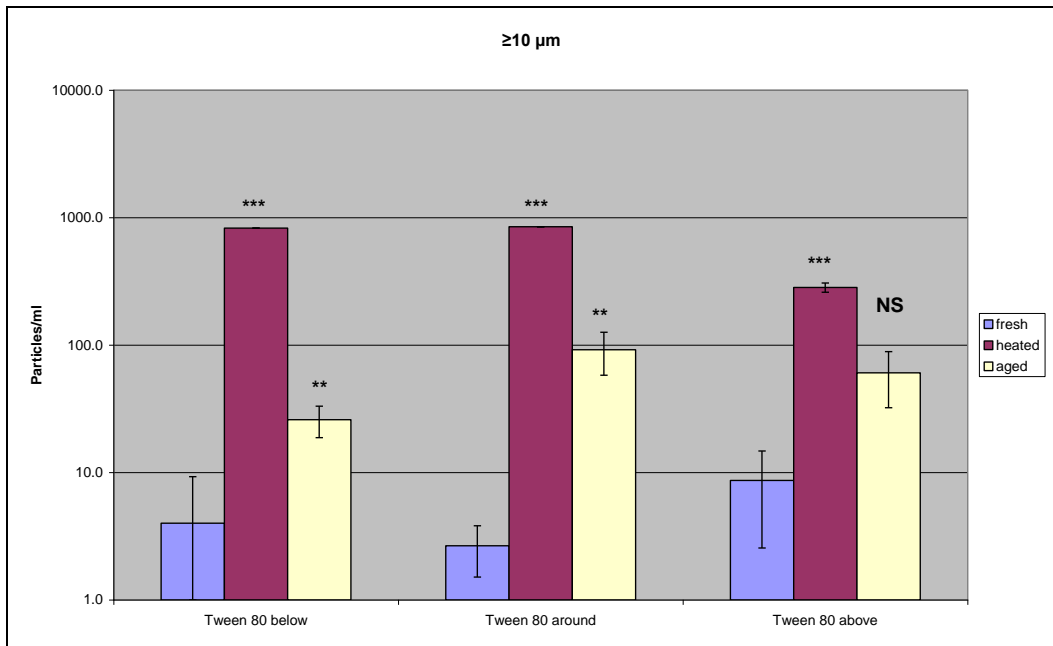
(A)



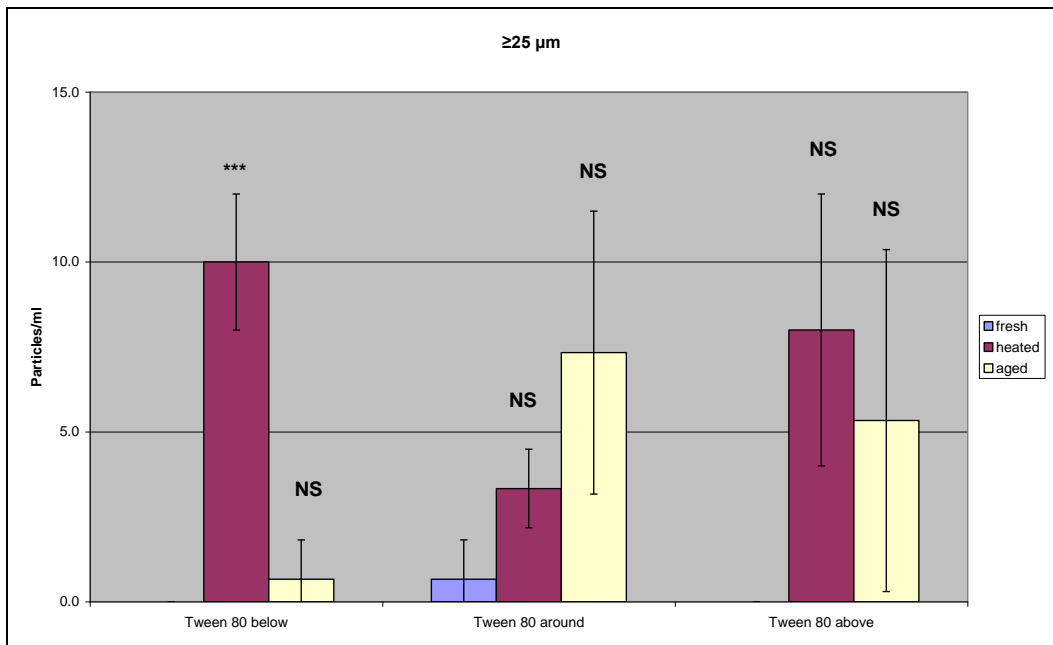
(B)



(C)



(D)



(E)

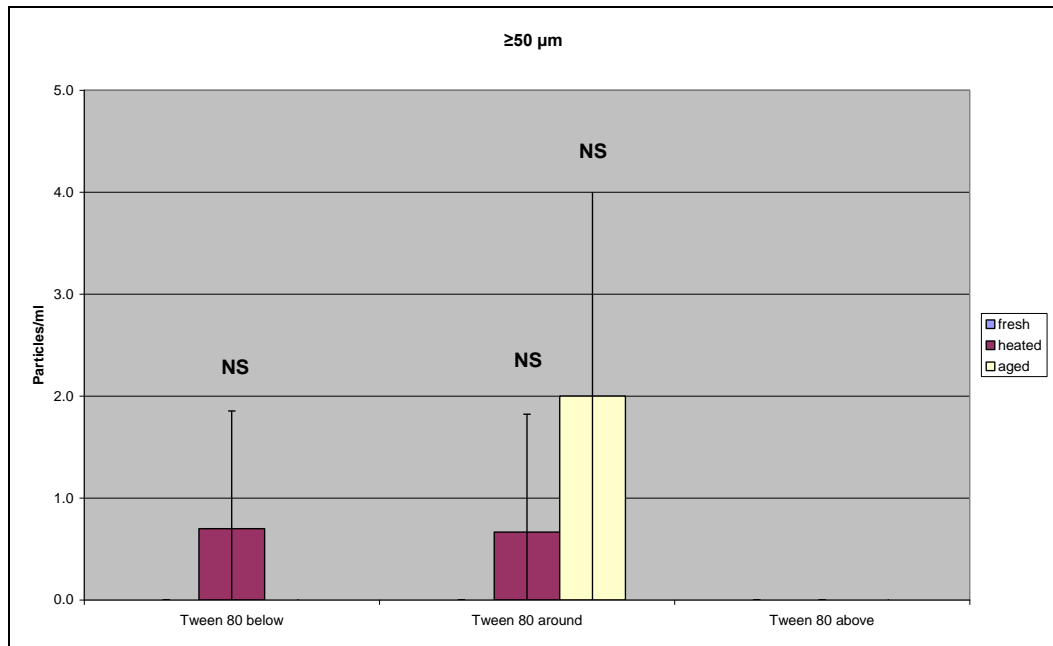


Figure 5.14. Particle concentrations at size ranges of: (A) $\geq 2 \mu\text{m}$, (B) $\geq 5 \mu\text{m}$, (C) $\geq 10 \mu\text{m}$, (D) $\geq 25 \mu\text{m}$, (E) $\geq 50 \mu\text{m}$ measured by HIAC for fresh, heated and aged IgG2 with Tween 80 present below, around and above CMC. Data are expressed as the mean \pm Std. Deviation. * $P<0.05$, ** $P<0.01$, * $P<0.001$; significant difference in particles per ml compared with fresh IgG2 with Tween 80 samples.**

Illustrated in Figure 5.14, one-way ANOVA analysis, using Bonferroni correction showed a significant effect of heat stress and aging on samples for IgG2 with Tween 80 surfactant present at below, around and above CMC levels for at particle count data obtained at $\geq 2 \mu\text{m}$. The mean difference is significant ($P<0.001$) for Tween 80 at levels around and above CMC compared to fresh samples. The difference between fresh and heated samples is statistically significant ($P<0.001$) and between fresh and aged samples ($P<0.01$) of IgG2 with Tween 80 present at levels below CMC (Figure 5.14 A).

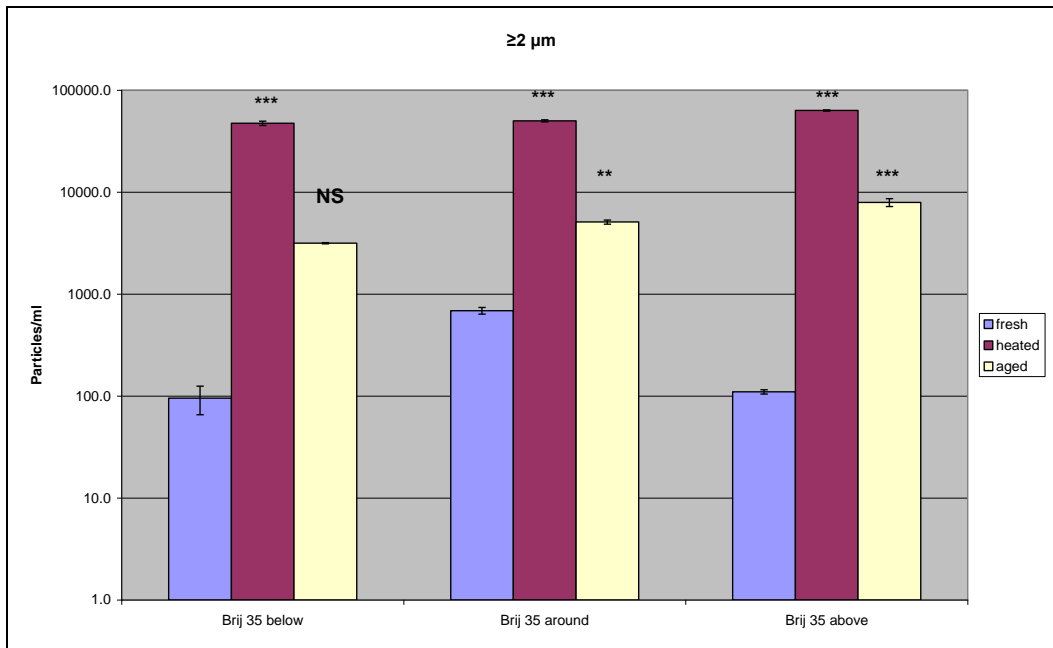
For particle count data of size $\geq 5 \mu\text{m}$, statistical analysis showed that heat treatment had a significant effect ($P < 0.001$) for IgG2 samples containing Tween 80 below, around and above CMC, whereas aging effect had no significant effect ($P > 0.05$) for these samples (Figure 5.14 B).

For particle count data of size $\geq 10 \mu\text{m}$, heat treatment had a significant effect on count number ($P < 0.001$) compared to fresh samples. The difference between fresh and aged samples of IgG2 with Tween 80 present below and around CMC was statistically significant ($P < 0.01$). Aging treatment had no significant effect on particle counts of this size for the IgG2 sample with Tween 80 present above CMC when compared to the initial sample (Figure 5.14 C).

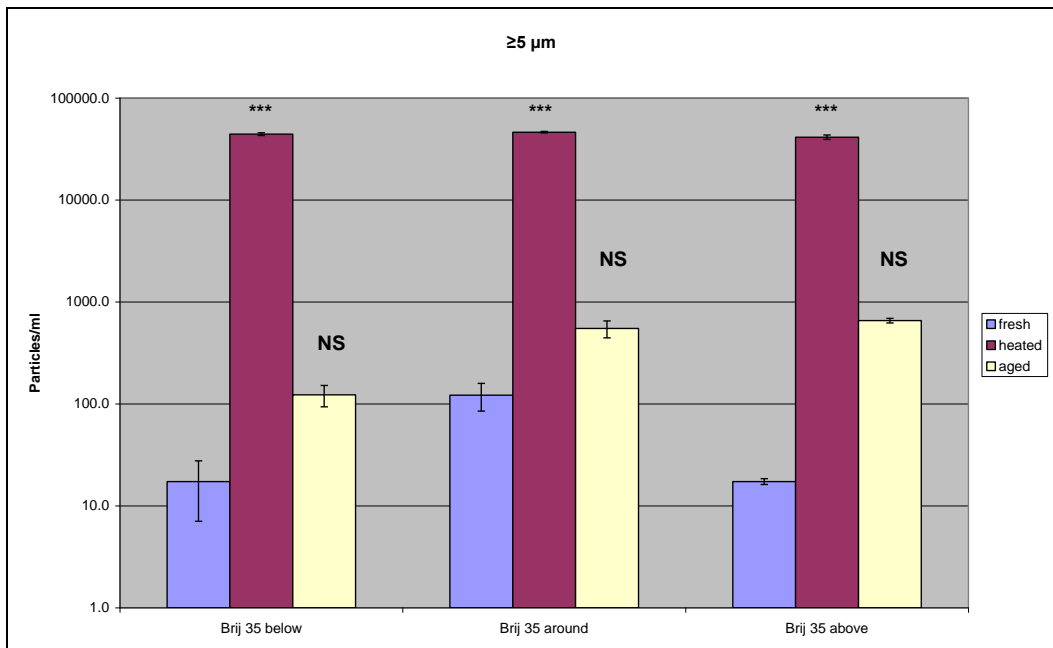
For particle count data of size $\geq 25 \mu\text{m}$, Bonferroni test analysis showed that heat treatment had a statistically significant effect ($P < 0.001$) only in the presence of Tween 80 at low concentration. No significant heat effect was detected for IgG2 in the presence of Tween 80 at around and above its CMC. Comparing fresh and aged IgG2 with Tween 80 levels below, around and above CMC, no significance difference in particle count was shown (Figure 5.14 D).

For particle count data of size $\geq 50 \mu\text{m}$ no statistical difference ($P > 0.05$) was detected between fresh and aged IgG2 samples containing Tween 80 at levels below, around and above its CMC (Figure 5.14 E).

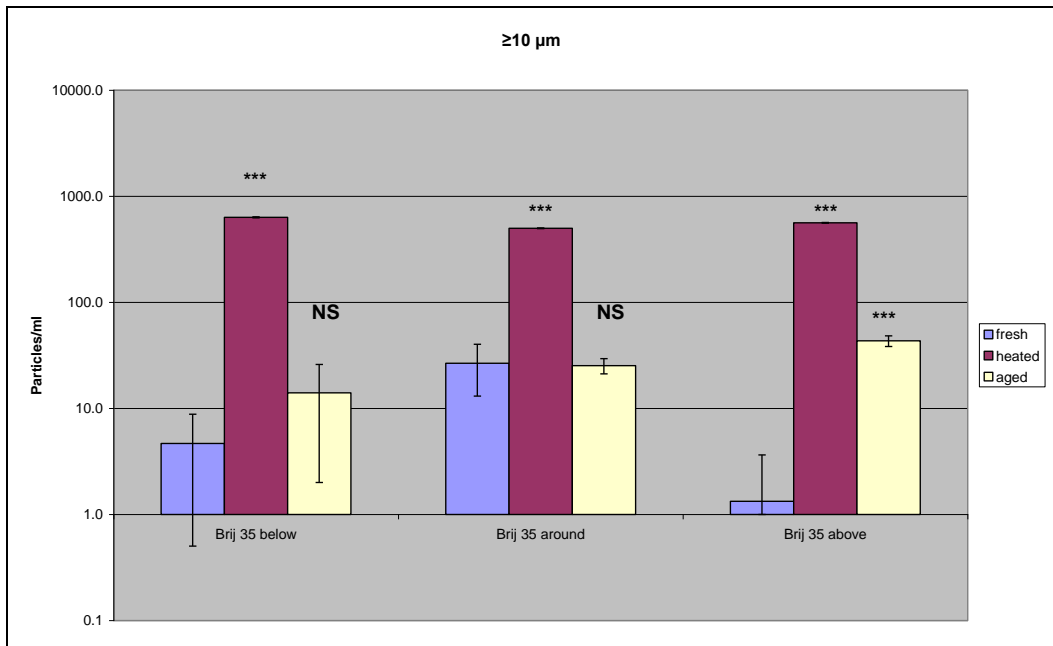
(A)



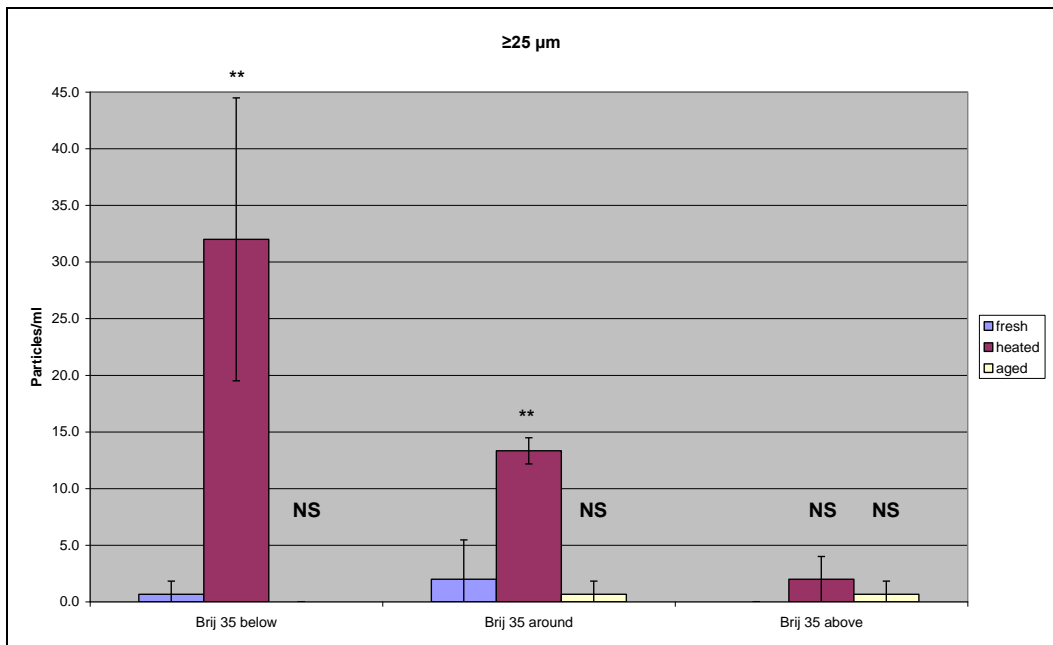
(B)



(C)



(D)



(E)

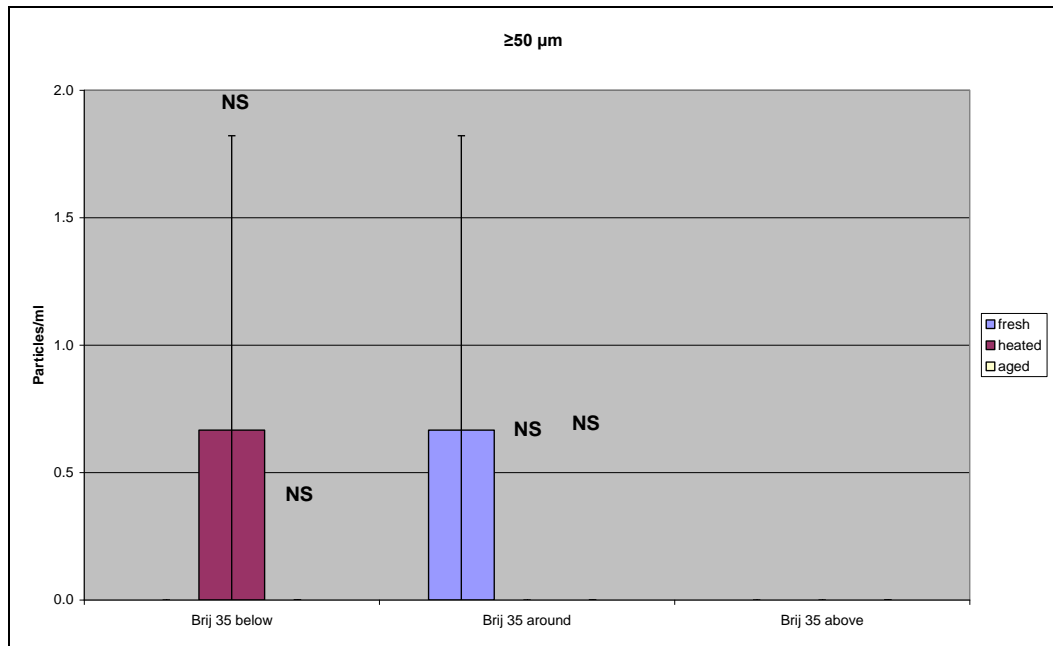


Figure 5.15. Particle concentrations at size ranges of: (A) $\geq 2 \mu\text{m}$, (B) $\geq 5 \mu\text{m}$, (C) $\geq 10 \mu\text{m}$, (D) $\geq 25 \mu\text{m}$, (E) $\geq 50 \mu\text{m}$ measured by HIAC for fresh, heated and aged IgG2 with added Brij 35 below, around and above its CMC level. Data are expressed as the mean \pm Std. Deviation. * $P<0.05$, ** $P<0.01$, * $P<0.001$; significant difference in particles per ml compared with fresh IgG2 with Brij 35 samples.**

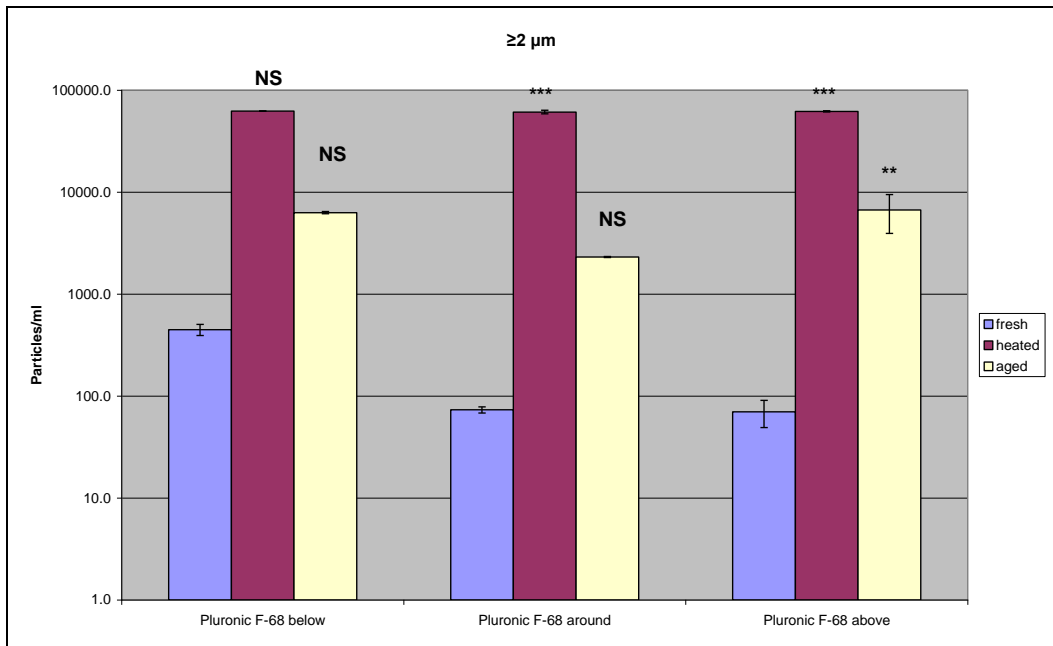
Figure 5.15 illustrates statistical analysis results for fresh, heated and aged IgG2 with Brij 35 present. One-way ANOVA analysis, Bonferroni test, showed a significant effect of heat stress for IgG2 with Brij 35 surfactant present at levels below, around and above CMC on the production of particles of size $\geq 2 \mu\text{m}$. The mean difference is significant ($P<0.001$) comparing the above samples' to fresh sample data. There is no significant difference between data for fresh and aged IgG2 samples with Brij 35 added at below CMC (Figure 5.15 A).

For particle count data of size $\geq 5 \mu\text{m}$ and $\geq 10 \mu\text{m}$ statistical analysis showed that the difference is significant ($P < 0.001$) between data for fresh and heated samples of IgG2 with Brij 35 below, around and above its CMC and between data from samples of fresh and aged IgG2 with Brij 35 present at above CMC for count data of particles $\geq 10 \mu\text{m}$. There is no statistical difference between fresh and aged IgG2 data for particles of $\geq 5 \mu\text{m}$ with Brij 35 present (Figure 5.15 B and C).

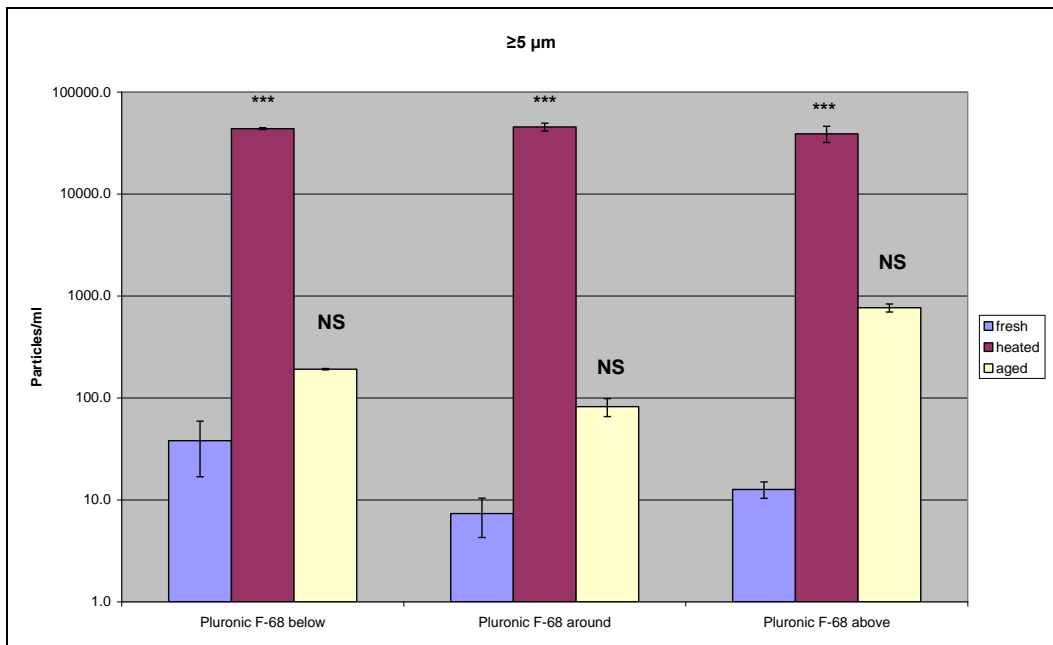
For particle count data of size ≥ 25 , Bonferroni test analysis showed that heat treatment effect on particle count is statistically significant ($P < 0.01$) for IgG2 with Brij 35 present at below and around CMC when compared to unheated samples. Aging does not statistically increase particle level for IgG2 with Brij 35 (Figure 5.15 D).

For particle count data of size $\geq 50 \mu\text{m}$ no statistical difference ($P > 0.05$) was detected between fresh and heated, and between fresh and aged samples of IgG2 with Brij 35 (Figure 5.15 E).

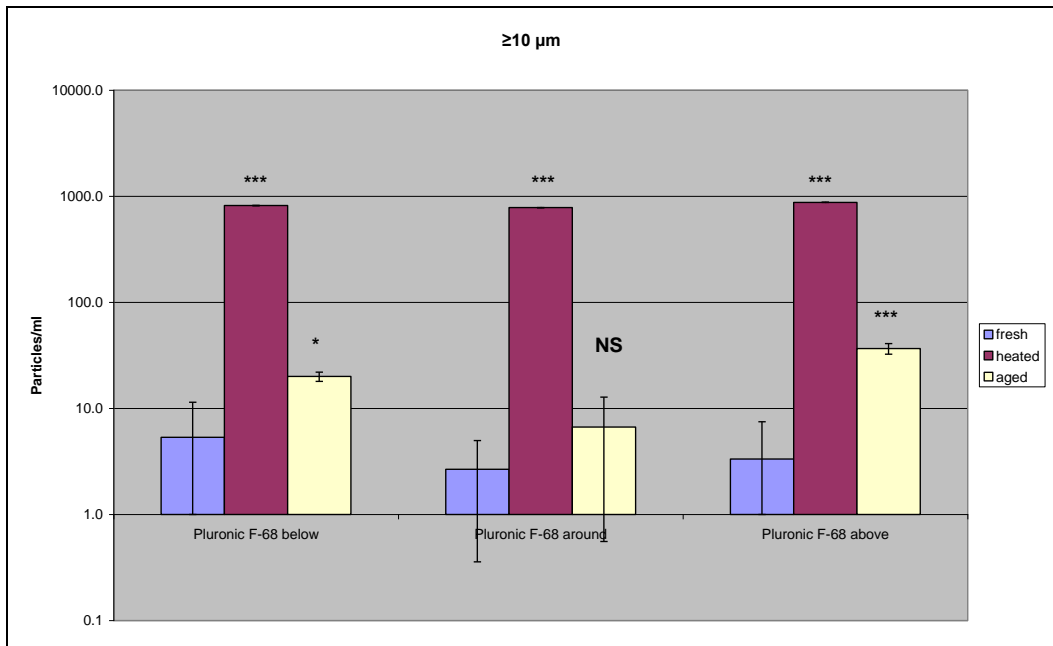
(A)



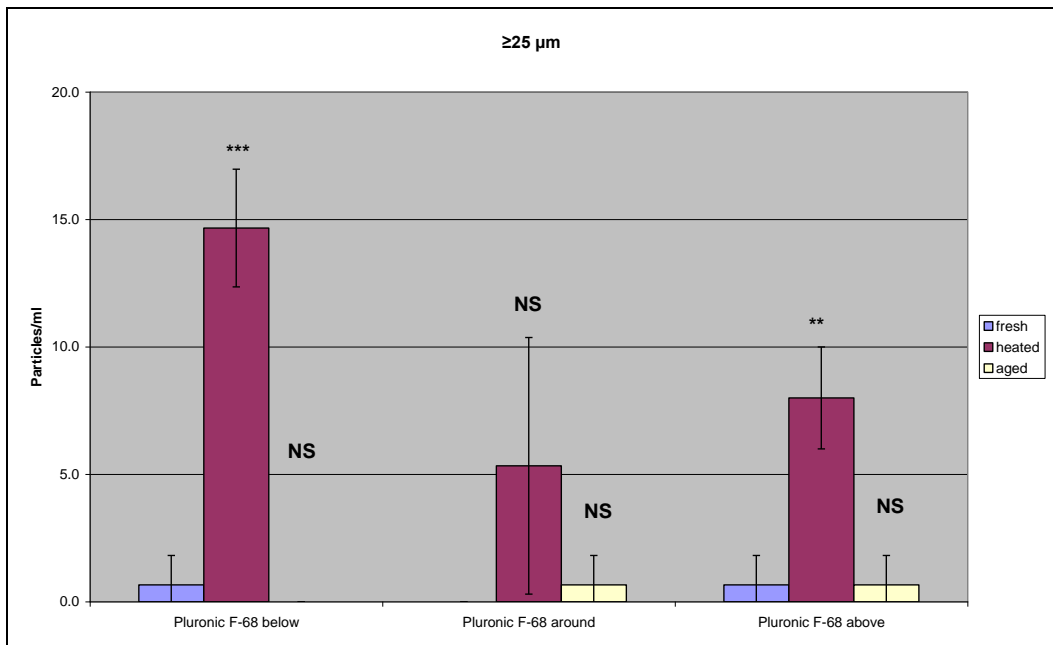
(B)



(C)



(D)



(E)

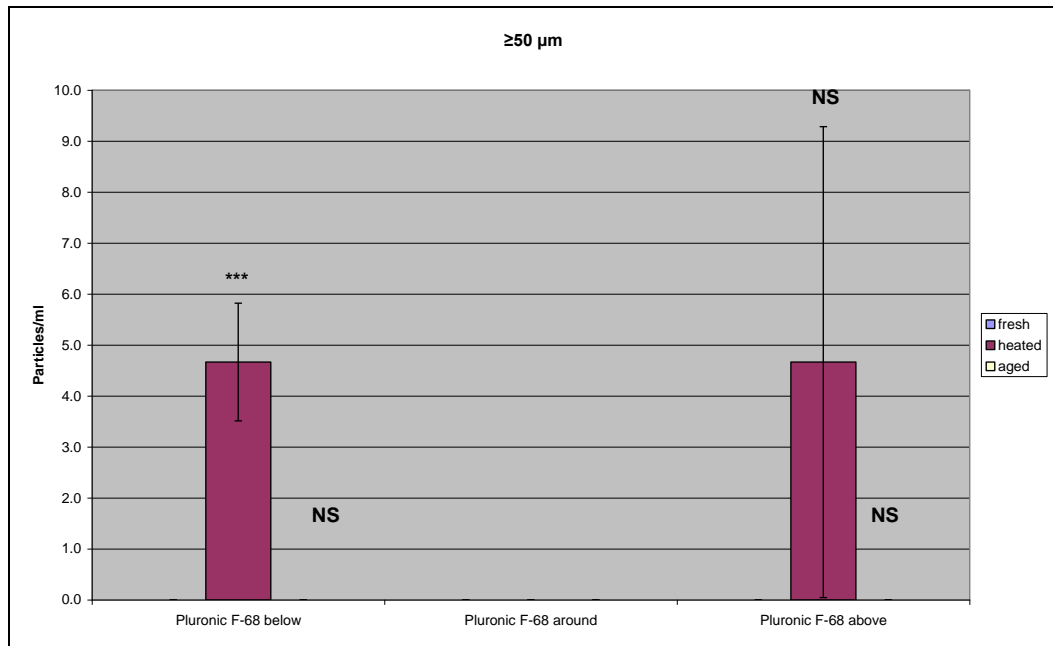


Figure 5.16. Particle concentrations at size ranges of: (A) $\geq 2 \mu\text{m}$, (B) $\geq 5 \mu\text{m}$, (C) $\geq 10 \mu\text{m}$, (D) $\geq 25 \mu\text{m}$, (E) $\geq 50 \mu\text{m}$ measured by HIAC for fresh, heated and aged IgG2 samples with Pluronic F-68 added below, around and above CMC level. Data are expressed as the mean \pm Std. Deviation. * $P < 0.05$, ** $P < 0.01$, * $P < 0.001$; significant difference in particles per ml compared with fresh IgG2 with Pluronic F-68 samples.**

From results presented in Figure 5.16 (A) for particle counts of particles with size $\geq 2 \mu\text{m}$, one-way ANOVA analysis, post-hoc Bonferroni test, showed a significant difference ($P < 0.001$) between fresh and heated samples of IgG2 with Pluronic F-68 present at around and above CMC. The mean difference is also significant at ($P < 0.01$) between fresh and aged IgG2 samples with Pluronic F-68 above CMC. No statistical difference was observed between fresh and aged samples with Pluronic F-68 at below and around CMC (Figure 5.16 A).

For particle count data of size $\geq 5 \mu\text{m}$, statistical analysis showed that heat stress is statistically significant ($P < 0.001$) on particle number for IgG2 samples with Pluronic F-68 present at below, around and above CMC. Aging has no statistically significant effect on particle count (Figure 5.16 B).

For particle count data of size $\geq 10 \mu\text{m}$, the difference is significant ($P < 0.001$) between fresh and heat stressed samples of IgG2 with Pluronic F-68 at below, around and above CMC. Significance at the same statistical level was found between the particle counts of fresh and aged IgG2 with Pluronic F-68 at above CMC. Figure 5.16 (C) illustrates these findings.

For particle count data of size $\geq 25 \mu\text{m}$ particles per ml, Bonferroni test showed that particle count difference is statistically significant ($P < 0.001$) between fresh and heated samples of IgG2 with Pluronic F-68 below its CMC and significant ($P < 0.01$) between fresh and heated IgG2 samples with Pluronic F-68 above CMC. No significant difference is detected between data obtained for samples of fresh and heated IgG2 with Pluronic F-68 around CMC and between the same for fresh and aged samples of IgG2 with Pluronic F-68 (Figure 5.16 D).

For particle count data of size $\geq 50 \mu\text{m}$ no statistical difference ($P > 0.05$) was detected in particle count between fresh and aged samples of IgG2 with Pluronic F-68 at below and above CMC levels. Post-hoc analysis showed a significant difference ($P < 0.001$) between data for samples of fresh and heated IgG2 with Pluronic F-68 below its CMC (Figure 5.16 E).

5.4.2 Micro-flow imaging (MFI) measurements

5.4.2.1 Micro-flow measurements for fresh, heated and aged BSA surfactant free and BSA with Tween 20, Tween 80, Brij 35 and Pluronic F-68 surfactants at below, around and above CMC levels

Micro-flow imaging (MFI) analysis assesses sub-visible particle count per ml, particle size and morphological characteristics for protein particles. The methods used are as described in Chapter 2, Section 2.2.

BSA (10 mg/ml) particles and aggregates were observed to be high in number and heterogeneous in shape, ranging from small dense fibres to large ribbon like aggregates (Figure 5.17).




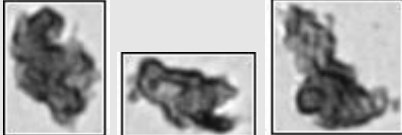
Particle size (μm)	BSA (10 mg/ml)
≥ 2	
≥ 10	
≥ 25	
≥ 50	

Figure 5.17. Representative micro-flow imaging (MFI) example images for BSA (10 mg/ml) particles.

Figure 5.18 shows particle concentration per ml measured for fresh, heated and aged BSA (10 mg/ml) samples.

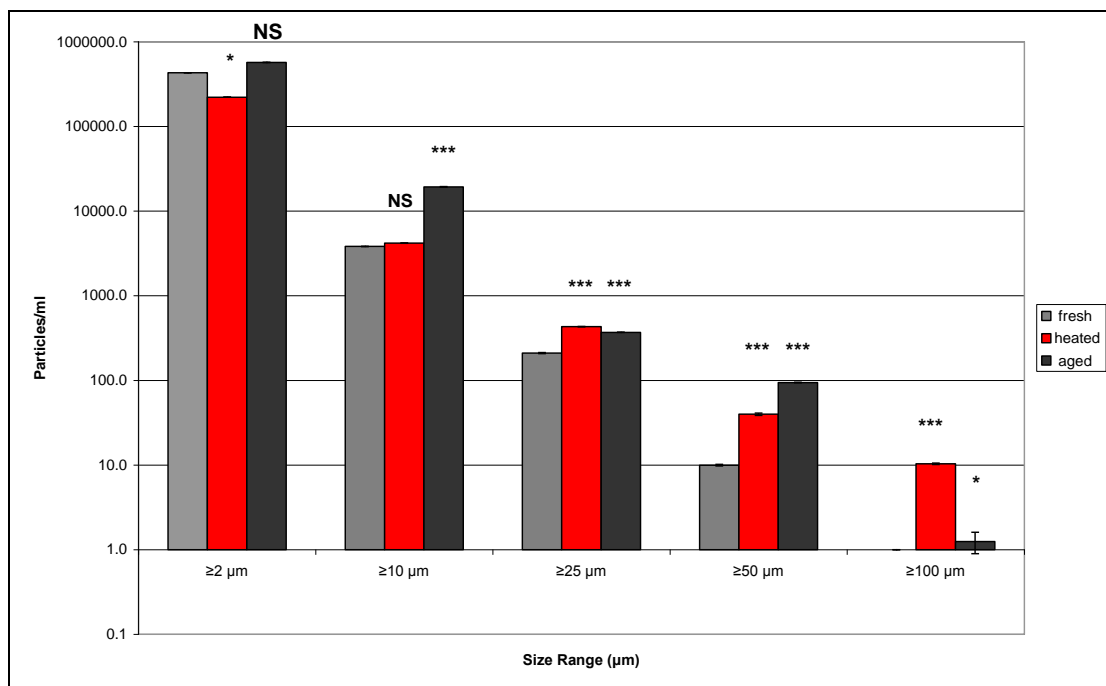


Figure 5.18. Particle concentrations measured by MFI for fresh, heated and aged BSA samples. Data are expressed as the mean \pm Std. Deviation. * $P < 0.05$, ** $P < 0.01$, * $P < 0.001$; significant difference in particles per ml compared with fresh BSA samples.**

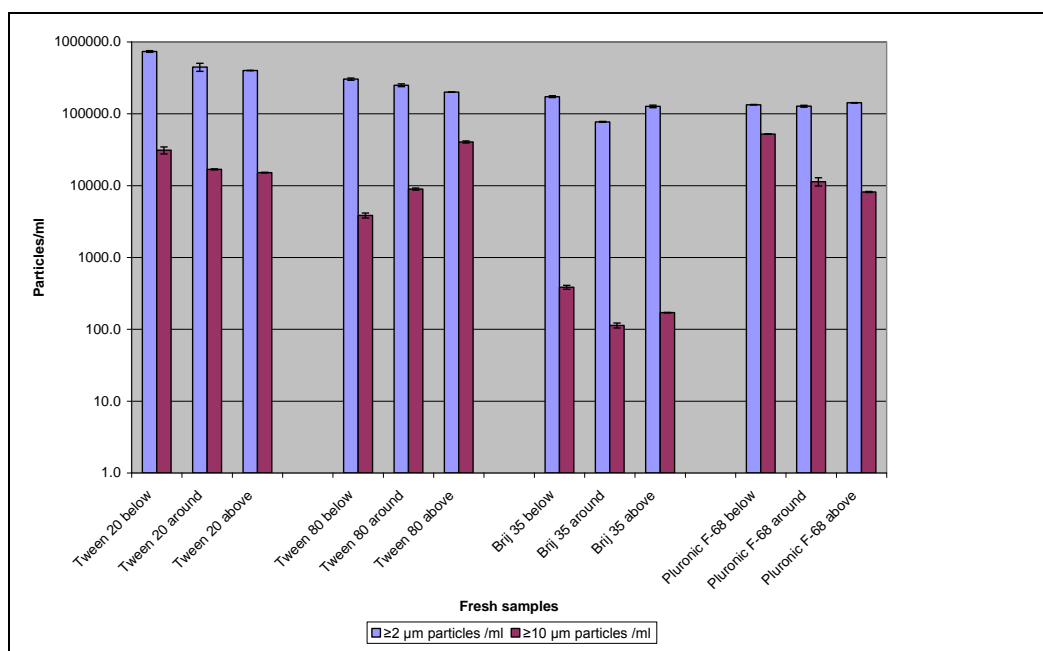
Heat stressed and aged BSA surfactant free formulations produced data with greater numbers of particles per ml of sizes greater than or equal to 10, 25, 50 and 100 μm than that determined for the fresh BSA sample (Figure 5.18). One-way ANOVA analysis showed a significant effect of heat treatment and storage on the number of particles determined per ml of size $\geq 2 \mu\text{m}$, $\geq 10 \mu\text{m}$, $\geq 25 \mu\text{m}$, $\geq 50 \mu\text{m}$ and $\geq 100 \mu\text{m}$. Post-hoc tests, Bonferroni correction showed a significant increase in the number of particles per ml of sizes $\geq 25 \mu\text{m}$ and $\geq 50 \mu\text{m}$ ($P < 0.001$) for heated and aged samples compared to fresh BSA.

For particle count data of size $\geq 10 \mu\text{m}$ size range Bonferroni statistical results showed that the mean increase is significant ($P < 0.001$) for aged BSA samples, but there was no statistical significance between fresh and heated

samples ($P > 0.05$). For particle count data of size $\geq 100 \mu\text{m}$ heated BSA samples showed a statistically significant increase in particle count ($P < 0.001$), whereas aged BSA samples had statistical significance at a lower level ($P < 0.05$) when compared to fresh samples (Figure 5.18).

Figure 5.19 shows the number of particles for size ranges of $\geq 2 \mu\text{m}$, $\geq 10 \mu\text{m}$, $\geq 25 \mu\text{m}$, $\geq 50 \mu\text{m}$ and $\geq 100 \mu\text{m}$ per ml measured by Micro-Flow Imaging for fresh samples of BSA with added Tween 20, Tween 80, Brij 35 and Pluronic F-68 surfactants.

(A)



(B)

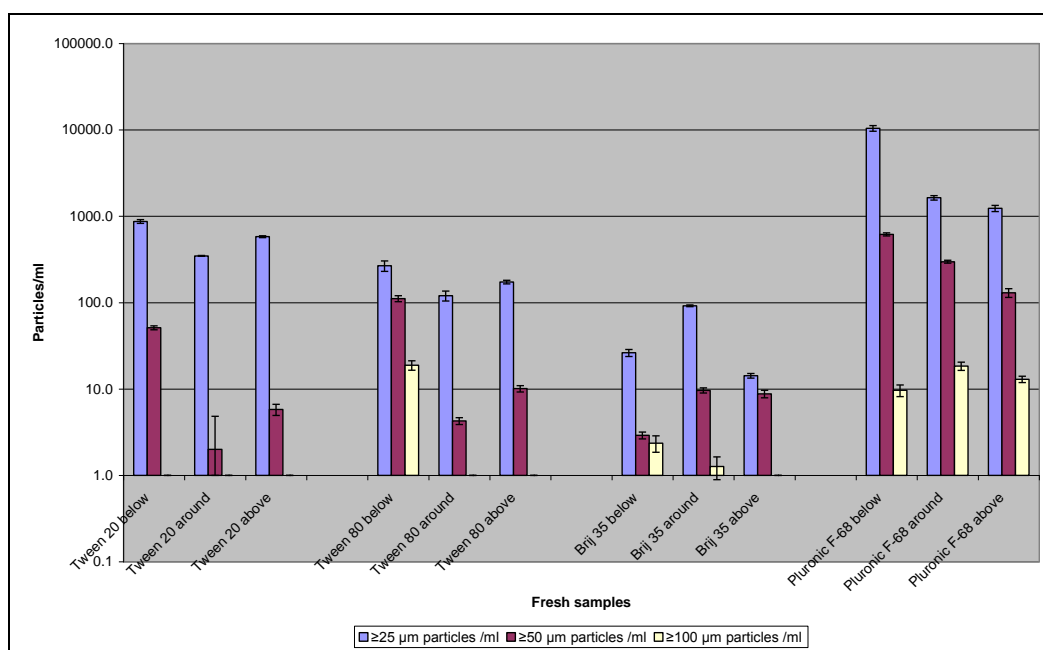


Figure 5.19. Particle concentrations in size ranges: (A) $\geq 2 \mu\text{m}$ and $\geq 10 \mu\text{m}$, (B) $\geq 25 \mu\text{m}$, $\geq 50 \mu\text{m}$ and $\geq 100 \mu\text{m}$ per ml measured by MFI for fresh BSA samples with added Tween 20, Tween 80, Brij 35 and Pluronic F-68 surfactants at levels below, around and above their CMC. Data are expressed as the mean \pm Std. Deviation.

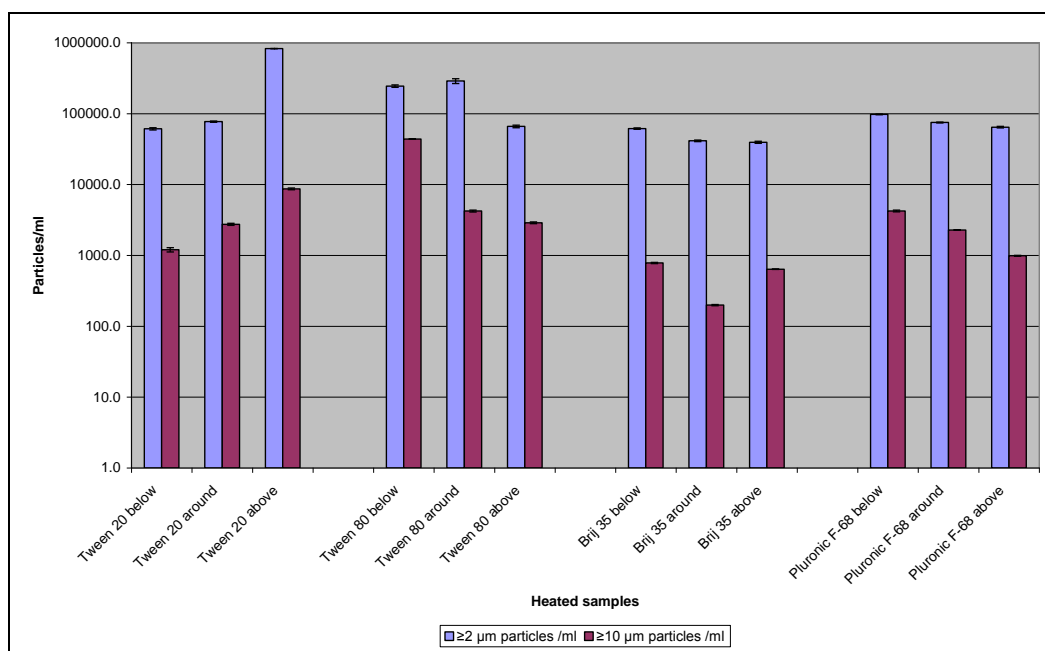
Data obtained for formulations of BSA containing Tween 20 at below and around CMC showed an increase in the number of particles $\geq 2 \mu\text{m}$ compared to fresh BSA surfactant free formulations (Figure 5.19 A).

BSA formulations with Tween 20, Brij 35 and Pluronic F-68 at all concentrations, and formulations containing Tween 80 at concentrations around and above CMC showed an increase in the number of particles per ml of size greater than or equal to $10 \mu\text{m}$ compared to fresh surfactant-free BSA samples (Figure 5.19).

For particle count data of size greater than or equal to $25 \mu\text{m}$, BSA with Tween 20 and Pluronic F-68 at all concentrations, and with Tween 80 below its CMC, produced an increase in particle count compared to BSA surfactant free samples (Figure 5.19 B). For particle count data of size $\geq 50 \mu\text{m}$, BSA solutions with Tween 20 and Tween 80 below their CMC and Pluronic F-68 at all concentrations showed an increase in particle count. For particle count data of size $\geq 100 \mu\text{m}$, an increase in particle count was detected for samples containing Tween 80 and Brij 35 below their CMC and for Pluronic F-68 samples at around and above its CMC when compared to BSA surfactant free solution.

Figure 5.20 shows particle count per ml data measured for heated BSA with Tween 20, Tween 80, Brij 35 and Pluronic F-68 surfactants present at below, around and above CMC.

(A)



(B)

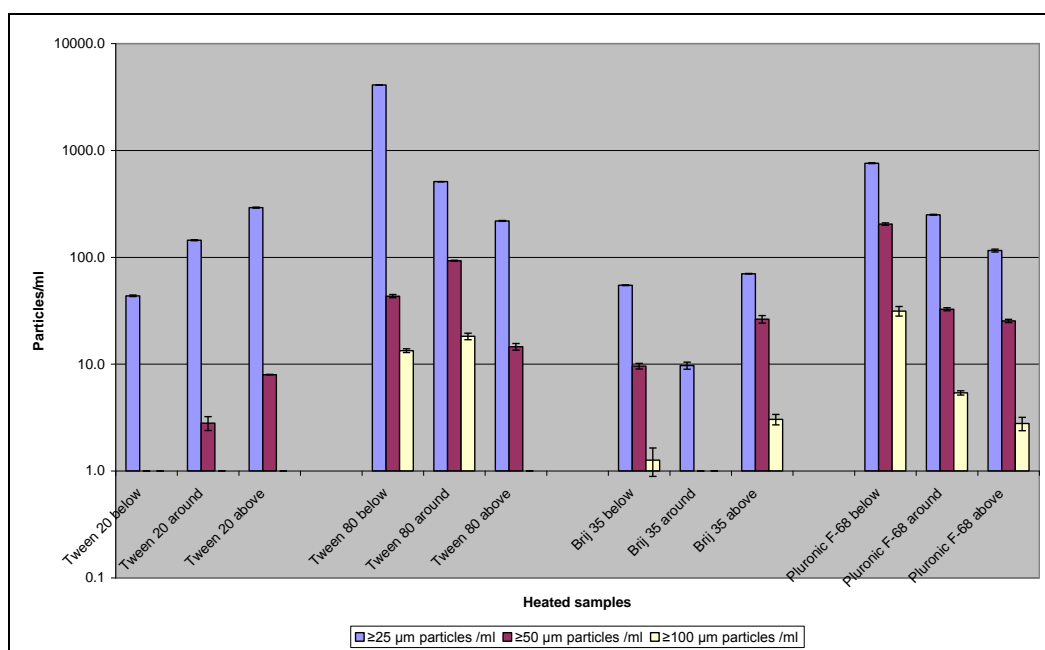


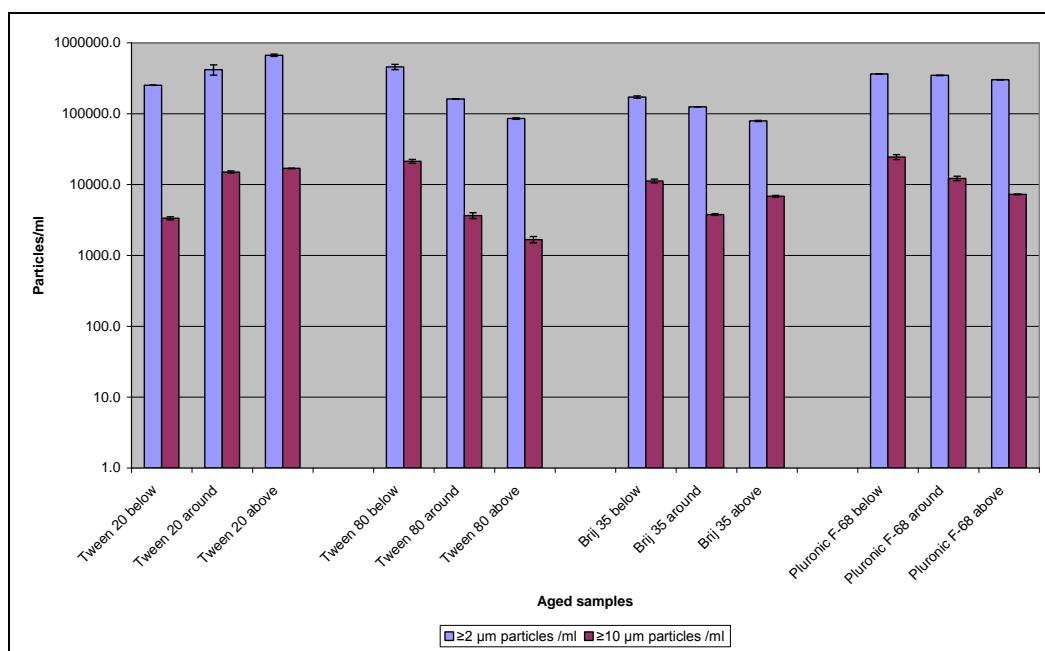
Figure 5.20. Particle concentrations in size ranges: (A) $\geq 2 \mu\text{m}$ and $\geq 10 \mu\text{m}$, (B) $\geq 25 \mu\text{m}$, $\geq 50 \mu\text{m}$ and $\geq 100 \mu\text{m}$ per ml measured by MFI for heated BSA samples with added Tween 20, Tween 80, Brij 35 and Pluronic F-68 surfactants at below, around and above their CMC levels. Data are expressed as the mean \pm Std. Deviation.

Heat stressed BSA (10 mg/ml) formulations showed a slight increase in the number of particles per ml greater than or equal to 2 μm for formulations containing Tween 20 above its CMC and containing Tween 80 below and around its CMC level. Data obtained when the other surfactants were employed showed a decrease in particle count for particles $\geq 2 \mu\text{m}$ when compared to the heated BSA surfactant free sample.

For particle count data of size $\geq 10 \mu\text{m}$, BSA with Tween 20 above and Tween 80 below their CMC showed an increase in particle count compared to the other surfactants and heat stressed surfactant free BSA (Figure 5.20 A, Figure 5.18).

Heated BSA formulations with Tween 80 below and around its CMC and Pluronic F-68 below its CMC showed an increase in the number of particles greater than or equal to 25 μm , 50 μm and 100 μm compared to other surfactants and a BSA surfactant free sample (Figure 5.20 B).

(A)



(B)

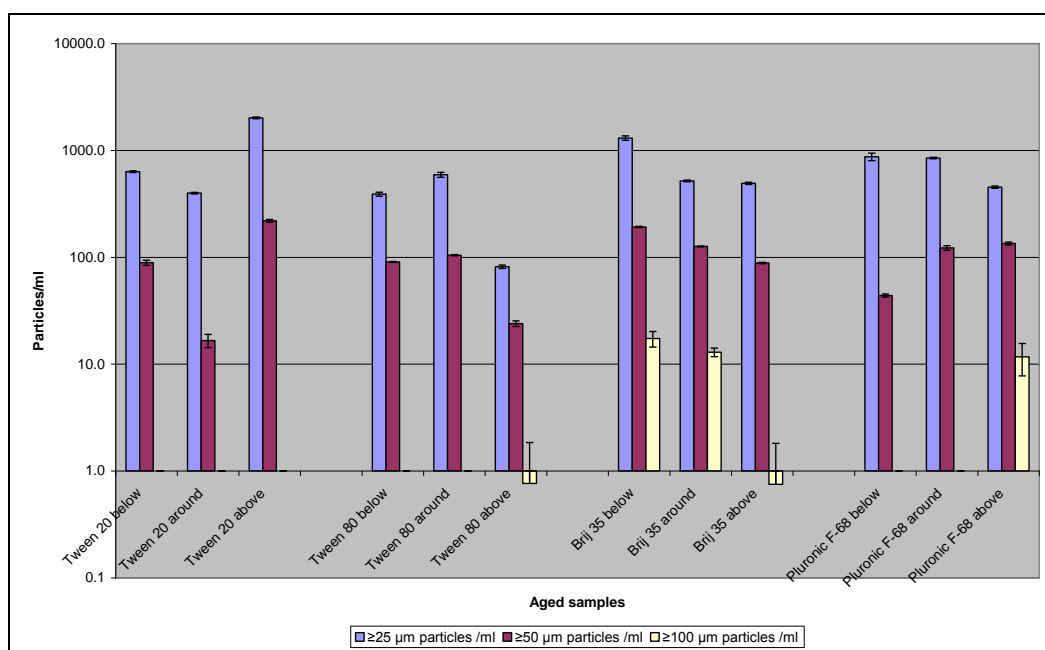


Figure 5.21. Particle concentration for size ranges: (A) $\geq 2 \mu\text{m}$ and $\geq 10 \mu\text{m}$, (B) $\geq 25 \mu\text{m}$, $\geq 50 \mu\text{m}$ and $\geq 100 \mu\text{m}$ measured by MFI for aged BSA samples with Tween 20, Tween 80, Brij 35 and Pluronic F-68 surfactants at below, around and above their CMC levels. Data are expressed as the mean \pm Std. Deviation.

For aged formulations of BSA containing Tween 20 at above its CMC, data showed an increase in particle count for particles $\geq 2 \mu\text{m}$ (Figure 5.21 A).

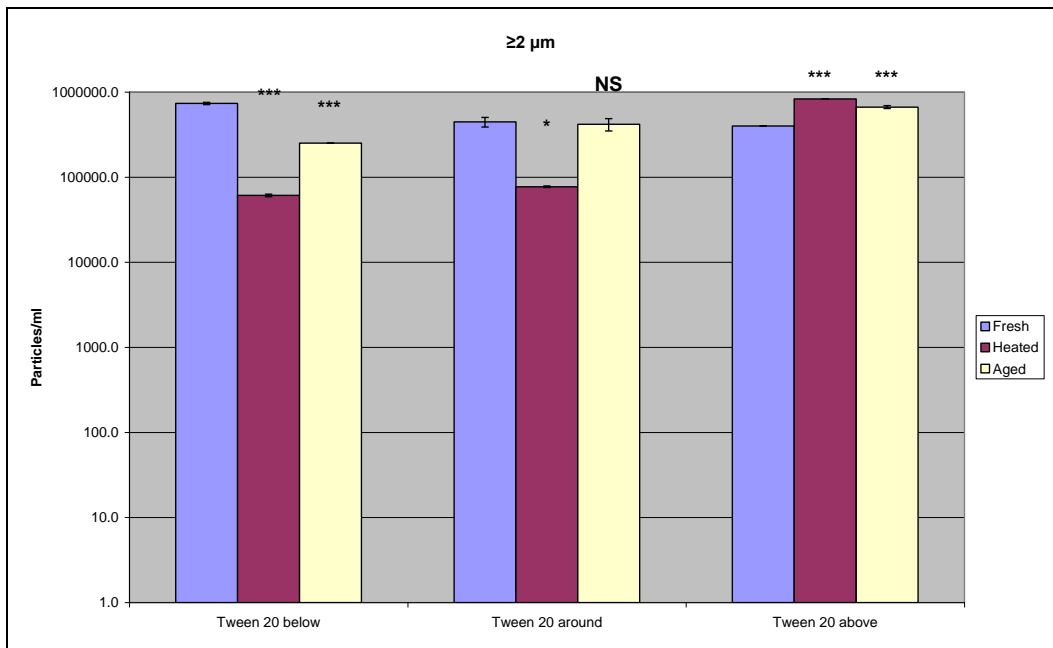
For particle count data of size $\geq 10 \mu\text{m}$, samples with Tween 80 and Pluronic F-68 showed a slight increase in particle count compared to other surfactant and aged BSA surfactant free samples.

The number of $\geq 25 \mu\text{m}$ particles measured for the aged BSA sample with Tween 80 above its CMC was lower compared to the remainder of the surfactants and surfactant free samples which showed an increase in particle count per ml (Figure 5.18). For particle count data of size $\geq 50 \mu\text{m}$, samples of aged BSA with Tween 20 above, Tween 80 around, Brij 35 below and around, and Pluronic F-68 around and above their respective CMC, all showed an increased particle count number compared to aged surfactant free BSA (Figure 5.21 B).

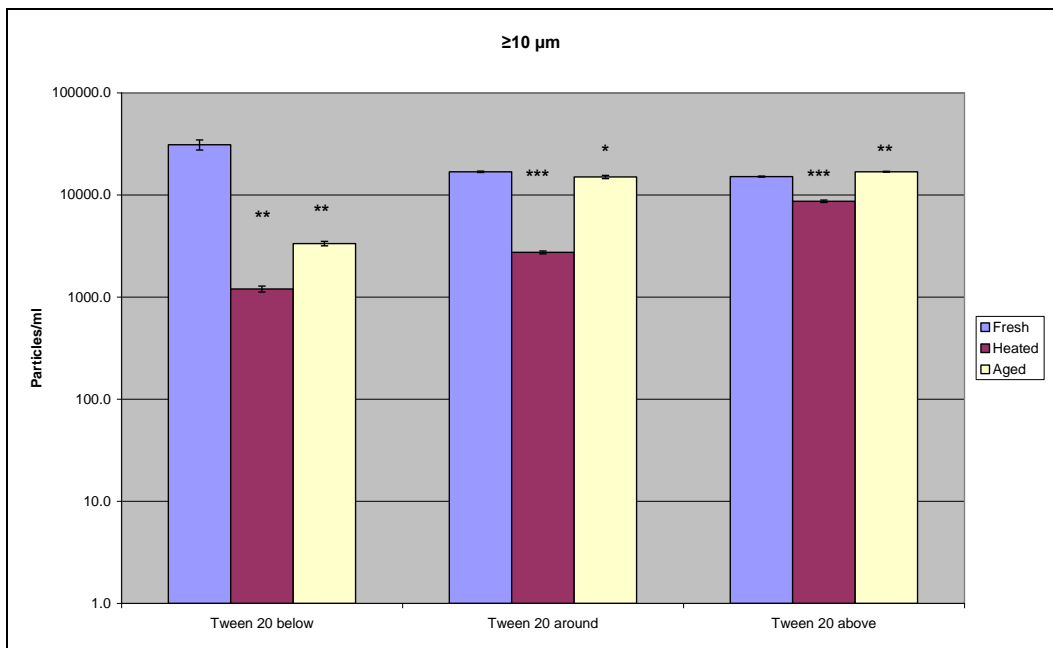
For particle count data of size $\geq 100 \mu\text{m}$ samples of aged BSA with Brij 35 below and around its CMC and Pluronic F-68 above its CMC displayed an increase in particle count compared to the other surfactants and aged BSA surfactant free formulations.

Figures 5.22 to 5.25 illustrate how particle count data of size of $\geq 2 \mu\text{m}$, $\geq 10 \mu\text{m}$, $\geq 25 \mu\text{m}$, $\geq 50 \mu\text{m}$ and $\geq 100 \mu\text{m}$ are affected by heat stress and aging of BSA with each surfactant at below, around and above its CMC levels.

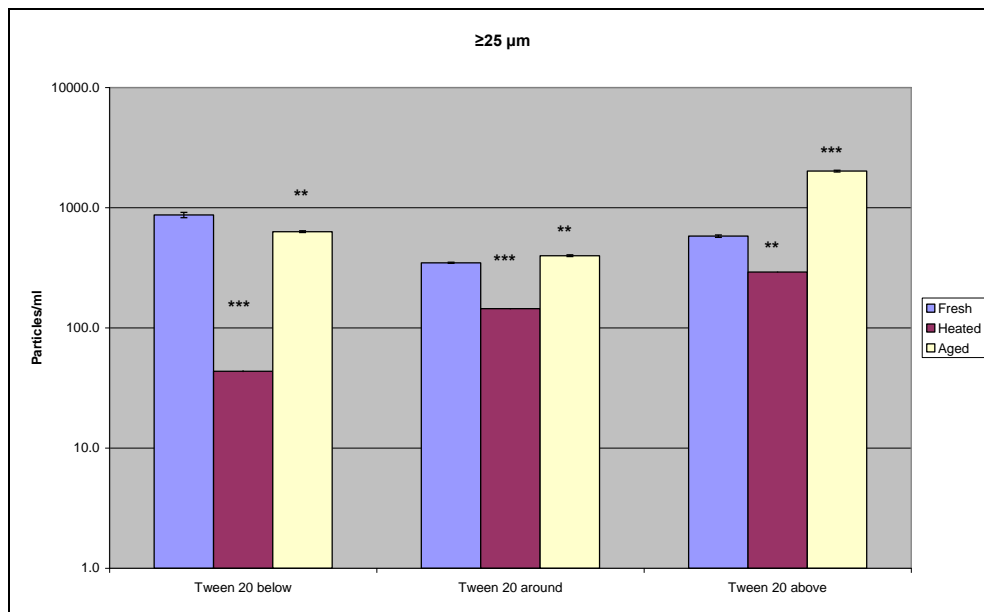
(A)



(B)



(C)



(D)

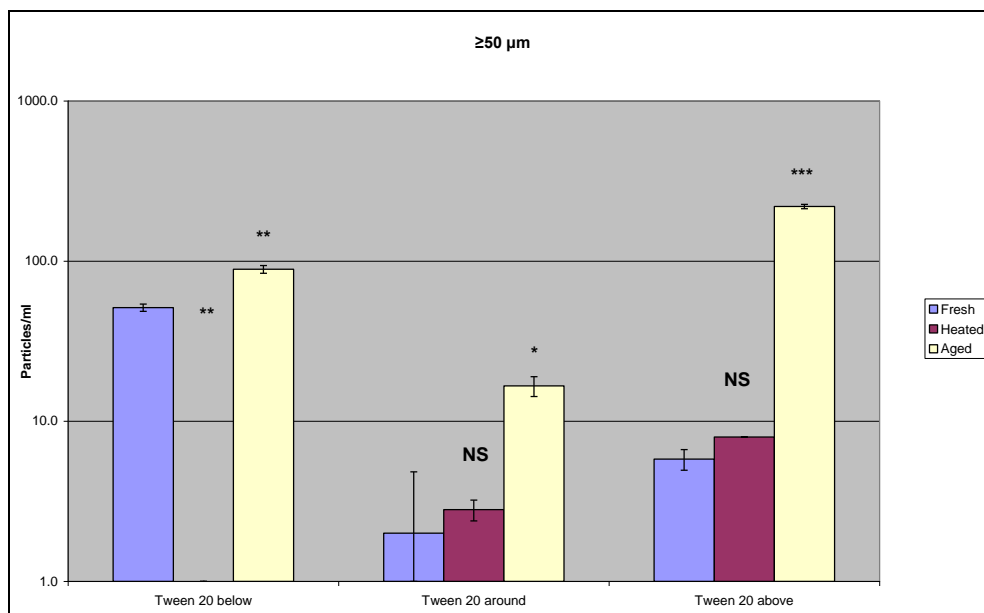


Figure 5.22. Particle concentrations at size ranges of: (A) $\geq 2 \mu\text{m}$, (B) $\geq 10 \mu\text{m}$, (C) $\geq 25 \mu\text{m}$, (D) $\geq 50 \mu\text{m}$ measured by MFI for fresh, heated and aged BSA with added Tween 20 below, around and above its CMC level. Data are expressed as the mean \pm Std. Deviation. * $P < 0.05$, ** $P < 0.01$, * $P < 0.001$; significant difference in particles per ml compared with fresh BSA with Tween 20 samples.**

One-way ANOVA analysis, using the Bonferroni correction, showed a significant effect of the effect of heat stress and aging samples of BSA with added Tween 20 surfactant at below, around and above its CMC on particle count at a particle size range $\geq 2 \mu\text{m}$ particles. The mean difference in particle count is significant ($P < 0.001$) between fresh and heated BSA samples with Tween 20 added below and above its CMC, and is also significant ($P < 0.05$) between fresh and heated BSA samples with Tween 20 added at around CMC (Figure 5.22 A).

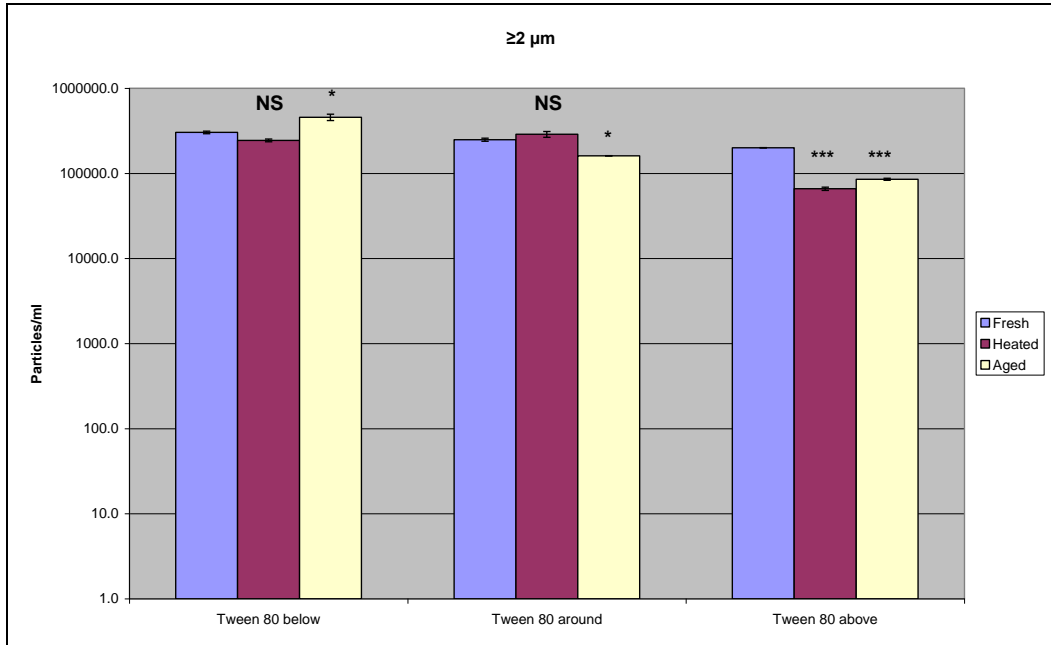
For particle count data of size $\geq 10 \mu\text{m}$, statistical analysis showed that the difference in count is significant ($P < 0.01$) between fresh and heated BSA samples with Tween 20 present below its CMC. The mean difference is also significant ($P < 0.001$) between data obtained for fresh and heated samples of BSA with Tween 20 present at around and above its CMC (Figure 5.22 B).

For particle count data of size ≥ 25 , Bonferroni test analysis showed that the count difference is statistically significant ($P < 0.001$) between fresh and heated BSA with Tween 20 present at below and around its CMC and also significant ($P < 0.01$) between fresh and heated BSA samples with Tween 20 present at around its CMC and similarly significant between fresh and aged BSA with Tween 20 added below and around its CMC (Figure 5.22 C).

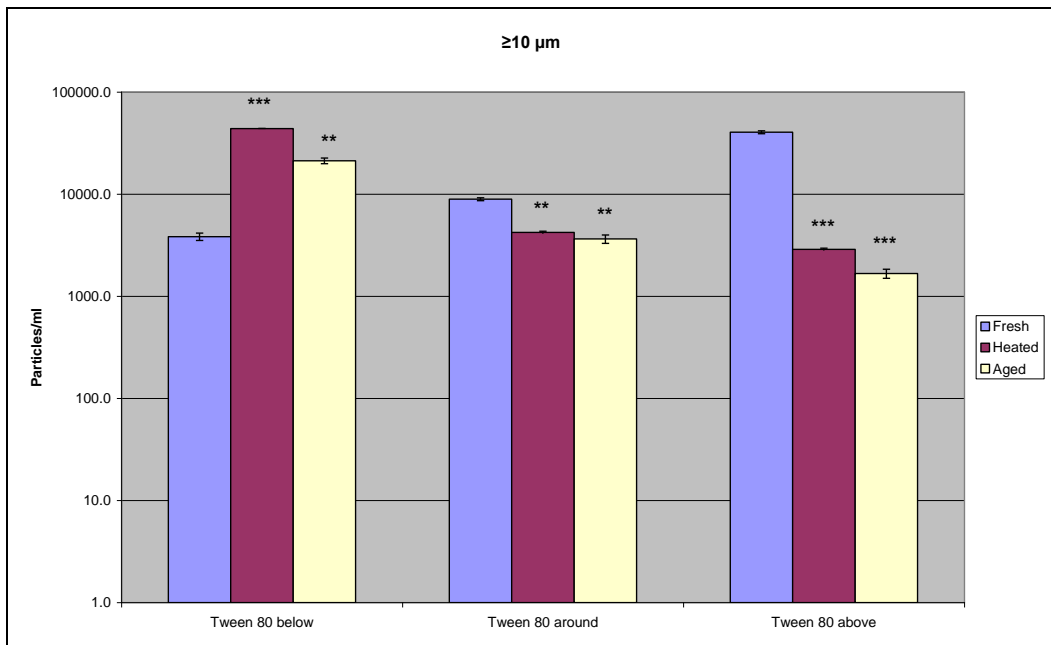
For particle count data of size $\geq 50 \mu\text{m}$ no statistical difference ($P > 0.05$) was detected between fresh and heated BSA samples with Tween 20 present at around and above its CMC. Post-hoc analysis showed a significant difference ($P < 0.001$) between particle counts of fresh and aged BSA samples with Tween 20 present at above its CMC and also a significant difference

($P < 0.01$) between fresh and heated samples, and fresh and aged samples of BSA with Tween 20 present below its CMC (Figure 5.22 D).

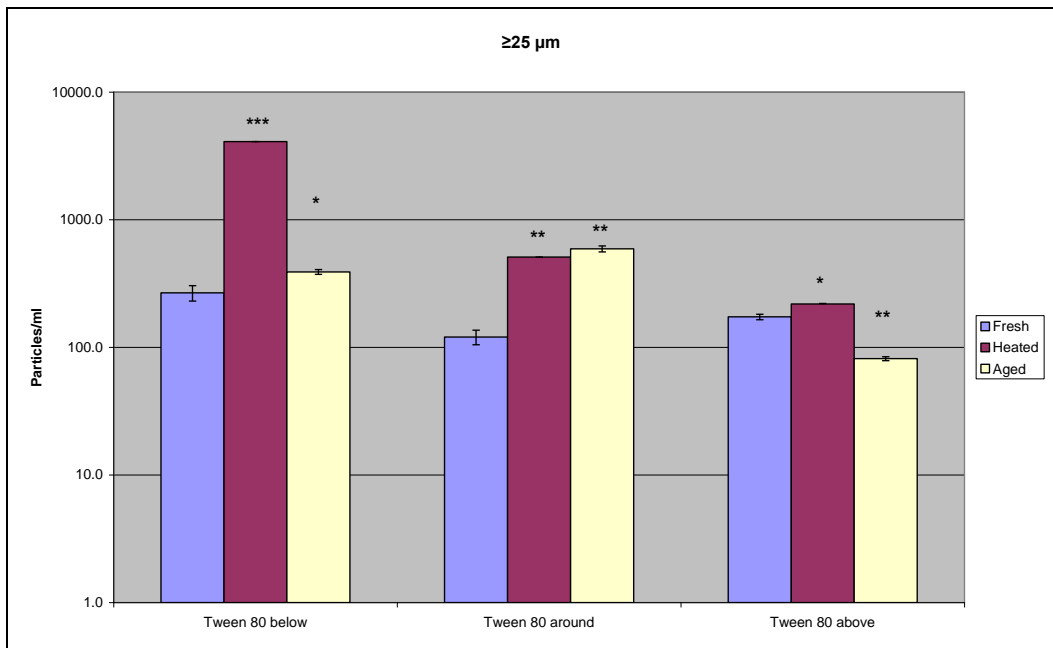
(A)



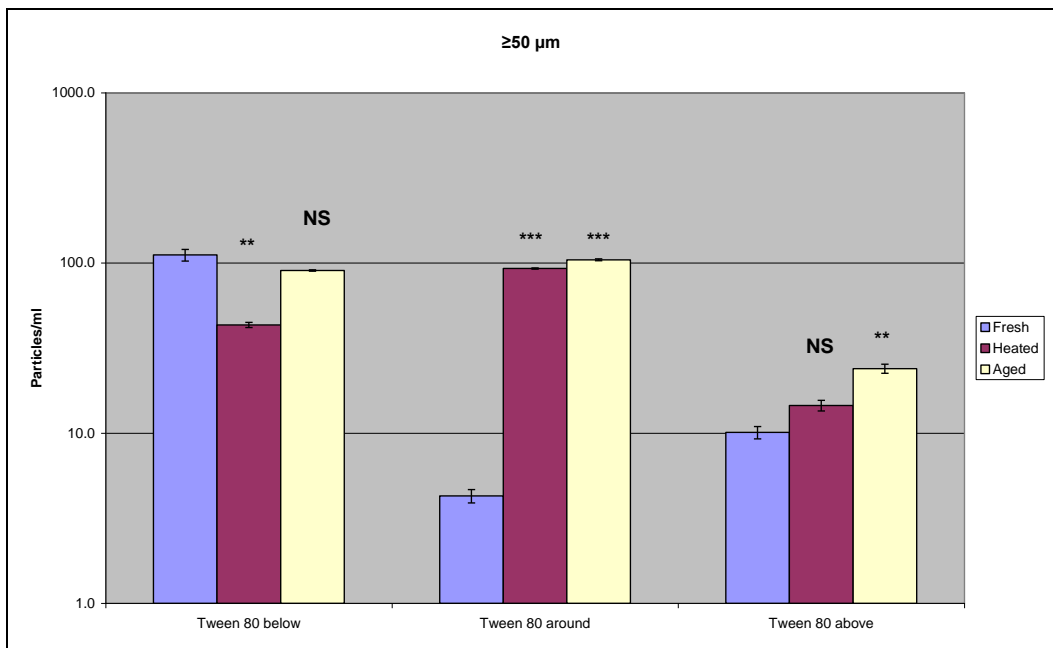
(B)



(C)



(D)



(E)

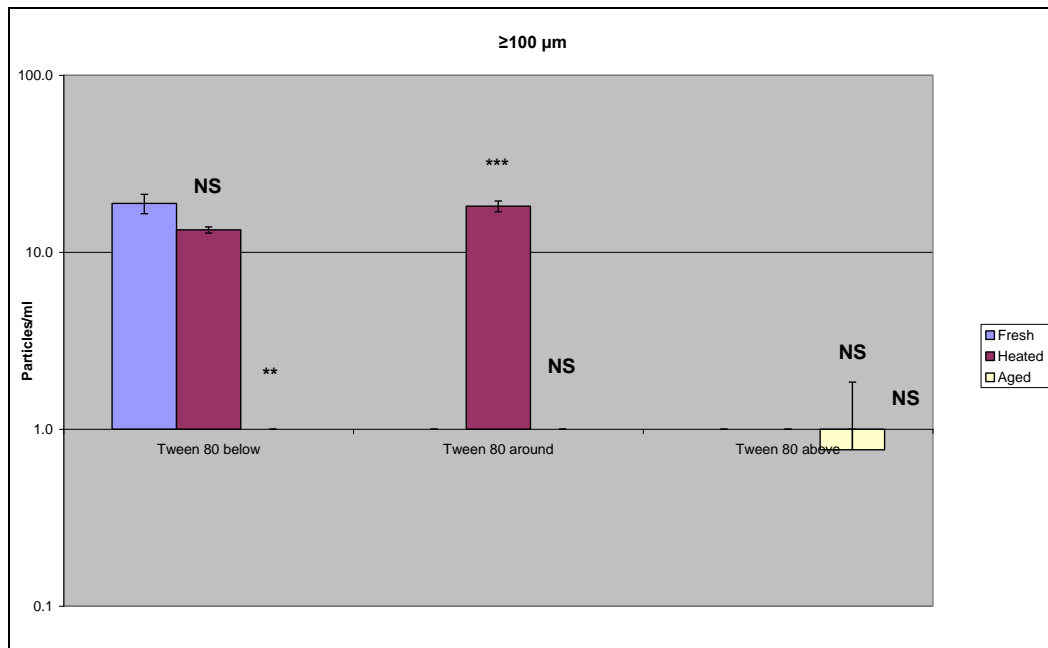


Figure 5.23. Particle concentrations at size ranges of: (A) $\geq 2 \mu\text{m}$, (B) $\geq 10 \mu\text{m}$, (C) $\geq 25 \mu\text{m}$, (D) $\geq 50 \mu\text{m}$ and (E) $\geq 100 \mu\text{m}$ measured by MFI for fresh, heated and aged BSA with added Tween 80 below, around and above its CMC level. Data are expressed as the mean \pm Std. Deviation. * $P < 0.05$, ** $P < 0.01$, * $P < 0.001$; significant difference in particles per ml compared with fresh BSA with Tween 80 samples.**

Figure 5.23 illustrates results from a One-way ANOVA analysis for fresh, heated and aged BSA samples in the presence of with Tween 80. Bonferroni correction analysis showed a significant effect of the effect of heat stress and aging treatment on the particle count of BSA samples with Tween 80 surfactant present at below, around and above its CMC for particles $\geq 2 \mu\text{m}$ particles per ml. The mean difference in particle count was ($P < 0.001$). The particle count difference between fresh and aged Tween 80 samples with below and around CMC levels is significant ($P < 0.05$). No significant

difference is detected between fresh and heated BSA samples with Tween 80 present at levels below and around its CMC (Figure 5.23 A).

For particle count data of size $\geq 10 \mu\text{m}$, statistical analysis showed that heat treatment had a significant effect ($P < 0.01$) for BSA samples with Tween 80 present at around its CMC, whereas for BSA samples with Tween 80 below and above its CMC, heat stress had a more significant effect ($P < 0.001$). Aging of samples of BSA with Tween 80 present below and around its CMC showed a significant effect ($P < 0.01$) and also showed significance for samples with Tween 80 above its ($P < 0.001$) level when comparing particle counts with that of the fresh samples (Figure 5.23 B).

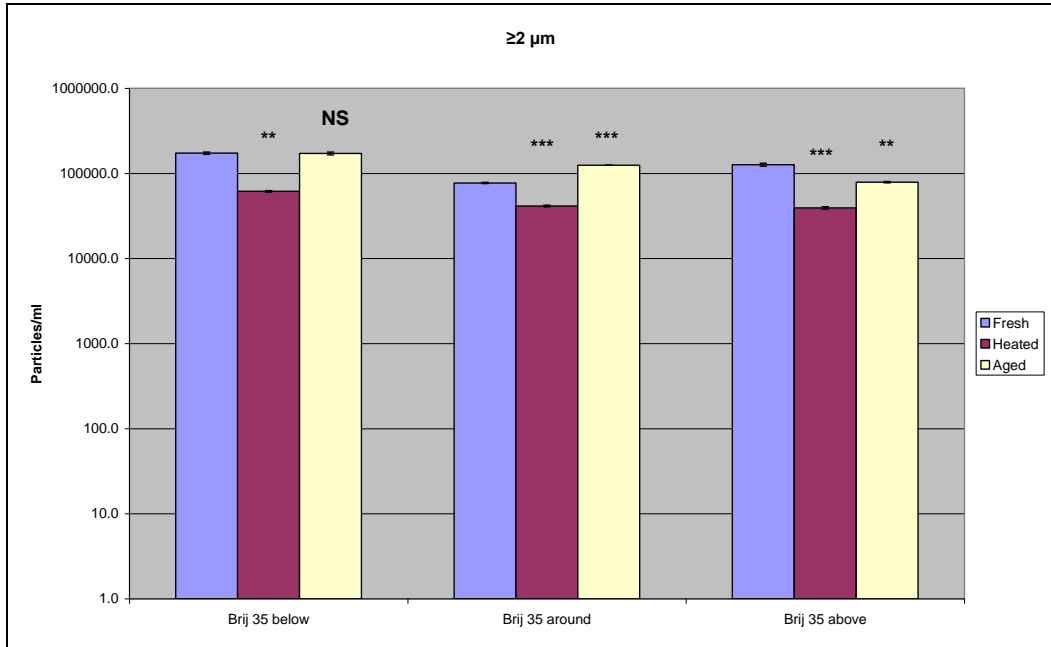
For particle count data of size $\geq 25 \mu\text{m}$ shown in Figure 5.23 C, Bonferroni test results showed that heat treatment has a statistically significant effect ($P < 0.001$) only for samples including Tween 80 at below CMC concentrations. Aging has statistically significant effect at the 0.01 level for BSA with Tween 80 present at around and above its CMC

For particle count data of size $\geq 50 \mu\text{m}$ no statistical difference ($P > 0.05$) was detected between the particle counts of fresh and aged BSA samples with Tween 80 below its CMC and between fresh and heated BSA samples with Tween 80 above its CMC. Both heat treatment and aging had a significant effect ($P < 0.001$) on particle count for BSA samples with Tween 80 present at around its CMC (Figure 5.23 D).

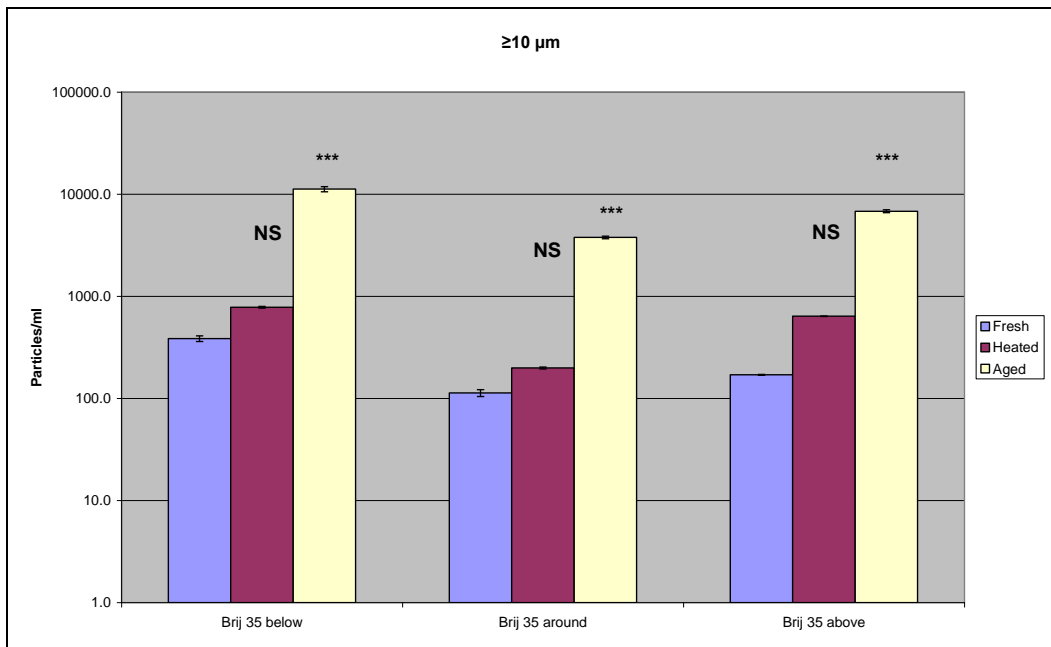
For particle count data of size $\geq 100 \mu\text{m}$, post-hoc test analysis showed that heat stress has a statistically significant effect ($P < 0.001$) for samples with Tween 80 present at around its CMC. Aging has a significant effect at the

0.01 level ($P < 0.01$) for samples of BSA with Tween 80 present at below its CMC (Figure 5.23 E).

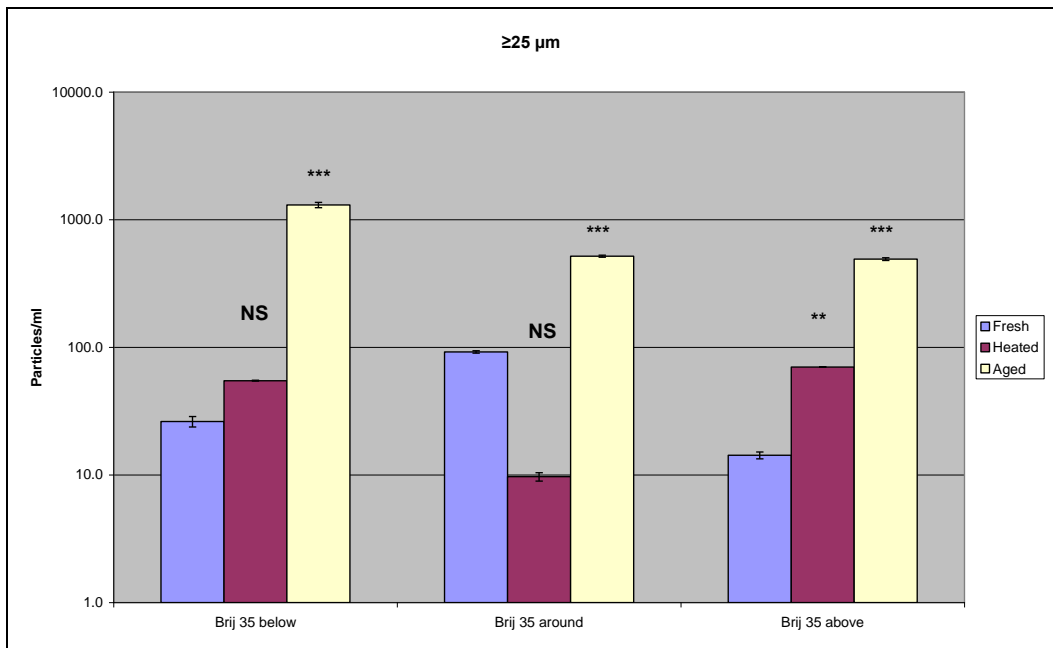
(A)



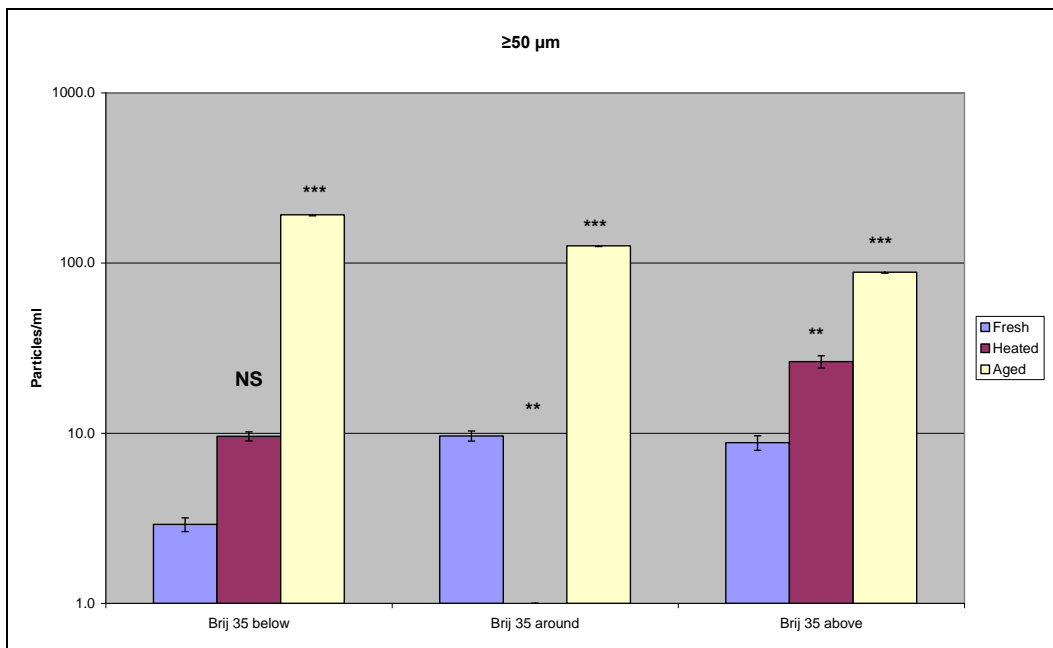
(B)



(C)



(D)



(E)

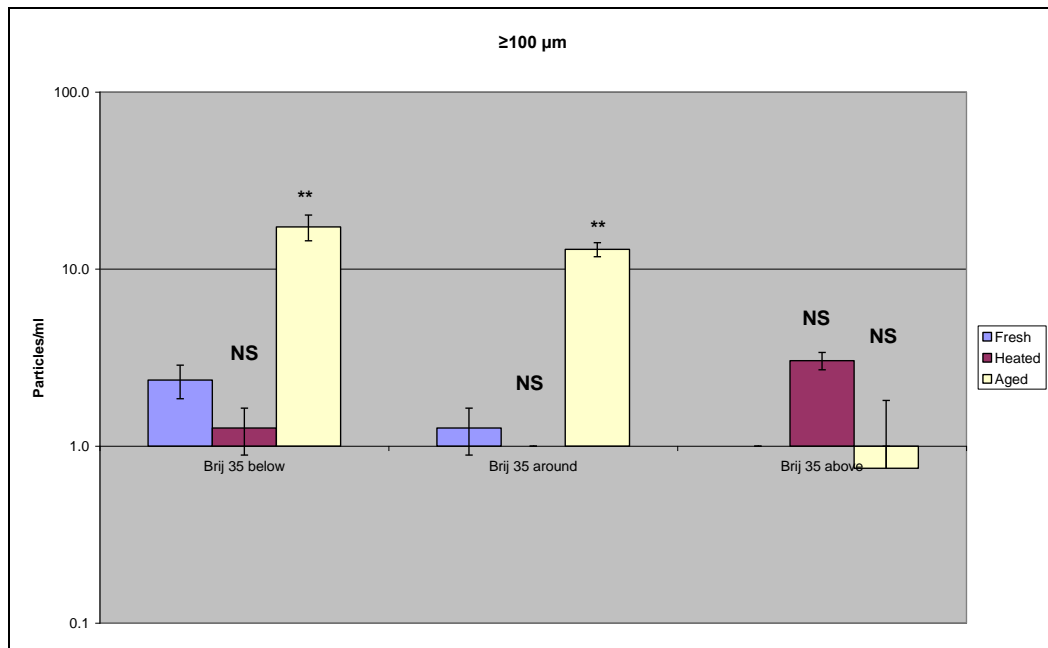


Figure 5.24. Particle concentrations at size ranges of: (A) $\geq 2 \mu\text{m}$, (B) $\geq 10 \mu\text{m}$, (C) $\geq 25 \mu\text{m}$, (D) $\geq 50 \mu\text{m}$ and (E) $\geq 100 \mu\text{m}$ measured by MFI for fresh, heated and aged BSA with added Brij 35 at below, around and above its CMC. Data are expressed as the mean \pm Std. Deviation. * $P < 0.05$, ** $P < 0.01$, * $P < 0.001$; significant difference in particles per ml compared with fresh BSA with Brij 35 samples.**

One-way ANOVA analysis, Bonferroni test results illustrated in Figure 5.24 show the significant effect of heat stress on particle count for BSA samples with Brij 35 surfactant present at below, around and above its CMC for particles $\geq 2 \mu\text{m}$. The mean difference in count is significant at the 0.001 level ($P < 0.001$) for BSA samples with Brij 35 present at around and above its CMC. The particle count difference between fresh and aged BSA samples with Brij 35 present at above its CMC is significant at the 0.01 level ($P < 0.01$) and for samples of BSA with Brij 35 at around its CMC the count difference is significant at the 0.01 level ($P < 0.01$) (Figure 5.24 A).

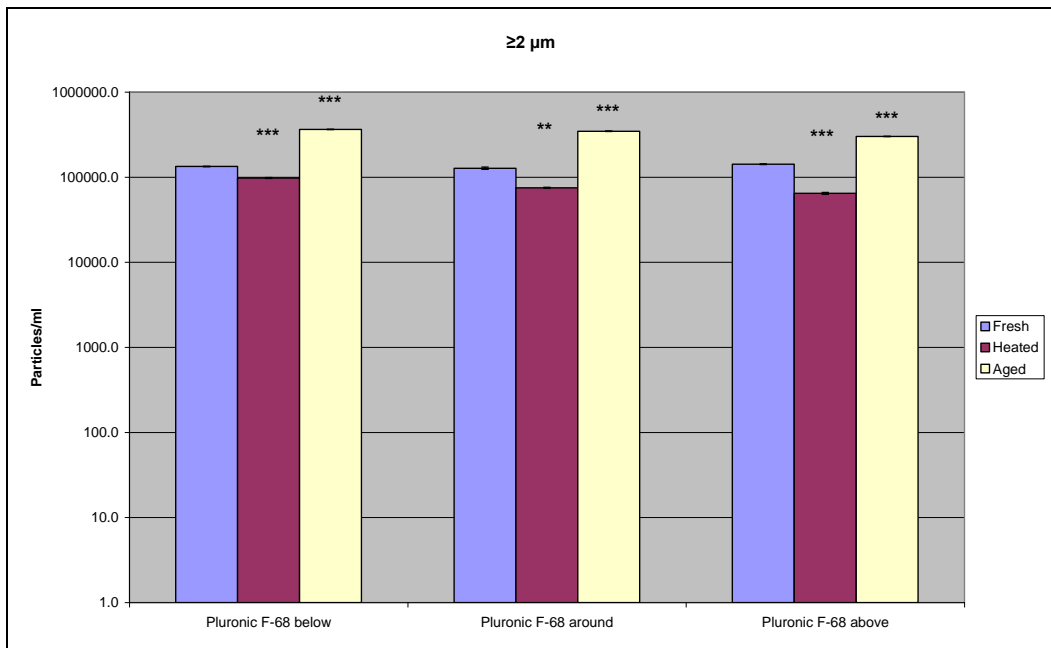
For particle count data of size $\geq 10 \mu\text{m}$, statistical analysis showed a significant difference ($P < 0.001$) between fresh and aged samples of BSA with Brij 35 at concentrations below, around and above its CMC. There is no significant difference between the particle counts of fresh and heated BSA with Brij 35 present at below, around and above its CMC (Figure 5.24 B).

For particle count data of size $\geq 25 \mu\text{m}$ particles, Bonferroni test analysis showed that the effect of heat treatment on particle count is statistically significant at the 0.01 level ($P < 0.01$) for BSA samples with Brij 35 above at levels above its CMC. No statistical difference was observed between fresh and heated BSA with Brij 35 present at concentrations below and around its CMC. Aging treatment produced a statistically significant effect on particle count ($P < 0.001$) for samples of BSA with Brij 35 at levels below, around and above its CMC (Figure 5.24 C).

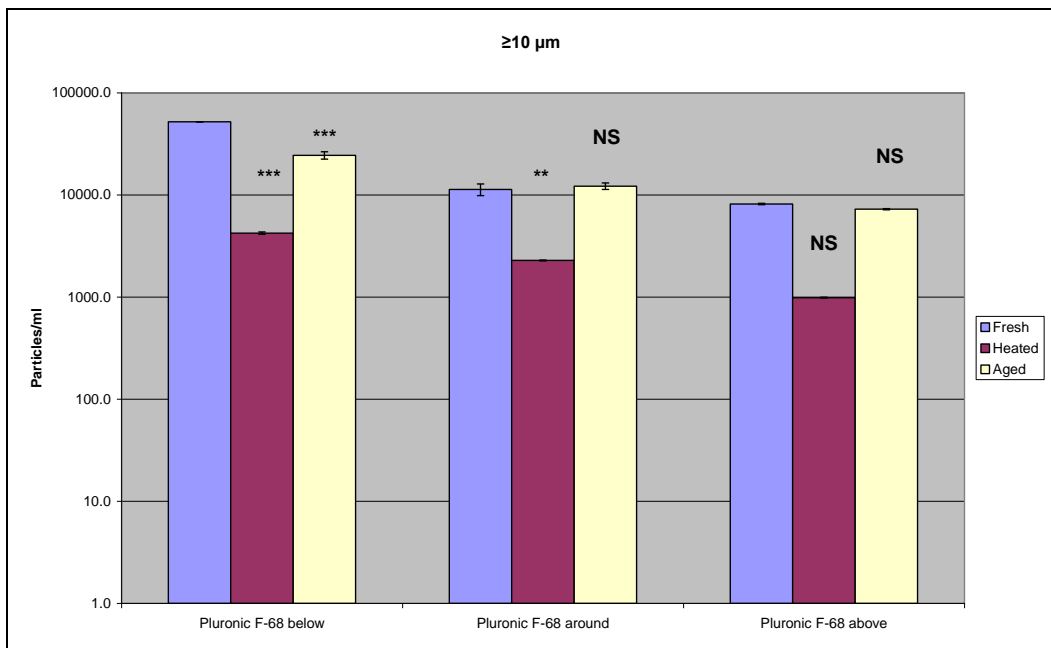
For particle count data of size $\geq 50 \mu\text{m}$ no statistical difference ($P > 0.05$) on count was detected between fresh and heated BSA samples with Brij 35 at below CMC. Aging treatment produced a statistically significant effect at the 0.001 level ($P < 0.001$) for samples of BSA with Brij 35 at levels below, around and above its CMC (Figure 5.24 D).

For particle count data of size $\geq 100 \mu\text{m}$ statistical analysis showed no statistical difference between fresh and heated BSA samples with Brij 35. Aging of samples produced a significant effect on particle count at the 0.01 level ($P < 0.01$) for BSA samples with Brij 35 present at below and around its CMC compared to fresh samples (Figure 5.24 E).

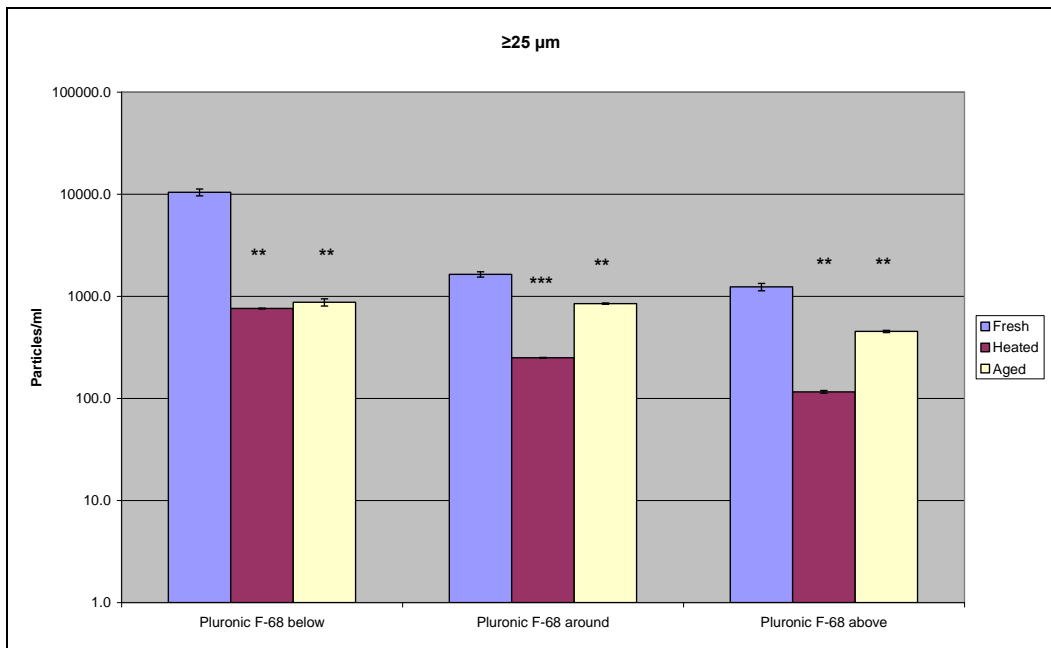
(A)



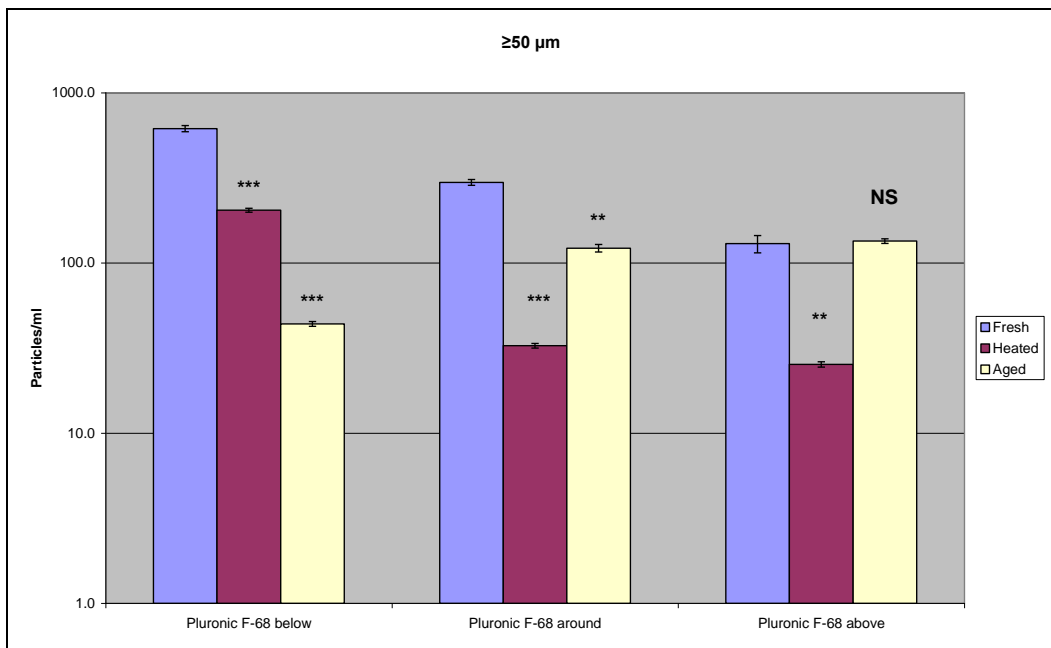
(B)



(C)



(D)



(E)

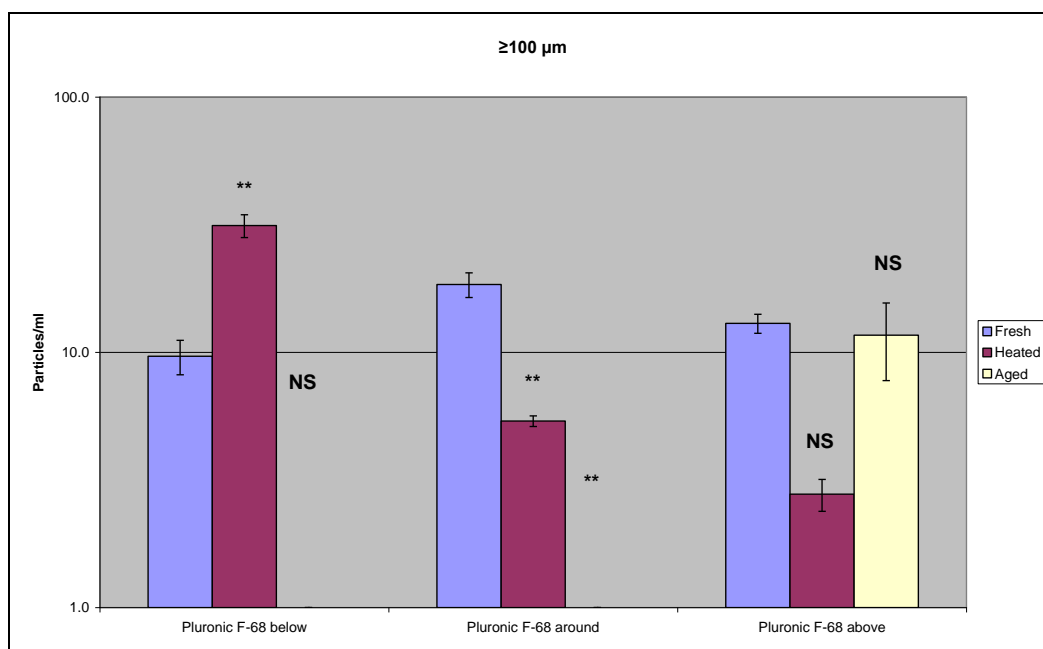


Figure 5.25. Particle concentrations at size ranges of: (A) $\geq 2 \mu\text{m}$, (B) $\geq 10 \mu\text{m}$, (C) $\geq 25 \mu\text{m}$, (D) $\geq 50 \mu\text{m}$ and (E) $\geq 100 \mu\text{m}$ measured by MFI for fresh, heated and aged BSA with added Pluronic F-68 at concentrations below, around and above its CMC. Data are expressed as the mean \pm Std. Deviation. * $P < 0.05$, ** $P < 0.01$, * $P < 0.001$; significant difference in particles per ml compared with fresh BSA with Pluronic F-68 samples.**

Figure 5.25 illustrates the results of heat treatment and aging effects on BSA with added Pluronic F-68 surfactant.

For particle count data of size $\geq 2 \mu\text{m}$, one-way ANOVA analysis, Bonferroni test showed a significant difference at the 0.01 level ($P < 0.01$) between fresh and heated BSA sample particle count with Pluronic F-68 present at around and above its CMC. The difference in mean count is significant at the 0.001 level ($P < 0.001$) between fresh and aged BSA samples with Pluronic F-68 added below, around and above its CMC compared to fresh samples (Figure 5.25 A).

For particle count data of size $\geq 10 \mu\text{m}$, statistical analysis showed that the effects of heat stress and aging are statistically significant at 0.001 level ($P < 0.001$) for BSA samples with Pluronic F-68 present at below CMC. Aging treatment was statistically significant at the 0.01 level ($P < 0.01$) for BSA samples with Pluronic F-68 present at around CMC (Figure 5.25 B).

For particle count data of size $\geq 25 \mu\text{m}$ Bonferroni test analysis showed that the difference is statistically significant at the 0.001 level ($P < 0.001$) between fresh and heated BSA samples with Pluronic F-68 present at around its CMC and significant at the 0.01 level ($P < 0.01$) for BSA samples with Pluronic F-68 added below and above its CMC. The mean difference in particle count is significant at the 0.01 level ($P < 0.01$) between fresh and aged samples of BSA with added Pluronic F-68 at below, around and above its CMC (Figure 5.25 C).

For particle count data of size $\geq 50 \mu\text{m}$, the mean particle count difference is significant at the 0.001 level ($P < 0.001$) between fresh and heat stressed samples of BSA with added Pluronic F-68 at below and around its CMC. Also significant at the same level was the count difference between fresh and aged samples with Pluronic F-68 present at below its CMC. No statistical difference ($P > 0.05$) was detected between fresh and aged BSA samples with Pluronic F-68 added at around and above its CMC. Figure 5.25 (D) illustrates these findings.

For particle count data of size $\geq 100 \mu\text{m}$ size range no statistical difference ($P > 0.05$) was detected between the particle count of fresh and heated BSA with Pluronic F-68 at above its CMC and between fresh and aged BSA samples with Pluronic F-68 below and above its CMC. Post-hoc analysis

showed a significant difference at the 0.01 level ($P < 0.01$) between the particle count data for fresh and heated BSA samples with Pluronic F-68 present at below and around its CMC and between fresh and aged samples including Pluronic F-68 at around its CMC (Figure 5.25 E).

5.4.2.2 Micro-flow measurements for fresh, heated and aged IgG2 surfactant free and IgG2 with Tween 20, Tween 80, Brij 35 and Pluronic F-68 surfactants present at below, around and above their CMC levels

Figure 5.26 shows particle concentration per ml measured for fresh, heated and aged IgG2 (10 mg/ml) samples.

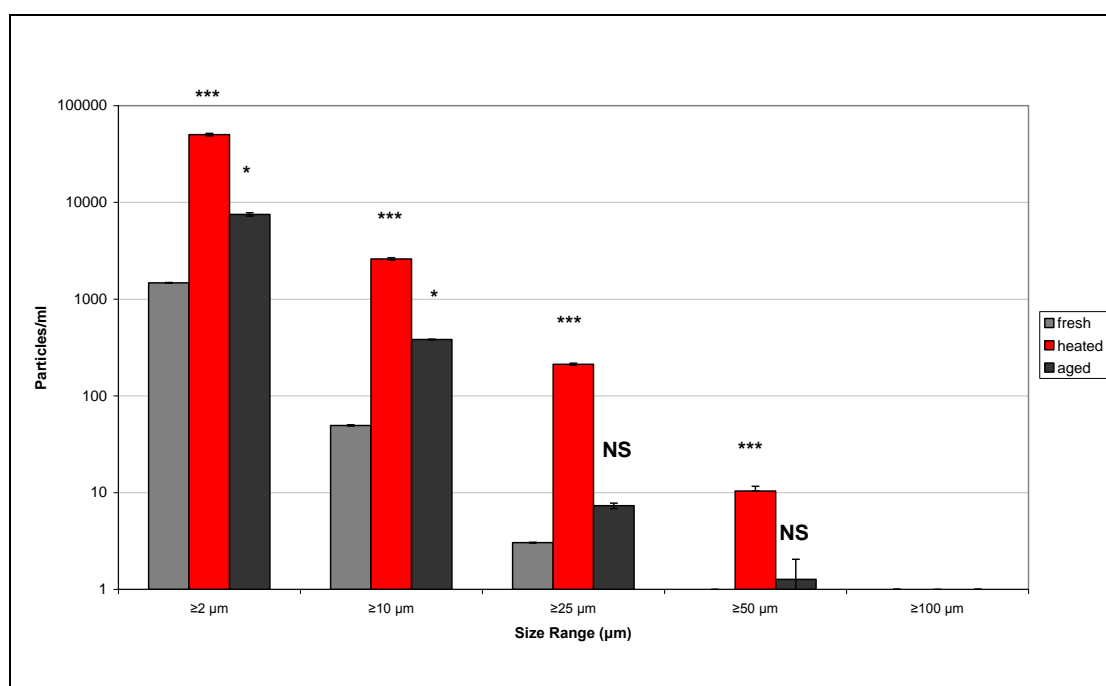


Figure 5.26. Particle concentrations measured by MFI for fresh, heated and aged IgG2 samples. Data are expressed as the mean \pm Std. Deviation. * $P < 0.05$, ** $P < 0.01$, *** $P < 0.001$; significant difference in particles per ml compared with fresh IgG2 samples.

Heated IgG2 (10 mg/ml) samples show their highest increase in particle count per ml for the size class $\geq 2 \mu\text{m}$ size range (50216.8 ± 1614.1 particles per ml). Heat stressed and aged IgG2 surfactant free formulations show increased numbers of particles per ml of a size greater than or equal to 2 and 10 μm than that determined for fresh IgG2 samples (Figure 5.26).

One-way ANOVA analysis showed a significant effect on particle count of heat treatment and storage on particles of the size ranges of $\geq 2 \mu\text{m}$, $\geq 10 \mu\text{m}$, $\geq 25 \mu\text{m}$ and $\geq 50 \mu\text{m}$. Post-hoc tests, using the Bonferroni correction, showed a significant increase ($P < 0.001$) in particle count for particles sized $\geq 2 \mu\text{m}$, $\geq 10 \mu\text{m}$, $\geq 25 \mu\text{m}$ and $\geq 50 \mu\text{m}$ for heated IgG2 samples compared to data for fresh samples.

For particle count data of size $\geq 2 \mu\text{m}$ and $\geq 10 \mu\text{m}$, Bonferroni statistical analysis results showed that the mean particle count increase is significant at 0.05 level ($P < 0.05$) for aged IgG2 samples, but there was no statistically significant difference between fresh and aged IgG2 samples ($P > 0.05$) particle count at $\geq 25 \mu\text{m}$ and $\geq 50 \mu\text{m}$ size ranges (Figure 5.26).

Figure 5.27 shows the number of particles in a size range of $\geq 2 \mu\text{m}$, $\geq 10 \mu\text{m}$, $\geq 25 \mu\text{m}$, $\geq 50 \mu\text{m}$ and $\geq 100 \mu\text{m}$ measured by Micro-Flow Imaging for fresh IgG2 with added Tween 20, Tween 80, Brij 35 and Pluronic F-68 surfactants at below, around and above their CMC levels.

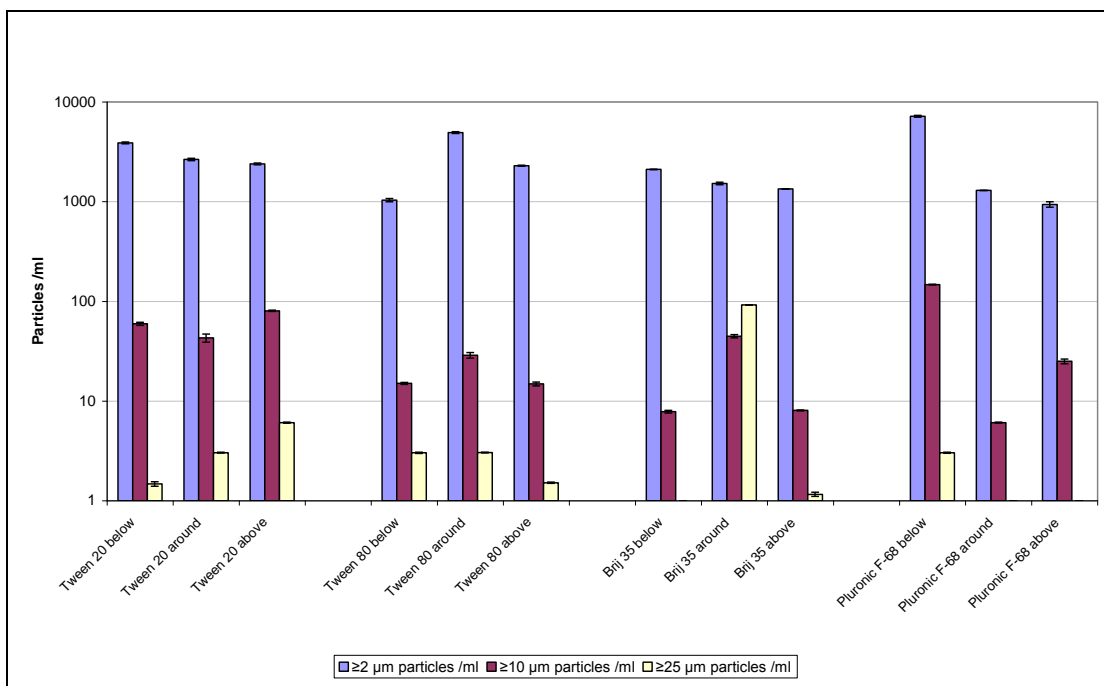


Figure 5.27. Particle concentrations in size ranges of $\geq 2 \mu\text{m}$, $\geq 10 \mu\text{m}$ and $\geq 25 \mu\text{m}$ per ml measured by MFI for fresh IgG2 samples with added Tween 20, Tween 80, Brij 35 and Pluronic F-68 surfactants at below, around and above their CMC levels. Data are expressed as the mean \pm Std. Deviation.

In fresh formulations of IgG2 containing Tween 20 at below, around and above its CMC, Tween 80 at around and above its CMC, Brij 35 at below and around its CMC and Pluronic F-68 at below its CMC, an increase in the number of particles $\geq 2 \mu\text{m}$ was determined. For Tween 80 at below CMC levels, Brij 35 at concentrations above its CMC and Pluronic F-68 at concentrations around and above its CMC a decrease in particle count of this size was observed compared to fresh IgG2 surfactant free samples (Figure 5.27).

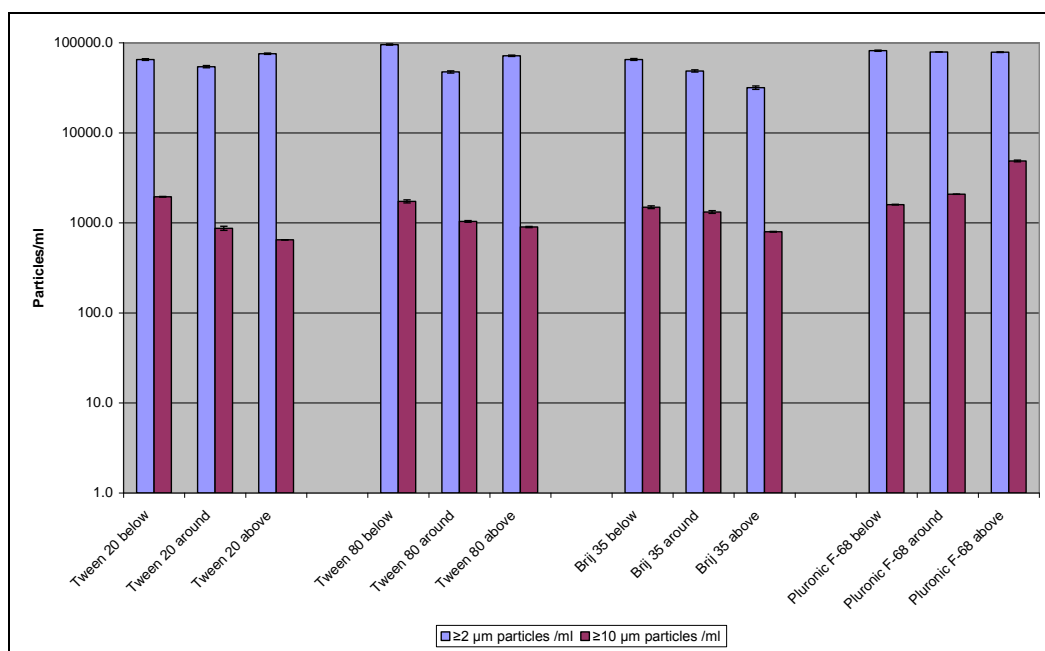
IgG2 formulations with Tween 20 present at levels below and above CMC and Pluronic F-68 present below its CMC showed an increase in particle

count of particles greater than or equal to 10 μm compared to the fresh surfactant-free IgG2 sample (Figure 5.26).

For particle count data of size $\geq 25 \mu\text{m}$, IgG2 samples with all four surfactants have a decreased particle count compared to that obtained for fresh IgG2 surfactant free samples. For particle count data of size $\geq 50 \mu\text{m}$ and $\geq 100 \mu\text{m}$ no particles were observed.

Figure 5.28 shows particle count data measured for heated IgG2 with Tween 20, Tween 80, Brij 35 and Pluronic F-68 surfactants at below, around and above their CMC.

(A)



(B)

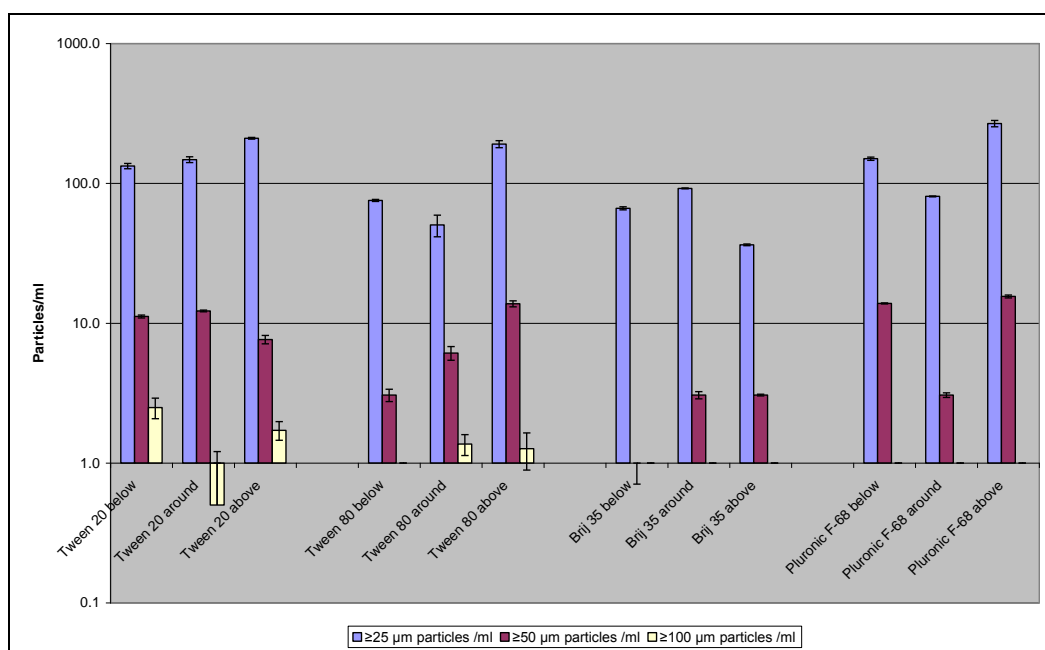


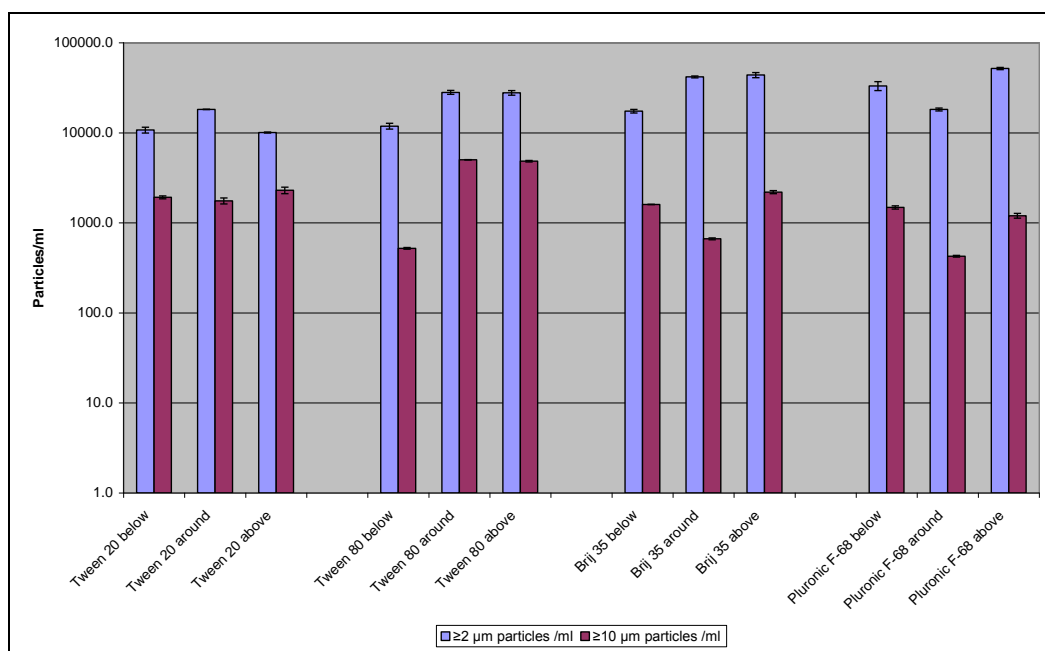
Figure 5.28. Particle concentrations in size range: (A) $\geq 2 \mu\text{m}$ and $\geq 10 \mu\text{m}$; (B) $\geq 25 \mu\text{m}$, $\geq 50 \mu\text{m}$ and $\geq 100 \mu\text{m}$ per ml measured by MFI for heated IgG2 samples with Tween 20, Tween 80, Brij 35 and Pluronic F-68 surfactants at below, around and above their CMC levels. Data are expressed as the mean \pm Std. Deviation.

Heat stressed IgG2 (10 mg/ml) formulations showed an increase in the number of particles greater than or equal to 2 μm with Tween 20 and Pluronic F-68 at below, around and above their CMC, Tween 80 below and above its CMC and Brij 35 below and around its CMC compared to heated IgG2 surfactant free samples.

For particle count data of size $\geq 10 \mu\text{m}$ and $\geq 25 \mu\text{m}$, IgG2 with Pluronic F-68 above its CMC produced a slight increase in particle count compared to heated IgG2 surfactant free samples. All other surfactants produced decreases in particle count at these size ranges (Figure 5.28 A and B).

Heated IgG2 formulations with Tween 20 present at below and around CMC Tween 80 above its CMC and Pluronic F-68 below and above its CMC, all showed an increase in the number of particles greater than or equal to 50 μm . For particle count data of size $\geq 100 \mu\text{m}$, only formulations of heated IgG2 solutions with Tween 20 at below and above its CMC and Tween 80 at around and above its CMC produced an increase in particle count per ml. For all other surfactant samples, no particles were detected at this size range (Figure 5.28 B).

(A)



(B)

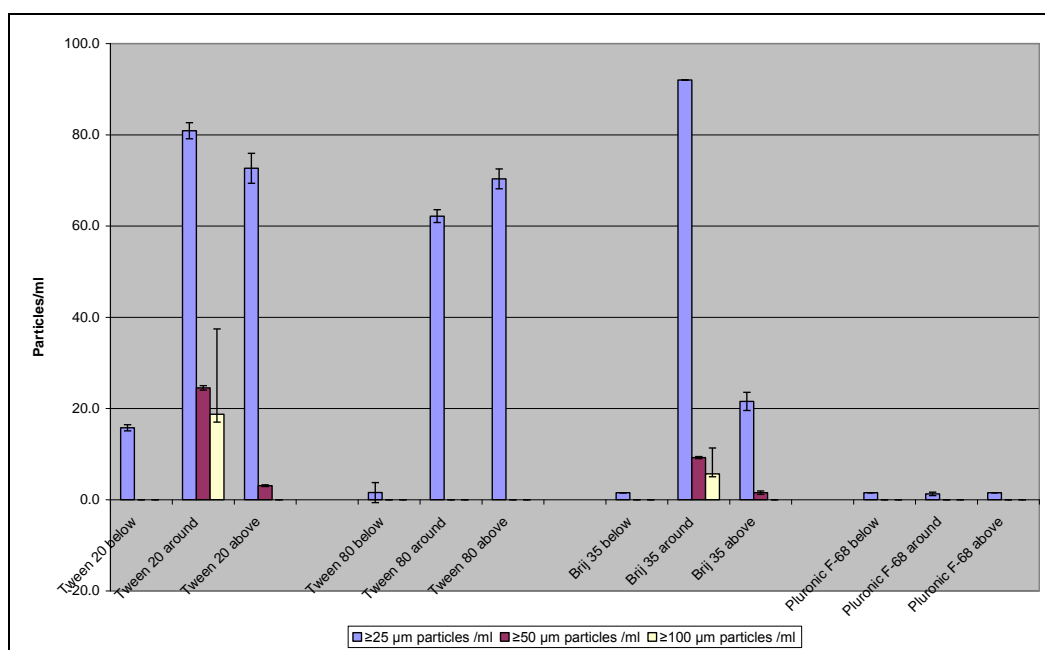


Figure 5.29. Particle concentrations in size range: (A) $\geq 2 \mu\text{m}$ and $\geq 10 \mu\text{m}$; (B) $\geq 25 \mu\text{m}$, $\geq 50 \mu\text{m}$ and $\geq 100 \mu\text{m}$ per ml measured by MFI for aged IgG2 samples with added Tween 20, Tween 80, Brij 35 and Pluronic F-68 surfactants at below, around and above their CMC. Data are expressed as the mean \pm Std. Deviation.

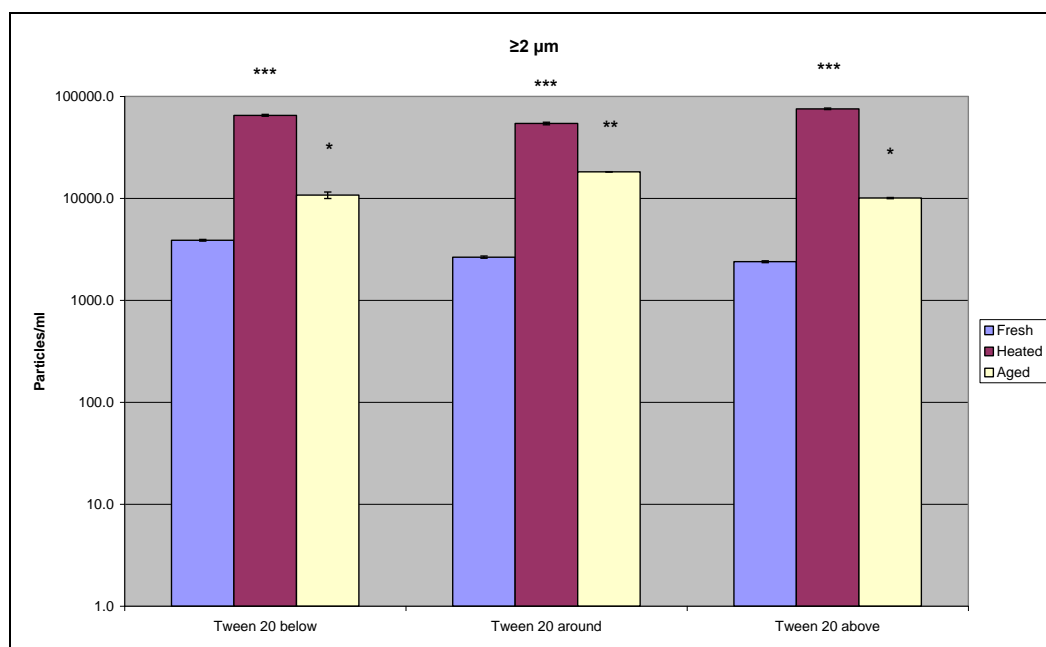
All four surfactant samples at any concentration on aging produced an increase in the number of particles at $\geq 2 \mu\text{m}$ and $\geq 10 \mu\text{m}$ (Figure 5.29 A).

The increase in the number of $\geq 25 \mu\text{m}$ particles was measured for aged IgG2 with Tween 20 present at all CMC concentrations, and for Tween 80 and Brij 35 at around and above their CMC . The particle count of particles at $\geq 50 \mu\text{m}$ for IgG2 with Tween 20 present at around and above and for Brij 35 present at around their CMC increased (Figure 5.29 B).

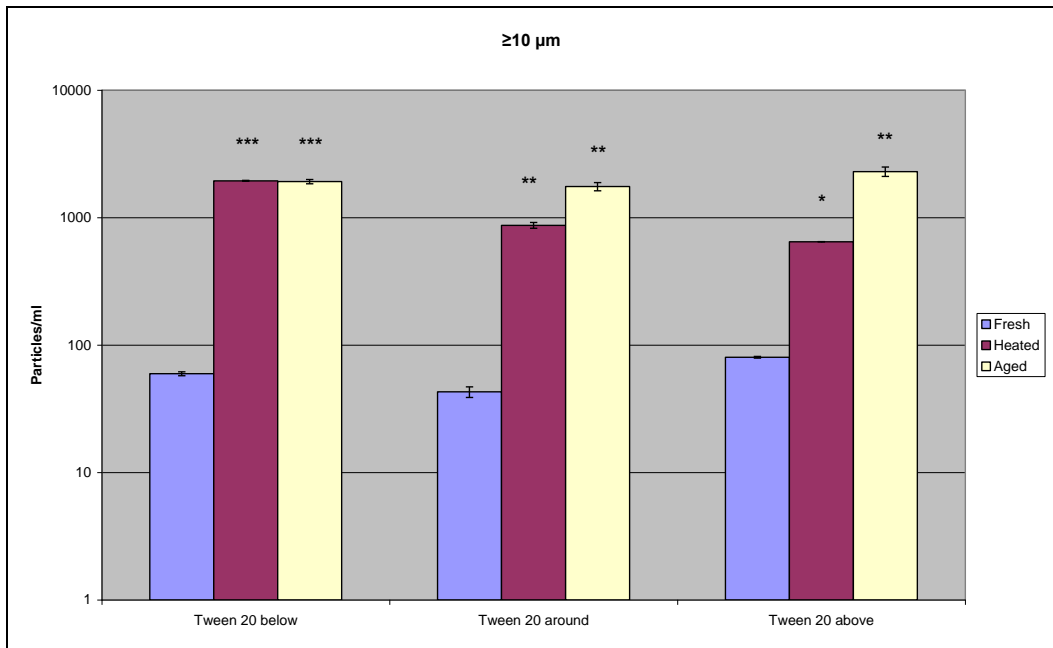
For particle count data of size $\geq 100 \mu\text{m}$, aged IgG2 with Tween 20 and Brij 35 around their CMC produced an increase comparing to other surfactants and aged IgG2 surfactant free formulations (Figures 5.26 and 5.29 B).

Figures 5.30 to 5.33 illustrate how particle count over the size ranges $\geq 2 \mu\text{m}$, $\geq 10 \mu\text{m}$, $\geq 25 \mu\text{m}$, $\geq 50 \mu\text{m}$ and $\geq 100 \mu\text{m}$ changed after heat stress and aging of IgG2 with each surfactant at below, around and above CMC levels.

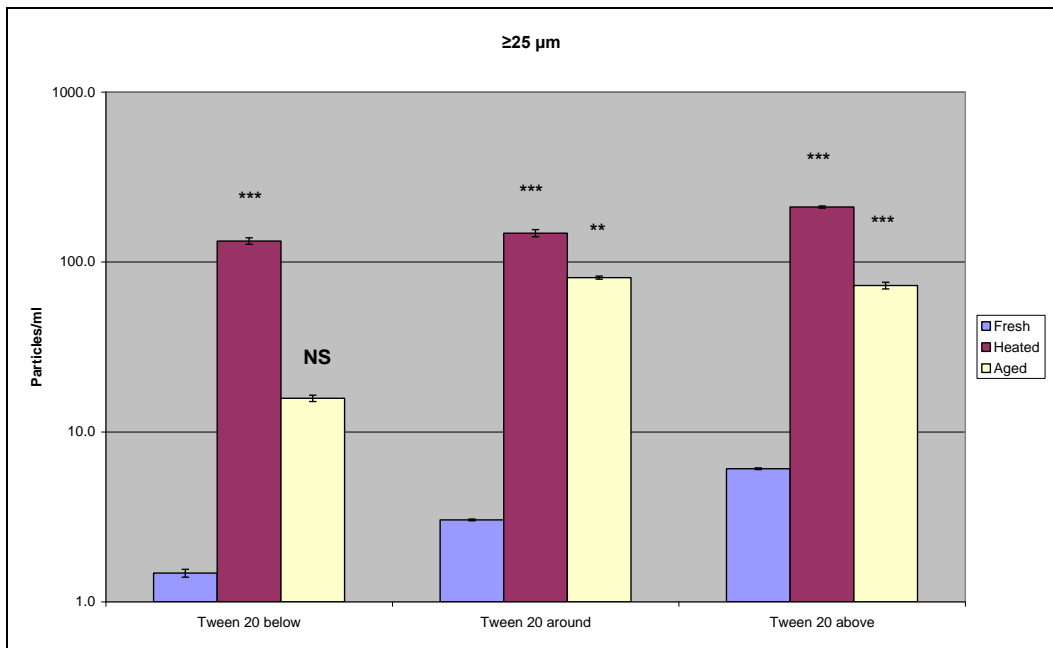
(A)



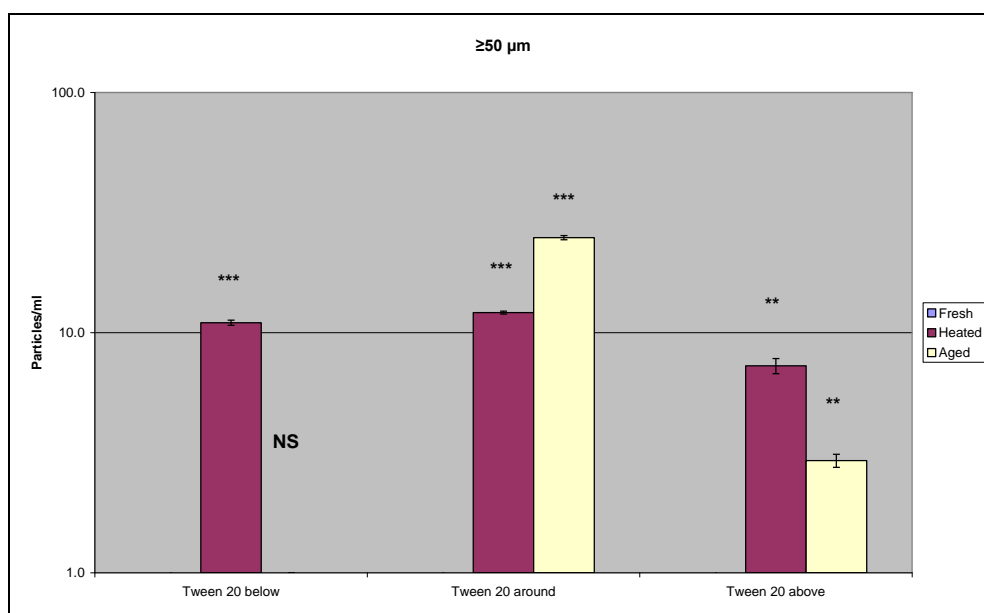
(B)



(C)



(D)



(E)

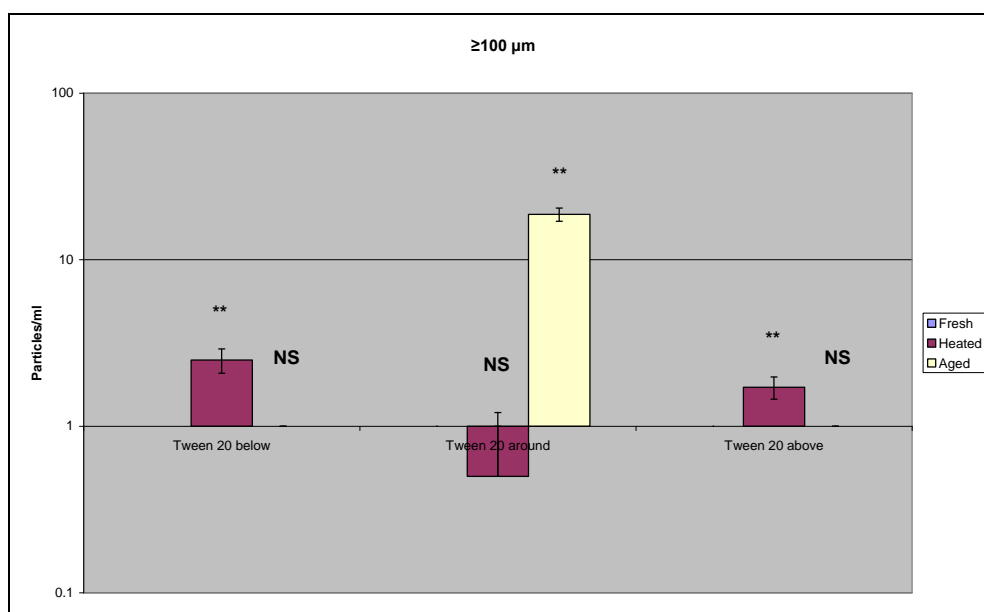


Figure 5.30. Particle concentrations at size ranges of: (A) $\geq 2 \mu\text{m}$, (B) $\geq 10 \mu\text{m}$, (C) $\geq 25 \mu\text{m}$, (D) $\geq 50 \mu\text{m}$ and (E) $\geq 100 \mu\text{m}$ measured by MFI for fresh, heated and aged IgG2 with Tween 20 at concentrations below, around and above CMC. Data are expressed as the mean \pm Std. Deviation. * $P < 0.05$, ** $P < 0.01$, *** $P < 0.001$; significant difference in particles per ml compared with fresh IgG2 with Tween 20 samples.

One-way ANOVA analysis, post-hoc Bonferroni correction, showed a significant effect of heat stress on particle count data for IgG2 samples with Tween 20 surfactant at below, around and above its CMC levels for particles $\geq 2 \mu\text{m}$. The mean difference in particle count was significant at the 0.001 level ($P < 0.001$) for IgG2 samples with Tween 20 present at below, around and above its CMC on comparing fresh and heated samples. Significance was observed at the 0.01 level ($P < 0.01$) between particle count data for IgG2 with Tween 20 present at around its CMC and at the 0.05 level ($P < 0.05$) between fresh and aged IgG2 samples with Tween 20 present below and above its CMC (Figure 5.30 A).

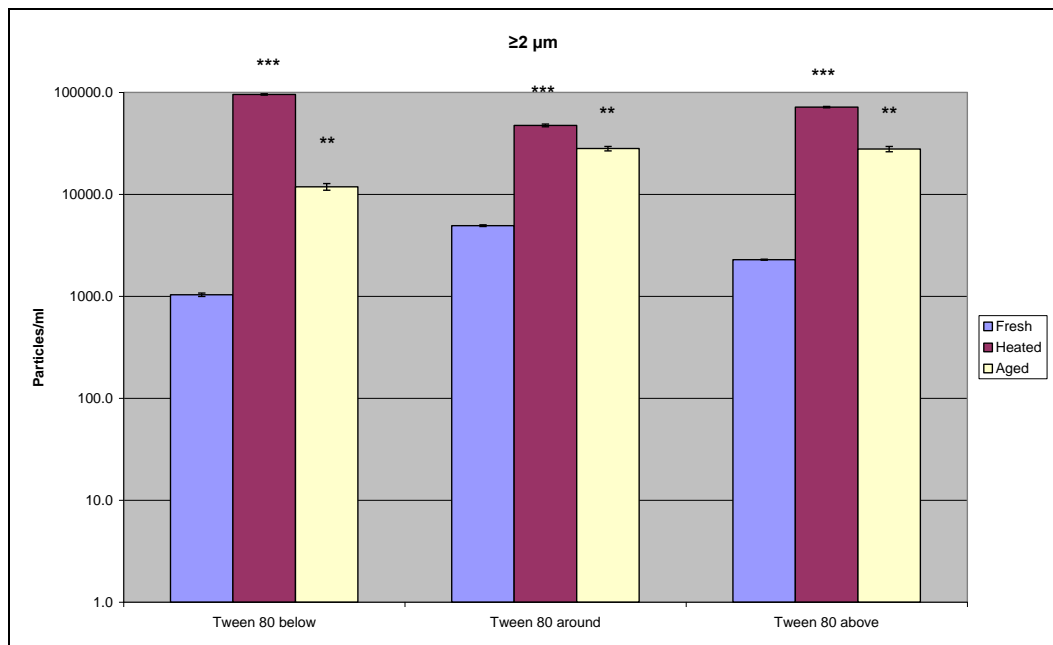
For particle count data of size $\geq 10 \mu\text{m}$, statistical analysis showed that the difference in count is significant at the 0.001 level ($P < 0.001$) between fresh and heated and between fresh and aged IgG2 with Tween 20 present below CMC. The difference in count is significant at a 0.01 level ($P < 0.01$) for IgG2 samples with Tween 20 present at around its CMC. Also the mean difference in count is significant at the 0.01 level ($P < 0.01$) between fresh and aged IgG2 samples with Tween 20 present above its CMC. Figure 5.30 (B) illustrates these findings.

For particle count data of size $\geq 25 \mu\text{m}$, Bonferroni test analysis showed that the difference in particle count is statistically significant at the 0.001 level ($P < 0.001$) between fresh and heated IgG2 samples with Tween 20 concentrations below, around and above CMC and at a 0.01 level ($P < 0.01$) between fresh and aged IgG2 samples with Tween 20 present at around CMC (Figure 5.30 C).

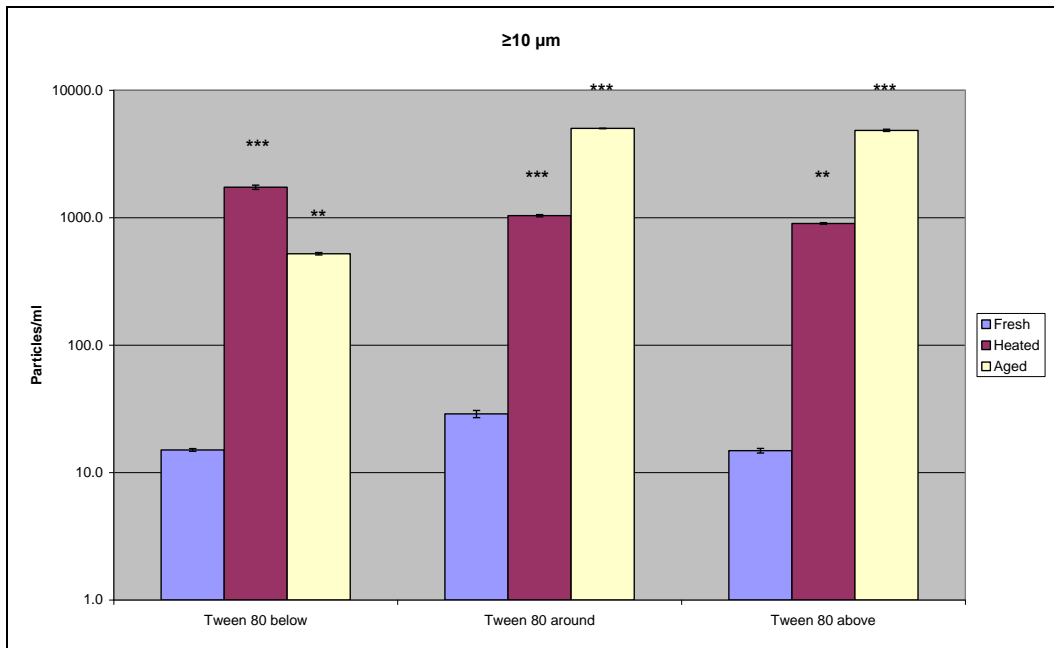
For particle count data of size $\geq 50 \mu\text{m}$ no statistical difference ($P>0.05$) was detected between fresh and aged samples of IgG2 with Tween 20 present at below CMC measurements. Post-hoc analysis showed a significant difference at 0.001 level ($P<0.001$) between the particle counts of fresh and heated IgG2 samples with Tween 20 at below and around CMC and significance at 0.01 level ($P<0.01$) was detected between fresh and heated, and fresh and aged samples with Tween 20 present above its CMC (Figure 5.30 D).

For particle count data of size $\geq 100 \mu\text{m}$, heat stress showed a significant effect on particle count at the level of 0.01 level ($P<0.01$) for samples with Tween 20 below and above its CMC. No significant effect was detected by aging samples containing Tween 20 below and above its CMC (Figure 5.30 E).

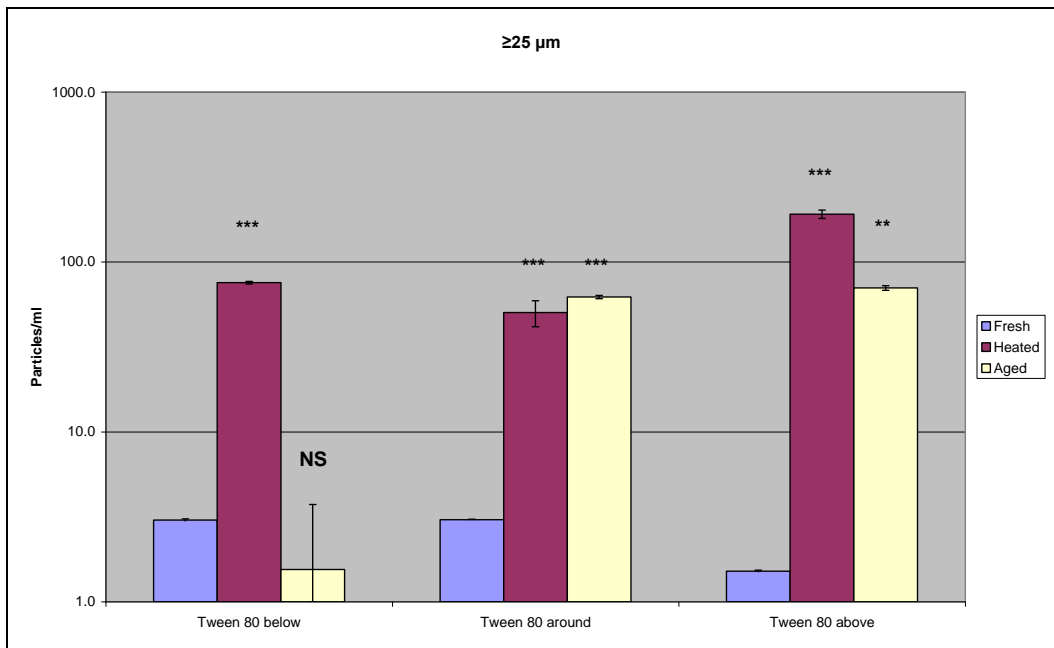
(A)



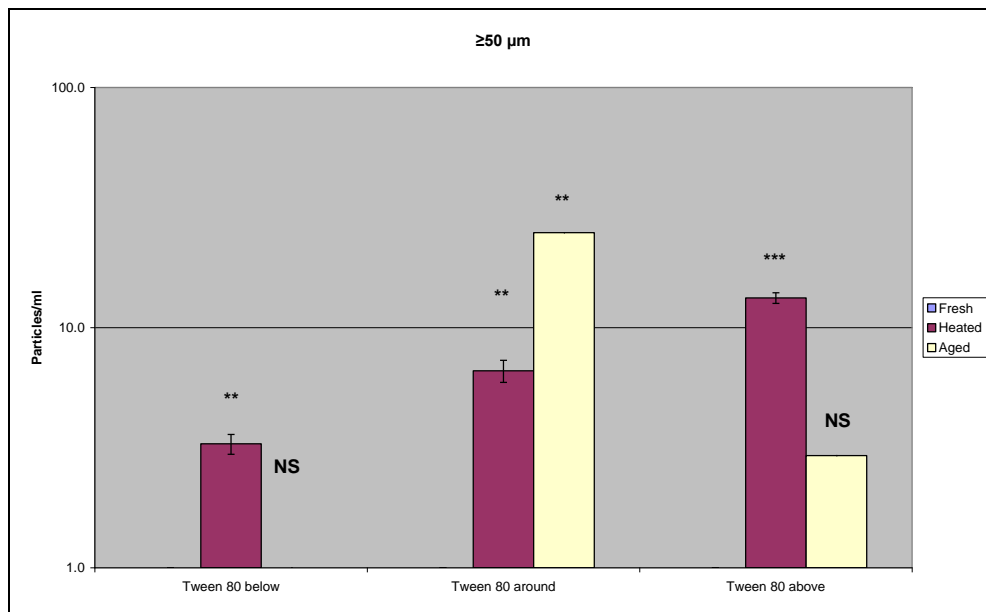
(B)



(C)



(D)



(E)

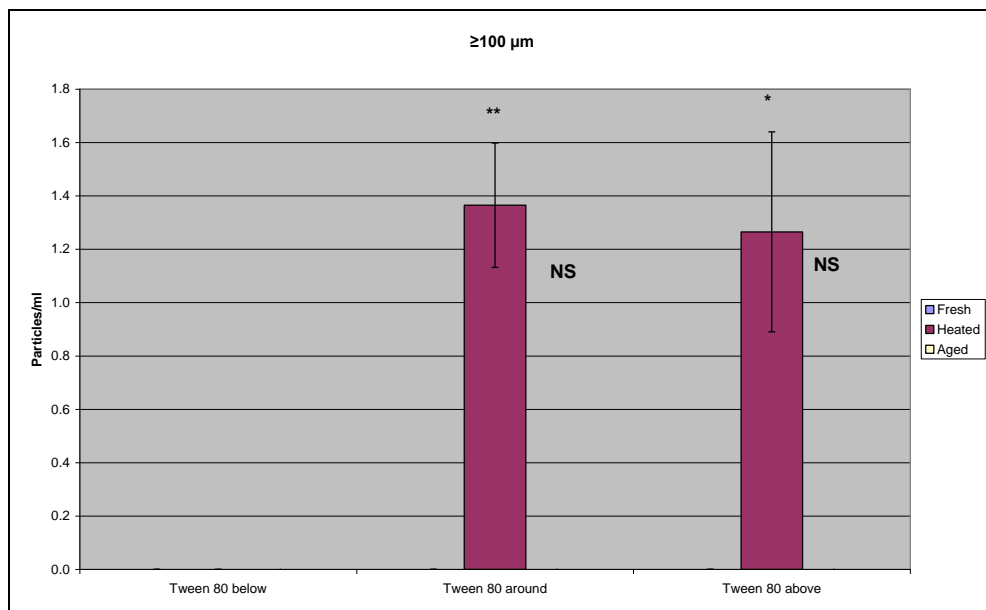


Figure 5.31. Particle concentrations at size ranges of: (A) $\geq 2 \mu\text{m}$, (B) $\geq 10 \mu\text{m}$, (C) $\geq 25 \mu\text{m}$, (D) $\geq 50 \mu\text{m}$ and (E) $\geq 100 \mu\text{m}$ measured by MFI for fresh, heated and aged IgG2 with Tween 80 present below, around and above CMC. Data are expressed as the mean \pm Std. Deviation. * $P < 0.05$, ** $P < 0.01$, * $P < 0.001$; significant difference in particles per ml compared with fresh IgG2 with Tween 80 samples.**

One-way ANOVA analysis, Bonferroni correction, showed a significant effect of heat stress on particle count for IgG2 samples with Tween 80 surfactant present at below, around and above CMC for particles $\geq 2 \mu\text{m}$ particle size. The difference in count was significant at 0.001 level ($P < 0.001$) for samples containing Tween 80 below, around and above its CMC. The difference in count between fresh and aged samples containing Tween 80 below, around and above CMC was significant at the 0.01 level ($P < 0.01$) (Figure 5.31 A).

For particle count data of size $\geq 10 \mu\text{m}$, statistical analysis showed that heat treatment had significant effect on particle count at the 0.001 level ($P < 0.001$) for IgG2 samples with Tween 80 present below and around its CMC. For IgG2 samples with Tween 80 above its CMC the statistical difference was reduced to the 0.01 level ($P < 0.01$) between fresh and heated samples. Aging of IgG2 with Tween 80 present at around and above CMC produced a significant effect at 0.001 level ($P > 0.001$) on particle numbers compared to fresh samples (Figure 5.31 B).

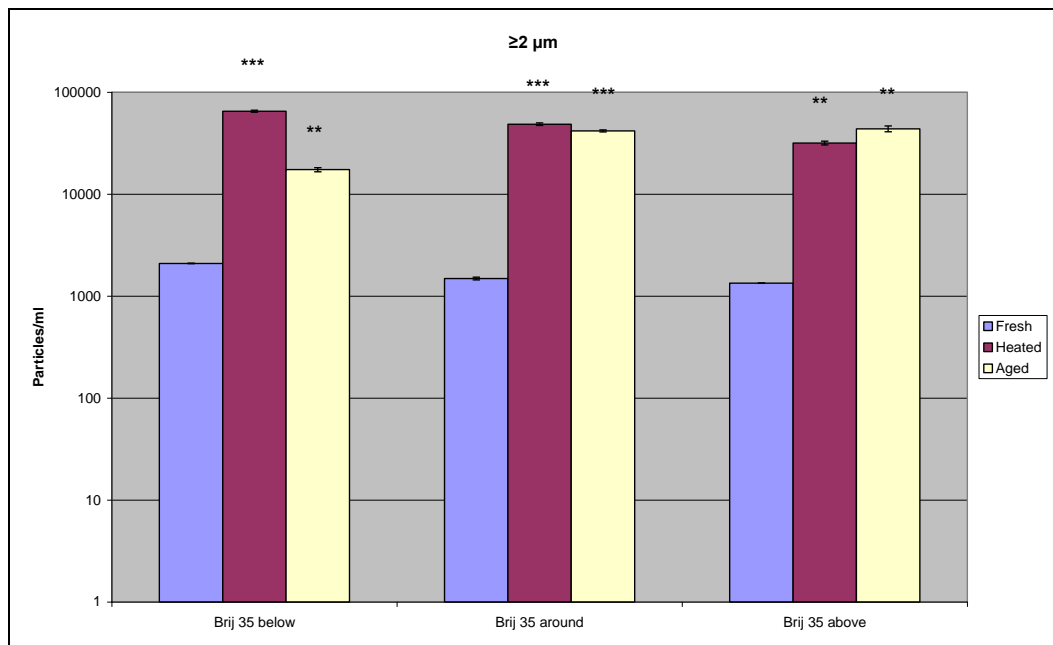
For particle count data of size $\geq 25 \mu\text{m}$, Bonferroni test analysis showed that heat treatment had a statistically significant effect on particle count at the 0.001 level ($P < 0.001$) for IgG2 samples with Tween 80 present at all levels tested. Aging had a statistically significant effect at 0.001 level on the particle count for samples with Tween 80 at around CMC and at a significance level of 0.01 for samples with Tween 80 present above CMC (Figure 5.31 C).

For particle count data of size $\geq 50 \mu\text{m}$ no statistical difference ($P > 0.05$) was detected between fresh and aged IgG2 with Tween 80 below and above CMC. Both heat treatment and aging had significant effects at the 0.01 level

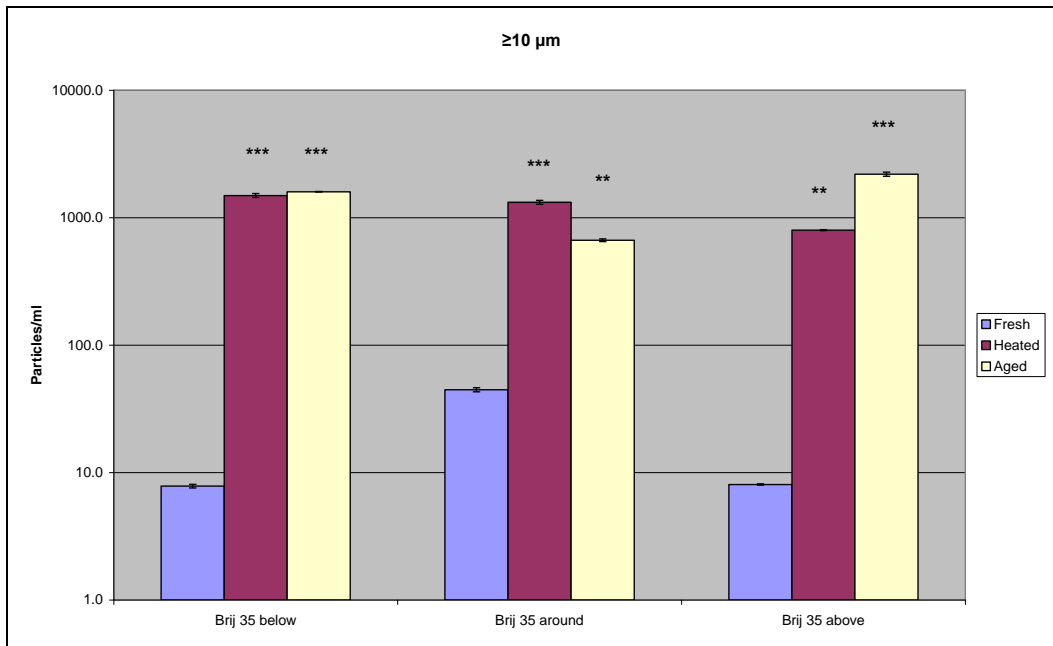
($P < 0.01$) for IgG2 samples with Tween 80 at around its CMC concentration (Figure 5.31 D).

For particle count data of size $\geq 100 \mu\text{m}$, post-hoc test results showed that heat treatment has statistically significant effect on particle count at a 0.01 level ($P < 0.01$) for samples with Tween 80 around CMC and at a 0.05 level ($P < 0.05$) for samples with Tween 80 present above CMC. Aging has no significant effect on particle count IgG2 with Tween 80 present at around and above CMC (Figure 5.31 E).

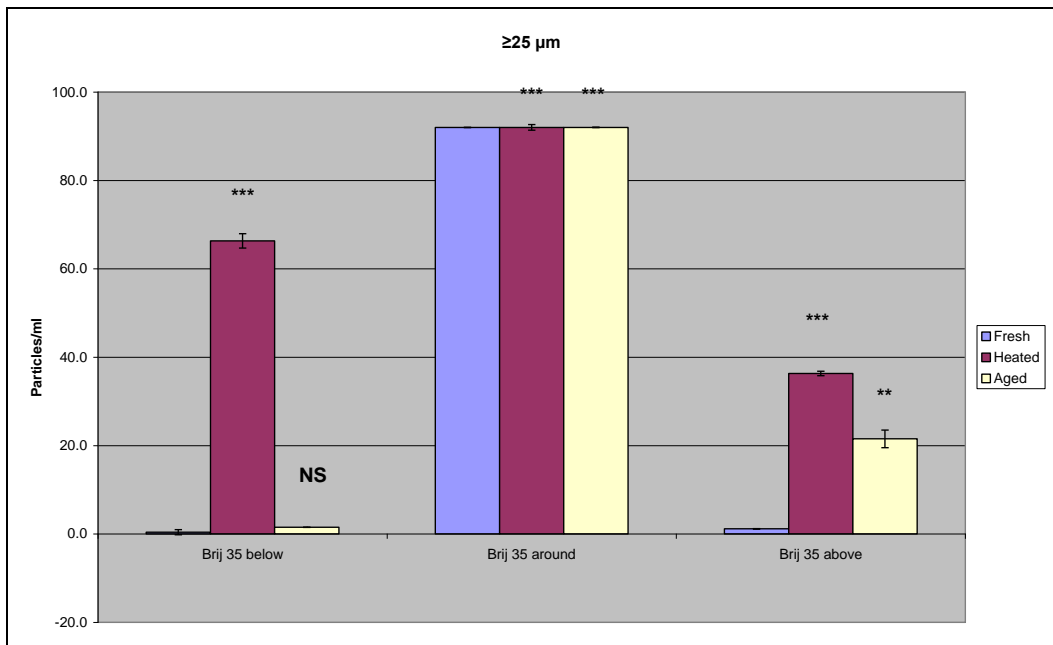
(A)



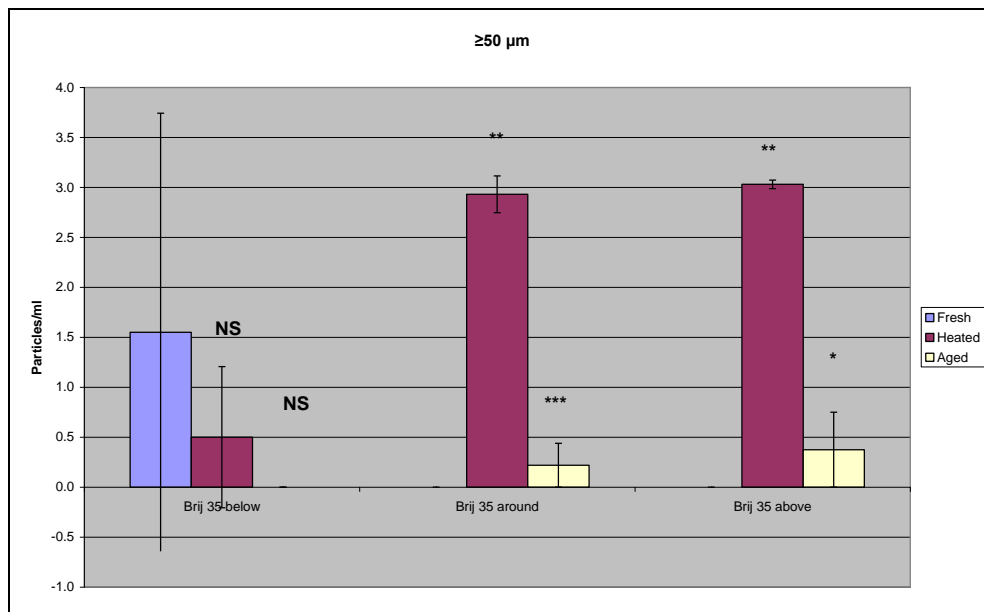
(B)



(C)



(D)



(E)

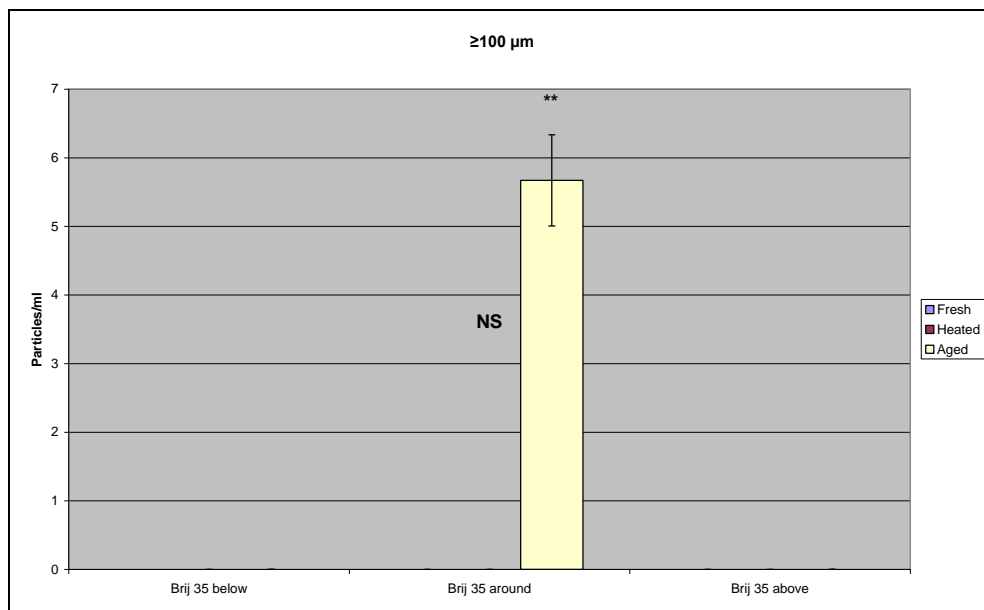


Figure 5.32. Particle concentrations at size ranges of: (A) $\geq 2 \mu\text{m}$, (B) $\geq 10 \mu\text{m}$, (C) $\geq 25 \mu\text{m}$, (D) $\geq 50 \mu\text{m}$ and (E) $\geq 100 \mu\text{m}$ measured by MFI for fresh, heated and aged IgG2 with Brij 35 below, around and above CMC levels. Data are expressed as the mean \pm Std. Deviation. * $P < 0.05$, ** $P < 0.01$, * $P < 0.001$; significant difference in particles per ml compared with fresh IgG2 with Brij 35 samples.**

One-way ANOVA analysis, Bonferroni test data showed a significant effect of heat stress and aging on particle numbers $\geq 2 \mu\text{m}$ for IgG2 samples with Brij 35 surfactant present at below, around and above CMC. Between fresh and heated IgG2 samples with Brij 35 present below and around CMC, the mean count difference was significant at the 0.001 level ($P < 0.001$). The difference in count, between fresh and aged IgG2 with Brij 35 present below and above CMC was significant at the 0.01 level ($P < 0.01$) and for IgG2 with Brij 35 present at around CMC a 0.001 level ($P < 0.001$) significance was determined (Figure 5.32 A).

For particle count data of size $\geq 10 \mu\text{m}$ particles, statistical analysis showed that the count difference is significant at a 0.001 level ($P < 0.001$) between fresh and heated IgG2 samples with Brij 35 present at below and around CMC. Also between fresh and aged IgG2 samples with Brij 35 present at below and above CMC the difference in particle count was found to be significant at 0.001 level ($P < 0.001$) (Figure 5.32 B).

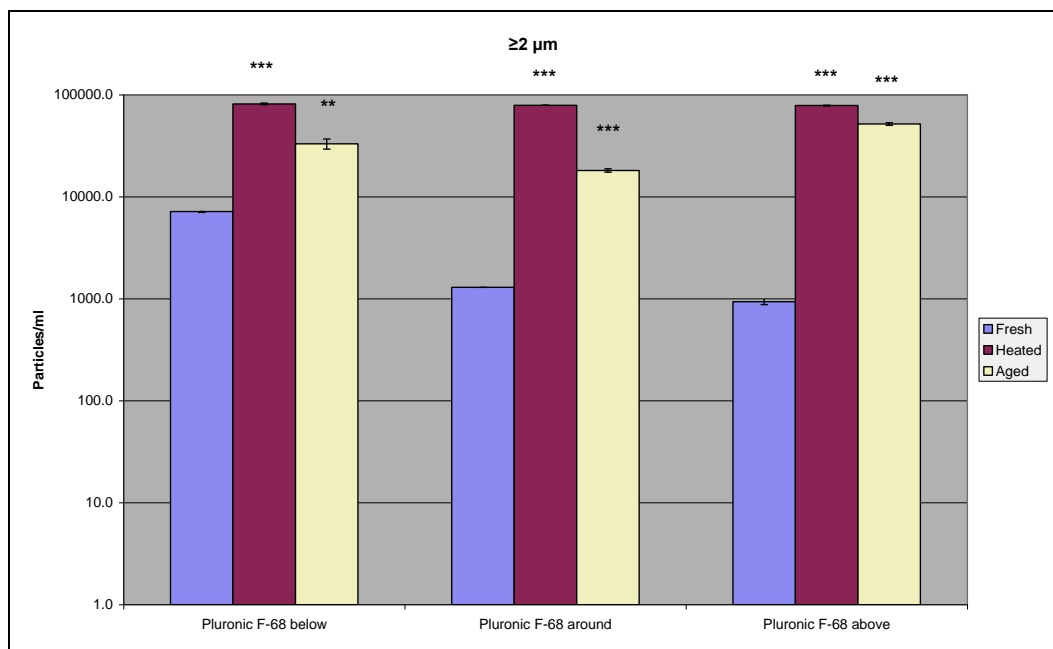
For particle count data of size $\geq 25 \mu\text{m}$ size range, Bonferroni test analysis showed that heat treatment effect on count is statistically significant at a 0.01 level ($P < 0.01$) for IgG2 samples with Brij 35 at around CMC and the effect is significant at a 0.001 level ($P < 0.001$) for IgG2 samples with Brij 35 present at below, around and above CMC samples comparing to fresh ones. Aging treatment has a statistically significant effect at the 0.001 level ($P < 0.001$) for IgG2 with Brij 35 present at around CMC (Figure 5.32 C).

For particle count data of size $\geq 50 \mu\text{m}$ no statistical difference ($P > 0.05$) was detected between fresh and heated and fresh and aged IgG2 with Brij 35 present at levels below CMC. Heat treatment had a statistically significant

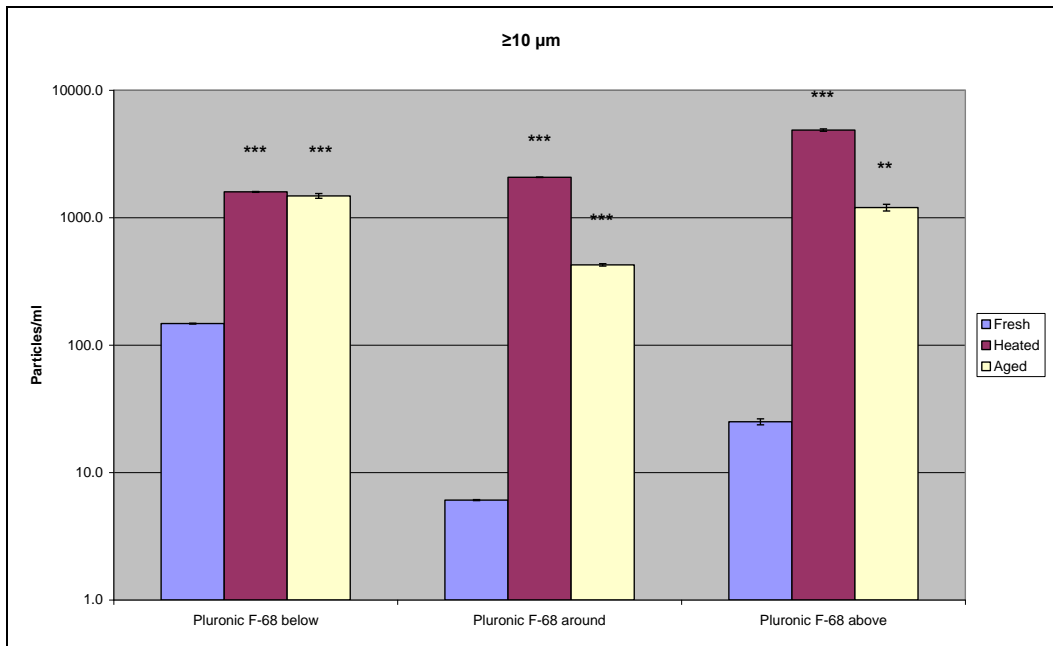
effect at the 0.01 level ($P < 0.01$) for IgG2 samples with Brij 35 at around and above CMC. Aging had a significant effect at the 0.001 level ($P < 0.001$) for samples with Brij 35 around CMC and at the 0.05 level ($P < 0.05$) for samples containing Brij 35 above its CMC (Figure 5.32 D).

For particle count data of size $\geq 100 \mu\text{m}$ statistical analysis showed no statistical difference ($P > 0.05$) between fresh and heated IgG2 with Brij 35 at around its CMC. Aging samples produced a significant effect on count at the 0.01 level ($P < 0.01$) for samples of IgG2 with Brij 35 present at around CMC (Figure 5.32 E).

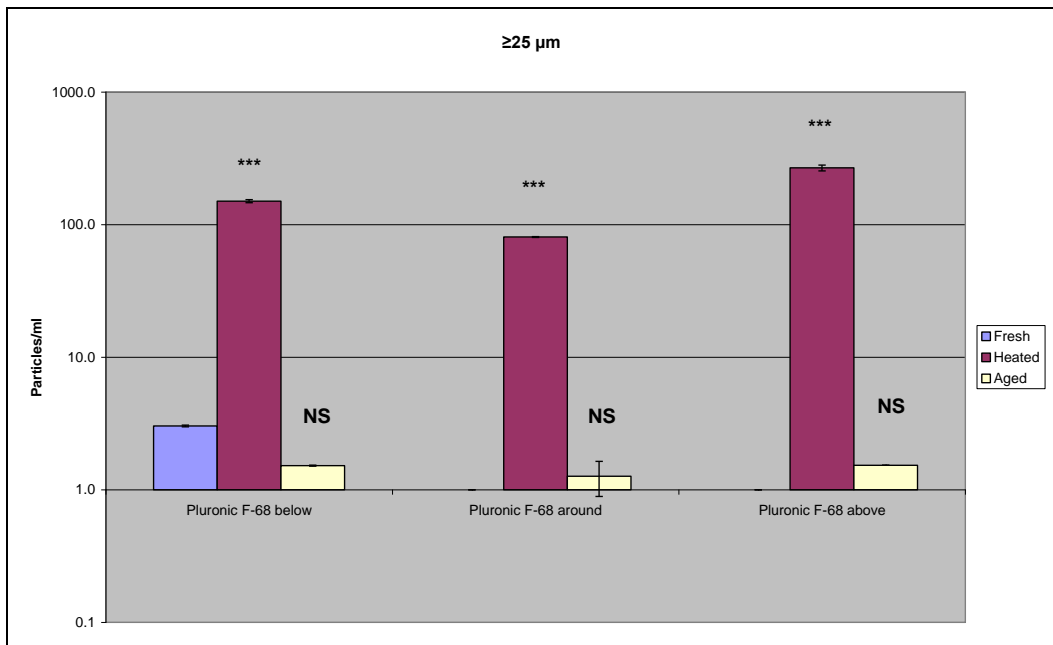
(A)



(B)



(C)



(D)

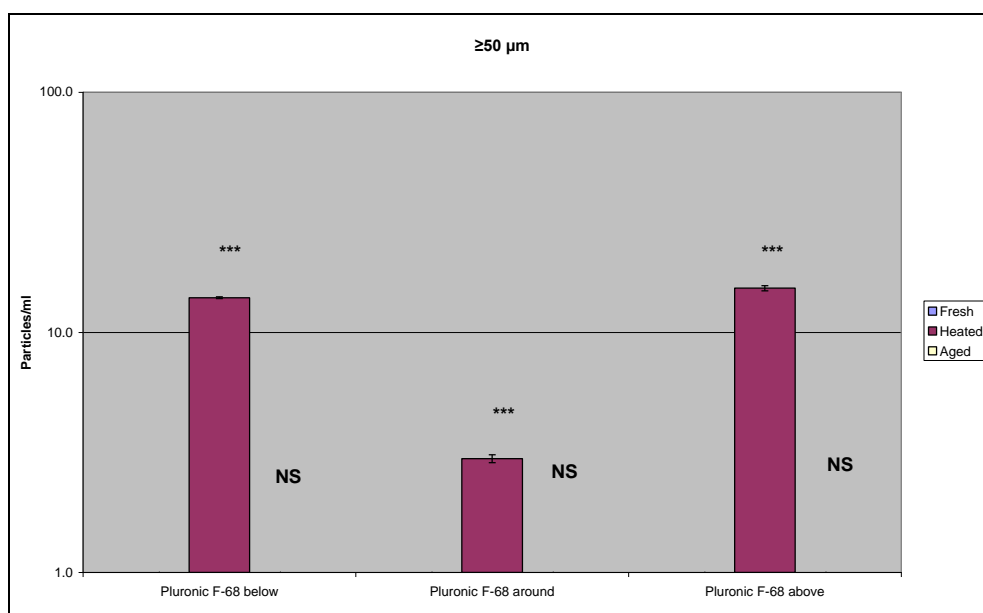


Figure 5.33. Particle concentrations at size ranges of: (A) $\geq 2 \mu\text{m}$, (B) $\geq 10 \mu\text{m}$, (C) $\geq 25 \mu\text{m}$, (D) $\geq 50 \mu\text{m}$ measured by MFI for fresh, heated and aged IgG2 with Pluronic F-68 below, around and above CMC levels. Data are expressed as the mean \pm Std. Deviation. * $P < 0.05$, ** $P < 0.01$, * $P < 0.001$; significant difference in particles per ml compared with fresh IgG2 with Pluronic F-68 samples.**

Figure 5.33 illustrates the effect of heat and aging treatments on IgG2 with Pluronic F-68 samples.

For particle count data of size $\geq 2 \mu\text{m}$ particles size range, one-way ANOVA analysis, Bonferroni test showed a significant difference at the 0.001 level ($P < 0.001$) between fresh and heated samples of IgG2 with Pluronic F-68 present at below, around and above CMC. The mean count difference was significant at the 0.001 level ($P < 0.001$) between fresh and aged IgG2 samples with Pluronic F-68 at around and above CMC and at the 0.01 level ($P < 0.01$) for samples containing Pluronic F-68 below its CMC (Figure 5.33 A).

For particle count data of size $\geq 10 \mu\text{m}$, statistical analysis showed that the heat stress effect on particle count is statistically significant at 0.001 level ($P < 0.001$) for IgG2 samples with Pluronic F-68 present at below, around and above CMC. Aging treatment had a statistically significant effect on count at 0.01 level ($P < 0.01$) for IgG2 samples with Pluronic F-68 above CMC and at 0.001 level ($P < 0.001$) for samples containing Pluronic F-68 at below and around CMC (Figure 5.33 B).

For particle count data of size $\geq 25 \mu\text{m}$ and $\geq 50 \mu\text{m}$ size Bonferroni test analysis showed that the difference in particle count is statistically significant at the 0.001 level ($P < 0.001$) between fresh and heated IgG2 samples with Pluronic F-68 present below, around and above its CMC. No significant count difference was detected between samples of fresh and aged IgG2 with Pluronic F-68 present below, around and above CMC samples (Figure 5.33 C and D).

5.5 General discussion

Based on the results obtained from Light Obscuration (HIAC) and Micro-flow Imaging (MFI) analysis, heat treatment and storage stress showed a significant effect on BSA and IgG2 protein particle size stability.

BSA surfactant free samples after storage treatment showed slightly higher numbers and statistically significantly different values of particles than those obtained after heat stress when compared to freshly prepared BSA. Also both heat stress and storage treatments induced an increase in particle count per ml for IgG2 surfactant free samples at particle size ranges from $\geq 2 \mu\text{m}$ to $\geq 10 \mu\text{m}$. For particle count data of size $\geq 25 \mu\text{m}$ measured by both HIAC and MFI methods, heat treatment produced higher, more statistically significant increases in particle count, whereas storage showed no statistical difference at this size range for IgG2 surfactant free samples.

Considering the effect of different surfactant type and concentration on BSA protein particle size stability as explored by HIAC and MFI experiments, all four surfactants at above their CMC produced a decrease in particle count of particles $\geq 2 \mu\text{m}$. On heating and storage, Tween 80 at above its CMC, Brij 35 at above its CMC and Pluronic F-68 at around and above its CMC showed the highest decrease in particle count of size $\geq 2 \mu\text{m}$ compared to BSA surfactant free samples.

For particle count data of size $\geq 5 \mu\text{m}$ to $\geq 10 \mu\text{m}$, the addition of the surfactant Brij 35 at around and above its CMC produced the lowest particle count level compared to the other surfactants and BSA surfactant free formulations. Very similar results were obtained for size ranges $\geq 25 \mu\text{m}$, ≥ 50

μm and $\geq 100 \mu\text{m}$. The use of surfactant Brij 35 at around and above its CMC is the most effective in bringing about a particle count decrease.

According to results obtained from HIAC and MFI analysis for IgG2 samples, considering the $\geq 2 \mu\text{m}$ size range, the most effective surfactant was Brij 35 above its CMC. This surfactant showed the highest decrease in particle count per ml after both heat and storage stress when compared to the other surfactants and IgG2 surfactant free samples.

For particle count data of size $\geq 10 \mu\text{m}$, Tween 20, Tween 80, Brij 35 and Pluronic F-68 at high CMC concentration effectively reduced the particle count per ml. For particle count data of size $\geq 25 \mu\text{m}$, $\geq 50 \mu\text{m}$ and $\geq 100 \mu\text{m}$ the surfactant Brij 35 used above its CMC level showed the highest decrease in particle count after heating and storage.

Chapter 6
General Discussion

6.1 General discussion

The overall aim of this project was to identify improved methods of particle characterisation within protein formulations and enhance understanding of the mechanisms of particle formation.

The development of liquid therapeutic protein drugs imposes the requirement of specific stabilisation agents to prevent protein aggregation in order to meet quality attributes and provide an acceptable drug shelf life for at least 2 years stored at 2-8°C. Non-ionic surfactants are used to avoid protein adsorption and the formation of protein aggregates. Depending on the protein and excipient used the stabilisation effect is quite different and cannot be predicted to date (Garidel et al., 2009). One reason for this is the lack of understanding of the process of particle formation and the influence of different surfactant type and concentration in relation to CMC and the consequent effect on protein stability and protein size stability.

In this thesis Bovine serum albumin BSA and immunoglobulin IgG2 were studied in order to assess the effect of Tween 20, Tween 80, Brij 35 and Pluronic F-68 at concentrations below, around and above their CMC on the protein conformational stability and protein size stability. The selection of the proteins and the different levels of Tween 20, Tween 80, Brij 35 and Pluronic F-68 surfactants was reported in Chapters 1 and 2.

In Chapter 3 the effect of Tween 20, Tween 80, Brij 35 and Pluronic F-68 surfactants on conformational stability of BSA and IgG2 was investigated. Single protein-surfactant free and protein-surfactant solutions were examined

for thermal stability employing HSDSC. Thermal stability was assessed by both unfolding and re-folding experiments.

Thermal unfolding experiments revealed that for surfactant free BSA (10 mg/ml) a single unfolding peak at T_m of $66.91 \pm 0.085^\circ\text{C}$ was observed, which was similar to the published value of 67°C (Nishimura et al., 2001). Moreover, results showed that conformational stability of the protein BSA was dependent on Tween 20, Tween 80, Brij 35 and Pluronic F-68 surfactants. The presence of the surfactants induced T_m to shift to lower unfolding temperatures for BSA, with the interactions of Brij 35 at a concentration around CMC being stronger compared to other types and level of surfactants.

Thermal unfolding experiments for surfactant free immunoglobulin IgG2 (10 mg/ml) showed two unfolding peaks, where T_{m1} was $69.38 \pm 0.057^\circ\text{C}$ and T_{m2} was at $77.53 \pm 0.113^\circ\text{C}$, which is the result of the melting of two independent domains of immunoglobulin as described in Chapter 3, Section 3.4.2. Two unfolding endotherms were previously reported (Tischenko et al., 1998, Kravchuk et al., 1998, Tischenko et al., 2003).

Thermal unfolding experiments indicated a very weak surfactant-immunoglobulin IgG2 interaction, compared to much stronger interactions for the bovine serum albumin-surfactant systems. However, the presence of Brij 35 at a concentration below its CMC and Pluronic F-68 at a concentration around its CMC induced a shift in the unfolding transition T_{m1} to lower temperatures. Similarly, the presence of Tween 80 below its CMC, Brij 35 below and around its CMC and Pluronic F-68 at around its CMC induced the IgG2 unfolding temperature T_{m2} to shift to a lower temperature.

In general, thermal unfolding experiments for both BSA and IgG2 with surfactant systems revealed that the conformational stabilisation in BSA and IgG2 solutions was surfactant type and concentration dependent. The interactions between protein and surfactants have been previously studied by several workers including Putnam (1948), Steinhardt and Reynolds (1969), Jones et al. (1991), Ananthapadamanabhan (1993) and Vermeer and Norde (2000). The nature of the protein-surfactant interaction was reported to be very complex and it was emphasised that surfactant binding may lead to partial denaturation of proteins and sometimes even complete unfolding, but then again it depends on surfactant. In order to prevent such surfactant-induced unfolding, better understanding of the binding characteristics is required.

Experiments conducted to look at how the proteins refold in the presence of surfactants (Chapter 3), revealed that the transitions for BSA and IgG2 with all four surfactants were irreversible and no thermal transitions were noted on subsequent scans of the same samples after cooling. It has been previously reported that unfolded proteins can easily aggregate during the refolding process as they go through the various intermediate states. Thermally induced protein unfolding is often followed or accompanied by immediate aggregation due to exposure of the hydrophobic residues (Wang et al., 2010).

Experiments in Chapter 4 were designed to investigate how particle size distribution measurements as determined by Dynamic Light Scattering (DLS) were affected by the presence and concentration of Tween 20, Tween 80, Brij 35 and Pluronic F-68 surfactants in relation to surfactant CMC.

Additionally, heat treatment and storage effects on particle size distribution for different surfactant concentration were investigated.

Dynamic Light Scattering (DLS) has been widely utilised in the area of protein characterisation, including bovine serum albumin (Adel et al. 2008) and immunoglobulin G (Ahrer et al. 2006, Bermudez and Forciniti 2004).

Protein alone solutions of BSA and IgG2 as well as protein-surfactant combinations were employed. From DLS experimental data represented in Chapter 4, it had been observed that for fresh BSA – surfactant systems, the presence of Tween 20 at above CMC produced the lowest increase in particle diameter (nm) compared to other surfactants, whereas for IgG2 – surfactant systems, the presence of all surfactants brought an increase in particle size. However the lowest increase was observed for Tween 80 at a concentration below and Pluronic F-68 at a concentration below their CMC.

To establish the heat treatment stability of the samples, BSA alone and BSA – surfactant systems were heated at 66°C. Solutions containing IgG2 alone and IgG2 – surfactant systems were heated to 60°C (Chapter 2, Section 2.2.1) to promote stress change within the samples. It has been previously reported that heat treatment of BSA and IgG induces strong aggregation which results in precipitation of the proteins (Padlan, 1997, Vermeer and Norde, 2000). However, the presence of Tween 20 above its CMC and Brij 35 above its CMC produced the highest relative decrease in particle size diameter of the BSA – surfactant systems. For IgG2-surfactant systems, the presence of Pluronic F-68 at below and around its CMC, showed a decreased in diameter on heating compared to IgG2 alone and the other surfactant systems.

To establish the storage stability of the samples, both fresh samples of BSA and IgG2 alone and with the four surfactants present were stored for 8 weeks in the fridge (Chapter 2, Section 2.2.2). DLS results indicated that all BSA – surfactant systems on storage displayed larger sized particles. The greatest increase in particle size diameter was observed for BSA in the presence of Tween 80 at around its CMC, Brij 35 below its CMC and Pluronic F-68 below and around its CMC. Interestingly IgG2 – surfactant systems displayed a different behaviour. Only IgG2 systems with Tween 80 present below its CMC and Pluronic F-68 at around its CMC showed an increase in particle size with storage.

Globally considering the data presented in Chapter 4, it can be said, that for both BSA and IgG2 alone the aggregate growth is much stronger than when certain surfactants at different concentrations are added to the systems. For the protein size stability of BSA in solution, results showed that the presence of Tween 20 above its CMC was preferable, because of the fewer aggregate formed for initial and heated BSA samples. Considering the data for initial IgG2 formulations; the presence of Tween 20 below its CMC and Pluronic F-68 at around its CMC were preferable. In terms of minimising heat stress Pluronic F-68 below and around its CMC performed well. The presence of Tween 80 at below and Pluronic-68 at around its CMC gave the best performance in terms of lower particle growth for the aged samples of IgG2. Dynamic light scattering experiments revealed that particle formation strongly depends on surfactant type and concentration. The difference between the behaviour of BSA and IgG2 in this study, and the difference in the results for the different stress approaches in the presence of the surfactants samples

could be due to the fact, that either the CMC concentration of Tween 20, Tween 80, Brij 35 and Pluronic F-68 surfactants are not sufficient to stabilize or because the stress methods used: heating and storage are too rigorous to enable surfactants to exhibit their full stabilizing effect (Mahler et al., 2005). All four surfactants used in this study, namely Tween 20, Tween 80, Brij 35 and Pluronic F-68, are non-ionic surfactants. The ability of a surfactant to participate in a specific biological/biochemical function is related to its structure. Non-ionic surfactants are characterised by uncharged hydrophilic head groups. These surfactants are mild and non-denaturing because they disrupt protein-lipid and lipid-lipid interactions. Short chain (i.e., C₇ – C₁₀) non-ionic surfactants are typically more deactivating than longer chain (i.e., C₁₂ – C₁₄) non-ionic surfactants (Seddon et al., 2004; le Maire et al., 2000). A pertinent question to ask is how is surfactant function in formulations affected by the structure of the hydrophobic group? The hydrophobic tail of a surfactant allows the molecule to partition into the apolar lipid bilayer during the solubilisation of membrane proteins. It also masks the hydrophobic portions of the membrane proteins once they have been solubilised and thus prevents protein aggregation. Although the hydrophilic head group and hydrophobic tail each affect the properties of the surfactant molecule differently. Together their total effect is known as the Hydrophilic-Lipophilic Balance (HLB), which is defined by a number that ranges from 0 to 40. In general, an HLB number <10 indicates that a surfactant has low solubility in water while an HLB number between 10 and 20 indicates that the detergent is readily soluble in water (Anatrace Inc., 2008).

The values of HLB for Tween 20, Tween 80, Brij 35 and Pluronic F-68 are shown in table 6.1.

Table 6.1 Hydrophilic-Lipophilic Balance values for Tween 20, Tween 80, Brij 35 and Pluronic F-68 surfactants (Anatrace, 2006; Griffin, 1954; Sigma Aldrich).

Surfactant type	HLB value
Tween 20	16.7
Tween 80	15
Brij 35	16.9
Pluronic F-68	29

All four surfactants used in this work are conferred with a high HLB (greater than about 12) value and Tween 20, Tween 80, Brij 35 and Pluronic F-68 surfactants are predominantly hydrophilic and water-soluble. Trends relating HLB value to surfactant benefit in terms of protein size stabilisation are not readily discernable.

Dynamic Light Scattering requires limited sample preparation and provides a relatively quick analysis time. However, the use of DLS often has to be combined with other analytical techniques as the higher sensitivity of the instrument to larger particles can make analysis of some solutions problematic. This is particularly so if larger particles or dust are present.

In Chapter 5, the preliminary experimental work focussed on sub-visible particle count by employing Light Obscuration (HIAC) and Micro-Flow Imaging (MFI) measurements. In the recently published commentary, it was noted that there are critical gaps in the detection and control of sub-visible particles, especially in the size range from 0.1 μm to 10 μm and that it is important to be able to effectively monitor and control these particles during formulation development (Carpenter et al., 2008; Sharma et al., 2010). In

Chapter 5, the effect of Tween 20, Tween 80, Brij 35 and Pluronic F-68 surfactants at concentrations below, around and above their CMC level on BSA and IgG2 proteins' size stability was investigated.

Results showed that heat shock and storage treatment had a significant effect on particle formation of BSA and IgG2 surfactant free solutions. According to the results obtained from HIAC and MFI analysis in Chapter 5, BSA surfactant-free samples after storage treatment showed slightly higher and statistically significantly different particle counts and distribution than that after heat stress when compared to freshly prepared BSA. Also both heat stress and storage treatments induced an increase in particle count for IgG2 surfactant free samples for particles of sizes $\geq 2 \mu\text{m}$ to $\geq 10 \mu\text{m}$. For particles $\geq 25 \mu\text{m}$, measured by both HIAC and MFI methods, heat treatment produced a statistically significant increase in particle count, whereas storage treatment showed no statistical difference at this size range for IgG2 surfactant free samples.

On considering the results obtained for the different surfactants on BSA and IgG2 protein particle size stability as explored by HIAC and MFI experiments, it can be noted, that the presence of Brij 35 at above its CMC was the most effective. The high concentration of Brij 35 decreased particle count at all size ranges for fresh, heated and aged samples when compared to other surfactants and surfactant free systems of both proteins. However, this might be due to Brij 35 being in excess at high concentrations. Surfactant – protein ratio should be considered.

In Chapter 5 BSA and IgG2 proteins were investigated by HIAC and MFI methods. It is prudent to compare the results obtained from the two methods.

Figures 6.1 and 6.2 present the comparative particle count data obtained for HIAC and MFI methods for fresh BSA and IgG2 solutions respectively. Results are reported as an average \pm standard deviation.

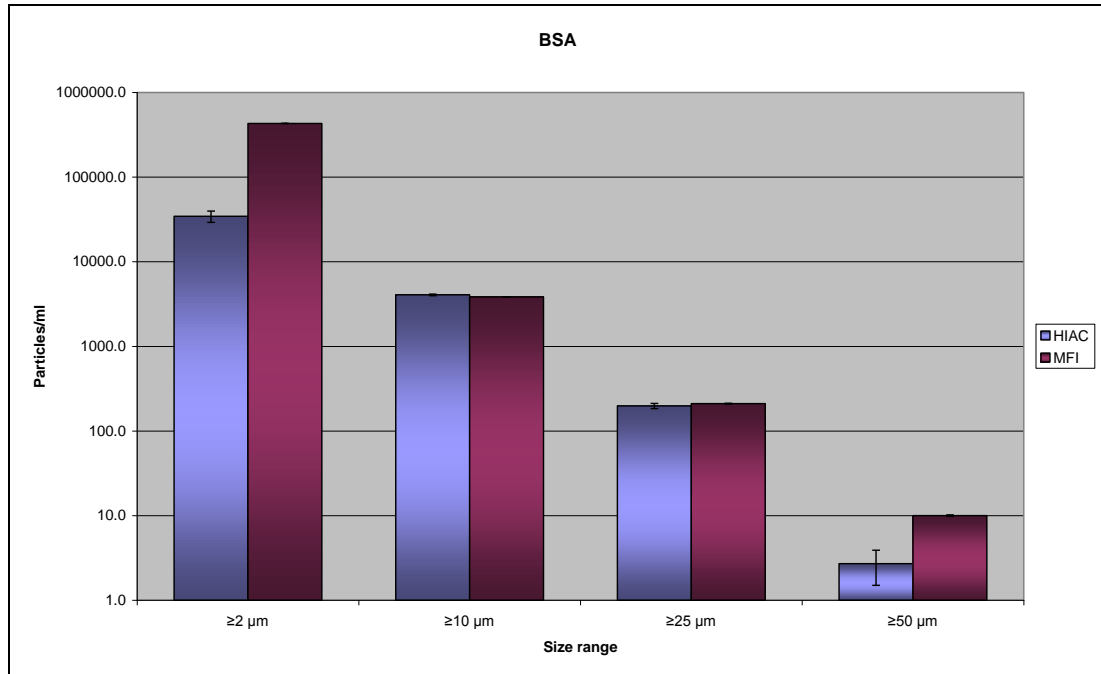


Figure 6.1. Comparison of particle count per ml measured by HIAC and MFI methods for fresh BSA protein.

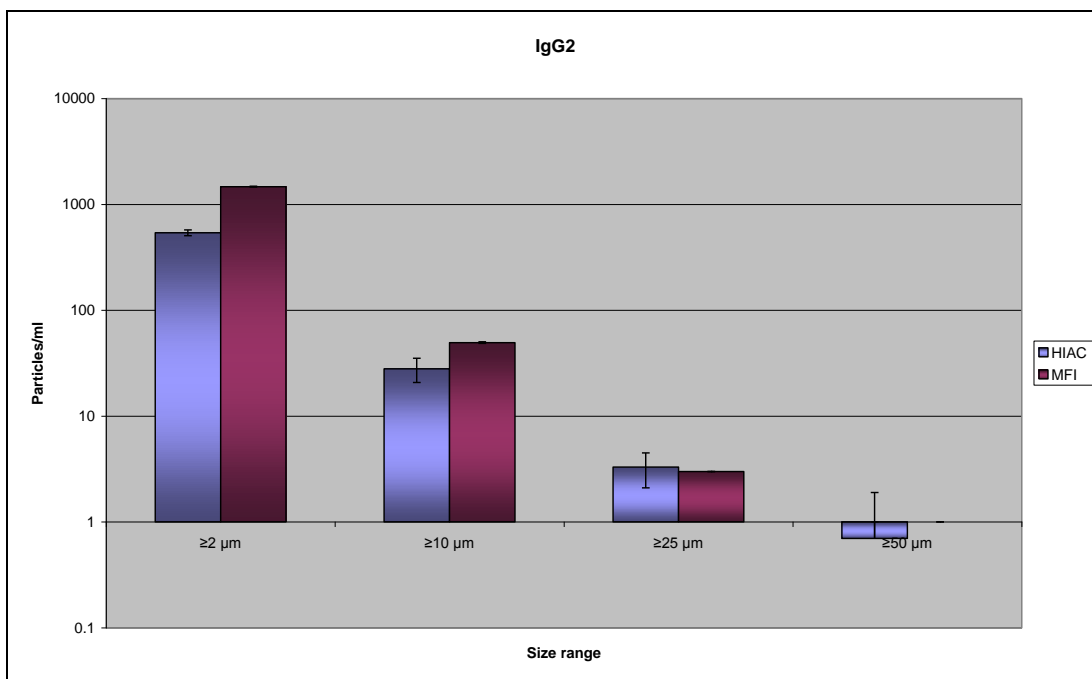


Figure 6.2. Comparison of particle count per ml measured by HIAC and MFI methods for fresh IgG2 protein.

Both instruments were expected to show similar particle counts. However, from Figures 6.1 and 6.2, it can be seen, that generally Light Obscuration (HIAC) reported lower particle counts data than Micro-flow imaging, especially at the size range of $\geq 2 \mu\text{m}$. It has been previously published by Demeule et al., 2010, Huang et al., 2009, Sharma et al., 2010, that Light Obscuration technique tended to report lower particle count numbers per ml than MFI (Demeule et al., 2010; Huan et al., 2009, Sharma et al., 2010).

However both HIAC and MFI techniques showed similar trends regarding particle count values. Using statistical analysis the Pearson correlation test showed that there was no relationship between HIAC and MFI methods for BSA and IgG2 particle count per ml ($P > 0.05$). However, there was a strong relationship at the 0.01 level ($P < 0.01$) between the data obtained for the HIAC and MFI methods from the fresh and heated BSA-surfactant formulations for particles $\geq 2 \mu\text{m}$. Pearson correlation analysis also showed

that there was a significant relationship at the 0.05 level ($P < 0.05$) between the particle count data for particles $\geq 50 \mu\text{m}$ obtained by the two methods for aged BSA – surfactant systems. For the particle count data for particles $\geq 25 \mu\text{m}$ the same level of significance was determined between the two methods for initial and aged IgG2-surfactant systems. Figures 6.3 to 6.8 represent the scatter plots between HIAC and MFI for fresh, heated and aged BSA and IgG2 – surfactant systems for particle count data at $\geq 2 \mu\text{m}$, $\geq 10 \mu\text{m}$, $\geq 25 \mu\text{m}$ and $\geq 50 \mu\text{m}$.

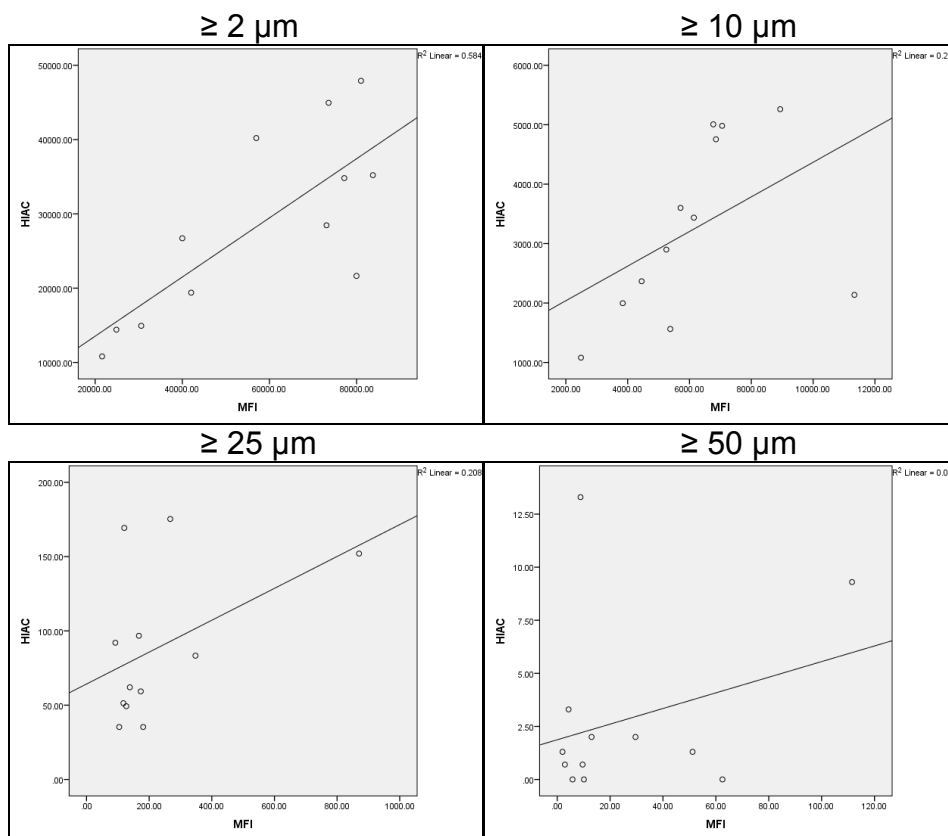


Figure 6.3. Scatter plots of particle count per ml at $\geq 2 \mu\text{m}$, $\geq 10 \mu\text{m}$, $\geq 25 \mu\text{m}$ and $\geq 50 \mu\text{m}$ as measured by HIAC and MFI for fresh BSA – surfactant formulations.

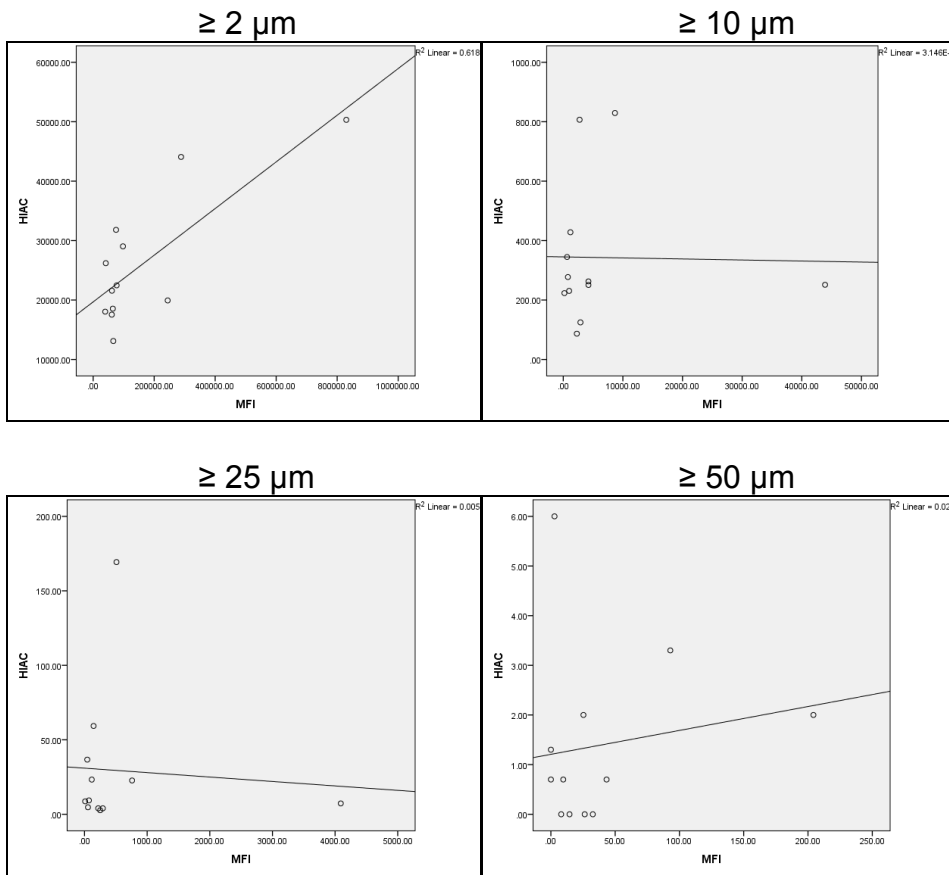


Figure 6.4. Scatter plots of particle count per ml at $\geq 2 \mu\text{m}$, $\geq 10 \mu\text{m}$, $\geq 25 \mu\text{m}$ and $\geq 50 \mu\text{m}$ as measured by HIAC and MFI for heated BSA – surfactant formulations.

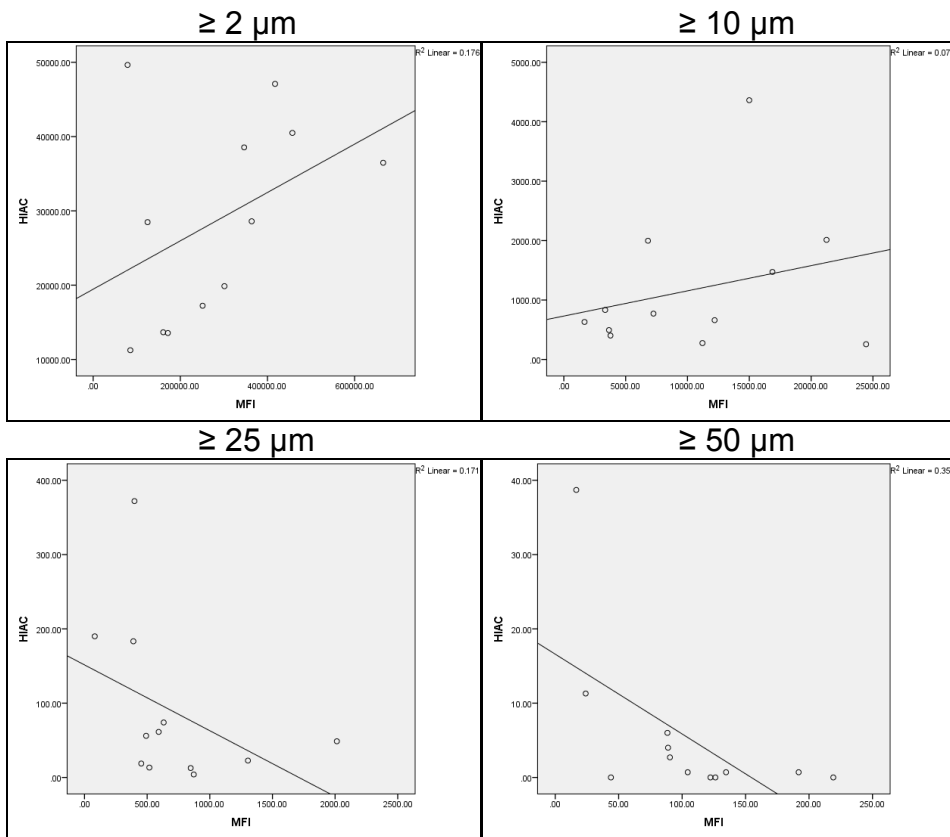


Figure 6.5. Scatter plots of particle count per ml at $\geq 2 \mu\text{m}$, $\geq 10 \mu\text{m}$, $\geq 25 \mu\text{m}$ and $\geq 50 \mu\text{m}$ measured by HIAC and MFI for aged BSA – surfactant formulations.

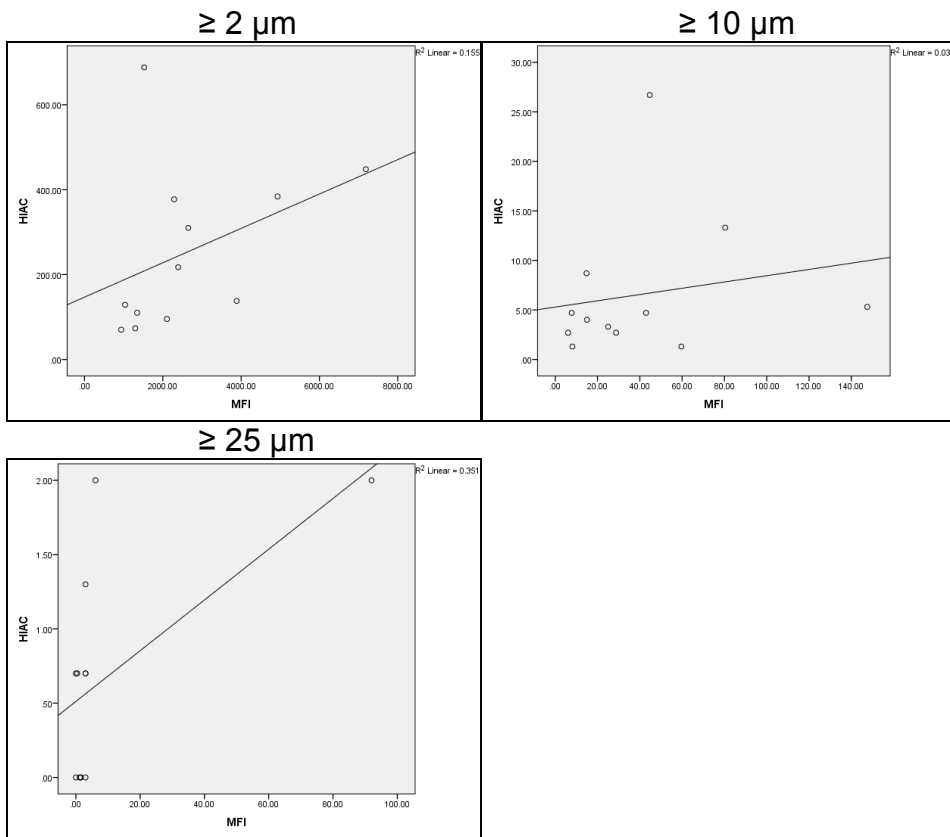


Figure 6.6. Scatter plots of particle count per ml at $\geq 2 \mu\text{m}$, $\geq 10 \mu\text{m}$, $\geq 25 \mu\text{m}$ and $\geq 50 \mu\text{m}$ as measured by HIAC and MFI for fresh IgG2 – surfactant formulations.

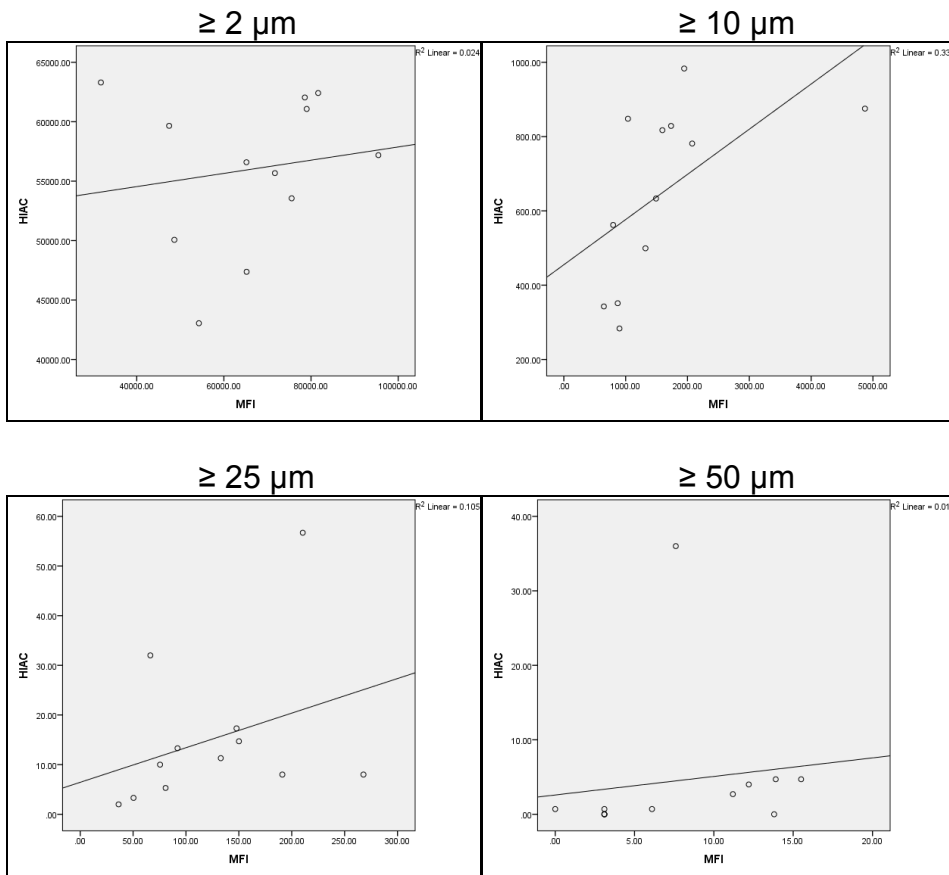


Figure 6.7. Scatter plots of particle count per ml at $\geq 2 \mu\text{m}$, $\geq 10 \mu\text{m}$, $\geq 25 \mu\text{m}$ and $\geq 50 \mu\text{m}$ as measured by HIAC and MFI for heated IgG2 – surfactant formulations.

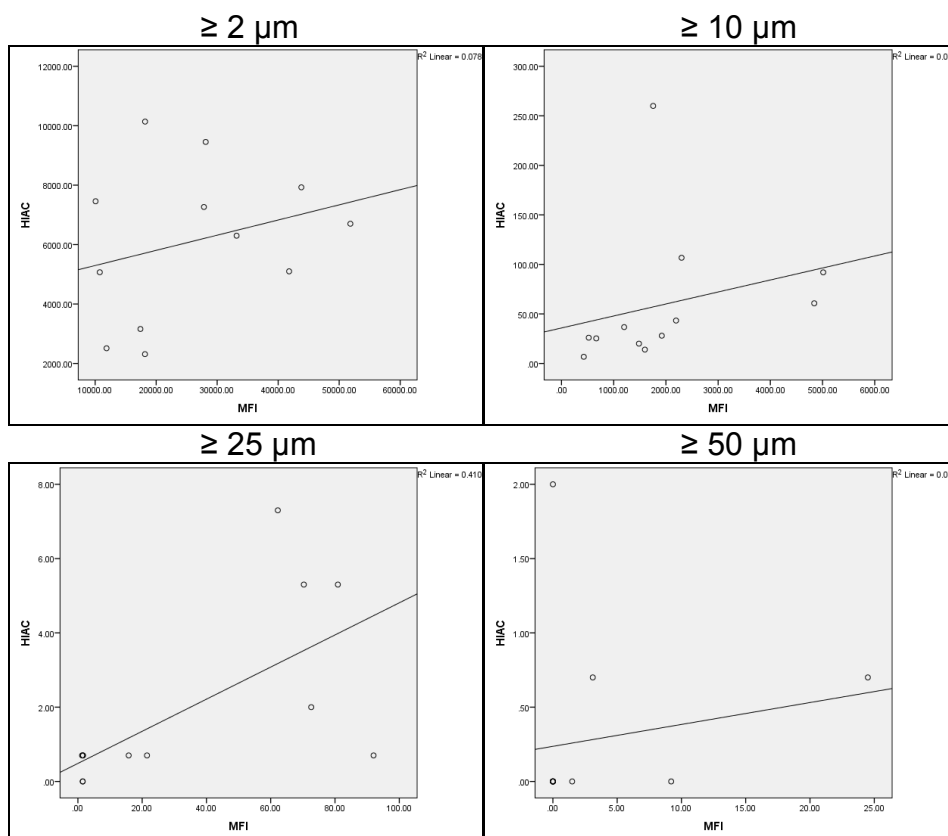


Figure 6.8. Scatter plots of particle count per ml at $\geq 2 \mu\text{m}$, $\geq 10 \mu\text{m}$, $\geq 25 \mu\text{m}$ and $\geq 50 \mu\text{m}$ as measured by HIAC and MFI for aged IgG2 – surfactant formulations.

In recent studies, Huang et al., 2009 and Sharma et al., 2010, compared the sizing and counting accuracy of HIAC and MFI and found that while the two methods gave similar results, MFI detected significantly more particles than HIAC. Both articles considered that the difference in Light Obscuration and Micro-flow Imaging measurements might be due to the under-estimation of sub-visible particles by the light obscuration technique (Huang et al., 2009; Sharma et al., 2010).

The different analytical methods applied in this thesis provide different aspects and insight into BSA and IgG2 conformational stability and protein size stability. The T_m value measured by High Sensitivity Differential Scanning calorimetry HSDSC was used as a stability indicator. DLS analysis

was used for detection of small sized aggregates in the range of 1 – 450 nm size. The Light Obscuration (HIAC) and Micro-flow Imaging (MFI) techniques were used in this study to detect large aggregates of 2 – 100 μm . The question is do these different methods have any relationship between each other? Does T_m predict particle formation measured by DLS, HIAC and MFI? Does level of small particle size measured by DLS predict levels of larger aggregates measured by HIAC and MFI?

Statistical data analysis using Pearson Correlation (See Chapter 2, Section 2.2.7) was used to describe the relationship between HSDSC temperature T_m and main peak diameter (nm) measured by DLS for fresh, heated and aged BSA and IgG2 surfactant systems (Figures 6.9, 6.10 and 6.11).

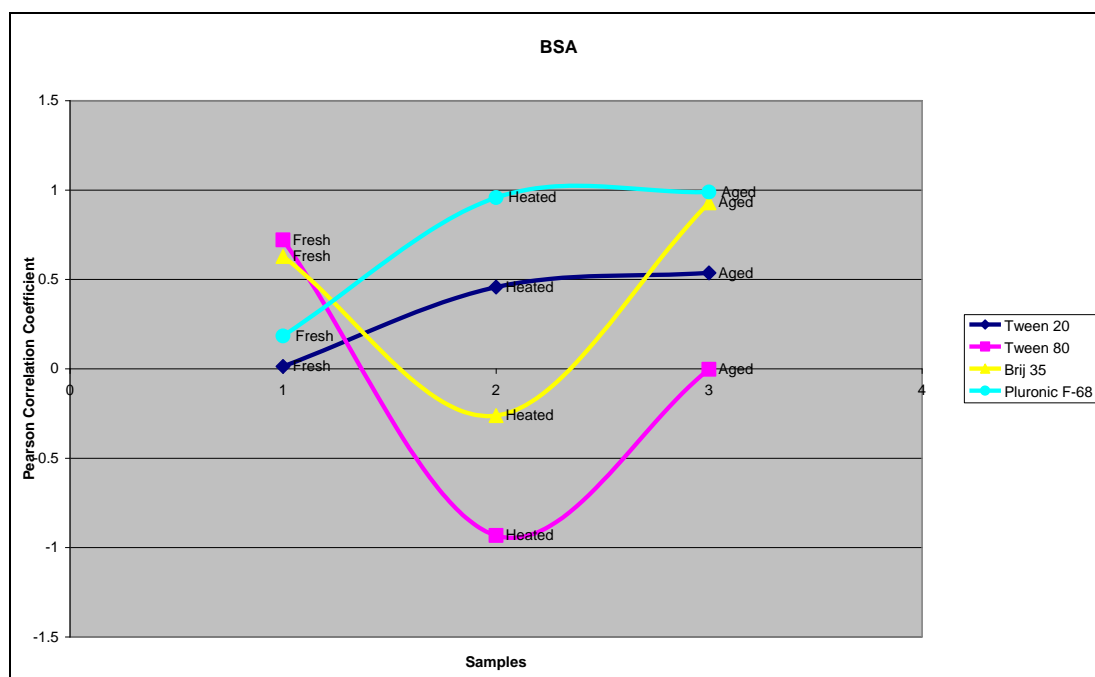


Figure 6.9. The Pearson Correlation Coefficient between HSDSC unfolding temperature T_m and main peak diameter (nm) measured by DLS for: (1) fresh, (2) heated and (3) aged BSA with Tween 20, Tween 80, Brij 35 and Pluronic F-68 surfactants.



Figure 6.10. The Pearson Correlation Coefficient between HSDSC unfolding temperature T_{m1} and main peak diameter (nm) measured by DLS for: (1) fresh, (2) heated and (3) aged IgG2 with Tween 20, Tween 80, Brij 35 and Pluronic F-68 surfactants.

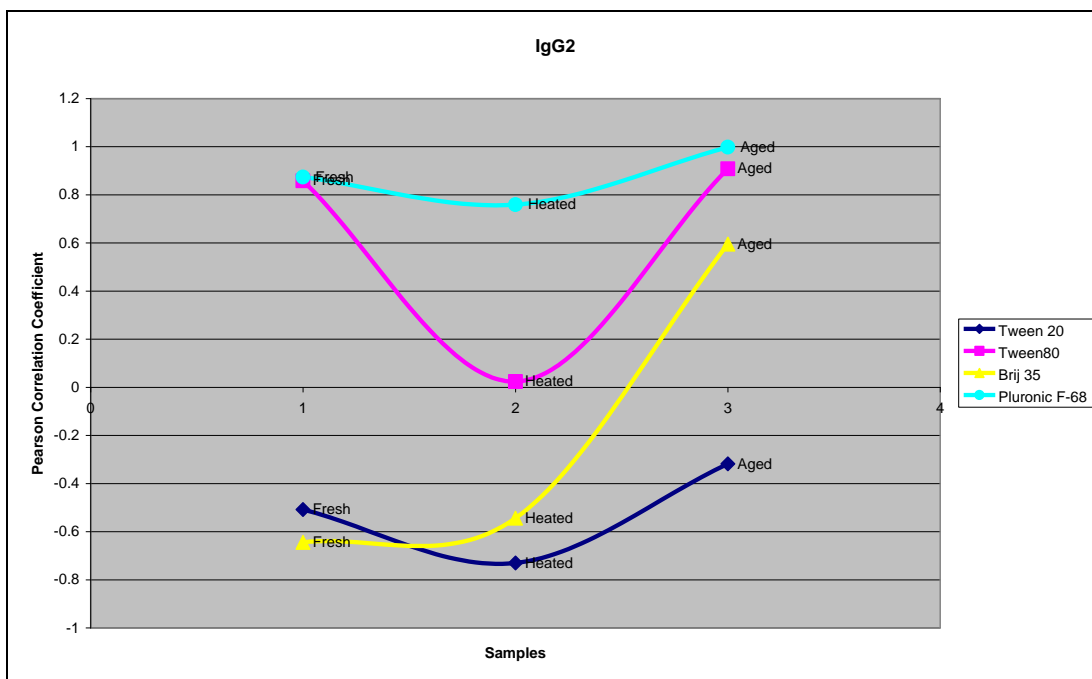


Figure 6.11. The Pearson Correlation Coefficient between HSDSC unfolding temperature T_{m2} and main peak diameter (nm) measured by DLS for: (1) fresh, (2) heated and (3) aged IgG2 with Tween 20, Tween 80, Brij 35 and Pluronic F-68 surfactants.

The Pearson Correlation Coefficient was closest to +1.00 for heated BSA with Pluronic F-68 surfactant and aged BSA with Brij 35 and Pluronic F-68 surfactant and was closest to -1.00 for heated BSA with Tween 80 (Figure 6.9). Such values would denote the perfect linear relationship and that both variables rise and fall sympathetically. However for all fresh, heated and aged BSA – surfactants systems the statistical significance failed to meet the 0.05 ($P > 0.05$) criteria, and confirmed that temperature T_m measured by HSDSC and main peak diameter (nm) measured by DLS were uncorrelated (zero correlation).

On analysing the correlation between IgG2 – surfactant systems T_{m1} and main peak diameter, the Pearson Correlation Coefficient was found to be +0.992 for aged IgG2 with Pluronic F-68 surfactant (Figure 6.10). However,

for fresh, heated and aged IgG2 – surfactants systems the statistical significance failed to meet the 0.05 ($P > 0.05$) criteria, and confirmed that temperature T_{m1} and main peak diameter have zero correlation.

There was no statistically significant relationship detected for IgG2 – surfactant system data between main peak diameter (nm) and temperature T_{m2} (Figure 6.11), except aged IgG2 with Pluronic F-68 surfactant showed significance ($P < 0.05$) between main peak diameter and temperature T_{m2} . The Pearson Correlation Coefficient was found to be +0.998, which tells us that both variables rise and fell sympathetically.

In general, the results from statistical data analysis identified that T_m measured by HSDSC can not predict the formation of smaller particle size particles measured by DLS.

To probe if there is any relationship between T_m and the particle count data at $\geq 2 \mu\text{m}$, $\geq 5 \mu\text{m}$, $\geq 10 \mu\text{m}$, $\geq 25 \mu\text{m}$ and $\geq 50 \mu\text{m}$ size ranges measured by HIAC and MFI, a statistical data analysis using the Pearson correlation test was used to measure the “degree of linearity” and relationship between these variables.

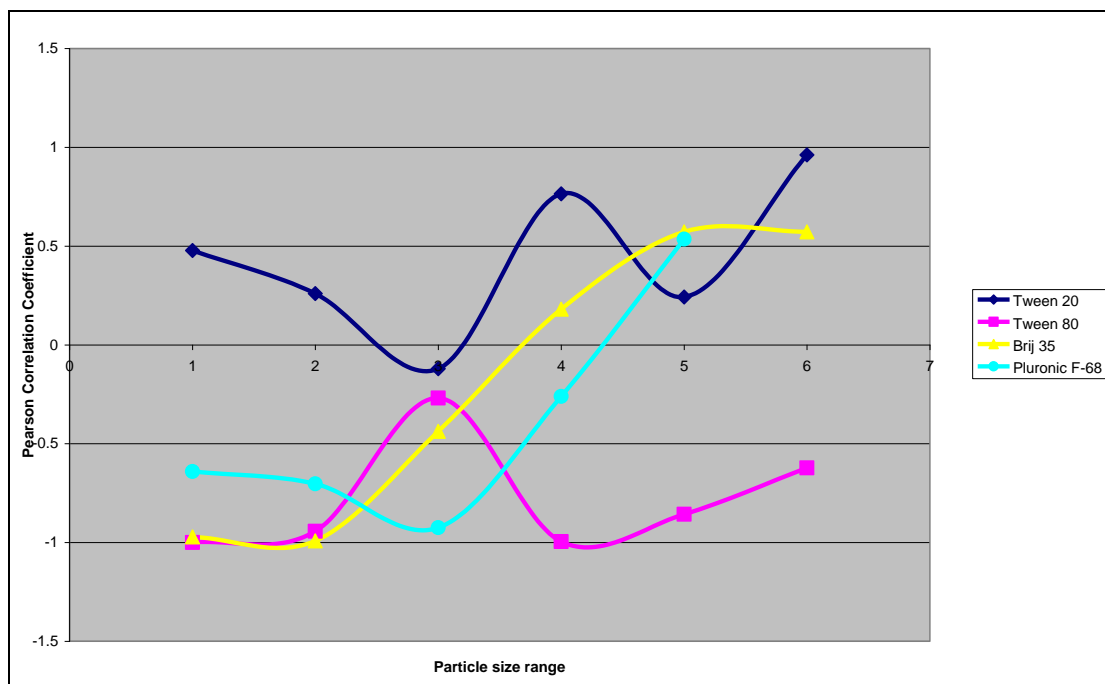


Figure 6.12. The Pearson Correlation Coefficient measured between T_m (HSDSC) and particle count (HIAC) for fresh BSA with Tween 20, Tween 80, Brij 35 and Pluronic F-68 surfactants at (1) $\geq 2 \mu\text{m}$, (2) $\geq 5 \mu\text{m}$, (3) $\geq 10 \mu\text{m}$, (4) $\geq 25 \mu\text{m}$, (5) $\geq 50 \mu\text{m}$ and (6) $\geq 100 \mu\text{m}$ particle size ranges.

The Pearson Correlation Coefficient was found to be -0.992 for fresh BSA with Brij 35 at $\geq 5 \mu\text{m}$ size range, -0.995 for Tween 80 at $\geq 25 \mu\text{m}$ particle size range. The magnitude of the coefficient was close to its maximum -1.00 (which would denote a perfect relationship), however the significance value was greater than 0.05 ($P > 0.05$), confirming that there was no relationship between T_m and particle count for these surfactants. The Pearson Correlation Coefficient was at -1.00 for fresh Tween 80 at $\geq 2 \mu\text{m}$ particle size range (Figure 6.12). The correlation between T_m and particle count for this surfactant is significant at the 0.05 level ($P < 0.05$). For all other initial protein-surfactant solutions, T_m measured by HSDSC and particle count measured by HIAC are uncorrelated (Figure 6.12).

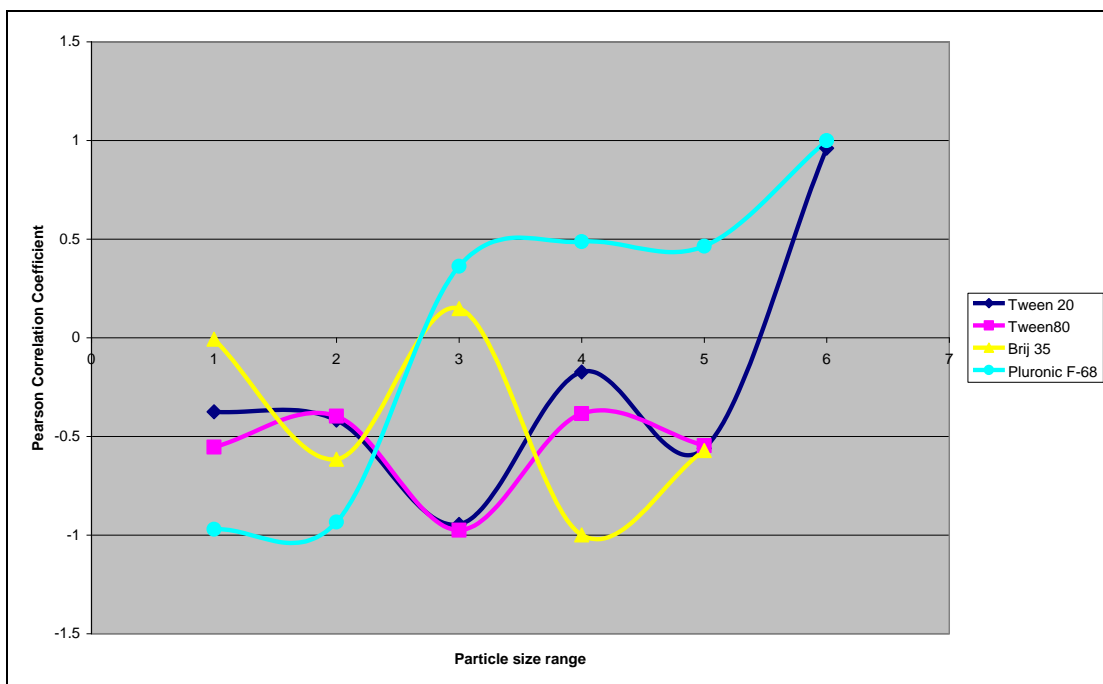


Figure 6.13. The Pearson Correlation Coefficient measured between T_m (HSDSC) and particle count (HIAC) for heated BSA with Tween 20, Tween 80, Brij 35 and Pluronic F-68 surfactants at (1) $\geq 2 \mu\text{m}$, (2) $\geq 5 \mu\text{m}$, (3) $\geq 10 \mu\text{m}$, (4) $\geq 25 \mu\text{m}$, (5) $\geq 50 \mu\text{m}$ and (6) $\geq 100 \mu\text{m}$ particle size ranges.

For samples of heated BSA with surfactant present, the Pearson Correlation Coefficient is found to be -0.999 for heated BSA with Brij 35 at $\geq 25 \mu\text{m}$ size range and +0.999 for heated BSA with Pluronic F-68 at $\geq 100 \mu\text{m}$ particle size range. The significance value for both of these examples were below 0.05 ($P < 0.05$). This indicates evidence that T_m and particle count at these cases are indeed correlated. For the remainder of the heated samples a significance value greater than 0.05 ($P > 0.05$) was obtained and indicated zero correlation (Figure 6.13).

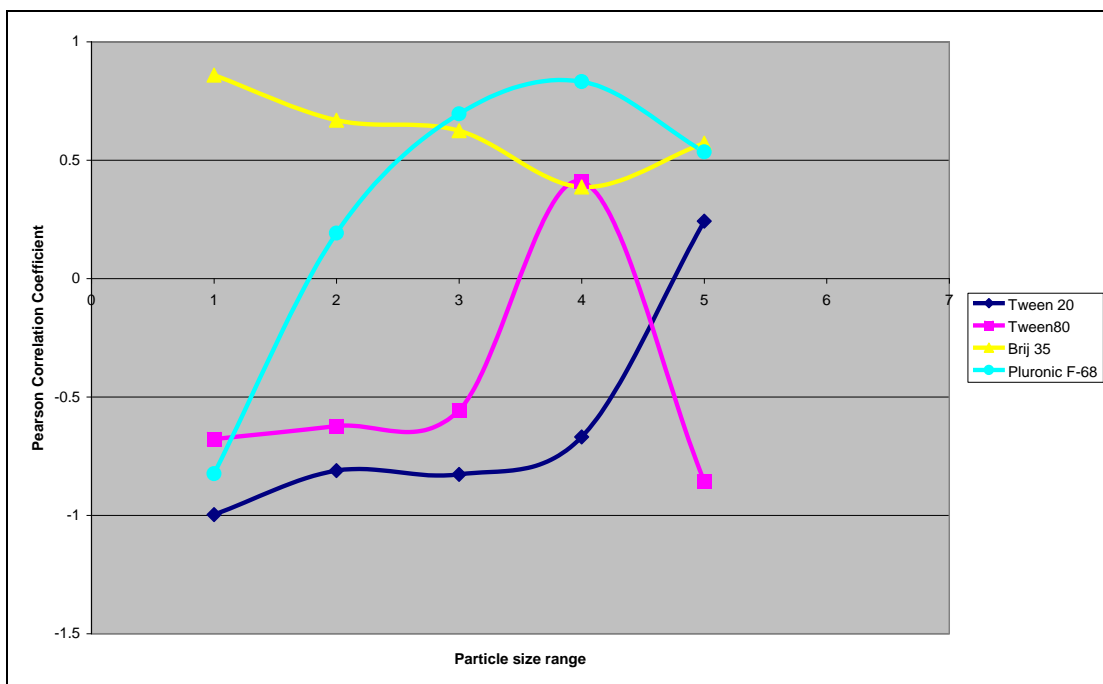


Figure 6.14. The Pearson Correlation Coefficient measured between T_m (HSDSC) and particle count (HIAC) for aged BSA with Tween 20, Tween 80, Brij 35 and Pluronic F-68 surfactants at (1) $\geq 2 \mu\text{m}$, (2) $\geq 5 \mu\text{m}$, (3) $\geq 10 \mu\text{m}$, (4) $\geq 25 \mu\text{m}$, (5) $\geq 50 \mu\text{m}$ and (6) $\geq 100 \mu\text{m}$ particle size ranges.

For samples of aged BSA with surfactant present, the Pearson Correlation Coefficient is found to be +0.999 for aged BSA with Pluronic F-68 and particle count data at $\geq 50 \mu\text{m}$ particle size range. That tells us that in this case both variables: T_m and particle count rise and fall sympathetically and that the magnitude of the coefficient is very close to maximum of +1.00, which would denote a perfect relationship. The significance value was quoted as 0.026, which is below 0.05. This indicates that in this case the correlation between T_m and particle count is significant at 0.05 level ($P < 0.05$). For all other surfactants at different size ranges the correlation coefficient was not close to -1.00 or +1.00, so that indicates zero correlation between T_m and particle count (Figure 6.14).

Statistical analysis, using Pearson correlation was used to describe the relationship between IgG2 unfolding temperatures T_{m1} , T_{m2} measured by HSDSC and particle count data for particles of size $\geq 2 \mu\text{m}$, $\geq 5 \mu\text{m}$, $\geq 10 \mu\text{m}$, $\geq 25 \mu\text{m}$ and $\geq 50 \mu\text{m}$ measured by Light Obscuration. The Pearson Correlation Coefficient results for fresh, heated and aged IgG2 with Tween 20, Tween 80, Brij 35 and Pluronic F-68 are summarised in Figures 6.15-6.20.

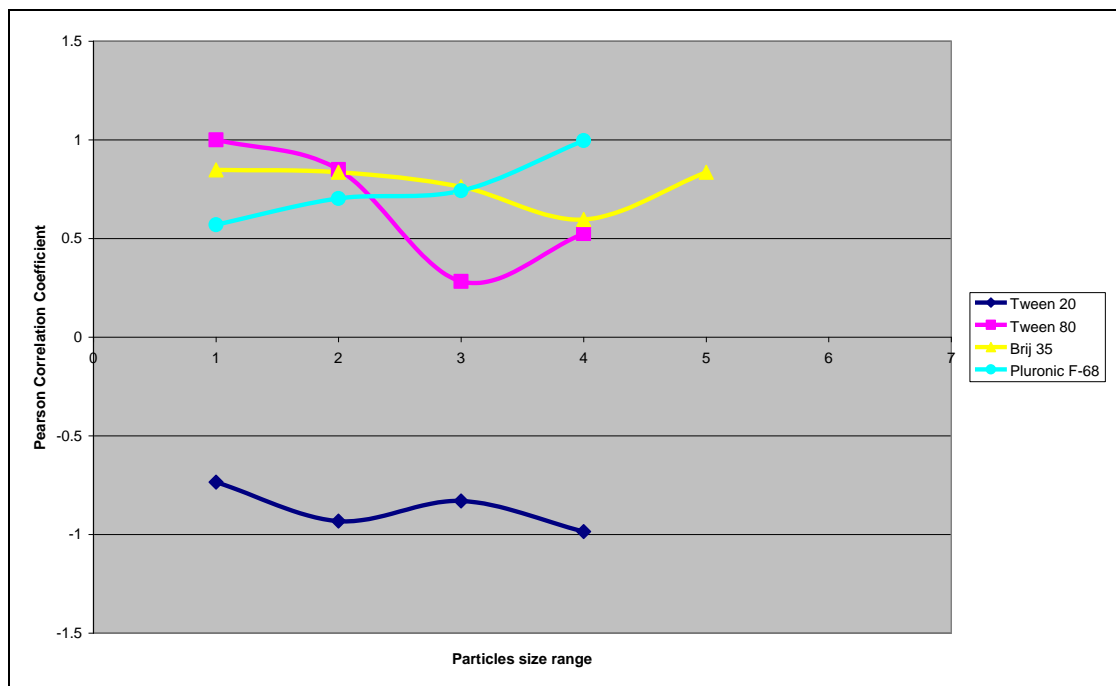


Figure 6.15. The Pearson Correlation Coefficient measured between T_{m1} (HSDSC) and particle count (HIAC) for fresh IgG2 with Tween 20, Tween 80, Brij 35 and Pluronic F-68 surfactants at (1) $\geq 2 \mu\text{m}$, (2) $\geq 5 \mu\text{m}$, (3) $\geq 10 \mu\text{m}$, (4) $\geq 25 \mu\text{m}$, (5) $\geq 50 \mu\text{m}$ and (6) $\geq 100 \mu\text{m}$ particle size ranges.

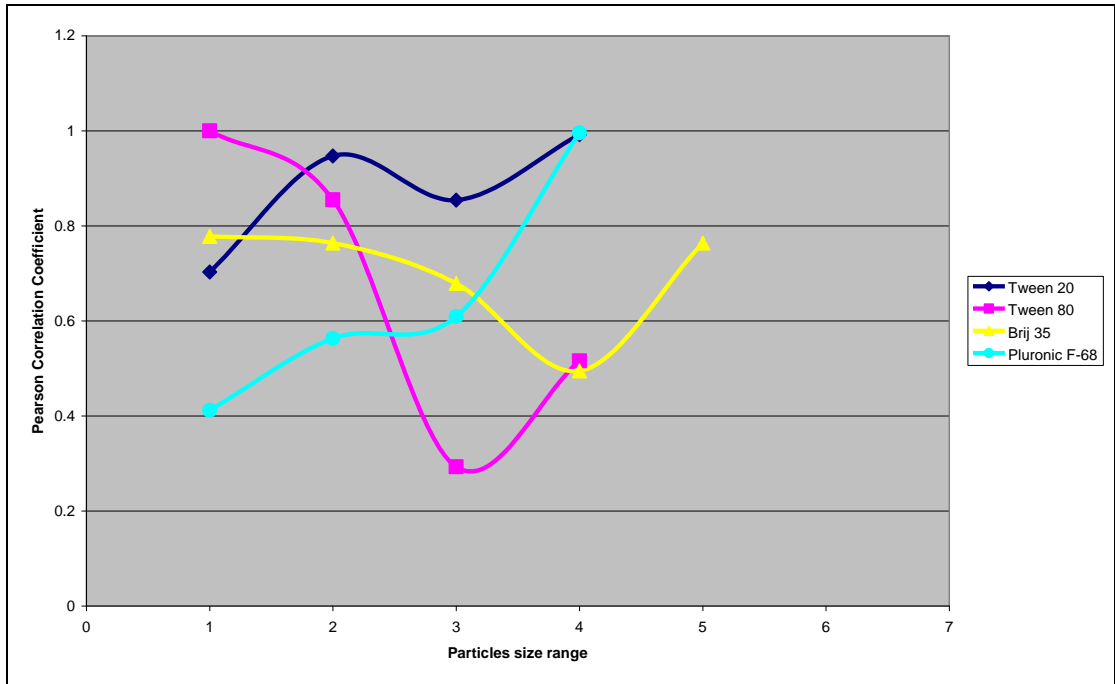


Figure 6.16. The Pearson Correlation Coefficient measured between T_{m2} (HSDSC) and particle count (HIAC) for fresh IgG2 with Tween 20, Tween 80, Brij 35 and Pluronic F-68 surfactants at (1) $\geq 2 \mu\text{m}$, (2) $\geq 5 \mu\text{m}$, (3) $\geq 10 \mu\text{m}$, (4) $\geq 25 \mu\text{m}$, (5) $\geq 50 \mu\text{m}$ and (6) $\geq 100 \mu\text{m}$ particle size ranges.

The Pearson Correlation Coefficient between T_{m1} , T_{m2} and particle count was found to be +1.00 for fresh IgG2 with Tween 80 at $\geq 2 \mu\text{m}$ size range (Figures 6.15 and 6.16). The magnitude of the coefficient is at its maximum +1.00, which denotes a perfect relationship between T_{m1} and particle count and T_{m2} and particle count per ml. In this case both variables rise and fall sympathetically. And the significance value in both these cases quoted as 0.003. This indicates very strong evidence that these variable are indeed correlated at the level of the 0.01 ($P < 0.01$). The Pearson Correlation Coefficient for all other fresh IgG2 with different surfactants was less than -1.00 or +1.00 and significance value was greater than 0.05 ($P > 0.05$), so T_{m1} , T_{m2} measured by HSDSC and particle count measured by HIAC in all

these cases was found to be statistically uncorrelated (Figures 6.15 and 6.16).

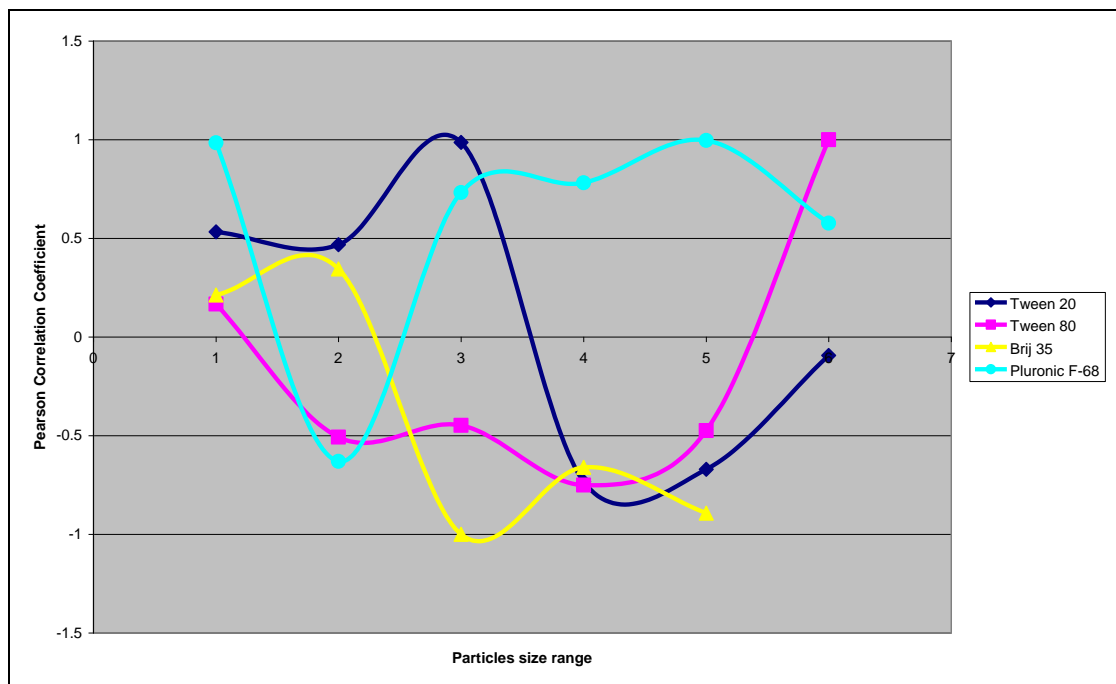


Figure 6.17. The Pearson Correlation Coefficient measured between T_{m1} (HSDSC) and particle count (HIAC) for heated IgG2 with Tween 20, Tween 80, Brij 35 and Pluronic F-68 surfactants at (1) $\geq 2 \mu\text{m}$, (2) $\geq 5 \mu\text{m}$, (3) $\geq 10 \mu\text{m}$, (4) $\geq 25 \mu\text{m}$, (5) $\geq 50 \mu\text{m}$ and (6) $\geq 100 \mu\text{m}$ particle size ranges.

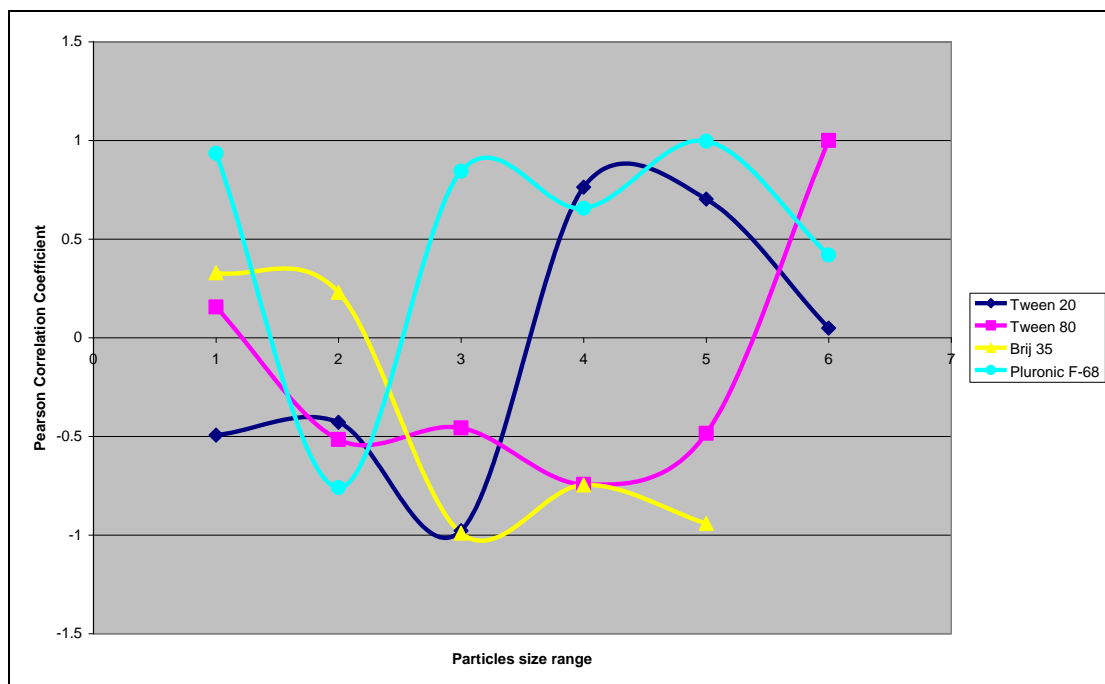


Figure 6.18. The Pearson Correlation Coefficient measured between T_{m2} (HSDSC) and particle count (HIAC) for heated IgG2 with Tween 20, Tween 80, Brij 35 and Pluronic F-68 surfactants at (1) $\geq 2 \mu\text{m}$, (2) $\geq 5 \mu\text{m}$, (3) $\geq 10 \mu\text{m}$, (4) $\geq 25 \mu\text{m}$, (5) $\geq 50 \mu\text{m}$ and (6) $\geq 100 \mu\text{m}$ particle size ranges.

For samples of heated IgG2 with surfactants present, the Pearson Correlation Coefficient between T_{m1} and particle count was found to be -1.00 for heated IgG2 with Brij 35 for particles $\geq 10 \mu\text{m}$ size and at +1.00 for IgG2 with Tween 80 for particles $\geq 100 \mu\text{m}$ (Figure 6.17). The significance value for these samples were below 0.05 ($P < 0.05$). The coefficient between T_{m2} and particle count was found to be +1.00 for Tween 80 for particles $\geq 100 \mu\text{m}$ (Figure 6.18). This indicates evidence that T_{m1} and particle count and T_{m2} and particle count at these cases are indeed correlated. For the remainder of the heated samples, no significant correlation was found between T_{m1} and particle count nor between T_{m2} and particle count (Figures 6.17 and 6.18).

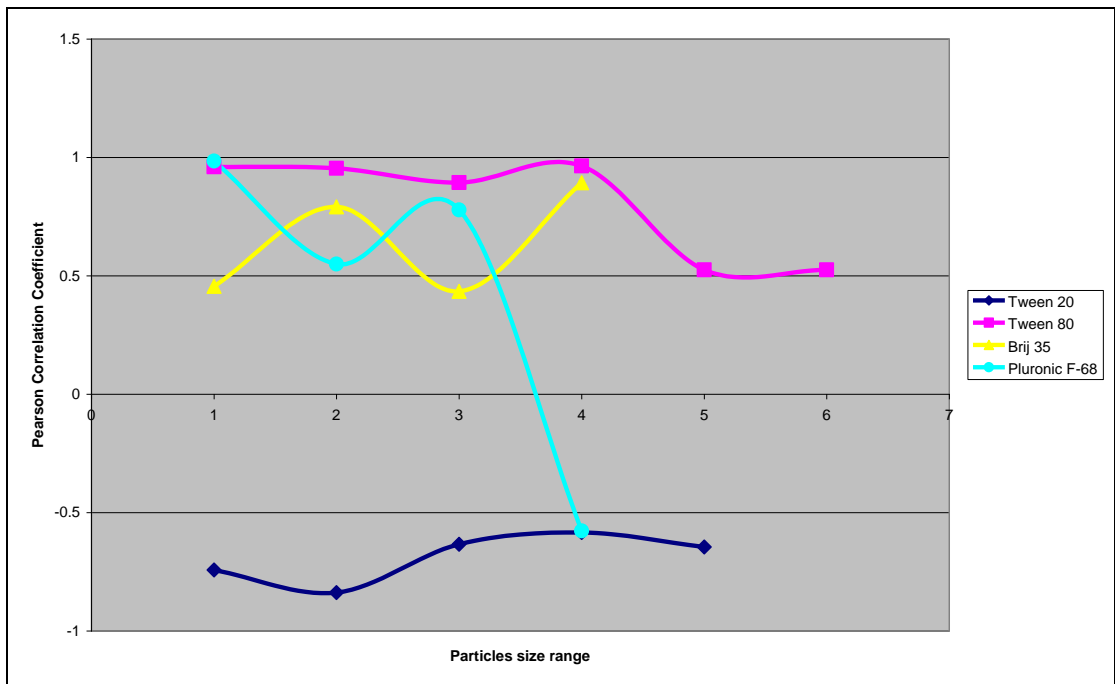


Figure 6.19. The Pearson Correlation Coefficient measured between T_{m1} (HSDSC) and particle count (HIAC) for aged IgG2 with Tween 20, Tween 80, Brij 35 and Pluronic F-68 surfactants at (1) $\geq 2 \mu\text{m}$, (2) $\geq 5 \mu\text{m}$, (3) $\geq 10 \mu\text{m}$, (4) $\geq 25 \mu\text{m}$, (5) $\geq 50 \mu\text{m}$ and (6) $\geq 100 \mu\text{m}$ particle size ranges.

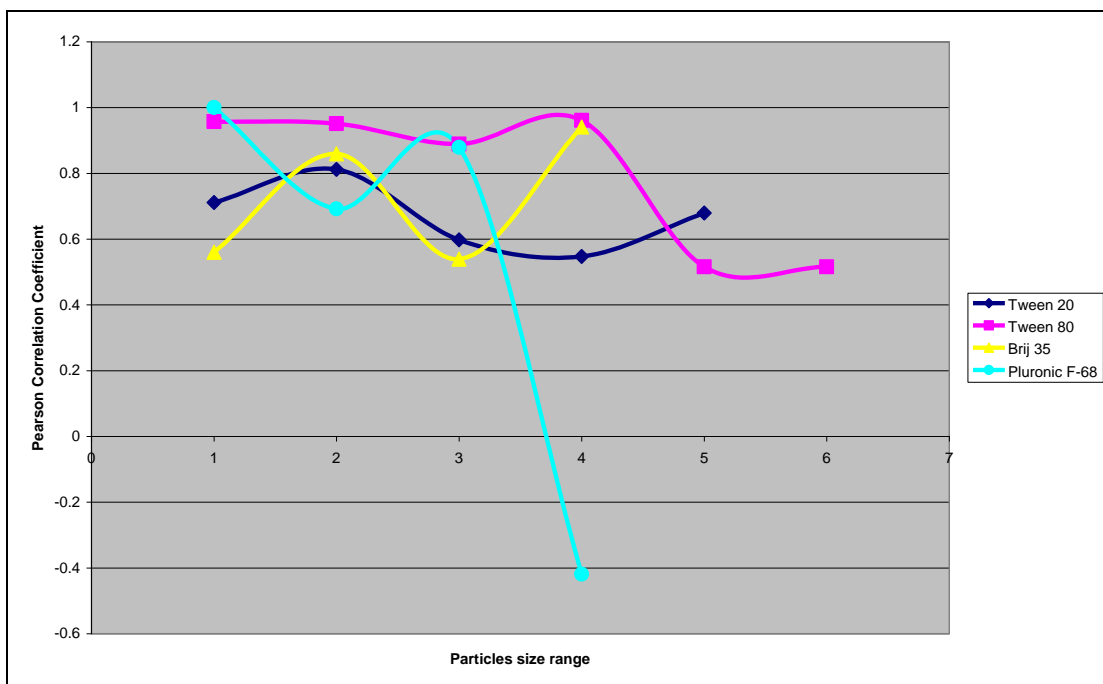


Figure 6.20. The Pearson Correlation Coefficient measured between T_{m2} (HSDSC) and particle count (HIAC) for aged IgG2 with Tween 20, Tween 80, Brij 35 and Pluronic F-68 surfactants at (1) $\geq 2 \mu\text{m}$, (2) $\geq 5 \mu\text{m}$, (3) $\geq 10 \mu\text{m}$, (4) $\geq 25 \mu\text{m}$, (5) $\geq 50 \mu\text{m}$ and (6) $\geq 100 \mu\text{m}$ particle size ranges.

For samples of aged IgG2 with surfactant present, the Pearson Correlation Coefficient for T_{m1} and particle count was found to be +0.999 for aged IgG2 with Pluronic F-68 for particles sized $\geq 100 \mu\text{m}$ (Figure 6.19). The Pearson Coefficient between T_{m2} and particle count was +1.00 for aged IgG2 with Pluronic F-68 present for particles $\geq 2 \mu\text{m}$ (Figure 6.20). In both these cases, the variables: T_{m1} , T_{m2} and particle count rise and fall sympathetically and that the magnitude of the coefficient is very close to maximum of +1.00, which would denote a perfect relationship. The statistical value was determined as 0.026 between T_{m1} and particle count, which is below 0.05. This indicates that in this case the correlation between T_m and particle count is significant at 0.05 level ($P < 0.05$).

The statistical significance value obtained for the correlation between T_{m2} and particle count was 0.005, which indicated that the correlation between those two variables is significant at 0.01 level ($P < 0.01$). For all other surfactants at any particle count size, the correlation coefficient was not close to -1.00 or +1.00 indicating no correlation between T_{m1} , T_{m2} and particle count (Figures 6.19 and 6.20).

The results of statistical analyses using the Pearson correlation test for T_m measured by HSDSC and particle count per ml measured by MFI for particles of size $\geq 2 \mu\text{m}$, $\geq 10 \mu\text{m}$, $\geq 25 \mu\text{m}$, $\geq 50 \mu\text{m}$ and $\geq 100 \mu\text{m}$ for fresh, heated and aged BSA and IgG2 surfactant systems are presented in Figures 6.21-6.29.

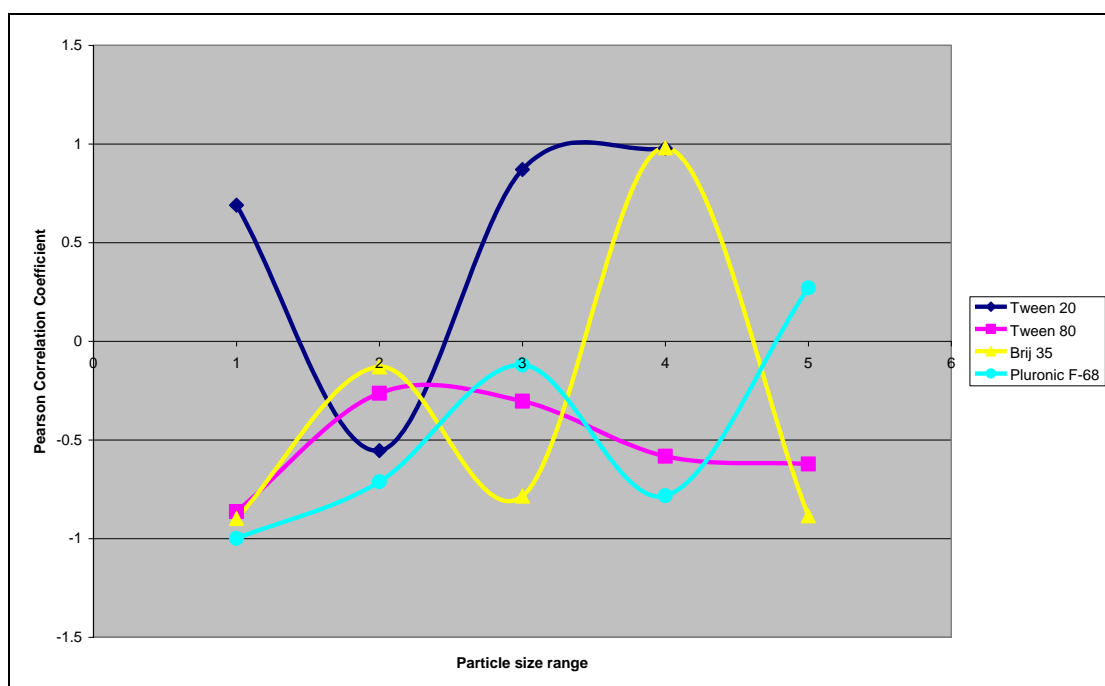


Figure 6.21. The Pearson Correlation Coefficient measured between T_m (HSDSC) and particle count (MFI) at (1) $\geq 2 \mu\text{m}$, (2) $\geq 10 \mu\text{m}$, (3) $\geq 25 \mu\text{m}$, (4) $\geq 50 \mu\text{m}$ and (5) $\geq 100 \mu\text{m}$ particle size ranges for fresh BSA with Tween 20, Tween 80, Brij 35 and Pluronic F-68 surfactant.

The Pearson Correlation Coefficient between T_m and particle count of particles size $\geq 10 \mu\text{m}$ was found to be -0.999 for fresh BSA with Pluronic F-68 present. The magnitude of the coefficient is close to its maximum -1.00, which denotes a perfect relationship between T_m and particle count measured by MFI, and the correlation is significant at the 0.05 level ($P < 0.05$). The significance value for all other surfactants and counts of different particle size ranges was greater than 0.05 ($P > 0.05$), and thus there was not significant (Figure 6.21).

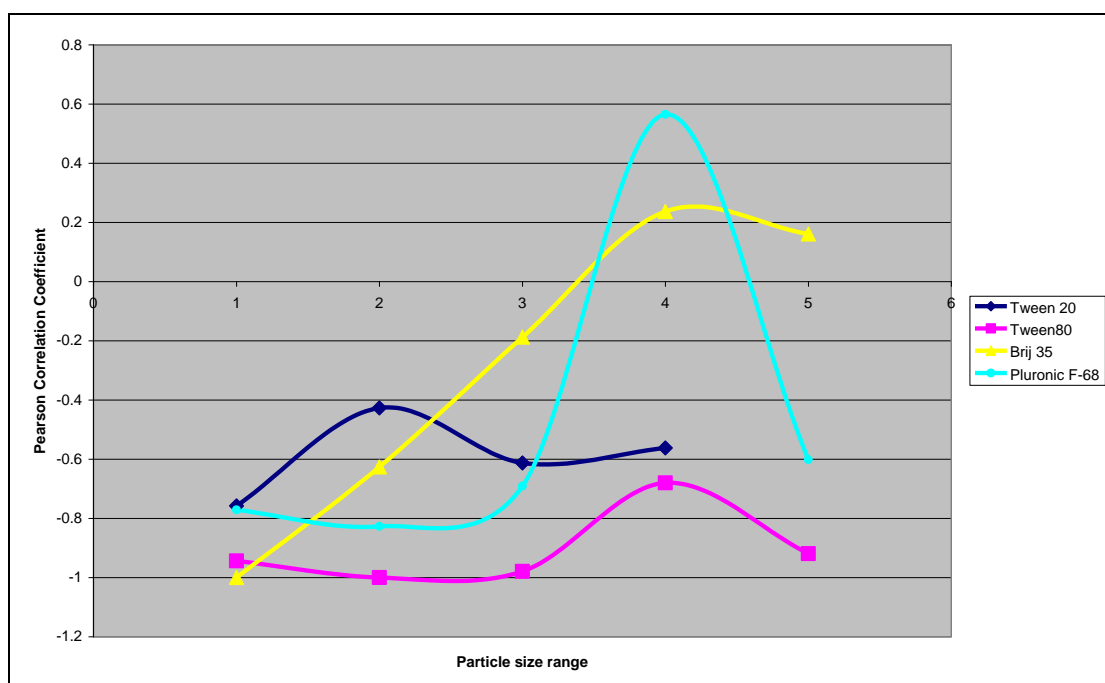


Figure 6.22. The Pearson Correlation Coefficient measured between T_m (HSDSC) and particle count (MFI) for heated BSA with Tween 20, Tween 80, Brij 35 and Pluronic F-68 surfactants at (1) $\geq 2 \mu\text{m}$, (2) $\geq 10 \mu\text{m}$, (3) $\geq 25 \mu\text{m}$, (4) $\geq 50 \mu\text{m}$ and (5) $\geq 100 \mu\text{m}$ particle size ranges.

For heated BSA with surfactant samples, the Pearson Correlation Coefficient is found to be -1.00 for heated BSA with Brij 35 at the $\geq 2 \mu\text{m}$ size range and -1.00 for heated BSA with Tween 80 at the $\geq 10 \mu\text{m}$ particle size range. The significance value for heated BSA with Brij 35 was below 0.01 level ($P < 0.01$)

and for heated BSA with Tween 80 was below 0.05 level ($P < 0.05$). T_m and particle count in these cases are indeed correlated. For the remainder of the heated samples no significant correlation was found (Figure 6.22).

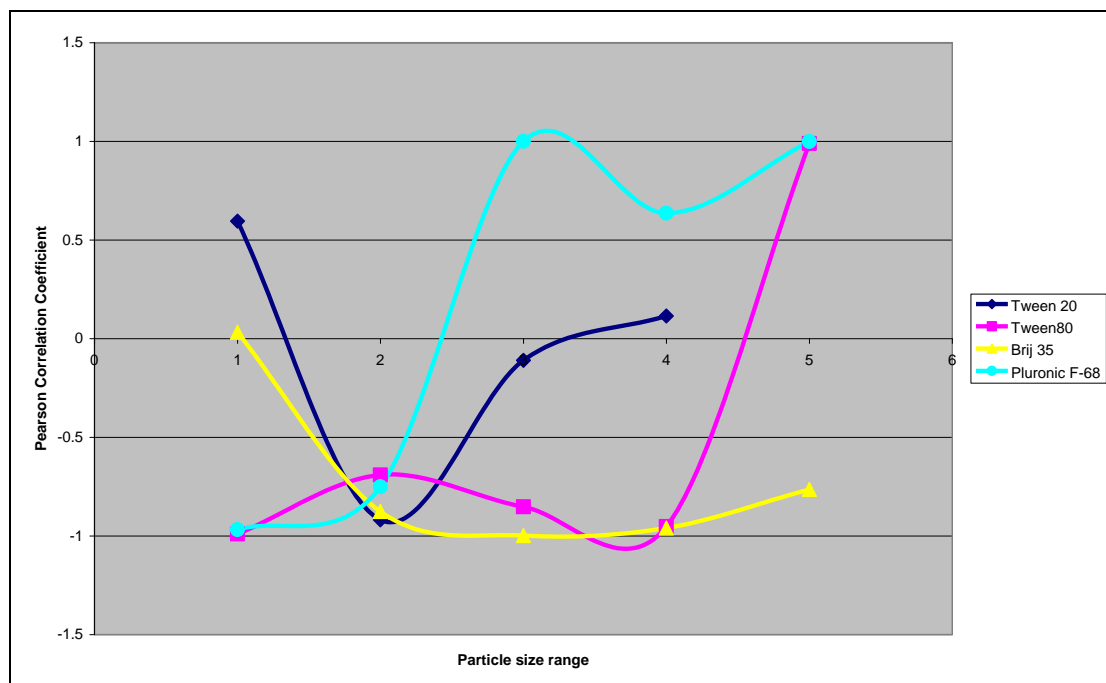


Figure 6.23. The Pearson Correlation Coefficient measured between T_m (HSDSC) and particle count (MFI) for aged BSA with Tween 20, Tween 80, Brij 35 and Pluronic F-68 surfactants at (1) $\geq 2 \mu\text{m}$, (2) $\geq 10 \mu\text{m}$, (3) $\geq 25 \mu\text{m}$, (4) $\geq 50 \mu\text{m}$ and (5) $\geq 100 \mu\text{m}$ particle size ranges.

For aged BSA with surfactant samples, the Pearson Correlation Coefficient is found to be -0.998 for aged BSA with Brij 35 and at +1.00 for aged BSA with Pluronic F-68 at the $\geq 25 \mu\text{m}$ particle size range, and at +0.999 for aged BSA with Pluronic F-68 at $\geq 100 \mu\text{m}$ particle size range (Figure 6.23).. The significance value was determined to be 0.036 for Brij 35 at $\geq 25 \mu\text{m}$ size range and 0.026 for Pluronic F-68 at $\geq 100 \mu\text{m}$ particle size range, which are below 0.05. This indicates that in these cases the correlation between T_m and particle count is significant at the 0.05 level ($P < 0.05$). The significance value quoted as 0.008 for aged BSA with Pluronic F-68 at $\geq 25 \mu\text{m}$, which indicated

that correlation is significant at the 0.01 level ($P < 0.01$). No other significant correlations were found for this system between T_m and particle count measured by MFI (Figure 6.23).

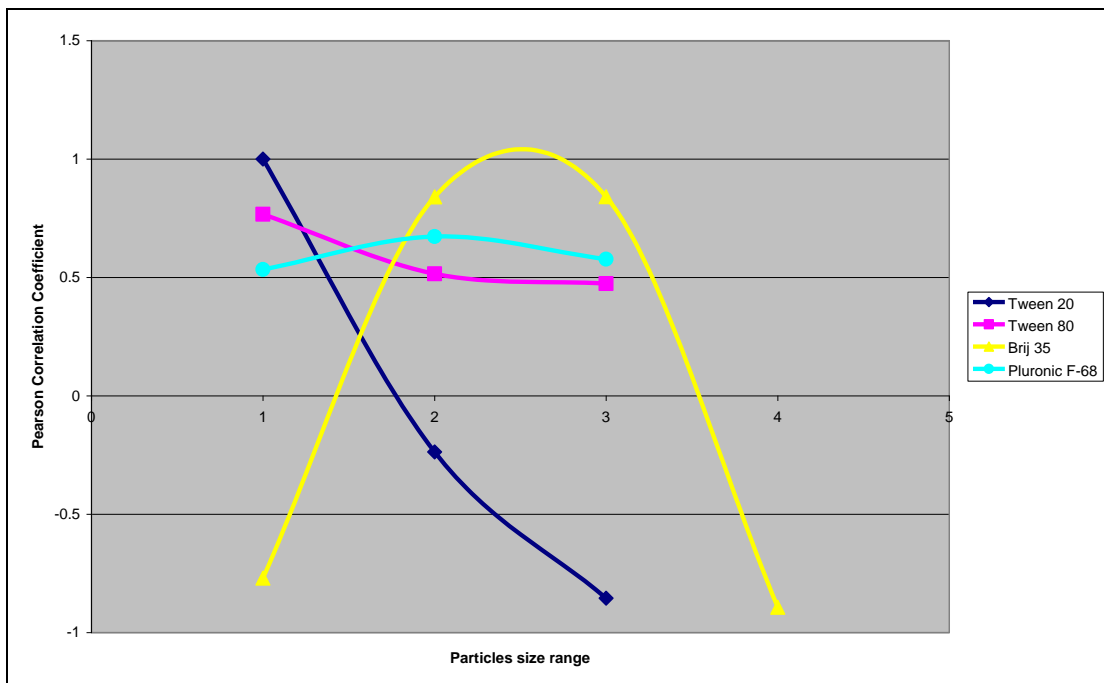


Figure 6.24. The Pearson Correlation Coefficient measured between T_{m1} (HSDSC) and particle count (MFI) for fresh IgG2 with Tween 20, Tween 80, Brij 35 and Pluronic F-68 surfactants at (1) $\geq 2 \mu\text{m}$, (2) $\geq 10 \mu\text{m}$, (3) $\geq 25 \mu\text{m}$, (4) $\geq 50 \mu\text{m}$ and (5) $\geq 100 \mu\text{m}$ particle size ranges.

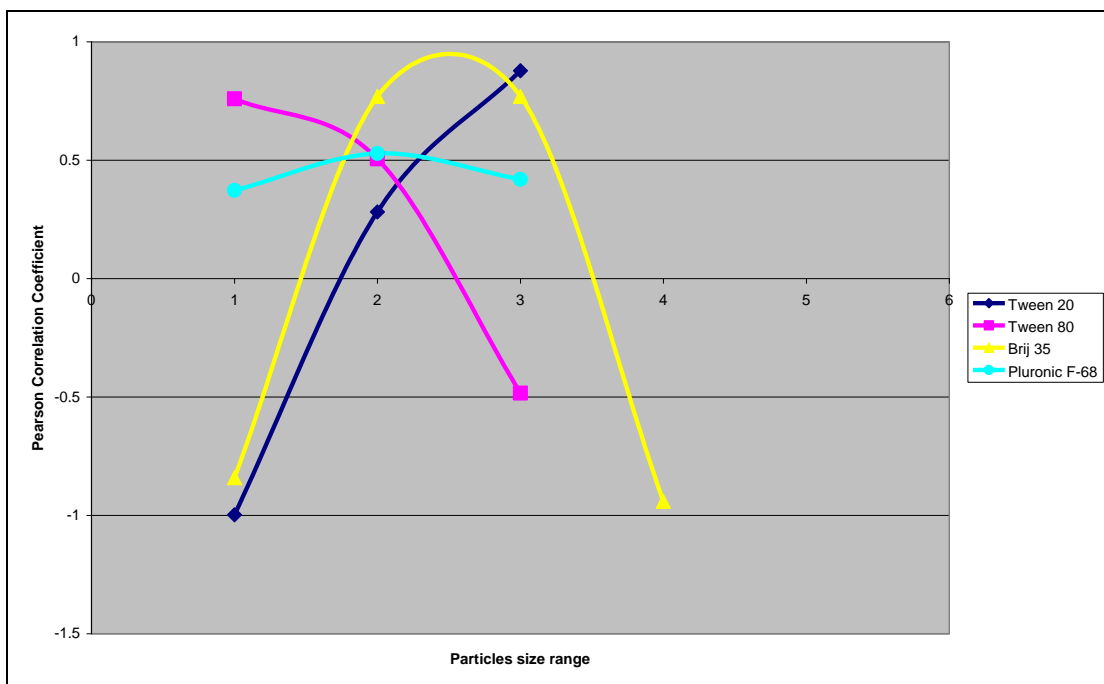


Figure 6.25. The Pearson Correlation Coefficient measured between T_{m2} (HSDSC) and particle count (MFI) for fresh IgG2 with Tween 20, Tween 80, Brij 35 and Pluronic F-68 surfactants at (1) $\geq 2 \mu\text{m}$, (2) $\geq 10 \mu\text{m}$, (3) $\geq 25 \mu\text{m}$, (4) $\geq 50 \mu\text{m}$ and (5) $\geq 100 \mu\text{m}$ particle size ranges.

The Pearson Correlation Coefficient between T_{m1} and particle count measured by MFI, at the various sizes was found to be +1.00 for fresh IgG2 with Tween 20 at the $\geq 2 \mu\text{m}$ size range (Figure 6.24). The magnitude of the coefficient is at its maximum +1.00, which denotes a perfect relationship between T_{m1} and particle count. The Correlation Coefficient between T_{m2} and particle count was found to be -0.998 for fresh IgG2 with Tween 20 at $\geq 2 \mu\text{m}$ size range (Figure 6.25). In this case both variables rise and fall sympathetically. The significance value determined for T_{m1} with particle count was 0.009. This indicates very strong evidence that these variables are indeed correlated at the level of the 0.01 ($P < 0.01$). The Pearson Correlation Coefficient for all other fresh IgG2 with different surfactants was less than -1.00 or +1.00 and the significance value was greater than 0.05 ($P > 0.05$), so

T_{m1} , T_{m2} measured by HSDSC and particle count measured by MFI in these cases were uncorrelated (Figures 6.24 and 6.25).

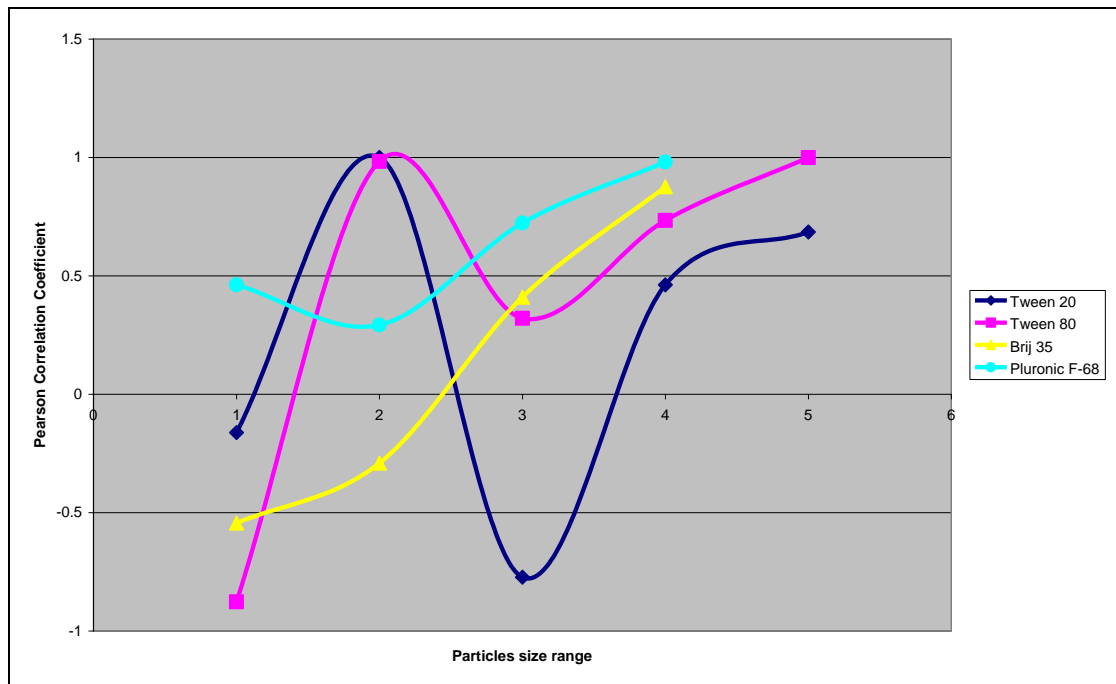


Figure 6.26. The Pearson Correlation Coefficient measured between T_{m1} (HSDSC) and particle count (MFI) for heated IgG2 with Tween 20, Tween 80, Brij 35 and Pluronic F-68 surfactants at (1) $\geq 2 \mu\text{m}$, (2) $\geq 10 \mu\text{m}$, (3) $\geq 25 \mu\text{m}$, (4) $\geq 50 \mu\text{m}$ and (5) $\geq 100 \mu\text{m}$ particle size ranges.

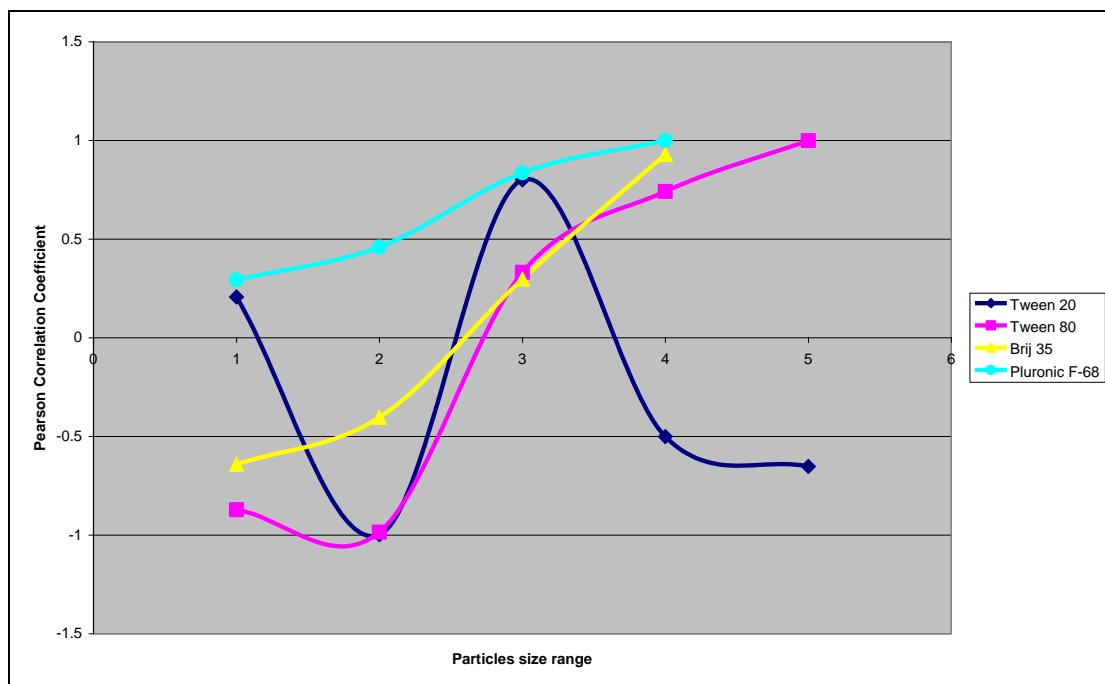


Figure 6.27. The Pearson Correlation Coefficient measured between T_{m2} (HSDSC) and particle count (MFI) for heated IgG2 with Tween 20, Tween 80, Brij 35 and Pluronic F-68 surfactants at (1) $\geq 2 \mu\text{m}$, (2) $\geq 10 \mu\text{m}$, (3) $\geq 25 \mu\text{m}$, (4) $\geq 50 \mu\text{m}$ and (5) $\geq 100 \mu\text{m}$ particle size ranges.

For heated IgG2 with surfactant samples, the Pearson Correlation Coefficient between T_{m1} and particle count per ml was found to be +1.00 for heated IgG2 with Tween 20 at $\geq 10 \mu\text{m}$ size range and +0.999 for IgG2 with Tween 80 and particle count data $\geq 100 \mu\text{m}$ (Figure 6.26). The significance values for these samples were below 0.05 ($P < 0.05$). The coefficient between T_{m2} and particle count was found to be -0.998 for Tween 20 at $\geq 10 \mu\text{m}$, +1.00 for Pluronic F-68 at $\geq 50 \mu\text{m}$ and +0.999 for Tween 80 at $\geq 100 \mu\text{m}$ particle size range (Figure 6.27). The findings indicate that T_{m1} and particle count and T_{m2} and particle count are indeed correlated. For the other heated samples no significant correlation was found between T_{m1} and particle count, or T_{m2} and particle count (Figures 6.26 and 6.27).

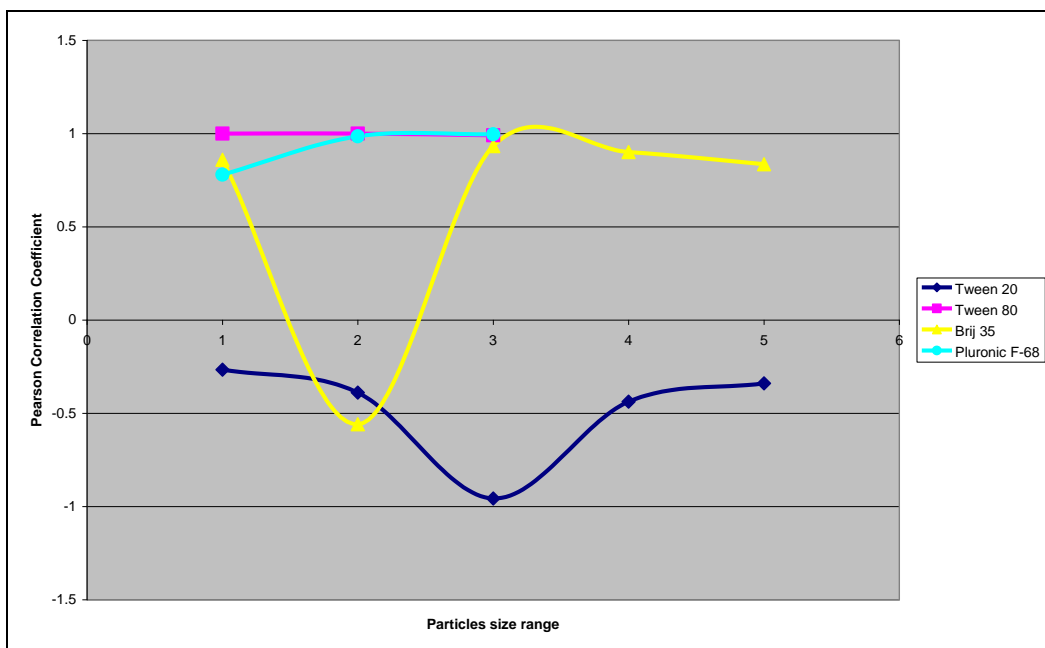


Figure 6.28. The Pearson Correlation Coefficient measured between T_{m1} (HSDSC) and particle count (MFI) for aged IgG2 with Tween 20, Tween 80, Brij 35 and Pluronic F-68 surfactants at (1) $\geq 2 \mu\text{m}$, (2) $\geq 10 \mu\text{m}$, (3) $\geq 25 \mu\text{m}$, (4) $\geq 50 \mu\text{m}$ and (5) $\geq 100 \mu\text{m}$ particle size ranges.

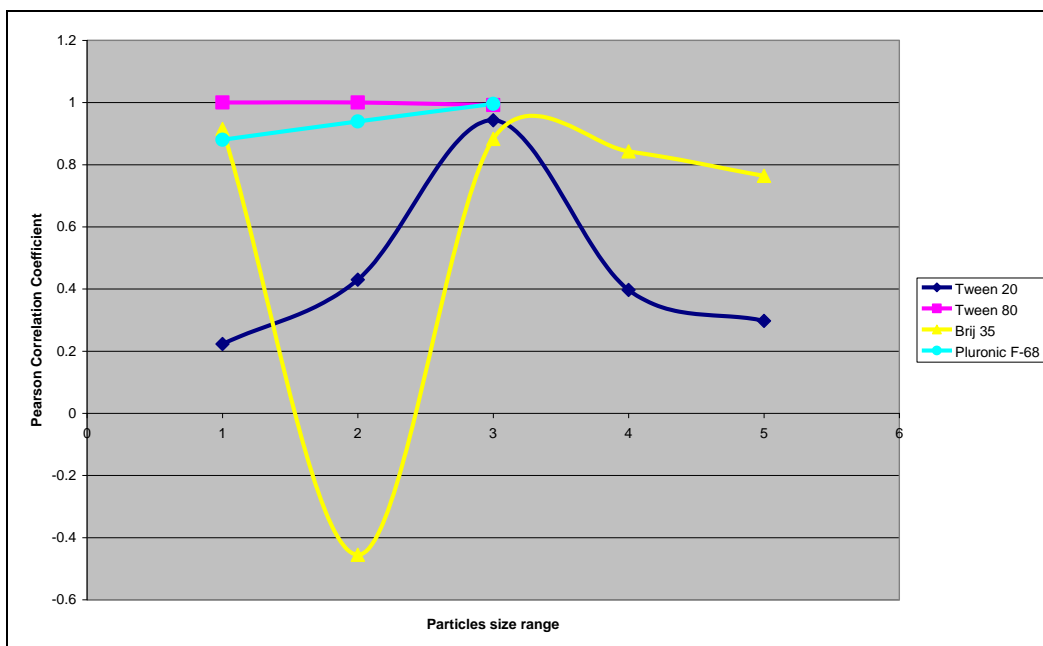


Figure 6.29. The Pearson Correlation Coefficient measured between T_{m2} (HSDSC) and particle count (MFI) for aged IgG2 with Tween 20, Tween 80, Brij 35 and Pluronic F-68 surfactants at (1) $\geq 2 \mu\text{m}$, (2) $\geq 10 \mu\text{m}$, (3) $\geq 25 \mu\text{m}$, (4) $\geq 50 \mu\text{m}$ and (5) $\geq 100 \mu\text{m}$ particle size ranges.

For aged IgG2 with surfactant samples, the Pearson Correlation Coefficient for T_{m1} and particle count and for T_{m2} and particle count is found to be +1.00 for aged IgG2 with Tween 80 particle count at $\geq 2 \mu\text{m}$ and at $\geq 10 \mu\text{m}$ (Figures 6.28 and 6.29). The significance values were below 0.01, which indicates that the correlation between T_m and particle count is significant at 0.01 level ($P < 0.01$).

The significance value between T_{m2} and particle count was 0.005, which indicated that correlation between those two variables is significant at 0.01 level ($P < 0.01$). For all other surfactants conditions the correlation coefficient was not close to -1.00 or +1.00, and so that indicated no significant correlation between T_{m1} , T_{m2} and particle count (Figures 6.28 and 6.29).

To investigate if formation of larger aggregates measured by HIAC and MFI comply with the results of smaller particles measurements by DLS, the Pearson Correlation statistical test was once again employed. Tables 6.2 – 6.5 present the results of Pearson Correlation Coefficient measured between main peak measured by DLS and different size range measured by HIAC and MFI for fresh, heated and aged BSA and IgG2 surfactant systems.

Table 6.2. Pearson Correlation Coefficient measured between main peak diameter (nm) (DLS) and particle count per ml (HIAC) for fresh, heated and aged BSA samples.

BSA samples	$\geq 2 \mu\text{m}$	$\geq 5 \mu\text{m}$	$\geq 10 \mu\text{m}$	$\geq 25 \mu\text{m}$	$\geq 50 \mu\text{m}$
Fresh	0.017	-0.149	-0.233	-0.245	0.263
Heated	0.022	0.202	-0.159	0.519	0.478
Aged	0.062	-0.178	0.502	0.519	0.336

Table 6.3. Pearson Correlation Coefficient measured between main peak diameter (nm) (DLS) and particle count per ml (MFI) for fresh, heated and aged BSA samples.

BSA samples	$\geq 2 \mu\text{m}$	$\geq 10 \mu\text{m}$	$\geq 25 \mu\text{m}$	$\geq 50 \mu\text{m}$
Fresh	-0.137	0.490	0.000	-0.270
Heated	-0.147	0.311	0.241	0.845
Aged	0.363	-0.016	-0.409	-0.269

Table 6.4. Pearson Correlation Coefficient measured between main peak diameter (nm) (DLS) and particle count per ml (HIAC) fresh, heated and aged IgG2 samples. (*) – Pearson Correlation is significant at 0.05 level (P<0.05).

IgG2 samples	≥ 2 μm	≥ 5 μm	≥ 10 μm	≥ 25 μm	≥ 50 μm
Fresh	-0.054	-0.328	-0.418	-0.266	-0.325
Heated	-0.171	-0.465	-0.157	-0.146	0.056
Aged	0.573*	0.146	-0.095	-0.011	0.377

Table 6.5. Pearson Correlation Coefficient measured between main peak diameter (nm) (DLS) and particle count per ml (MFI) for fresh, heated and aged IgG2 samples. (*) – Pearson Correlation is significant at 0.05 level (P<0.05).

IgG2 samples	≥ 2 μm	≥ 10 μm	≥ 25 μm	≥ 50 μm
Fresh	0.380	0.040	-0.109	-
Heated	0.052	-0.110	0.235	0.189
Aged	0.679*	0.531	0.085	-0.137

The Pearson Correlations Coefficient results presented in tables 6.2-6.5 indicated that formation of small aggregates measured by Dynamic Light Scattering does not correlate statistically with the results of sub-visible particle analysis. Only the relationship between main peak diameter (DLS) and particle count per ml (HIAC and MFI) particle count of size ≥ 2 μm for HIAC and MFI for aged IgG2 samples was significant at the 0.05 level (P<0.05) (Table 6.4 and 6.5; Figure 6.30 and 6.31).

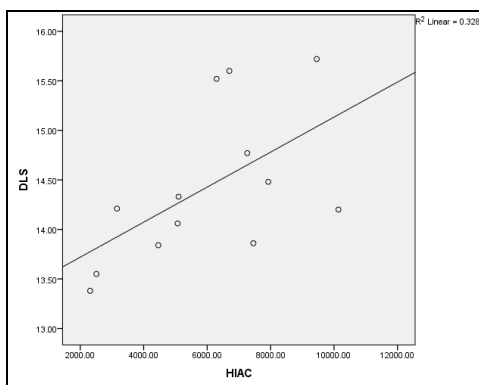


Figure 6.30. Scatter plot for aged IgG2 samples between main peak diameter (nm) (DLS) and particle count per ml (HIAC) at $\geq 2 \mu\text{m}$ size range using Pearson correlation test.

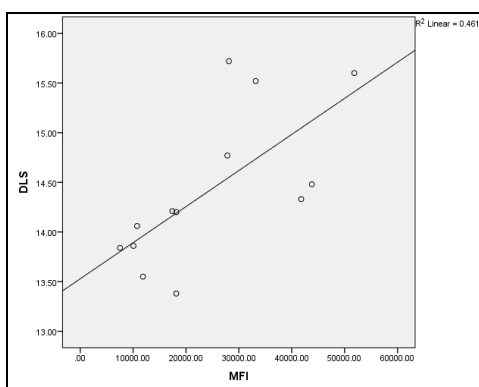


Figure 6.31. Scatter plot for aged IgG2 samples between main peak diameter (nm) (DLS) and particle count per ml (MFI) at $\geq 2 \mu\text{m}$ size range using Pearson correlation test.

Summing up, all the methods used in this thesis are suitable as screening methods for proteins formulation studies, because they are reproducible and require small volumes of protein material. However, as it was reported by Mahler et al. (2005), a single technique is not sufficient to describe the aggregation process completely, due to the different particle sizes of aggregated protein (Mahler et al., 2005). The exclusive use of Dynamic Light Scattering analysis may even result in invalid conclusions regarding protein size stability. In order to analyse the amount and size of induced aggregation products, a combination of different, but complementary analytical techniques

such as HSDSC, DLS, HIAC and MFI measurements can be used in order to assess the extent of aggregation and different size of protein aggregates. However, further evaluations of other methods should be taken into consideration.

Chapter 7

General Conclusions and Recommendations for Future Research

7.1 General Conclusions

A constant challenge in the development of biopharmaceutical products is the phenomenon generally known as protein aggregation. In order to control protein aggregation, it is important to understand the cause of aggregate formation, and to apply appropriate analytical methods. Due to the variety of aggregated species, a major challenge for the analysis of protein particles is that no single analytical method exists to cover the entire size range and type in which particles may appear (Mahler et al., 2009).

Therefore, the overall aim of this project was to identify improved methods of particle characterisation and enhance understanding the mechanisms of their formation in biopharmaceutical formulations.

Bovine serum albumin BSA and immunoglobulin IgG2 were studied in order to assess the effect of Tween 20, Tween 80, Brij 35 and Pluronic F-68 below, around and above CMC levels on protein conformational stability and size stability.

In Chapter 3 thermal unfolding experiments employing HSDSC method showed that for surfactant free BSA single unfolding peak at T_m of $66.91 \pm 0.085^\circ\text{C}$ was observed, which was similar to the published value of 67°C (Nishimura et al., 2001). Also the presence of all four surfactants induced the T_m shifts to lower unfolding temperatures for BSA protein. Considering the effect of all four surfactants, Brij 35 at around CMC produced slightly stronger interactions with BSA.

For surfactant free IgG2 – two unfolding peaks at $T_{m1}=69.38 \pm 0.057^\circ\text{C}$ and $T_{m2}=77.53 \pm 0.113^\circ\text{C}$ were determined. Similar unfolding temperature values

for IgG2 were previously reported by Tischenko et al., (1998), Kravchuk et al., (1998), Tischenko et al., (2003).

To the best of the authors' knowledge, our study is the most extensive study of the effect of a range of surfactants and range of concentrations on protein T_m . The results showed that the presence of any surfactant at different concentrations with immunoglobulin IgG2 was negligible. No notable changes of the T_{m1} and T_{m2} were observed.

Thermal unfolding experiments indicated a very weak surfactant-immunoglobulin IgG2 interaction, compared to much stronger interactions for the bovine serum albumin-surfactant systems. These results are consistent with published results by Garidel et al., (2009), who found out that the binding of some of the surfactants we employed on IgG2 are negligible. Also weak binding of some surfactants has been confirmed by fluorescence spectroscopic measurements done by Hoffman, 2007 (Hoffman, 2007).

Refolding experiments revealed that the transitions for BSA and IgG2 with all the surfactants were irreversible and no thermal transitions were noted on subsequent scans of the same samples after cooling. A different experimental design may have produced different results.

In Chapter 4 the role of surfactant type and concentration on BSA and IgG2 size stability as assessed by Dynamic Light Scattering was investigated. The DLS measurements revealed that BSA with IgG2 with the surfactants at below, around and above CMC concentrations produced different levels of particle size growth. The reported size of native BSA is 7.83 nm (Yu et al, 2011), which is similar to the 7.69 nm obtained for freshly prepared BSA for this study. BSA with added Tween 20, Tween 80 and Brij 35 surfactants at all

concentrations and Pluronic F-68 at below and above its CMC, yielded trimodal distributions with the main peak consistently around 8 nm diameter.

DLS results for fresh samples of IgG2 surfactant free produced a bimodal distribution with a main peak at 14.44 nm diameter, which is significantly higher than the 10 nm reported for native IgG (Song et al., 2001, Bermudez et al., 2004). However the IgG2 is not the same variant. DLS measurements for the IgG2 in the presence of all four nonionic surfactants produced a low increase in particle size.

To establish the heat treatment stability of the samples, BSA alone and BSA – surfactant systems were heated at 66°C and IgG2 alone, IgG2 – surfactant systems were heated at 60°C (Chapter 2, Section 2.2.1) to promote changes within the samples. It has been previously reported that heat treatment of BSA and IgG induces strong aggregation which results in precipitation of the proteins (Padlan, 1997, Vermeer and Norde, 2000). However, in the presence of Tween 20 above CMC and Brij 35 above CMC significant decreases in particle size diameter for BSA – surfactant systems were observed. For IgG2-surfactant systems, Pluronic F-68 at concentrations below and around its CMC, yielded decreases in diameter compared to IgG2 alone and other surfactant systems.

To establish the storage stability of the samples, both fresh samples of BSA and IgG2 alone and proteins with Tween 20, Tween 80, Brij 35 and Pluronic F-68 surfactants were stored refrigerated at 4°C for 8 weeks (Chapter 2, Section 2.2.2) to promote changes within the samples. DLS data for all BSA – surfactant systems displayed particle growth. The greatest increase in particle size diameter was observed for BSA samples with Tween 80 at

around its CMC, Brij 35 at below CMC and Pluronic F-68 at below and around its CMC. For IgG2 – surfactant systems an opposing effect was observed in that only IgG2 systems with Tween 80 present below its CMC and Pluronic F-68 at around its CMC showed an increase in particle size.

Compared to BSA, IgG2 did not aggregate as readily under storage conditions. Storage and heat stress bears the potential to generate aggregates and particles, but this depends on protein and surfactant type and concentration (Schmidt, 2009).

The use of DLS often has to be combined with other analytical techniques with higher sensitivity for measuring larger particles.

In Chapter 5 the role of surfactant type and level on BSA and IgG2 protein size stability as assessed by HIAC and MFI was investigated. As was the case for the DLS measurements, for sub-visible particle measurements by HIAC and MFI the effect of heat treatment and storage stress were assessed. Heat treatment and storage stress showed a significant effect on BSA and IgG2 protein particle size stability. BSA surfactant free samples on storage treatment showed statistically different numbers and sizes of particles than those obtained after heat stress when compared to freshly prepared BSA. Also both heat stress and storage treatments induced an increase in particle count per ml for IgG2 surfactant free samples at particle size ranges from $\geq 2 \mu\text{m}$ to $\geq 10 \mu\text{m}$. For particle count data of size $\geq 25 \mu\text{m}$ measured by both HIAC and MFI methods, heat treatment produced higher, more statistically significant increases in particle count, whereas storage showed no statistical difference at this size range for IgG2 surfactant free samples.

Considering the effect of different surfactant type and concentration on BSA protein particle size stability as explored by HIAC and MFI experiments, all four surfactants at above their CMC produced a decrease in particle count of particles $\geq 2 \mu\text{m}$. On heating and storage, Tween 80 at above its CMC, Brij 35 at above its CMC and Pluronic F-68 at around and above its CMC showed the highest decrease in particle count of size $\geq 2 \mu\text{m}$ compared to BSA surfactant free samples.

For particle count data of size $\geq 5 \mu\text{m}$ and $\geq 10 \mu\text{m}$, the addition of the surfactant Brij 35 at around and above its CMC produced the lowest particle count level compared to the other surfactants and BSA surfactant free formulations. Very similar results were obtained for size ranges $\geq 25 \mu\text{m}$, $\geq 50 \mu\text{m}$ and $\geq 100 \mu\text{m}$. The use of surfactant Brij 35 at around and above its CMC is the most effective in bringing about a particle count decrease.

According to results obtained from HIAC and MFI analysis for IgG2 samples, considering the $\geq 2 \mu\text{m}$ size range, the most effective surfactant was Brij 35 above its CMC. This surfactant showed the highest decrease in particle count per ml after both heat and storage stress when compared to the other surfactants and IgG2 surfactant free samples.

For particle count data of size $\geq 10 \mu\text{m}$, Tween 20, Tween 80, Brij 35 and Pluronic F-68 at high CMC concentration effectively reduced the particle count per ml. For particle count data of size $\geq 25 \mu\text{m}$, $\geq 50 \mu\text{m}$ and $\geq 100 \mu\text{m}$ the surfactant Brij 35 used above its CMC level showed the highest decrease in particle count after heating and storage.

The difference in sub-visible particle counts between the different type of surfactants and their CMC levels may suggest that either the concentration of

surfactants in the formulation was not capable in stabilizing the protein against the induction of aggregates via heat treatment and storage stress, or that aggregation caused by these stresses can not be completely prevented by Tween 20, Tween 80, Brij 35 and Pluronic F-68 surfactants (Mahler et al., 2005).

Also it was shown in previous studies that sub-visible particle count measured by HIAC and MFI increases in the presence of different types of stresses (Sluzky et al., 1991; Mahler et al., 2005; Sharma et al., 2010; Demeule et al., 2010). It is difficult to compare data in this thesis to the data published in these papers because the authors in the above publications have used different proteins and different surfactants to our study. However the work in this thesis adds to the body of work that surfactant protein effects on particle formation are difficult to predict. Additionally, different stresses were used in the above publications, including shear stress, horizontal shaking and stirring and thus the nature of particle formation will be affected by the type of stress as shown in this thesis too. Data from HIAC and MFI instruments were expected to be consistent in particle count measurements for each of the BSA and IgG2 surfactant formulations. However Light Obscuration (HIAC) reported lower particle count than Micro-flow Imaging (MFI), especially for the particle count at $\geq 2 \mu\text{m}$ size range. The lower particle count per ml measured by HIAC than MFI has been previously reported in recent publications (Demeule et al., 2010; Huan et al., 2009; Sharma et al., 2010). In Chapter 6 statistical analysis using Pearson Correlation test showed no strong relationship between HIAC and MFI methods ($P > 0.05$) confirming the above. However, there was a strong

relationship at the 0.01 level ($P < 0.01$) between the data obtained for the HIAC and MFI methods from the fresh and heated BSA-surfactant formulations for particles $\geq 2 \mu\text{m}$. Pearson correlation analysis also showed that there was a significant relationship at the 0.05 level ($P < 0.05$) between the particle count data for particles $\geq 50 \mu\text{m}$ obtained by the two methods for aged BSA – surfactant systems

In recent studies, Huang et al., 2009 and Sharma et al., 2010, compared the sizing and counting accuracy of HIAC and MFI and found that while the two methods gave similar results, MFI detected significantly more particles than HIAC. These authors considered that such difference in Light Obscuration and Micro-flow Imaging measurements might be due to the under-estimation of sub-visible particles by the light obscuration technique (Huang et al., 2009; Sharma et al., 2010). The results in this thesis would support their findings.

The different analytical methods applied in this thesis provide different aspects and insight into BSA and IgG2 conformational stability and protein size stability. The T_m value measured by High Sensitivity Differential Scanning calorimetry HSDSC was used as a stability indicator for proteins. DLS analysis was used for detection of small sized aggregates in the range of 1 – 450 nm size. The Light Obscuration (HIAC) and Micro-flow Imaging (MFI) techniques were used in this study to detect large aggregates of 2 – 100 μm .

One aim of the thesis was to explore the relationship between the different analytical approaches. For example, is the surfactant effect on thermal unfolding predictive of sub-micron particle formation detected by DLS or sub-visible particle formation as determined by HIAC and MFI methods? Or

indeed is DLS data predictive of larger particle formation (HIAC and MFI) on stressing formulations? It was hoped that where such correlations exist mechanistic insight into aggregation would be forthcoming. In Chapter 6 statistical analysis via measurement of the Pearson correlation coefficient was applied in correlating the results from each method to obtain the relationship between HSDSC, DLS, HIAC and MFI measurements. Statistical analysis results revealed that T_m measured by HSDSC can not predict the smaller particle size formation as measured by DLS since there was no statistically significant correlation.

Statistical analysis of the relationship between HSDSC and HIAC measurements in a few cases showed a reliable correlation. HSDSC measurements were correlated at the 0.05 significance level ($P < 0.05$) with HIAC measurements of particle count for particles of size $\geq 25 \mu\text{m}$ for heated BSA samples with Brij 35 and particle count for particles of size $\geq 100 \mu\text{m}$ for BSA samples with Pluronic F-68 and particle count for particles of size $\geq 50 \mu\text{m}$ for aged BSA samples with Pluronic F-68.

Pearson correlation test results indicated that there was a relationship significant at the 0.01 level ($P < 0.01$) between unfolding temperatures and particle count measured by HIAC for fresh IgG2 with Tween 80 for particles sized $\geq 2 \mu\text{m}$. Likewise, a significant relationship at the 0.05 level ($P < 0.05$) was found for heated IgG2 with Brij 35 present for particles $\geq 10 \mu\text{m}$ and also with Tween 80 present for particles $\geq 100 \mu\text{m}$. For aged IgG2 surfactant systems, unfolding temperature and particle count per ml as measured by HIAC was correlated at the 95% level: between T_{m1} and particle count per ml

for particles sized $\geq 100 \mu\text{m}$, and similarly for IgG2 with Pluronic F-68 present between T_{m2} and particle count for particles sized $\geq 2 \mu\text{m}$.

Also statistical analysis showed an excellent linear relationship between HSDSC data and MFI count measurements for particles sized $\geq 10 \mu\text{m}$ for fresh BSA with Pluronic F-68 present. A similar correlation was found between T_m and particle count data of particles $\geq 2 \mu\text{m}$ for heated BSA with Brij 35 present and for particle count data of particles $\geq 10 \mu\text{m}$ for heated BSA with Tween 80. The Pearson correlation test showed excellent relationships between HSDSC data and MFI count measurements for particles sized $\geq 25 \mu\text{m}$ size range for aged BSA with Brij 35 or Pluronic F-68 present. A similar correlation was found between T_m and particle count data of particles sized $\geq 100 \mu\text{m}$ for aged BSA with Pluronic F-68.

The relationship between HSDSC and MFI measurements was significant at 0.01 level ($P < 0.01$) for fresh IgG2 samples with Tween 20 present and particle count data for particle size $\geq 2 \mu\text{m}$ and for aged IgG2 with Tween 80 present and particle count data for particle size $\geq 2 \mu\text{m}$ and $\geq 10 \mu\text{m}$.

The same relationship was significant at 0.05 level ($P < 0.05$) for heated IgG2 with Tween 20 present for size data $\geq 10 \mu\text{m}$ and Tween 80 size data $\geq 100 \mu\text{m}$.

Pearson correlation coefficient results calculated for relationship between DLS and HIAC and MFI, indicated that the size of small aggregates measured by DLS is not generally predictive of the initial results obtained from sub-visible particle analysis (HIAC and MFI) or on stressing. Only the relationship between main peak diameter (DLS) and particle count per ml

(HIAC and MFI) particle count of size $\geq 2 \mu\text{m}$ for HIAC and MFI for aged IgG2 samples was significant at the 0.05 level ($P < 0.05$).

In summary, this project was able to analyse the role of different surfactant type and level on protein conformational stability as assessed by HSDSC and on protein size stability as assessed by DLS, HIAC and MFI under heat treatment and storage conditions. To the best of the authors' knowledge this is the first such systematic study. It can be concluded that each protein will interact differently with each surfactant and that the type and concentration of surfactant is important for the level of particle formation and effect on conformational stability. Whilst sporadic correlations existed no global relationships could be determined between T_m and size data and between DLS data and sub-visible count data. As such from the data presented in this thesis no clear mechanistic insights are readily apparent as to the links between small aggregates and sub-visible particles and between conformational thermal stability and sub-visible particulate formation. This first systematic comparison of four structurally different surfactants on particle formation for BSA and IgG2 may lead to other systems being explored with the result that such mechanistic insights may be determined.

7.2 Recommendations for future research

As a result of conducting the experiment in this project, possibilities and ideas for further research arose:

The HSDSC unfolding temperature measurements carried out in chapter 3 could be improved by extending the range of nonionic surfactants employed. Chapters 3, 4 and 5 clearly indicated that BSA and IgG2 interact differently towards the surfactants. It would therefore be desirable to extend the range of proteins and monoclonal antibodies studied. It would also be useful to include ionic surfactants as an alternative to the non-ionic excipients used in this work.

The stress conditions in chapters 4 and 5 made it possible to determine the effects of heat treatment and storage on the stability of the protein-surfactant systems. It would seem important to repeat the experiments under different stress conditions such as shaking, stirring, thermal, UV and fluorescence light. It might be useful to characterize extensively particulates before, during and after the addition of the surfactants. The range and length of storage conditions could be extended.

In chapter 5 HIAC and MFI techniques gave different results of particle growth for BSA and IgG2 surfactant systems. This difference is worthy of further investigation.

All methods used in this project have their own advantages and disadvantages, there is no “gold standard method” for the analysis of proteins aggregates due to the complexity of the subject. Therefore it would be very useful to employ Nanoparticle Tracking Analysis (NTA) technique to compare

it with Dynamic Light Scattering (DLS). Also more techniques of measuring sub-visible particles in solutions, such additional techniques of measuring aggregates in solutions, such as Size Exclusion Chromatography (SEC) and Taylor Dispersion Analysis may be useful.

Experiments could also explore the formation of visible particles and appropriate methods such as filtration and staining techniques for visible particle characterization. The links between sub-visible and visible particle formation could be explored.

References

Adel, A., Nadia, M., Mohamed, O., Abdelhafid H. (2008) Study of thermally and chemically unfolded conformations of bovine serum albumin by means of dynamic light scattering. *Mat. Sci. Eng. C* 28, 594-600.

Ahrer, K., Buchacher, A., Iberer, G., Jungbauer, A. (2006) Thermodynamic stability and formation of aggregates of human immunoglobulin G characterised by differential scanning calorimetry and dynamic light scattering. *J. Biochem. Bioph. Methods* 66, 73-86.

Alliance Protein Laboratories Inc. (2014) *Sedimentation velocity*. Alliance Protein Laboratories Inc. Available from:

http://www.ap-lab.com/sedimentation_velocity.htm (Accessed 23 October 2014).

Analytical Ventura. (2013) *Chromatography. SE-HPLC*. Analytical Ventura. Available from :

<http://analyticalventura.com/services/chromatography/se-hplc/> (Accessed 15 June 2013).

Anatrace Inc. (2008). Detergents and their uses in Membrane Protein Science. Anatrace Inc. Available from:

http://wolfson.huji.ac.il/purification/PDF/detergents/ANATRACE_DetergentsUse.pdf (Accessed 10 June 2013).

Andya, J. D., Hsu, C. C., Shire S. J. (2003) Mechanisms of aggregate formation and carbohydrate excipient stabilisation of lyophilized humanized monoclonal antibody formulations. *AAPS Pharm. Sci.* 5:E10. PubMed DOI: 10, 1208.

Arakawa, T., Philo, J. S., Ejima, D., Tsumoto, K., Arisaka, F. (2007) Aggregation analysis of therapeutic proteins, part 2. *Analytical*

ultracentrifugation and Dynamic Light Scattering. *Bioprocess Technol.*, 38-47.

Barber, T. A. (2000) Control of particulate matter contamination in healthcare manufacturing. Denver, CO: Interpharm. Press., USA.

Barth, H.C. (2004) High performance SEC column technology. *LC GC LC Column Technol. Suppl.*, 38-43.

Beck, A. (2008) Trends in glycosylation, glycoanalysis and glycoengineering of therapeutic antibodies and Fc-fusion proteins. *Curr. Pharm. Biotechnol.* 9, 482-501.

Beck, A., Reichert, J. M., Wurch, T. (2010) 5th European Antibody Congress 2009: November 30 – December 2, MAbs 2, 108-128.

Beck, A., Wurch, T., Corvala, N. (2008) Editorial: therapeutic antibodies and derivatives: from the bench to the clinic. *Curr. Pharm. Biotechnol.* 9, 421-422.

Beckman Coulter. (2008) *Particle technologies. Laser diffraction*. Beckman Coulter Available from:

<https://www.beckmancoulter.com/wsrportal/wsr/industrial/particle-technologies/laser-diffraction/index.htm> (Accessed 15 June 2013).

Behan, N. (1999) Nanomedicine and drug delivery at the University of Limerick. Department of Materials Science and Technology.

Berkowitz, S.A. (2006) Role of analytical ultracentrifugation in assessing the aggregation of protein pharmaceuticals. *AAPS J.* 8, 590-605.

Bermudez, O., Forciniti, D. (2004) Aggregation and denaturation of antibodies: a capillary electrophoresis, dynamic light scattering and aqueous two-phase partitioning study. Chemical Engineering department. *J. Chromatogr. B.* 807, 17-24.

Branchu, S., Forbes, R. T., York, P., Nyqvist, H. (1999) A central composite design to investigate the thermal stability of lysozyme. *Pharm. Res.* 16, 702-708.

Brightwell Technologies Inc. (2006) *Application of Micro-Flow Imaging to the analysis of particles in parenteral fluids*. Brightwell Technologies Inc. Available from: <http://www.brightwelltech.com/Campaigns/Parenterals.html> (Accessed 14 March 2013).

Carpenter, J., Randolph, T. W., Jiskoot, W., Crommelin, D., Middlaugh, C., Winter, G. et al. (2008) Overlooking sub-visible particles in therapeutic protein products: gaps that may compromise product quality. *J. Pharm. Sci.* 98 (4), 1201-1205.

Chen, S. H., Teixeira, J. (1986) Structure and fractal dimension of protein-detergent complexes. *Phys. Rev. Lett.* 57, 2583-2586.

Chen, X., Liu, Y. D., Flynn, G. C. (2009) The effect of Fc glycan forms on human IgG2 antibody clearance in humans. *Glycobiology* 19, 240-249.

Chi, E. Y., Krishnan, S., Randolph, T. W., Carpenter, J. F. (2003) Physical stability of proteins in aqueous solution: mechanism and driving forces in non-native proteins aggregation. *Pharm. Res.* 20, 1325-1336.

Chodankar, S., Aswal, V. K., Hassan, P. A., Wagh, A. G. (2007) Structure of protein-surfactant complexes as studied by small-angle neutron scattering and dynamic light scattering. *Physica B* 398, 112-117.

Cromwell, M. E., Hilario, E., Jacobson, F. (2006) Protein aggregation and bioprocessing. *AAPS J.* 8 (3), E572-579.

Cueto, M., Dorta, M. J, Munguia, O., Llabres, M. (2003) New approaches to stability assessment of protein solution formulations by differential scanning calorimetry. *Int. J. Pharm.* 252, 159-166.

Das, A., Chitra, R., Choudhury, R. R, Ramanadham, M. (2004) Structural changes during the unfolding of bovine serum albumin in the presence of urea: a small angle neutron scattering study. *J. Phys.* 63 (2), 363-368.

Das, T., Nema, S. (2007) Protein particulate issues in biologics development. Particle sizing. Pfizer Global Biologics Presentation. *American Pharmaceutical Review*, 52-57.

Davies, D. R., Chacko, S. (1993) Antibody structure. *Acc. Chem. Res.* 26, 421-427.

Demeule, B., Lawrence, M. J., Drake, A. F., Gurny, R., Arvinte, T. (2007) Characterization of protein aggregation: the case of a therapeutic immunoglobulin. *Biochem. Biophys. Acta Proteins Proteomics* 1774, 146-153.

Demeule, B., Messick, S., Shire, S. J., Liu, J. (2010) Characterization of particles in protein solutions: reaching the limits of current technologies. *AAPS* 12 (4), 708-715.

Edge BioSystems Inc. Performa 96 well short plates. Available from: <https://www.edgebio.com/products/performa%C2%AE-dtr-v3-96-well-short-plates-no-receiver-plates-80808> (Accessed 13 March 2013).

European Pharmacopoeia 5.0 (2005) Particulate contamination : visible particles. 01/2005, 20920, 255.

Flaugh, S. L., Kosinski-Collins, M. S., King, J. (2005a) Interdomain side chain interactions in human γ D crystallin influencing folding and stability. *Protein Sci.* 14, 2030-2043.

Flaugh, S. L., Kosinski-Collins, M. S., King, J. (2005b) Contributions of hydrophobic domain interface interactions to the folding and stability of human γ D-crystallin. *Protein Sci.* 14, 569-581.

Fraunhofer, W. and Winter, G. (2004) The use of asymmetrical flow field-flow fractionation in pharmaceuticals and biopharmaceuticals. *Eur. J. Phar. Biopharm.* 58, 369-383.

Gabrielson, J. P., Arthur, K.K., Stoner, M. R, Winn, B. C., Kendrick, B. S., Razinkov, V., Svitel, J., Jiang, Y., Voelker, P., Fernandes, C. A., Ridgeway, R. (2009) Analytical Sciences, Amgen Inc. 19782040.

Gabrielson, J.P., Brader, M.L., Pekar, A.H., Mathis, K.B., Winter, G., Carpenter, J.F. and Randolph, T.W. (2007) Quantitation of aggregate levels in a recombinant humanized monoclonal antibody formulation by size exclusion chromatography, asymmetrical flow field fractionation, and sedimentation velocity. *J. Pharm. Sci.* 96, 268-279.

Garg, R. (2012) *Supramolecular Chemistry of host-guest inclusion complexes*. GRIN Publishing GmbH. Available from:
<http://www.grin.com/en/e-book/187894/supramolecular-chemistry-of-host-guest-inclusion-complexes> (Accessed 22 June 2013).

Garidel, P., Hegyu, M., Bassarab, M., Weichel, M. (2008) A rapid, sensitive and economical assessment of monoclonal antibody conformational stability by intrinsic tryptophan fluorescence spectroscopy. *Biotechnol. J.* 3, 1201-1211.

Garidel, P., Hoffmann, C., Blume, A. (2009) A thermodynamic analysis of the binding interaction between polysorbate 20 and 80 with human serum albumins and immunoglobulins: a contribution to understand colloidal protein stabilisation. *Biophys. Chem.* 143, 70-78.

Georgalis, Y., Zouni, A., Eberstein, W., Saenger, W. (1993) Formation dynamics of protein precrystallization fractal clusters. *J. Crystal. Growth* 126, 245-260.

Giancola, C., De Sena, C., Fessas, D., Granziano, G., Barone, G. (1997) DSC studies on bovine serum albumin denaturation. Effects of ionic strength and SDS concentration. *Int. Biol. Macromol.* 20, 193-204.

Giddings, J. C., Yang, F. J., Myers, M. N. (1976) Flow-field-flow fractionation: new separation method. *Science* 193.4259, 1244-1245.

Giddings, J.C. (1993) Field-flow fractionation: Analysis of macromolecular, colloidal, and particulate materials. *Science* 260, 1456-1465.

Hermeling, S., Crommelin, D. J., Schellekens, H., Jiskoot, W. (2004) Structure-immunogenicity relationships of therapeutic proteins. *Pharm. Res.* 21(6), 897-903.

Huang, C. T., Sharma, D., Oma, P., Krishnamurthy, R. (2009) Quantitation of protein particles in parenteral solutions using micro-flow imaging. *J. Pharm. Sci.* 98(9), 3058-3071.

Ionescu, R. M., Vlasak, J., Price, M., Kirchmeier, M. (2007) Contribution of variable domains to the stability of humanised IgG monoclonal antibodies. *J. Pharm. Sci.* 97, 1414-1426.

ISO 13322-2 (2006) Particle size analysis. Dynamic image analysis methods.

Ives, C. Soderquist, R., Stoner, M., Kendrick, B. (2007) Light obscuration particulate analysis for protein solutions: challenges and limitations. Protein stability conference.

Izutsu, K. I., Yoshioka, S., Takeda, Y. (1990) Protein denaturation in dosage forms measured by differential scanning calorimetry. *Chem. Pharm. Bull.*, 28, 800-803.

Jiang, Y. (2009) Analysis of aggregates and sub-visible particles in protein solutions. *PubMed* 10(4), 373-381.

Jones, M. N. (1992) Surfactant interactions with biomembranes and proteins. *Chem. Soc. Rev.* 21, 127.

Jones, M. N., Brass A. (1991). *Food Polymers, Gels and Colloids*, Royal Society of Chemistry, Cambridge, 65.

Kaszuba, M., McKnight, D., Connah, M.T., Mc Neil-Watson, F.K., Nobbomann, A.U. (2007) Measuring sub nanometre sizes using dynamic light scattering. *J. Nanopart. Res* 10: 823-829.

Katakam, M., Bell, L. N., Banga, A. K. (1995) Effect of surfactants on the physical stability of recombinant human growth hormone. *J. Pharm. Sci.* 84 (6), 713-716.

Kendrick, B. S., Cleland, J. L., Lam, X., Nguyen, T., Randolph, T. W., Manning, M. C., Carpenter, J. F. (1998) Aggregation of recombinant human interferon gamma: kinetics and structural transitions. *J. Pharm. Sci.* 1069-1076.

Kerwin, B. A. (2008) Polysorbates 20 and 80 used in the formulation of protein biotherapeutics: Structure and degradation pathways. *J. Pharm. Sci.* 97, 2924-2935.

Kiese S., Pappenberg A., Friess W, Mahler HC. Equilibrium studies of protein aggregates and homogeneous nucleation in protein formulation. *J Pharm Sci.* 2010; 99(2): 532-44.

Kravchuk, Z. I., Chumanevich, A. A., Vlasov, A. P. (1998) Two high-affinity monoclonal IgG2a antibodies with differing thermodynamic stability demonstrate distinct antigen-induced changes in protein A-binding affinity. *J. Immunol. Methods* 217, 131-141.

Krielgaard, L., Jones, L.S., Randolph, T.W., Frokjaer, S., Flink., J.M, Manning, M.C., Carpenter, J.F. (2000) Effect of tween 20 on freeze-thawing and agitation induced aggregation of recombinant human factor XIII. *J. Pharm. Sci.* Vol. 87, Issue 12, 1593-1603.

Krishnan, S. (2009) Effect of formulation and container-closure aspects on particle formation in proteins based drug product. AMGEN. AAPS National Biotechnology Conference, June 24th 2009 Presentation.

Larsericsdotter, H., Oscarsson, S., Buijs, J. (2004) Thermodynamic analysis of lysozyme adsorbed on silica. *J. Coll. and Int. Sci.* 276 (2), 261-268.

Liu, J. and Shire, S.J. (1999) Analytical ultracentrifugation in the pharmaceutical industry. *J. Pharm. Sci.* 88, 1237-1241.

Liu, J., Andya, J.D. and Shire, S.J. (2006) A critical review of analytical ultracentrifugation and field flow fractionation methods for measuring protein aggregation. *AAPS J.* 8, 580-589.

Liu, X., Huo, Q. (2009) A washing – free and amplification – free one – step homogeneous assay for protein detection using gold nanoparticle probes and dynamic light scattering. *J. Immunol. Meth.* 349, 38-44.

Maggio, E. T. (2012) Polysorbates, peroxides, protein aggregation, and immunogenicity – a growing concern. *J. Excipients and Food Chem.*, 3 (2), 45-53.

Mahler, H. C., Frieß, W., Grauschopf, U., Kiese, S. (2009). Protein Aggregation: Pathways, Induction Factors and Analysis. *J. Pharm. Sci.* 98 (9), 2909-2934.

Mahler, H-C., Jiskoot W. (2011) Analysis of aggregates and particles in protein pharmaceuticals. 1-14.

Mahler, H-C., Muller, R, Frieß, W., Delille, A., Matheus, S. (2005) Induction and analysis of aggregates in a liquid IgG1-antibody formulation. *Eur. J. Pharm. Biopharm.* 59, 407-417.

Malvern Instruments Limited. (2011) *Dynamic light scattering common terms defined*. Malvern Instruments Ltd. Available from:
http://www.biophysics.bioc.cam.ac.uk/wpcontent/uploads/2011/02/DLS_Terms_defined_Malvern.pdf (Accessed 1 June 2013).

Malvern Instruments Ltd. (2006) *Zetasizer nano application note. Surfactant micelle characterization using dynamic light scattering*. Malvern Instruments Ltd. Available from:
<http://quimica.udea.edu.co/~coloides/Anexo1.pdf> (Accessed 5 June 2013).

Malvern Instruments Ltd. (2010) *Flow particle image analysis of size and shape*. Malvern Instruments Ltd. Available from:
<http://www.atomikateknik.com/pdf/Sysmex%20FPIA%203000.pdf> (Accessed 20 June 2013).

Mayer, G., (2009) Immunoglobulins – structure and function. *Immunology* 7th Edition, Chapter 4.

Michnik, A. (2003) Thermal stability of bovine serum albumin DSC study. *J. Therm. Anal. Calorim.* 71, 509-519.

Narayanan, J., Deotare, V. W. (1999) Salt induced liquid-liquid phase separation of protein-surfactant complexes. *Phys. Rev. E* 60, 4597.

Narhi, L. O., Jiang, Y., Cao, S., Benedek, K., Schnek, D (2009) A critical review of analytical methods for subvisible and visible particles. *Curr. Pharm. Biotechnol.*10(4), 3302-3321.

Nishimura, K., Goto, M., Higasa, T., Kawase S-J., Matsumura Y. (2001) Aggregation behaviour of bovine serum albumin as a cause of sauce liquid separation by heating. *J. Agric. Food. Chem.* 81 (1), 76-81.

Onuma, K., Kanzaki, N. (2003) Size distribution and intermolecular interaction of laminin-1 in physiological solutions. *J. Phys. Chem.* 107, 11799-11804.

Onuma, K., Kanzaki, N. (2005) Aggregation dynamics of laminin-1 in a physiological solution: a time resolved static light scattering study. *J. Cryst. Growth* 284, 530-537.

Padlan, E. A. (1997) Anatomy of the antibody molecule. *Mol. Immunol.* 31, 149.

Pico, G .A. (1997) Thermodynamic features of the thermal unfolding of human serum albumin. *Int. J. Biol. Macromol.* 20, 63-73.

Plakoutsi, G., Bemporad, F., Calamai, M., Taddei, N., Dobson, C. M., Chiti, F. (2005) Evidence for a mechanism of amyloid formation involving molecular reorganization within native-like precursor aggregates. *J. Mol. Biol.* 351, 910-922.

Qian, R. L., Mhatre, R., Krull, I. S. (1997) Characterization of antigen-antibody complexes by size exclusion chromatography coupled with low-angle light-scattering photometry and viscometry. *J. Chromatogr. A.* 787, 101-109.

Rangel-Yagui, C. O., Pessoa Junior, A., Costa Tavares, L. (2005) Micellar solubilization of drugs. *J. Pharm. Pharmaceut. Sci.* 8(2), 147-163.

Remmele, R. L., Bhat, S. D., Phan, D. H., Gombotz, W. R. (1999) Minimization of recombinant human Flt3 ligand aggregation at the T_m plateau: a matter of thermal reversibility. *Biochem.* 38, 5241-5247.

Remmele, R. L., Nightlinger, N. S., Srinivasan, S., Gombotz, W. R. (1998) Interleukin-1 receptor (IL-1R) liquid formulation development using differential scanning calorimetry. *Pharm. Res.* 15, 200.

Remmele, R.L. (2005) Microcalorimetric approaches to biopharmaceutical development. *Anal. Tech. Biopharm. Dev.* Marcel Dekker, Inc., 327-381.

Reschiglian, P., Zattoni, A., Roda, B., Michelini, E., Roda, A. (2005) Field-flow fractionation and biotechnology. *Biotechnol.* 23, 475-483.

Reynolds, J. A., Tanford, C. (1970) Binding of Dodecyl Sulfate to Proteins at High Binding Ratios. Possible Implications for the State of Proteins in Biological Membranes. *J. Biol. Chem.* 245 (3), 1002-1007.

Roberts, Ch. J., Das, T. P., Sahin, E. (2011) Predicting solution aggregation rates for therapeutic proteins: Approaches and challenges. *Int. J. Pharm.* 418, 318-333.

Robson, H., Craig, D. Q. M., Deutch, D. (2000) An investigation into the release of cefuroxime axetil from taste-masked stearic acid microspheres. III. The use of DSC and HSDSC as means of characterising the interaction of the microspheres with buffered media. *Int. J. Pharm.*, 201, 211-219.

Rosen, M. J. (2004) *Surfactants and interfacial phenomena*. 3rd edition.

Sahin, E., Grillo, A. O., Perkins, M. D., Roberts, C. J. (2010) Comparative effects of pH and ionic strength on protein-protein interactions, unfolding, and aggregation for IgG1 antibodies. *J. Pharm. Sci.* 99, 4830-4848.

Sahu, K., Roy, D., Mondal, S. K., Karmakar, R., Bhattacharyya, K. (2005) Slow solvation dynamics of 4-AP and DCM in binary mixtures, *J. Photochem. Photobiol.* 404, 341.

Santander-Ortega, M. J., Jodar-Reyes, A. B., Csaba, N., Bastos-Gonzalez, D., Ortega-Vinuesa, J. L. (2006) Colloidal stability of Pluronic F68-coated PLGA nanoparticles: A variety of stabilisation mechanisms. *J. Colloid Interface Sci.* 302 (2), 522–529.

Schmidt, R. (2009) Detecting aggregates without samples separation or dilution by low angle light scattering. PEGSummit April 6th-10th 2009. Boston USA.

Seddon, A. M, Curnow, P., Booth, P. J. (2004) Membrane proteins, lipids and detergents: not just a soap opera. *Biochim Biophys Acta* 2004, 1666(1-2), 105-117.

Sharma, D, King, D., Moore, P., Oma, P., Thomas, D.(2007) Flow Microscopy for particulate analysis in parenteral and pharmaceutical fluids. *Eur. J. Parent. Pharm. Sci.* 12(4), 97-101.

Sharma, D. K., King, D., Oma, P., Merchant, C. (2010) Micro-flow imaging: flow microscopy applied to sub-visible particulate analysis in protein formulations. *AAPS* 12 (3), 455-464.

Sharma, D. K., Oma, P., Pollo, M. J., Sukumar, M. (2009) Quantification and characterization of subvisible proteinaceous particles in opalescent mAb formulations using micro-flow imaging. *J. Pharm. Sci.* 99 (6), 2628-2642.

Shire, S.J., Shahrokh, Z., Liu, J. (2004) Challenges in the development of high protein concentration formulations. *J. Pharm Sci.* 93(6), 1390-1420.

Sluzky, V., Tamada, J. A., Klibanov, A. M., Langer, R. (1991) Kinetics of insulin aggregation in aqueous solutions upon agitation in the presence of hydrophobic surfaces. *Proc. Natl. Acad. Sci. USA.* 88 (21), 9377-9381.

Solids Wiki. (2013) *Particle counter top down view*. Solids Wiki. Available from: http://solidswiki.com/index.php?title=File:Particle_counter_top_down_view.jpg (Accessed 25 May 2013).

Song, D., Forciniti, J. (2001) Monte Carlo simulations of peptide adsorption on solid surfaces. *J. Chem. Phys.* 115, 8089-8101.

Stavroudis, C. (2009) Sorting out surfactants. *WAAC Newsletter.* 31 (1), 18-21.

Stefani, M. (2004) Protein misfolding and aggregation: new examples in medicine and biology of the dark side of the protein world. *Biochem. Biophys. Acta.* 1739(1), 5-25.

Steinhardt, J., Reynolds J. A. (1969) *Multiple Equilibria in Proteins*. Academic Press, New York.

The Nanobiotechnology Centre (2009) *Zetasizer*. The Nanobiotechnology Centre. Cornell University. Available from: <http://www.nbtc.cornell.edu/facilities/downloads/Zetasizer%20chapter%204.pdf> (Accessed 28 February 2013).

Tischenko, V. M., Abramov, V. M., Zav'yalov, V. P. (1998) Investigation of the cooperative structure of Fc fragments from myeloma immunoglobulin G. *Biochemistry* 37, 5576.

Tischenko, V. M., Zav'yalov, V. P. (2003) Core hinge of human immunoglobulin G3 as a system of four independent cooperative blocks. *Immunol.* 86, 281.

Tyagi, A. K., Randolph, T. W., Dong, A., Maloney, K. M., Hitscherich Jr, C., Carpenter, J. F. (2009) IgG particle formation during filling pump operation: a case study of heterogeneous nucleation on stainless steel nanoparticles. *J. Pharm. Sci.* 98(1), 94-104.

Valstar, A., Almgren, M., Brown, W. (2000) The Interaction of Bovine Serum Albumin with Surfactants Studied by Light Scattering *Langmuir* 16, 922.

Valstar, A., Brown, W., Almgren, M. (1999) The Lysozyme–Sodium Dodecyl Sulfate System Studied by Dynamic and Static Light Scattering *Langmuir* 15, 4597.

Vankeirsblick, T., Vercauteren, A., Baeyens, W., Van der Weken, G., Verpoort, F., Vergote, G., Remon, J.P. (2002) *Trends Anal. Chem.* 21, 869-877.

Vermeer, A. W. P., Norde W. (2000) The influence of the binding of low molecular weight surfactants on the thermal stability and secondary structure of IgG1. *Physiochem. Engineering Aspects* 161, 139-150.

Vidanovic, D., Milic Askrabic J., Stankovic, M., Poprzen, V. (2003) Effects of non-ionic surfactants on the physical stability of immunoglobulin G in aqueous solution during mechanical agitation. *Pharmazie* 58, 399.

Virden, A. (2010) Method development for laser diffraction particle size analysis. *Pharm. Technol.*, 100-106.

Wang, W. (2005) Protein aggregation and its inhibition in biopharmaceutics. *Int. J. Pharm.* 289, 1 – 30.

Wang, W., Nema, S., Teagarden, D. (2010) Protein aggregation-pathways and influencing factors. *Int. J. Pharm.* 290, 89-99.

Wang, W., Singh, S., Zeng, D.L., King, K., Nema, S. (2006) Antibody structure, instability, and formulation. *J. Pharm. Sci.* 96 (1), 1-26.

Warterwig, S., Neubert, R. H. (2005) *Adv. Drug. Deliv. Rev.* 57(8), 1144-1170.

Wei, G., Lu, L. F., Lu, W. Y. (2007) Stabilization of recombinant human growth hormone against emulsification-induced aggregation by Pluronic surfactants during microencapsulation. *Int. J. Pharm.* 338 (1-2), 125-132.

Wei, Y.L., Li, J.D., Shuang, S., Liu, D., Huie, C.W. (2006) Investigation of the association behaviours between biliverdin and bovine serum albumin by fluorescence spectroscopy. *J. Pharm. Sci.* 70 (2), 377-382.

Weichel, M., Bassarab, S., Garidel, P. (2008) Probing thermal stability of MAbs by intrinsic tryptophan fluorescence. A practical approach for preformulation development. *J. Pharm. Sci.* 6, 42-52.

Wissing, S., Craig, Q. M., Barker, S.A, Moore, W.D. (2000) An investigation into the use of stepwise isothermal high sensitivity DSC as a means of detecting drug-exciipient incompatibility. *Int. J. Pharm.* 199, 141-150.

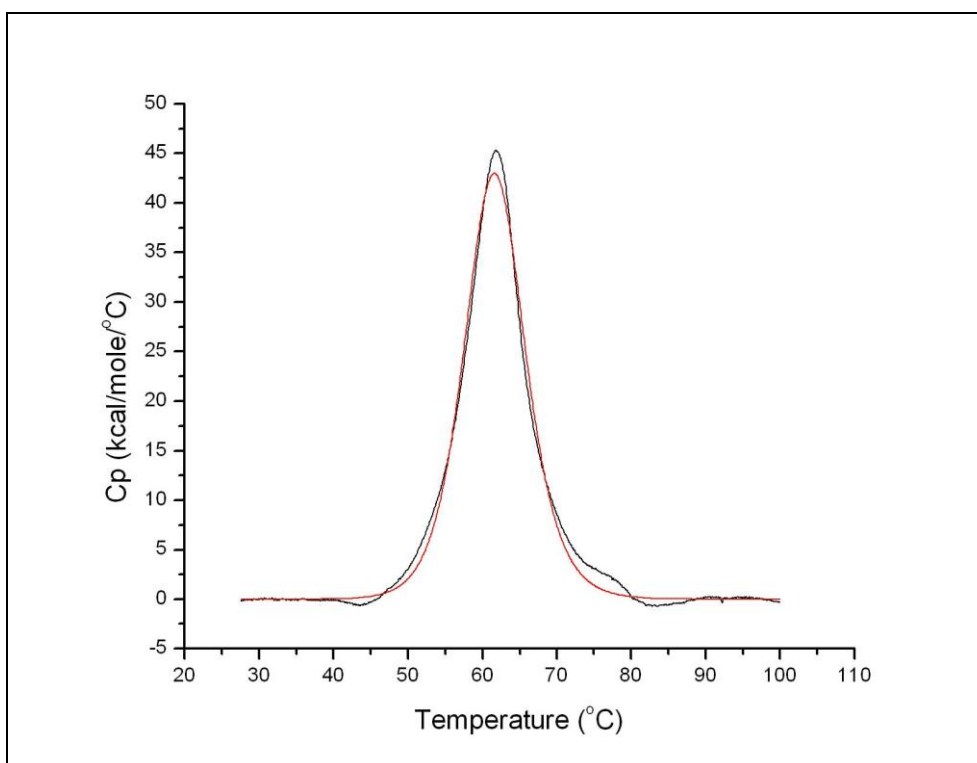
Wuchner, K., Buchler, J., Spycher, R., Dalmonte, P., Volkin, D. B. (2010) Development of a microflow imaging assay to characterize protein particulates during storage of a high concentration IgG1 monoclonal antibody formulation. *J. Pharm. Sci.* 99 (8), 3343-3361.

Ye, H. (2006) Simultaneous determination of protein aggregation, degradation, and absolute molecular weight by size exclusion chromatography-multiangle laser light scattering. *Anal. Biochem.* 356, 76-85.

Yu, M., Ding, Z., Jiang, F., Ding, X., Sun, J., Chen, S., Lv, G. (2011) Analysis of binding interaction between pegylated puerarin and bovine serum albumin by spectroscopic methods and dynamic light scattering. *Spectrochimica Acta Part A* 83, 453-460.

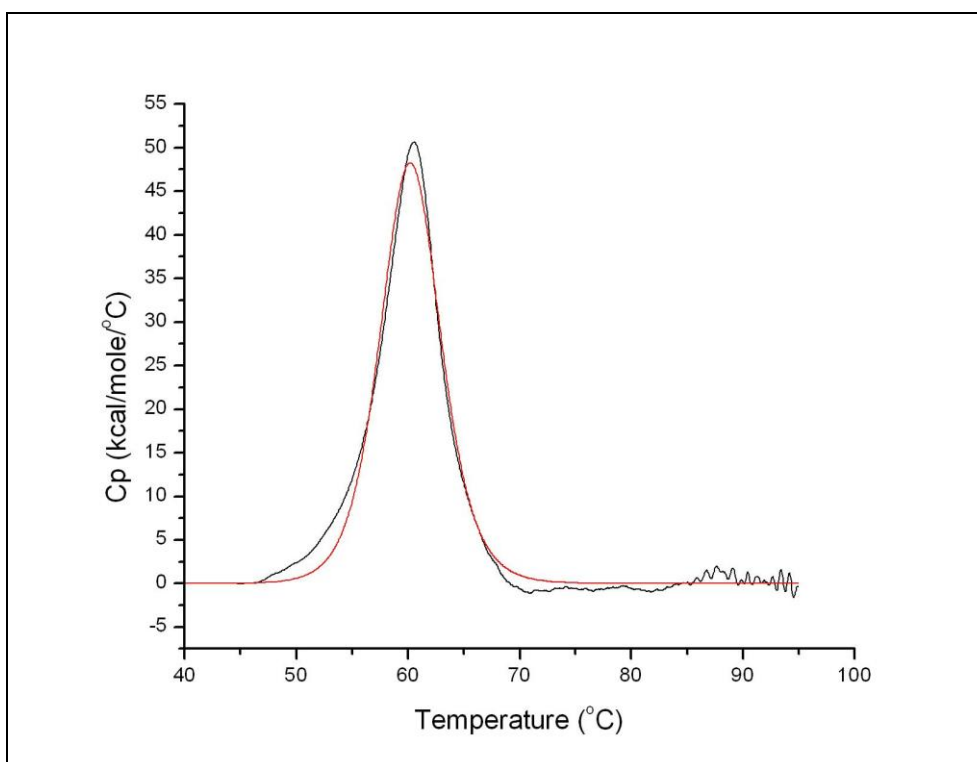
Appendices

APPENDIX 1.



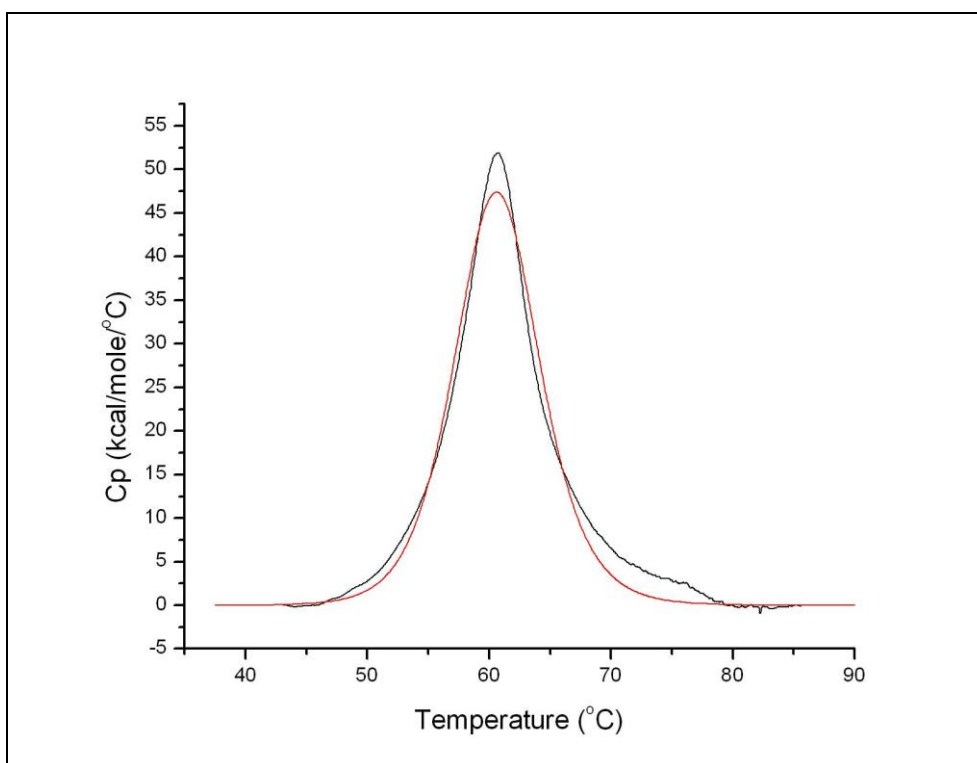
Thermal unfolding profile of BSA with Tween 20 below CMC.

APPENDIX 2.



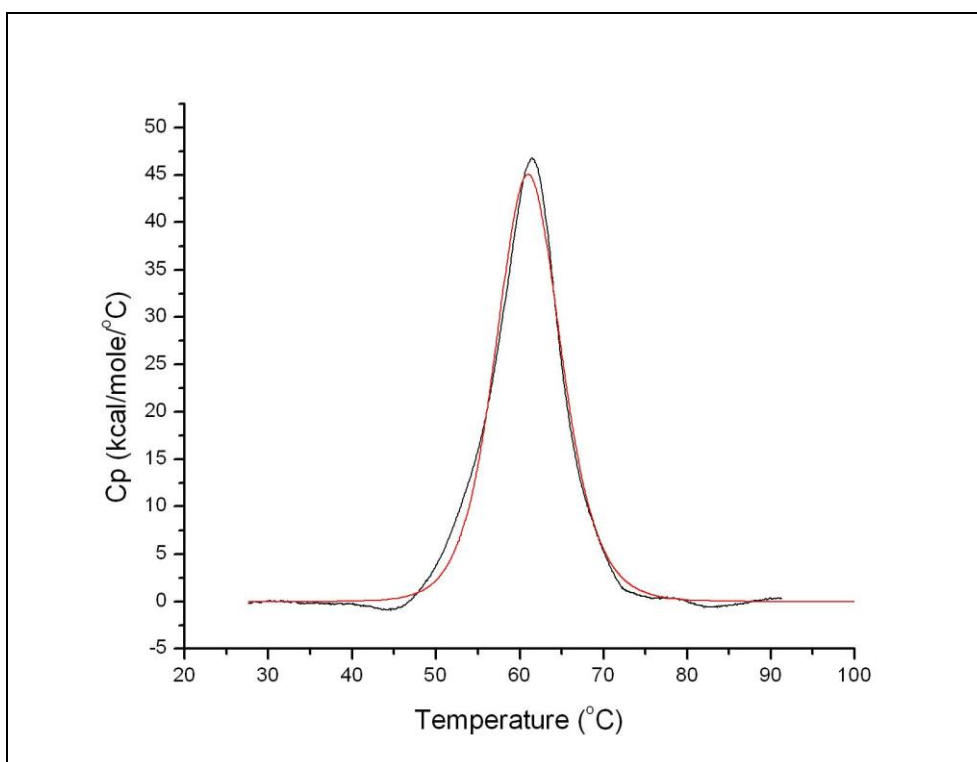
Thermal unfolding profile of BSA with Tween 20 around CMC.

APPENDIX 3.



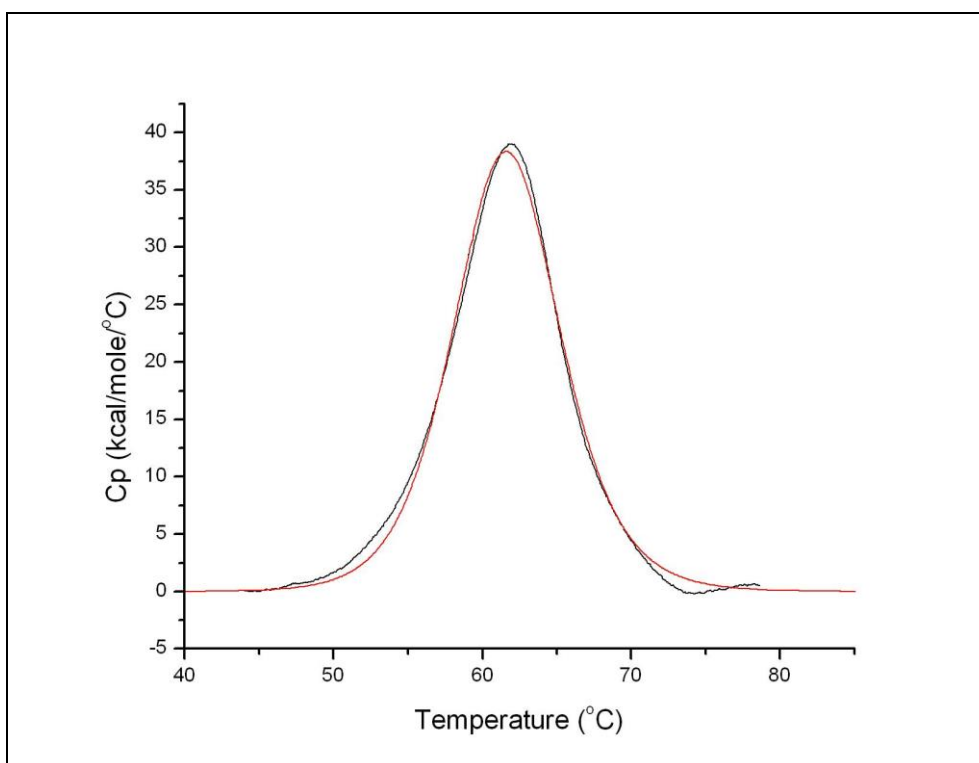
Thermal unfolding profile of BSA with Tween 20 above CMC.

APPENDIX 4.



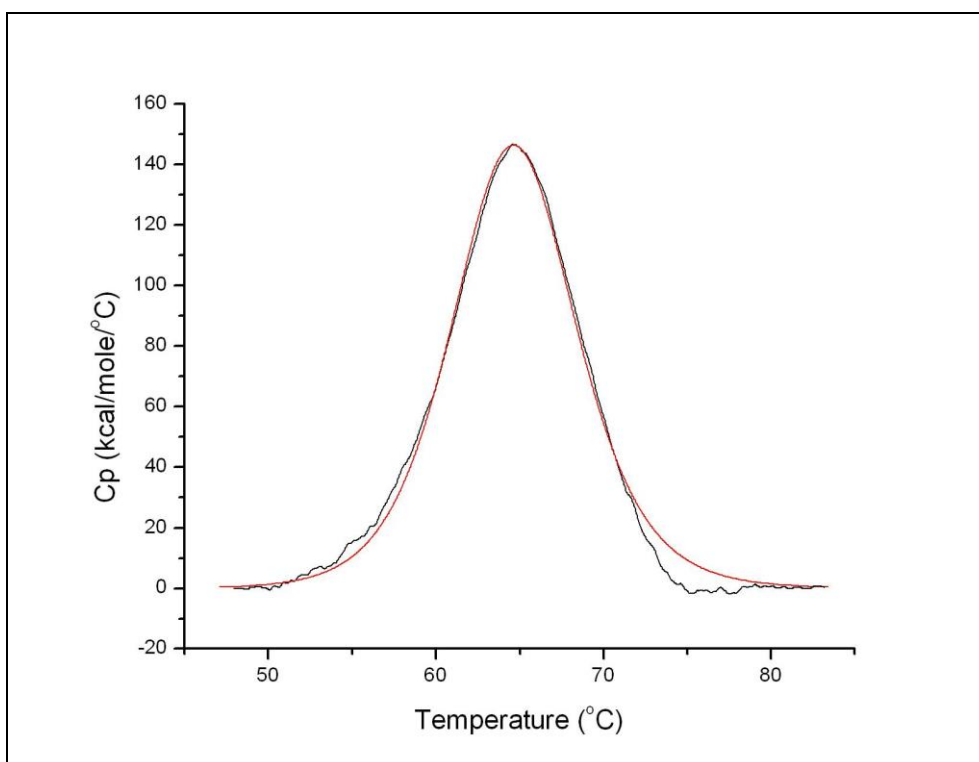
Thermal unfolding profile of BSA with Tween 80 below CMC.

APPENDIX 5.



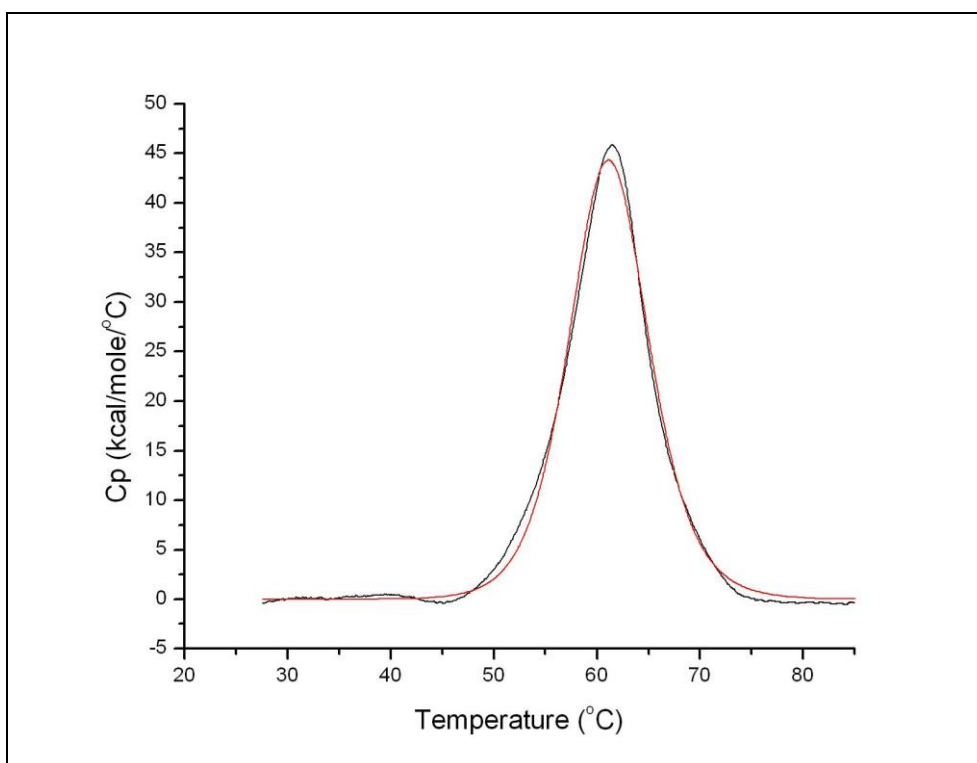
Thermal unfolding profile of BSA with Tween 80 around CMC.

APPENDIX 6.



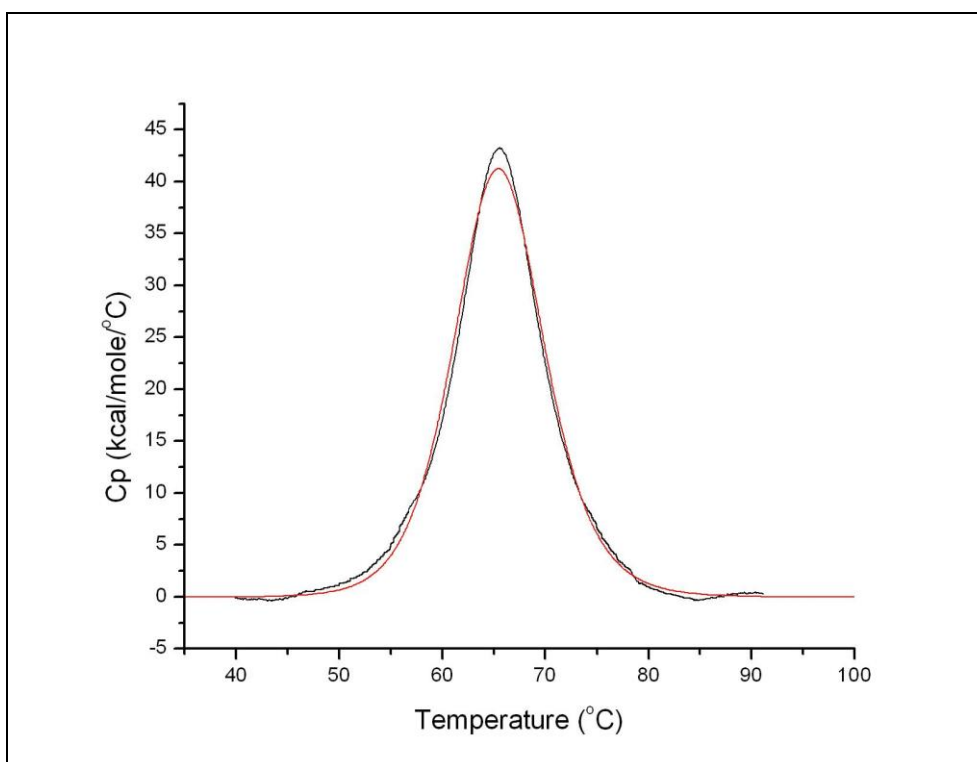
Thermal unfolding profile of BSA with Tween 80 above CMC.

APPENDIX 7.



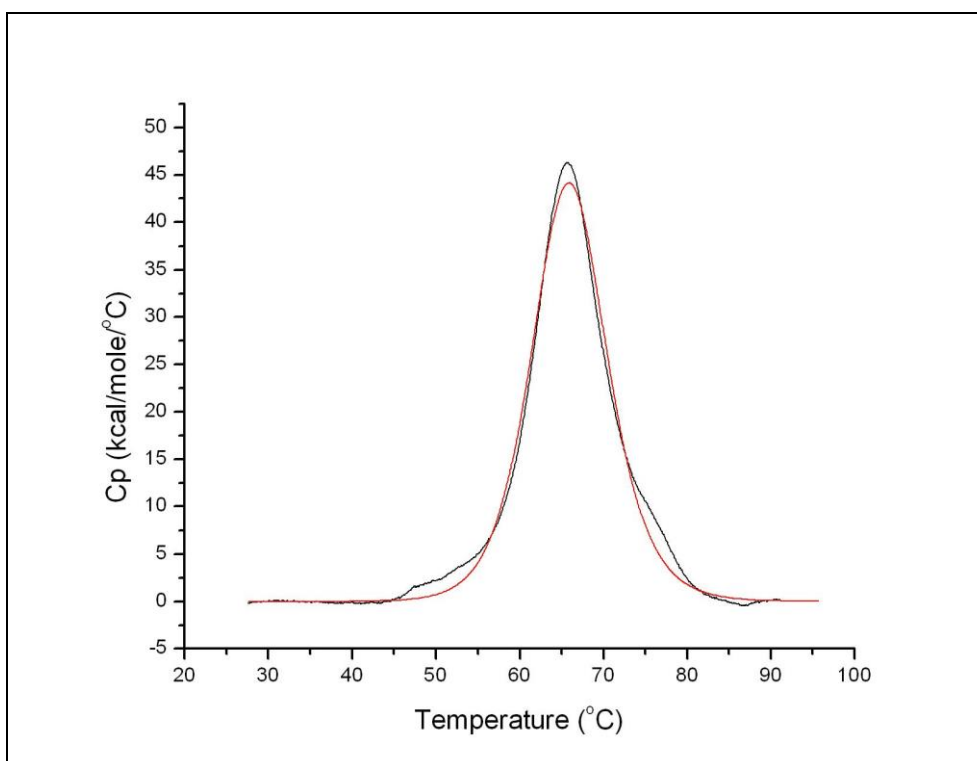
Thermal unfolding profile of BSA with Brij 35 below CMC.

APPENDIX 8.



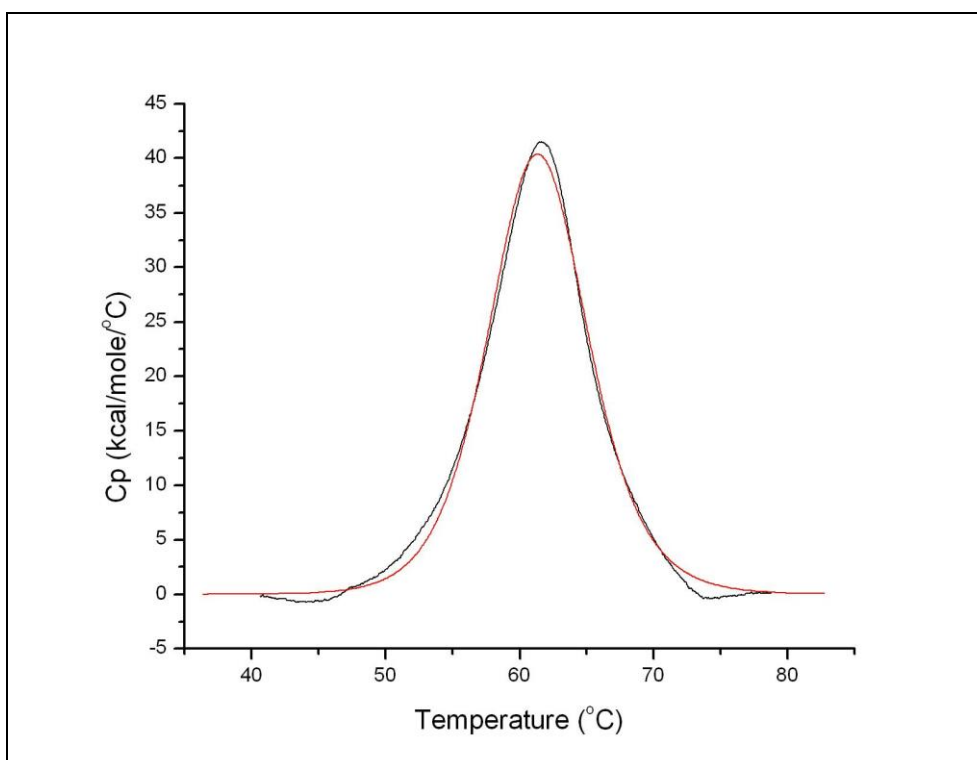
Thermal unfolding profile of BSA with Brij 35 around CMC.

APPENDIX 9.



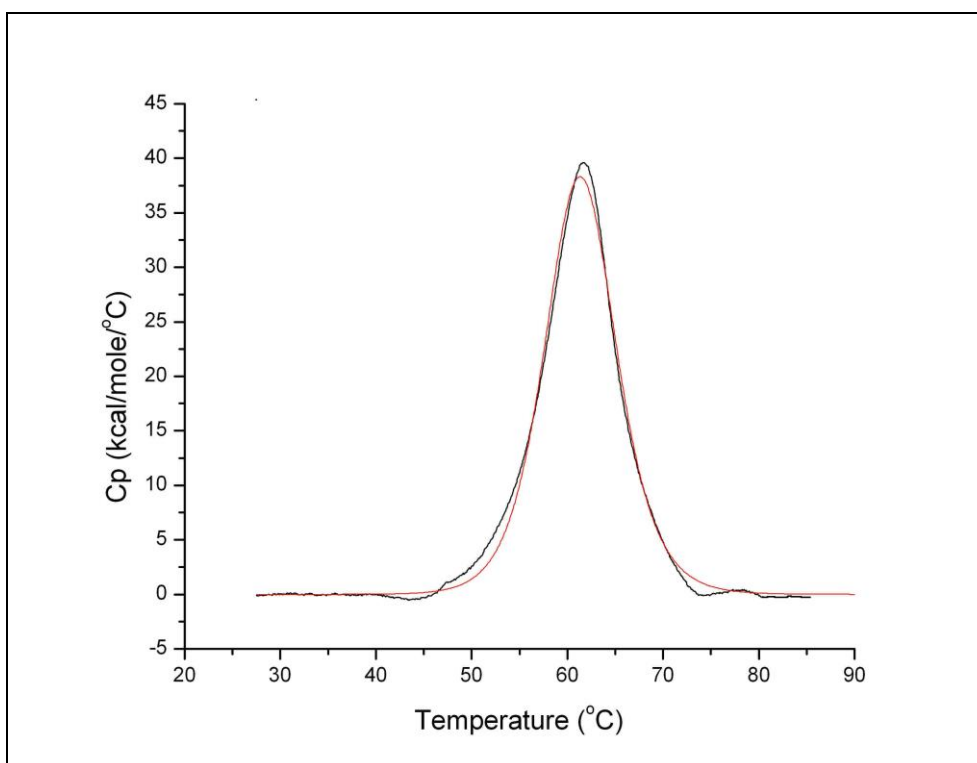
Thermal unfolding profile of BSA with Brij 35 above CMC.

APPENDIX 10.



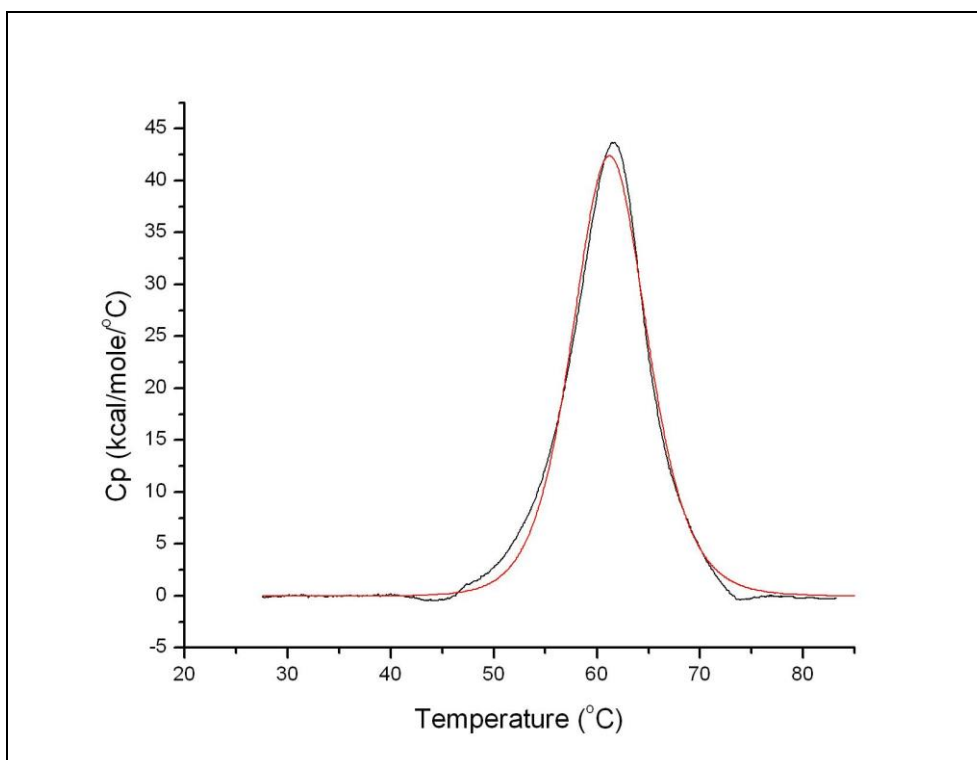
Thermal unfolding profile of BSA with Pluronic F-68 below CMC.

APPENDIX 11.



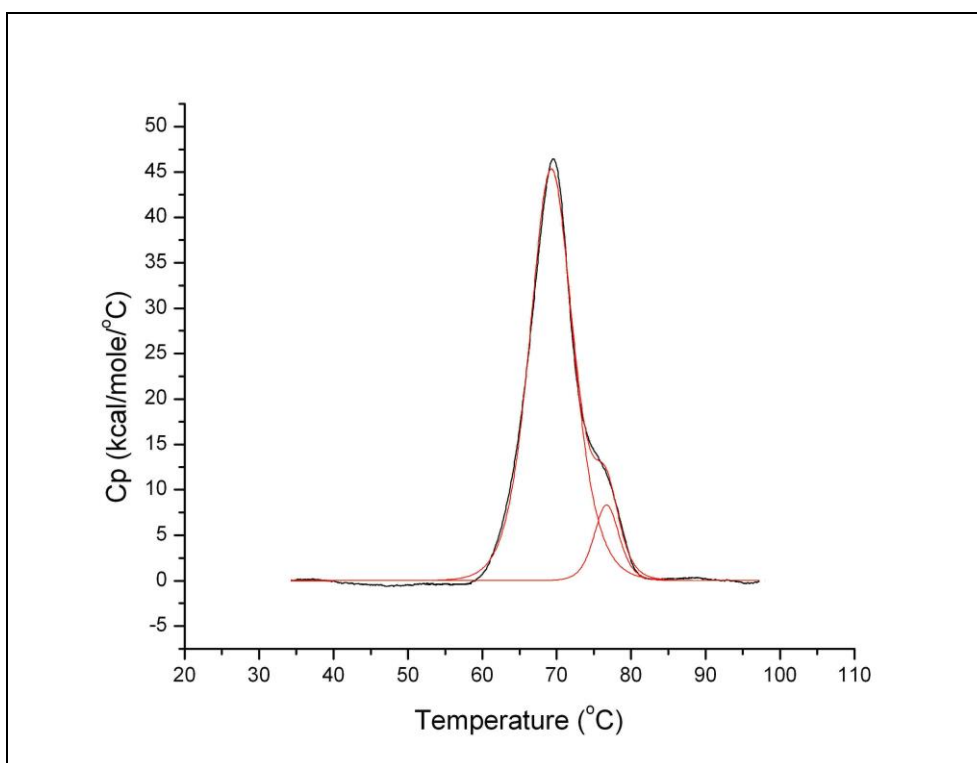
Thermal unfolding profile of BSA with Pluronic F-68 around CMC.

APPENDIX 12.



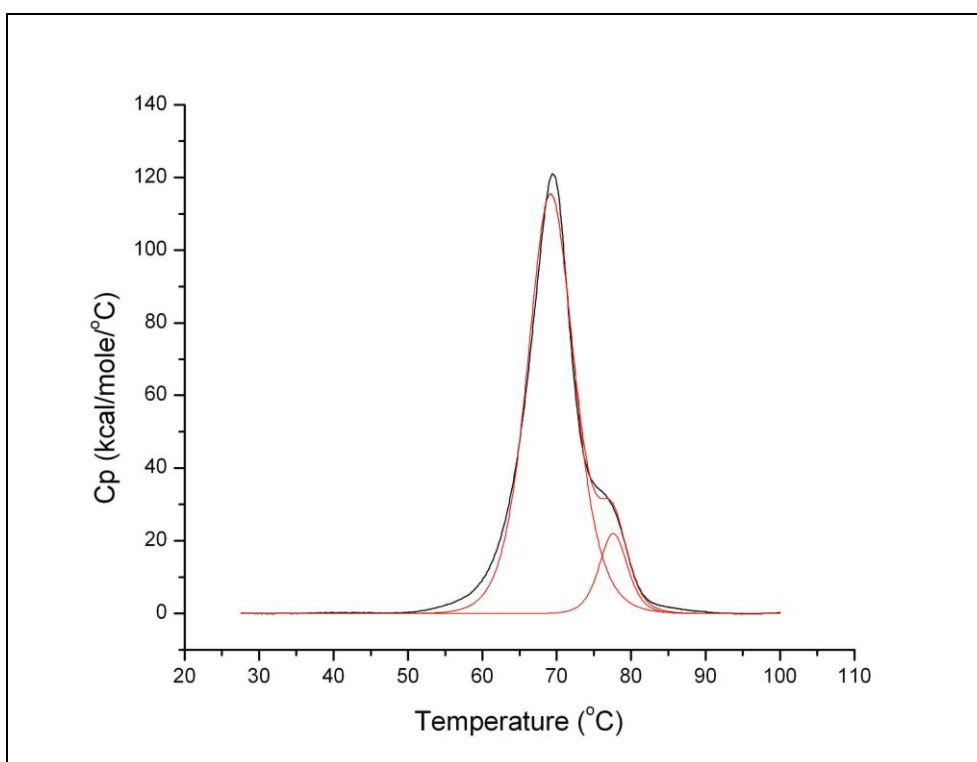
Thermal unfolding profile of BSA with Pluronic F-68 above CMC.

APPENDIX 13.



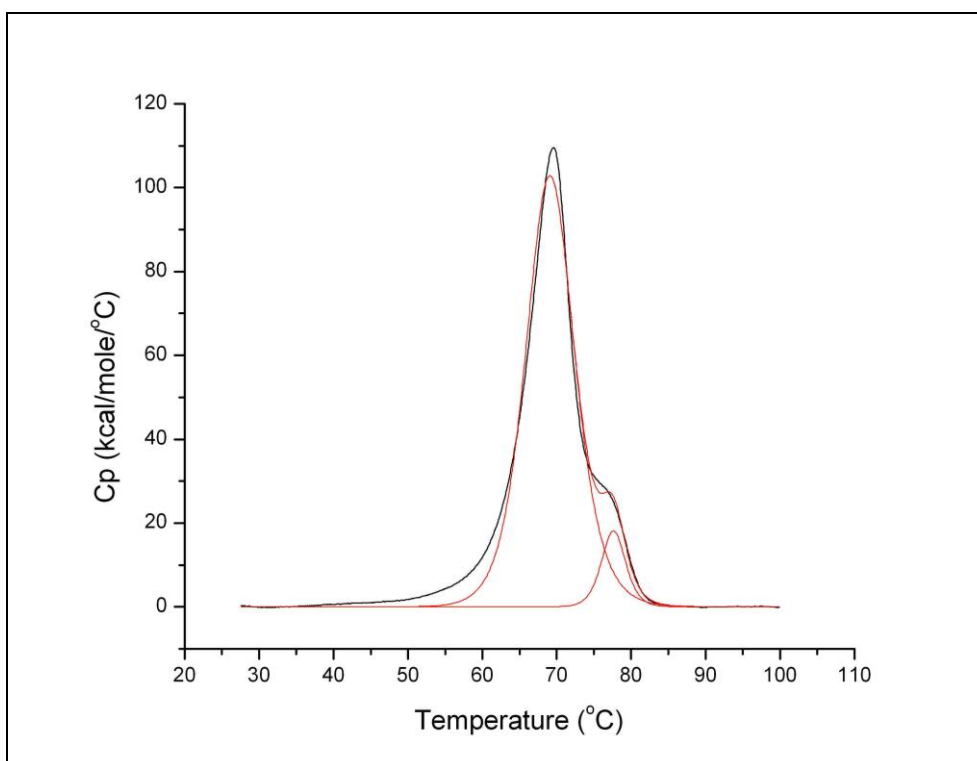
Thermal unfolding profile of IgG2 with Tween 20 below CMC.

APPENDIX 14.



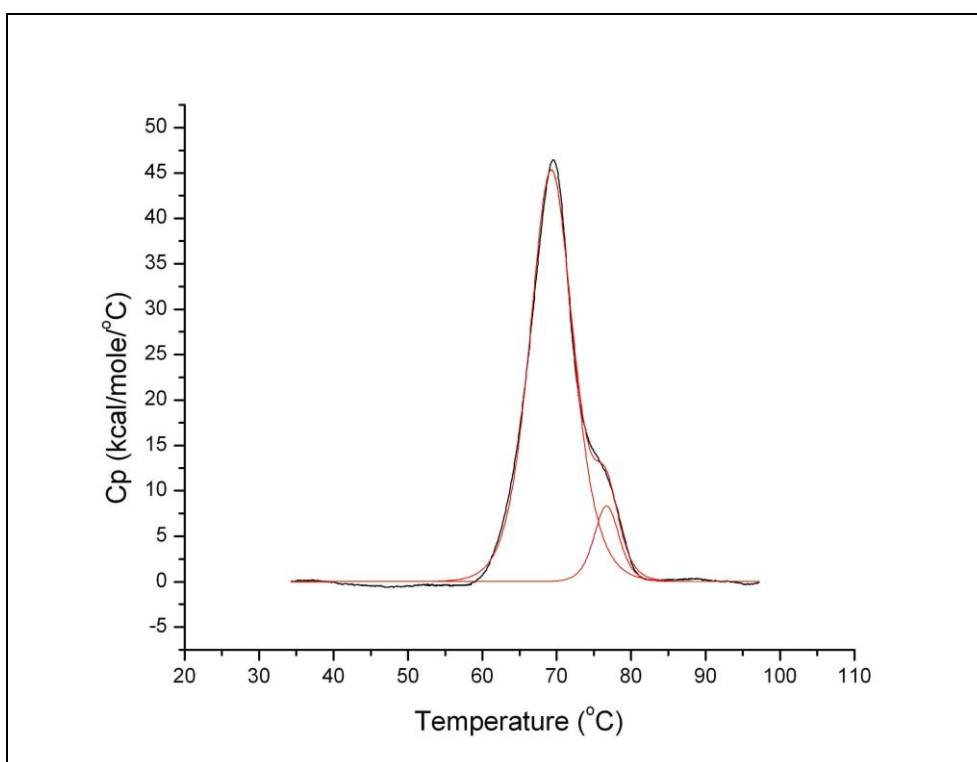
Thermal unfolding profile of IgG2 with Tween 20 around CMC.

APPENDIX 15.



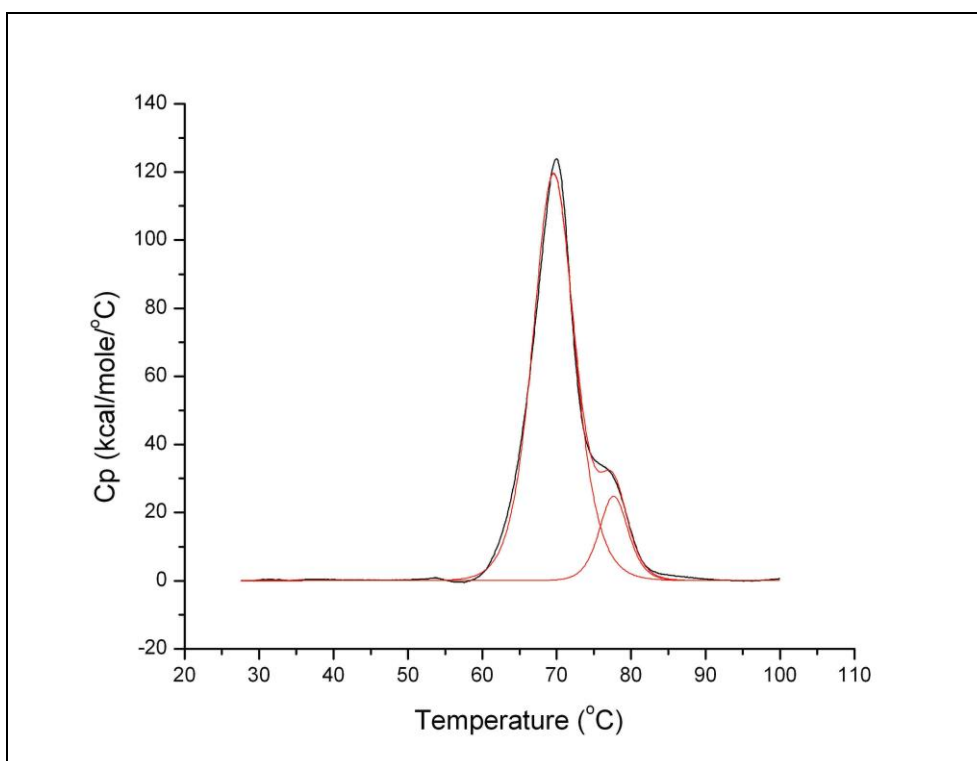
Thermal unfolding profile of IgG2 with Tween 20 above CMC.

APPENDIX 16.



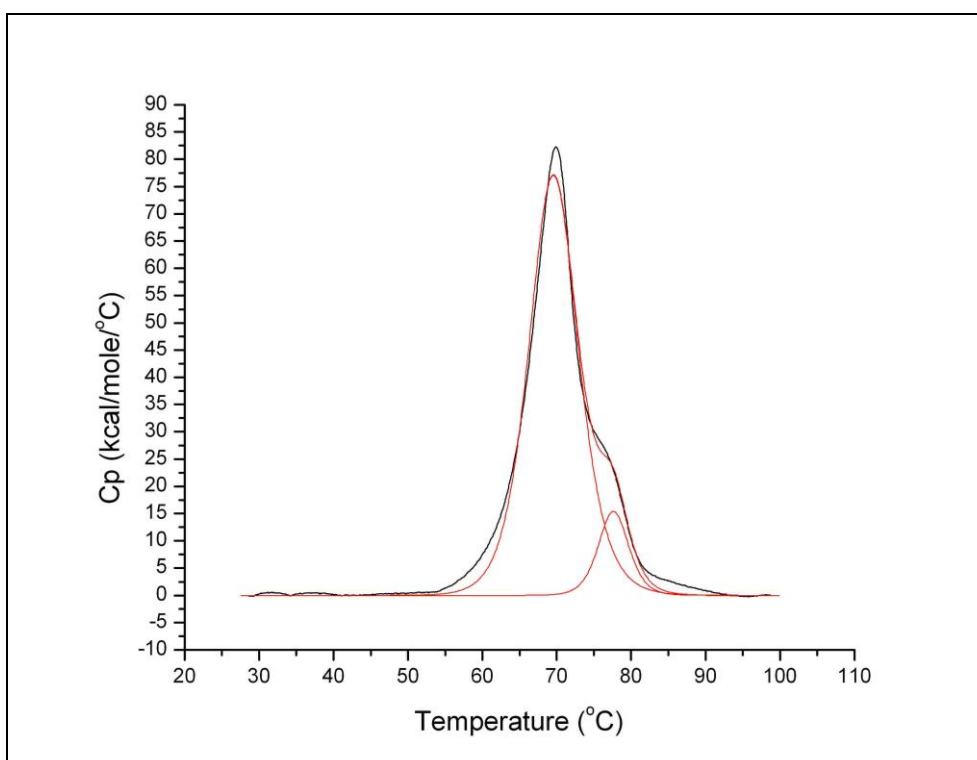
Thermal unfolding profile of IgG2 with Tween 80 below CMC.

APPENDIX 17.



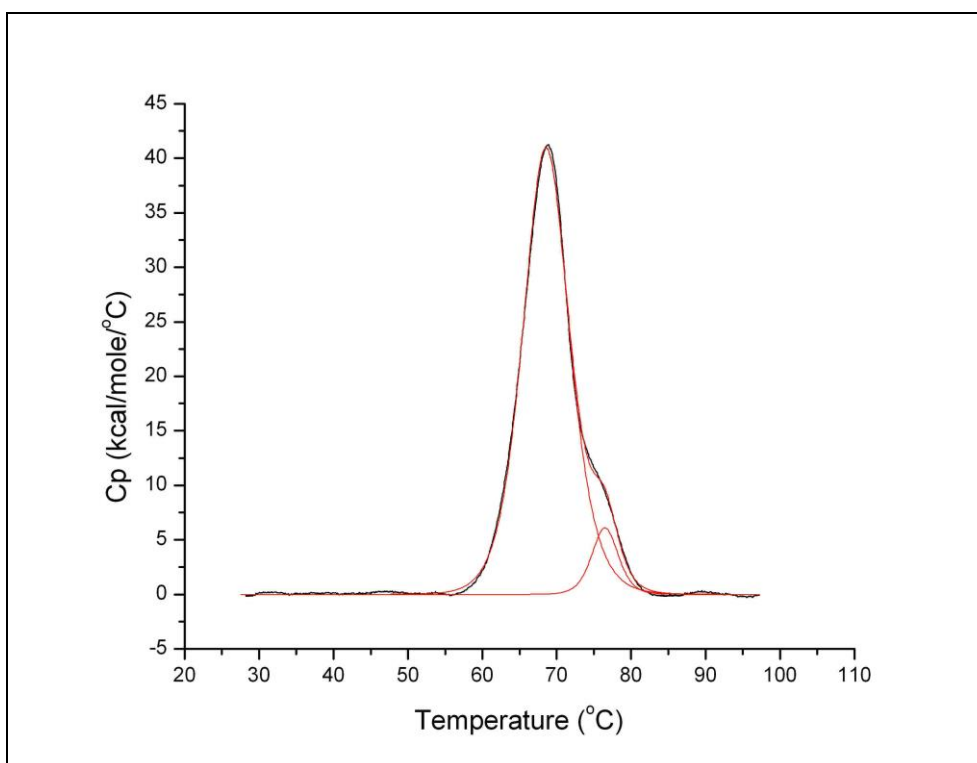
Thermal unfolding profile of IgG2 with Tween 80 around CMC.

APPENDIX 18.



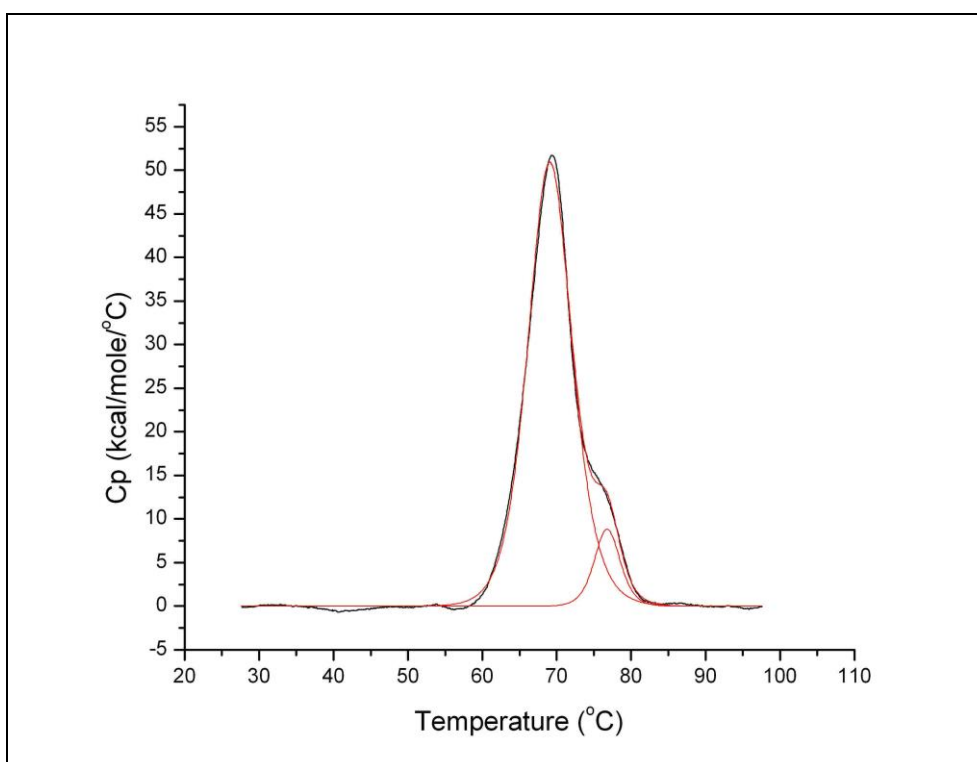
Thermal unfolding profile of IgG2 with Tween 80 above CMC.

APPENDIX 19.



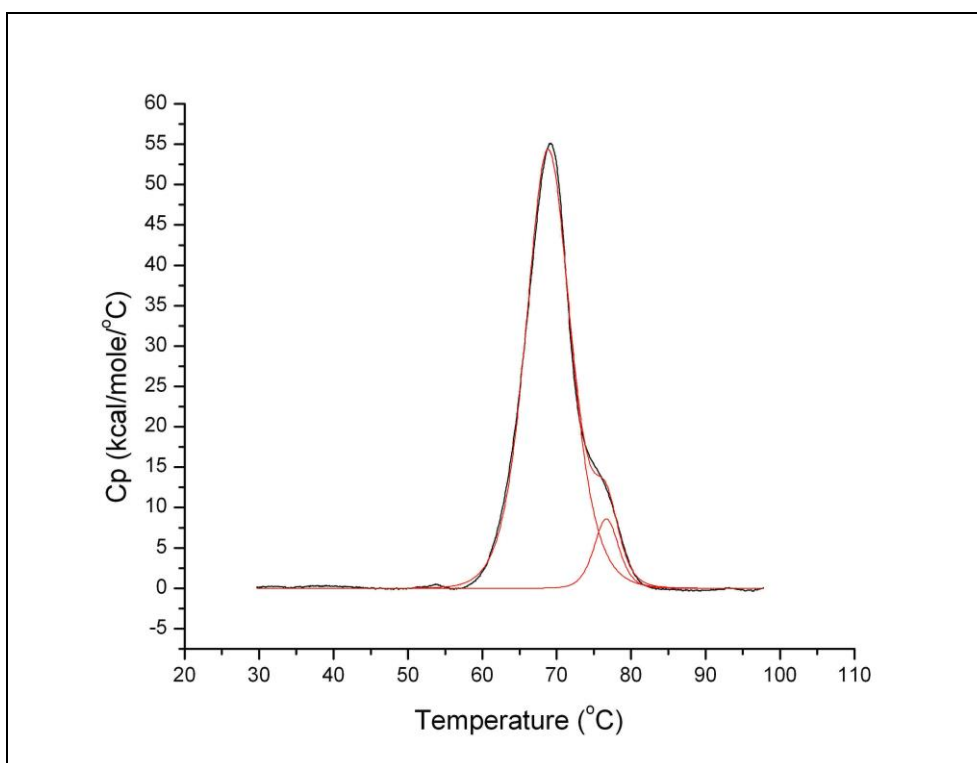
Thermal unfolding profile of IgG2 with Brij 35 below CMC.

APPENDIX 20.



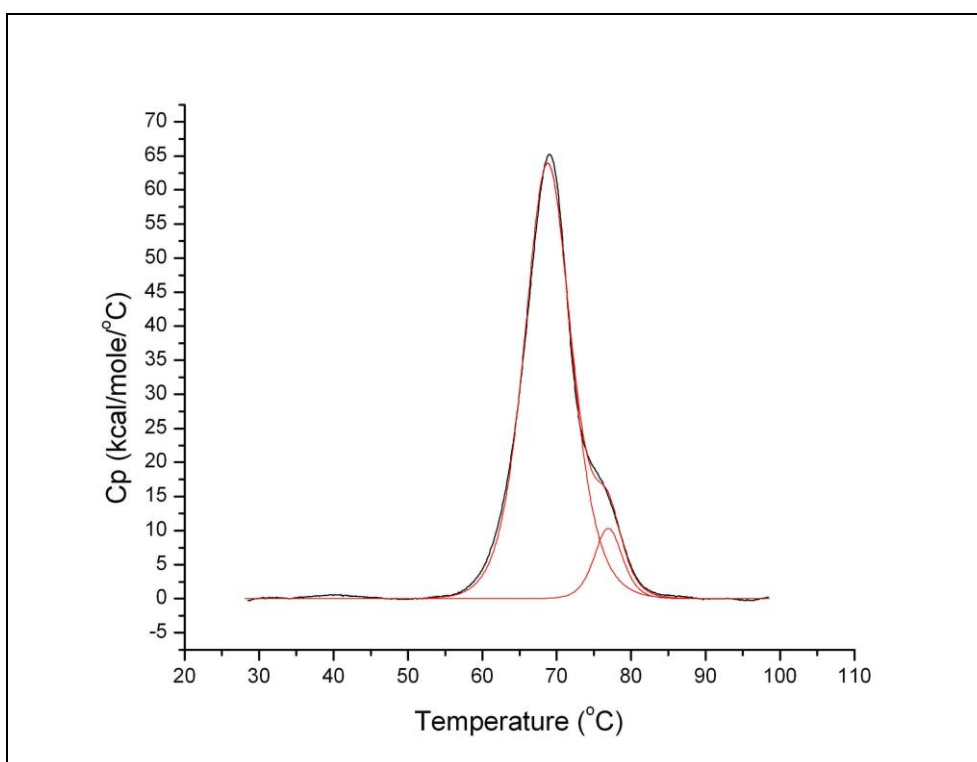
Thermal unfolding profile of IgG2 with Brij 35 around CMC.

APPENDIX 21.



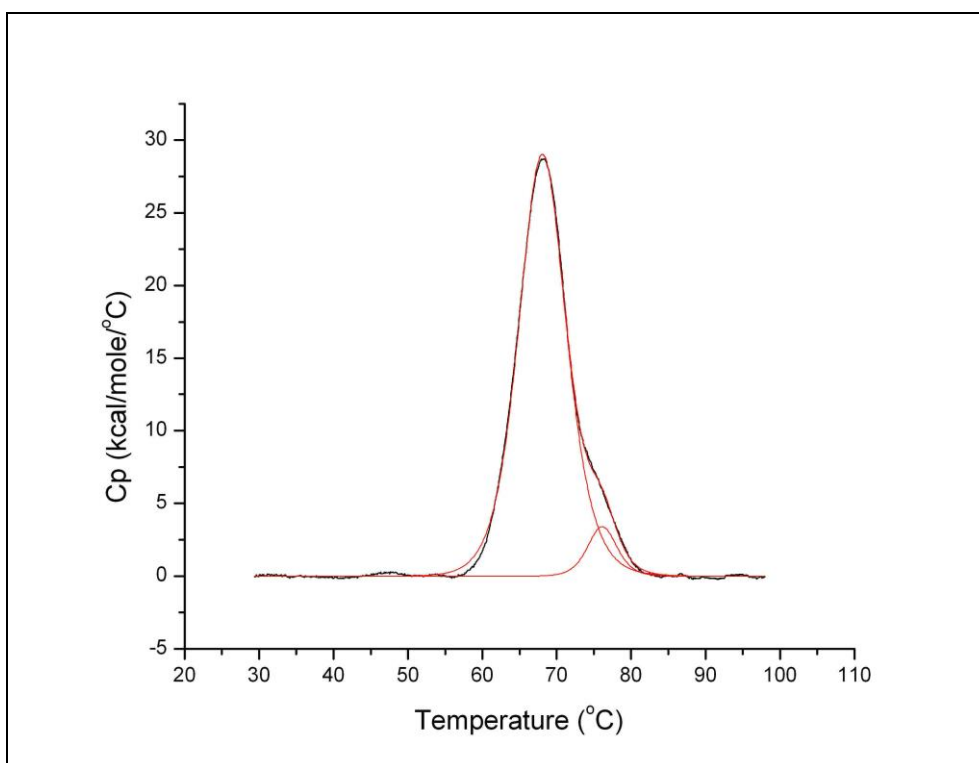
Thermal unfolding profile of IgG2 with Brij 35 above CMC.

APPENDIX 22.



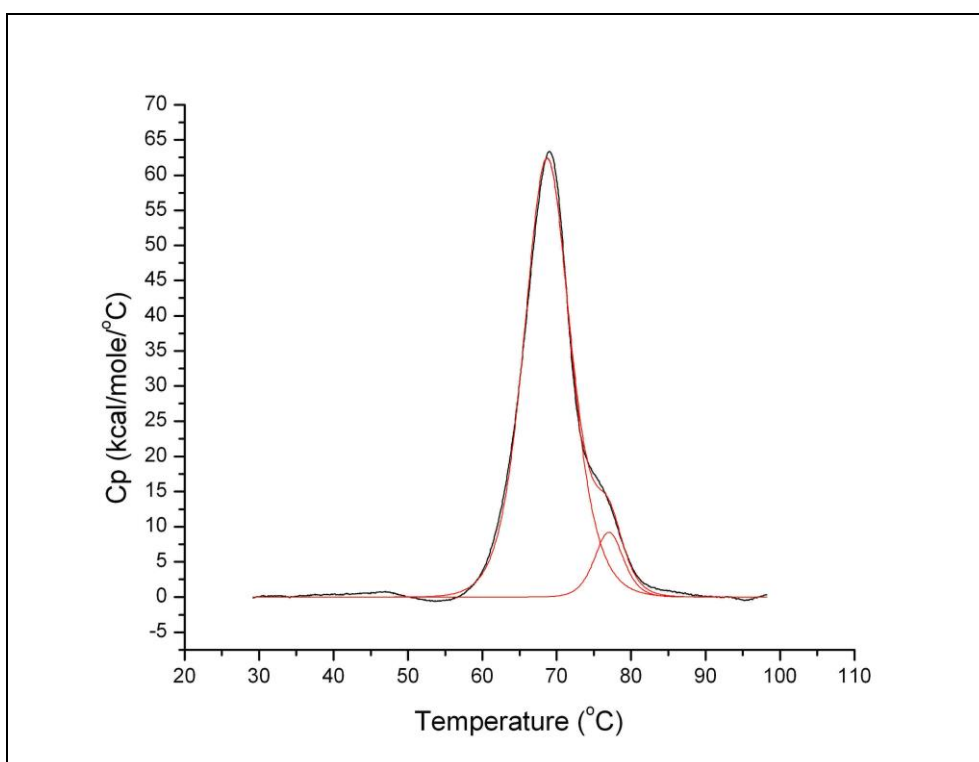
Thermal unfolding profile of IgG2 with Pluronic F-68 below CMC.

APPENDIX 23.



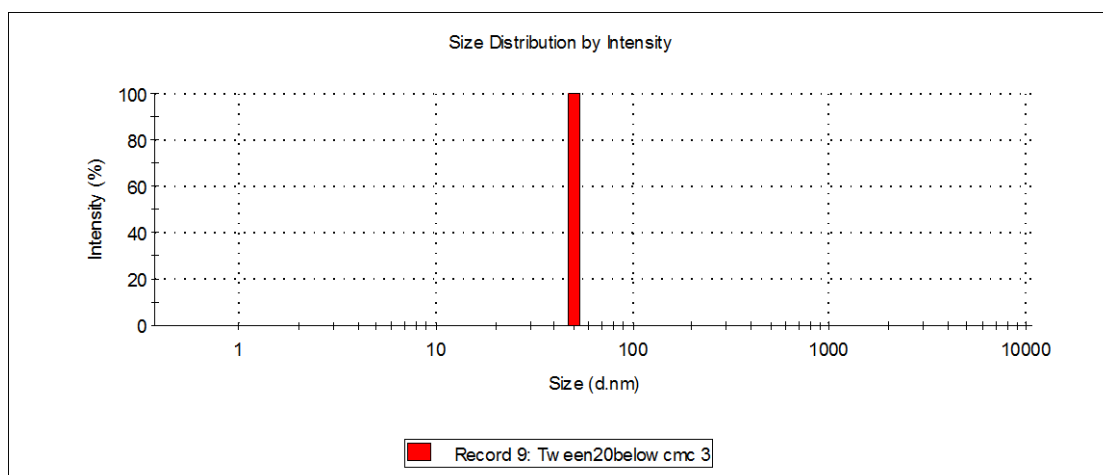
Thermal unfolding profile of IgG2 with Pluronic F-68 around CMC.

APPENDIX 24.



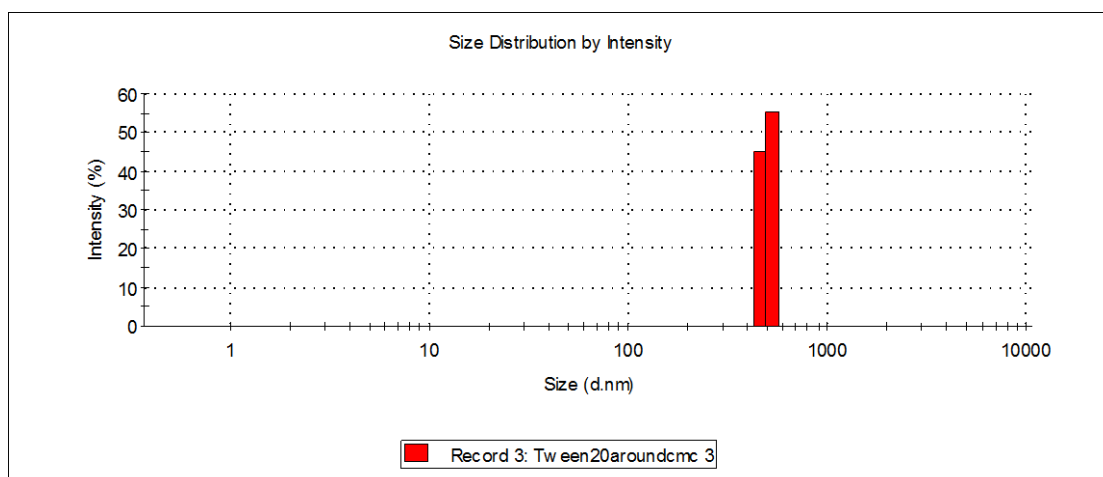
Thermal unfolding profile of IgG2 with Pluronic F-68 above CMC.

APPENDIX 25.



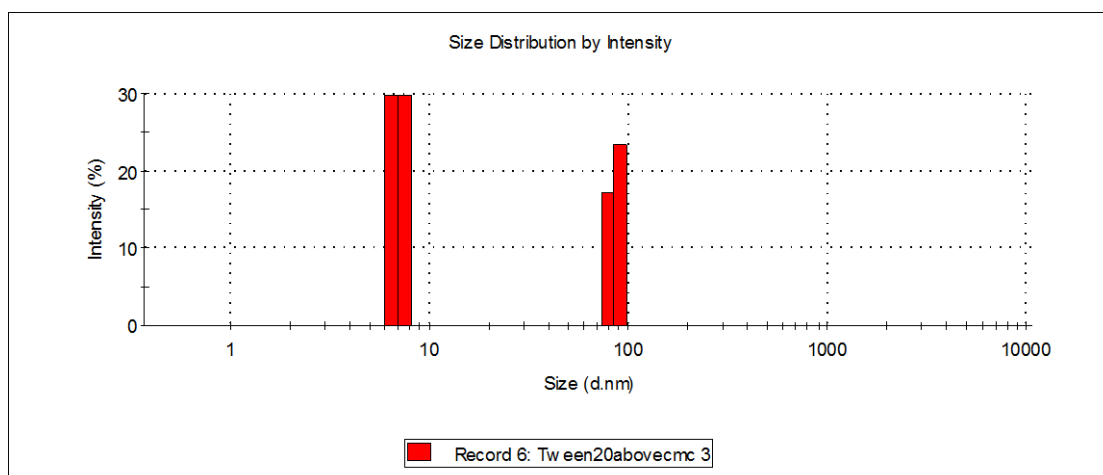
Particle size distribution by intensity for Tween 20 below CMC.

APPENDIX 26.



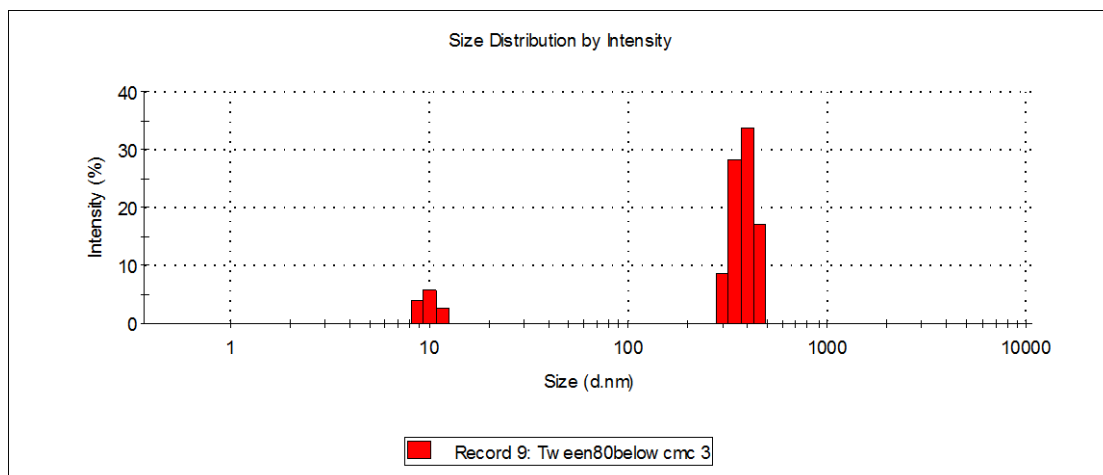
Particle size distribution by intensity for Tween 20 around CMC.

APPENDIX 27.



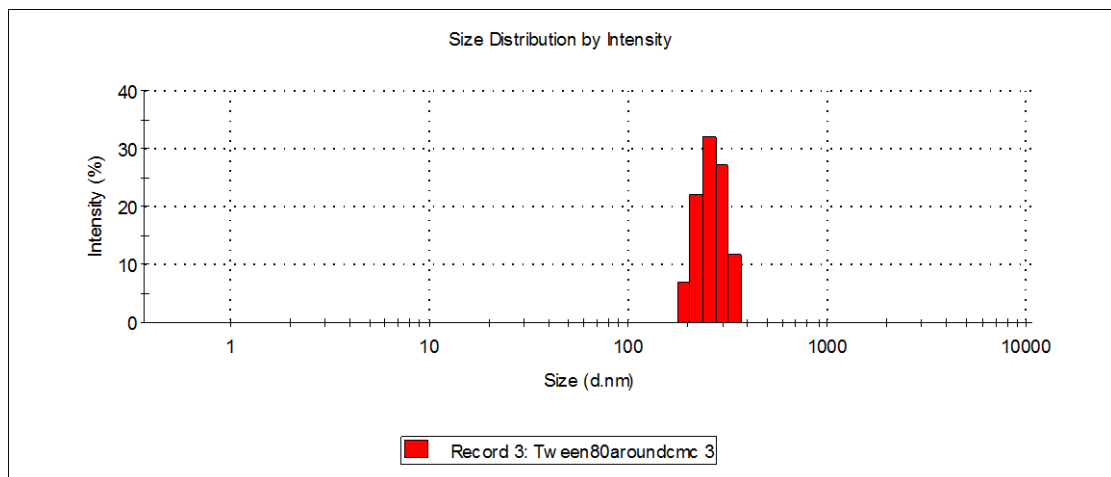
Particle size distribution by intensity for Tween 20 above CMC.

APPENDIX 28.



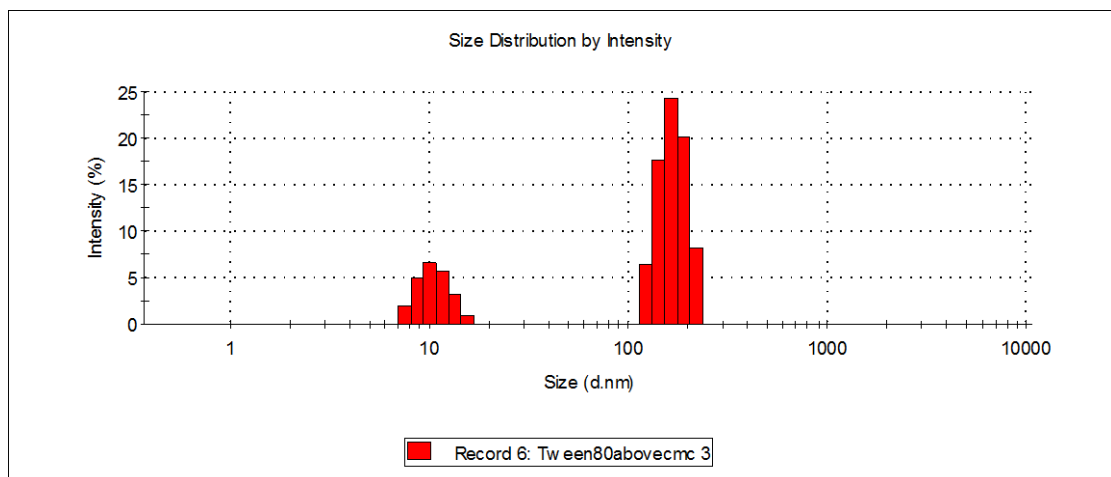
Particle size distribution by intensity for Tween 80 below CMC.

APPENDIX 29.



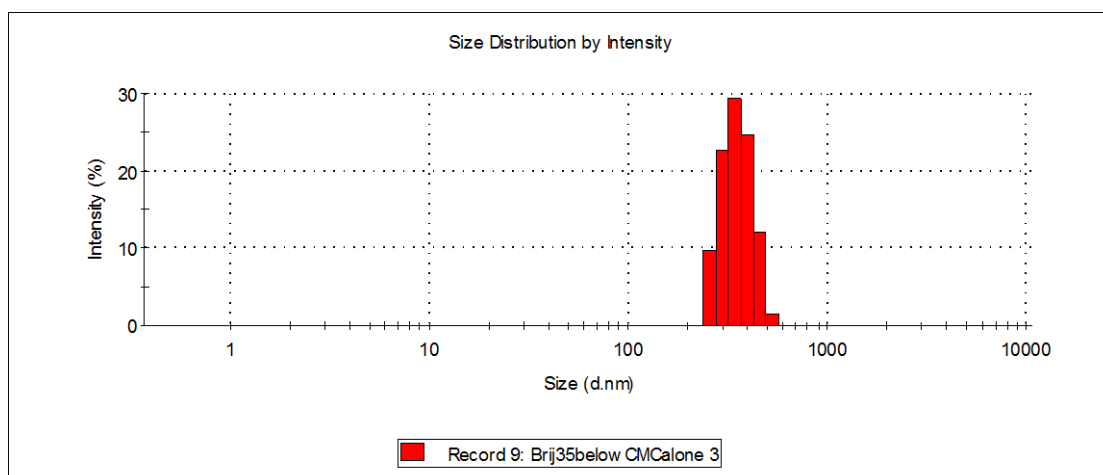
Particle size distribution by intensity for Tween 80 around CMC.

APPENDIX 30.



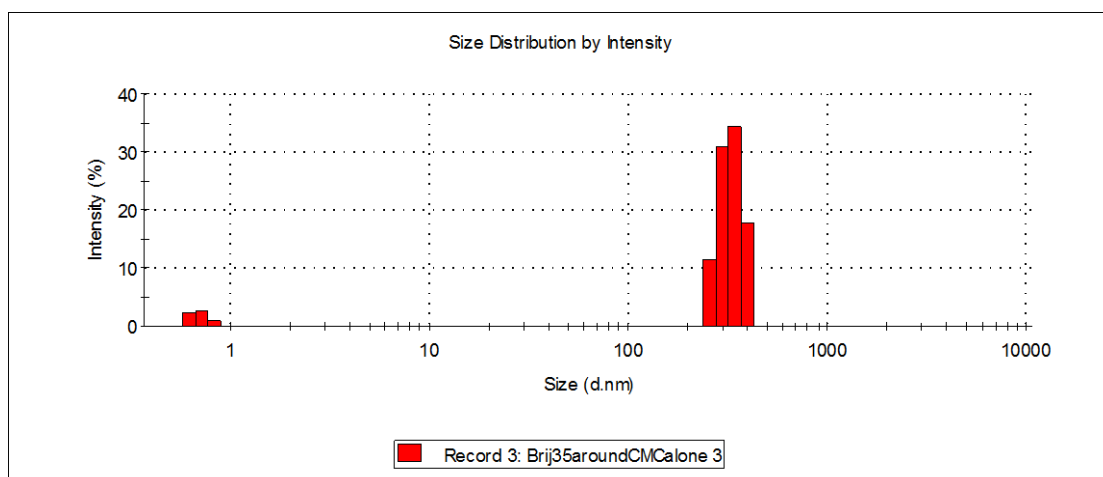
Particle size distribution by intensity for Tween 80 above CMC.

APPENDIX 31.



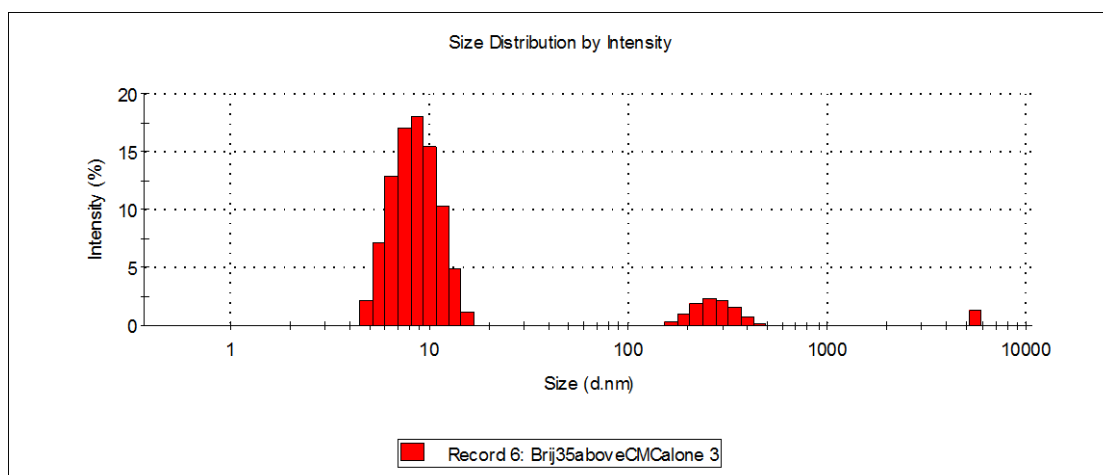
Particle size distribution by intensity for Brij 35 below CMC.

APPENDIX 32.



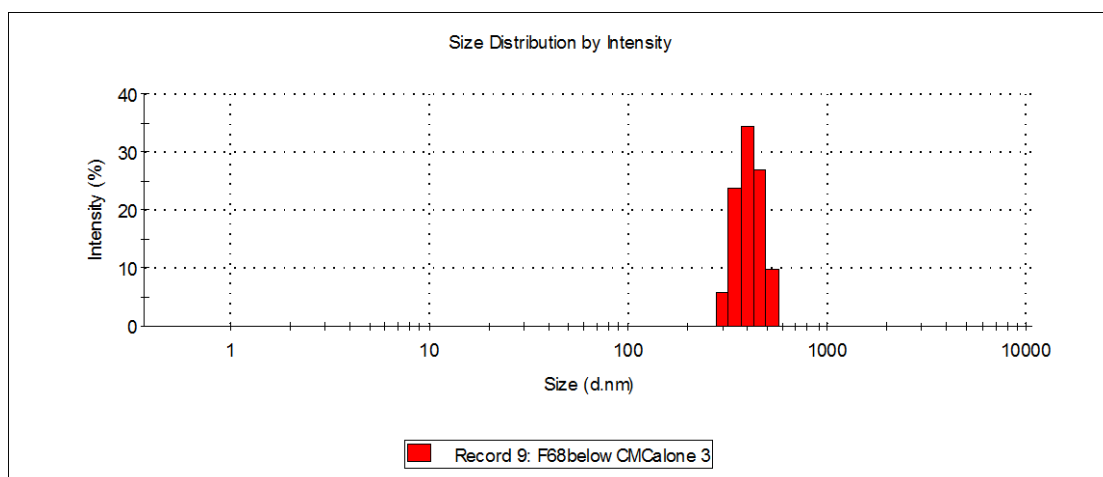
Particle size distribution by intensity for Brij 35 around CMC.

APPENDIX 33.



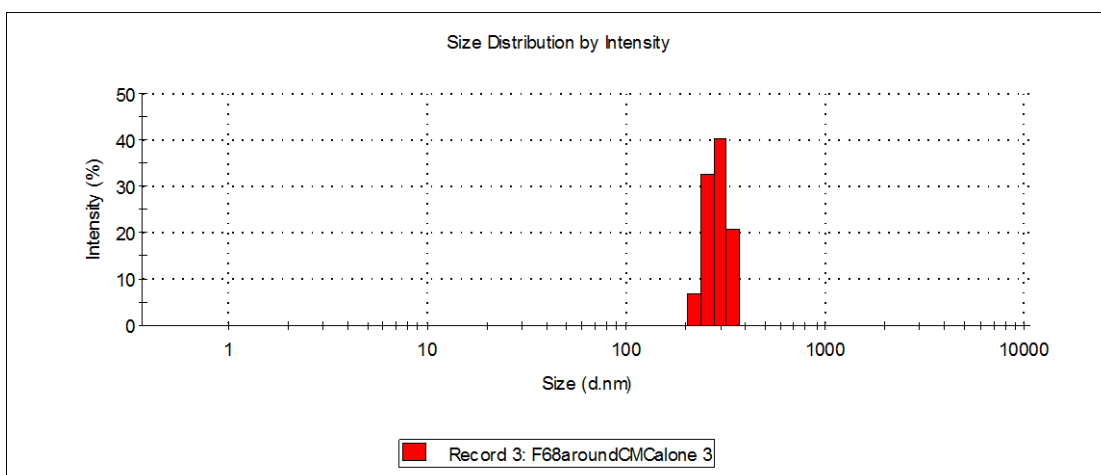
Particle size distribution by intensity for Brij 35 above CMC.

APPENDIX 34.



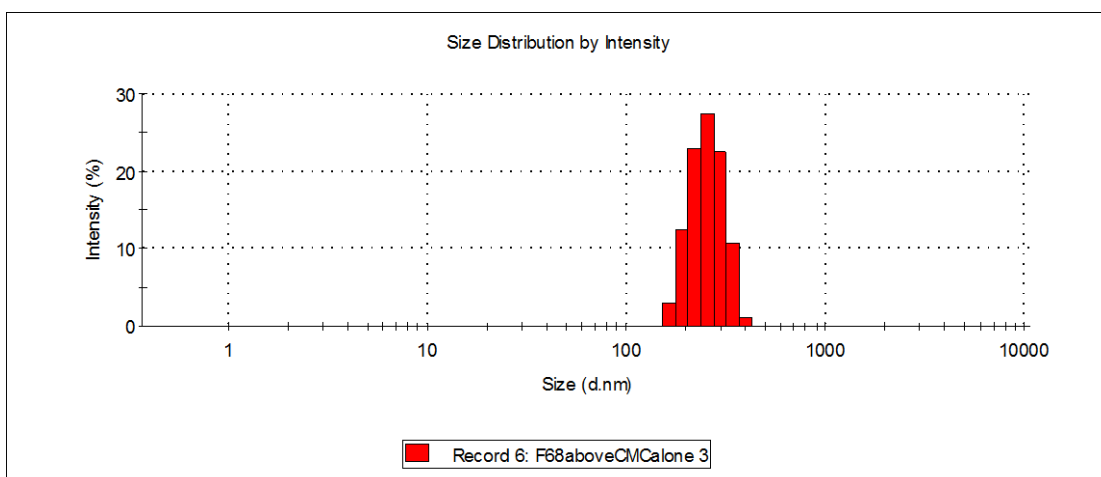
Particle size distribution by intensity for Pluronic F-68 below CMC.

APPENDIX 35.



Particle size distribution by intensity for Pluronic F-68 around CMC.

APPENDIX 36.



Particle size distribution by intensity for Pluronic F-68 above CMC.

